



ESCOLA DE DOUTORAMENTO  
INTERNACIONAL DA USC

Érika  
Diz Pita

Tese de doutoramento

Qualitative dynamics of planar  
and spatial Lotka-Volterra and  
Kolmogorov systems

Santiago de Compostela, 2022

Programa de Doutoramento en Matemáticas

TESE DE DOUTORAMENTO

**QUALITATIVE DYNAMICS OF PLANAR  
AND SPATIAL LOTKA-VOLTERRA AND  
KOLMOGOROV SYSTEMS**

Érika Diz Pita

ESCOLA DE DOUTORAMENTO INTERNACIONAL DA UNIVERSIDADE DE SANTIAGO DE COMPOSTELA  
PROGRAMA DE DOUTORAMENTO EN MATEMÁTICAS

SANTIAGO DE COMPOSTELA

ANO 2022





## DECLARACIÓN DA AUTORA DA TESE

### **Qualitative dynamics of planar and spatial Lotka-Volterra and Kolmogorov systems**

Dna. Érika Diz Pita

Presento a miña tese, seguindo o procedemento adecuado ao Regulamento, e declaro que:

- 1) A tese abarca os resultados da elaboración do meu traballo.
- 2) No seu caso, na tese faise referencia ás colaboracións que tivo este traballo.
- 3) Confirmo que a tese non incorre en ningún tipo de plaxio doutros autores nin de traballos presentados por min para a obtención doutros títulos.
- 4) A tese é a versión definitiva presentada para a súa defensa e coincide a versión impresa coa presentada en formato electrónico.

E comprométome a presentar o Compromiso Documental de Supervisión no caso de que o orixinal non estea na Escola.

En Santiago de Compostela, 16 de maio de 2022



## AUTORIZACIÓN DOS DIRECTORES DA TESE

### **Qualitative dynamics of planar and spatial Lotka-Volterra and Kolmogorov systems**

D. Jaume Llibre Saló

Dna. M. Victoria Otero Espinar

#### INFORMAN:

*Que a presente tese correspóndese co traballo realizado por Dna. Érika Diz Pita , baixo a nosa dirección, e autorizamos a súa presentación, considerando que reúne os requisitos esixidos no Regulamento de Estudos de Doutoramento da USC, e que como directores desta non incorremos nas causas de abstención establecidas na lei 40/2015.*

*De acordo co indicado no Regulamento de Estudos de Doutoramento, declaramos tamén que a presente tese de doutoramento é idónea para ser defendida en base á modalidade monográfica con reprodución de publicacións, nas que a participación da doutoranda foi decisiva para a súa elaboración e as publicacións se axustan ao Plan de Investigación.*

En Santiago de Compostela, 16 de maio de 2022

Asdo. Jaume Llibre Saló

Asdo. M. Victoria Otero Espinar



*A todos los que me alegráis los días,  
porque con vosotros cerca es como si siempre fuese mi cumpleaños.*



# Agradecimientos

---

Gracias, en primer lugar, a mis directores de tesis. Porque toda la culpa de que yo haya escrito una tesis la tiene Viví, que creyó en mí desde el principio, y me acompañó y apoyó cada día a lo largo de estos años. Jaume ha estado siempre presente, aportando la calma y la seguridad, encontrando siempre una solución a todos mis problemas. Gracias a los dos por haberlo hecho posible.

Gracias a mi familia. A mis padres, por enseñarme las cosas más importantes, por vuestro cariño y vuestra alegría, que hacen que siga queriendo volver siempre a casa. Gracias a mi abuela, porque aún no sé qué voy a ser de mayor, pero lo que quiero es ser como tú. Gracias a Dani, a Sarahit y a Flavia, porque también sois mi familia, y porque incluso en los momentos en los que todo salía mal y quería dejar la tesis, estar con vosotros me hacía feliz.

Gracias a mis compañeros del departamento, incluídos los del módulo siete, porque el silencio y la tranquilidad están sobrevalorados. Gracias por hacer que este sea el mejor lugar para trabajar, por preocuparos por mí y estar siempre dispuestos a ayudarme en todo.

Gracias a todos los que habéis compartido conmigo el día a día en la facultad, a los que compartís los planes, las comidas y las cenas, los cafés aunque yo solo tome té, los congresos sean en la ciudad que sean, las quejas y los dramas, la navidad y el carnaval, y tantas otras cosas. Porque sois sin duda la mejor parte de todos estos años.

Gracias a María y a Paula, por acompañarme tan de cerca este último año. Porque teneros en casa cada día lo ha hecho todo mucho más fácil y divertido.

Gracias a Gelu, María, Sabe y Sara. Por quererme, por confiar siempre en mí, por apoyarme, animarme, y aconsejarme, pero también por reñirme; por escucharme, pero también por mandarme callar; por compartir los días (y los años) buenos y también los malos. Gracias por ser mis amigas, con todo lo que eso significa.

Gracias a Bea por escucharme, entenderme y animarme siempre. Por darme consejos y recordarme qué es lo correcto, incluso cuando sabes que haré todo lo contrario.

Y gracias a Laura. Porque has sido a veces directora de tesis, a veces familia y a veces compañera de departamento. Pero siempre amiga. Gracias por compartirlo todo.





# Contents

---

<b>Introduction</b>	<b>v</b>
Aims and objectives . . . . .	ix
Methodology . . . . .	x
<b>Resumo</b>	<b>xiii</b>
<b>Resumen</b>	<b>xxiii</b>
<b>Summary</b>	<b>xxxiii</b>
<b>1 Preliminaries</b>	<b>1</b>
1.1 Vector fields . . . . .	1
1.2 Singular points . . . . .	2
1.3 Poincaré compactification . . . . .	12
1.4 Topological equivalence and phase portraits . . . . .	16
1.5 Normally hyperbolic submanifolds . . . . .	18
1.6 Indices of singular points . . . . .	18
1.7 Invariants and application of the Darboux theory of integrability . . . . .	18
1.8 Limit cycles: bifurcation and averaging theory . . . . .	25
<b>2 First Kolmogorov family (I)</b>	<b>29</b>
2.1 Properties of the systems . . . . .	34
2.2 Finite singular points . . . . .	37
2.3 Infinite singular points . . . . .	46
2.3.1 Case $c_1$ non-zero . . . . .	50
2.3.2 Case $c_1$ zero . . . . .	59
2.4 Global phase portraits . . . . .	67
2.4.1 Cases with a totally-determined local phase portrait at infinity . . . . .	67
2.4.2 Cases with undetermined sectors at infinity . . . . .	68
2.4.3 Cases with three possible global phase portraits . . . . .	69
2.5 Topological equivalences . . . . .	81

<b>3</b>	<b>First Kolmogorov family (II)</b>	<b>89</b>
3.1	Local study of finite singular points . . . . .	91
3.2	Local study of infinite singular points . . . . .	94
3.2.1	Case with $\tilde{O}_1$ semi-hyperbolic . . . . .	95
3.2.2	Case with $\tilde{O}_1$ linearly zero . . . . .	97
3.3	Global phase portraits . . . . .	102
<b>4</b>	<b>Second Kolmogorov family (I)</b>	<b>109</b>
4.1	Properties of the systems . . . . .	112
4.2	Finite singular points . . . . .	113
4.3	Local study of infinite singular points in chart $U_1$ . . . . .	117
4.3.1	Nondicritical case . . . . .	119
4.3.2	Dicritical case . . . . .	126
4.4	Local study of infinite singular points in chart $U_2$ . . . . .	127
4.5	Global phase portraits . . . . .	133
4.5.1	Cases with a totally-determined local phase portrait at infinity . . . . .	133
4.5.2	Cases with undetermined sectors at infinity . . . . .	134
4.5.3	Cases with three possible global phase portraits . . . . .	137
4.6	Topological equivalences . . . . .	147
<b>5</b>	<b>Second Kolmogorov family (II)</b>	<b>155</b>
5.1	Local study of finite singular points . . . . .	157
5.2	Local study of infinite singular points . . . . .	158
5.2.1	Study of the origin of chart $U_1$ . . . . .	160
5.2.2	Study of the origin of chart $U_2$ . . . . .	162
5.3	Global phase portraits . . . . .	162
5.4	Topological equivalences . . . . .	166
<b>6</b>	<b>Zero-Hopf bifurcation on Kolmogorov systems</b>	<b>171</b>
6.1	Kolmogorov systems under conditions (ii) . . . . .	173
6.1.1	Examples of Theorem 6.1.1 . . . . .	177
6.2	Kolmogorov systems under conditions (iii) and (iv) . . . . .	179
6.2.1	Examples of Theorem 6.2.1 . . . . .	182
6.3	Kolmogorov systems under conditions (v) . . . . .	183
6.3.1	Examples of Theorem 6.3.1 . . . . .	186
6.4	Notation . . . . .	188
<b>7</b>	<b>Applications</b>	<b>193</b>
7.1	Predator-prey systems: a review on some recent advances . . . . .	194
7.2	The Rosenzweig-MacArthur model as a Kolmogorov system . . . . .	198
7.2.1	Finite singular points . . . . .	199
7.2.2	Infinite singular points . . . . .	201
7.2.3	Cases with no singular points in the positive quadrant . . . . .	202
7.2.4	Cases with singular points in the positive quadrant . . . . .	203
7.2.5	Phase portraits on the positive quadrant of the Poincaré disk . . . . .	206

7.2.6	Conclusions . . . . .	207
7.3	A two prey and one predator system . . . . .	207
7.3.1	Analysis of the system on the invariant planes . . . . .	209
7.3.2	Existence and stability analysis of equilibria . . . . .	216
7.3.3	Some remarks about coexistence of the three species . . . . .	223
7.3.4	Hopf bifurcation . . . . .	226
7.3.5	Conclusions . . . . .	230
<b>General conclusions and future work</b>		<b>231</b>
<b>Bibliography</b>		<b>234</b>
<b>Further information</b>		<b>245</b>



# Introduction

---

In recent years we have all become convinced of the importance of being able to understand the evolution of a contagious disease that is spreading among the population. We also find it interesting, in a world increasingly committed to the environment, to study how the populations of different species that coexist in an habitat can evolve in the future. We want to know how the economy works and how different actors or decisions may affect it and cause changes that affect society; how different languages evolve and coexist in a territory; how the chemical reactions, which are necessary to give rise to all those materials or medicines that we need in our daily lives, are regulated and developed. We are also curious about things that are much further away from us: astronomical phenomena, star movements or black holes. All these subjects have something in common, and that is that we can approach, understand and analyze them through differential equations. Then, it seems to be clear that the study of differential equations is of great interest.

In this work, our aim is to accomplish the qualitative study of some ordinary differential systems. Besides its fundamental role on applied mathematics, because they are an important tool for modeling problems from other sciences, their study is also interesting on pure mathematics. Particularly, we will study polynomial differential systems, with special emphasis on the Lotka-Volterra and Kolmogorov systems.

The Lotka-Volterra systems have been used for modeling many natural phenomena, such as the time evolution of conflicting species in biology [84, 97, 141], chemical reactions [63], physical problems as the coupling of waves in laser physics [80] or the evolution of neutral species, electrons and ions in plasma physics [81], hydrodynamics [19], just as other problems from social science and economics [54, 124].

These systems, which are polynomial differential equations of degree two, were initially proposed, independently, by Alfred J. Lotka in 1925 and Vito Volterra in 1926, both in the context of competing species.

The first contributions of Alfred J. Lotka were in 1910 in the field of autocatalytic chemical reactions, studying models similar to the logistic equation. In 1920, Lotka extended the model to organic systems, using a plant species and a herbivorous animal species. The application to the study of the dynamics of a predator-prey system was proposed in 1925, in a work which today we would consider to be included in the field called Biomathematics [92].

On his behalf, Volterra considered the same model simultaneously, in his case, to explain some observations made by her son-in-law, the marine biologist Umberto D'Ancona. D'Ancona studied the fish catches in the Adriatic Sea and had noticed that the percentage of predatory fish caught had increased during the years of World War I. This fact seemed confus-

ing, because the fishing effort had been reduced during that years, so Volterra was interested in studying this situation.

In order to explain this behavior, Volterra stated a system of ordinary differential equations. He considered  $x(t)$  and  $y(t)$  the densities of prey and predators, respectively, and reasoned about the growth rates in the next way: the growth rate of prey,  $\dot{x}/x$ , must be a decreasing function on  $y$ , positive in absence of predators; furthermore, the growth rate of predators,  $\dot{y}/y$ , must be an increasing function on  $x$ , negative in absence of prey. Assuming the functions are linear, and taking positive constants  $a, b, c$  and  $d$ , the model stated by Volterra was

$$\begin{aligned}\dot{x} &= x(a - by), \\ \dot{y} &= y(-c + dx).\end{aligned}$$

For this first model, the phase portrait on the positive quadrant, the unique region which is interesting in the case of populations, consists on periodic orbits surrounding a singular point  $(\tilde{x}, \tilde{y}) = (c/d, a/b)$ . The means of population densities along the orbits coincide with the values at the singular point. The decrease of the parameter  $a$ , which represents the growth rate of prey in absence of predators, and the increase of  $c$ , the decrease rate of predators in absence of prey, without changing the parameters  $b$  and  $d$ , has an effect on the means of the densities of both populations, which corresponds with the observation of D'Ancona.

Volterra employed elegant reasonings, included in [132], nevertheless, his equations were simple and unrealistic. For instance, the system implies that a prey population, in absence of predators, would grow exponentially towards infinity.

Later, Lotka-Volterra systems were generalized and considered on arbitrary dimension, it is:

$$\dot{x}_i = x_i \left( a_{i0} + \sum_{j=1}^n a_{ij} x_j \right), \quad i = 1, \dots, n.$$

Consequently, the applications of these systems started to multiply. On economic theory, Lotka-Volterra systems are applied to many problems and, although their first appearance in this field is usually attributed to Richard Goodwin in 1967 [60], as can be found in [37], previous applications have been found. The Italian economist Giuseppe Palomba used these equations on 1939 (see [56]). More recent applications on this field can be found on [55] and [136].

In the field of hydrodynamics (see [19]), already in the decade of 1970, became evident that low order systems of ordinary differential equations, particularly Lotka-Volterra systems, were suitable for the simulation, at least qualitative, of many phenomena related with transition to turbulence in fluid flows. This turned out surprising because of the infinite number of degrees of freedom of a fluid and the fact that the basic equations of motion are partial differential equations.

From a more theoretical point of view, Brening and Goriely proved in [15, 16] that many other differential systems coming from different sciences can be transformed into Lotka-Volterra systems on dimension three. For example, these systems are equivalent to the replicator differential equations used in game theory, economics and evolution, as can be seen in [67].

On the other side, in [76], Kolmogorov extended Lotka-Volterra systems to others of arbitrary degree, i.e.,

$$\dot{x}_i = x_i P_i(x_1, \dots, x_n), i = 1, \dots, n,$$

where  $P_i$  are polynomials of degree at most  $m$ . These systems have also interesting applications in science, as in the study of black holes in cosmology. In [1] the qualitative analysis of a Kolmogorov system on dimension three is performed, which appears in a natural way while studying black holes with a Higgs field, see [14] for specific details.

While many other applications were appearing, for both the Kolmogorov and Lotka-Volterra systems, the applications in the original field in which the original Lotka-Volterra system appeared, population dynamics, continued developing. In [43] we have reviewed some recently studied predator-prey systems, focusing on some of the features that have been of special interest for the researchers.

For the mathematicians which have been interested in the study of these systems throughout history, one of the fundamental objectives was the study of integrability, which is only possible for a very restricted set of parameters.

In [21] some integrable cases of the Lotka-Volterra systems were obtained, using a generalized Carleman method, which can be consulted in [27], and the results were extended to dimension  $n$ . In [29] the study of integrability of Lotka-Volterra systems on dimension two was continued.

Certainly, the qualitative analysis of these systems has a special interest due to the difficulty of studying their integrability. Qualitative theory of differential equations, which was initiated by Poincaré in [109], studies the behavior of differential equations by other means which are not finding their solutions, and allows us, using tools from analysis and topology, to solve them in a qualitative way, obtaining information about their properties.

For Lotka-Volterra systems on dimension two, D. Schlomiuk and N. Vulpe have carried out a complete study of the global qualitative dynamics, classifying all possible phase portraits on the Poincaré disk, as it appears in [117]. For that purpose, they have used theory of invariants. This theory has been developed for polynomial systems of arbitrary degree and dimension but so far, only for the planar polynomial systems of degree two all the necessary invariants are known. Those invariants have been obtained for first time in [8].

Regarding Lotka-Volterra systems on dimension three, there exist some partial results for special cases in which the systems are simpler. For instance, it have been studied the May-Leonard systems, a particular case in which only two parameters appear, that was proposed in [98], representing the competition between three species. The fact that these systems have only two parameters, instead of the twelve that present the general Lotka-Volterra systems on dimension three, simplifies the study of the global dynamics, which has been carried out in [12].

Despite the intricacy of their study, Lotka-Volterra equations on dimension three are really interesting and have many applications, as mentioned above. However, there are not general results about global dynamics on dimension three.

In this work, we accomplish the study of the global dynamics of Lotka-Volterra systems



on dimension three, i.e.,

$$\begin{aligned}\dot{x} &= x(a_0 + a_1x + a_2y + a_3z), \\ \dot{y} &= y(b_0 + b_1x + b_2y + b_3z), \\ \dot{z} &= z(c_0 + c_1x + c_2y + c_3z),\end{aligned}$$

which have a rational first integral of degree two of the form  $x^{\lambda_1}y^{\lambda_2}z^{\lambda_3}$ . In Chapter 1, in addition to the introduction of all the necessary preliminaries to make the work self-contained, we use the Darboux theory of integrability to obtain a characterization of these systems. As a result, we reduce the initial problem to a problem on dimension two, the study of the global dynamics of the next two Kolmogorov families:

$$\begin{aligned}\dot{x} &= x(a_0 + a_1x + a_2z^2 + a_3z), & \dot{y} &= y(b_0 + b_1yz + b_2y + b_3z), \\ \dot{z} &= z(c_0 + c_1x + c_2z^2 + c_3z), & \dot{z} &= z(c_0 + c_1yz + c_2y + c_3z).\end{aligned}$$

These families depend on eight parameters, which is a big number in order to classify all their distinct topological phase portraits. Then we require that these Kolmogorov systems have a Darboux invariant of the form  $e^{st}x^{\lambda_1}z^{\lambda_2}$  for the first one and  $e^{st}y^{\lambda_1}z^{\lambda_2}$  for the second, and applying the Darboux theory of integrability, we reduce the study of the two previous families to the study of the two following:

$$\begin{aligned}\dot{x} &= x(a_0 - \mu(c_1x + c_2z^2 + c_3z)), & \dot{y} &= y(b_0 + b_1yz + b_2y + b_3z), \\ \dot{z} &= z(c_0 + c_1x + c_2z^2 + c_3z), & \dot{z} &= z(c_0 - \mu(b_1yz + b_2y + b_3z)),\end{aligned}$$

which now depend on six parameters. For these Kolmogorov systems we give the topological classification of all their phase portraits in the Poincaré disk. The Poincaré disk is the closed unit disc where the plane  $\mathbb{R}^2$  is identified with its interior and its boundary, the circle  $\mathbb{S}^1$ , is identified with the infinity of  $\mathbb{R}^2$ . Note that in the plane  $\mathbb{R}^2$  we can go to infinity in as many directions as points has the circle  $\mathbb{S}^1$ .

In Chapter 2 we study the first family in the case it has only isolated singular points, and in Chapter 3 we study the global phase portraits with infinitely many singular points at infinity. The same is done with the second family in Chapters 4 and 5.

We also deal with the study of limit cycles in the Kolmogorov systems. Limit cycles, i.e., isolated periodic orbits in the set of all periodic orbits of a differential system, play an important role in the qualitative theory of differential equations. The behavior of many real-world oscillatory systems have been modeled by limit cycles, see for instance the famous limit cycle of van der Pol [110]. The study of the limit cycles was initiated by Poincaré [108] and a great interest in their study was motivated by the famous 16th Hilbert problem [65, 72, 82], which concerns the determination of the upper bound for the number of limit cycles in polynomial vector fields of dimension two and degree  $n$ , and the investigation of their relative positions.

We want to study the limit cycles of the Kolmogorov systems of degree three in  $\mathbb{R}^3$  which bifurcate in the zero-Hopf bifurcations of the singular points  $(a, b, c)$  which are not on the invariant planes  $x = 0$ ,  $y = 0$  and  $z = 0$  of the Kolmogorov systems

$$\dot{x} = xP(x, y, z), \quad \dot{y} = yQ(x, y, z), \quad \dot{z} = zR(x, y, z),$$

with  $P$ ,  $Q$  and  $R$  polynomials of degree two. This study is carried out in Chapter 6.

To conclude we focus our attention on the applications. In Chapter 7, first of all, we briefly present a review work which gives us a better understanding of how predator-prey models have advanced in recent years and which are the topics and characteristics that have particularly attracted the attention of researchers. Next, we study a predator-prey system in the plane, for which we obtain its global phase portraits in the positive quadrant of the Poincaré disk. Finally, we present a model in dimension three, with two prey and one predator, whose restriction to only two of the variables coincides with the previous model. For this three-dimensional model we study different aspects of its qualitative dynamics, including the existence of limit cycles.

We see, therefore, that population models have come a long way and are becoming more and more realistic. Even so, and after having analyzed the literature, there are still many open problems that are of interest to improve the existing models and that we would like to address in the future.

## Aims and objectives

The main goal of the PhD thesis is to accomplish the qualitative study of some ordinary differential systems, particularly, the Lotka-Volterra and Kolmogorov systems. We work on the following specific goals:

### O1 *Contribution to the qualitative study of the Lotka-Volterra systems on dimension three.*

There are not general results about global dynamics of Lotka-Volterra systems on dimension three, despite their interest and the multiple applications that they have. To make some progress in this field, we want to study the global dynamics of Lotka-Volterra systems on dimension three, i.e.,

$$\begin{aligned}\dot{x} &= x(a_0 + a_1x + a_2y + a_3z), \\ \dot{y} &= y(b_0 + b_1x + b_2y + b_3z), \\ \dot{z} &= z(c_0 + c_1x + c_2y + c_3z),\end{aligned}$$

which have a rational first integral of degree two of the form  $x^{\lambda_1}y^{\lambda_2}z^{\lambda_3}$ . To this end, we must address the following objectives:

#### O1.A *Application of the Darboux theory of integrability to obtain a characterization of these systems.*

Through the work carried out to achieve this objective, we reduce the initial problem to a problem on dimension two, the study of the global dynamics of two Kolmogorov families. This objective is addressed in Chapter 1.

#### O1.B *Reduction of the number of parameters through the requirement of suitable conditions.*

We must determine and impose conditions that allow us to reduce the number of parameters, in order to face a manageable problem. This leads us to obtain two Kolmogorov families in the plane. This objective is also addressed in Chapter 1.

**O1.C** *Study and topological classification of the global phase portraits of the obtained families.*

We study the two families of Kolmogorov systems obtained, distinguishing the cases in which the singular points are isolated and the ones with a continuum of singular points at infinity. These objectives are addressed for the first family in chapters 2 and 3, respectively, and for the second family in chapters 4 and 5.

**O2** *Study of the limit cycles in the Kolmogorov systems.*

Limit cycles are the isolated periodic orbits in the set of all periodic orbits of a differential system, and they play an important role in the qualitative theory of differential equations. Specifically, we want to study the limit cycles of the Kolmogorov systems of degree three in  $\mathbb{R}^3$  which bifurcate in the zero-Hopf bifurcations of the singular points  $(a, b, c)$  which are not on the invariant planes  $x = 0$ ,  $y = 0$  and  $z = 0$  of the Kolmogorov systems

$$\dot{x} = xP(x, y, z), \quad \dot{y} = yQ(x, y, z), \quad \dot{z} = zR(x, y, z),$$

with  $P$ ,  $Q$  and  $R$  polynomials of degree two. This study is carried out in Chapter 6.

**O3** *Analysis of the applications of polynomial systems to problems from other sciences, and study of some concrete models.*

**O3.A** *Review of the predator-prey models studied in recent years.*

Since Lotka-Volterra systems, in which this work focuses, were proposed in the context of population dynamics, especially predator-prey dynamics, our aim is to review the current development of this kind of systems.

**O3.B** *Study of some predator-prey systems in dimensions two and three.*

We want to study some predator-prey models from a qualitative point of view, by analyzing, for example, the existence of limit cycles and the topological classification of their global phase portraits.

## Methodology

This thesis follows the classic methodology in basic research in mathematics. In general, the research begins by carrying out a comprehensive study of the topics to be addressed and reviewing some classical and recent bibliographical references. Here we describe the methods used in the development of the objectives O1-O3.

**O1** *Contribution to the qualitative study of the Lotka-Volterra systems on dimension three.*

**O1.A** *Apply the Darboux theory of integrability to obtain a characterization of these systems.*

**O1.B** *Reduction of the number of parameters through the requirement of suitable conditions.*

To achieve these two objectives, our methodology is based on applying the results of Darboux theory of integrability, which can be found in [50, Chapter 8].

*O1.C Study and topological classification of the global phase portraits of the obtained families.*

For the classification of the finite and infinite singular points in the Poincaré disk, we use the local chart formulation of the Poincaré disk, which can be found, for example, in [50, Chapter 5]. For the study of the local phase portraits of these singular points, we use the results for hyperbolic, semi-hyperbolic and nilpotent singular points, which can be found in [50, Chapter 5]. For the singular points whose linear part is identically zero we use the blow up technique (see [4, 5, 49, 125, 130]).

For the study of the possible global phase portraits in the Poincaré disk, according to the Theorem of Markus-Neumann-Peixoto, we determine all the possible  $\alpha$  and  $\omega$ -limits of the separatrices of the considered Kolmogorov systems.

Then, from all the possible global phase portraits in the Poincaré disk obtained, we classify those that are realizable and from among them, we study which are the topological equivalence classes by using, among other tools, invariants, symmetries or rotations.

*O2 Study of the limit cycles in the Kolmogorov systems.*

In Chapter 6 we deal with this objective and, in order to accomplish it, we use the averaging theory of first order (see [17, 18, 86, 131]) to study the limit cycles bifurcating from the zero-Hopf bifurcations of the Kolmogorov systems of degree three in  $\mathbb{R}^3$ .

*O3 Analysis of the applications of polynomial systems to problems from other sciences, and study of some concrete models.*

*O3.A Review of the predator-prey models studied in recent years.*

To develop this objective, we carried out a review of the recent work in the field of population dynamics, specifically in predator-prey systems, selecting some characteristics that seemed relevant for the researchers in the last years. We compare different models, analyzing their differences and similarities as well as the different behaviors they show.

*O3.B Study of some predator-prey systems in dimensions two and three.*

To achieve this objective, the techniques and methodologies used in the development of the previous objectives are combined to study some specific predator-prey models.

The use of computers is an essential tool in different parts of the thesis. We use the algebraic manipulator Mathematica 12.0.0.0 (for Mac OS X x86) to perform symbolic calculations and represent graphics of solutions and phase portraits obtained numerically. All the global and local phase portraits obtained as a result of the objective O1.C included in this thesis are done with the software Inkscape. The software P4 [7] is used as a support in Chapters 2 to 5, especially to study the feasibility of global phase portraits.



# Resumo

---

Os contidos desta tese, titulada *Dinámica cualitativa de sistemas Lotka-Volterra e Kolmogorov no plano e no espazo*, son o resultado do traballo realizado por Érika Diz Pita durante os estudos correspondentes ao Programa de Doutoramento en Matemáticas da Universidade de Santiago de Compostela. Este traballo foi realizado en colaboración cos seus directores de tese Jaume Llibre Saló (Universitat Autònoma de Barcelona) e M. Victoria Otero Espinar (Universidade de Santiago de Compostela), así como coa profesora Claudia Valls Anglès (Universidade de Lisboa), responsable da estancia de investigación preceptiva para optar á mención internacional, e co profesor Renato Colucci (Università Politecnica delle Marche).

Esta tese céntrase no estudo da dinámica cualitativa de sistemas de ecuacións diferenciais en dimensión dous e tres, especialmente de sistemas Lotka-Volterra e Kolmogorov. Estes sistemas permiten modelizar moitos procesos e fenómenos da natureza, así como problemas que xorden noutras ciencias ou cuestións de carácter social. Por iso, o coñecemento da dinámica destes sistemas resulta de interese non só dende un punto de vista teórico, senón tamén polas súas múltiples aplicacións.

Fixéronse importantes avances no estudo destes sistemas, por exemplo, a dinámica dos sistemas Lotka-Volterra en dimensión dous foi totalmente estudada en [117]. Con todo, para os sistemas Lotka-Volterra en dimensión tres estudáronse só algunhas familias moi concretas, como é o caso dos sistemas de May-Leonard [98], que dependen só de dous parámetros.

Nesta tese preténdese avanzar no estudo dos sistemas Lotka-Volterra en dimensión tres, considerando unha familia máis xeral e cun maior número de parámetros. A caracterización desta familia realízase no Capítulo 1, xunto coa introdución dos resultados preliminares necesarios para o desenvolvemento dos capítulos posteriores. Nos Capítulos 2–5 estúdase completamente a dinámica global dos sistemas Kolmogorov planos obtidos como resultado desa caracterización.

No Capítulo 6 abórdase o estudo dos ciclos límite, un dos elementos máis importantes dentro da teoría cualitativa. Concretamente, caracterizamos os sistemas Kolmogorov de grao tres en dimensión tres que posúen ciclos límite que aparecen a través dunha bifurcación zero-Hopf. Empregamos para iso a técnica dos promedios de orden un.

Por último, no Capítulo 7, centrámonos nalgúns aplicacións no ámbito da dinámica de poboacións. Comezamos facendo unha revisión na que se comparan distintos modelos poboacionais, analizando como estes son cada vez máis realistas e van incorporando distintas características relativas ao comportamento das poboacións estudadas. Por último estudamos dous modelos poboacionais, un en dimensión dous e outro en dimensión tres, con dúas presas e un depredador, aplicando algunhas das técnicas introducidas con anterioridade.

A continuación resumimos con máis detalle os contidos de cada un dos capítulos.

## Capítulo 1: Preliminares

Neste primeiro capítulo, e co fin de que o traballo sexa autocontido, introducimos os conceptos e resultados que son necesarios para o desenvolvemento dos capítulos seguintes.

Comezamos incluíndo algunhas nocións elementais sobre campos vectoriais e puntos singulares nas Seccións 1.1 e 1.2. Nesta última sección presentamos tamén os resultados que permiten caracterizar localmente as singularidades non dexeneradas, semihiperbólicas e nilpotentes dos sistemas polinomiais planos. Para estudar as singularidades cuxa parte lineal é idénticamente nula recorreremos á técnica dos blow up's, que introducimos tamén na Sección 1.2. En liñas xerais, esta técnica consiste en explotar ditas singularidades, converténdoa nunha recta mediante un cambio de variable, de forma que o estudo das novas singularidades que aparecen sobre esa recta permita determinar como é o comportamento das órbitas nunha veciñanza do punto orixinal.

A continuación, na Sección 1.3, presentamos a compactificación de Poincaré, que nos permite estudar o comportamento das órbitas no infinito, a partir dunha proxección do campo en  $\mathbb{R}^2$  sobre a esfera unidade  $\mathbb{S}^2$ , á que chamamos esfera de Poincaré. Grazas a esta técnica podemos estudar os retratos de fases no disco de Poincaré, un espazo limitado obtido ao proxectar a esfera sobre o plano  $z = 0$ , en lugar de en todo o plano  $\mathbb{R}^2$ . Identificamos o interior do disco de Poincaré con  $\mathbb{R}^2$  e a súa fronteira co infinito de  $\mathbb{R}^2$ , podendo así estudar a dinámica dos sistemas nun veciñanza do infinito.

Nos retratos de fases que obtemos no disco de Poincaré, distinguimos as súas rexións canónicas, as súas separatrices, e a configuración das separatrices, conceptos que se introducen na Sección 1.4. Nesta mesma sección enunciámos o Teorema de Markus-Neumann-Peixoto, o fundamento teórico que nos permite facer a clasificación topolóxica dos retratos de fases no disco de Poincaré en función das súas configuracións de separatrices.

Na Sección 1.5 presentamos un resultado que permite estudar as subvariedades formadas por singularidades, en concreto as subvariedades normalmente hiperbólicas. Utilizamos este resultado para o estudo dos casos nos que todos os puntos do infinito, que se corresponden cos puntos da circunferencia  $\mathbb{S}^1$ , son singularidades.

Na Sección 1.6 introducimos o concepto de índice dunha singularidade, e enunciámos o Teorema de Poincaré-Hopf, que garante que a suma dos índices de todas as singularidades dun campo sobre a esfera  $\mathbb{S}^2$  é igual a dous. Este resultado, aplicado aos campos sobre a esfera de Poincaré, permítenos determinar o comportamento das órbitas nalgúns rexións do plano, onde non podemos concluír por outros métodos.

Un primeiro punto clave no noso traballo é a aplicación da teoría de Darboux para a caracterización dos sistemas diferenciais. Na Sección 1.7 introducimos algúns conceptos e resultados relacionados coa integrabilidade e as superficies invariantes e, ademais, aplicámoslos para obter unha caracterización do noso problema. Recordamos que nos propoñemos estudar os sistemas Lotka-Volterra en dimensión tres, é dicir, os sistemas

$$\begin{aligned}\dot{x} &= x(a_0 + a_1x + a_2y + a_3z), \\ \dot{y} &= y(b_0 + b_1x + b_2y + b_3z), \\ \dot{z} &= z(c_0 + c_1x + c_2y + c_3z),\end{aligned}$$

que teñen unha integral primeira racional de grado dous da forma  $x^{\lambda_1} y^{\lambda_2} z^{\lambda_3}$ . Aplicando o teorema de integrabilidade de Darboux para sistemas polinomiais, logramos reducir o estudo destes sistemas en dimensión tres ao estudo das seguintes dúas familias de sistemas Kolmogorov no plano:

$$\begin{aligned}\dot{x} &= x(a_0 + a_1x + a_2z^2 + a_3z), & \dot{y} &= y(b_0 + b_1yz + b_2y + b_3z), \\ \dot{z} &= z(c_0 + c_1x + c_2z^2 + c_3z), & \dot{z} &= z(c_0 + c_1yz + c_2y + c_3z).\end{aligned}$$

Estas familias dependen de oito parámetros, o cal supón aínda un número moi elevado para levar a cabo a clasificación de todos os seus distintos retratos de fases globais. Esiximos que estes sistemas Kolmogorov teñan un invariante de Darboux da forma  $e^{st} x^{\lambda_1} z^{\lambda_2}$  no caso da primeira familia, e da forma  $e^{st} y^{\lambda_1} z^{\lambda_2}$  no caso da segunda. Aplicando de novo o teorema de integrabilidade de Darboux reducimos o estudo das dúas familias previas ao estudo das dúas seguintes, que tamén son de tipo Kolmogorov:

$$\begin{aligned}\dot{x} &= x(a_0 - \mu(c_1x + c_2z^2 + c_3z)), & \dot{y} &= y(b_0 + b_1yz + b_2y + b_3z), \\ \dot{z} &= z(c_0 + c_1x + c_2z^2 + c_3z), & \dot{z} &= z(c_0 - \mu(b_1yz + b_2y + b_3z)).\end{aligned}$$

O estudo da dinámica global destas familias, que agora dependen de seis parámetros, lévase a cabo nos Capítulos 2–5.

Por último, na Sección 1.8, incluímos os resultados empregados para o estudo de ciclos límite, tanto os relativos á técnica dos promedios, como ás bifurcacións de Hopf.

## Capítulo 2: Clasificación da primeira familia Kolmogorov con singularidades illadas

Neste capítulo estudamos a dinámica global da primeira das familias Kolmogorov obtidas previamente, é dicir,

$$\begin{aligned}\dot{x} &= x(a_0 - \mu(c_1x + c_2z^2 + c_3z)), \\ \dot{z} &= z(c_0 + c_1x + c_2z^2 + c_3z).\end{aligned}\tag{1}$$

O resultado principal relativo a esta familia é o seguinte:

**Teorema 1.** *Os sistemas Kolmogorov (1) baixo as condicións  $H_2^1$  teñen 78 retratos de fases topoloxicamente distintos no disco de Poincaré, dados na Figura 2.0.1.*

Ao longo do capítulo lévase a cabo a proba deste resultado, realizando a clasificación topolóxica global de todos os retratos de fases no disco de Poincaré.

Comenzamos estudando algunhas das propiedades dos sistemas na Sección 2.1, o que nos permite impoñer certas condicións sobre os parámetros. En particular, consideraremos  $c_2 \neq 0$  para que os sistemas non se reduzan a sistemas Lotka-Volterra en dimensión dous, os cales xa están estudados. Ademais, como esiximos que  $e^{-t(a_0+c_0\mu)}xz^\mu$  sexa un invariante de Darboux, debemos considerar a condición  $a_0 + c_0\mu \neq 0$ . Estudando as simetrías dos sistemas podemos garantir que é suficiente estudar esta familia Kolmogorov cos parámetros verificando

$$H^1 = \{c_2 \neq 0, a_0 \geq 0, c_1 \geq 0, c_3 \geq 0, a_0 + c_0\mu \neq 0\},$$



pois en calquera outro caso obteríanse retratos simétricos respecto a algún dos xa obtidos. Polo mesmo motivo, cando  $a_0 = 0$ , podemos limitar o noso estudo ao caso con  $c_0 > 0$ . Podemos garantir tamén que nos casos nos que  $c_1 = 0$  ou  $c_3 = 0$ , os retratos globais obtidos deben ser simétricos con respecto ao eixo  $z$  ou  $x$ , respectivamente. Estudamos tamén a existencia de rectas invariantes e de puntos de contacto sobre as rectas  $z = cte$ . Isto axudaranos a determinar, máis adiante, cales dos retratos de fases globais son realizables.

Na Sección 2.2 calculamos as singularidades finitas, estudamos todos os posibles retratos de fases locais en torno a cada unha delas e facemos unha clasificación recollida nas Táboas 2.2.2 a 2.2.7. Probamos tamén que non existen ciclos límite. Eliminamos os casos nos que existe un continuo de puntos singulares, nos cales os nosos sistemas poden reducirse a outros máis sinxelos xa estudados, e traballamos entón con parámetros que satisfan as condicións:

$$H_1^1 = \{c_2 \neq 0, a_0 \geq 0, c_1 \geq 0, c_3 \geq 0, a_0 + c_0\mu \neq 0, a_0^2 + c_1^2\mu^2 \neq 0\}.$$

Na Sección 2.3 estudamos as singularidades infinitas, traballando coa compactificación de Poincaré dos sistemas.

En primeiro lugar estudamos a compactificación na carta local  $U_1$  da esfera, onde obtemos que, ou ben a única singularidade infinita é a orixe da carta, ou ben todos os puntos do infinito son singularidades. Este caso particular no que todo o infinito está formado por puntos singulares, e que se corresponde coa condición  $\mu = -1$ , estúdase de forma independente no Capítulo 3. Considerando polo tanto as condicións

$$H_2^1 = \{c_2 \neq 0, a_0 \geq 0, c_1 \geq 0, c_3 \geq 0, a_0 + c_0\mu \neq 0, a_0^2 + c_1^2\mu^2 \neq 0, \mu \neq -1\},$$

estudamos todos os posibles retratos de fases locais da orixe da carta  $U_1$ , empregando a técnica dos blow up's. En concreto, realizamos dous blow up's verticais e distinguimos casos dicríticos e non dicríticos. Como resultado de estudar as singularidades existentes sobre o divisor excepcional tras o segundo blow up, aparecen algúns casos nos que os retratos de fases non están ben definidos, polo que é preciso realizar tamén un blow up horizontal. Como resultado deste proceso obtemos un total de 47 retratos de fases locais distintos para a orixe da carta  $U_1$ , incluídos na Figura 2.3.1. Cabe mencionar que nalgúns casos queda aínda unha indeterminación en certos sectores ao rematar o proceso. Eses sectores poden ser elípticos ou hiperbólicos, e aínda que esta indeterminación podería solucionarse a nivel local aplicando outros métodos, no noso caso optamos por resolvelo a nivel global baseándonos na teoría do índice.

O estudo da compactificación na carta  $U_2$  resulta máis sinxelo. A orixe desta carta é un punto singular hiperbólico, que pode ser un nodo ou un punto de sela.

A continuación facemos o paso do estudo local desenvolvido ata o momento ao estudo global. Para iso recompilamos toda a información local obtida, partindo da clasificación nas Táboas 2.2.2 a 2.2.7. Nalgúns dos casos recollidos nestas táboas as condicións determinan un único retrato local nos puntos do infinito, pero en moitos outros temos que distinguir distintas posibilidades.

Empregamos a teoría do índice e o Teorema de Poincaré-Hopf para completar o estudo das singularidades infinitas realizado por medio de blow up's, probando se as rexións non determinadas corresponden a sectores elípticos ou hiperbólicos.

Cando as separatrices se poden conectar dunha única forma, obtemos un único retrato global a partir da información local, mais en 14 casos aparecen tres posibles retratos globais.

Empregando os resultados relativos á existencia de curvas invariantes e puntos de contacto, probamos que en cada un deses 14 casos só un dos retratos globais é realizable.

Por último, na Sección 2.5, realizamos a clasificación topolóxica dos 102 retratos globais obtidos. En primeiro lugar determinamos 19 clases de equivalencia en función de dous invariantes: o número de rexións canónicas e o número de separatrices. Dentro de cada unha das clases, seleccionamos os invariantes apropiados para distinguir aqueles retratos topoloxicamente distintos, e buscamos os homeomorfismos entre aqueles topoloxicamente iguais mediante o uso, entre outros, de xiros ou simetrías.

Concluimos así a proba do resultado principal, obtendo a clasificación topolóxica global de todos os retratos de fases no disco de Poincaré dos sistemas (1) que non teñen un continuo de singularidades no infinito.

### Capítulo 3: Clasificación da primeira familia Kolmogorov con singularidades non illadas

Neste capítulo estudamos a primeira das familias de sistemas Kolmogorov cando todos os puntos do infinito son singularidades. Este caso correspóndese co valor do parámetro  $\mu = -1$ , polo que estudamos os sistemas

$$\begin{aligned}\dot{x} &= x(a_0 + c_1x + c_2z^2 + c_3z), \\ \dot{z} &= z(c_0 + c_1x + c_2z^2 + c_3z).\end{aligned}\tag{2}$$

A partir dos resultados obtidos no capítulo previo obtemos algunhas propiedades dos sistemas, e determinamos unha serie de condicións que podemos impoñer aos parámetros sen perda de xeneralidade, en concreto:

$$\tilde{H}^1 = \{c_2 \neq 0, a_0 \geq 0, c_1 \geq 0, c_3 \geq 0, a_0 \neq c_0, a_0^2 + c_1^2 \neq 0\}.$$

O noso resultado principal sobre a dinámica global dos sistemas (2) é o seguinte:

**Teorema 2.** *Os sistemas Kolmogorov (2) baixo as condicións  $\tilde{H}^1$  teñen 22 retratos de fases topoloxicamente distintos no disco de Poincaré, dados na Figura 3.0.1.*

A existencia de singularidades finitas así como a clasificación dos seus retratos de fases locais, realízase a partir dos resultados do Capítulo 2.

Na Sección 3.2, empregando a compactificación de Poincaré, estudamos a dinámica no infinito. Neste caso, como xa se mencionou, todos os puntos do infinito son singularidades. En primeiro lugar estudamos a orixe da carta  $U_2$ , na cal a matriz Xacobiana ten un autovalor nulo e outro non nulo. Isto permítenos aplicar o Teorema 1.5.1 e concluír que, ou ben hai exactamente unha órbita que sae dese punto singular, ou ben unha única órbita que chega a él.

Considerando a expresión da compactificación na carta  $U_1$  estudamos todos os demais puntos do infinito. Nos puntos distintos da orixe estamos en condicións de aplicar o Teorema 1.5.1 e distinguir casos nos que a cada un deses puntos chega exactamente unha órbita e outros nos que de cada punto sae exactamente unha órbita.

Por outra parte, para a orixe da carta  $U_1$  obtemos 12 retratos de fases locais distintos, incluíndo casos nos que a singularidade é semihiperbólica e outros nos que é linealmente cero. Nestes últimos recorreremos ao emprego de blow up's para realizar a desingularización.

Combinando a información local, determinamos os retratos de fases globais a partir da análise das posibles conexións das separatrizes. En seis casos, as separatrizes poden conectarse de tres modos distintos. En cada un deses casos, probamos que solo un dos tres retratos globais é realizable, obtendo finalmente un total de 29 retratos no disco de Poincaré.

Por último realizamos a clasificación topolóxica. Inicialmente consideramos o número de singularidades finitas e a suma dos índices en todas as singularidades finitas como invariantes, e con eles determinamos 14 clases. Analizando as coincidencias topolóxicas dentro de cada unha desas clases, obtemos finalmente 22 retratos globais topoloxicamente distintos, probando así o resultado principal deste capítulo.

## Capítulo 4: Clasificación da segunda familia Kolmogorov con singularidades illadas

Neste capítulo abordamos o estudo da segunda das familias Kolmogorov, é dicir

$$\begin{aligned}\dot{y} &= y(b_0 + b_1 yz + b_2 y + b_3 z), \\ \dot{z} &= z(c_0 - \mu(b_1 yz + b_2 y + b_3 z)).\end{aligned}\tag{3}$$

Para estes sistemas obtemos o seguinte resultado sobre a súa dinámica global:

**Teorema 3.** *Os sistemas Kolmogorov (3) baixo as condicións  $H_2^2$  teñen 52 retratos de fases topoloxicamente distintos no disco de Poincaré, dados na Figura 4.0.1.*

A estrutura da demostración é similar á descrita no Capítulo 2. Comenzamos estudando propiedades dos sistemas, especialmente simetrías, que nos permiten traballar no seguinte espacio de parámetros:

$$H^2 = \{b_1 \neq 0, c_0 + b_0\mu \neq 0, b_0 \geq 0, b_2 \geq 0, b_3 \geq 0\}.$$

Despois estudamos a existencia de singularidades finitas e os seus retratos de fases locais, obtendo a clasificación dada nas Táboas 4.2.2 a 4.2.5. Traballamos baixo as condicións

$$H_1^2 = \{b_1 \neq 0, b_0\mu + c_0 \neq 0, b_0 \geq 0, b_2 \geq 0, b_3 \geq 0, \mu^2 b_3^2 + c_0^2 \neq 0, b_2^2 + b_0^2 \neq 0\},$$

eliminando así os casos nos que existe un continuo de puntos singulares finitos, e que poden reducirse a outros sistemas cuxa dinámica global xa foi estudada.

De novo, baixo a condición  $\mu = -1$  existe un continuo de singularidades no infinito, e estudamos ese caso de forma independente no seguinte capítulo, traballando agora baixo as condicións

$$H_2^2 = \{b_1 \neq 0, b_0\mu + c_0 \neq 0, b_0 \geq 0, b_2 \geq 0, b_3 \geq 0, \mu^2 b_3^2 + c_0^2 \neq 0, b_2^2 + b_0^2 \neq 0, \mu \neq -1\}.$$

Unha das diferencias respecto ao estudo da primeira familia, levado a cabo no Capítulo 2, é que neste caso é necesario realizar dous procesos de desingularización mediante blow up's, un para a orixe da carta  $U_1$  e outro para a orixe da carta  $U_2$ . Obtéñense 27 retratos locais no primeiro caso e 26 no segundo, como se amosa nas Figuras 4.3.1. e 4.4.1. Neste caso tamén se require combinar blow up's verticais e horizontais.

A partir da información local obtida, estudamos os retratos de fases globais no disco de Poincaré. Nalgúns casos, a información local é completa e determina unívocamente un retrato de fases a través dunha única conexión posible das separatrices. Noutros casos, aplicamos teoría do índice para determinar se certos sectores dos retratos de fases locais son elípticos ou hiperbólicos, obtendo de novo un único retrato global ao conectar as separatrices. Noutros 11 casos podemos conectar as separatrices de tres formas diferentes, dando lugar a tres retratos de fases globais. A diferenza do que ocorría coa primeira familia Kolmogorov, probamos en cada un dos 11 casos que os tres retratos globais son realizables. Para iso, en cada caso demostramos que para certos valores dos parámetros a conexión das separatrices ten lugar sobre unha recta invariante, e perturbando os parámetros obtemos as outras dúas configuracións. Compróbase tamén numericamente co programa P4, e se inclúen valores para os que cada un dos retratos se realiza.

Para concluír a demostración realizamos a clasificación topolóxica dos 106 retratos globais obtidos, comezando por determinar clases de equivalencia en función do número de rexións canónicas e separatrices. Finalmente probamos que existen un total de 52 retratos globais topoloxicamente distintos no disco de Poincaré.

## Capítulo 5: Clasificación da segunda familia Kolmogorov con singularidades non illadas

Neste capítulo terminamos a clasificación dos retratos globais das familias Kolmogorov abordando o caso no que na segunda familia todos os puntos do infinito son singularidades. Neste caso, no que o parámetro  $\mu = -1$ , estudamos os sistemas

$$\begin{aligned}\dot{y} &= y(b_0 + b_1 yz + b_2 y + b_3 z), \\ \dot{z} &= z(c_0 + b_1 yz + b_2 y + b_3 z),\end{aligned}\tag{4}$$

baixo as condicións

$$\tilde{H}^2 = \{b_1 \neq 0, c_0 - b_0 \neq 0, b_0 \geq 0, b_2 \geq 0, b_3 \geq 0, b_3^2 + c_0^2 \neq 0, b_2^2 + b_0^2 \neq 0\},$$

que podemos asumir baseándonos nos resultados obtidos no capítulo anterior. O resultado principal é o seguinte:

**Teorema 4.** *Os sistemas Kolmogorov (4) baixo as condicións  $\tilde{H}^2$  teñen 13 retratos de fases topoloxicamente distintos no disco de Poincaré, dados na Figura 5.0.1.*

Seguindo unha estrutura similar á dos capítulos anteriores, estudamos as singularidades finitas e os seus retratos de fases locais. Despois estudamos os puntos de equilibrio infinitos empregando a compactificación de Poincaré. Obtemos resultados sobre a dinámica en veciñanzas das singularidades infinitas empregando o Teorema 1.5.1 para subvariedades normalmente hiperbólicas, o Teorema 1.2.3 para singularidades semihiperbólicas e o Teorema 1.2.5 para singularidades nilpotentes.

A partir da información local obtemos os posibles retratos globais, realizando posteriormente unha clasificación topolóxica da que concluímos que existen 13 retratos globais topoloxicamente distintos no disco de Poincaré.

## Capítulo 6: Bifurcación Zero-Hopf nos sistemas Kolmogorov en $\mathbb{R}^3$

Os ciclos límite teñen un importante papel na teoría cualitativa dos sistemas diferenciais, pois aparecen no estudo de moitos fenómenos e procesos do mundo real.

Neste capítulo centrámonos no estudo dos ciclos límite nos sistemas Kolmogorov. En concreto, estudamos os ciclos límite dos sistemas Kolmogorov de grao tres en  $\mathbb{R}^3$  que aparecen a través dunha bifurcación zero-Hopf en calquera punto singular  $(a, b, c)$  que non está sobre os planos invariantes  $x = 0$ ,  $y = 0$ ,  $z = 0$ . Estes sistemas teñen a forma xeral

$$\dot{x} = xP(x, y, z), \quad \dot{y} = yQ(x, y, z), \quad \dot{z} = zR(x, y, z),$$

onde  $P$ ,  $Q$  e  $R$  son polinomios de grao dous.

Facendo un reescalado do sistema, asumimos sen perda de xeneralidade que a singularidade estudada é o punto  $(1, 1, 1)$ . Caracterizamos cando esta singularidade é de tipo zero-Hopf na Proposición 6.0.1, obtendo cinco casos distintos. O primeiro deles xa tiña sido estudado en [85], polo que abordamos o estudo de todos os demais casos.

En cada unha das seccións seguimos unha organización similar, enunciando e probando un teorema que caracteriza a existencia de dous ciclos límite que bifurcan do punto  $(1, 1, 1)$  en cada caso: os Teoremas 6.1.1, 6.2.1 e 6.3.1. O Teorema 6.2.1 foi elaborado de forma que permite unificar dous dos casos sen máis que redefinir algunhas constantes.

Para a demostración dos resultados, perturbamos os parámetros que definen o equilibrio zero-Hopf, e realizamos transformacións sobre os sistemas para chegar á forma normalizada. En liñas xerais, calculamos os sistemas con parte lineal en forma canónica de Jordan, facemos un cambio a coordenadas cilíndricas, reescalamos co parámetro de perturbación e eliximos  $\theta$  como nova variable independente.

Unha vez que os sistemas están na súa forma normalizada, aplicamos a teoría dos promedios. Para iso calculamos a función promedio de primeira orde,  $f_1 = (f_{11}, f_{12})$  e calculamos e estudamos as solucións da ecuación  $(f_{11}, f_{12}) = (0, 0)$ . O Teorema 1.8.3 permítenos concluir a existencia de ciclos límite.

Unha vez garantida a existencia dos ciclos límite, estudamos a súa estabilidade analizando os autovalores da matriz Xacobiana nas solucións obtidas para a anterior ecuación.

Dentro de cada sección incluimos tamén unha subsección na cal se proporcionan exemplos concretos, a través dos valores dos parámetros, que proban que todos os conxuntos de condicións incluídas nos resultados son non vacíos, e que, polo tanto, todos os casos que contemplan as afirmacións dos teoremas son realizables.

## Capítulo 7: Aplicacións

No último capítulo, aplicando as técnicas e resultados tratados nos capítulos anteriores, consideramos algúns problemas específicos no campo da biomatemática. Dado que os sistemas Lotka-Volterra e Kolmogorov teñen a súa orixe no campo da dinámica de poboacións, e xa que as súas aplicacións neste ámbito seguen sendo de interese na actualidade e continúan desenvolvéndose, centramos a nosa atención nesta área.

En primeiro lugar, na Sección 7.1 presentamos un traballo de revisión que nos proporciona unha mellor comprensión de como os modelos depredador-presa avanzaron nos últimos anos e cales son os temas e características que atraeron especialmente a atención dos investigadores.

Despois, na Sección 7.2 estudamos un modelo depredador-presa no plano dado por un sistema Kolmogorov obtido a partir do sistema de Rosenzweig e MacArthur. Para este sistema estudamos a súa dinámica no cuadrante positivo do disco de Poincaré, analizando os posibles retratos de fases globais. Estudamos as singularidades finitas e infinitas e incluimos un estudo da bifurcación de Hopf.

Finalmente, na Sección 7.3 estudamos un modelo en dimensión tres, con dúas especies de presas e unha especie depredadora. A restrición deste sistema a dúas variables coincide co modelo no plano estudado anteriormente. Para este modelo tridimensional, estudamos distintos aspectos da súa dinámica cualitativa, incluíndo a existencia de singularidades e a súa estabilidade, a existencia de ciclos límite e a bifurcación de Hopf ou as propiedades de persistencia do sistema.



# Resumen

---

Los contenidos de esta tesis, titulada *Dinámica cualitativa de sistemas Lotka-Volterra y Kolmogorov en el plano y en el espacio*, son el resultado del trabajo realizado por Érika Diz Pita durante los estudios correspondientes al Programa de Doctorado en Matemáticas de la Universidad de Santiago de Compostela. Este trabajo ha sido realizado en colaboración con sus directores de tesis Jaume Llibre Saló (Universitat Autònoma de Barcelona) y M. Victoria Otero Espinar (Universidade de Santiago de Compostela), así como con la profesora Claudia Valls Anglès (Universidade de Lisboa), responsable de la estancia de investigación preceptiva para optar a la mención internacional, y con el profesor Renato Colucci (Università Politecnica delle Marche).

Esta tesis se centra en el estudio de la dinámica cualitativa de sistemas de ecuaciones diferenciales en dimensión dos y tres, especialmente de sistemas Lotka-Volterra y Kolmogorov. Estos sistemas permiten modelizar muchos procesos y fenómenos de la naturaleza, así como problemas que surgen en otras ciencias o cuestiones de carácter social. Por ello, el conocimiento de la dinámica de estos sistemas resulta de interés no solo desde un punto de vista teórico, si no también por sus múltiples aplicaciones.

Se han hecho importantes avances en el estudio de estos sistemas, por ejemplo, la dinámica de los sistemas Lotka-Volterra en dimensión dos ha sido totalmente estudiada en [117]. Sin embargo, para los sistemas Lotka-Volterra en dimensión tres se han estudiado solo algunas familias muy concretas, como es el caso de los sistemas de May-Leonard [98], definidos con tan solo dos parámetros.

En esta tesis se pretende avanzar en el estudio de los sistemas Lotka-Volterra en dimensión tres, considerando una familia más general y con un mayor número de parámetros. La caracterización de esta familia se realiza en el Capítulo 1, junto con la introducción de los resultados preliminares necesarios para el desarrollo de los capítulos posteriores. En los Capítulos 2–5 se estudia completamente la dinámica global de los sistemas Kolmogorov planos obtenidos como resultado de esa caracterización.

En el Capítulo 6 se aborda el estudio de los ciclos límite, uno de los elementos más importantes dentro de la teoría cualitativa. Concretamente, caracterizamos los sistemas Kolmogorov de grado tres en dimensión tres que poseen ciclos límite que aparecen a través de una bifurcación zero-Hopf. Empleamos para ello la técnica de los promedios de orden uno.

Por último, en el Capítulo 7, nos centramos en algunas aplicaciones en el ámbito de la dinámica de poblaciones. Comenzamos haciendo una revisión en la que se comparan distintos modelos poblacionales, analizando como estos son cada vez más realistas y van incorporando distintas características reales relativas al comportamiento de las poblaciones estudiadas. Por



último estudiamos dos modelos poblacionales, uno en dimensión dos y otro en dimensión tres, con dos presas y un depredador, aplicando algunas de las técnicas introducidas con anterioridad.

A continuación resumimos con más detalle los contenidos de cada uno de los capítulos.

## Capítulo 1: Preliminares

En este primer capítulo, y con el fin de que el trabajo sea autocontenido, introducimos los conceptos y resultados que son necesarios para el desarrollo de los capítulos siguientes.

Comenzamos incluyendo algunas nociones elementales sobre campos vectoriales y puntos singulares en las Secciones 1.1 y 1.2. En esta última sección presentamos también los resultados que permiten caracterizar localmente las singularidades no degeneradas, semihiperbólicas y nilpotentes de los sistemas polinomiales planos. Para estudiar las singularidades cuya parte lineal es idénticamente nula recurrimos a la técnica de blowup's, que introducimos también en la Sección 1.2. A grandes rasgos, esta técnica consiste en explotar dichas singularidades, convirtiéndolas en una recta mediante un cambio de variable, de forma que el estudio de las nuevas singularidades que aparecen sobre esa recta nos permita determinar como es el comportamiento de las órbitas en un entorno del punto original.

A continuación, en la Sección 1.3, presentamos la compactificación de Poincaré, que nos permite estudiar el comportamiento de las órbitas en el infinito, a partir de una proyección del campo en  $\mathbb{R}^2$  sobre la esfera unidad  $\mathbb{S}^2$ , a la que llamaremos esfera de Poincaré. Gracias a esta técnica podemos estudiar los retratos de fases en el disco de Poincaré, un espacio acotado obtenido al proyectar la esfera sobre el plano  $z = 0$ , en lugar de en todo el plano  $\mathbb{R}^2$ . Identificaremos el interior del disco de Poincaré con  $\mathbb{R}^2$  y su frontera con el infinito de  $\mathbb{R}^2$ , pudiendo así estudiar la dinámica de los sistemas en un entorno del infinito.

En los retratos de fases que obtenemos en el disco de Poincaré, distinguiremos sus regiones canónicas, sus separatrices, y la configuración de las separatrices, conceptos que se introducen en la Sección 1.4. En esta misma sección enunciamos el Teorema de Markus-Neumann-Peixoto, el fundamento teórico que nos permite hacer la clasificación topológica de los retratos de fases en el disco de Poincaré en función de sus configuraciones de separatrices.

En la Sección 1.5 presentamos un resultado que permite estudiar las subvariedades formadas por singularidades, en concreto las subvariedades normalmente hiperbólicas. Utilizamos este resultado para el estudio de los casos en los que todos los puntos del infinito, que se corresponden con los puntos de la circunferencia  $\mathbb{S}^1$ , son singularidades.

En la Sección 1.6 introducimos el concepto de índice de una singularidad, y enunciamos el Teorema de Poincaré-Hopf, que garantiza que la suma de los índices de todas las singularidades de un campo sobre la esfera  $\mathbb{S}^2$  es igual a dos. Este resultado, aplicado a los campos sobre la esfera de Poincaré, nos permite determinar el comportamiento de las órbitas en algunas regiones del plano, donde otros métodos no son concluyentes.

Un primer punto clave en nuestro trabajo es la aplicación de la teoría de Darboux para la caracterización de los sistemas diferenciales. En la Sección 1.7 introducimos algunos conceptos y resultados relacionados con la integrabilidad y las superficies invariantes y, además, los aplicamos para obtener una caracterización de nuestro problema. Recordamos que nos proponemos estudiar los sistemas Lotka-Volterra en dimensión tres, es decir, los sistemas

$$\begin{aligned}\dot{x} &= x(a_0 + a_1x + a_2y + a_3z), \\ \dot{y} &= y(b_0 + b_1x + b_2y + b_3z), \\ \dot{z} &= z(c_0 + c_1x + c_2y + c_3z),\end{aligned}$$

que tienen una integral primera racional de grado dos de la forma  $x^{\lambda_1}y^{\lambda_2}z^{\lambda_3}$ . Aplicando el teorema de integrabilidad de Darboux para sistemas polinomiales, logramos reducir el estudio de estos sistemas en dimensión tres al estudio de las siguientes dos familias de sistemas Kolmogorov en el plano:

$$\begin{aligned}\dot{x} &= x(a_0 + a_1x + a_2z^2 + a_3z), & \dot{y} &= y(b_0 + b_1yz + b_2y + b_3z), \\ \dot{z} &= z(c_0 + c_1x + c_2z^2 + c_3z), & \dot{z} &= z(c_0 + c_1yz + c_2y + c_3z).\end{aligned}$$

Estas familias dependen de ocho parámetros, lo cual supone todavía un número muy elevado para llevar a cabo la clasificación de todos sus distintos retratos de fases globales. Exigimos que estos sistemas Kolmogorov tengan un invariante de Darboux de la forma  $e^{st}x^{\lambda_1}z^{\lambda_2}$  en el caso de la primera familia, y de la forma  $e^{st}y^{\lambda_1}z^{\lambda_2}$  en el caso de la segunda. Aplicando de nuevo el teorema de integrabilidad de Darboux reducimos el estudio de las dos familias previas al estudio de las dos siguientes, que también son de tipo Kolmogorov:

$$\begin{aligned}\dot{x} &= x(a_0 - \mu(c_1x + c_2z^2 + c_3z)), & \dot{y} &= y(b_0 + b_1yz + b_2y + b_3z), \\ \dot{z} &= z(c_0 + c_1x + c_2z^2 + c_3z), & \dot{z} &= z(c_0 - \mu(b_1yz + b_2y + b_3z)).\end{aligned}$$

El estudio de la dinámica global de estas familias, que ahora dependen de seis parámetros, se lleva a cabo en los Capítulos 2–5.

Por último, en la Sección 1.8, incluimos los resultados empleados para el estudio de ciclos límite, tanto los relativos a la técnica de los promedios, como a la bifurcación de Hopf.

## Capítulo 2: Clasificación de la primera familia Kolmogorov con singularidades aisladas

En este capítulo estudiamos la dinámica global de la primera de las familias Kolmogorov obtenidas previamente, es decir,

$$\begin{aligned}\dot{x} &= x(a_0 - \mu(c_1x + c_2z^2 + c_3z)), \\ \dot{z} &= z(c_0 + c_1x + c_2z^2 + c_3z).\end{aligned}\tag{1}$$

Nuestro resultado principal es el siguiente:

**Teorema 1.** *Los sistemas Kolmogorov (1) bajo las condiciones  $H_2^1$  tienen 78 retratos de fases topológicamente distintos en el disco de Poincaré, dados en la Figura 2.0.1.*

A lo largo del capítulo se lleva a cabo la prueba de este resultado, realizando la clasificación topológica global de todos los retratos de fases en el disco de Poincaré.

Comenzamos estudiando algunas de las propiedades de los sistemas en la Sección 2.1, lo que nos permite imponer ciertas condiciones sobre los parámetros. En particular, consideraremos  $c_2 \neq 0$  para que los sistemas no se reduzcan a sistemas Lotka-Volterra en dimensión dos, los cuales ya están estudiados. Además, como exigimos que  $e^{-t(a_0+c_0\mu)}xz^\mu$  sea un invariante

de Darboux, debemos considerar la condición  $a_0 + c_0\mu \neq 0$ . Estudiando las simetrías de los sistemas podemos garantizar que es suficiente estudiar esta familia Kolmogorov con los parámetros verificando

$$H^1 = \{c_2 \neq 0, a_0 \geq 0, c_1 \geq 0, c_3 \geq 0, a_0 + c_0\mu \neq 0\},$$

pues en cualquier otro caso se obtendrían retratos simétricos respecto a alguno de los ya obtenidos. Por el mismo motivo, cuando  $a_0 = 0$  podremos limitar nuestro estudio al caso con  $c_0 > 0$ . Podemos garantizar también que en los casos en los que  $c_1 = 0$  o  $c_3 = 0$ , los retratos globales obtenidos deben ser simétricos con respecto al eje  $z$  o  $x$ , respectivamente. Estudiamos también la existencia de rectas invariantes y de puntos de contacto sobre las rectas  $z = cte$ . Esto nos ayudará a determinar, más adelante, cuales de los retratos de fases globales son realizables.

En la Sección 2.2 calculamos las singularidades finitas, estudiamos todos los posibles retratos de fases locales en torno a cada una de ellas y damos una clasificación en las Tablas 2.2.2 a 2.2.7. Probamos también que no existen ciclos límite. Eliminamos los casos en los que existe un continuo de equilibrios, en los cuales nuestros sistemas pueden reducirse a otros más sencillos ya estudiados, y trabajamos así con parámetros que satisfacen las condiciones:

$$H_1^1 = \{c_2 \neq 0, a_0 \geq 0, c_1 \geq 0, c_3 \geq 0, a_0 + c_0\mu \neq 0, a_0^2 + c_1^2\mu^2 \neq 0\}.$$

En la Sección 2.3 estudiamos las singularidades infinitas, trabajando con la compactificación de Poincaré de los sistemas.

En primer lugar estudiamos la compactificación en la carta local  $U_1$  de la esfera, donde obtenemos que, o bien la única singularidad infinita es el origen de la carta, o bien todos los puntos del infinito son singularidades. Este caso particular en el que todo el infinito está formado por puntos singulares, y que se corresponde con la condición  $\mu = -1$ , se estudia de forma independiente en el Capítulo 3. Considerando por tanto las condiciones

$$H_2^1 = \{c_2 \neq 0, a_0 \geq 0, c_1 \geq 0, c_3 \geq 0, a_0 + c_0\mu \neq 0, a_0^2 + c_1^2\mu^2 \neq 0, \mu \neq -1\},$$

estudiamos todos los posibles retratos de fases locales del origen de la carta  $U_1$ , empleando la técnica de blow up's. En concreto, realizamos dos blow up's verticales y distinguimos casos dicríticos y no dicríticos. Como resultado de estudiar las singularidades existentes sobre el divisor excepcional tras el segundo blow up, aparecen algunos casos en los que los retratos de fases no están bien definidos, por lo que es necesario realizar también un blow up horizontal. Como resultado de este proceso obtenemos un total de 47 retratos de fases locales distintos para el origen de la carta  $U_1$ , incluídos en la Figura 2.3.1. Cabe mencionar que en algunos casos queda todavía una indeterminación en ciertos sectores al terminar el proceso. Esos sectores podrían ser elípticos o hiperbólicos, y aunque esta indeterminación podría solventarse a nivel local aplicando otros métodos, en nuestro caso hemos optado por resolverlo a nivel global basándonos en la teoría del índice.

El estudio de la compactificación en la carta  $U_2$  resulta más sencillo. El origen de esta carta es un punto singular hiperbólico, que puede ser un nodo o un punto de silla.

A continuación hacemos el paso del estudio local desarrollado hasta el momento al estudio global. Para ello recopilamos toda la información local obtenida, partiendo de la clasificación en las Tablas 2.2.2 a 2.2.7. En algunos de los casos recogidos en estas tablas las

condiciones determinan un único retrato local en los puntos del infinito, pero en muchos otros debemos distinguir distintas posibilidades.

Empleamos la teoría del índice y el Teorema de Poincaré-Hopf para completar el estudio de las singularidades infinitas realizado por medio de blow up's, probando si las regiones no determinadas se corresponden con sectores elípticos o hiperbólicos.

Cuando las separatrices se pueden conectar de una única forma, obtenemos un único retrato global a partir de la información local, pero en 14 casos aparecen tres posibles retratos globales. Empleando los resultados relativos a la existencia de curvas invariantes y puntos de contacto, probamos que en cada uno de esos 14 casos solo uno de los retratos globales es realizable.

Por último, en la Sección 2.5, realizamos la clasificación topológica de los 102 retratos globales obtenidos. En primer lugar determinamos 19 clases de equivalencia en función de dos invariantes: el número de regiones canónicas y el número de separatrices. Dentro de cada una de las clases, seleccionamos los invariantes apropiados para distinguir aquellos retratos topológicamente distintos, y buscamos los homeomorfismos entre aquellos topológicamente iguales mediante el uso, entre otros, de giros o simetrías.

Concluimos así la prueba de nuestro resultado principal, obteniendo la clasificación topológica global de todos los retratos de fases en el disco de Poincaré de los sistemas (1) que no tienen un continuo de singularidades en el infinito.

### Capítulo 3: Clasificación de la primera familia Kolmogorov con singularidades no aisladas

En este capítulo estudiamos la primera de las familias de sistemas Kolmogorov cuando todos los puntos del infinito son singularidades. Este caso se corresponde con el valor del parámetro  $\mu = -1$ , por lo que estudiamos los sistemas

$$\begin{aligned}\dot{x} &= x(a_0 + c_1x + c_2z^2 + c_3z), \\ \dot{z} &= z(c_0 + c_1x + c_2z^2 + c_3z).\end{aligned}\tag{2}$$

A partir de los resultados obtenidos en el capítulo previo obtenemos algunas propiedades de los sistemas, y determinamos una serie de condiciones que podemos imponer a los parámetros sin pérdida de generalidad, en concreto:

$$\tilde{H}^1 = \{c_2 \neq 0, a_0 \geq 0, c_1 \geq 0, c_3 \geq 0, a_0 \neq c_0, a_0^2 + c_1^2 \neq 0\}.$$

Nuestro resultado principal sobre la dinámica global de los sistemas (2) es el siguiente:

**Teorema 2.** *Los sistemas Kolmogorov (2) bajo las condiciones  $\tilde{H}^1$  tienen 22 retratos de fases topológicamente distintos en el disco de Poincaré, dados en la Figura 3.0.1.*

La existencia de singularidades finitas así como la clasificación de sus retratos de fases locales, se realiza a partir de los resultados del Capítulo 2.

En la Sección 3.2, empleando la compactificación de Poincaré, estudiamos la dinámica en el infinito. En este caso, como ya se ha mencionado, todos los puntos del infinito son singularidades. En primer lugar estudiamos el origen de la carta  $U_2$ , en el cual la matriz Jacobiana tiene un autovalor nulo y otro no nulo. Esto nos permite aplicar el Teorema 1.5.1

y concluir que, o bien hay exactamente una órbita que sale de ese punto singular, o bien una única órbita que llega a él.

Considerando la expresión de la compactificación en la carta  $U_1$  estudiamos todos los demás puntos del infinito. En los puntos distintos del origen estamos en condiciones de aplicar el Teorema 1.5.1 y distinguir casos en los que a cada uno de esos puntos llega exactamente una órbita y otros en los que de cada punto sale exactamente una órbita.

Por otra parte, para el origen de la carta  $U_1$  obtenemos 12 retratos de fases locales distintos, incluyendo casos en los que la singularidad es semihiperbólica y otros en los que es linealmente cero. En estos últimos recurrimos al empleo de blow up's para realizar la desingularización.

Combinando la información local, determinamos los retratos de fases globales a partir del análisis de las posibles conexiones de las separatrices. En seis casos, las separatrices pueden conectarse de tres modos distintos. En cada uno de esos casos, probamos que solo uno de los tres retratos globales es realizable, obteniendo finalmente un total de 29 retratos en el disco de Poincaré.

Por último realizamos la clasificación topológica. Inicialmente consideramos el número de singularidades finitas y la suma de los índices en todas las singularidades finitas como invariantes, y con ellos determinamos 14 clases. Analizando las coincidencias topológicas dentro de cada una de esas clases, obtenemos finalmente 22 retratos globales topológicamente distintos, probando así nuestro resultado principal de este capítulo.

## Capítulo 4: Clasificación de la segunda familia Kolmogorov con singularidades aisladas

En este capítulo abordamos el estudio de la segunda de las familias Kolmogorov, es decir

$$\begin{aligned}\dot{y} &= y(b_0 + b_1 yz + b_2 y + b_3 z), \\ \dot{z} &= z(c_0 - \mu(b_1 yz + b_2 y + b_3 z)).\end{aligned}\tag{3}$$

Para estos sistemas obtenemos el siguiente resultado sobre su dinámica global:

**Teorema 3.** *Los sistemas Kolmogorov (3) bajo las condiciones  $H_2^2$  tienen 52 retratos de fases topológicamente distintos en el disco de Poincaré, dados en la Figura 4.0.1.*

La estructura de la demostración es similar a la descrita en el Capítulo 2. Comenzamos estudiando propiedades de los sistemas, especialmente simetrías, que nos permiten trabajar en el siguiente espacio de parámetros:

$$H^2 = \{b_1 \neq 0, c_0 + b_0\mu \neq 0, b_0 \geq 0, b_2 \geq 0, b_3 \geq 0\}.$$

Después estudiamos la existencia de singularidades finitas y sus retratos de fases locales, obteniendo la clasificación dada en las Tablas 4.2.2 a 4.2.5. Trabajamos bajo las condiciones

$$H_1^2 = \{b_1 \neq 0, b_0\mu + c_0 \neq 0, b_0 \geq 0, b_2 \geq 0, b_3 \geq 0, \mu^2 b_3^2 + c_0^2 \neq 0, b_2^2 + b_0^2 \neq 0\},$$

eliminando así los casos en los que existe un continuo de puntos singulares finitos, y que pueden reducirse a otros sistemas cuya dinámica global ya ha sido estudiada.

De nuevo, bajo la condición  $\mu = -1$  existe un continuo de singularidades en el infinito, y estudiamos ese caso de forma independiente en el siguiente capítulo, trabajando ahora bajo las condiciones

$$H_2^2 = \{b_1 \neq 0, b_0\mu + c_0 \neq 0, b_0 \geq 0, b_2 \geq 0, b_3 \geq 0, \mu^2 b_3^2 + c_0^2 \neq 0, b_2^2 + b_0^2 \neq 0, \mu \neq -1\}.$$

Una de las diferencias respecto al estudio de la primera familia, llevado a cabo en el Capítulo 2, es que en este caso es necesario realizar dos procesos de desingularización mediante blow up's, un para el origen de la carta  $U_1$  y otro para el origen de la carta  $U_2$ . Se obtienen 27 retratos locales en el primer caso y 26 en el segundo, como se muestra en las Figuras 4.3.1 y 4.4.1. En este caso también se requiere combinar blow up's verticales y horizontales.

A partir de la información local obtenida, estudiamos los retratos de fases globales en el disco de Poincaré. En algunos casos, la información local es completa y determina unívocamente un retrato de fases a través de una única conexión posible de las separatrices. En otros casos, aplicamos teoría del índice para determinar si ciertos sectores de los retratos de fases locales son elípticos o hiperbólicos, obteniendo de nuevo un único retrato global al conectar las separatrices. En otros 11 casos podemos conectar las separatrices de tres formas diferentes, dando lugar a tres retratos de fases globales. A diferencia de lo que ocurría con la primera familia Kolmogorov, probamos en cada uno de los 11 casos que los tres retratos globales son realizables. Para ello, en cada caso demostramos que para ciertos valores de los parámetros la conexión de separatrices tiene lugar sobre una recta invariante, y perturbando los parámetros obtenemos las otras dos configuraciones. Se comprueba también numéricamente con el programa P4, y se incluyen valores para los que cada uno de los retratos se realiza.

Para concluir la demostración realizamos la clasificación topológica de los 106 retratos globales obtenidos, comenzando por determinar clases de equivalencia en función del número de regiones canónicas y separatrices. Finalmente probamos que existen un total de 52 retratos globales topológicamente distintos en el disco de Poincaré.

## Capítulo 5: Clasificación de la segunda familia Kolmogorov con singularidades no aisladas

En este capítulo terminamos la clasificación de los retratos globales de las familias Kolmogorov abordando el caso en el que en la segunda familia todos los puntos del infinito son singularidades. En este caso, en el que el parámetro  $\mu = -1$ , estudiamos los sistemas

$$\begin{aligned}\dot{y} &= y(b_0 + b_1 yz + b_2 y + b_3 z), \\ \dot{z} &= z(c_0 + b_1 yz + b_2 y + b_3 z),\end{aligned}\tag{4}$$

bajo las condiciones

$$\tilde{H}^2 = \{b_1 \neq 0, c_0 - b_0 \neq 0, b_0 \geq 0, b_2 \geq 0, b_3 \geq 0, b_3^2 + c_0^2 \neq 0, b_2^2 + b_0^2 \neq 0\},$$

que podemos asumir basándonos en los resultados obtenidos en el capítulo anterior. Nuestro resultado principal es el siguiente:

**Teorema 4.** *Los sistemas Kolmogorov (4) bajo las condiciones  $\tilde{H}^2$  tienen 13 retratos de fases topológicamente distintos en el disco de Poicaré, dados en la Figura 5.0.1.*

Siguiendo una estructura similar a los capítulos anteriores, estudiamos las singularidades finitas y sus retratos de fases locales. Después estudiamos los puntos de equilibrio infinitos empleando la compactificación de Poincaré. Obtenemos resultados sobre la dinámica en entornos de las singularidades infinitas empleando el Teorema 1.5.1 para subvariedades normalmente hiperbólicas formadas por singularidades, el Teoremas 1.2.3 para singularidades semihiperbólicas y el Teorema 1.2.5 para singularidades nilpotentes.

A partir de la información local obtenemos los posibles retratos globales, realizando posteriormente una clasificación topológica de la que concluimos que existen 13 retratos globales topológicamente distintos en el disco de Poincaré.

## Capítulo 6: Bifurcación Zero-Hopf en los sistemas Kolmogorov en $\mathbb{R}^3$

Los ciclos límite tienen un importante papel en la teoría cualitativa de los sistemas diferenciales, pues aparecen en el estudio de muchos fenómenos y procesos del mundo real.

En este capítulo nos centramos en el estudio de los ciclos límite en los sistemas Kolmogorov. En concreto, estudiamos los ciclos límite de los sistemas Kolmogorov de grado tres en  $\mathbb{R}^3$  que aparecen a través de una bifurcación zero-Hopf en cualquier punto singular  $(a, b, c)$  que no está sobre los planos invariantes  $x = 0$ ,  $y = 0$ ,  $z = 0$ . Estos sistemas tienen la forma general

$$\dot{x} = xP(x, y, z), \quad \dot{y} = yQ(x, y, z), \quad \dot{z} = zR(x, y, z),$$

donde  $P$ ,  $Q$  y  $R$  son polinomios de grado dos.

Haciendo un reescalado del sistema, asumimos sin pérdida de generalidad que la singularidad estudiada es el punto  $(1, 1, 1)$ . Caracterizamos cuando esta singularidad es de tipo zero-Hopf en la Proposición 6.0.1, obteniendo cinco casos distintos. El primero de ellos ya había sido estudiado en [85], por lo que abordamos el estudio de todos los demás casos.

En cada una de las secciones seguimos una organización similar, enunciando y probando un teorema que caracteriza la existencia de dos ciclos límite que bifurcan del punto  $(1, 1, 1)$  en cada caso, los Teoremas 6.1.1, 6.2.1 y 6.3.1. El Teorema 6.2.1 ha sido elaborado de forma que permite unificar dos de los casos sin más que redefinir algunas constantes.

Para la demostración de los resultados, perturbamos los parámetros que definen el equilibrio zero-Hopf, y realizamos transformaciones sobre los sistemas para llegar a la forma normalizada. A grandes rasgos, calculamos los sistemas con parte lineal en forma de Jordan, hacemos un cambio a coordenadas cilíndricas, reescalamos con el parámetro de perturbación y elegimos  $\theta$  como nueva variable independiente.

Una vez que los sistemas están en su forma normalizada, aplicamos la teoría de los promedios. Para ello calculamos la función promedio de primer orden,  $f_1 = (f_{11}, f_{12})$  y calculamos y estudiamos las soluciones de la ecuación  $(f_{11}, f_{12}) = (0, 0)$ . El teorema 1.8.3 nos permite concluir la existencia de ciclos límite.

Una vez garantizada la existencia de los ciclos límite, estudiamos su estabilidad analizando los autovalores de la matriz Jacobiana en las soluciones obtenidas para la anterior ecuación.

Dentro de cada sección incluimos también una subsección en la cual se proporcionan ejemplos concretos, a través de los valores de los parámetros, que prueban que todos los

conjuntos de condiciones incluidas en los resultados son no vacíos, y que por tanto, todos los casos que contemplan las afirmaciones de los teoremas son realizables.

## Capítulo 7: Aplicaciones

En el último capítulo, aplicando las técnicas y resultados tratados en los capítulos anteriores, consideramos algunos problemas específicos en el campo de la biomatemática. Dado que los sistemas Lotka-Volterra y Kolmogorov tienen su origen en el campo de la dinámica de poblaciones, y ya que sus aplicaciones en este ámbito siguen siendo de interés en la actualidad y continúan desarrollándose, centramos nuestra atención en esta área.

En primer lugar, en la Sección 7.1 presentamos un trabajo de revisión que nos proporciona una mejor comprensión de como los modelos depredador-presa han avanzado en los últimos años y cuales son los temas y características que han atraídos especialmente la atención de los investigadores.

Después, en la Sección 7.2 estudiamos un modelo depredador-presa en el plano dado por un sistema Kolmogorov obtenido a partir del sistema de Rosenzweig y MacArthur. Para este sistema estudiamos su dinámica en el cuadrante positivo del disco de Poincaré, analizando los posibles retratos de fases globales. Estudiamos las singularidades finitas e infinitas e incluimos un estudio de la bifurcación de Hopf.

Finalmente, en la Sección 7.3 estudiamos un modelo en dimensión tres, con dos especies de presas y una especie depredadora. La restricción de este sistema a dos variables coincide con el modelo en el plano estudiado anteriormente. Para este modelo tridimensional, estudiamos distintos aspectos de su dinámica cualitativa, incluyendo la existencia de singularidades y su estabilidad, la existencia de ciclos límite y de bifurcación de Hopf o las propiedades de persistencia del sistema.





# Summary

---

The contents of this thesis, entitled *Qualitative dynamics of planar and spatial Lotka-Volterra and Kolmogorov systems*, are the result of the work developed by Érika Diz Pita during the PhD studies in Mathematics at the Universidade de Santiago de Compostela. This work has been carried out in collaboration with her thesis advisors Jaume Llibre Saló (Universitat Autònoma de Barcelona) and M. Victoria Otero Espinar (Universidade de Santiago de Compostela), as well as with Professor Claudia Valls Anglès (Universidade de Lisboa), responsible for the research stay required to qualify for international mention, and with Professor Renato Colucci (Università Politecnica delle Marche).

This thesis focuses on the study of the qualitative dynamics of differential systems in dimension two and three, particularly of Lotka-Volterra and Kolmogorov systems. These systems model many processes and phenomena of nature, as well as problems from other sciences or social problems. Therefore, the study of the dynamics of these systems is of interest not only from a theoretical point of view, but also for its multiple applications.

Important advances have been made in the study of these systems, for example, the dynamics of Lotka-Volterra systems in dimension two has been totally studied in [117]. However, for Lotka-Volterra systems in dimension three only some very specific families have been studied, as is the case of the May-Leonard systems [98], defined with only two parameters.

In this thesis we want to advance in the study of Lotka-Volterra systems in dimension three, considering a more general family with a larger number of parameters. The characterization of this family is carried out in Chapter 1, together with the introduction of the preliminary results necessary for the development of the subsequent chapters. In Chapters 2 to 5 the global dynamics of the planar Kolmogorov systems obtained as a result of the characterization is totally studied.

In Chapter 6 we deal with the study of limit cycles, one of the most important elements within the qualitative theory. Specifically, we characterize Kolmogorov systems of degree three in dimension three that have limit cycles appearing through a zero-Hopf bifurcation. For this purpose we use the averaging theory of first order.

Finally, in Chapter 7, we focus on some applications in the field of population dynamics. We begin with a review comparing different population models, analyzing how they are becoming more realistic and incorporating different characteristics related to the behavior of the populations. Finally, we study two population models, one in dimension two and the other in dimension three, with two prey and one predator, applying some of the techniques previously introduced.

Below we summarize with more detail the contents of each one of the chapters.

## Chapter 1: Preliminaries

In the first chapter, and in order to make the work self-contained, we introduce the concepts and results that are necessary for the development of the following chapters.

We begin by including some elementary notions about vector fields and singular points in Sections 1.1 and 1.2. In the latter section we also present some results that allow us to locally characterize nondegenerate, semi-hyperbolic and nilpotent singular points of planar polynomial systems. To study singular points whose linear part is identically zero we resort to the blowup's technique, which we introduce also in Section 1.2. Roughly speaking, this technique consists of exploding these singularities, transforming them into a straight line by means of a variable change, so that the study of the new singularities that appear on this straight line allows us to determine the behavior of the orbits in a neighborhood of the original point.

Next, in Section 1.3, we present the Poincaré compactification, which allows us to study the behavior of the orbits at infinity, starting from a projection of the field in  $\mathbb{R}^2$  on the unit sphere  $\mathbb{S}^2$ , which we call Poincaré sphere. Thanks to this technique we can study the phase portraits on the Poincaré disk, a bounded space obtained by projecting the sphere onto the plane  $z = 0$ , instead of on the whole plane  $\mathbb{R}^2$ . We identify the interior of the Poincaré disk with  $\mathbb{R}^2$  and its boundary with the infinity of  $\mathbb{R}^2$ , thus being able to study the dynamics of the systems in a neighborhood of the infinity.

In the phase portraits that we obtain in the Poincaré disk, we distinguish their canonical regions, their separatrices, and the configuration of the separatrices, concepts that are introduced in Section 1.4. In this same section we state the Markus-Neumann-Peixoto Theorem, the theoretical basis that allows us to do the topological classification of the global phase portraits in the Poincaré disk by studying their separatrix configurations.

In Section 1.5 we present a result that allows us to study submanifolds formed by singular points, in particular normally hyperbolic submanifolds. We use this result to study the cases in which all points at infinity, which correspond to the points of  $\mathbb{S}^1$ , are singular points.

In Section 1.6 we introduce the concept of index of a singularity, and state the Poincaré-Hopf Theorem, which guarantees that the sum of the indices of all singularities of a field on the sphere  $\mathbb{S}^2$  is equal to two. This result, applied to fields on the Poincaré sphere, allows us to determine the behavior of orbits in some regions of the plane, where other methods are inconclusive.

A first key point in our work is the application of Darboux theory of integrability to the characterization of differential systems. In Section 1.7 we introduce some concepts and results related to integrability and invariant surfaces and, in addition, we apply them to obtain a characterization of our problem. We recall that we propose to study Lotka-Volterra systems in dimension three, i.e., systems

$$\dot{x} = x(a_0 + a_1x + a_2y + a_3z),$$

$$\dot{y} = y(b_0 + b_1x + b_2y + b_3z),$$

$$\dot{z} = z(c_0 + c_1x + c_2y + c_3z),$$

which have a rational first integral of degree two of the form  $x^{\lambda_1}y^{\lambda_2}z^{\lambda_3}$ . Applying Darboux's integrability theorem for polynomial systems, we reduce the study of these systems in

dimension three to the study of the two following families of planar Kolmogorov systems:

$$\begin{aligned}\dot{x} &= x (a_0 + a_1x + a_2z^2 + a_3z), & \dot{y} &= y (b_0 + b_1yz + b_2y + b_3z), \\ \dot{z} &= z (c_0 + c_1x + c_2z^2 + c_3z), & \dot{z} &= z (c_0 + c_1y + c_2y + c_3z).\end{aligned}$$

These families depend on eight parameters, which is still a very large number to carry out the topological classification of all their different global phase portraits. We require that these Kolmogorov systems have a Darboux invariant of the form  $e^{st}x^{\lambda_1}z^{\lambda_2}$  in the case of the first family, and of the form  $e^{st}y^{\lambda_1}z^{\lambda_2}$  in the case of the second one. Applying again Darboux's integrability theorem we reduce the study of the two previous families to the study of the next two, which are also of Kolmogorov type:

$$\begin{aligned}\dot{x} &= x (a_0 - \mu(c_1x + c_2z^2 + c_3z)), & \dot{y} &= y (b_0 + b_1yz + b_2y + b_3z), \\ \dot{z} &= z (c_0 + c_1x + c_2z^2 + c_3z), & \dot{z} &= z (c_0 - \mu(b_1yz + b_2y + b_3z)).\end{aligned}$$

The study of the global dynamics of these families, which now depend on six parameters, is carried out in Chapters 2 to 5.

Finally, in Section 1.8, we include the results used for the study of limit cycles, both those related to the averaging theory and to the Hopf bifurcations.

## Chapter 2: Classification of the first Kolmogorov family with isolated singularities

In this chapter we study the global dynamics of the first Kolmogorov family obtained in the previous chapter, that is,

$$\begin{aligned}\dot{x} &= x (a_0 - \mu(c_1x + c_2z^2 + c_3z)), \\ \dot{z} &= z (c_0 + c_1x + c_2z^2 + c_3z).\end{aligned}\tag{1}$$

Our main result is the following:

**Theorem 1.** *Kolmogorov systems (1) under conditions  $H_2^1$  have 78 topologically distinct phase portraits in the Poincaré disk, given in Figure 2.0.1.*

Throughout the chapter we develop the proof of this result by performing the global topological classification of all phase portraits in the Poincaré disk.

We begin by studying some of the properties of the systems in Section 2.1, which allows us to impose certain conditions on the parameters. In particular, we will consider  $c_2 \neq 0$  so that the systems do not reduce to Lotka-Volterra systems in dimension two, which are already studied. Moreover, since we require that  $e^{-t(a_0+c_0\mu)}xz^\mu$  be a Darboux invariant, we must consider the condition  $a_0 + c_0\mu \neq 0$ . By studying the symmetries of the systems we can guarantee that it is sufficient to study this Kolmogorov family with the parameters satisfying

$$H^1 = \{c_2 \neq 0, a_0 \geq 0, c_1 \geq 0, c_3 \geq 0, a_0 + c_0\mu \neq 0\},$$

because in any other case we would obtain phase portraits symmetrical to some of those already obtained. For the same reason, when  $a_0 = 0$  we can limit our study to the case with

$c_0 > 0$ . We can also guarantee that in the cases where  $c_1 = 0$  or  $c_3 = 0$ , the global phase portraits obtained must be symmetric with respect to the  $z$  or  $x$  axis, respectively. We also study the existence of invariant lines and contact points on the straight lines  $z = cte$ . This help us to determine, later, which of the global phase portraits are realizable.

In Section 2.2 we obtain the finite singularities, we study all possible local phase portraits in each of them and give a classification in Tables 2.2.2 to 2.2.7. We also prove that there are no limit cycles. We eliminate the cases where a continuum of singular points exists, in which our systems can be reduced to simpler ones already studied, and thus we work with parameters that satisfy the conditions:

$$H_1^1 = \{c_2 \neq 0, a_0 \geq 0, c_1 \geq 0, c_3 \geq 0, a_0 + c_0\mu \neq 0, a_0^2 + c_1^2\mu^2 \neq 0\}.$$

In Section 2.3 we study the infinite singular points, working with the Poincaré compactification of the systems.

We first study the compactification on local chart  $U_1$  of the sphere, where we obtain that either the only infinite singularity is the origin of the chart, or all points at the infinity are singularities. This particular case in which the entire infinity consists of singular points, and which corresponds to the condition  $\mu = -1$ , is studied independently in Chapter 3. Then, considering conditions

$$H_2^1 = \{c_2 \neq 0, a_0 \geq 0, c_1 \geq 0, c_3 \geq 0, a_0 + c_0\mu \neq 0, a_0^2 + c_1^2\mu^2 \neq 0, \mu \neq -1\},$$

we study all possible local phase portraits at the origin of  $U_1$ , employing the blow up technique. Specifically, we perform two vertical blow up's and distinguish dicritical and nondicritical cases. As a result of studying the singularities existing on the exceptional divisor after the second blow up, we find some cases in which the phase portraits are not well defined, so it is necessary to perform also a horizontal blow up. As a result of this process we obtain a total of 47 distinct local phase portraits for the origin of  $U_1$ , included in Figure 2.3.1. It is worth mentioning that in some cases there is still a indeterminacy in certain sectors at the end of the process. These sectors could be elliptic or hyperbolic, and although this indeterminacy could be solved locally by applying other methods, in our case we have chosen to solve it when studying the global phase portraits by using index theory.

The study of the compactification in chart  $U_2$  is simpler. The origin of this chart is a hyperbolic singular point, which can be a node or a saddle point.

Next we go from the local study developed so far to the global study. For this we combine all the local information obtained, starting from the classification in Tables 2.2.2 to 2.2.7. In some of the cases in these tables the conditions determine just one local phase portrait at the infinity singular points, but in many others we must distinguish different possibilities.

We employ index theory and the Poincaré-Hopf Theorem to complete the study of infinite singularities performed by the blow up technique, by proving whether the undetermined regions correspond to elliptic or hyperbolic sectors.

When the separatrices can be connected in a unique way, we obtain one global phase portrait from the local information, but in 14 cases three possible global phase portraits appear. Employing the results concerning the existence of invariant curves and contact points, we prove that in each of those 14 cases only one of the global phase portraits is realizable.

Finally, in Section 2.5, we perform the topological classification of the 102 global phase portraits obtained. We first determine 19 equivalence classes based on two invariants: the

number of canonical regions and the number of separatrices. Within each of the classes, we select appropriate invariants to distinguish those phase portraits that are topologically distinct, and we search for homeomorphisms between those that are topologically equal by using, among others, rotations or symmetries.

We thus conclude the proof of our main result, obtaining the global topological classification of all phase portraits in the Poincaré disk of systems (1) that do not have a continuum of singular points at infinity.

### Chapter 3: Classification of the first Kolmogorov family with non-isolated singularities

In this chapter we study the first family of Kolmogorov systems when all points at infinity are singular points. This case corresponds with the value of the parameter  $\mu = -1$ , so we study the systems

$$\begin{aligned}\dot{x} &= x(a_0 + c_1x + c_2z^2 + c_3z), \\ \dot{z} &= z(c_0 + c_1x + c_2z^2 + c_3z).\end{aligned}\tag{2}$$

From the results obtained in the previous chapter we obtain some properties of the systems, and we determine some conditions that we can impose on the parameters without loss of generality, namely:

$$\tilde{H}^1 = \{c_2 \neq 0, a_0 \geq 0, c_1 \geq 0, c_3 \geq 0, a_0 \neq c_0, a_0^2 + c_1^2 \neq 0\}.$$

Our main result on the global dynamics of systems (2) is as follows:

**Theorem 2.** *Kolmogorov systems (2) under conditions  $\tilde{H}^1$  have 22 topologically distinct phase portraits in the Poincaré disk, given in Figure 3.0.1.*

The existence of finite singular points and the classification of their local phase portraits is carried out based on the results of Chapter 2.

In Section 3.2, by using the Poincaré compactification, we study the dynamics at infinity. In this case, as already mentioned, all points at infinity are singularities. We first study the origin of chart  $U_2$ , in which the Jacobian matrix has a zero eigenvalue and a nonzero eigenvalue. This allows us to apply Theorem 1.5.1 and conclude that either there is exactly one orbit leaving that singular point, or there is exactly one orbit that arrives at it.

Considering the expression of the compactification in chart  $U_1$  we study all other points at infinity. At the points which are not the origin we can apply Theorem 1.5.1 and distinguish cases in which to each one of these points arrives exactly one orbit and others in which from each point leaves exactly one orbit.

On the other hand, for the origin of chart  $U_1$  we obtain 12 different local phase portraits, distinguishing cases in which the singularity is semi-hyperbolic and others in which it is linearly zero. In the latter we resort to the use of blow up's to perform the desingularization.

Combining local information, we determine the global phase portraits from the analysis of the possible connections of the separatrices. In six cases, the separatrices can be connected in three different ways. In each of these cases, we prove that only one of the three global

phase portraits is realizable, finally obtaining a total of 29 phase portraits in the Poincaré disk.

Finally, we perform the topological classification. First we consider the number of finite singularities and the sum of the indices on all the finite singularities as invariants, and with them we determine 14 equivalence classes. By analyzing the topological coincidences within each of these classes, we finally obtain 22 topologically distinct global portraits, thus proving the main result of this chapter.

## Chapter 4: Classification of the second Kolmogorov family with isolated singularities

In this chapter we address the study of the second Kolmogorov family, i.e.,

$$\begin{aligned}\dot{y} &= y(b_0 + b_1 yz + b_2 y + b_3 z), \\ \dot{z} &= z(c_0 - \mu(b_1 yz + b_2 y + b_3 z)).\end{aligned}\tag{3}$$

For these systems we obtain the following result about their global dynamics:

**Theorem 3.** *Kolmogorov systems (3) under conditions  $H_2^2$  have 52 topologically distinct phase portraits in the Poincaré disk, given in Figure 4.0.1.*

The structure of the proof is similar to that described in Chapter 2. We begin by studying properties of the systems, especially symmetries, which allow us to work in the following parameter space:

$$H^2 = \{b_1 \neq 0, c_0 + b_0\mu \neq 0, b_0 \geq 0, b_2 \geq 0, b_3 \geq 0\}.$$

Then we study the existence of finite singular points and their local phase portraits, obtaining the classification given in Tables 4.2.2 to 4.2.5. We work under conditions

$$H_1^2 = \{b_1 \neq 0, b_0\mu + c_0 \neq 0, b_0 \geq 0, b_2 \geq 0, b_3 \geq 0, \mu^2 b_3^2 + c_0^2 \neq 0, b_2^2 + b_0^2 \neq 0\},$$

thus eliminating the cases in which there is a continuum of finite singular points, in which the systems can be reduced to others whose global dynamics have already been studied.

Under condition  $\mu = -1$  there exists a continuum of infinite singular points, and we study that case independently in the following chapter, considering here the conditions

$$H_2^2 = \{b_1 \neq 0, b_0\mu + c_0 \neq 0, b_0 \geq 0, b_2 \geq 0, b_3 \geq 0, \mu^2 b_3^2 + c_0^2 \neq 0, b_2^2 + b_0^2 \neq 0, \mu \neq -1\}.$$

One of the differences with respect to the study of the first family, carried out in Chapter 2, is that in this case it is necessary to perform two desingularization processes using blow up's, one for the origin of chart  $U_1$  and another for the origin of chart  $U_2$ . We obtain 27 local phase portraits in the first case and 26 in the second case, as shown in Figures 4.3.1 and 4.4.1. In this case it is also necessary to combine vertical and horizontal blow up's.

From the local information obtained, we study the global phase portraits in the Poincaré disk. In some cases, the local information is complete and univocally determines a global phase portrait through a unique possible connection of the separatrices. In other cases, we apply index theory to determine whether certain sectors of the local phase portraits are elliptic

or hyperbolic, and then we obtain again a unique global phase portrait by connecting the separatrices. In 11 other cases we can connect the separatrices in three different ways, obtaining three global phase portraits. In contrast to the first Kolmogorov family, we prove in each of the 11 cases that all the three global phase portraits are realizable. For this, in each case we show that for certain values of the parameters the connection of separatrices takes place over an invariant line, and by perturbing the parameters we obtain the two other configurations. We also check it numerically with the program P4, and include values for which each of the phase portraits is realized.

To conclude the proof we perform the topological classification of the 106 global portraits obtained, starting by determining equivalence classes according to the number of canonical regions and separatrices. Finally, we prove that there are a total of 52 topologically distinct global phase portraits in the Poincaré disk.

## Chapter 5: Classification of the second Kolmogorov family with non-isolated singularities

In this chapter we finish the classification of the global phase portraits of the Kolmogorov families by addressing the case in which in the second family all points at infinity are singularities. In this case, in which the parameter  $\mu = -1$ , we study the systems

$$\begin{aligned}\dot{y} &= y(b_0 + b_1 yz + b_2 y + b_3 z), \\ \dot{z} &= z(c_0 + b_1 yz + b_2 y + b_3 z),\end{aligned}\tag{4}$$

under conditions

$$\tilde{H}^2 = \{b_1 \neq 0, c_0 - b_0 \neq 0, b_0 \geq 0, b_2 \geq 0, b_3 \geq 0, b_3^2 + c_0^2 \neq 0, b_2^2 + b_0^2 \neq 0\},$$

that we can assume based on the results obtained in the previous chapter. Our main result is as follows:

**Theorem 4.** *Kolmogorov systems (4) under conditions  $\tilde{H}^2$  have 13 topologically distinct phase portraits in the Poincaré disk, given in Figure 5.0.1.*

Following a similar structure to the previous chapters, we study finite singularities and their local phase portraits. Then we study infinite singular points using the Poincaré compactification. We obtain results on the dynamics in neighborhoods of infinite singularities by employing Theorem 1.5.1 for normally hyperbolic submanifolds consisting on singular points, Theorem 1.2.3 for semi-hyperbolic singularities and Theorem 1.2.5 for nilpotent singularities.

From the local information we obtain the possible global phase portraits, subsequently performing a topological classification from which we conclude that there are 13 topologically distinct global portraits in the Poincaré disk.

## Chapter 6: Zero-Hopf bifurcation on Kolmogorov systems in $\mathbb{R}^3$

Limit cycles play an important role in the qualitative theory of differential equations, since they appear in the study of many phenomena and processes of the real world.



In this chapter we focus on the study of limit cycles in the Kolmogorov systems. Specifically, we study the limit cycles of the Kolmogorov systems of degree three in  $\mathbb{R}^3$  that appear through a zero-Hopf bifurcation at any singular point  $(a, b, c)$  that is not on the invariant planes  $x = 0, y = 0, z = 0$ . These systems have the general form

$$\dot{x} = xP(x, y, z), \quad \dot{y} = yQ(x, y, z), \quad \dot{z} = zR(x, y, z),$$

where  $P, Q$  and  $R$  are polynomials of degree two.

Doing a rescaling we assume without loss of generality that we study the singular point  $(1, 1, 1)$ . We characterize when this singularity is zero-Hopf in Proposition 6.0.1, obtaining five different cases. The first of them has already been studied in [85], so we address the study of the other cases.

In each one of the sections we follow a similar organization, stating and proving a theorem characterizing the existence of two limit cycles emerging from the point  $(1, 1, 1)$  in each case: Theorems 6.1.1, 6.2.1 and 6.3.1. Theorem 6.2.1 has been done in such a way that unifies two of the cases by simply redefining some constants.

For the proof of the results, we perturb the parameters defining the zero-Hopf equilibrium and perform transformations on the systems to obtain the normalized form. Roughly speaking, we compute the systems whose linear part is in Jordan canonical form, make a change to cylindrical coordinates, rescale with the perturbation parameter, and choose  $\theta$  as the new independent variable.

Once the systems are in its normalized form, we apply averaging theory. For this we compute the first order average function,  $f_1 = (f_{11}, f_{12})$  and compute and study the solutions of the equation  $(f_{11}, f_{12}) = (0, 0)$ . Theorem 1.8.3 allows us to conclude the existence of limit cycles.

Once the existence of limit cycles is guaranteed, we study their stability by analyzing the eigenvalues of the Jacobian matrix in the solutions obtained from the previous equation.

Within each section we also include a subsection in which concrete examples are provided, through the parameter values, that prove that all sets of conditions included in the results are non-empty, and that therefore, all cases in the statements of the theorems are realizable.

## Chapter 7: Applications

In the last chapter, applying the techniques and results discussed in the previous chapters, we consider some specific problems in the field of biomathematics. Since the Lotka-Volterra and Kolmogorov systems have their origin in the field of population dynamics, and since their applications in this field are still of interest nowadays and continue to be developed, we focus our attention on this area.

First, in Section 7.1, we present a review that provides us with a better understanding of how predator-prey models have advanced in recent years and which are the topics and features that have attracted particular attention from researchers.

Then, in Section 7.2, we study a planar predator-prey model given by a Kolmogorov system obtained from the Rosenzweig and MacArthur system. For this system we study its dynamics in the positive quadrant of the Poincaré disk, analyzing all the possible global phase portraits. We study finite and infinite singularities and include a study of the Hopf bifurcation.

Finally, in Section 7.3 we study a model in dimension three, with two prey species and one predator species. The restriction of this system to two variables coincides with the planar model previously studied. For this three-dimensional model, we study different aspects of its qualitative dynamics, including the existence of singularities and their stability, the existence of limit cycles, the Hopf bifurcation or the persistence properties of the system.



---

# Chapter 1

## Preliminaries

---

In this first chapter we present some results that will be needed throughout the manuscript. First we introduce some notions about vector fields and singular points, particularly focusing on the results and methods that will allow us to determine the local phase portraits at the singular points. Later, we introduce the Poincaré compactification and the main ideas of topological equivalence, as this will be essential for the objective addressed in chapters 2 to 5. The results about index theory will be used also throughout those chapters. We also include a brief section about normally hyperbolic submanifolds, as it is needed to study the particular cases addressed in Chapters 3 and 5. Then we present some basic notions and results of the Darboux theory of integrability, and further we apply them to the characterization of one of our main problems, as a preliminary step for its complete study in later chapters. Finally, we include the results about limit cycles, bifurcations and averaging theory that we need in Chapters 6 and 7. All these results are included here as this work aspires to be self-contained.

### 1.1 Vector fields

Let  $D$  be an open subset of the euclidean plane  $\mathbb{R}^2$ . We define a *vector field of class  $C^r$*  on  $D$  as a  $C^r$  map  $X : D \rightarrow \mathbb{R}^2$  where  $X(x)$  represents the free part of a vector attached at the point  $x \in D$ . The  $r$  can be a positive integer,  $+\infty$  or  $\omega$ , in which case  $C^\omega$  represents the class of the analytic functions. A vector field defines a *differential equation*

$$\dot{x} = X(x), \quad (1.1.1)$$

where  $x \in D$ , and  $\dot{x}$  denotes the derivative of  $x$  with respect to  $t$ . We say that  $x$  is the *dependent variable* and  $t$  the *independent variable*, although we usually also refer to  $t$  as the *time*.

The differential equation (1.1.1) is *autonomous* since  $X = X(x)$  does not depend on  $t$ , and along this manuscript we will always work with this kind of equations.

The *solutions* of this differential equation are differentiable maps  $\varphi : I \rightarrow D$  such that

$$\frac{d\varphi}{dt}(t) = X(\varphi(t)),$$

where  $I$  is an interval on which the solution is defined and  $t \in I$ .

Let  $p \in D$  and  $\varphi : I \rightarrow D$  be a solution of (1.1.1) such that  $\varphi(0) = p$ . The solution  $\varphi$  is called *maximal* if for every solution  $\psi : J \rightarrow D$  such that  $I \subset J$  and  $\varphi = \psi|_I$  then  $I = J$  and, consequently  $\varphi = \psi$ . In this case we denote the interval of definition as  $I_p$  and call it the *maximal interval*.

A point  $p \in D$  is a *singular point*, a *singularity* or an *equilibrium point* if  $X(p) = 0$  and it is a *regular point* if  $X(p) \neq 0$ . If  $x$  is a singular point of  $X$ , then  $\varphi(t) = x$ , with  $t \in \mathbb{R}$ , is a solution of (1.1.1), that is,  $\dot{\varphi}(t) = X(\varphi(t)) = X(x) = 0$ . If  $L$  is a straight line and  $q$  is a point of  $L$ , we say that  $q$  is a *contact point* of  $L$  with the vector field  $X$  if  $X(q)$  is parallel to  $L$ .

If  $\varphi : I_p \rightarrow D$  is a maximal solution, it is either regular or constant (if it consist only on a singular point). The image  $\gamma_p = \gamma(p) = \{\varphi(t) : t \in I_p\} \subset D$  endowed with the orientation induced by  $\varphi$ , in case  $\varphi$  is regular, is called the *trajectory* or *orbit* associated to the maximal solution  $\varphi$  or to the point  $p$ . We will denote  $\gamma^+ = \{\varphi(t) : t \in I_p \cap \mathbb{R}^+\}$  and  $\gamma^- = \{\varphi(t) : t \in I_p \cap \mathbb{R}^-\}$ .

We say that an orbit  $\varphi_p(t)$  of  $X$  is *periodic* if there exists a real number  $c > 0$  such that  $\varphi_p(t+c) = \varphi_p(t)$  for every  $t \in \mathbb{R}$ .

We introduce now the concepts of  $\alpha$  and  $\omega$ - limit sets of an orbit. Let  $\varphi_p(t)$  be the orbit passing through the point  $p$  defined on its maximal interval  $I_p = (a_p, b_p)$ . If  $b_p = \infty$ , we can define the set

$$\omega(p) = \{q \in D : \text{there exist } \{t_n\} \text{ with } t_n \rightarrow \infty \text{ and } \varphi(t_n) \rightarrow q \text{ when } n \rightarrow \infty\},$$

and in the same way, if  $a_p = -\infty$ , we can define the set

$$\alpha(p) = \{q \in D : \text{there exist } \{t_n\} \text{ with } t_n \rightarrow -\infty \text{ and } \varphi(t_n) \rightarrow q \text{ when } n \rightarrow \infty\}.$$

These sets  $\omega(p)$  and  $\alpha(p)$  are called the  $\omega$ -*limit* set and the  $\alpha$ -*limit* set of  $p$ , respectively.

We say that a periodic orbit  $\gamma_1$  is a *limit cycle* if there exists another orbit  $\gamma_2$  such that  $\alpha(\gamma_2) = \gamma_1$  or  $\omega(\gamma_2) = \gamma_1$ .

## 1.2 Singular points

Now we focus on singular points, defining the different types and introducing the results for studying them. Consider a planar  $C^r$  vector field  $X = (P, Q)$  and a singular point  $p$ . We say that the matrix

$$DX(p) = \begin{pmatrix} \frac{\partial P}{\partial x}(p) & \frac{\partial P}{\partial y}(p) \\ \frac{\partial Q}{\partial x}(p) & \frac{\partial Q}{\partial y}(p) \end{pmatrix}$$

is the *linear part* of the vector field  $X$  at the singular point  $p$ , and it will allow us to classify the point  $p$ . According to the eigenvalues of this matrix the singular point  $p$  can be of one of the following types:

- *Hyperbolic* if the two eigenvalues have real part different from zero.
- *Semi-hyperbolic* if exactly one eigenvalue is equal to zero.
- *Nilpotent* if both eigenvalues are equal to zero but  $DX(p) \neq 0$ .
- *Linearly zero* if  $DX(p) \equiv 0$ .

- *Linearly a center* if the eigenvalues of  $DX(p)$  are purely imaginary without being zero. In that case, and if the vector field  $X$  is analytic, it can have either a center or a focus at  $p$ . We say that it is a *center* if there is an open neighborhood consisting, besides the singularity, of periodic orbits. It is a *focus* if there is an open neighborhood such that the orbit through any of its points tends to the singular point spirally in positive or negative time.

We will say that  $p$  is *non-degenerate* if it is either hyperbolic or linearly a center, i.e., if zero is not an eigenvalue. We also call hyperbolic and semi-hyperbolic singularities *elementary singular points*.

In order to study the different cases systematically, we introduce some definitions and results. Let us consider now that the vector field  $X$  is defined in a compact neighborhood  $V$  of  $p$  such that  $X(p) = 0$  and  $X(q) \neq 0$  for all  $q \in V \setminus \{p\}$ .

- We say that  $p$  is a *center* if there exists a neighborhood  $W \subseteq V$  of  $p$  such that  $\partial W$  is a periodic orbit and all orbits in  $W \setminus \{p\}$  are periodic.
- We say that  $p$  is an *attracting focus* or *node* if there exists a neighborhood  $W \subseteq V$  of  $p$  such that at all points of  $\partial W$  the vector field points inward and for all  $q \in V \setminus \{p\}$ ,  $\omega(q) = \{p\}$  and  $\gamma^-(q) \cap \partial V \neq \emptyset$ .
- We say that  $p$  is a *repelling focus* or *node* if there exists a neighborhood  $W \subseteq V$  of  $p$  such that at all points of  $\partial W$  the vector field points outward and for all  $q \in V \setminus \{p\}$ ,  $\alpha(q) = \{p\}$  and  $\gamma^+(q) \cap \partial V \neq \emptyset$ .
- We say that  $p$  has a *non-trivial finite sectorial decomposition* if we are not in the previous cases and if there exist a finite number of orbits tending to  $p$ , namely  $c_0, \dots, c_{n-1}$ , each cutting  $\partial V$  transversely at one point  $p_i$ , in the sense that  $\partial V$  is a transverse section near  $p_i$ , and with the property that between  $c_i$  and  $c_{i+1}$  (with  $c_n = c_0$ ), we have one of the following situations with respect to the sector  $S_i$ , defined as the compact region bounded by the point  $p$ ,  $c_i$ ,  $c_{i+1}$  and the piece of  $\partial V$  between  $p_i$  and  $p_{i+1}$ :
  - Attracting parabolic sector.* At all points of  $[p_i, p_{i+1}] \subset \partial V$  the vector field points inward, and for all  $q \in S_i \setminus \{p\}$ ,  $\omega(q) = \{p\}$  and  $\gamma^-(q) \cap \partial V \neq \emptyset$ . See Figure 1.2.1(a).
  - Repelling parabolic sector.* At all points of  $[p_i, p_{i+1}] \subset \partial V$  the vector field points outward, and for all  $q \in S_i \setminus \{p\}$ ,  $\alpha(q) = \{p\}$  and  $\gamma^+(q) \cap \partial V \neq \emptyset$ . See Figure 1.2.1(b).
  - Hyperbolic sector.* There exists a point  $q_i \in (p_i, p_{i+1}) \subset \partial V$  with the property that at all points of  $[p_i, q_i)$  the vector field points inward (respectively outward) while at all points of  $(q_i, p_{i+1}]$  the vector field points outward (respectively inward). At  $q_i$  the vector field is tangent at  $\partial V$  and the tangency is external in the sense that the orbit of  $q_i$  stays outside  $V$ , and for all  $q \in S_i \setminus \bar{c}_i \cup c_{i+1} \cup q_i$  we have  $\gamma^+(q) \cap \partial V \neq \emptyset$  and  $\gamma^-(q) \cap \partial V \neq \emptyset$ . See Figure 1.2.1(c).
  - Elliptic sector.* There exists a point  $q_i \in (p_i, p_{i+1}) \subset \partial V$  with the property that  $\gamma(q_i) \subset V$  with  $\omega(q_i) = \alpha(q_i) = \{p\}$ . At all points  $q \in [p_i, q_i)$  the

vector field points inward,  $\gamma^+(q) \subset V$  and  $\omega(q) = p$ . We denote by  $S_{[p_i, q_i]} = \bigcup_{q \in [p_i, q_i]} \gamma^+(q)$ . At all points  $q \in (q_i, p_{i+1}]$  the vector field points outward,  $\gamma^-(q) \subset V$  and  $\alpha(q) = \{p\}$ . We denote by  $S_{[q_i, p_{i+1}]} = \bigcup_{q \in [q_i, p_{i+1}]} \gamma^-(q)$ . At all points  $q$  of  $S \setminus (S_{[p_i, q_i]} \cup S_{[q_i, p_{i+1}]} \cup \{p\})$  we have  $\gamma(q) \subset V$  with  $\omega(q) = \alpha(q) = \{p\}$ . The same may also be true for  $[p_i, q_i]$  and  $[q_i, p_{i+1}]$  interchanged. See Figure 1.2.1(d).

If  $X$  is defined in a neighborhood  $U$  of the singular point  $p$  we say that  $X$  has the *finite sectorial decomposition property* at  $p$  if there exists some neighborhood  $V \subset U$  of  $p$  such that  $X|_V$  satisfies one of the conditions (i), (ii), (iii) or (iv).

In the first three cases there is only one sector, so we speak about a *trivial sectorial decomposition*. In the last case, we denote respectively by  $e$ ,  $h$  and  $r$  the number of elliptic, hyperbolic and parabolic sectors. Since we are not in the cases (i), (ii) or (iii), we need that  $e$ ,  $h$  or both are different from zero. We try to maintain  $r$  as small as possible, both by joining two adjacent parabolic sectors and by adding a parabolic sector to an elliptic one if it is adjacent to it. Hence the remaining parabolic sectors can only be the ones lying between two hyperbolic sectors. We call this a *minimal sectorial decomposition*. Since  $X(p_i)$  and  $X(p_{i+1})$  cannot both be pointing inward (or outward) if  $S_i$  is a hyperbolic or an elliptic sector, it is clear that  $e + h$  is always even.

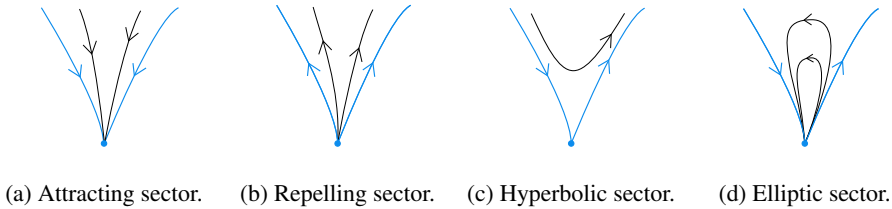


Figure 1.2.1: Sectors near a singular point.

Once we have defined the different types of singular points we will introduce the results to study them. These results provide the local phase portrait at the origin of systems which are in a normal form, so if we want to apply them to a general polynomial differential system we have to move the singular point we want to study to the origin and then put the system in the required normal form. Then, before stating the results, we remind some basic but important tools. First note that we can always move a singular point  $p = (x_0, y_0)$  to the origin of coordinates. If  $p$  is a singular point of the differential system

$$\dot{x} = P(x, y), \quad \dot{y} = Q(x, y),$$

then the point  $(0, 0)$  is a singular point of the system

$$\dot{\bar{x}} = P(\bar{x}, \bar{y}), \quad \dot{\bar{y}} = Q(\bar{x}, \bar{y}),$$

## 1.2 Singular points

where  $x = \bar{x} + x_0$  and  $y = \bar{y} + y_0$ , and the functions  $P(\bar{x}, \bar{y})$  and  $Q(\bar{x}, \bar{y})$  start with terms of order one in  $\bar{x}$  and  $\bar{y}$ . Thus we get a system of the form

$$\dot{x} = ax + by + F(x, y), \quad \dot{y} = cx + dy + G(x, y),$$

where the first partial derivatives of  $F$  and  $G$  are zero at the origin.

Also we recall that by a linear change of coordinates the linear part  $DX(0, 0)$  can be placed in real Jordan canonical form. If the singularity is hyperbolic, the Jordan form is

$$\begin{pmatrix} \lambda_1 & 0 \\ 0 & \lambda_2 \end{pmatrix} \text{ or } \begin{pmatrix} \lambda_1 & 1 \\ 0 & \lambda_1 \end{pmatrix} \text{ or } \begin{pmatrix} \alpha & \beta \\ -\beta & \alpha \end{pmatrix},$$

with  $\lambda_1 \lambda_2 \neq 0$ ,  $\alpha \neq 0$  and  $\beta > 0$ . In the semi-hyperbolic case and the linearly center case, we obtain, respectively

$$\begin{pmatrix} \lambda & 0 \\ 0 & 0 \end{pmatrix} \text{ and } \begin{pmatrix} 0 & \beta \\ -\beta & 0 \end{pmatrix},$$

with  $\lambda \neq 0$  and  $\beta > 0$ . And finally, in the nilpotent case and the linearly zero case, we obtain, respectively,

$$\begin{pmatrix} 0 & 1 \\ 0 & 0 \end{pmatrix} \text{ and } \begin{pmatrix} 0 & 0 \\ 0 & 0 \end{pmatrix}.$$

If we allow a time rescaling introducing a new time variable  $u = \gamma t$  for some  $\gamma > 0$ , then we can also suppose that in the hyperbolic case one of the eigenvalues  $\lambda_1$  or  $\lambda_2$  is equal to  $\pm 1$  and either  $\alpha = \pm 1$  or  $\beta = 1$ , while in the semi-hyperbolic case  $\lambda = \pm 1$  and in the linearly center case  $\beta = 1$ .

These considerations will be necessary to apply the following results to our polynomial differential systems. Now let state the results that provide the local phase portraits in the cases of non-degenerated, semi-hyperbolic and nilpotent singular points, except for linear centers, in which case other tools must be used, as Lyapunov constants, but we will not deal with this situation in our work.

**Theorem 1.2.1** (Non-Degenerated Singular Points Theorem). *Let  $(0, 0)$  be an isolated singular point of the vector field  $X$ , given by*

$$\begin{aligned} \dot{x} &= ax + by + A(x, y), \\ \dot{y} &= cx + dy + B(x, y), \end{aligned} \tag{1.2.2}$$

where  $A$  and  $B$  are analytic in a neighborhood of the origin with  $A(0, 0) = B(0, 0) = DA(0, 0) = DB(0, 0) = 0$ . Let  $\lambda_1$  and  $\lambda_2$  be the eigenvalues of the linear part  $DX(0, 0)$  of the system at the origin. Then the following statements hold.

- (i) If  $\lambda_1$  and  $\lambda_2$  are real and  $\lambda_1 \lambda_2 < 0$ , then  $(0, 0)$  is a saddle (see Figure 1.2.2(a)). If we denote by  $E_1$  and  $E_2$  the eigenspaces of respectively  $\lambda_1$  and  $\lambda_2$ , then one can find two invariant analytic curves, tangent respectively to  $E_1$  and  $E_2$  at the origin, on one of which points are attracted towards the origin, and on one of which points are repelled away from the origin. On these invariant curves  $X$  is  $C^\omega$ -linearizable. There exists a  $C^\infty$  coordinate change transforming (1.2.2) into one of the following normal forms:

$$\dot{x} = \lambda_1 x, \quad \dot{y} = \lambda_2 y,$$



in the case  $\lambda_2/\lambda_1 \in \mathbb{R} \setminus \mathbb{Q}$ , and

$$\dot{x} = x(\lambda_1 + f(x^k y^l)), \quad \dot{y} = y(\lambda_2 + g(x^k y^l)),$$

in the case  $\lambda_2/\lambda_1 = -k/l \in \mathbb{Q}$  with  $k, l \in \mathbb{N}$  and where  $f$  and  $g$  are  $C^\infty$  functions. In this case systems (1.2.2) are  $C^0$ -conjugate to

$$\dot{x} = x, \quad \dot{y} = -y.$$

- (ii) If  $\lambda_1$  and  $\lambda_2$  are real with  $|\lambda_1| \geq |\lambda_2|$  and  $\lambda_1 \lambda_2 > 0$ , then  $(0, 0)$  is a node (see Figure 1.2.2(b)). If  $\lambda_1 > 0$  (respectively  $\lambda_1 < 0$ ) then it is repelling or unstable (respectively attracting or stable). There exists a  $C^\infty$  coordinate change transforming (1.2.2) into

$$\dot{x} = \lambda_1 x, \quad \dot{y} = \lambda_2 y,$$

in case  $\lambda_2/\lambda_1 \notin \mathbb{N}$ , and into

$$\dot{x} = \lambda_1 x, \quad \dot{y} = \lambda_2 y + \delta x^m,$$

for some  $\delta = 0$  or  $1$ , in case  $\lambda_2 = m\lambda_1$  with  $m \in \mathbb{N}$  and  $m \geq 1$ . In this case systems (1.2.2) are  $C^0$ -conjugate to

$$\dot{x} = \delta x, \quad \dot{y} = \delta y,$$

with  $\delta = \pm 1$  and  $\lambda_1 \delta > 0$ .

- (iii) If  $\lambda_1 = \alpha + i\beta$  and  $\lambda_2 = \alpha - i\beta$  with  $\alpha, \beta \neq 0$ , then  $(0, 0)$  is a “strong” focus (see Figure 1.2.2(c)). If  $\alpha > 0$  (respectively  $\alpha < 0$ ), it is repelling or unstable (respectively attracting or stable). There exists a  $C^\infty$  coordinate change transforming (1.2.2) into

$$\dot{x} = \alpha x + \beta y, \quad \dot{y} = -\beta x + \alpha y.$$

In this case systems (1.2.2) are  $C^0$ -conjugate to

$$\dot{x} = \delta x, \quad \dot{y} = \delta y,$$

with  $\delta = \pm 1$  and  $\alpha \delta > 0$ .

- (iv) If  $\lambda_1 = i\beta$  and  $\lambda_2 = -i\beta$  with  $\beta \neq 0$ , then  $(0, 0)$  is a linear center, topologically, a “weak” focus or a center (see Figures 1.2.2(c) and (d)).

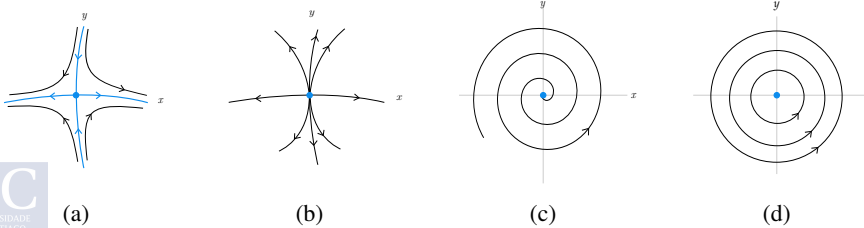


Figure 1.2.2: Phase portraits of non-degenerate singular points.

**Remark 1.2.2.** The denomination strong focus in (iii) is used to describe singular points whose linear part  $DX(0,0)$  is already a focus, while the denomination weak focus is used in the case  $DX(0,0)$  is a center.

**Theorem 1.2.3** (Semi-Hyperbolic Singular Points Theorem). *Let  $(0,0)$  be an isolated singular point of the vector field  $X$  given by*

$$\begin{aligned}\dot{x} &= A(x, y), \\ \dot{y} &= \lambda y + B(x, y),\end{aligned}$$

where  $A$  and  $B$  are analytic in a neighborhood of the origin with  $A(0,0) = B(0,0) = DA(0,0) = DB(0,0) = 0$  and  $\lambda > 0$ . Let  $y = f(x)$  be the solution of the equation  $\lambda y + B(x, y) = 0$  in a neighborhood of the point  $(0,0)$ , and suppose that the function  $g(x) = A(x, f(x))$  has the expression  $g(x) = a_m x^m + o(x^m)$ , where  $m \geq 2$  and  $a_m \neq 0$ . Then there always exists an invariant analytic curve, called the strong unstable manifold, tangent at the origin to the  $y$ -axis, on which  $X$  is analytically conjugate to

$$\dot{y} = \lambda y;$$

it represents repelling behavior since  $\lambda > 0$ . Moreover the following statements hold.

- (i) If  $m$  is odd and  $a_m < 0$ , then  $(0,0)$  is a topological saddle (see Figure 1.2.3(a)). Tangent to the  $x$ -axis there is a unique invariant  $C^\infty$  curve, called the center manifold, on which  $X$  is  $C^\infty$ -conjugate to

$$\dot{x} = -x^m(1 + ax^{m-1}), \quad (1.2.3)$$

for some  $a \in \mathbb{R}$ . If this invariant curve is analytic, then on it  $X$  is  $C^\omega$ -conjugate to (1.2.3).

System  $X$  is  $C^\infty$ -conjugate to

$$\dot{x} = -x^m(1 + ax^{m-1}), \quad \dot{y} = \lambda y,$$

and is  $C^0$ -conjugate to

$$\dot{x} = -x, \quad \dot{y} = y.$$

- (ii) If  $m$  is odd and  $a_m > 0$ , then  $(0,0)$  is an unstable topological node (see Figure 1.2.3(b)). Every point not belonging to the strong unstable manifold lies on an invariant  $C^\infty$  curve, called a center manifold, tangent to the  $x$ -axis at the origin, and on which  $X$  is  $C^\infty$ -conjugate to

$$\dot{x} = x^m(1 + ax^{m-1}), \quad (1.2.4)$$

for some  $a \in \mathbb{R}$ . All these center manifolds are mutually infinitely tangent to each other, and hence at most one of them can be analytic, in which case  $X$  is  $C^\omega$ -conjugate on it to (1.2.4).

System  $X$  is  $C^\infty$ -conjugate to

$$\dot{x} = x^m(1 + ax^{m-1}), \quad \dot{y} = \lambda y,$$

and is  $C^0$ -conjugate to

$$\dot{x} = x, \quad \dot{y} = y.$$

(iii) If  $m$  is even, then  $(0, 0)$  is a saddle-node, that is, a singular point whose neighborhood is the union of one parabolic and two hyperbolic sectors (see Figure 1.2.3(c)). Modulo changing  $x$  into  $-x$ , we suppose that  $a_m > 0$ . Every point to the right of the strong unstable manifold (side  $x > 0$ ) lies on an invariant  $C^\infty$  curve, called a center manifold, tangent to the  $x$ -axis at the origin, and on which  $X$  is  $C^\infty$ -conjugate to

$$\dot{x} = x^m(1 + ax^{m-1}), \quad (1.2.5)$$

for some  $a \in \mathbb{R}$ . All these center manifolds coincide on the side  $x \leq 0$  and are hence infinitely tangent at the origin. At most one of these center manifolds can be analytic, in which case  $X$  is  $C^\omega$ -conjugate on it to (1.2.5). System  $X$  is  $C^\infty$ -conjugate to

$$\dot{x} = x^m(1 + ax^{m-1}), \quad \dot{y} = \lambda y,$$

and is  $C^0$ -conjugate to

$$\dot{x} = x^2, \quad \dot{y} = y.$$

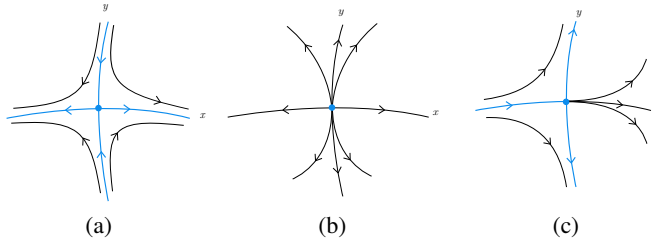


Figure 1.2.3: Phase portraits of semi-hyperbolic singular points.

**Remark 1.2.4.** The case  $\lambda < 0$  can be reduced to  $\lambda > 0$  by changing  $X$  into  $-X$ . We also recall that in case  $g(x) = A(x, f(x))$ , as defined in Theorem 1.2.3, is identically zero, then there exists an analytic curve consisting of singularities.

**Theorem 1.2.5** (Nilpotent Singular Points Theorem). *Let  $(0, 0)$  be an isolated singular point of the vector field  $X$  given by*

$$\begin{aligned} \dot{x} &= y + A(x, y), \\ \dot{y} &= B(x, y), \end{aligned}$$

where  $A$  and  $B$  are analytic in a neighborhood of the origin and also  $DA(0, 0) = DB(0, 0) = 0$ . Let  $y = f(x)$  be the solution of the equation  $y + A(x, y) = 0$  in a neighborhood of the point  $(0, 0)$  and consider the functions

$$F(x) = B(x, f(x)) \quad \text{and} \quad G(x) = (\partial A / \partial x + \partial B / \partial y)(x, f(x)).$$

Then the following statements hold.

- (i) If  $F(x) \equiv G(x) \equiv 0$ , then the phase portrait of  $X$  is given by 1.2.4(a).
- (ii) If  $F(x) \equiv 0$  and  $G(x) = bx^n + o(x^n)$  for  $n \in \mathbb{N}$  with  $n \geq 1$  and  $b \neq 0$ , then the phase portrait of  $X$  is given by Figure 1.2.4(b) or (c).
- (iii) If  $G(x) \equiv 0$  and  $F(x) = ax^m + o(x^m)$  for  $m \in \mathbb{N}$  with  $m \geq 1$  and  $a \neq 0$ , then
  - (a) If  $m$  is odd and  $a > 0$ , then the origin of  $X$  is a saddle as in Figure 1.2.4(d) and if  $a < 0$ , then it is a center or a focus as in Figure 1.2.4(e-g).
  - (b) If  $m$  is even then the origin of  $X$  is a cusp as in Figure 1.2.4(h).
- (iv) If  $F(x) = ax^m + o(x^m)$  and  $G(x) = bx^n + o(x^n)$  with  $m \in \mathbb{N}$ ,  $m \geq 2$ ,  $n \in \mathbb{N}$ ,  $n \geq 1$ ,  $a \neq 0$  and  $b \neq 0$ , then we have
  - (a) If  $m$  is even, and
    - (a1)  $m < 2n + 1$ , then the origin of  $X$  is a cusp as in Figure 1.2.4(h).
    - (a2)  $m > 2n + 1$ , then the origin of  $X$  is a saddle-node as in Figure 1.2.4(i) or (j).
  - (b) If  $m$  is odd and  $a > 0$  then the origin of  $X$  is a saddle as in Figure 1.2.4(d).
  - (c) If  $m$  is odd,  $a < 0$  and
    - (c1) Either  $m < 2n + 1$ , or  $m = 2n + 1$  and  $b^2 + 4a(n + 1) < 0$ , then the origin of  $X$  is a center or a focus as in Figure 1.2.4(e-g).
    - (c2)  $n$  is odd and either  $m > 2n + 1$ , or  $m = 2n + 1$  and  $b^2 + 4a(n + 1) \geq 0$ , then the phase portrait of the origin of  $X$  consist of one hyperbolic and one elliptic sector as in Figure 1.2.4(k).
    - (c3)  $n$  is even and either  $m > 2n + 1$ , or  $m = 2n + 1$  and  $b^2 + 4a(n + 1) \geq 0$ , then the origin of  $X$  is a node as in Figure 1.2.4(l) or (m). The node is attracting if  $b < 0$  and repelling if  $b > 0$ .

The previous results provide a total classification of non-degenerated, semi-hyperbolic and nilpotent singular points, except, as we said before, for the linear centers. All these results and their proofs can be found in Chapters 2 and 3 of [50]. Whereas, to study a singular point for which the Jacobian matrix is identically zero, the only possibility is studying each singular point case by case. The main technique to perform the desingularization of a linearly zero singular point is the blow up technique.

The desingularization theorem for planar vector fields was first stated by Bendixson in 1901 without proof. Seidenberg gave the first rigorous proof of the theorem for the analytic case (see [125]). The desingularization procedure was extended to  $C^\infty$  vector fields of “Lojasiewicz” type in [49]. Van den Essen found a transformed proof of the desingularization theorem for analytic vector fields (see [130]).

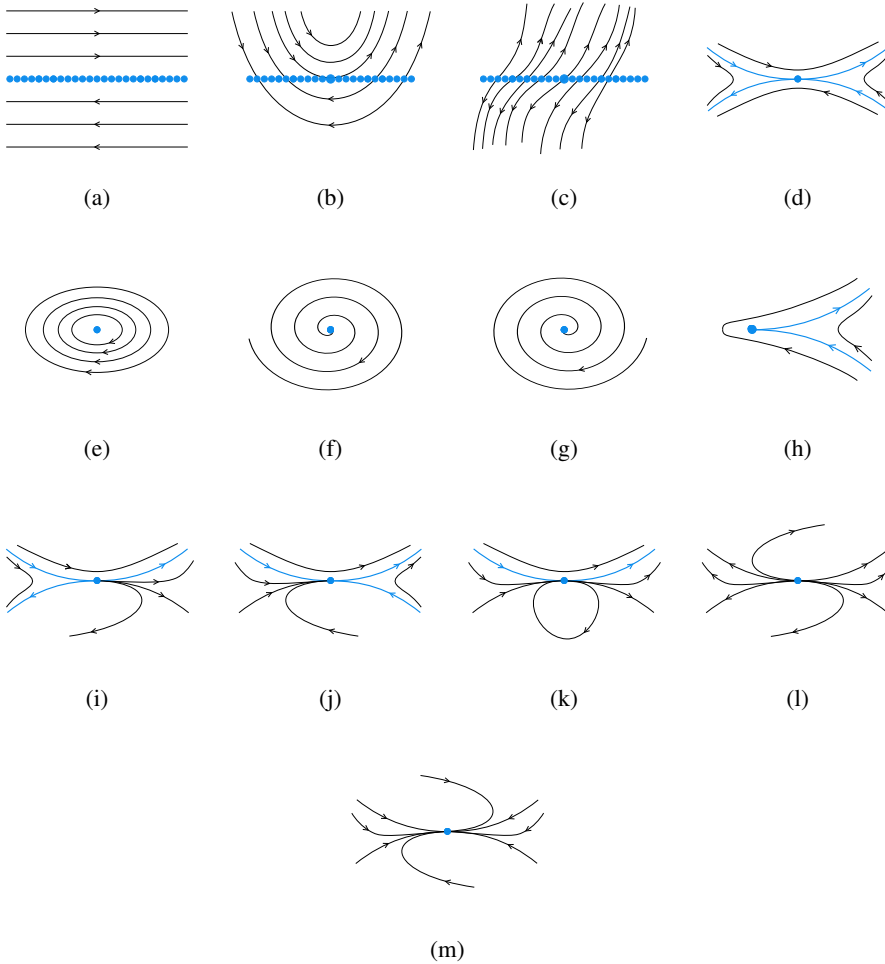


Figure 1.2.4: Phase portraits of nilpotent singular points.

Roughly speaking the idea behind the blow up technique is to explode, through a change of variables that is not a diffeomorphism, the singularity to a line. Then, for studying the original singular point, one studies the new singular points that appear on this line, and this is simpler. If some of these new singular points are linearly zero, the process is repeated. Dumortier proved that this iterative process of desingularization is finite (see [49]).

Consider a real planar polynomial differential system of the form

$$\begin{aligned}\dot{x} &= P(x, y) = P_m(x, y) + \dots, \\ \dot{y} &= Q(x, y) = Q_m(x, y) + \dots,\end{aligned}\tag{1.2.6}$$

where  $P$  and  $Q$  are coprime polynomials,  $P_m$  and  $Q_m$  are homogeneous polynomials of degree  $m \in \mathbb{N}$  and the dots mean higher order terms in  $x$  and  $y$ . Note that we are assuming

that the origin is a singular point because  $m > 0$ . We define the *characteristic polynomial* of (1.2.6) as

$$\mathcal{F}(x, y) := xQ_m(x, y) - yP_m(x, y),$$

and we say that the origin is a *nondicritical* singular point if  $\mathcal{F} \not\equiv 0$  and a *dicritical* singular point if  $\mathcal{F} \equiv 0$ . In this last case  $P_m = xW_{m-1}$  and  $Q_m = yW_{m-1}$ , where  $W_{m-1} \not\equiv 0$  is a homogeneous polynomial of degree  $m - 1$ . If  $y - vx$  is a factor of  $W_{m-1}$  and  $v = \tan \theta^*$ ,  $\theta^* \in [0, 2\pi)$ , then  $\theta^*$  is a *singular direction*.

The *homogeneous directional blow up in the vertical direction* (resp. in the horizontal direction) is the mapping  $(x, y) \rightarrow (x, z) = (x, y/x)$  (resp.  $(x, y) \rightarrow (z, y) = (x/y, y)$ ), where  $z$  is a new variable. This map transforms the origin of (1.2.6) into the line  $x = 0$  (resp.  $y = 0$ ), which is called the *exceptional divisor*. The expression of system (1.2.6) after the blow up in the vertical direction is

$$\dot{x} = P(x, xz), \quad \dot{z} = \frac{Q(x, xz) - zP(x, xz)}{x}, \quad (1.2.7)$$

that is always well-defined since we are assuming that the origin is a singular point. After the blow up, we cancel an appearing common factor  $x^{m-1}$  ( $x^m$  if  $\mathcal{F} \equiv 0$ ). Moreover, the mapping swaps the second and third quadrants in the vertical directional blow up and the third and fourth quadrants in the horizontal blow up, after which the system writes as

$$\dot{z} = \frac{P(yz, y) - zQ(yz, y)}{y}, \quad \dot{x} = P(yz, y).$$

The two following results provide the relationship between the original singular point of system (1.2.6) and the new singularities of system (1.2.7). For more details see [5].

**Proposition 1.2.6.** *Let  $\varphi_t = (x(t), y(t))$  be a trajectory tending to the origin of system (1.2.6), in forward or backward time. Suppose that  $\mathcal{F} \not\equiv 0$ . Assume that  $\varphi_t$  is tangent to one of the two angle directions  $\tan \theta = v$ ,  $v \neq \infty$ . Then the following statements hold.*

1. *The two angle directions  $\theta = \arctan v$  (in  $[0, 2\pi)$ ) are characteristic directions.*
2. *The point  $(0, v)$  on the  $(x, z)$ -plane is an isolated singular point of system (1.2.7).*
3. *The trajectory  $\varphi_t$  corresponds to a solution of system (1.2.7) tending to the singular point  $(0, v)$ .*
4. *Conversely, any solution of system (1.2.7) tending to the singular point  $(0, v)$  on the  $(x, z)$ -plane corresponds to a solution of system (1.2.6) tending to the origin in one of the two angle directions  $\tan \theta = v$ .*

**Proposition 1.2.7.** *Consider system (1.2.6) and suppose that  $\mathcal{F} \equiv 0$ . Then for every non-singular direction  $\theta$  there exists exactly one semipath tending to the origin in the direction  $\theta$  in forward or backward time. If  $\theta^*$  is a singular direction, there may be either no semipaths tending to the origin in the direction  $\theta^*$ , or a finite number, or infinitely many.*

Finally, to study the behavior of the solutions around the origin of system (1.2.6), it is necessary to study the singular points of system (1.2.7) on the exceptional divisor. They correspond to either characteristic directions in the nondicritical case, or singular directions in the dicritical case. It may happen that some of these singular points are linearly zero, in which case we have to repeat the process. As we said before, it is proved in [49] that this chain of blow ups is finite.

### 1.3 Poincaré compactification

In order to study a planar vector field and to draw its phase portrait, working over the complete real plane  $\mathbb{R}^2$  is not easy. If the functions defining the vector field are polynomials, we can use the Poincaré compactification, which allows us to control the orbits which tend to or come from infinity, and to draw the phase portrait in a finite region. For this reason we will work on the Poincaré sphere, introduced by Poincaré [109].

In this section we introduce the Poincaré compactification and we shall use the coordinates  $(x_1, x_2)$  instead of  $(x, y)$ . Consider two polynomials  $P$  and  $Q$  of arbitrary degree in the variables  $x_1$  and  $x_2$  and let  $d$  be the maximum of the degrees of  $P$  and  $Q$ . The polynomial vector field of degree  $d$

$$X = P \frac{\partial}{\partial x_1} + Q \frac{\partial}{\partial x_2}$$

defines the differential system

$$\begin{aligned} \dot{x}_1 &= P(x_1, x_2), \\ \dot{x}_2 &= Q(x_1, x_2). \end{aligned} \tag{1.3.8}$$

We consider  $\mathbb{R}^2$  as the plane in  $\mathbb{R}^3$  defined by  $(y_1, y_2, y_3) = (x_1, x_2, 1)$ . We also consider the sphere  $\mathbb{S}^2 = \{y \in \mathbb{R}^3 : y_1^2 + y_2^2 + y_3^2 = 1\}$ , which we call *Poincaré sphere*. This sphere is tangent to  $\mathbb{R}^2$  at the point  $(0, 0, 1)$ . We may divide this sphere into  $H_+ = \{y \in \mathbb{S}^2 : y_3 > 0\}$  (the northern hemisphere),  $H_- = \{y \in \mathbb{S}^2 : y_3 < 0\}$  (the southern hemisphere) and  $\mathbb{S}^1 = \{y \in \mathbb{S}^2 : y_3 = 0\}$  (the equator). We consider the projection of the vector field  $X$  from  $\mathbb{R}^2$  to  $\mathbb{S}^2$  given by the central projections  $f^+ : \mathbb{R}^2 \rightarrow \mathbb{S}^2$  and  $f^- : \mathbb{R}^2 \rightarrow \mathbb{S}^2$ . By definition,  $f^+(x)$  is the intersection of the straight line passing through the point  $x$  and the origin with the northern hemisphere of  $\mathbb{S}^2$ , and respectively for  $f^-(x)$  with the southern hemisphere:

$$f^+(x) = \left( \frac{x_1}{\Delta(x)}, \frac{x_2}{\Delta(x)}, \frac{1}{\Delta(x)} \right), \quad f^-(x) = \left( \frac{-x_1}{\Delta(x)}, \frac{-x_2}{\Delta(x)}, \frac{-1}{\Delta(x)} \right),$$

where  $\Delta(x) = \sqrt{x_1^2 + x_2^2 + 1}$ .

In this way we obtain induced vector fields in each hemisphere. The induced vector field on  $H_+$  is

$$\bar{X}(y) = Df^+(x)X(x), \text{ where } y = f^+(x),$$

and the one in  $H_-$  is

$$\bar{X}(y) = Df^-(x)X(x), \text{ where } y = f^-(x).$$

We remark that  $\bar{X}$  is a vector field on  $\mathbb{S}^2 \setminus \mathbb{S}^1$  that is everywhere tangent to  $\mathbb{S}^2$ . Note that the points at infinity of  $\mathbb{R}^2$  (two for each direction) are in bijective correspondence with the points of the equator of  $\mathbb{S}^2$ .

Now we would like to extend the induced vector field  $\bar{X}$  from  $\mathbb{S}^2 \setminus \mathbb{S}^1$  to  $\mathbb{S}^2$ . Unfortunately it does not in general stay bounded as we get close to  $\mathbb{S}^1$ , obstructing the extension. It turns out, however, that if we multiply the vector field by the factor  $\rho(x) = x_3^{d-1}$  then, as we will check in a moment, the extension becomes possible. The extended vector field on  $\mathbb{S}^2$  is called the *Poincaré compactification* of the vector field  $X$  on  $\mathbb{R}^2$  and it is denoted by  $\rho(X)$ .

To make calculations we use the six local charts of  $\mathbb{S}^2$  given by

$$U_k = \{y \in \mathbb{S}^2 \mid y_k > 0\}, \quad V_k = \{y \in \mathbb{S}^2 \mid y_k < 0\},$$

for  $k = 1, 2, 3$ , and the corresponding local maps

$$\phi_k : U_k \longrightarrow \mathbb{R}^2 \quad \text{and} \quad \psi_k : V_k \longrightarrow \mathbb{R}^2,$$

which are defined as

$$\phi_k(y) = \psi_k(y) = \left( \frac{y_m}{y_k}, \frac{y_n}{y_k} \right),$$

for  $m < n$  and  $m, n \neq k$ . We denote by  $z = (u, v)$  the value of  $\phi_k(y)$  or  $\psi_k(y)$ , for any  $k$ , such that  $(u, v)$  will play different roles depending on the local chart we are considering. Geometrically the coordinates  $(u, v)$  can be expressed as in Figure 1.3.1. The points of  $\mathbb{S}^1$  in any chart have  $v = 0$ .

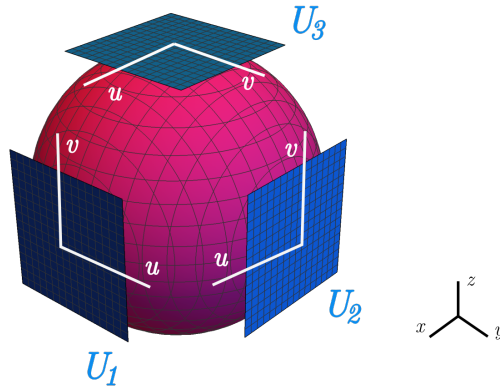


Figure 1.3.1: The local charts  $(U_k, \phi_k)$  for  $k = 1, 2, 3$  of the Poincaré sphere.

In what follows we make a detailed calculation of the expression of  $\rho(X)$  in the local chart  $U_1$ . We have  $X(x) = (P(x_1, x_2), Q(x_1, x_2))$  and  $\bar{X}(y) = Df^+(x)X(x)$  with  $y = f^+(x)$ , then

$$D\phi_1(y)\bar{X}(y) = D\phi_1(y) \circ Df^+(x)X(x) = D(\phi_1 \circ f^+)(x)X(x).$$



Let  $\bar{X}|_{U_1}$  denote the system defined as  $D\phi_1(y)\bar{X}(y)$ . Then

$$(\phi_1 \circ f^+)(x) = \phi_1 \left( \frac{x_1}{\Delta(x)}, \frac{x_2}{\Delta(x)}, \frac{1}{\Delta(x)} \right) = \left( \frac{x_2}{x_1}, \frac{1}{x_1} \right) = (u, v),$$

and

$$D(\phi_1 \circ f^+)(x) = \begin{pmatrix} -\frac{x_2}{x_1^2} & \frac{1}{x_1} \\ -\frac{1}{x_1^2} & 0 \end{pmatrix}.$$

We have

$$\begin{aligned} \bar{X}|_{U_1} &= \begin{pmatrix} -\frac{x_2}{x_1^2} & \frac{1}{x_1} \\ -\frac{1}{x_1^2} & 0 \end{pmatrix} \begin{pmatrix} P(x_1, x_2) \\ Q(x_1, x_2) \end{pmatrix} \\ &= \left( -\frac{x_2}{x_1^2} P(x_1, x_2) + \frac{1}{x_1} Q(x_1, x_2), -\frac{1}{x_1^2} P(x_1, x_2) \right) \\ &= \frac{1}{x_1^2} (-x_2 P(x_1, x_2) + x_1 Q(x_1, x_2), -P(x_1, x_2)) \\ &= v^2 \left( -\frac{u}{v} P\left(\frac{1}{v}, \frac{u}{v}\right) + \frac{1}{v} Q\left(\frac{1}{v}, \frac{u}{v}\right), -P\left(\frac{1}{v}, \frac{u}{v}\right) \right). \end{aligned}$$

Also

$$\rho(y) = y_3^{d-1} = \left( \frac{1}{\Delta(x)} \right)^{d-1} = \frac{v^{d-1}}{\Delta(z)^{d-1}} = v^{d-1} m(z),$$

where  $m(z) = (1 + u^2 + v^2)^{\frac{1-d}{2}}$ . Therefore we can multiply the field  $\bar{X}|_{U_1}$  by  $\rho(y)$ , which is equivalent to change the time variable  $t$  for a new variable  $s$ , so that  $dt = \rho(y)ds$ . This does not make any changes on the phase portrait, except the velocity at which orbits are traveled. Now we have a compactification of the field on the local charts that has a well defined polynomial expression:

$$\rho(y)(\bar{X}|_{U_1}) = v^{d+1} m(z) \left( -\frac{u}{v} P\left(\frac{1}{v}, \frac{u}{v}\right) + \frac{1}{v} Q\left(\frac{1}{v}, \frac{u}{v}\right), -P\left(\frac{1}{v}, \frac{u}{v}\right) \right).$$

We notice that while  $\bar{X}|_{U_1}$  is not well defined when  $v = 0$ ,  $p(X)|_{U_1} = \rho\bar{X}|_{U_1}$  is well defined along  $v = 0$ , since the multiplying factor  $v^{d+1}$  cancels any factor of  $v$  which could appear in the denominator, so the extension of  $\rho\bar{X}$  to  $p(X)$  is defined on the whole of  $\mathbb{S}^1$ . In order to simplify the extended vector field we also make a change in the time variable and remove the factor  $m(z)$ . Similar arguments can be applied to the rest of the local charts.

Summarizing, the Poincaré compactification of the vector field  $X$  is given by the following expressions. In local chart  $(U_1, \phi_1)$  the expression is

$$\begin{aligned} \dot{u} &= v^d \left[ -u P\left(\frac{1}{v}, \frac{u}{v}\right) + Q\left(\frac{1}{v}, \frac{u}{v}\right) \right], \\ \dot{v} &= -v^{d+1} P\left(\frac{1}{v}, \frac{u}{v}\right), \end{aligned} \tag{1.3.9}$$

in  $(U_2, \phi_2)$  we have

$$\begin{aligned}\dot{u} &= v^d \left[ P\left(\frac{u}{v}, \frac{1}{v}\right) - uQ\left(\frac{u}{v}, \frac{1}{v}\right) \right], \\ \dot{v} &= -v^{d+1} Q\left(\frac{u}{v}, \frac{1}{v}\right),\end{aligned}\tag{1.3.10}$$

and finally, in  $(U_3, \phi_3)$ :

$$\begin{aligned}\dot{u} &= P(u, v), \\ \dot{v} &= Q(u, v).\end{aligned}\tag{1.3.11}$$

Note that we do not need to go through the complete geometrical construction in order to get these expressions. The expressions in (1.3.11) do not need any elaboration. To obtain (1.3.9) we start with (1.3.8) and introduce coordinates  $(u, v)$  by the formulas  $(x_1, x_2) = (1/v, u/v)$ . This leads to a vector field  $\bar{X}^u$  which we multiply by  $v^{d-1}$ . To obtain (1.3.10) we start with (1.3.8) and introduce coordinates  $(u, v)$  by the formulas  $(x_1, x_2) = (u/v, 1/v)$ . We again multiply the obtained vector field  $\bar{X}^v$  by  $v^{d-1}$ .

In the charts  $(V_k, \psi_k)$ , with  $k = 1, 2, 3$ , the expression for  $\rho(X)$  is the same as for  $(U_k, \phi_k)$  multiplied by  $(-1)^{d-1}$ . Therefore, it is not necessary to study the system in these charts independently, as it is enough to determine the behavior of the orbits based on the behavior on charts  $(U_i, \phi_i)$ , with  $i = 1, 2, 3$ .

The equator  $\mathbb{S}^1$  is invariant by the vector field  $\rho(X)$  and all the singular points of  $\rho(X)$  which lie in this equator are called the *infinite singular points* of  $X$ . If  $y \in \mathbb{S}^1$  is an infinite singular point, then  $-y$  is also an infinite singular point and they have the same (respectively opposite) stability if the degree of vector field is odd (respectively even).

The image of the northern hemisphere of  $\mathbb{S}^2$  onto the plane  $y_3 = 0$  under the orthogonal projection  $\pi$  is called the *Poincaré disk*, and we denote it by  $\mathbb{D}^2$ . Since the orbits of  $\rho(X)$  on  $\mathbb{S}^2$  are symmetric with respect to the origin of  $\mathbb{R}^3$ , we only need to consider the flow of  $\rho(X)$  in the closed northern hemisphere, and we can project the phase portrait of  $\rho(X)$  on the northern hemisphere onto the Poincaré disk. We shall present the phase portraits of the polynomial differential systems in the Poincaré disk, which is covered by charts  $U_1, V_1, U_2$  and  $V_2$  as in Figure 1.3.2.

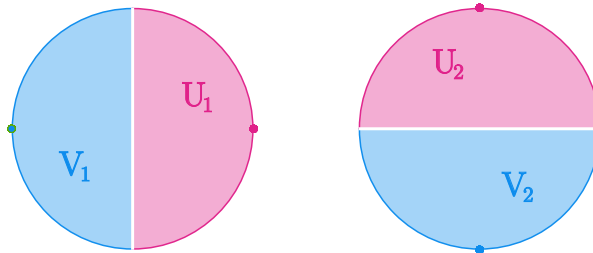


Figure 1.3.2: The projection of the northern hemisphere on the Poincaré disk, with charts  $U_1$ ,  $V_1$ ,  $U_2$  and  $V_2$ .

## 1.4 Topological equivalence and phase portraits

We introduce the notion of equivalence between two vector fields which allows us to compare their phase portraits. Let  $X_1$  and  $X_2$  be two vector fields defined on open subsets  $D_1$  and  $D_2$  of  $\mathbb{R}^2$ , respectively. We say that  $X_1$  is *topologically equivalent* to  $X_2$  when there exists a homeomorphism  $h : D_1 \rightarrow D_2$  which sends orbits of  $X_1$  to orbits of  $X_2$  preserving (or reversing) the orientation. More precisely, let  $p \in D_1$  and  $\gamma_p^1$  be the oriented orbit of  $X_1$  passing through  $p$ ; then  $h(\gamma_p^1)$  is an oriented orbit of  $X_2$  passing through  $h(p)$ . Such a homeomorphism  $h$  is called a *topological equivalence* between  $X_1$  and  $X_2$ .

A topological equivalence  $h$  defines an equivalence relation between vector fields defined on open sets  $D_1$  and  $D_2 = h(D_1)$  of  $\mathbb{R}^2$ . A topological equivalence  $h$  between  $X_1$  and  $X_2$  maps singular points to singular points, and periodic orbits to periodic orbits.

Since we will be working on the Poincaré disk, we will say that two polynomial vector fields  $X_1$  and  $X_2$  on  $\mathbb{R}^2$  are topologically equivalent if there exists a homeomorphism on the Poincaré disk which preserves the infinity  $\mathbb{S}^1$  and sends the trajectories of the flow of  $\pi(\rho(X_1))$  to the trajectories of the flow of  $\pi(\rho(X_2))$ , preserving or reversing the orientation of all the orbits.

Our objective is to give a topological classification of the phase portraits of some differential systems. Generally, by a *phase portrait of the vector field*  $X$ , we mean the set of oriented orbits of  $X$ . It consists of singularities and regular orbits, oriented according to the maximal solutions describing them, hence in the sense of increasing  $t$ . Usually the phase portrait is represented by drawing a number of significant orbits, representing the orientation by arrows (in case of regular orbits).

For linear vector fields it is possible to describe all conjugacy classes, but this is not for nonlinear vector fields. However, there exists a general characterization of the topological equivalence classes for vector fields on the plane. In order to present it, we introduce some definitions. The vector field  $X$  needs only to be sufficiently regular to admit the existence of a continuous flow (local Lipschitz continuity suffices). We consider a differential equation  $\dot{x} = X(x)$  where  $X$  is a locally Lipschitz function on  $\mathbb{R}^2$  and let  $\phi(s, x)$  be the flow defined by the differential equation. Following the notation of the works of Markus and Neumann, we denote by  $(\mathbb{R}^2, \phi)$  the flow defined by the differential equation. By the theorem of continuous dependence on initial conditions, the flow  $(\mathbb{R}^2, \phi)$  is continuous. We say that a flow  $(\mathbb{R}^2, \phi)$  is a *parallel flow* if it is topologically equivalent to one of the following flows:

- (i) The flow defined on  $\mathbb{R}^2$  by the differential system

$$\dot{x} = 1, \quad \dot{y} = 0,$$

which we denote by *strip flow*.

- (ii) The flow defined on  $\mathbb{R}^2 \setminus \{0\}$  by the differential system given in polar coordinates

$$r' = 0, \quad \theta' = 1,$$

which we denote by *annulus flow*.

(iii) The flow defined on  $\mathbb{R}^2 \setminus \{0\}$  by the differential system given in polar coordinates

$$r' = r, \quad \theta' = 1,$$

which we denote by *spiral flow*.

Given a maximal open region on  $\mathbb{R}^2$  on which the flow is parallel, it is interesting to know the orbit structure of its boundary, where we can find the following types of orbits:

- (i) a singular point,
- (ii) a periodic orbit for which there does not exist a neighborhood entirely consisting of periodic orbits,
- (iii) an orbit  $\gamma(p)$ , homeomorphic to  $\mathbb{R}$  for which there does not exist a neighborhood  $N$  of  $\gamma(p)$  such that
  - (1) for all  $q \in N$   $\alpha(q) = \alpha(p)$  and  $\omega(q) = \omega(p)$ ,
  - (2) the boundary  $\partial N$  of  $N$ , that is  $\partial N = \overline{N} \setminus N$ , is formed by  $\alpha(p)$ ,  $\omega(p)$  and two orbits  $\gamma(q_1)$  and  $\gamma(q_2)$  such that  $\alpha(p) = \alpha(q_1) = \alpha(q_2)$  and  $\omega(p) = \omega(q_1) = \omega(q_2)$ .

We will call *separatrix* to a orbit satisfying (i), (ii) or (iii). The set of all separatrices of  $X$  is closed and we denote it by  $\Sigma_X$ . We call  $V$  a *canonical region* if it is a maximal connected component of  $\mathbb{R}^2 \setminus \Sigma_X$ , in which case it necessarily is invariant under the flow.

**Proposition 1.4.1.** *Every canonical region of  $(\mathbb{R}^2, \phi)$  is parallel, given by either a strip, an annular or a spiral flow.*

On the Poincaré disk we consider as separatrices of  $\pi(\rho(X))$  the finite singular points, the limit cycles, the orbits on the boundary of a hyperbolic sector at a finite or an infinite singular point, and also any orbit at the infinity  $\mathbb{S}^1$ . The *separatrix configuration* of  $\pi(\rho(X))$  is the union of an orbit of each canonical region with the set  $\Sigma_X$ , and it is denoted by  $\Sigma'_X$ . We denote by  $S$  (respectively  $R$ ) the number of separatrices (respectively canonical regions) of a vector field  $\pi(\rho(X))$ .

We say that two separatrix configurations  $\Sigma'_{X_1}$  and  $\Sigma'_{X_2}$  are *topologically equivalent* if there is a homeomorphism  $h : \mathbb{D}^2 \rightarrow \mathbb{D}^2$  such that  $h(\Sigma'_{X_1}) = \Sigma'_{X_2}$ . We say that two separatrix configurations are *topologically distinct* if they are not topologically equivalent.

The following theorem of Markus [96], Neumann [103] and Peixoto [106] allows us to investigate only the separatrix configuration of a polynomial differential system in order to determine its global phase portrait.

**Theorem 1.4.2.** *The phase portraits in the Poincaré disk of two compactified polynomial vector fields  $\pi(\rho(X_1))$  and  $\pi(\rho(X_2))$  with finitely many separatrices are topologically equivalent if and only if their separatrix configurations  $\Sigma'_{X_1}$  and  $\Sigma'_{X_2}$  are topologically equivalent.*

## 1.5 Normally hyperbolic submanifolds

Here we summarize a result that allows us to study systems which have a submanifold consisting of singular points, for more details see [38, 66]. If we have a smooth flow  $\varphi_t$  on a manifold  $M$  and  $C$  is a submanifold of  $M$  consisting entirely of singular points, we say that  $C$  is *normally hyperbolic* if the tangent bundle to  $M$  over  $C$  splits into three subbundles  $TC$ ,  $E^s$  and  $E^u$  invariant under the flow and satisfying that  $d\varphi_t$  contracts  $E^s$  exponentially,  $d\varphi_t$  expands  $E^u$  exponentially and  $TC$  is the tangent bundle of  $C$ . For these submanifolds the following result holds:

**Theorem 1.5.1.** *Let  $C$  be a normally hyperbolic submanifold consisting of singular points for a flow  $\varphi_t$ . Then there exist smooth stable and unstable manifolds tangent along  $C$  to  $E^s \oplus TC$  and  $E^u \oplus TC$  respectively. Furthermore, both  $C$  and the stable and unstable manifolds are permanent under small perturbations of the flow.*

## 1.6 Indices of singular points

Given an isolated singularity  $q$  of a vector field  $X$ , defined on an open subset of  $\mathbb{R}^2$  or  $\mathbb{S}^2$ , we define the index of  $q$  by means of the Poincaré Index Formula. We assume that  $q$  has the finite sectorial decomposition property. Let  $e$ ,  $h$  and  $r$  denote the number of elliptic, hyperbolic and parabolic sectors of  $q$ , respectively, and suppose that  $e + h + r > 0$ . Then the *index* of  $q$  is

$$i_q = (e - h)/2 + 1.$$

The index is always integer, we only need to see that in the previous definition  $e - h$  is always even since, as we said in Section 1.2,  $e + h$  is always even. Moreover, given any integer  $n \in \mathbb{Z}$ , there exists a singular point which index is  $n$ .

In Section 1.2 we have defined the different type of sectors: parabolic, hyperbolic and elliptic, and the finite sectorial decomposition property for an isolated singular point different from a center or a focus. By definition, we say that a center and a focus have neither elliptic, hyperbolic, nor parabolic sectors and their index is  $+1$ .

If  $X$  is a vector field on  $\mathbb{S}^2$ , it is called a *tangent vector field* to  $\mathbb{S}^2$  if for every  $p \in \mathbb{S}^2$ ,  $X(p)$  belongs to the tangent plane  $T_p\mathbb{S}^2$  to  $\mathbb{S}^2$  at the point  $p$ . We recall that the Poincaré compactification of a vector field on  $\mathbb{R}^2$  introduced in Section 1.3 is a tangent vector field on the sphere, so the next result will be useful in our work.

**Theorem 1.6.1** (Poincaré-Hopf). *For every tangent vector field on  $\mathbb{S}^2$  with a finite number of singular points, the sum of their indices is 2.*

## 1.7 Invariants and application of the Darboux theory of integrability

In order to characterize the Lotka-Volterra systems that we want to study, we use the Darboux theory of integrability, which provides a link between the integrability of polynomial

vector fields and the number of invariant algebraic surfaces that they have. The basic results on dimension two can be found in Chapter 8 of [50], and these results have been extended to  $\mathbb{R}^n$  and  $\mathbb{C}^n$  in [88–90]. We apply this theory to general Lotka-Volterra systems on dimension three, and then to the Kolmogorov resulting systems in dimension two. We state the definitions and results in dimension three, their restriction to  $\mathbb{R}^2$  being analogous.

We consider a real polynomial differential system in dimension three, that is, a system of the form

$$\begin{aligned}\dot{x} &= P(x, y, z), \\ \dot{y} &= Q(x, y, z), \\ \dot{z} &= R(x, y, z),\end{aligned}\tag{1.7.12}$$

where  $P, Q$  and  $R$  are polynomials in the variables  $x, y$  and  $z$ . The degree of the polynomial system is  $m = \max \{\deg P, \deg Q, \deg R\}$  and we assume that these polynomials are relatively prime in the ring of complex polynomials in the variables  $x, y$  and  $z$ . The vectorial field associated to system (1.7.12) can be represented by the differential operator

$$X = P \frac{\partial}{\partial x} + Q \frac{\partial}{\partial y} + R \frac{\partial}{\partial z}.$$

**Definition 1.7.1.** The polynomial system (1.7.12) is *integrable* on an open subset  $U$  of  $\mathbb{R}^3$  if there exists a nonconstant analytic function  $H : U \rightarrow \mathbb{R}$ , called a *first integral* of the system on  $U$ , which is constant on all trajectories  $(x(t), y(t), z(t))$  of system (1.7.12) contained in  $U$ , that is,  $H(x(t), y(t), z(t))$  is constant for all values of  $t$  for which the solution  $(x(t), y(t), z(t))$  is defined and contained in  $U$ .

**Definition 1.7.2.** Let  $U \subset \mathbb{R}^3$  be an open set. We say that an analytic function  $H(x, y, z, t) : U \times \mathbb{R} \rightarrow \mathbb{R}$  is an *invariant* of the polynomial vector field  $X$  on  $U$  if  $H(x, y, z, t)$  is constant for all values of  $t$  for which the solution  $(x(t), y(t), z(t))$  is defined and contained in  $U$ .

Obviously, if an invariant  $H$  is independent of  $t$ , then it is a first integral. The information provided by an invariant is weaker than the one provided by a first integral. An invariant, in general, gives information only about either the  $\alpha$  or the  $\omega$ -limit set of the orbits of the system.

If the first integral  $H$  is a rational function, then we say that  $H$  is a *rational first integral*. For a rational first integral we always assume that the polynomials in the numerator and the denominator are coprime. If the maximum between the degrees of the polynomials of the numerator and the denominator of a rational first integral is  $d$ , then we say that the rational first integral  $H$  has *degree*  $d$ .

**Definition 1.7.3.** Let  $f \in \mathbb{R}[x, y, z]$ ,  $f$  not identically zero. The algebraic surface  $f(x, y, z) = 0$  is an *invariant algebraic surface* of the polynomial system (1.7.12) if for some polynomial  $K \in \mathbb{R}[x, y, z]$  we have

$$Xf = P \frac{\partial f}{\partial x} + Q \frac{\partial f}{\partial y} + R \frac{\partial f}{\partial z} = Kf.$$

The polynomial  $K$  is called *cofactor* of the invariant algebraic surface  $f = 0$ . We note that, since the polynomial system has degree  $m$ , any cofactor has degree at most  $m - 1$ .

On the points of the algebraic surface  $f = 0$  the gradient  $(\partial f/\partial x, \partial f/\partial y, \partial f/\partial z)$  of  $f$  is orthogonal to the vector field  $X$ . Hence at every point of  $f = 0$  the vector field  $X$  is tangent to the curve  $f = 0$ , so this surface is formed by trajectories of the vector field  $X$ . This justifies the name invariant algebraic surface, since it is invariant under the flow defined by  $X$ .

**Definition 1.7.4.** An irreducible invariant algebraic surface  $f = 0$  is an invariant algebraic surface such that  $f$  is an irreducible polynomial in the ring  $\mathbb{R}[x, y, z]$ .

Clearly  $H$  is a first integral of system (1.7.12) on  $U$  if and only if  $XH = PH_x + QH_y + RH_z \equiv 0$  on  $U$ .

**Definition 1.7.5.** Let  $f, g \in \mathbb{R}[x, y, z]$  such that  $f$  and  $g$  are relatively prime in the ring  $\mathbb{R}[x, y, z]$ , or that  $g = 1$ . Then the function  $\exp(f/g)$  is a *exponential factor* of system (1.7.12) if there exists a polynomial  $L \in \mathbb{R}[x, y, z]$  of degree at most  $m - 1$  such that

$$P \frac{\partial \exp(f/g)}{\partial x} + Q \frac{\partial \exp(f/g)}{\partial y} + R \frac{\partial \exp(f/g)}{\partial z} = L \exp(f/g).$$

The polynomial  $L$  is called the *cofactor* of the exponential factor  $\exp(f/g)$ .

**Definition 1.7.6.** A *Darboux invariant* for system (1.7.12) is an invariant  $H$  of the form

$$H(x, y, z, t) = f_1^{\lambda_1} \dots f_p^{\lambda_p} F_1^{\mu_1} \dots F_q^{\mu_q} e^{st},$$

where  $f_i = 0$  are invariant algebraic surfaces of system (1.7.12) for  $i = 1, \dots, p$ , and  $F_j$  are exponential factors of system (1.7.12) for  $j = 1, \dots, q$ ,  $\lambda_i, \mu_j \in \mathbb{R}$  and  $s \in \mathbb{R} \setminus \{0\}$ .

**Theorem 1.7.7** (Darboux Integrability Theorem for Polynomial Systems). *Suppose that a polynomial system (1.7.12) of degree  $m$  admits  $p$  irreducible invariant algebraic surfaces  $f_i = 0$ , with cofactors  $K_i$  for  $i = 1, \dots, p$ . Then, the next statements hold:*

- (i) *There exist  $\lambda_i \in \mathbb{R}$  not all zero such that  $\sum_{i=1}^p \lambda_i K_i = 0$  if and only if the function  $f_1^{\lambda_1} \dots f_p^{\lambda_p}$  is a first integral of system (1.7.12).*
- (ii) *There exist  $\lambda_i \in \mathbb{R}$  not all zero such that  $\sum_{i=1}^p \lambda_i K_i = -s$  for some  $s \in \mathbb{R} \setminus \{0\}$  if and only if the function  $f_1^{\lambda_1} \dots f_p^{\lambda_p} \exp(st)$  is an invariant of system (1.7.12).*

As previously stated, our objective is to study the global dynamics of Lotka-Volterra systems on dimension three, it is,

$$\begin{aligned} \dot{x} &= x(a_0 + a_1x + a_2y + a_3z), \\ \dot{y} &= y(b_0 + b_1x + b_2y + b_3z), \\ \dot{z} &= z(c_0 + c_1x + c_2y + c_3z), \end{aligned} \tag{1.7.13}$$

which have a rational first integral of degree two of the form  $x^{\lambda_1} y^{\lambda_2} z^{\lambda_3}$ . The Darboux theory of integrability allows us to obtain a characterization of these systems, which can be classified into three families.

We consider the irreducible invariant algebraic surfaces  $f_1(x, y, z) = x$ ,  $f_2(x, y, z) = y$  and  $f_3(x, y, z) = z$ , with cofactors  $K_1$ ,  $K_2$  and  $K_3$ , respectively. As  $K_i$  is the cofactor of  $f_i$  we have that

$$Xf_i = P \frac{\partial f_i}{\partial x} + Q \frac{\partial f_i}{\partial y} + R \frac{\partial f_i}{\partial z} = K_i f_i.$$

For  $f_1 = x$  we have

$$Xx = P \frac{\partial x}{\partial x} + Q \frac{\partial x}{\partial y} + R \frac{\partial x}{\partial z} = P = K_1 x,$$

and so we get the first cofactor  $K_1 = a_0 + a_1x + a_2y + a_3z$ . Similarly, for  $f_2$  and  $f_3$  we obtain cofactors  $K_2 = b_0 + b_1x + b_2y + b_3z$  and  $K_3 = c_0 + c_1x + c_2y + c_3z$ , respectively.

Applying Theorem 1.7.7, since we assume that  $x^{\lambda_1}y^{\lambda_2}z^{\lambda_3}$  is a first integral of the system, we get that there exist  $\lambda_i \in \mathbb{R}$ , with  $i \in \{1, 2, 3\}$ , not all zero, such that  $\sum_{i=1}^3 \lambda_i K_i = 0$ , it is,

$$\lambda_1 \cdot (a_0 + a_1x + a_2y + a_3z) + \lambda_2 \cdot (b_0 + b_1x + b_2y + b_3z) + \lambda_3 \cdot (c_0 + c_1x + c_2y + c_3z) = 0.$$

Apart from the trivial solution  $\{\lambda_1 = 0, \lambda_2 = 0, \lambda_3 = 0\}$ , there are three solutions of this equation:

$$\begin{aligned} S_1 &= \{c_0 = 0, c_1 = 0, c_2 = 0, c_3 = 0, \lambda_2 = 0, \lambda_1 = 0\}, \\ S_2 &= \left\{ b_0 = -\frac{c_0\lambda_3}{\lambda_2}, b_1 = -\frac{c_1\lambda_3}{\lambda_2}, b_2 = -\frac{c_2\lambda_3}{\lambda_2}, b_3 = -\frac{c_3\lambda_3}{\lambda_2}, \lambda_1 = 0 \right\}, \text{ and} \\ S_3 &= \left\{ a_0 = \frac{-b_0\lambda_2 - c_0\lambda_3}{\lambda_1}, a_1 = \frac{-b_1\lambda_2 - c_1\lambda_3}{\lambda_1}, a_2 = \frac{-b_2\lambda_2 - c_2\lambda_3}{\lambda_1}, \right. \\ &\quad \left. a_3 = \frac{-b_3\lambda_2 - c_3\lambda_3}{\lambda_1} \right\}, \end{aligned}$$

which give rise to three families of Lotka-Volterra polynomial differential systems of degree two in  $\mathbb{R}^3$ , with a first integral of the form  $x^{\lambda_1}y^{\lambda_2}z^{\lambda_3}$ . Now we will characterize each one of these families.

At first we consider the family given by solution  $S_1$ . As the parameters  $c_i$ ,  $i = 0, \dots, 3$ , are zero, we have that  $\dot{z} = 0$  and Lotka-Volterra systems (1.7.13) are reduced to:

$$\begin{aligned} \dot{x} &= x (a_0 + a_1x + a_2y + a_3z), \\ \dot{y} &= y (b_0 + b_1x + b_2y + b_3z), \\ \dot{z} &= 0. \end{aligned}$$

As  $\dot{z} = 0$ ,  $z$  is constant and these systems have  $H = z$  as a first integral. Note that if we consider the first integral  $H = x^{\lambda_1}y^{\lambda_2}z^{\lambda_3}$ , and we apply the conditions given by  $S_1$ , it is  $\lambda_1 = \lambda_2 = 0$ , we obtain  $H = z^{\lambda_3}$  with  $\lambda_3 = 2$ , for getting the degree two, but we will consider the simplest first integral. In each invariant plane  $z = \text{constant}$ , we have a Lotka-Volterra polynomial differential system in  $\mathbb{R}^2$ . The phase portrait of these systems has been studied in [117], so we are not going to deal with this case.



Let us consider now the second family, given by the solution  $S_2$ . This solution provides the values of parameters  $b_i$  as a function of the parameters  $\lambda_2$ ,  $\lambda_3$  and  $c_i$ , with  $i = 0, \dots, 3$ , so we can replace them in the expression of  $\dot{y}$ , obtaining

$$\dot{y} = y \left( -\frac{c_0\lambda_3}{\lambda_2} - \frac{c_1\lambda_3}{\lambda_2}x - \frac{c_2\lambda_3}{\lambda_2}y - \frac{c_3\lambda_3}{\lambda_2}z \right).$$

If we denote  $\lambda = -\lambda_3/\lambda_2$ , then the original Lotka-Volterra systems become

$$\begin{aligned}\dot{x} &= x(a_0 + a_1x + a_2y + a_3z), \\ \dot{y} &= \lambda y(c_0 + c_1x + c_2y + c_3z), \\ \dot{z} &= z(c_0 + c_1x + c_2y + c_3z).\end{aligned}$$

Given that  $\lambda_1 = 0$ , the first integral  $H = x^{\lambda_1}y^{\lambda_2}z^{\lambda_3}$  is reduced to  $H = y^{\lambda_2}z^{\lambda_3}$ , but if this is a first integral, also

$$H = (y^{\lambda_2}z^{\lambda_3})^{-\frac{1}{\lambda_2}} = y^{-1}z^{-\frac{\lambda_3}{\lambda_2}} = y^{-1}z^\lambda = \frac{z^\lambda}{y}.$$

is a first integral. If we want  $H$  to be rational of degree two, we must take  $\lambda = 2$ . In each level  $H = 1/h$ , with  $h \neq 0$ , we will have

$$\frac{1}{h} = \frac{z^2}{y} \implies y = hz^2,$$

and then, for each  $h$ , the initial Lotka-Volterra systems on dimension three reduce to the systems on dimension two

$$\begin{aligned}\dot{x} &= x(a_0 + a_1x + a_2h z^2 + a_3z), \\ \dot{z} &= z(c_0 + c_1x + c_2h z^2 + c_3z).\end{aligned}$$

We must study the phase portrait of the systems of this family, but it is equivalent to study the phase portraits of the family of Kolmogorov systems on dimension two

$$\begin{aligned}\dot{x} &= x(a_0 + a_1x + a_2z^2 + a_3z), \\ \dot{z} &= z(c_0 + c_1x + c_2z^2 + c_3z).\end{aligned}$$

In the particular cases in which  $H$  is zero or infinity, the differential systems on dimension three are reduced to Lotka-Volterra systems on dimension two, having in each case  $z = 0$  and  $y = 0$ , respectively. We recall that these systems had already been studied in [117].

At last we consider the family given by solution  $S_3$ , which provides the values of parameters  $a_i$  in function of parameters  $\lambda_i$ ,  $b_i$  and  $c_i$ , with  $i = 0, \dots, 3$ . Replacing them in the expression of  $\dot{x}$  we obtain:

$$\dot{x} = x \left( \frac{-b_0\lambda_2 - c_0\lambda_3}{\lambda_1} + \frac{x(-b_1\lambda_2 - c_1\lambda_3)}{\lambda_1} + \frac{y(-b_2\lambda_2 - c_2\lambda_3)}{\lambda_1} + \frac{z(-b_3\lambda_2 - c_3\lambda_3)}{\lambda_1} \right),$$

and if we denote

$$\lambda = -\frac{\lambda_2}{\lambda_1} \quad \text{and} \quad \mu = -\frac{\lambda_3}{\lambda_1},$$

and replace it again in the previous expression, we obtain that in this case the initial Lotka-Volterra systems have the form:

$$\dot{x} = x (b_0\lambda + c_0\mu + x(b_1\lambda + c_1\mu) + y(b_2\lambda + c_2\mu) + z(b_3\lambda + c_3\mu)),$$

$$\dot{y} = y (b_0 + b_1x + b_2y + b_3z),$$

$$\dot{z} = z (c_0 + c_1x + c_2y + c_3z).$$

By hypothesis, we have the first integral  $H = x^{\lambda_1} y^{\lambda_2} z^{\lambda_3}$ . Thus, we also can consider as a first integral

$$H = (x^{\lambda_1} y^{\lambda_2} z^{\lambda_3})^{-\frac{1}{\lambda_1}} = x^{-1} y^{-\frac{\lambda_2}{\lambda_1}} z^{-\frac{\lambda_3}{\lambda_1}} = \frac{y^\lambda z^\mu}{x}.$$

We want  $H$  to be rational of degree two so we must take  $\lambda = \mu = 1$ . In each level  $H = 1/h$ , with  $h \neq 0$ , we will have

$$\frac{1}{h} = \frac{yz}{x} \implies x = h y z,$$

and then, for each  $h$ , the initial Lotka-Volterra systems on dimension three are reduced to the differential systems on dimension two

$$\dot{y} = y (b_0 + b_1 h y z + b_2 y + b_3 z),$$

$$\dot{z} = z (c_0 + c_1 h y z + c_2 y + c_3 z).$$

As in the previous case, we must study the phase portrait of this family of differential systems, which is equivalent to study the phase portraits of the following Kolmogorov family on dimension two:

$$\dot{y} = y (b_0 + b_1 y z + b_2 y + b_3 z),$$

$$\dot{z} = z (c_0 + c_1 y z + c_2 y + c_3 z).$$

In conclusion, we have reduced the initial problem, the study of the global dynamics of Lotka-Volterra systems on dimension three with a rational first integral of degree two, to another problem on dimension two: study the global dynamics of the next two Kolmogorov families:

$$\dot{x} = x(a_0 + a_1x + a_2z^2 + a_3z),$$

(1.7.14)

$$\dot{y} = y(b_0 + b_1yz + b_2y + b_3z),$$

(1.7.15)

$$\dot{z} = z(c_0 + c_1x + c_2z^2 + c_3z),$$

$$\dot{z} = z(c_0 + c_1yz + c_2y + c_3z).$$

These systems depend on eight parameters and the classification of all their distinct topological phase portraits is huge. For this reason we study a subclass of them.

For systems (1.7.14) we study the subclass of them having a Darboux invariant of the form  $e^{st} x^{\lambda_1} z^{\lambda_2}$ . By Theorem 1.7.7(ii), the expression  $\lambda_1 K_x + \lambda_2 K_z + s$  must be zero, where  $K_x$  and  $K_y$  are the cofactors of the invariant planes  $x = 0$  and  $z = 0$ , respectively. Note that  $s$  and  $\lambda_1^2 + \lambda_2^2$  can not be zero.

We obtain the cofactors  $K_x = a_0 + a_1x + a_2z^2 + a_3z$  and  $K_z = c_0 + c_1x + c_2z^2 + c_3z$  and then, solving the equation  $\lambda_1 K_x + \lambda_2 K_z + s = 0$ , we get the two following non-trivial solutions

$$\tilde{S}_1 = \left\{ s = -a_0\lambda_1 - c_0\lambda_2, a_1 = -\frac{c_1\lambda_2}{\lambda_1}, a_2 = -\frac{c_2\lambda_2}{\lambda_1}, a_3 = -\frac{c_3\lambda_2}{\lambda_1} \right\} \text{ and}$$

$$\tilde{S}_2 = \{s = -c_0\lambda_2, c_1 = 0, c_2 = 0, c_3 = 0, \lambda_1 = 0\}.$$

Therefore, we get two subfamilies from the initial one (1.7.14). According to the conditions given by solution  $\tilde{S}_1$ , the first subfamily is

$$\dot{x} = x \left( a_0 - \frac{c_1\lambda_2}{\lambda_1}x - \frac{c_2\lambda_2}{\lambda_1}z^2 - \frac{c_3\lambda_2}{\lambda_1}z \right),$$

$$\dot{z} = z (c_0 + c_1x + c_2z^2 + c_3z).$$

If we denote  $\lambda_2/\lambda_1 = \mu$  and  $\lambda_1 = \lambda$ , these systems become

$$\dot{x} = x (a_0 - \mu(c_1x + c_2z^2 + c_3z)),$$

$$\dot{z} = z (c_0 + c_1x + c_2z^2 + c_3z),$$

and the Darboux invariant is  $x^\lambda z^{\lambda\mu} e^{-t\lambda(a_0+c_0\mu)}$ . But if this is a Darboux invariant, also it is  $xxz^\mu e^{-t(a_0+c_0\mu)}$ . Note that in order that we have a Darboux invariant  $a_0 + c_0\mu$  cannot be zero.

If we consider now the solution  $\tilde{S}_2$ , we get the subfamily

$$\dot{x} = x (a_0 + a_1x + a_2z^2 + a_3z),$$

$$\dot{z} = c_0z,$$

which is equivalent to the previous one, taking  $\mu = 0$  and interchanging the variables  $x$  and  $z$ , so it is sufficient to study the first system, and we deal with that problem in Chapters 2 and 3.

For systems (1.7.15) we study the subclass having a Darboux invariant of the form  $e^{st}y^{\lambda_1}z^{\lambda_2}$ , and we proceed in the same way that we did with systems (1.7.14).

At first, the expression  $\lambda_1 K_y + \lambda_2 K_z + s$  must be zero by Theorem 1.7.7(ii), with  $K_y$  and  $K_z$  the cofactors of the invariant planes  $y = 0$  and  $z = 0$ , respectively. We recall that  $s$  and  $\lambda_1^2 + \lambda_2^2$  can not be zero.

We obtain the cofactors  $K_y = b_0 + b_1yz + b_2y + b_3z$  and  $K_z = c_0 + c_1yz + c_2y + c_3z$  and solving the equation  $\lambda_1 K_x + \lambda_2 K_z + s = 0$ , we get the following non-trivial solution

$$\left\{ c_1 = -\frac{b_1\lambda_1}{\lambda_2}, c_2 = -\frac{b_2\lambda_1}{\lambda_2}, c_3 = -\frac{b_3\lambda_1}{\lambda_2}, s = -b_0\lambda_1 - c_0\lambda_2 \right\},$$

which leads to the systems

$$\dot{y} = y (b_0 + b_1yz + b_2y + b_3z),$$

$$\dot{z} = z \left( c_0 - \frac{b_1yz\lambda_1}{\lambda_2} - \frac{b_2y\lambda_1}{\lambda_2} - \frac{b_3z\lambda_1}{\lambda_2} \right).$$

If we denote  $\lambda_2 = \lambda$  and  $\lambda_1 = \lambda\mu$ , then the systems become

$$\begin{aligned}\dot{y} &= y(b_0 + b_1 yz + b_2 y + b_3 z), \\ \dot{z} &= z(c_0 - \mu(b_1 yz + b_2 y + b_3 z)),\end{aligned}$$

and the Darboux invariant is  $y^{\lambda\mu} z^{\lambda} e^{-t\lambda(c_0 + b_0\mu)}$ . But if this is a Darboux invariant, also it is  $y^{\mu} z e^{-t(c_0 + b_0\mu)}$ . Note that in order that we have a Darboux invariant  $c_0 + b_0\mu$  cannot be zero. We study these systems in Chapters 4 and 5.

## 1.8 Limit cycles: bifurcation and averaging theory

As defined in Section 1.1, a limit cycle is a periodic orbit  $\gamma_1$  such that there exists another orbit  $\gamma_2$  satisfying  $\alpha(\gamma_2) = \gamma_1$  or  $\omega(\gamma_2) = \gamma_1$ . In this section we introduce some concepts related to limit cycles and techniques for studying their existence.

Let us consider an autonomous system

$$\dot{x} = f(x), \quad x \in \mathbb{R}^n, \quad (1.8.16)$$

and let  $L_0$  be a periodic orbit of (1.8.16). Given a point  $x_0 \in L_0$  we consider a cross-section  $\Gamma$  to the periodic orbit, i.e., a smooth hypersurface of dimension  $n - 1$  intersecting  $L_0$  and nowhere tangent to it. The simplest choice of  $\Gamma$  is a hyperplane orthogonal to  $L_0$  at the point  $x_0$ . Consider now orbits of (1.8.16) near  $L_0$ . The periodic orbit  $L_0$  is an orbit that starts at the point  $x_0$  on  $\Gamma$  and returns to  $\Gamma$  at the same point  $x_0$ . As the solutions depend smoothly on their initial conditions, an orbit starting at a point  $x \in \Gamma$  sufficiently close to  $x_0$  also returns to  $\Gamma$  at some point  $\tilde{x} \in \Gamma$  near  $x_0$ . Moreover, nearby orbits also intersect  $\Gamma$  transversally. Then we have a map  $P : \Gamma \rightarrow \Gamma$  that sends  $x$  into  $P(x) = \tilde{x}$ . This map  $P$  is called the *Poincaré map* associated with  $L_0$ . The point  $x_0$  is a fixed point of the Poincaré map as  $P(x_0) = x_0$ , and the stability of this fixed point is equivalent to the stability of the periodic orbit  $L_0$ . More details can be found, for example, in [78, 87, 107].

**Definition 1.8.1.** Given the autonomous differential equation (1.8.16) with periodic solution  $\varphi(t)$ , transversal  $\Gamma$  and Poincaré map  $P$  with fixed point  $a$ . The solution  $\varphi(t)$  is *stable* if for each  $\varepsilon > 0$  we can find  $\delta(\varepsilon)$  such that

$$||x_0 - a|| \leq \delta, \quad x_0 \in \Gamma \Rightarrow ||P^n(x_0) - a|| \leq \varepsilon, \quad n = 1, 2, 3, \dots$$

**Definition 1.8.2.** Given the autonomous differential equation (1.8.16) with periodic solution  $\varphi(t)$ , transversal  $\Gamma$  and Poincaré map  $P$  with fixed point  $a$ . The solution  $\varphi(t)$  is *asymptotically stable* if it is stable and if there exists  $\delta > 0$  such that

$$||x_0 - a|| \leq \delta, \quad x_0 \in \Gamma \Rightarrow \lim_{n \rightarrow \infty} P^n(x_0) = a.$$

Now we present some results that we use to study the existence of limit cycles. Let us consider a system that depends on some parameters

$$\dot{x} = f(x, \alpha),$$

where  $x \in \mathbb{R}^n$  and  $\alpha \in \mathbb{R}^m$  represent the variables and the parameters, respectively. As the parameters vary, the phase portrait of the system also varies, and there are two possibilities: the system can remain topologically equivalent to the original one, or it can change its topology. The appearance of a topologically nonequivalent phase portrait under a variation of parameters is called a *bifurcation*.

We say that a singular point of an autonomous system in  $\mathbb{R}^n$  is a *Hopf singular point* if it is an isolated singular point with linear part having a pair of purely imaginary eigenvalues  $\pm i\beta$  with  $\beta \in \mathbb{R}^+$ . We say that a singular point of an autonomous system in  $\mathbb{R}^3$  is *zero-Hopf* if it is an isolated singular point with linear part having one zero eigenvalue and a pair of purely imaginary eigenvalues  $\pm i\beta$  with  $\beta \in \mathbb{R}^+$ . These points are important because under some assumptions a small-amplitude limit cycle bifurcates from them.

On chapter 6 we study limit cycles emerging from a zero-Hopf singular point in the interior of the positive octant of the Kolmogorov systems of degree three in  $\mathbb{R}^3$ . On Chapter 7 we study the Hopf bifurcation on two systems in the context of population dynamics: a planar Kolmogorov system obtained from the Rosenzweig-MacArthur system, and a three-dimensional system which represents a two prey and one predator ecosystem.

We summarize the averaging theory of first order, which provides sufficient conditions for the existence of periodic orbits for a periodic differential system depending on small parameters. This result is applied in Chapter 7 to study when a limit cycle appears by Hopf bifurcation on the Kolmogorov systems of degree three and dimension three. For additional details and the proof of the result see [17, 18, 86] and [131, Theorems 11.5, 11.6].

**Theorem 1.8.3.** *We consider the following differential system*

$$x'(t) = \varepsilon F_1(t, x) + \varepsilon^2 R(t, x, \varepsilon), \quad (1.8.17)$$

where  $F_1 : \mathbb{R} \times D \rightarrow \mathbb{R}^n$  and  $R : \mathbb{R} \times D \times (-\varepsilon_f, \varepsilon_f) \rightarrow \mathbb{R}^n$  are continuous functions,  $T$ -periodic in the first variable and  $D$  is an open subset of  $\mathbb{R}^n$ . We define  $f_1 : D \rightarrow \mathbb{R}^n$  as

$$f_1(z) = \int_0^T F_1(s, z) ds,$$

and assume that:

1.  $F_1$  and  $R$  are locally Lipschitz with respect to  $x$ ;
2. for  $a \in D$  with  $f_1(a) = 0$ , there exists a neighborhood  $V$  of  $a$  such that  $f_1(z) \neq 0$  for all  $z \in \bar{V} \setminus \{a\}$  and  $d_B(f_1, V, 0) \neq 0$ , where  $d_B(f_1, V, 0)$  is the Brouwer degree.

Then for  $|\varepsilon| > 0$  sufficiently small, there exists a  $T$ -periodic solution  $\varphi(\cdot, \varepsilon)$  of system (1.8.17) such that  $\varphi(\cdot, \varepsilon) \rightarrow a$  as  $\varepsilon \rightarrow 0$ . The kind of stability of the limit cycle is given by the eigenvalues of the Jacobian matrix at the point  $a$ .

Note that a sufficient condition for showing that the Brouwer degree of a function  $f$  at a point  $a$  is nonzero, is that the Jacobian of the function  $f$  at  $a$ , when it is defined, is nonzero (see [91]).

With this result, in Chapter 6, we are able to prove the existence of limit cycles that appear by a Hopf bifurcation. Then we also study the stability of the limit cycles by analyzing the

the eigenvalues at the critical point of the averaged function  $f_1$ ; see Theorem 11.6 in [131] for more theoretical details.

But this is not the only way to study this bifurcation. Now we introduce the theoretical basis that allow us to study it in Chapter 7. More details can be found in [78, Chapter 3].

Consider a system depending on one parameter of the form:

$$\begin{aligned}\dot{x}_1 &= \alpha x_1 - x_2 - x_1(x_1^2 + x_2^2), \\ \dot{x}_2 &= x_1 + \alpha x_2 - x_2(x_1^2 + x_2^2).\end{aligned}\tag{1.8.18}$$

The origin is a singular point for all the values of the parameter, and the Jacobian matrix at this point is

$$A = \begin{pmatrix} \alpha & -1 \\ 1 & \alpha \end{pmatrix},$$

with eigenvalues  $\lambda_{1,2} = \alpha \pm i$ . We can write the system in polar form as

$$\begin{aligned}\dot{\rho} &= \rho(\alpha - \rho^2), \\ \dot{\varphi} &= 1.\end{aligned}\tag{1.8.19}$$

Bifurcations of the phase portrait of this system when  $\alpha$  passes through zero can be analyzed since the equations in (1.8.19) are uncoupled. For any value of  $\alpha$ , the first equation has the singular point  $\rho = 0$ , which is stable if  $\alpha < 0$ , remains stable at  $\alpha = 0$  but with a rate of solution convergence to zero which is not exponential, and is unstable for  $\alpha > 0$ . There is another stable singular point  $\rho = \sqrt{\alpha}$  for  $\alpha > 0$ . The second equation represents a rotation with constant speed. Then, combining the motions defined by both equations we obtain that system (1.8.18) has a singular point at the origin which is a stable focus for  $\alpha < 0$  and an unstable focus for  $\alpha > 0$ . At  $\alpha = 0$  the singular point is topologically equivalent to the stable focus. For  $\alpha > 0$  the singular point is surrounded by one stable limit cycle. All orbits except the origin tend to the limit cycle as  $t$  tends to infinity. This is a Hopf bifurcation.

In the same way we can analyze the system

$$\begin{aligned}\dot{x}_1 &= \alpha x_1 - x_2 + x_1(x_1^2 + x_2^2), \\ \dot{x}_2 &= x_1 + \alpha x_2 + x_2(x_1^2 + x_2^2),\end{aligned}\tag{1.8.20}$$

which undergoes a Hopf bifurcation at  $\alpha = 0$ . In this case there is an unstable limit cycle surrounding the origin which disappears when  $\alpha$  crosses zero from negative to positive values. The singular point at the origin has the same stability that for system (1.8.18).

The bifurcation in system (1.8.18) is called *supercritical* because the limit cycle exists for positive values of the parameter  $\alpha$ , while the bifurcation in system (1.8.20) is called *subcritical* since the limit cycle appears for negative values of  $\alpha$ .

Later we will state two theorems that characterize when we can put a two-dimensional system in the normal forms that we have analyzed, but first it is necessary to have a formula to compute the so called *first Lyapunov coefficient*,  $\ell_1$ .

Let us write the system in the form

$$\dot{x} = A(\alpha)x + \frac{1}{2}B(x, x) + \frac{1}{6}C(x, x, x) + O(\|x\|^4),$$

where  $A$  is the Jacobian matrix, and  $B$  and  $C$  are symmetric multilinear vector functions. We consider two complex eigenvectors  $p, q$  of the matrix  $A$  satisfying

$$Aq = i\omega q, \quad A^T p = -i\omega p, \quad \text{and} \quad \langle p, q \rangle = 1,$$

where  $\langle \cdot, \cdot \rangle$  means the standard scalar product in  $\mathbb{C}^2$ . Then the first Lyapunov coefficient is

$$\ell_1(0) = \frac{1}{2\omega_0} \operatorname{Re}(ig_{20}g_{11} + \omega_0 g_{21}),$$

where

$$g_{20} = \langle p, B(q, q) \rangle, \quad g_{11} = \langle p, B(q, \bar{q}) \rangle \quad \text{and} \quad g_{21} = \langle p, C(q, q, \bar{q}) \rangle.$$

**Theorem 1.8.4.** *Suppose that two-dimensional system*

$$\frac{dx}{dt} = f(x, \alpha), \quad x \in \mathbb{R}^2, \quad \alpha \in \mathbb{R}, \quad (1.8.21)$$

*with smooth  $f$ , has for all sufficiently small  $|\alpha|$  the equilibrium  $x = 0$  with eigenvalues*

$$\lambda_{1,2}(\alpha) = \mu(\alpha) \pm i\omega(\alpha),$$

*where  $\mu(0) = 0$ ,  $\omega(0) = \omega_0 > 0$ . Let the following conditions be satisfied:*

*(B.1)  $\ell_1(0) \neq 0$ ;*

*(B.2)  $\mu'(0) \neq 0$ .*

*Then, there are invertible coordinate and parameter changes and a time reparametrization transforming (1.8.21) into*

$$\frac{d}{d\tau} \begin{pmatrix} y_1 \\ y_2 \end{pmatrix} = \begin{pmatrix} \beta & -1 \\ 1 & \beta \end{pmatrix} \begin{pmatrix} y_1 \\ y_2 \end{pmatrix} \pm (y_1^2 + y_2^2) \begin{pmatrix} y_1 \\ y_2 \end{pmatrix} + O(\|y\|^4).$$

By dropping the  $O(\|y\|^4)$  terms it can be obtained the following result:

**Theorem 1.8.5.** *A generic system in dimension two with one parameter*

$$\dot{x} = f(x, \alpha)$$

*having at  $\alpha = 0$  the singular point  $x = 0$  with eigenvalues*

$$\lambda_{1,2}(0) = \pm i\omega_0, \quad \omega_0 > 0,$$

*is locally topologically equivalent near the origin to one of the following normal forms:*

$$\begin{pmatrix} \dot{y}_1 \\ \dot{y}_2 \end{pmatrix} = \begin{pmatrix} \beta & -1 \\ 1 & \beta \end{pmatrix} \begin{pmatrix} y_1 \\ y_2 \end{pmatrix} \pm (y_1^2 + y_2^2) \begin{pmatrix} y_1 \\ y_2 \end{pmatrix}.$$

These two theorems together with the formula for computing the first Lyapunov coefficient and the analysis of the normal forms previously summarized, provide us the necessary tools for studying the Hopf bifurcation in the planar systems presented in Chapter 7. We also study the Hopf bifurcation numerically, in Section 7.3.4, for a system in dimension three. The results included here can be generalized to dimension  $n$ , as can be seen in [78, Chapter 5], but we do not include the generalization here as we do not perform a general bifurcation analysis for the three-dimensional system.

---

## Chapter 2

# Classification of the first Kolmogorov family with isolated singularities

---

In this chapter we study the global dynamics of the first family of Kolmogorov systems obtained in Chapter 1, i.e.,

$$\begin{aligned}\dot{x} &= x \left( a_0 - \mu(c_1x + c_2z^2 + c_3z) \right), \\ \dot{z} &= z \left( c_0 + c_1x + c_2z^2 + c_3z \right),\end{aligned}\tag{2.0.1}$$

for which we give the topological classification of all their global phase portraits in the Poincaré disk. We work under conditions

$$H_2^1 = \{c_2 \neq 0, a_0 \geq 0, c_1 \geq 0, c_3 \geq 0, a_0 + c_0\mu \neq 0, a_0^2 + c_1^2\mu^2 \neq 0, \mu \neq -1\},$$

as the case with  $\mu = -1$ , in which there are a continuum of singular points at the infinity, is studied in Chapter 3, and we prove that in any other case the systems can be reduced to simpler systems already studied. Our main result is the following:

**Theorem 2.0.1.** *Kolmogorov systems (2.0.1) under conditions  $H_2^1$  have 78 topologically distinct phase portraits in the Poincaré disk, given in Figure 2.0.1.*

The complete proof of Theorem 2.0.1, which includes the contents of the research article [42]<sup>1</sup>, is given in this chapter and organized as follows. In Section 2.1 we give some properties of the systems that allow us to simplify the topological classification by reducing the number of phase portraits appearing. In Section 2.2 we study the local phase portraits of the finite singular points applying Theorems 1.2.1 and 1.2.3 and in Section 2.3 we study the singular points at infinity, for which is necessary to apply the blow up technique. Finally, in Section 2.4 we study all the possible global phase portraits and we determine the different topological equivalence classes, proving Theorem 2.0.1.

---

<sup>1</sup>Erika Diz-Pita (Departamento de Estadística, Aálise Matemática e Optimización, Universidade de Santiago de Compostela), Jaume Llibre (Departament de Matemàtiques, Universitat Autònoma de Barcelona) and María Victoria Otero-Espinar (Departamento de Estadística, Aálise Matemática e Optimización, Universidade de Santiago de Compostela), *Phase portraits of a family of Kolmogorv systems depending on six parameters*, Electronic Journal of Differential Equations (ISSN: 1072-6691), **35** (2021). Published by Texas State University. The final authenticated version is available online at: <https://ejde.math.txstate.edu/Volumes/2021/35/diz.pdf>.



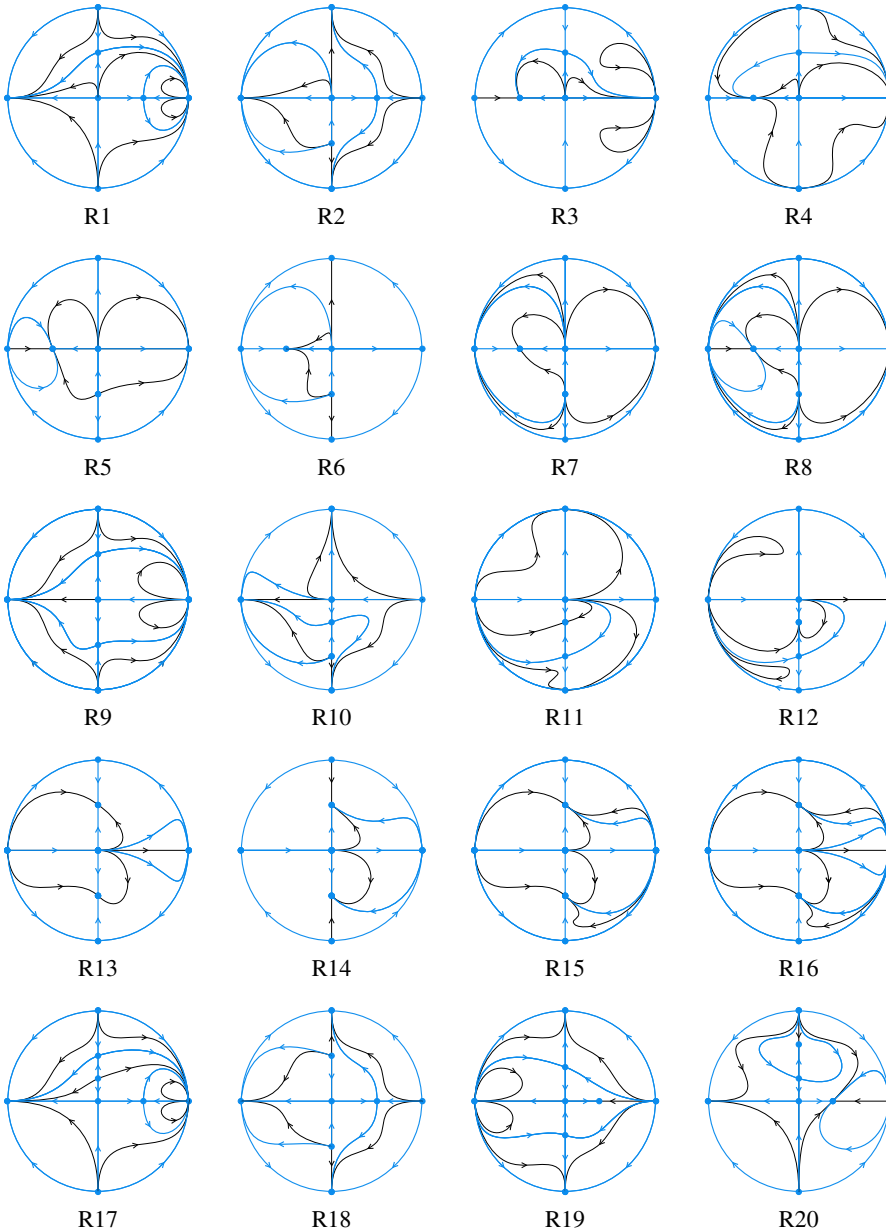


Figure 2.0.1 (1 out of 4): The topologically distinct phase portraits of systems (2.0.1) in the Poincaré disk.

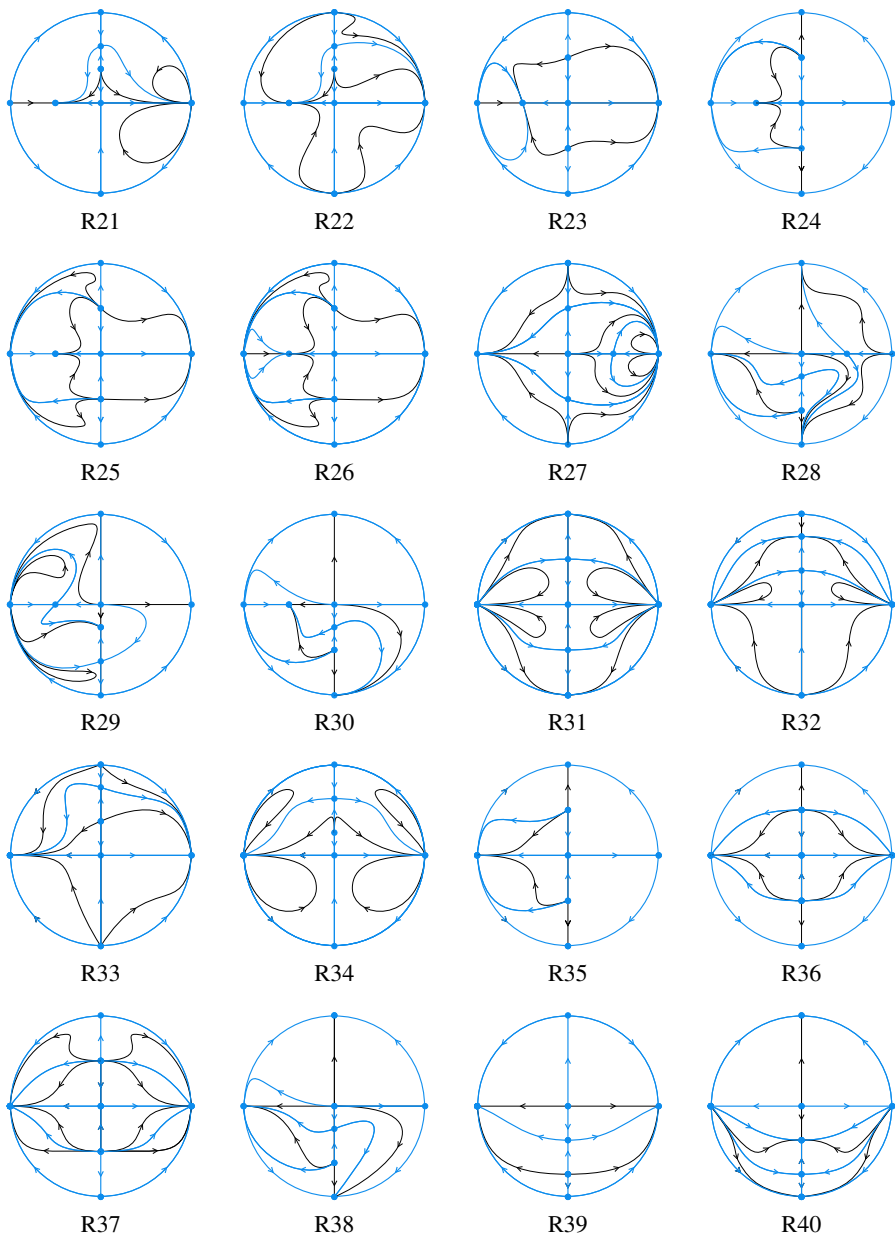


Figure 2.0.1 (2 out of 4): The topologically distinct phase portraits of systems (2.0.1) in the Poincaré disk.

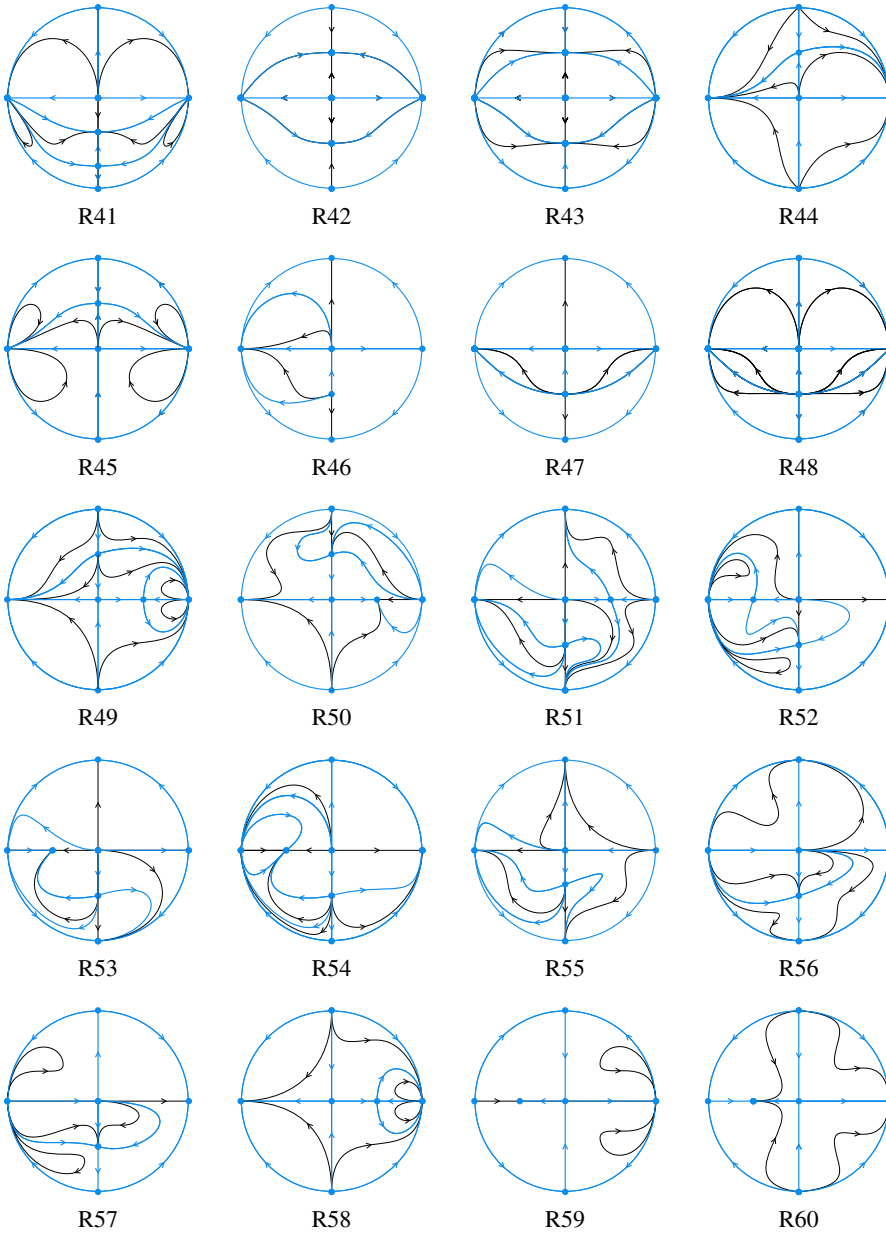


Figure 2.0.1 (3 out of 4): The topologically distinct phase portraits of systems (2.0.1) in the Poincaré disk.

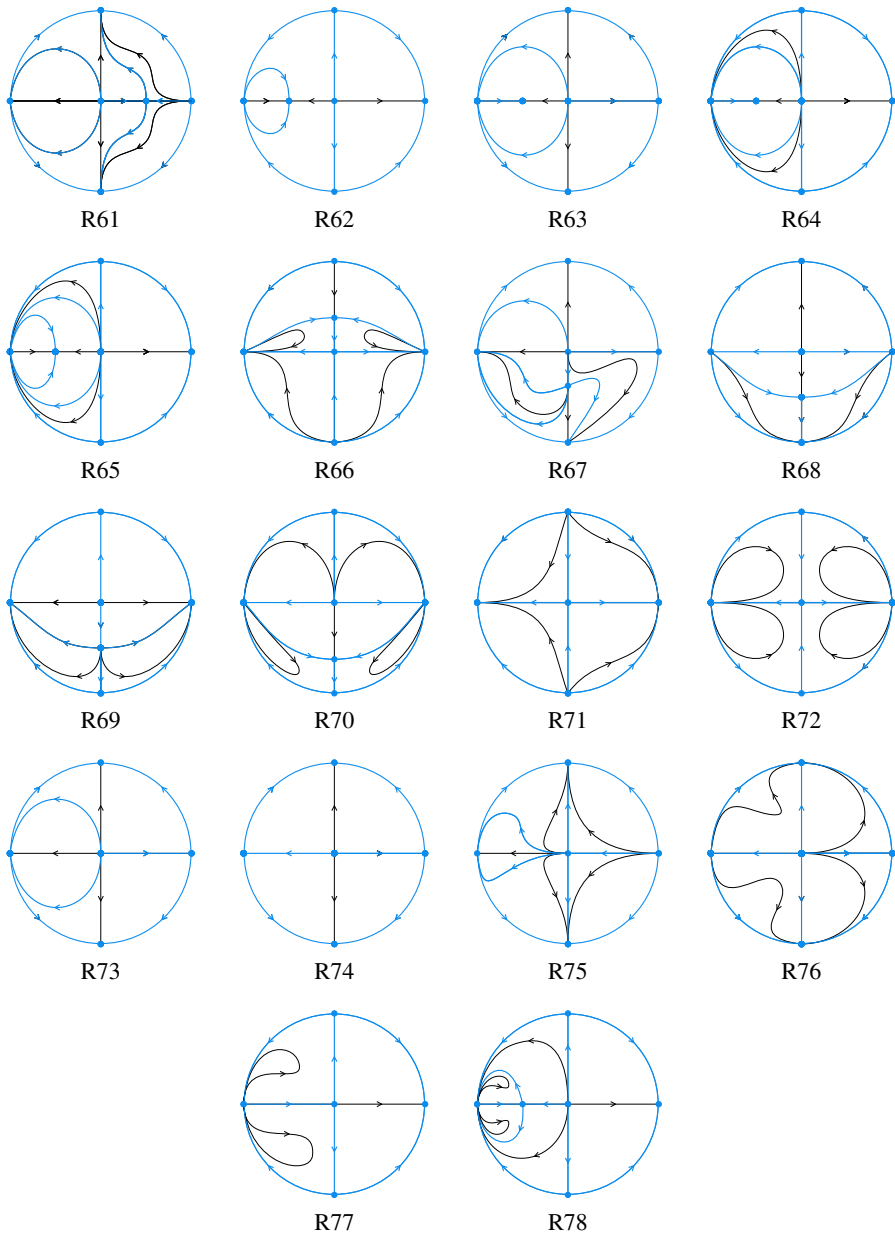


Figure 2.0.1 (4 out of 4): The topologically distinct phase portraits of systems (2.0.1) in the Poincaré disk.

## 2.1 Properties of the systems

In this section we state some results that will be used on the classification in order to reduce the number of phase portraits appearing. At first, note that if  $c_2 = 0$ , then systems (2.0.1) are Lotka-Volterra systems in dimension two. A global topological classification of these systems has been completed in [117], so we limit our study to the case  $c_2 \neq 0$ . We recall that, for obtaining systems (2.0.1), we have supposed that systems (1.7.14) have a Darboux invariant  $e^{-t(a_0+c_0\mu)}xz^\mu$ , so it is required that  $a_0 + c_0\mu \neq 0$ .

**Proposition 2.1.1.** *Consider systems (2.0.1) and suppose that  $(\tilde{x}(t), \tilde{z}(t))$  is a solution of these systems. If we change  $c_1$  by  $-c_1$ , we get the systems*

$$\begin{aligned}\dot{x} &= x (a_0 - \mu(-c_1x + c_2z^2 + c_3z)), \\ \dot{z} &= z (c_0 - c_1x + c_2z^2 + c_3z),\end{aligned}\tag{2.1.2}$$

for which  $(-\tilde{x}(t), \tilde{z}(t))$  is a solution.

*Proof.* In order to prove that  $(-\tilde{x}, \tilde{z})$  is a solution of (2.1.2), we must verify that

$$\begin{aligned}-\dot{\tilde{x}} &= -\tilde{x} (a_0 - \mu(+c_1\tilde{x} + c_2z^2 + c_3z)), \\ \dot{\tilde{z}} &= \tilde{z} (c_0 + c_1\tilde{x} + c_2z^2 + c_3z),\end{aligned}$$

which can be obtained immediately from the fact that  $(\tilde{x}, \tilde{z})$  is a solution of (2.0.1).  $\square$

**Proposition 2.1.2.** *Consider systems (2.0.1) and suppose  $(\tilde{x}, \tilde{z})$  is a solution of these systems. If we change  $c_3$  by  $-c_3$ , we get the systems*

$$\begin{aligned}\dot{x} &= x (a_0 - \mu(c_1x + c_2z^2 - c_3z)), \\ \dot{z} &= z (c_0 + c_1x + c_2z^2 - c_3z),\end{aligned}\tag{2.1.3}$$

for which  $(\tilde{x}, -\tilde{z})$  is a solution.

*Proof.* In order to prove that  $(\tilde{x}, -\tilde{z})$  is a solution of (2.1.3), we must verify that

$$\begin{aligned}\dot{\tilde{x}} &= \tilde{x} (a_0 - \mu(+c_1\tilde{x} + c_2z^2 + c_3z)), \\ -\dot{\tilde{z}} &= -\tilde{z} (c_0 + c_1\tilde{x} + c_2z^2 + c_3z),\end{aligned}$$

which is deduced immediately from the fact that  $(\tilde{x}, \tilde{z})$  is a solution of (2.0.1).  $\square$

**Remark 2.1.3.** *By Propositions 2.1.1 and 2.1.2 we can limit our study to Kolmogorov systems (2.0.1) with  $c_1$  and  $c_3$  non negatives. In the cases with these parameters negatives, we will obtain phase portraits symmetric to the ones obtained in the positive cases, with respect to the  $z$ -axis when we change the sign of  $c_1$ , and with respect to the  $x$ -axis when we change the sign of  $c_3$ .*

**Corollary 2.1.4.** *Consider systems (2.0.1) and suppose  $(\tilde{x}(t), \tilde{z}(t))$  is a solution. If  $c_1 = 0$ , then  $(-\tilde{x}(t), \tilde{z}(t))$  is also a solution.*

**Corollary 2.1.5.** Consider systems (2.0.1) and suppose  $(\tilde{x}(t), \tilde{z}(t))$  is a solution. If  $c_3 = 0$ , then  $(\tilde{x}(t), -\tilde{z}(t))$  is also a solution.

**Remark 2.1.6.** The previous corollaries simplify the study of the cases with  $c_1 = 0$  or  $c_3 = 0$ , because they prove that the phase portraits have to be symmetric with respect to the  $z$ -axis and the  $x$ -axis respectively, and this fact is useful in the process of obtaining the global phase portraits from the local results.

**Theorem 2.1.7.** Let  $(x(t), z(t))$  be a solution of systems (2.0.1). In the next cases we obtain another systems with solution  $(-\tilde{x}(-t), -\tilde{z}(-t))$ .

1. If  $a_0, c_0$  and  $c_2$  are not zero, and we change the sign of all of them.
2. If  $a_0 = 0$  and we change the sign of  $c_0$  and  $c_2$ , which are not zero.
3. If  $c_0 = 0$  and we change the sign of  $a_0$  and  $c_2$ , which are not zero.

*Proof.* In the first case, by changing the sign of  $a_0, c_0$  and  $c_2$ , we get the systems

$$\begin{aligned}\dot{x} &= x(-a_0 - \mu(c_1x - c_2z^2 + c_3z)), \\ \dot{z} &= z(-c_0 + c_1x - c_2z^2 + c_3z).\end{aligned}\tag{2.1.4}$$

We must prove that these equations hold for  $(-\tilde{x}, -\tilde{z}, -t)$ . At first, for  $(-\tilde{x}, -\tilde{z})$  we get

$$\begin{aligned}-\dot{\tilde{x}} &= -\tilde{x}(-a_0 - \mu(-c_1\tilde{x} - c_2\tilde{z}^2 - c_3\tilde{z})), \\ -\dot{\tilde{z}} &= -\tilde{z}(-c_0 - c_1\tilde{x} - c_2\tilde{z}^2 - c_3\tilde{z}),\end{aligned}$$

it is

$$\begin{aligned}\dot{\tilde{x}} &= -\tilde{x}(a_0 - \mu(c_1\tilde{x} + c_2\tilde{z}^2 + c_3\tilde{z})), \\ \dot{\tilde{z}} &= -\tilde{z}(c_0 + c_1\tilde{x} + c_2\tilde{z}^2 + c_3\tilde{z}),\end{aligned}$$

Then by changing the sense in which orbits are described, i.e., changing  $t$  by  $-t$ , we obtain that  $(-\tilde{x}, -\tilde{z}, -t)$  is a solution for systems (2.1.4). Similar arguments prove cases 2 and 3.  $\square$

**Remark 2.1.8.** In order to classify all the phase portraits of the Kolmogorov systems (2.0.1), according to the previous results, it is sufficient to consider  $a_0 \geq 0$ , and when  $a_0 = 0$  we can also consider  $c_0 > 0$ .

**Remark 2.1.9.** In short, according to the previous results and considerations, from now on it will be sufficient to study the Kolmogorov systems (2.0.1) with their parameters satisfying

$$H^1 = \{c_2 \neq 0, a_0 \geq 0, c_1 \geq 0, c_3 \geq 0, a_0 + c_0\mu \neq 0\}.$$

**Theorem 2.1.10.** For systems (2.0.1) the next statements hold.

1. If  $c_1 \neq 0$ , then on any straight line  $z = cte \neq 0$ , there exists only one contact point.

2. Suppose  $c_1 = 0$ . Then if  $c_3^2 > 4c_0c_2$ , there exist two invariant straight lines  $z = (\sqrt{c_3^2 - 4c_0c_2} - c_3)/(2c_2)$  and  $z = -(\sqrt{c_3^2 - 4c_0c_2} + c_3)/(2c_2)$  and there are not contact points on any other line  $z = cte \neq 0$ ; if  $c_3^2 = 4c_0c_2$ , there exists one invariant straight line  $z = -c_3/(2c_2)$  and there are not contact points on any other line  $z = cte \neq 0$ . If  $c_3^2 < 4c_0c_2$ , there are not contact points in any line  $z = cte \neq 0$ .

*Proof.* First we suppose  $c_1 \neq 0$  and consider a straight line  $z = z_0 \neq 0$ . Then the contact points on this straight line are those on which  $\dot{z} = 0$  and, as  $z_0 \neq 0$ , the only possible contact point is the one that satisfies  $c_0 + c_1x + c_2z_0^2 + c_3z_0 = 0$ , i.e., the point such that its first coordinate is  $x = -(c_2z_0^2 + c_3z_0 + c_0)/c_1$ .

We consider now the case with  $c_1 = 0$ . Then looking for the points on the straight line  $z = z_0 \neq 0$  satisfying  $\dot{z} = 0$ , we obtain that they must satisfy the condition  $c_0 + c_2z_0^2 + c_3z_0 = 0$ , and solving this equation we get that either there are no contact points, or a full straight line of contact points, or two straight lines of contact points, depending on the solutions  $z_0$  of that equation.  $\square$

**Proposition 2.1.11.** *For systems (2.0.1) the following statements hold.*

- (i) *If  $a_0 + c_0\mu > 0$  and  $\mu > 0$ , then for orbits which are not on the axes their  $\omega$ -limit is one of the singular points at infinity and their  $\alpha$ -limit is one of the singular points on the axes.*
- (ii) *If  $a_0 + c_0\mu > 0$  and  $\mu < 0$ , then for orbits which are not on the axes their  $\omega$ -limit is over the  $x$ -axis and their  $\alpha$ -limit is over the  $z$ -axis, and they can be either finite or infinite singular points.*
- (iii) *If  $a_0 + c_0\mu < 0$  and  $\mu > 0$ , then for orbits which are not on the axes their  $\omega$ -limit is one of the singular points on the axes and their  $\alpha$ -limit is one of the singular points at infinity.*
- (iv) *If  $a_0 + c_0\mu < 0$  and  $\mu < 0$ , then for orbits which are not on the axes their  $\omega$ -limit is over the  $z$ -axis and their  $\alpha$ -limit is over the  $x$ -axis, and they can be either finite or infinite singular points.*

*Proof.* At first we recall that  $e^{-t(a_0+c_0\mu)}xz^\mu$  is a Darboux invariant of systems (2.0.1), so that it is constant and non zero on the orbits  $(x(t), z(t))$  which are not on the axes.

If  $a_0 + c_0\mu > 0$ , then  $\lim_{t \rightarrow \infty} e^{-t(a_0+c_0\mu)} = 0$ , so necessarily  $\lim_{t \rightarrow \infty} x(t)z(t)^\mu = \pm\infty$ . If  $\mu > 0$ , then or  $\lim_{t \rightarrow \infty} x(t) = \pm\infty$  or  $\lim_{t \rightarrow \infty} z(t) = \pm\infty$ , so the  $\omega$ -limit of the orbits has to be an infinite singular point. If  $\mu < 0$ , then or  $\lim_{t \rightarrow \infty} x(t) = \pm\infty$  or  $\lim_{t \rightarrow \infty} z(t) = 0$ , so the  $\omega$ -limit of the orbits has to be over the  $x$ -axis, but it can be a finite or infinite singular point.

Also we have  $\lim_{t \rightarrow -\infty} e^{-t(a_0+c_0\mu)} = +\infty$ , so necessarily  $\lim_{t \rightarrow -\infty} x(t)z(t)^\mu = 0$ . If  $\mu > 0$ , then or  $\lim_{t \rightarrow -\infty} x(t) = 0$  or  $\lim_{t \rightarrow -\infty} z(t) = 0$ , so the  $\alpha$ -limit of the orbits has to be over the axes. If  $\mu < 0$ , then or  $\lim_{t \rightarrow -\infty} x(t) = 0$  or  $\lim_{t \rightarrow -\infty} z(t) = \pm\infty$ , so the  $\alpha$ -limit of the orbits has to be over the  $z$ -axis, but it can be a finite or infinite singular point.

An analogous reasoning is valid in the case  $a_0 + c_0\mu < 0$ .  $\square$

## 2.2 Finite singular points

**Lemma 2.2.1.** *Systems (2.0.1) have the following finite singular points:*

- $P_0 = (0, 0)$ , under any conditions.
- $P_1 = \left(0, \frac{-c_3 + \sqrt{c_3^2 - 4c_0c_2}}{2c_2}\right)$  and  $P_2 = \left(0, \frac{-c_3 - \sqrt{c_3^2 - 4c_0c_2}}{2c_2}\right)$  if  $c_3^2 > 4c_0c_2$ .
- $P_3 = \left(0, -\frac{c_3}{2c_2}\right)$  if  $c_3^2 = 4c_0c_2$ .
- $P_4 = \left(\frac{a_0}{c_1\mu}, 0\right)$  if  $c_1\mu \neq 0$ .

Moreover, if  $a_0 = 0$  and  $c_1\mu = 0$ , all the points on the  $z$ -axis are singular points.

*Proof.* The condition  $x = 0$  makes zero the first component of the vector field, and the same does  $z = 0$  with the second component, so the origin is always a singularity.

If we look for the singularities on  $z$ -axis, then  $c_0 + c_2z^2 + c_3z$  must be zero. If  $c_3^2 > 4c_0c_2$ , this equation has two different solutions,  $z = (-c_3 \pm \sqrt{c_3^2 - 4c_0c_2})/2c_2$ , that lead to the singularities  $P_1$  and  $P_2$ . If  $c_3^2 = 4c_0c_2$ , the equation has only one solution,  $z = -c_3/2c_2$ , that leads to the singularity  $P_3$ .

If we look for the other singularities on  $x$ -axis, then we must solve  $a_0 - \mu c_1x = 0$ . If  $c_1\mu \neq 0$ , we get the unique solution  $x = a_0/\mu c_1$ , which leads to the singular point  $P_4$ . If  $a_0 \neq 0$  and  $c_1\mu = 0$ , there is no solution so new singularities do not appear. At last, if  $c_1\mu = 0$  and  $a_0 = 0$ , then all the points on  $z = 0$  are singularities.

Finally, if there exists some singular point not on the axes, it must satisfy that

$$\begin{aligned} a_0 - \mu(c_1x + c_2z^2 + c_3z) &= 0, \\ c_0 + c_1x + c_2z^2 + c_3z &= 0. \end{aligned}$$

From these equations we get that  $a_0 + c_0\mu = 0$ , which contradicts our hypothesis. We conclude that there are not singular points outside the axes.  $\square$

**Remark 2.2.2.** *As we have said, if  $c_1\mu = 0$  and  $a_0 = 0$ , all the points on  $z = 0$  are singular points. In this case systems (2.0.1) are of the form*

$$\begin{aligned} \dot{x} &= -\mu x z (c_2 z + c_3), \\ \dot{y} &= z (c_0 + c_2 z^2 + c_3 z). \end{aligned}$$

*If we introduce the time variable  $s$  such that  $ds = zdt$ , then we get systems*

$$\begin{aligned} \frac{dx}{ds} &= -\mu x (c_2 z + c_3), \\ \frac{dz}{ds} &= c_0 + c_2 z^2 + c_3 z, \end{aligned}$$



which are quadratic systems with an invariant straight line  $x = 0$ . These systems have been studied in [6] so it is not necessary to consider this case.

According to this, from now on we will add the restriction that  $a_0^2 + (c_1\mu)^2 \neq 0$ , so we will consider the hypothesis

$$H_1^1 = \{c_2 \neq 0, a_0 \geq 0, c_1 \geq 0, c_3 \geq 0, a_0 + c_0\mu \neq 0, a_0^2 + c_1^2\mu^2 \neq 0\}.$$

Furthermore, we will use the notation  $R_c = \sqrt{c_3^2 - 4c_0c_2}$ , in order to simplify the expressions appearing.

**Theorem 2.2.3.** *Systems (2.0.1) have no limit cycles.*

*Proof.* The straight lines  $x = 0$  and  $z = 0$  are invariant sets, and by Lemma 2.2.1, all the singular points of systems (2.0.1) are over these axes. If there were any periodic orbit in the plane it would be surrounding one of the singular points and therefore it would intersect an invariant set, which is not possible.  $\square$

As a result, assuming  $H_1^1$  there are 6 different cases according to the finite singular points existing for systems (2.0.1), which are given in Table 2.2.1.

Case	Conditions	Finite singular points
1	$c_3^2 > 4c_0c_2, c_1\mu \neq 0$	$P_0, P_1, P_2, P_4$
2	$c_3^2 > 4c_0c_2, c_1\mu = 0, a_0 > 0$	$P_0, P_1, P_2$
3	$c_3^2 = 4c_0c_2, c_1\mu \neq 0$	$P_0, P_3, P_4$
4	$c_3^2 = 4c_0c_2, c_1\mu = 0, a_0 > 0$	$P_0, P_3$
5	$c_3^2 < 4c_0c_2, c_1\mu \neq 0$	$P_0, P_4$
6	$c_3^2 < 4c_0c_2, c_1\mu = 0, a_0 > 0$	$P_0$

Table 2.2.1: The different cases for the finite singular points.

Once we have obtained the singular points, we will study their local phase portraits. The results are summarized in the next lemmas.

**Lemma 2.2.4.** *Assuming  $H_1^1$ , the origin is always an isolated singular point for systems (2.0.1), and we have the next classification for its phase portraits:*

(1) *If  $a_0c_0 \neq 0$ , the singularity is hyperbolic and two cases are possible:*

(1.a) *If  $c_0 < 0$ , then the origin is a saddle point.*

(1.b) *If  $c_0 > 0$ , then the origin is an unstable node.*

(2) *If  $a_0 \neq 0$  and  $c_0 = 0$ , the singularity is semi-hyperbolic, and we must consider the following possibilities:*

(2.a) *If  $c_3 \neq 0$ , then the origin is a saddle-node.*

(2.b) If  $c_3 = 0$  and also

- $c_2 < 0$ , then the origin is a topological saddle.
- $c_2 > 0$ , then the origin is a topological unstable node.

(3) If  $a_0 = 0$ , the origin is a semi-hyperbolic saddle-node.

*Proof.* The eigenvalues of the linear part are  $a_0$  and  $c_0$ . At first, if  $a_0$  and  $c_0$  are not zero, the origin is hyperbolic. By Theorem 1.2.1, since  $a_0$  is non negative, we distinguish cases (1.a) and (1.b) according to the sign of  $c_0$ .

Suppose that  $c_0 = 0$ , in which case the singular point is semi-hyperbolic. Applying Theorem 1.2.3, and according to the notation employed, we get  $f(z) = 0$  and  $g(z) = c_2 z^3 + c_3 z^2$ .

If  $c_3 \neq 0$ , also the quadratic term is non-zero, so we get a saddle-node. If  $c_3 = 0$ , then we must distinguish the cases saddle and node, depending on the sign of  $c_2$ .

Finally, if  $a_0 = 0$ , the singular point is also semi-hyperbolic, and again by Theorem 1.2.3, with  $f(x) = 0$  and  $g(x) = -c_1 \mu x^2$ , we obtain that the origin is a saddle-node.

We recall that  $a_0 + c_0 \mu$  is not zero by hypothesis, so  $a_0$  and  $c_0$  can not be zero at the same time.

□

**Lemma 2.2.5.** Assuming  $H_1^1$ , let  $c_3^2 > 4c_0 c_2$ . Then,  $P_1$  is an isolated singularity of systems (2.0.1), and the next statements hold:

(1) If  $c_0 = 0$ , then  $P_1$  runs into the origin.

(2) If  $c_0 \neq 0$ , then  $P_1$  is hyperbolic. We distinguish the following phase portraits:

(2.a) If  $c_2(a_0 + c_0 \mu)(R_c - c_3) < 0$ , then  $P_1$  is a saddle.

(2.b) If  $a_0 + c_0 \mu < 0$  and  $c_2(R_c - c_3) < 0$ , then  $P_1$  is a stable node.

(2.c) If  $a_0 + c_0 \mu > 0$  and  $c_2(R_c - c_3) > 0$ , then  $P_1$  is an unstable node.

*Proof.* At first we move the singular point to the origin obtaining the systems

$$\begin{aligned}\dot{x} &= -c_2 \mu x z^2 - c_1 \mu x^2 - R_c \mu x z + (a_0 + c_0 \mu)x, \\ \dot{z} &= c_2 z^3 + c_1 x z + \frac{3R_c - c_3}{2} z^2 + \frac{c_1(R_c - c_3)}{2c_2} x + \frac{R_c(R_c - c_3)}{2c_2} z.\end{aligned}$$

The eigenvalues of the linear part of these systems are  $\lambda_1 = a_0 + c_0 \mu$  and  $\lambda_2 = R_c(R_c - c_3)/(2c_2)$ , so by hypothesis the first of them is non-zero.

Suppose that  $\lambda_2$  is zero. Then  $R_c - c_3$  must be zero, it is,  $\sqrt{c_3^2 - 4c_0 c_2} = c_3$ , but then,  $c_3^2 - 4c_0 c_2 = c_3^2$ , so  $c_0 c_2 = 0$ , and, since  $c_2 \neq 0$  by hypothesis,  $c_0 = 0$ . Assuming this condition we get that  $\sqrt{c_3^2} = c_3$ , so  $c_3$  must be non-negative. Given the expression of  $P_1$ , it is clear that in this case it coincides with the origin.

In any other case, the singular point  $P_1$  is hyperbolic, and by Theorem 1.2.1 we obtain the three possibilities (2.a)–(2.c).

□

**Lemma 2.2.6.** Assuming  $H_1^1$ , let  $c_3^2 > 4c_0c_2$ . Then  $P_2$  is a hyperbolic isolated singularity of systems (2.0.1), and the next statements hold:

- (1) If  $c_2(a_0 + c_0\mu) < 0$ , then  $P_2$  is a saddle.
- (2) If  $a_0 + c_0\mu < 0$  and  $c_2 < 0$ , then  $P_2$  is a stable node.
- (3) If  $a_0 + c_0\mu > 0$  and  $c_2 > 0$ , then  $P_2$  is an unstable node.

*Proof.* If we move the singular point to the origin we get the system

$$\begin{aligned}\dot{x} &= -c_2\mu xz^2 - c_1\mu x^2 + R_c\mu xz + (a_0 + c_0\mu)x, \\ \dot{z} &= +c_2z^3 + c_1xz - \frac{3R_c + c_3}{2}z^2 - \frac{c_1(R_c + c_3)}{2c_2}x + \frac{R_c(R_c + c_3)}{2c_2}z.\end{aligned}$$

The eigenvalues of the linear part are  $\lambda_1 = a_0 + c_0\mu$  and  $\lambda_2 = R_c(R_c + c_3)/(2c_2)$ . Proceeding in the same way as in Lemma 2.2.5, we obtain that  $\lambda_2 = 0$  if and only if  $c_0 = 0$  and  $c_3 < 0$ , which contradicts the hypothesis. Therefore the singular point  $P_2$  is always hyperbolic, and applying Theorem 1.2.1 we discern the cases (1)–(3). In order to simplify the conditions that define these cases, we note that  $R_c > 0$  and  $R_c + c_3 > 0$ , and so the sign of  $\lambda_2$  is the same as the sign of  $c_2$ . □

**Lemma 2.2.7.** Assuming  $H_1^1$ , let  $c_3^2 = 4c_0c_2$ . Then  $P_3$  is an isolated singularity of systems (2.0.1), and the next statements hold:

- (1) If  $c_3 = 0$ , then  $P_3$  runs into the origin.
- (2) If  $c_3 \neq 0$ , then  $P_3$  is a semi-hyperbolic saddle-node.

*Proof.* Moving the singular point to the origin we get the system

$$\begin{aligned}\dot{x} &= -c_2\mu xz^2 - c_1\mu x^2 + (a_0 + c_0\mu)x, \\ \dot{z} &= c_2z^3 + c_1xz - \frac{c_3}{2}z^2 - \frac{c_1c_3}{2c_2}x.\end{aligned}$$

The eigenvalues of the linear part are  $\lambda_1 = a_0 + c_0\mu$  and  $\lambda_2 = 0$ , so the singular point is always semi-hyperbolic. We obtain the systems associated to the Jordan canonical form of the linear part, which are

$$\begin{aligned}\dot{u} &= -\frac{c_1^2c_3^2\mu}{4c_2(a_0 + c_0\mu)^2}u^3 + \frac{c_1c_3\mu}{a_0 + c_0\mu}u^2v - c_2\mu uv^2 - c_1\mu u^2 + (a_0 + c_0\mu)u, \\ \dot{v} &= -\frac{c_1^3c_3^3(\mu + 1)}{8c_2^2(a_0 + c_0\mu)^3}u^3 + \frac{c_1^2c_3^2(\mu + \frac{3}{2})}{2c_2(a_0 + c_0\mu)^2}u^2v - \frac{c_1c_3(\mu + 3)}{2(a_0 + c_0\mu)}uv^2 + c_2v^3 \\ &\quad - \frac{4c_1^2c_2c_3(\mu + 1)(a_0 + c_0\mu) + c_1^2c_3^3}{8c_2^2(a_0 + c_0\mu)^2}u^2 + \frac{4c_1c_3^2 + 8(a_0 + c_0\mu)c_1c_2}{8c_2(a_0 + c_0\mu)}uv.\end{aligned}$$

## 2.2 Finite singular points

For these systems, we can apply Theorem 1.2.3. With  $f(v) = 0$  and  $g(v) = c_2v^3 - (c_3/2)v^2$ , we conclude that, if  $c_3 \neq 0$ , then the singular point is a saddle-node. Note that if  $c_3 = 0$ , then the singular point coincides with the origin.  $\square$

**Lemma 2.2.8.** *Assuming  $H_1^1$ , let  $c_1\mu \neq 0$ . Then  $P_4$  is an isolated singularity of systems (2.0.1), and the next statements hold:*

- (1) *If  $a_0 = 0$ , the singularity  $P_4$  runs into the origin.*
- (2) *If  $a_0 \neq 0$ , the singularity  $P_4$  is hyperbolic, and we distinguish the next phase portraits:*
  - (2.a) *If  $(a_0 + c_0\mu)\mu > 0$ ,  $P_4$  is a saddle.*
  - (2.b) *If  $\mu(a_0 + c_0\mu) < 0$ ,  $P_4$  is an stable node.*

*Proof.* Moving the singular point to the origin we get the systems

$$\begin{aligned}\dot{x} &= -c_2\mu xz^2 - c_1\mu x^2 - c_3\mu xz - \frac{a_0c_2}{c_1}z^2 - a_0x - \frac{a_0c_3}{c_1}z, \\ \dot{z} &= c_2z^3 + c_1xz + c_3z^2 + \left(\frac{a_0}{\mu} + c_0\right)z.\end{aligned}$$

We obtain the eigenvalues  $\lambda_1 = -a_0$  and  $\lambda_2 = (a_0 + c_0\mu)/\mu$ . Note that if  $a_0 = 0$ , then the singular point coincides with the origin. In any other case, the singular point is hyperbolic. By Theorem 1.2.1 we discern the cases saddle and node.  $\square$

**Lemma 2.2.9.** *Assuming the conditions  $H_1^1$ , there are 50 different cases according to the local phase portrait of finite singular points, which are given in Tables 2.2.2–2.2.7.*

*Proof.* We have to analyze cases 1 to 6 in Table 2.2.1 and determine the local phase portraits of the singular points existing in each one of them, according to their individual classification.

We start with the first one, in which the conditions,  $c_3^2 > 4c_0c_2$  and  $c_1\mu \neq 0$  hold. The singular points are  $P_0, P_1, P_2$  and  $P_4$ . We shall consider three subcases:  $a_0 = 0, c_0 = 0$  and  $a_0c_0 \neq 0$ .

Consider case  $c_0 = 0$  in which the origin is a saddle-node and  $P_1$  collides with the origin. Since  $c_0 = 0$  and  $a_0 > 0$ , the singular point  $P_2$  is a saddle if  $c_2 < 0$ , and an unstable node if  $c_2 > 0$ .

In these two cases  $P_4$  can be either a saddle if  $\mu > 0$ , or a stable node if  $\mu < 0$ . This leads to cases 1.1 to 1.4 in Table 2.2.2.

We continue with the case  $a_0 = 0$  in which  $P_0$  is again a saddle-node, but in this case it coincides with  $P_4$ . Suppose that  $P_1$  is an unstable node, then we have  $c_0\mu > 0$  and  $c_2(R_c - c_3) > 0$ . By Remark 2.1.8, we will only consider the case  $c_0 > 0$ . Then if  $c_2 > 0$ , also  $R_c - c_3 > 0$ , and taking into account the expression of  $R_c$  and squaring both terms, we get that  $c_3^2 - 4c_0c_2 > c_2^2$ , so  $c_0c_2 < 0$ , which leads to a contradiction. The same occurs if we suppose  $c_2 < 0$ . Therefore,  $P_1$  cannot be an unstable node. If  $P_1$  is a saddle, then  $P_2$  can be a saddle or an unstable node, but not a stable node, which is only possible if  $c_0 < 0$ , by an

analogous reasoning to the previous one. If  $P_1$  is a stable node, then  $c_0\mu < 0$ , so  $P_2$  can be a saddle or a stable node, but not an unstable node because it requires that  $c_0\mu > 0$ . This leads to cases 1.5 to 1.8.

The last case is  $a_0c_0 \neq 0$  in which the origin is a hyperbolic singular point. We start with the case in which  $P_0$  is a saddle, and then  $c_0 < 0$ . First we consider that  $P_1$  is also a saddle, and so  $c_2(a_0 + c_0\mu)(R_c - c_3) < 0$ . If  $P_2$  is a saddle, then  $c_2(a_0 + c_0\mu) < 0$ , and we get  $R_c - c_3 > 0$ . From this we deduce like in previous cases that  $c_0c_2 < 0$ , but we are supposing  $c_0 < 0$  and so  $c_2 > 0$  and  $a_0 + c_0\mu < 0$ . From the last inequality  $a_0 < -c_0\mu$ , and so  $\mu$  has to be positive. In short,  $\mu(a_0 + c_0\mu) < 0$  and consequently  $P_4$  can only be a stable node. If  $P_0$  and  $P_1$  are saddles, but  $P_2$  is a stable node, reasoning in an analogous way we get that  $P_4$  is again a stable node. This leads to cases 1.9 and 1.10.

Note that if  $P_0$  and  $P_1$  are saddles, it is impossible for  $P_2$  to be an unstable node. In that case we would have that  $c_0 < 0$ ,  $c_2 > 0$ ,  $a_0 + c_0\mu > 0$  and  $R_c - c_3 < 0$ . From this last inequality we get that  $c_0c_2 > 0$ , which is a contradiction.

We consider now the cases where  $P_0$  is saddle and  $P_1$  an unstable node, in which the conditions  $c_0 < 0$ ,  $a_0 + c_0\mu > 0$  and  $c_2(R_c - c_3) > 0$  hold. It is obvious that  $P_2$  cannot be a stable node because it requires that  $a_0 + c_0\mu < 0$ , so  $P_2$  is a saddle if  $c_2 < 0$  and an unstable node if  $c_2 > 0$ . In both cases  $P_4$  can be either a saddle if  $\mu > 0$ , or a stable node if  $\mu < 0$ . This leads to cases 1.11 to 1.14.

Note that the case with  $P_0$  a saddle and  $P_1$  a stable node is not possible, because we would have  $c_0 < 0$ ,  $a_0 + c_0\mu < 0$  and  $c_2(R_c - c_3) < 0$ . If  $c_2 > 0$ , then  $R_c - c_3 < 0$  whence we deduce  $c_0c_2 > 0$  and get a contradiction. The same argument is valid if  $c_2 < 0$ .

Let us study now the cases where  $P_0$  is an unstable node, i.e., the ones with  $c_0 > 0$ . First we prove that it is impossible that  $P_1$  is an unstable node. In that case we would have  $a_0 + c_0\mu > 0$  and  $c_2(R_c - c_3) > 0$ . If we suppose  $c_2 > 0$ , then  $R_c - c_3 > 0$  and we deduce  $c_0c_2 < 0$  which is a contradiction. The same reasoning is valid with  $c_2 < 0$ . We consider now the case with  $P_1$  saddle. If we suppose that  $P_2$  is a stable node, we arrive at a contradiction, so only the cases  $P_2$  saddle and unstable node are possible. In both of them,  $P_4$  can be either a saddle or a stable node. This leads to cases 1.15 to 1.18.

At last we have the case with  $P_1$  a stable node, in which we have  $a_0 + c_0\mu < 0$ , condition that makes not possible for  $P_2$  to be an unstable node. Then we have the cases with  $P_2$  a saddle or a stable node. In both cases, by the condition  $0 < a_0 < -c_0\mu$ , we get that  $\mu < 0$ , so  $\mu(a_0 + c_0\mu) > 0$  and therefore  $P_4$  is a saddle. This leads to cases 1.19 and 1.20.

Now we study case 2 of Table 2.2.1, in which  $c_3^2 > 4c_0c_2$ ,  $c_1\mu = 0$  and  $a_0 \neq 0$ . We shall consider three cases:  $c_0 < 0$ ,  $c_0 > 0$  and  $c_0 = 0$ .

We start with case  $c_0 < 0$  in which  $P_0$  is a saddle. If  $P_1$  is a saddle, then  $P_2$  can be a saddle or a stable node. If  $P_2$  is an unstable node, then we have the conditions  $c_2(a_0 + c_0\mu)(R_c - c_3) < 0$ ,  $c_2 > 0$  and  $a_0 + c_0\mu > 0$ , so  $R_c - c_3 < 0$ , and we deduce  $c_0c_2 > 0$  which is a contradiction.

$P_1$  cannot be a stable node, because in that case we would have the conditions  $c_0 < 0$ ,  $a_0 + c_0\mu < 0$  and  $c_2(R_c - c_3) < 0$  which lead to a contradiction in the following way: If  $c_2 > 0$ , then  $R_c - c_3 < 0$ , and squaring we deduce  $c_0c_2 > 0$ , which is not possible because  $c_0 < 0$  and we are supposing  $c_2 > 0$ . An analogous reasoning works in the case  $c_2 < 0$ . If  $P_1$  is an unstable node, then  $P_2$  can be either a saddle or an unstable node, but not a stable node because it requires  $a_0 + c_0\mu$  to be negative, but we already know that this expression is

positive because it is a condition in order that  $P_1$  be an unstable node. This leads to cases 2.1 to 2.4 of Table 2.2.3.

We continue with the subcase  $c_0 > 0$ , in which  $P_0$  is an unstable node. If  $P_1$  is a saddle, then  $P_2$  can be a saddle or an unstable node. If  $P_2$  is a stable node, then we have the conditions  $c_0 > 0$ ,  $c_2(a_0 + c_0\mu)(R_c - c_3) < 0$ ,  $a_0 + c_0\mu < 0$  and  $c_2 < 0$ . Thus we have  $R_c - c_3 < 0$  and squaring we obtain  $c_0c_2 > 0$  which is a contradiction. This leads to cases 2.5 and 2.6.

If  $P_1$  is a stable node, it can be proved similarly to previous cases that  $P_2$  cannot be an unstable node. This leads to cases 2.7 and 2.8.

$P_1$  cannot be an unstable node, because in that case we would have the conditions  $c_0 > 0$ ,  $a_0 + c_0\mu > 0$  and  $c_2(R_c - c_3) > 0$  which lead to a contradiction in the following way: If  $c_2 > 0$ , then  $R_c - c_3 > 0$ , and squaring we deduce  $c_0c_2 < 0$ , which is not possible because  $c_0 > 0$  and we are supposing  $c_2 > 0$ . An analogous reasoning works in the case  $c_2 < 0$ .

At last we have the subcase  $c_0 = 0$ . Necessarily  $c_3 \neq 0$  so the origin is a saddle-node. Also we have that  $P_1$  coincides with the origin. For the singular point  $P_2$  we have that it is a saddle if  $c_2 < 0$  and an unstable node if  $c_2 > 0$ . This leads to cases 2.9 and 2.10.

We study case 3 of Table 2.2.1 in which  $c_3^2 = 4c_0c_2$  and  $c_1\mu \neq 0$ . Then  $c_0 = 0$  if and only if  $c_3 = 0$ . We consider  $a_0 > 0$  and  $c_0 < 0$ , then the origin is a saddle and  $P_3$  a saddle-node (as  $c_3 \neq 0$ ). The singular point  $P_4$  is either a saddle or a stable node, depending on the sign of  $\mu(a_0 + c_0\mu)$ . The same is valid in the case  $a_0 > 0$  and  $c_0 < 0$ , except for the origin, which is now an unstable node. We get the cases 3.1 to 3.4 of Table 2.2.4.

We continue with the case in which  $a_0 = 0$  and so  $P_0$  is a saddle-node,  $P_4$  coincides with  $P_0$  and  $P_3$  is a saddle-node. This correspond with case 3.5.

At last we have the condition  $c_0 = 0$ , under which  $P_3$  coincides with  $P_0$ . If  $c_2 < 0$ , then it is a topological saddle and if  $c_2 > 0$ , it is a topological unstable node. In any case  $P_4$  can be either a saddle or a stable node. This leads to cases 3.6 to 3.9.

Now we address the case 4 of Table 2.2.1 in which  $c_3^2 = 4c_0c_2$ ,  $c_1\mu = 0$  and  $a_0 \neq 0$ . The origin is a saddle if  $c_0 < 0$  and an unstable node if  $c_0 > 0$ . If  $c_0 = 0$ , then  $c_3 = 0$  so we must distinguish two semi-hyperbolic possibilities for the origin: if  $c_2 < 0$ , it is a topological saddle and if  $c_2 > 0$ , it is a topological unstable node. The classification of  $P_3$  is totally determined by the one of  $P_0$ , because it only depends on whether  $c_3$  is zero or not. We get cases 4.1 to 4.4.

In case 5 of Table 2.2.1 the conditions  $c_3^2 < 4c_0c_2$  and  $c_1\mu \neq 0$  hold. The singular points are  $P_0$  and  $P_4$ . From condition  $c_3^2 < 4c_0c_2$  we get that  $c_0 \neq 0$ . If  $a_0 = 0$ , then the origin is a saddle-node and  $P_4$  coincides with the origin. If  $a_0 \neq 0$ , then both singular points are hyperbolic, and it leads to cases 5.2 to 5.5.

At last, in case 6 of Table 2.2.1, we have the conditions  $c_3^2 < 4c_0c_2$ ,  $c_1\mu = 0$  and  $a_0 \neq 0$ . The unique singular point is the origin and as  $c_0$  cannot be zero, it is either a saddle or an unstable node.

□

**Case 1:  $c_3^2 > 4c_0c_2$ ,  $c_1\mu \neq 0$** 

Sub.	Conditions	Classification
1.1	$a_0 > 0, c_0 = 0, \mu > 0, c_2 < 0$	$P_0 \equiv P_1$ saddle-node, $P_2$ saddle, $P_4$ saddle
1.2	$a_0 > 0, c_0 = 0, \mu > 0, c_2 > 0$	$P_0 \equiv P_1$ saddle-node, $P_2$ unstable node, $P_4$ saddle
1.3	$a_0 > 0, c_0 = 0, \mu < 0, c_2 < 0$	$P_0 \equiv P_1$ saddle-node, $P_2$ saddle, $P_4$ stable node
1.4	$a_0 > 0, c_0 = 0, \mu < 0, c_2 > 0$	$P_0 \equiv P_1$ saddle-node, $P_2$ unstable node, $P_4$ stable node
1.5	$a_0 = 0, c_0 > 0, c_2\mu < 0, R_c - c_3 > 0$	$P_0 \equiv P_4$ saddle-node, $P_1$ saddle, $P_2$ saddle
1.6	$a_0 = 0, c_0 > 0, R_c - c_3 < 0, \mu > 0, c_2 > 0$	$P_0 \equiv P_4$ saddle-node, $P_1$ saddle, $P_2$ unstable node
1.7	$a_0 = 0, c_0 > 0, \mu < 0, R_c - c_3 < 0, c_2 > 0$	$P_0 \equiv P_4$ saddle-node, $P_1$ stable node, $P_2$ saddle
1.8	$a_0 = 0, c_0 > 0, \mu < 0, c_2 < 0, R_c - c_3 > 0$	$P_0 \equiv P_4$ saddle-node, $P_1$ stable node, $P_2$ stable node
1.9	$a_0 > 0, c_0 < 0, \mu > 0, a_0 + c_0\mu < 0, c_2 > 0, R_c - c_3 > 0$	$P_0$ saddle, $P_1$ saddle, $P_2$ saddle, $P_4$ stable node
1.10	$a_0 > 0, c_0 < 0, c_2 < 0, \mu > 0, a_0 + c_0\mu < 0, R_c - c_3 < 0$	$P_0$ saddle, $P_1$ saddle, $P_2$ stable node, $P_4$ stable node
1.11	$a_0 > 0, c_0 < 0, c_2 < 0, \mu > 0, a_0 + c_0\mu > 0, R_c - c_3 < 0$	$P_0$ saddle, $P_1$ unstable node, $P_2$ saddle, $P_4$ saddle
1.12	$a_0 > 0, c_0 < 0, c_2 < 0, \mu < 0, a_0 + c_0\mu > 0, R_c - c_3 < 0$	$P_0$ saddle, $P_1$ unstable node, $P_2$ saddle, $P_4$ stable node
1.13	$a_0 > 0, c_0 < 0, \mu > 0, a_0 + c_0\mu > 0, c_2 > 0, R_c - c_3 > 0$	$P_0$ saddle, $P_1$ unstable node, $P_2$ unstable node, $P_4$ saddle
1.14	$a_0 > 0, c_0 < 0, \mu < 0, a_0 + c_0\mu > 0, c_2 > 0, R_c - c_3 > 0$	$P_0$ saddle, $P_1$ unstable node, $P_2$ unstable node, $P_4$ stable node
1.15	$a_0 > 0, c_0 > 0, \mu(a_0 + c_0\mu) > 0, c_2(a_0 + c_0\mu) < 0, R_c - c_3 > 0$	$P_0$ unstable node, $P_1$ saddle, $P_2$ saddle, $P_4$ saddle
1.16	$a_0 > 0, c_0 > 0, \mu(a_0 + c_0\mu) < 0, c_2(a_0 + c_0\mu) < 0, R_c - c_3 > 0$	$P_0$ unstable node, $P_1$ saddle, $P_2$ saddle, $P_4$ stable node
1.17	$a_0 > 0, c_0 > 0, \mu > 0, R_c - c_3 < 0, a_0 + c_0\mu > 0, c_2 > 0$	$P_0$ unstable node, $P_1$ saddle, $P_2$ unstable node, $P_4$ saddle
1.18	$a_0 > 0, c_0 > 0, \mu < 0, R_c - c_3 < 0, a_0 + c_0\mu > 0, c_2 > 0$	$P_0$ unstable node, $P_1$ saddle, $P_2$ unstable node, $P_4$ stable node
1.19	$a_0 > 0, c_0 > 0, \mu < 0, a_0 + c_0\mu < 0, R_c - c_3 < 0, c_2 > 0$	$P_0$ unstable node, $P_1$ stable node, $P_2$ saddle, $P_4$ saddle
1.20	$a_0 > 0, c_0 > 0, \mu < 0, a_0 + c_0\mu < 0, c_2 < 0, R_c - c_3 > 0$	$P_0$ unstable node, $P_1$ stable node, $P_2$ stable node, $P_4$ saddle

Table 2.2.2: Classification in case 1 of Table 2.2.1 according to the local phase portraits of finite singular points.

## 2.2 Finite singular points

**Case 2:**  $c_3^2 > 4c_0c_2$ ,  $c_1\mu = 0$ ,  $a_0 > 0$

Sub.	Conditions	Classification
2.1	$c_0 < 0$ , $c_2(a_0 + c_0\mu) < 0$ , $R_c - c_3 > 0$	$P_0$ saddle, $P_1$ saddle, $P_2$ saddle
2.2	$c_0 < 0$ , $R_c - c_3 < 0$ , $a_0 + c_0\mu < 0$ , $c_2 < 0$	$P_0$ saddle, $P_1$ saddle, $P_2$ stable node
2.3	$c_0 < 0$ , $a_0 + c_0\mu > 0$ , $R_c - c_3 < 0$ , $c_2 < 0$	$P_0$ saddle, $P_1$ unstable node, $P_2$ saddle
2.4	$c_0 < 0$ , $a_0 + c_0\mu > 0$ , $c_2 > 0$ , $R_c - c_3 > 0$	$P_0$ saddle, $P_1$ unstable node, $P_2$ unstable node
2.5	$c_0 > 0$ , $c_2(a_0 + c_0\mu) < 0$ , $R_c - c_3 > 0$	$P_0$ unstable node, $P_1$ saddle, $P_2$ saddle
2.6	$c_0 > 0$ , $R_c - c_3 < 0$ , $a_0 + c_0\mu > 0$ , $c_2 > 0$	$P_0$ unstable node, $P_1$ saddle, $P_2$ unstable node
2.7	$c_0 > 0$ , $a_0 + c_0\mu < 0$ , $R_c - c_3 < 0$ , $c_2 > 0$	$P_0$ unstable node, $P_1$ stable node, $P_2$ saddle
2.8	$c_0 > 0$ , $a_0 + c_0\mu < 0$ , $c_2 < 0$ , $R_c - c_3 > 0$	$P_0$ unstable node, $P_1$ stable node, $P_2$ stable node
2.9	$c_0 = 0$ , $a_0 > 0$ , $c_2 < 0$	$P_0 \equiv P_1$ saddle-node, $P_2$ saddle
2.10	$c_0 = 0$ , $a_0 > 0$ , $c_2 > 0$	$P_0 \equiv P_1$ saddle-node, $P_2$ unstable node

Table 2.2.3: Classification in case 2 of Table 2.2.1 according to the local phase portraits of finite singular points.

**Case 3:**  $c_3^2 = 4c_0c_2$ ,  $c_1\mu \neq 0$

Sub.	Conditions	Classification
3.1	$a_0 > 0$ , $c_0 < 0$ , $\mu(a_0 + c_0\mu) > 0$	$P_0$ saddle, $P_3$ saddle-node, $P_4$ saddle
3.2	$a_0 > 0$ , $c_0 < 0$ , $\mu(a_0 + c_0\mu) < 0$	$P_0$ saddle, $P_3$ saddle-node, $P_4$ stable node
3.3	$a_0 > 0$ , $c_0 > 0$ , $\mu(a_0 + c_0\mu) > 0$	$P_0$ unstable node, $P_3$ saddle-node, $P_4$ saddle
3.4	$a_0 > 0$ , $c_0 > 0$ , $\mu(a_0 + c_0\mu) < 0$	$P_0$ unstable node, $P_3$ saddle-node, $P_4$ stable node
3.5	$a_0 = 0$ , $c_0 > 0$	$P_0 \equiv P_4$ saddle-node, $P_3$ saddle-node
3.6	$c_0 = 0$ , $a_0 > 0$ , $c_2 < 0$ , $\mu > 0$	$P_0 \equiv P_3$ topological saddle, $P_4$ saddle
3.7	$c_0 = 0$ , $a_0 > 0$ , $c_2 < 0$ , $\mu < 0$	$P_0 \equiv P_3$ topological saddle, $P_4$ stable node
3.8	$c_0 = 0$ , $a_0 > 0$ , $c_2 > 0$ , $\mu > 0$	$P_0 \equiv P_3$ topological unstable node, $P_4$ saddle
3.9	$c_0 = 0$ , $a_0 > 0$ , $c_2 > 0$ , $\mu < 0$	$P_0 \equiv P_3$ topological unstable node, $P_4$ stable node

Table 2.2.4: Classification in case 3 of Table 2.2.1 according to the local phase portraits of finite singular points.



**Case 4:**  $c_3^2 = 4c_0c_2$ ,  $c_1\mu = 0$ ,  $a_0 > 0$

Sub.	Conditions	Classification
4.1	$c_0 < 0$	$P_0$ saddle, $P_3$ saddle-node
4.2	$c_0 > 0$	$P_0$ unstable node, $P_3$ saddle-node
4.3	$c_0 = 0$ , $c_2 < 0$	$P_0 \equiv P_3$ topological saddle
4.4	$c_0 = 0$ , $c_2 > 0$	$P_0 \equiv P_3$ topological unstable node

Table 2.2.5: Classification in case 4 of Table 2.2.1 according to the local phase portraits of finite singular points.

**Case 5:**  $c_3^2 < 4c_0c_2$ ,  $c_1\mu \neq 0$

Sub.	Conditions	Classification
5.1	$a_0 = 0$	$P_0 \equiv P_4$ saddle-node
5.2	$a_0 > 0$ , $c_0 < 0$ , $\mu(a_0 + c_0\mu) > 0$	$P_0$ saddle, $P_4$ saddle
5.3	$a_0 > 0$ , $c_0 < 0$ , $\mu(a_0 + c_0\mu) < 0$	$P_0$ saddle, $P_4$ stable node
5.4	$a_0 > 0$ , $c_0 > 0$ , $\mu(a_0 + c_0\mu) > 0$	$P_0$ unstable node, $P_4$ saddle
5.5	$a_0 > 0$ , $c_0 > 0$ , $\mu(a_0 + c_0\mu) < 0$	$P_0$ unstable node, $P_4$ stable node

Table 2.2.6: Classification in case 5 of Table 2.2.1 according to the local phase portraits of finite singular points.

**Case 6:**  $c_3^2 < 4c_0c_2$ ,  $c_1\mu = 0$ ,  $a_0 > 0$

Sub.	Conditions	Classification
6.1	$c_0 < 0$	$P_0$ saddle
6.2	$c_0 > 0$	$P_0$ unstable node

Table 2.2.7: Classification in case 6 of Table 2.2.1 according to the local phase portraits of finite singular points.

## 2.3 Infinite singular points

In order to study the behavior of the trajectories of systems (2.0.1) near infinity, we consider its Poincaré compactification. For the moment we assume the same hypothesis  $H_1^1$  than in previous sections. According to equations (1.3.9) and (1.3.10), we get the compactification in the local charts  $U_1$  and  $U_2$  respectively. From Section 1.3, it is enough to study the singular points over  $v = 0$  in chart  $U_1$  and the origin of chart  $U_2$ .

In chart  $U_1$  systems (2.0.1) write

$$\begin{aligned}\dot{u} &= c_2(\mu + 1)u^3 + c_3(\mu + 1)u^2v + (c_0 - a_0)uv^2 + c_1(\mu + 1)uv, \\ \dot{v} &= c_2\mu u^2v + c_3\mu uv^2 - a_0v^3 + c_1\mu v^2.\end{aligned}\tag{2.3.5}$$

## 2.3 Infinite singular points

Taking  $v = 0$  we get  $\dot{u}|_{v=0} = c_2(\mu + 1)u^3$  and  $\dot{v}|_{v=0} = 0$ . Therefore, if  $\mu = -1$ , all the points at infinity are singular points, and we will deal with this situation in Chapter 3. In other case, if  $\mu \neq -1$ , the only singular point is the origin of  $U_1$ , which we denote by  $O_1$ . The linear part of systems (2.3.5) at the origin is identically zero, so we must use the blow up technique to study it.

From now on we include the condition  $\mu \neq -1$  in our hypothesis, so we will work under conditions

$$H_2^1 = \{c_2 \neq 0, a_0 \geq 0, c_1 \geq 0, c_3 \geq 0, a_0 + c_0\mu \neq 0, a_0^2 + c_1^2\mu^2 \neq 0, \mu \neq -1\}.$$

The study of the local phase portraits of the singular point  $O_1$  by means of the blow up technique leads to the following result which is proved in Subsections 2.3.1 and 2.3.2.

**Lemma 2.3.1.** *Assuming hypothesis  $H_2^1$ , the origin of chart  $U_1$  is an infinite singular point of systems (2.0.1), and it has 47 distinct local phase portraits described in Figure 2.3.1.*

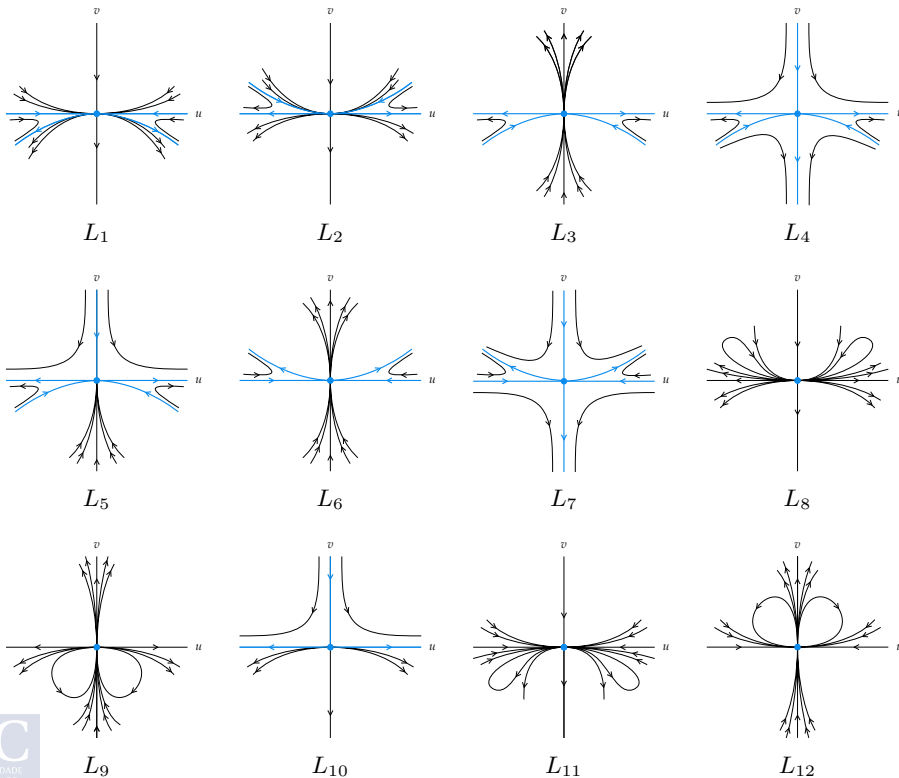
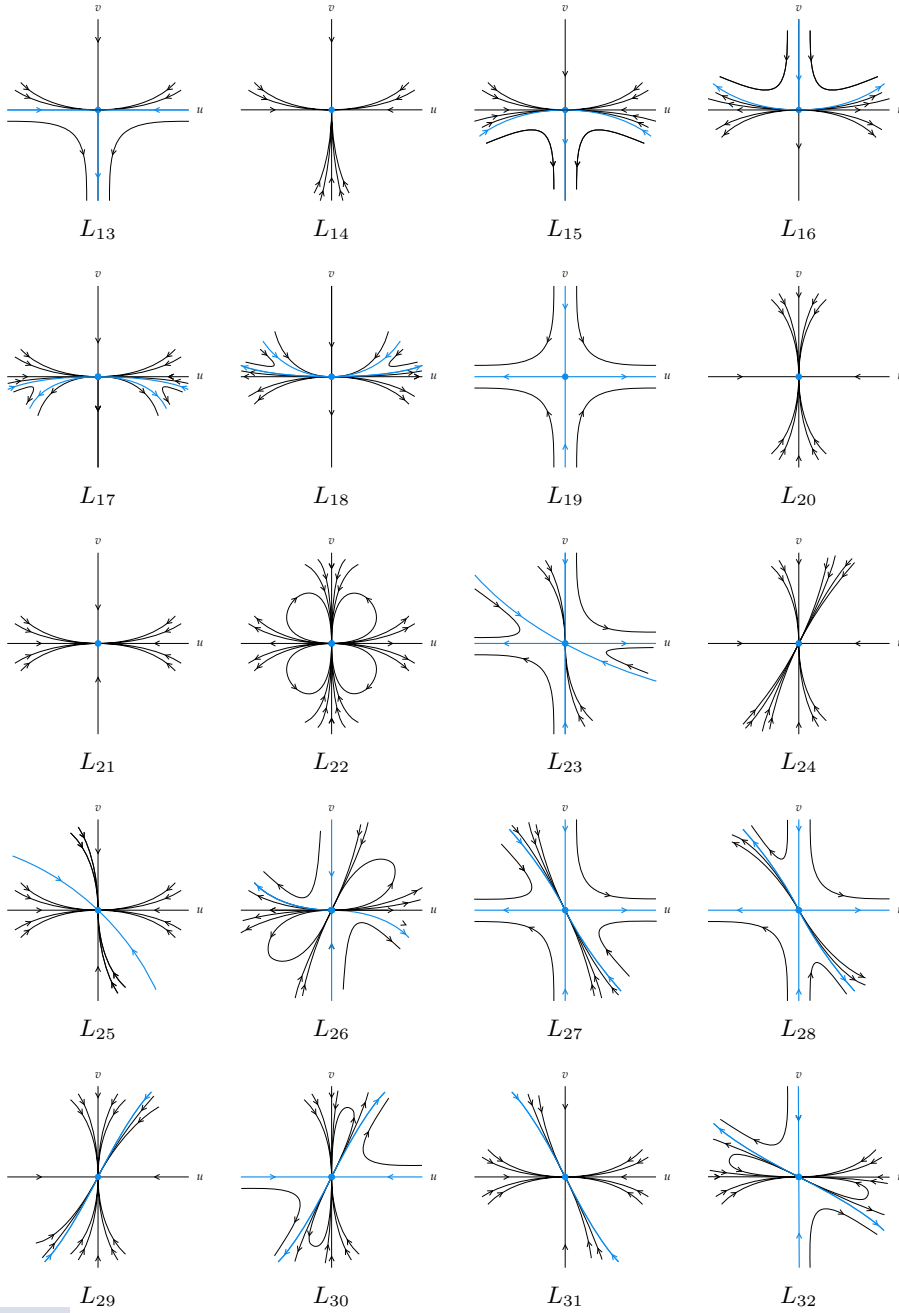


Figure 2.3.1 (1 out of 3): Local phase portraits of the infinite singular point  $O_1$ .


 Figure 2.3.1 (2 out of 3): Local phase portraits of the infinite singular point  $O_1$ .

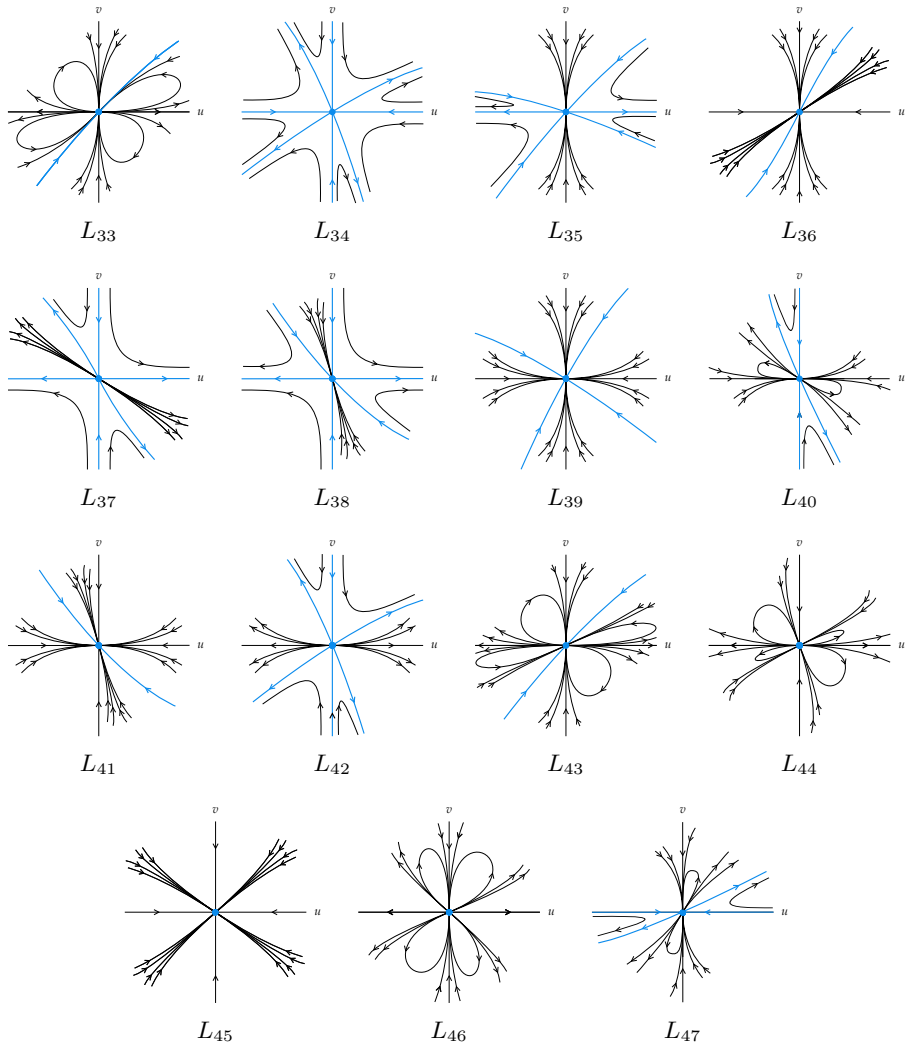


Figure 2.3.1 (3 out of 3): Local phase portraits of the infinite singular point  $O_1$ .

For systems (2.3.5), if  $c_1 \neq 0$ , the characteristic polynomial is  $\mathcal{F} = -c_1 uv^2 \neq 0$ , so the origin is a nondcritical singular point. If  $c_1 = 0$ , the characteristic polynomial is  $\mathcal{F} = -c_3 u^2 v - c_2 u^3 v - c_0 uv^3$ , which cannot be identically zero because  $c_2 \neq 0$ , so we have also a nondcritical singular point. We will study these two cases separately in Subsections 2.3.1 and 2.3.2.

### 2.3.1 Case $c_1$ non-zero

Consider  $c_1 \neq 0$ . We introduce the new variable  $w_1$  on systems (2.3.5) by means of the variable change  $uw_1 = v$ , and get the systems

$$\begin{aligned}\dot{u} &= (c_0 - a_0)u^3w_1^2 + c_3(\mu + 1)u^3w_1 + c_2(\mu + 1)u^3 + c_1(\mu + 1)u^2w_1, \\ \dot{w}_1 &= -c_0u^2w_1^3 - c_3u^2w_1^2 - c_2u^2w_1 - c_1uw_1^2.\end{aligned}\quad (2.3.6)$$

Now we cancel the common factor  $u$ , getting the systems

$$\begin{aligned}\dot{u} &= (c_0 - a_0)u^2w_1^2 + c_3(\mu + 1)u^2w_1 + c_2(\mu + 1)u^2 + c_1(\mu + 1)uw_1, \\ \dot{w}_1 &= -c_0uw_1^3 - c_3uw_1^2 - c_2uw_1 - c_1w_1^2,\end{aligned}\quad (2.3.7)$$

for which the only singular point on the exceptional divisor is the origin, and it is linearly zero, so we have to repeat the process. Now the characteristic polynomial is  $\mathcal{F} = -c_2(\mu + 2)u^2w_1 - c_1(\mu + 2)uw_1^2$ , so the origin is a non dicritical singular point if  $\mu \neq -2$  and it is dicritical if  $\mu = -2$ . In both cases we introduce the new variable  $w_2$  doing the change  $uw_2 = w_1$ , obtaining the systems

$$\begin{aligned}\dot{u} &= (c_0 - a_0)u^4w_2^2 + c_3(\mu + 1)u^3w_2 + c_2(\mu + 1)u^2 + c_1(\mu + 1)u^2w_2, \\ \dot{w}_2 &= (a_0 - 2c_0)u^3w_2^3 - c_3(\mu + 2)u^2w_2^2 - c_1(\mu + 2)uw_2^2 - c_2(\mu + 2)uw_2.\end{aligned}\quad (2.3.8)$$

In the nondicritical case we have to eliminate the common factor  $u$ , obtaining

$$\begin{aligned}\dot{u} &= (c_0 - a_0)u^3w_2^2 + c_3(\mu + 1)u^2w_2 + c_2(\mu + 1)u + c_1(\mu + 1)uw_2, \\ \dot{w}_2 &= (a_0 - 2c_0)u^2w_2^3 - c_3(\mu + 2)uw_2^2 - c_1(\mu + 2)w_2^2 - c_2(\mu + 2)w_2.\end{aligned}\quad (2.3.9)$$

But in the dicritical case, when  $\mu = -2$ , we must cancel the common factor  $u^2$  from systems (2.3.8), hence we obtain the systems

$$\begin{aligned}\dot{u} &= (c_0 - a_0)u^2w_2^2 - c_3uw_2 - c_2 - c_1w_2, \\ \dot{w}_2 &= (a_0 - 2c_0)uw_2^3.\end{aligned}\quad (2.3.10)$$

#### Nondicritical case

In this case it is necessary to study the singular points of systems (2.3.9) on the exceptional divisor. The origin is always a singular point, and we denote it by  $Q_0$ . As  $\mu + 2 \neq 0$ , there is another singular point,  $Q_1 = (0, -c_2/c_1)$ , and we shall determine their local phase portraits. For the origin, the eigenvalues of the linear part are  $\lambda_1 = c_2(\mu + 1)$  and  $\lambda_2 = -c_2(\mu + 2)$ , so they are both non-zero and the singular point is hyperbolic. By Theorem 1.2.1 we get the three following possibilities:

- If  $\mu \in (-\infty, -2) \cup (-1, +\infty)$ , the origin is a saddle.
- If  $c_2 > 0$  and  $\mu \in (-2, -1)$ , the origin a stable node.
- If  $c_2 < 0$  and  $\mu \in (-2, -1)$ , the origin is an unstable node.

For the singular point  $Q_1$ , after doing a translation to the origin, we obtain eigenvalues  $\lambda_1 = 0$  and  $\lambda_2 = c_2(\mu + 2)$ , so it is semi-hyperbolic. We place the systems in real Jordan canonical form and apply Theorem 1.2.3, which gives us the next classification:

- If  $c_2(a_0 + c_0\mu) > 0$ , then  $Q_1$  is a topological saddle.
- If  $c_2(\mu + 2) > 0$  and  $(\mu + 2)(a_0 + c_0\mu) < 0$ , then  $Q_1$  is a topological unstable node.
- If  $c_2(\mu + 2) < 0$  and  $(\mu + 2)(a_0 + c_0\mu) > 0$ , then  $Q_1$  is a topological stable node.

These conditions come together in the seven subcases (a) to (g) listed below:

- (a) If  $\mu \in (-\infty, -2) \cup (-1, +\infty)$  and  $c_2(a_0 + c_0\mu) > 0$ , then  $Q_0$  is a saddle and  $Q_1$  is a topological saddle.

In order to determine the phase portrait around the  $w_2$ -axis for systems (2.3.9), we must fix the sign of  $c_2$ , which determines the position of the singular point  $Q_1$  and also the sign of  $\mu + 1$ , which determines the sense of the flow along the  $x$ -axis. Thus, we deal with the following subcases.

**Subcase (a.1).** Let  $\mu < -2$  (so  $\mu + 1 < 0$ ), and  $c_2 > 0$ . Then the singular point  $Q_1$  is on the negative part of the  $w_2$ -axis and the expression  $\dot{u}|_{w_2=0} = c_2(\mu + 1)u$  determines the sense of the flow. The phase portrait is the one in Figure 2.3.3(a).

To return to systems (2.3.8) we multiply by  $u$ , thus the orbits in the second and third quadrants change their orientation. Moreover, all the points on the  $w_2$ -axis become singular points. The resultant phase portrait is given in Figure 2.3.3(b).

When going back to the  $(u, w_1)$ -plane, the second and third quadrants swap from the  $(u, w_2)$ -plane, the exceptional divisor shrinks to a point and hence the orbits are slightly modified. Attending to the expressions  $\dot{u}|_{w_1=0} = c_2(\mu + 1)u^2$  and  $\dot{w}_1|_{u=0} = -c_1w_1^2$ , we know the sense of the flow along the axes. Following Proposition 1.2.6, the separatrix of the singular point  $Q_1$  in the  $(u, w_2)$ -plane, becomes the separatrix with slope  $-c_2/c_1$  at the  $(u, w_1)$ -plane.

The phase portrait around the  $w_1$  is not determined with this blow up, so it is necessary to do a horizontal blow up in systems (2.3.7). We introduce the variable  $w_3 = u/w_1$  and obtain the systems

$$\begin{aligned}\dot{w}_3 &= (2c_0 - a_0)w_3^2w_1^3 + c_3(\mu + 2)w_1^2w_3^2 + c_2(\mu + 2)w_1w_3^2 + c_1(\mu + 2)w_1w_3, \\ \dot{w}_1 &= -c_0w_3w_1^4 - c_3w_3w_1^3 - c_2w_3w_1^2 - c_1w_1^2.\end{aligned}\tag{2.3.11}$$

Eliminating a common factor  $w_1$  we get

$$\begin{aligned}\dot{w}_3 &= (2c_0 - a_0)w_3^2w_1^2 + c_3(\mu + 2)w_1w_3^2 + c_2(\mu + 2)w_3^2 + c_1(\mu + 2)w_3, \\ \dot{w}_1 &= -c_0w_3w_1^3 - c_3w_3w_1^2 - c_2w_3w_1 - c_1w_1.\end{aligned}\tag{2.3.12}$$

The exceptional divisor is the line  $w_1 = 0$ , and the singular points over this line are the origin and the point  $(-c_1/c_2, 0)$ . Under the conditions of this subcase, the origin is a

stable node and the point  $(-c_1/c_2, 0)$  is a semi-hyperbolic saddle, with the configuration given in Figure 2.3.2(a). Now to return to systems (2.3.11) we multiply by  $w_1$  so the orbits in the third and fourth quadrants change their orientation. Moreover, all the points on the  $w_3$ -axis become singular points. The resultant phase portrait is given in Figure 2.3.2(b).

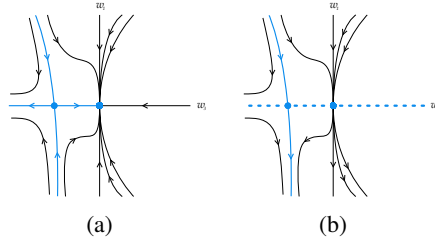


Figure 2.3.2: Horizontal blow up in nondicritical case (1.1).

Going back to the  $(u, w_1)$ -plane, the third and fourth quadrants swap from the  $(w_3, w_1)$ -plane, the exceptional divisor shrinks to a point and the orbits are modified. Attending to the sense of the flow along the axes and following again Proposition 1.2.6, the separatrix of the singular point  $(-c_1/c_2, 0)$  in the  $(w_3, w_1)$ -plane becomes the separatrix with slope  $-c_1/c_2$  at the  $(u, w_1)$ -plane, and now this Proposition determines totally the behavior in all the regions of the plane. We obtain that the phase portrait for systems (2.3.7) is the one given in Figure 2.3.3(c).

Lastly we multiply by  $u$  and undo the first vertical blow up to return to the  $(u, v)$ -plane. We swap the second and the third quadrants and contract the exceptional divisor to the origin. According to Proposition 1.2.6, the orbits tending to the origin in forward or backward time, become orbits tending to the origin in forward or backward time with slope zero, i.e., tangent to the  $u$ -axis. According to the expressions  $\dot{u}|_{v=0} = c_1\mu v^2 - a_0v^3$  and  $\dot{v}|_{v=0} = c_2(\mu + 1)u^3$ , which determine the sense of the flow along the axes, we get the local phase portrait  $L_1$  of Figure 2.3.1 at the origin of systems (2.3.5).

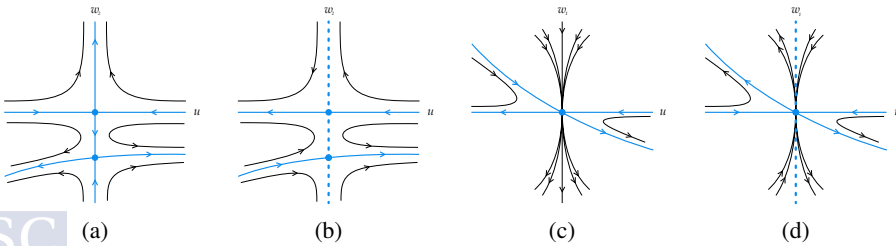


Figure 2.3.3: Desingularization of the origin of systems (2.3.5) with  $c_1 \neq 0$ . Nondicritical case (a.1).

### 2.3 Infinite singular points

**Subcase (a.2).** If we maintain  $\mu < -2$  but take  $c_2 < 0$ , the reasoning is essentially similar to the one we have given in the previous case, and we obtain the phase portrait  $L_2$  of Figure 2.3.1.

**Subcase (a.3).** Let  $\mu > -1$  and  $c_2 > 0$ . This determines the position of singular point  $Q_1$  and the sense of the flow along the axes, so around the  $w_2$ -axis we obtain the phase portrait given in Figure 2.3.4(a).

We multiply by  $u$  obtaining the phase portrait given in Figure 2.3.4(b), as the orbits in the second and third quadrants change their orientation and all the points in the  $w_2$ -axis become singular points.

In order to undo the variable change we analyze the sense of the flow along the axes according to the expressions  $\dot{u}|_{w_1=0} = c_2(\mu + 1)u^2$ , which determines that the flow goes in the positive sense of the  $u$ -axis, and  $\dot{w}_1|_{u=0} = -c_1w_1^2$  which determines that the flow goes in the negative sense of the  $w_1$ -axis. Moreover, we swap the second and third quadrants, and press the exceptional divisor into the origin, modifying the orbits in accordance with Proposition 1.2.6. We obtain the phase portrait given in Figure 2.3.4(c). Multiplying again by  $u$  we obtain the phase portrait 2.3.4(d).

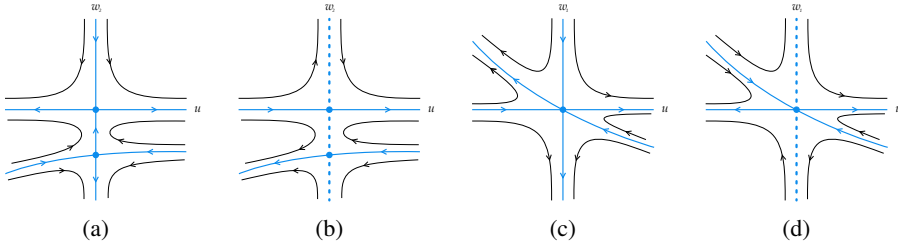


Figure 2.3.4: Desingularization of the origin of systems (2.3.5) with  $c_1 \neq 0$ . Nondicritical case (a.3).

Now we have to undo the second variable change. We note that  $\dot{u}|_{v=0} = c_2(\mu + 1)u^3$ , so the flow gets away from the origin along the  $u$ -axis. Nevertheless, the sense of the flow along the  $v$ -axis is not determined by  $\dot{v}|_{u=0} = c_1\mu v^2 - a_0v^3$ , it depends on the constant  $\mu$ . If  $\mu < 0$ , the flow goes in the negative sense of the  $v$ -axis and the phase portrait is totally determined, obtaining the  $L_4$  in Figure 2.3.1.

In the case with  $\mu = 0$  the phase portrait is not determined around the  $v$ -axis in the third and fourth quadrants, and in the case with  $\mu > 0$  it is not determined around the  $v$ -axis in none of the quadrants. The information we get in both cases is given in Figure 2.3.5, where the non determined regions are shaded in blue. To complete the phase portraits we must do a horizontal blow up. We introduce the variable  $w_4 = u/v$  on systems (2.3.5) obtaining the systems

$$\begin{aligned}\dot{w}_4 &= c_2w_4^3v^2 + c_3w_4^2v^2 + c_0w_4v^2 + c_1w_4v, \\ \dot{v} &= c_2\mu w_4^2v^3 + c_3\mu w_4v^3 - a_0v^3 + c_1\mu v^2.\end{aligned}$$



If we eliminate a common factor  $v$  we get

$$\begin{aligned}\dot{w}_4 &= c_2 w_4^3 v + c_3 w_4^2 v + c_0 w_4 v + c_1 w_4, \\ \dot{v} &= c_2 \mu w_4^2 v^2 + c_3 \mu w_4 v^2 - a_0 v^2 + c_1 \mu v,\end{aligned}\tag{2.3.13}$$

and the only singular point of these systems over the exceptional divisor  $v = 0$  is the origin. If  $\mu > 0$ , it is an unstable node and if  $\mu = 0$ , it is a semi-hyperbolic saddle-node.

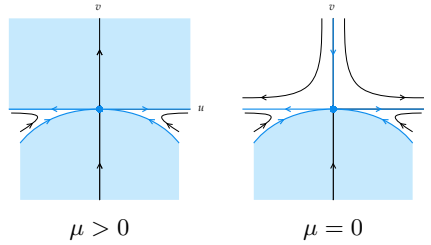


Figure 2.3.5: Information obtained from vertical blow up in nondicritical case (a.3).

We follow the same steps in the two cases, illustrated in Figures 2.3.6 and 2.3.7. We draw the phase portrait for systems (2.3.13) as can be seen in Subfigures (a); then we multiply by  $v$  obtaining phase portraits in Subfigures (b) and lastly we undo the variable change according to Proposition 1.2.6. The phase portraits in the  $(u, v)$ -plane are not determined around the  $u$ -axis in the third and fourth quadrants, i.e., in the regions colored in blue in Subfigures (c), but nevertheless combining this information with the obtained from the vertical blow ups, we can conclude that the phase portrait when  $\mu > 0$  is the  $L_3$  of Figure 2.3.1 and if  $\mu = 0$ , the phase portrait is the  $L_5$ .

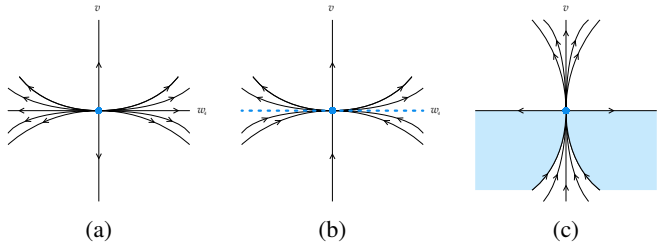


Figure 2.3.6: Horizontal blow up in the nondicritical case (a.3) with  $\mu > 0$ .

**Subcase (a.4).** Let  $\mu > -1$  and  $c_2 < 0$ . By a similar reasoning to the previous one, we obtain the phase portraits  $L_6$  and  $L_7$  of Figure 2.3.1 for  $\mu > 0$  and  $\mu < 0$ , respectively.

- (b) If  $\mu \in (-\infty, -2) \cup (-1, +\infty)$ ,  $c_2(\mu + 2) > 0$  and  $(\mu + 2)(a_0 + c_0\mu) < 0$ , then  $Q_0$  is a saddle and  $Q_1$  a topological unstable node. We must distinguish two cases according to the sign of  $c_2$ .

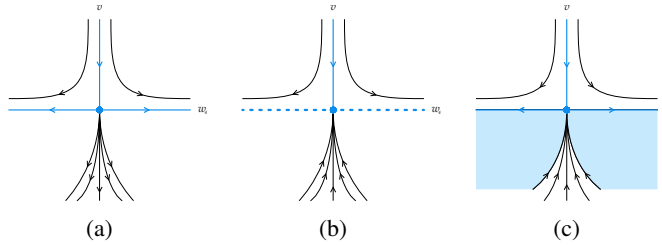


Figure 2.3.7: Horizontal blow up in the nondicritical case (a.3) with  $\mu = 0$ .

**Subcase (b.1).** We consider  $c_2 < 0$ , so  $\mu < -2$  and  $a_0 + c_0\mu > 0$ . The singular point  $Q_1$  is on the positive  $w_2$ -axis and it is an unstable node, so the sense of the flow along the axes is determined, and we obtain the phase portrait given in Figure 2.3.8(a). Multiplying by  $u$  we obtain Figure 2.3.8(b).

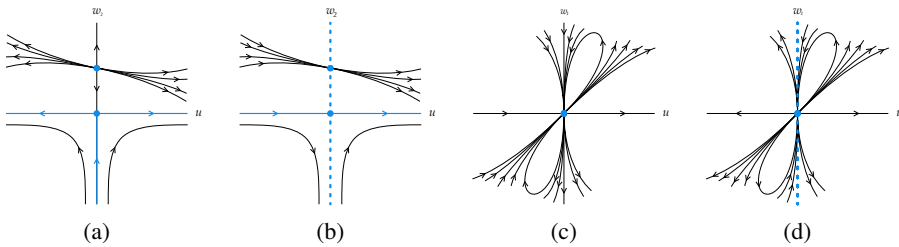


Figure 2.3.8: Desingularization of the origin of systems (2.3.5) with  $c_1 \neq 0$ . Nondicritical case (b.1).

We see that for systems (2.3.7) the flow goes in the negative sense along the  $w_1$ -axis and in the positive sense along the  $u$ -axis, according to the expressions  $\dot{u}|_{w_1=0} = c_2(\mu + 1)u^2$  and  $\dot{w}_1|_{u=0} = -c_1w_1^2$ . If we undo the variable change modifying the orbits in accordance with Proposition 1.2.6, the only information we get is that there are orbits that left the origin in the first quadrant and orbits that arrive to the origin in the third quadrant, all with slope  $-c_2/c_1$ , but also there must exist hyperbolic or elliptic sectors on these quadrants, and this is not well determined and neither is the phase portrait in the second and fourth quadrants. In any case, we would like to point that the determination of whether the sectors in the first and third quadrants are hyperbolic or elliptic can be done by means of index theory applied in the global phase portraits. More detailed explanations will be given in Section 2.4, but roughly speaking, we know that the index of the vector field on the sphere must be 2, and this index is the sum of the indices of all singularities, which depend on the sectors that they have, so if the index is 2 considering two elliptic sectors in a particular singular point, it cannot be 2 if we change those sectors for hyperbolic ones. This argument can be used to conclude in cases in which the only indeterminacy raised from the vertical blow up is of this type.

Here we study the phase portrait with a horizontal blow up. We must introduce the variable  $w_3 = u/w_1$  in systems (2.3.7) as done in subcase (a.1), so we obtain the same systems (2.3.11) and then (2.3.12) by eliminating a common factor  $w_1$ . The singular points over  $w_1 = 0$  are the origin, which is a stable node, and the point  $(-c_1/c_2, 0)$ , which is a semi-hyperbolic unstable node. The phase portrait is given in Figure 2.3.9(a). To return to systems (2.3.11) we multiply by  $w_1$  and obtain 2.3.9(b).

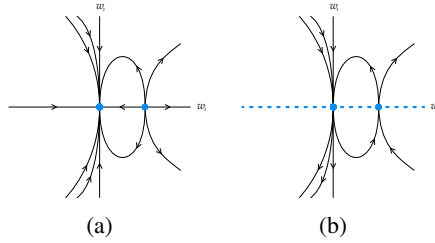


Figure 2.3.9: Horizontal blow up in nondicritical case (b.1).

We can go back from the  $(w_3, w_1)$ -plane to the  $(u, w_1)$ -plane of systems (2.3.7) undoing the variable change according to Proposition 1.2.6. Now the phase portrait is well defined in all the plane and we obtain that the separatrix of the singular point  $(-c_1/c_2, 0)$  in the  $(w_3, w_1)$ -plane, becomes the separatrix with slope  $-c_1/c_2$  at the  $(u, w_1)$ -plane, and the behavior is well determined in all the regions of the plane. We obtain that the phase portrait for systems (2.3.7) is the one given in Figure 2.3.8(c).

Multiplying by  $u$  we obtain the phase portrait in Figure 2.3.8(d) and undoing the first vertical blow up we return to the  $(u, v)$ -plane, concluding that the phase portrait of  $O_1$  is  $L_8$  of Figure 2.3.1.

From now on, we will omit the reasonings about how to undo the variable changes for obtaining the final phase portrait, because they are similar to the ones in the previous cases. The results obtained are the following.

**Subcase (b.2).** Let  $c_2 > 0$ , so  $\mu > -1$  and  $a_0 + c_0\mu < 0$ . We obtain the phase portraits  $L_9$  and  $L_{10}$  of Figure 2.3.1 for  $\mu > 0$  and  $\mu < 0$ , respectively. In  $L_9$  it is possible to consider hyperbolic sectors instead of the elliptic ones, but applying index theory in the global phase portraits obtained in our study, we note that only the phase portrait with elliptic sectors is feasible.

- (c) If  $\mu \in (-\infty, -2) \cup (-1, +\infty)$ ,  $c_2(\mu + 2) < 0$ ,  $(\mu + 2)(a_0 + c_0\mu) > 0$ , then  $Q_0$  is a saddle and  $Q_1$  a topological stable node. If  $c_2 > 0$ , we obtain the phase portrait  $L_{11}$  of Figure 2.3.1, and if  $c_2 < 0$ , we obtain the phase portraits  $L_{12}$ ,  $L_{13}$  and  $L_{14}$  of Figure 2.3.1 for  $\mu > 0$ ,  $\mu < 0$  and  $\mu = 0$ , respectively. In  $L_{11}$  and  $L_{12}$  it would be possible that the elliptic sectors appearing were hyperbolic sectors, but again we have proved in all the global phase portraits that only the elliptic option is feasible according to the index theory.
- (d) If  $c_2 > 0$ ,  $\mu \in (-2, -1)$  and  $a_0 + c_0\mu > 0$ , then  $Q_0$  is a stable node and  $Q_1$  a topological saddle. We obtain the phase portrait  $L_{15}$  of Figure 2.3.1.

- (e) If  $c_2 > 0$ ,  $\mu \in (-2, -1)$  and  $a_0 + c_0\mu < 0$ , then  $Q_0$  is a stable node and  $Q_1$  a topological unstable node. We obtain the phase portrait  $L_{11}$  of Figure 2.3.1.
- (f) If  $c_2 < 0$ ,  $\mu \in (-2, -1)$  and  $a_0 + c_0\mu < 0$ , then  $Q_0$  is an unstable node and  $Q_1$  a topological saddle. We obtain the phase portrait  $L_{16}$  of Figure 2.3.1.
- (g) If  $c_2 < 0$ ,  $\mu \in (-2, -1)$  and  $a_0 + c_0\mu > 0$ , then  $Q_0$  is an unstable node and  $Q_1$  a topological stable node. We obtain the phase portrait  $L_8$  of Figure 2.3.1.

#### Dicritical case

In the dicritical case, i.e., when  $\mu = -2$ , we must work with systems (2.3.10) and studying the singular points on the exceptional divisor. In this case there is only one singular point,  $R = (0, -c_2/c_1)$ . After moving the singular point to the origin, we obtain that the eigenvalues of the linear part are

$$\lambda_1 = \frac{c_2c_3 - c_2\sqrt{c_3^2 + 4c_2(a_0 - 2c_0)}}{2c_1} \quad \text{and} \quad \lambda_2 = \frac{c_2c_3 + c_2\sqrt{c_3^2 + 4c_2(a_0 - 2c_0)}}{2c_1},$$

and the determinant is  $-(c_3^2(a_0 - 2c_0))/c_1^2$ , so it is nonzero according to the hypothesis  $c_2 \neq 0$ ,  $a_0 + c_0\mu \neq 0$ , and so the singular point is non-degenerated. We will study separately the next subcases.

- (a) If  $c_3^2 < -4c_2(a_0 - 2c_0)$  and  $c_2c_3 < 0$ , then  $P$  is a stable focus. We shall distinguish two subcases depending on the sign of the parameter  $c_2$ , because it determines if the singular point is on the positive or negative  $u$ -axis. Let us consider  $c_2 > 0$ . In Figure 2.3.10 the blowing-down process is represented. The phase portrait around the  $u$ -axis is the one given in Figure 2.3.10(a), multiplying by  $u^2$  we obtain (b), undoing the second variable change we obtain (c), multiplying by  $u$  we get (d) and finally, undoing the first variable change we get the phase portrait  $L_{11}$  of Figure 2.3.1. Taking  $c_2 < 0$  and by the same method we obtain the phase portrait  $L_8$  of Figure 2.3.1.

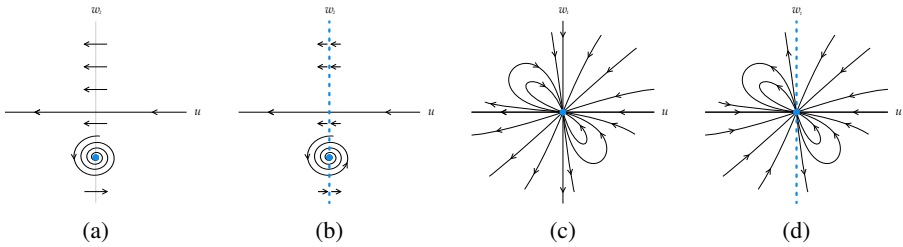


Figure 2.3.10: Desingularization of the origin of systems (2.3.5) with  $c_1 \neq 0$ . Dicritical case (a) with  $c_2 > 0$ .

- (b) If  $c_3^2 < -4c_2(a_0 - 2c_0)$  and  $c_2c_3 > 0$ , then  $P$  is an unstable focus. The reasoning is analogous to the one on the previous case and we obtain the same phase portraits:  $L_{11}$  of Figure 2.3.1 if  $c_2 > 0$  and  $L_8$  if  $c_2 < 0$ .

- (c) If  $c_3^2 = -4c_2(a_0 - 2c_0)$  and  $c_2c_3 < 0$ , or if  $c_2(c_3 - \sqrt{c_3^2 + 4c_2(a_0 - 2c_0)}) < 0$ ,  $c_3^2 > -4c_2(a_0 - 2c_0)$  and  $c_2(c_3 + \sqrt{c_3^2 + 4c_2(a_0 - 2c_0)}) < 0$ , then  $P$  is a stable node. Again, we study the case with  $c_2 > 0$ . The blowing-down process is represented in Figure 2.3.11, specifically, the phase portraits corresponding to systems (2.3.10), (2.3.8), (2.3.7) and (2.3.6).

The final phase portrait obtained is again  $L_{11}$  of Figure 2.3.1. If we consider  $c_2 < 0$  we obtain the phase portrait  $L_8$ .

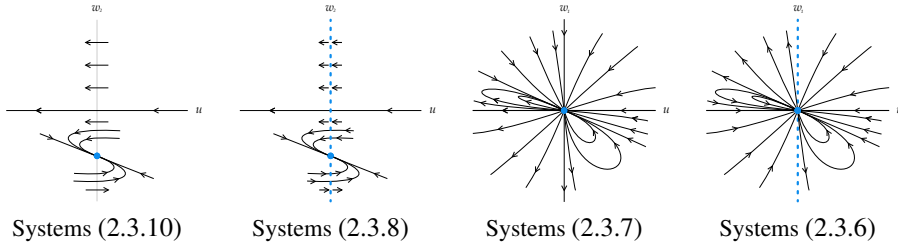


Figure 2.3.11: Desingularization of the origin of systems (2.3.5) with  $c_1 \neq 0$ . Dicritical case (c) with  $c_2 > 0$ .

- (d) If  $c_3^2 = -4c_2(a_0 - 2c_0)$  and  $c_2c_3 > 0$ , or if  $c_2(c_3 - \sqrt{c_3^2 + 4c_2(a_0 - 2c_0)}) > 0$ ,  $c_3^2 > -4c_2(a_0 - 2c_0)$  and  $c_2(c_3 + \sqrt{c_3^2 + 4c_2(a_0 - 2c_0)}) > 0$ , then  $P$  is an unstable node. Analogously to the stable case, we obtain the phase portrait  $L_{11}$  of Figure 2.3.1 if  $c_2 > 0$ , and  $L_8$  if  $c_2 < 0$ .
- (e) If  $c_3^2 > -4c_2(a_0 - 2c_0)$  and  $(c_3 - \sqrt{c_3^2 + 4c_2(a_0 - 2c_0)})(c_3 + \sqrt{c_3^2 + 4c_2(a_0 - 2c_0)}) < 0$ , or if  $c_3 = 0$  and  $c_2(a_0 - 2c_0) > 0$ , then  $P$  is a saddle. The blowing-down considering  $c_2 > 0$  is represented in Figure 2.3.12. The final result is  $L_{17}$  of Figure 2.3.1. If we take  $c_2 < 0$ , we obtain the phase portrait  $L_{18}$ .

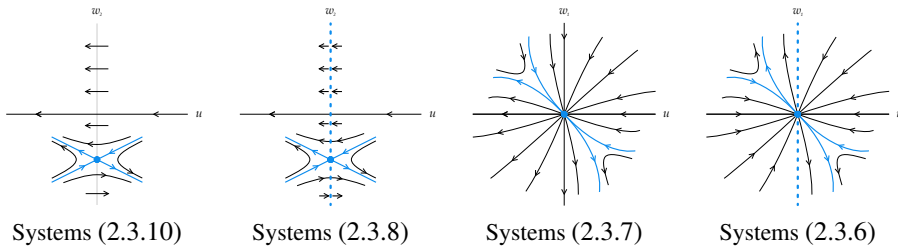


Figure 2.3.12: Desingularization of the origin of systems (2.3.5) with  $c_1 \neq 0$ . Dicritical case (e) with  $c_2 > 0$ .

- (f) If  $c_3 = 0$  and  $c_2(a_0 - 2c_0) < 0$ , then  $P$  is a linear center. In this case, the singular point  $P$  could be a center or a focus. The case with a focus has already been studied in subcases (a) and (b). Let us study now the center case, in particular the one with

$c_2 > 0$ . The blowing-down process is represented in Figure 2.3.13. Finally, we get to the same phase portrait as in the focus case, i.e.,  $L_{11}$  of Figure 2.3.1. In the same way, if we suppose  $c_2 < 0$ , we obtain the phase portrait  $L_8$  of Figure 2.3.1. Therefore, in the case in which  $P$  is a linear center, regardless of whether it is a center or a focus, qualitatively, the phase portrait obtained for  $O_1$  is  $L_{11}$  if  $c_2 > 0$  and  $L_8$  if  $c_2 < 0$ .

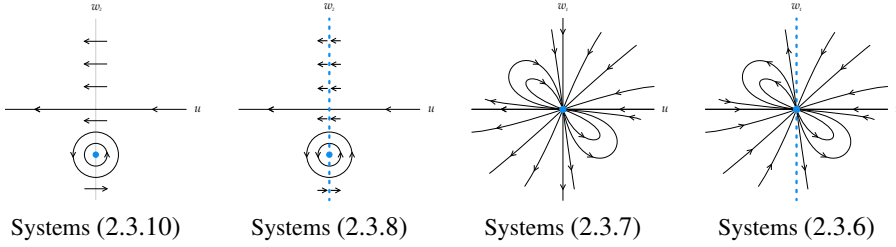


Figure 2.3.13: Desingularization of the origin of systems (2.3.5) with  $c_1 \neq 0$ . Dicritical case (f) with  $c_2 > 0$ .

### 2.3.2 Case $c_1$ zero

We consider systems (2.3.5) and do the same variable change that we do in the case with  $c_1 \neq 0$ . We obtain obviously the systems (2.3.6) but taking  $c_1 = 0$ , i.e.,

$$\begin{aligned} \dot{u} &= (c_0 - a_0)u^3w_1^2 + c_3(\mu + 1)u^3w_1 + c_2(\mu + 1)u^3, \\ \dot{w}_1 &= -c_0u^2w_1^3 - c_3u^2w_1^2 - c_2u^2w_1. \end{aligned}$$

In this case we can cancel a common factor  $u^2$ , getting the systems

$$\begin{aligned} \dot{u} &= (c_0 - a_0)uw_1^2 + c_3(\mu + 1)uw_1 + c_2(\mu + 1)u, \\ \dot{w}_1 &= -c_0w_1^3 - c_3w_1^2 - c_2w_1, \end{aligned} \quad (2.3.14)$$

for which we must study the singular points on the exceptional divisor, i.e., on the straight line  $u = 0$ .

The origin  $S_0 = (0, 0)$  is always a singular point. The other singular points on this line are those for which  $w_1$  is a solution of  $c_0w_1^2 + c_3w_1 + c_2 = 0$  so, if  $c_0 \neq 0$  and  $c_3^2 > 4c_0c_2$ , then

$$S_1 = (0, -(R_c + c_3)/(2c_0)) \quad \text{and} \quad S_2 = (0, (R_c - c_3)/(2c_0))$$

are singular points. If  $c_0 \neq 0$  and  $c_3^2 = 4c_0c_2$ , then

$$S_3 = (0, -c_3/(2c_0))$$

is a singular point, and finally, if  $c_0$  and  $c_3$  are non-zero,

$$S_4 = (0, -c_2/c_3)$$

is a singular point. In summary we shall study the five cases given in Table 2.3.1. For doing this we study separately the local phase portrait of each singular point assuming in each case the necessary hypothesis for its existence.

Case	Conditions	Singular points
(A)	$c_0 = 0, c_3 = 0.$	$S_0.$
(B)	$c_0 = 0, c_3 \neq 0.$	$S_0, S_4.$
(C)	$c_0 \neq 0, c_3^2 < 4c_0c_2.$	$S_0.$
(D)	$c_0 \neq 0, c_3^2 = 4c_0c_2.$	$S_0, S_3.$
(E)	$c_0 \neq 0, c_3^2 > 4c_0c_2.$	$S_0, S_1, S_2.$

Table 2.3.1: Cases according to singular points on the exceptional divisor of systems (2.3.14).

**Lemma 2.3.2.** *The local phase portraits for the singular points of systems (2.3.14) are the following:*

1. *The singular point  $S_0$  is hyperbolic and*
  - *If  $\mu > -1$ , it is a saddle.*
  - *If  $c_2 > 0$  and  $\mu < -1$ , it is a stable node.*
  - *If  $c_2 < 0$  and  $\mu < -1$ , it is an unstable node.*
2. *The singular point  $S_1$  is hyperbolic and*
  - *If  $c_0(a_0 + c_0\mu) < 0$ , it is a saddle.*
  - *If  $c_0 > 0$  and  $(a_0 + c_0\mu) > 0$ , it is a stable node.*
  - *If  $c_0 < 0$  and  $(a_0 + c_0\mu) < 0$ , it is an unstable node.*
3. *The singular point  $S_2$  is hyperbolic and*
  - *If  $c_0(a_0 + c_0\mu)(R_c - c_3) < 0$ , it is a saddle.*
  - *If  $c_0(R_c - c_3) > 0$  and  $(a_0 + c_0\mu) > 0$ , it is a stable node.*
  - *If  $c_0(R_c - c_3) < 0$  and  $(a_0 + c_0\mu) < 0$ , it is an unstable node.*
4. *The singular point  $S_3$  is a semi-hyperbolic saddle-node.*
5. *The singular point  $S_4$  is a hyperbolic saddle if  $c_2 > 0$  and a hyperbolic stable node if  $c_2 < 0$ .*

*Proof.*

1. For the linear part at the origin  $S_0$ , we get the eigenvalues  $\lambda_1 = c_2(\mu + 1)$  and  $\lambda_2 = -c_2$ , so it is hyperbolic and applying Theorem 1.2.1 we get the three possible phase portraits.
2. For the singular point  $S_1$  we get the eigenvalues  $\lambda_1 = (a_0 + c_0\mu)(2c_0c_2 - c_3^2 - c_3R_c)/(2c_0^2)$  and  $\lambda_2 = -R_c(R_c + c_3)/(2c_0)$ . It is immediate from the hypothesis that  $\lambda_2$  is not zero and, if  $\lambda_1$  was zero, then

$$2c_0c_2 - c_3^2 - c_3R_c = 0 \Rightarrow (2c_0c_2 - c_3^2)^2 = c_3^2R_c^2 \Rightarrow 4c_0^2c_2^2 - 4c_0c_2c_3^2 + c_3^4 = c_3^4 - 4c_0c_2c_3^2$$

and so  $4c_0^2c_2^2 = 0$ , which contradicts our hypothesis. We will prove that expressions  $2c_0c_2 - c_3^2 - c_3R_c$  and  $2c_0c_2 - c_3^2 + c_3R_c$  can not be positive. Suppose that  $c_0c_2 > 0$ , so

we have  $c_3^2 - 2c_0c_2 > c_3^2 - 4c_0c_2 > 0$  and then  $2c_0c_2 - c_3^2 < 0$ . If  $2c_0c_2 - c_3^2 - c_3R_c > 0$ , then  $2c_0c_2 - c_3^2 > c_3R_c > 0$  which is a contradiction, so  $2c_0c_2 - c_3^2 - c_3R_c$  must be negative. If  $2c_0c_2 - c_3^2 + c_3R_c > 0$ , then  $2c_0c_2 - c_3^2 > -c_3R_c$  so, in addition to the above we have  $|2c_0c_2 - c_3^2| < c_3R_c$  and squaring we get

$$(2c_0c_2 - c_3^2)^2 < c_3^2R_c^2 \Rightarrow 4c_0^2c_2^2 - 4c_0c_2c_3^2 + c_3^4 < c_3^4 - 4c_0c_2c_3^2 \Rightarrow 4c_0^2c_2^2 < 0$$

reaching again to a contradiction. Let us consider now the case  $c_0c_2 < 0$ . If  $2c_0c_2 - c_3^2 - c_3R_c > 0$ , then  $2c_0c_2 > c_3^2 + c_3R_c > 0$ , which is a contradiction, so again we have  $2c_0c_2 - c_3^2 - c_3R_c < 0$ , and by the same reasoning as in the previous case we conclude again that  $2c_0c_2 - c_3^2 + c_3R_c < 0$ . Thus,  $S_1$  is hyperbolic and applying again Theorem 1.2.1 we get the three possibilities and their corresponding conditions.

3. The reasoning is analogous to the one in the previous case.
4. The singular point  $S_3$  is semi-hyperbolic, and by Theorem 1.2.3 it is always a saddle-node.
5. The singular point  $S_4$  is hyperbolic and by Theorem 1.2.1 it can be a saddle if  $c_2 > 0$  or a stable node if  $c_2 < 0$ .

□

According to Lemma 2.3.2, we obtain the next 26 subcases from the five given in Table 2.3.1.

**Case (A).** The only singular point is the origin, so we have the next three possibilities.

- (A.1) If  $c_0 = c_3 = 0$  and  $\mu > -1$ , then  $S_0$  is a saddle. In order to define totally the phase portrait around the  $w_1$ -axis for systems (2.3.14), we must set the sign of  $c_2$ , which determines the sense of the flow along the axes.

**Subcase (A.1.1).** Considering  $c_2 > 0$ , on the  $v$ -axis the points are attracted towards the origin, and on the  $u$ -axis points are repelled away from the origin, so the phase portrait is the given in Figure 2.3.14(a). Then we have to multiply by  $u^2$ , and so all the points on the  $w_1$ -axis become singular points, getting the phase portrait in Figure 2.3.14(b).

We undo the variable change and verify the sense of the flow along the axes, concluding that the final phase portrait is the  $L_{19}$  given in Figure 2.3.1.

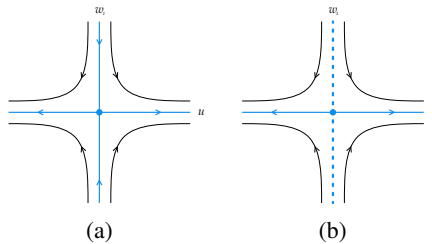


Figure 2.3.14: Desingularization of the origin of systems (2.3.5) with  $c_1 = 0$ . Subcase (A.1.1).



**Subcase (A.1.2).** Considering  $c_2 < 0$ , we obtain the phase portrait  $L_{20}$  of Figure 2.3.1.

(A.2) If  $c_0 = c_3 = 0$ ,  $\mu < -1$  and  $c_2 > 0$ , then  $S_0$  is a stable node. We obtain the phase portrait  $L_{21}$  of Figure 2.3.1.

(A.3) If  $c_0 = c_3 = 0$ ,  $\mu < -1$  and  $c_2 < 0$ , then  $S_0$  is an unstable node. We obtain the phase portrait  $L_{22}$  of Figure 2.3.1.

**Case (B).** Fixed the phase portrait of  $S_4$ , only two phase portraits are possible for the origin, as the sign of  $c_2$  is determined, and so we get the four following cases.

(B.1) If  $c_0 = 0$ ,  $c_3 \neq 0$ ,  $\mu > -1$  and  $c_2 > 0$ , then  $S_0$  and  $S_4$  are both saddle points and  $S_4$  is on the negative  $w_1$ -axis. According to the expression of systems (2.3.14), it is,  $\dot{u}|_{w_1=0} = c_2(\mu+1)u$  and  $\dot{w}_1|_{u=0} = -c_2w_1 - c_3w_1^2 - c_0w_1^3$ , we determine the sense of the flow along the axes. We get the phase portrait given in Figure 2.3.15(a). Multiplying by  $u^2$  we obtain the phase portrait in Figure 2.3.15(b), in which all the points on the  $w_1$ -axis are singular points. Now we undo the blow up according to the expression of systems (2.3.5) and Proposition 1.2.6. The separatrix of the saddle  $S_4$  which is not on the axes, become a separatrix on the second and fourth quadrants passing through the origin. The hyperbolic sector on the first quadrant remains the same, and the one on the second quadrant moves to the third quadrant. On second and fourth quadrants we have got two different sectors, in one of them remains the hyperbolic sector and in the other, colored in blue in Figure 2.3.15(c), the phase portrait is not defined.

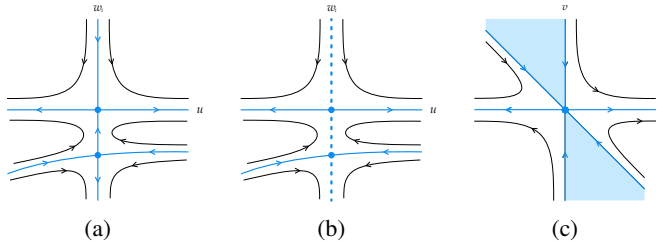


Figure 2.3.15: Desingularization of the origin of systems (2.3.5) with  $c_1 = 0$ . Case (B.1).

We do a horizontal blow up introducing the variable  $w_5 = u/v$  in systems (2.3.5), obtaining

$$\begin{aligned}\dot{w}_5 &= c_2w_5^3v^2 + c_3w_5^2v^2 + c_0w_5v^2, \\ \dot{v} &= c_2\mu w_5^2v^3 + c_3\mu w_5v^3 - a_0v^3,\end{aligned}$$

and eliminating a common factor  $v^2$  we get

$$\begin{aligned}\dot{w}_5 &= c_2w_5^3 + c_3w_5^2 + c_0w_5, \\ \dot{v} &= c_2\mu w_5^2v + c_3\mu w_5v - a_0v.\end{aligned}$$

The only singular point on the exceptional divisor  $v = 0$  is the origin which is a semi-hyperbolic saddle-node as represented in Figure 2.3.16(a). If we multiply by  $v^2$  the phase portrait is the same but with a line of singular points on the  $w_5$ -axis as shown in Figure 2.3.16(b). Now undoing the blow up there are also some regions where the phase portrait is not defined, but combining the information we get here, included in Figure 2.3.16(c) with the obtained previously in the vertical blow up, given in Figure 2.3.15(c), we can conclude that the phase portrait for  $O_1$  is  $L_{23}$  of Figure 2.3.1.

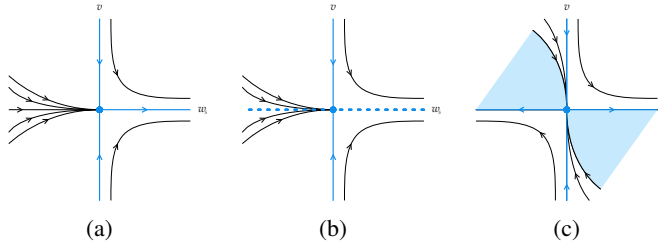


Figure 2.3.16: Horizontal blow up in the case (B.1).

- (B.2)** If  $c_0 = 0$ ,  $c_3 \neq 0$ ,  $\mu > -1$  and  $c_2 < 0$ , then  $S_0$  is a saddle and  $S_4$  a stable node. We obtain the phase portrait  $L_{24}$  of Figure 2.3.1.
- (B.3)** If  $c_0 = 0$ ,  $c_3 \neq 0$ ,  $\mu < -1$  and  $c_2 > 0$ , then  $S_0$  is a stable node and  $S_4$  is a saddle. We obtain the phase portrait  $L_{25}$  of Figure 2.3.1.
- (B.4)** If  $c_0 = 0$ ,  $c_3 \neq 0$ ,  $\mu < -1$  and  $c_2 < 0$ , then  $S_0$  is an unstable node and  $S_4$  is a stable node. We obtain the phase portrait  $L_{26}$  of Figure 2.3.1.

**Case (C).** The only singular point is the origin so we distinguish three cases, and obtain the same local phase portrait that in case (A), but under different conditions.

- (C.1)** If  $c_0 \neq 0$ ,  $c_3^2 < 4c_0c_2$  and  $\mu > -1$ , then  $S_0$  is a saddle. Attending to the sign of  $c_2$ , which determines the sense of the flow on the axes, we consider the following subcases: If  $c_2 > 0$ , we obtain the phase portrait  $L_{19}$  of Figure 2.3.1, and if  $c_2 < 0$ , we obtain the phase portrait  $L_{20}$  of Figure 2.3.1.
- (C.2)** If  $c_0 \neq 0$ ,  $c_3^2 < 4c_0c_2$ ,  $\mu < -1$  and  $c_2 > 0$ , then  $S_0$  is a stable node. We obtain the phase portrait  $L_{21}$  of Figure 2.3.1.
- (C.3)** If  $c_0 \neq 0$ ,  $c_3^2 < 4c_0c_2$ ,  $\mu < -1$  and  $c_2 < 0$ , then  $S_0$  is an unstable node. We obtain the phase portrait  $L_{22}$  of Figure 2.3.1.

**Case (D).** Apart from the origin, there exists the singular point  $S_3$ , which is always a saddle node, regardless of the conditions, so again we get only three subcases:

- (D.1)** If  $c_0 \neq 0$ ,  $c_3^2 = 4c_0c_2$  and  $\mu > -1$ , then  $S_0$  is a saddle and  $S_3$  is a saddle-node. We must distinguish four subcases according to the signs of  $c_0$  and  $a_0 + c_0\mu$ , which determine the position of the saddle-node  $S_3$  and its sectors. If  $c_0 > 0$  and  $a_0 + c_0\mu > 0$ , we obtain the phase portrait  $L_{27}$  of Figure 2.3.1; if  $c_0 > 0$  and  $a_0 + c_0\mu < 0$ , the phase portrait  $L_{28}$  of Figure 2.3.1; if  $c_0 < 0$  and  $a_0 + c_0\mu > 0$ , the phase portrait  $L_{29}$  and if  $c_0 < 0$  and  $a_0 + c_0\mu < 0$ , the phase portrait  $L_{30}$ .
- (D.2)** If  $c_0 \neq 0$ ,  $c_3^2 = 4c_0c_2$ ,  $\mu < -1$  and  $c_2 > 0$ , then  $S_0$  is a stable node and  $S_3$  is a saddle-node. We distinguish two subcases setting the sign of  $a_0 + c_0\mu$  which determines the position of the sectors of the saddle-node  $S_3$ . If  $a_0 + c_0\mu > 0$ , we obtain the phase portrait  $L_{31}$  of Figure 2.3.1, and if  $a_0 + c_0\mu < 0$ , we obtain the phase portrait  $L_{32}$  of Figure 2.3.1.
- (D.3)** If  $c_0 \neq 0$ ,  $c_3^2 = 4c_0c_2$ ,  $\mu < -1$  and  $c_2 < 0$ , then  $S_0$  is an unstable node and  $S_3$  is a saddle-node. The only possibility is that  $a_0 + c_0\mu > 0$ , so there are no subcases, and we obtain the phase portrait  $L_{33}$  of Figure 2.3.1.

**Case (E).** There exist three singular points, with three possible phase portraits for each of them, however, many of the combinations are not possible, and only 13 subcases will be feasible.

First, due to the conditions which define the local phase portrait in each singular point, it is obvious that if  $S_1$  is a stable node, then  $S_2$  can not be an unstable node, and if  $S_1$  is an unstable node,  $S_2$  can not be a stable node, due to the sign of  $a_0 + c_0\mu$ .

If  $S_0$  and  $S_2$  were stable nodes and  $S_1$  a saddle, the conditions  $c_2 > 0$ ,  $R_c - c_3 < 0$ , and  $c_0 < 0$  will hold. Squaring both terms in the condition  $R_c < c_3$  we obtain  $c_3^2 - 4c_0c_2 < c_3^2$ , and then  $c_0c_2 > 0$ , which is a contradiction. The same reasoning is valid in the next two cases. If  $S_0$  and  $S_2$  are unstable nodes and  $S_1$  a saddle, then the conditions  $c_2 < 0$ ,  $R_c - c_3 < 0$  and  $c_0 > 0$  hold, and if  $S_0$  is an unstable node,  $S_1$  a stable node and  $S_2$  a saddle, then the same three conditions hold.

If  $S_0$ ,  $S_1$  and  $S_2$  are stable nodes, the conditions  $c_2 > 0$ ,  $R_c - c_3 > 0$  and  $c_0 > 0$  hold. Now we take condition  $R_c < c_3$  and squaring both terms we obtain  $c_3^2 - 4c_0c_2 < c_3^2$ , and then  $c_0c_2 > 0$ , which is now a contradiction.

If  $S_0$  is a stable node and  $S_1$  an unstable node, the conditions  $\mu < -1$ ,  $c_0 < 0$  and  $a_0 + c_0\mu < 0$  hold. Then according to the signs of  $c_0$  and  $\mu$  which are fixed,  $a_0 < -c_0\mu < 0$  which contradicts the hypothesis  $H_2^1$ . The same reasoning is valid if  $S_0$  and  $S_1$  are unstable nodes, because the same conditions hold. Now we will study the feasible cases.

- (E.1)** If  $c_0 \neq 0$ ,  $c_3^2 > 4c_0c_2$ ,  $\mu > -1$ ,  $c_0(a_0 + c_0\mu)(2c_0c_2 - c_3^2 - c_3R_c) > 0$  and  $c_0(a_0 + c_0\mu)(R_c - c_3)(2c_0c_2 - c_3^2 + c_3R_c) > 0$ , then  $S_0$ ,  $S_1$  and  $S_2$  are saddles. We must distinguish two subcases depending on the position of singular points  $S_1$  and  $S_2$  on the  $w_1$ -axis. First, if  $S_1$  is on the negative  $w_1$ -axis and  $S_2$  on the positive  $w_1$ -axis, which corresponds with conditions  $c_0 > 0$ ,  $R_c - c_3 > 0$  and  $c_2 < 0$ , we obtain the phase portrait  $L_{34}$  of Figure 2.3.1. Note that if  $R_c - c_3 > 0$ , the singular points  $S_1$  and  $S_2$  are one on the positive part of the axis and other on the negative part, and in any case, the absolute value of the second coordinate of  $S_1$  is greater or equal than the absolute value

of the second coordinate of  $S_2$ , and this determines the relation between the slopes of the orbits in the phase portraits.

Conversely, if we have  $S_1$  on the positive  $w_1$ -axis and  $S_2$  on the negative one, i.e., under conditions  $c_0 < 0$ ,  $R_c - c_3 > 0$  and  $c_2 > 0$ , we obtain the phase portrait  $L_{35}$  of Figure 2.3.1.

- (E.2) If  $c_0 \neq 0$ ,  $c_3^2 > 4c_0c_2$ ,  $\mu > -1$ ,  $c_0(a_0 + c_0\mu)(2c_0c_2 - c_3^2 - c_3R_c) > 0$ ,  $c_0(R_c - c_3) > 0$  and  $(a_0 + c_0\mu)(2c_0c_2 - c_3^2 + c_3R_c) < 0$ , then  $S_0$  and  $S_1$  are saddles and  $S_2$  is a stable node. If  $c_0 > 0$  then  $R_c - c_3 > 0$  and so  $c_3^2 - 4c_0c_2 > c_3^2$  and  $c_0c_2 < 0$ . If  $a_0 + c_0\mu > 0$  then  $2c_0c_2 - c_3^2 - c_3R_c > 0$  which is not possible because  $2c_0c_2 < 0$  and we subtract two positive terms. Conversely, if  $a_0 + c_0\mu < 0$ , then  $2c_0c_2 - c_3^2 < c_3R_c$  and  $2c_0c_2 - c_3^2 > -c_3R_c$ , so  $|2c_0c_2 - c_3^2| < c_3R_c$ . Squaring we get  $4c_0^2c_2^2 < 0$  which is not possible. If  $c_0 < 0$ , then  $R_c - c_3 < 0$  and we deduce  $c_2 < 0$ . If  $a_0 + c_0\mu < 0$  then  $2c_0c_2 - c_3^2 - c_3R_c > 0$ , but  $c_3^2 - 2c_0c_2 > c_3^2 - 4c_0c_2 > 0$ , so  $2c_0c_2 - c_3^2 < 0$  and subtracting  $c_3R_c > 0$  the result can not be positive.

In conclusion we deduce that  $c_0, c_2 < 0$  and  $a_0 + c_0\mu > 0$ . Hence we have  $-(R_c + c_3)/(2c_0) > (R_c - c_3)/(2c_0) > 0$ . This determines the only possible position of singular points which are both in the positive  $w_1$ -axis,  $S_1$  under  $S_2$ . Undoing the blow up we obtain the phase portrait  $L_{36}$  of Figure 2.3.1.

- (E.3) If  $c_0 \neq 0$ ,  $c_3^2 > 4c_0c_2$ ,  $\mu > -1$ ,  $c_0(a_0 + c_0\mu)(2c_0c_2 - c_3^2 - c_3R_c) > 0$ ,  $c_0(R_c - c_3) < 0$  and  $(a_0 + c_0\mu)(2c_0c_2 - c_3^2 + c_3R_c) > 0$ , then  $S_0$  and  $S_1$  are saddles and  $S_2$  is an unstable node. Therefore we deduce that  $0 > (R_c - c_3)/2c_0 > -(R_c + c_3)/2c_0$ , so both singular points are on the negative  $w_1$  axis,  $S_1$  under  $S_2$ . We obtain the phase portrait  $L_{37}$  of Figure 2.3.1.

- (E.4) If  $c_0 \neq 0$ ,  $c_3^2 > 4c_0c_2$ ,  $\mu > -1$ ,  $c_0 > 0$ ,  $(a_0 + c_0\mu)(2c_0c_2 - c_3^2 - c_3R_c) < 0$  and  $c_0(R_c - c_3)(a_0 + c_0\mu)(2c_0c_2 - c_3^2 + c_3R_c) > 0$ , then  $S_0$  and  $S_2$  are saddles and  $S_1$  is a stable node. Then we deduce that  $-(R_c + c_3)/2c_0 < (R_c - c_3)/2c_0 < 0$ , so both singular points are on the negative  $w_1$  axis,  $S_1$  under  $S_2$ . We obtain the phase portrait  $L_{38}$  of Figure 2.3.1.

- (E.5) If  $c_0 \neq 0$ ,  $c_3^2 > 4c_0c_2$ ,  $\mu > -1$ ,  $c_0 > 0$ ,  $(a_0 + c_0\mu)(2c_0c_2 - c_3^2 - c_3R_c) < 0$ ,  $c_0(R_c - c_3) > 0$  and  $(a_0 + c_0\mu)(2c_0c_2 - c_3^2 + c_3R_c) < 0$ , then  $S_0$  is a saddle and  $S_1$  and  $S_2$  are stable nodes. We obtain the phase portrait  $L_{45}$  of Figure 2.3.1.

- (E.6) If  $c_0 \neq 0$ ,  $c_3^2 > 4c_0c_2$ ,  $\mu > -1$ ,  $c_0 < 0$ ,  $(a_0 + c_0\mu)(2c_0c_2 - c_3^2 - c_3R_c) > 0$  and  $(a_0 + c_0\mu)(R_c - c_3)(2c_0c_2 - c_3^2 + c_3R_c) < 0$ , then  $S_0$  and  $S_2$  are saddles and  $S_1$  is an unstable node. Hence we deduce that  $0 < (R_c - c_3)/2c_0 < -(R_c + c_3)/2c_0$ , so both singular points are on the positive  $w_1$  axis,  $S_2$  under  $S_1$ . We obtain the phase portrait  $L_{47}$  of Figure 2.3.1.

- (E.7) If  $c_0 \neq 0$ ,  $c_3^2 > 4c_0c_2$ ,  $\mu > -1$ ,  $c_0 < 0$ ,  $(a_0 + c_0\mu)(2c_0c_2 - c_3^2 - c_3R_c) > 0$ ,  $R_c - c_3 > 0$  and  $(a_0 + c_0\mu)(2c_0c_2 - c_3^2 + c_3R_c) > 0$ , then  $S_0$  is a saddle and  $S_1$  and  $S_2$  are unstable nodes. We obtain the phase portrait  $L_{46}$  of Figure 2.3.1.

- (E.8) If  $c_0 \neq 0$ ,  $c_3^2 > 4c_0c_2$ ,  $c_2 > 0$ ,  $\mu < -1$ ,  $c_0(a_0 + c_0\mu)(2c_0c_2 - c_3^2 - c_3R_c) > 0$  and  $c_0(a_0 + c_0\mu)(R_c - c_3)(2c_0c_2 - c_3^2 + c_3R_c) > 0$ , then  $S_0$  is a stable node and  $S_1$  and  $S_2$  are saddles. We obtain the phase portrait  $L_{39}$  of Figure 2.3.1.
- (E.9) If  $c_0 \neq 0$ ,  $c_3^2 > 4c_0c_2$ ,  $c_2 > 0$ ,  $\mu < -1$ ,  $c_0(a_0 + c_0\mu)(2c_0c_2 - c_3^2 - c_3R_c) > 0$ ,  $c_0(R_c - c_3) < 0$  and  $(a_0 + c_0\mu)(2c_0c_2 - c_3^2 + c_3R_c) > 0$ , then  $S_0$  is a stable node,  $S_1$  is a saddle and  $S_2$  is an unstable node. We obtain the phase portrait  $L_{40}$  of Figure 2.3.1.
- (E.10) If  $c_0 \neq 0$ ,  $c_3^2 > 4c_0c_2$ ,  $c_2 > 0$ ,  $\mu < -1$ ,  $c_0 > 0$ ,  $(a_0 + c_0\mu)(2c_0c_2 - c_3^2 - c_3R_c) < 0$  and  $(a_0 + c_0\mu)(R_c - c_3)(2c_0c_2 - c_3^2 + c_3R_c) > 0$ , then  $S_0$  and  $S_1$  are stable nodes and  $S_2$  is a saddle. We obtain the phase portrait  $L_{41}$  of Figure 2.3.1.
- (E.11) If  $c_0 \neq 0$ ,  $c_3^2 > 4c_0c_2$ ,  $c_2 < 0$ ,  $\mu < -1$ ,  $c_0(a_0 + c_0\mu)(2c_0c_2 - c_3^2 - c_3R_c) > 0$  and  $c_0(a_0 + c_0\mu)(R_c - c_3)(2c_0c_2 - c_3^2 + c_3R_c) > 0$ , then  $S_0$  is an unstable node and  $S_1$  and  $S_2$  are saddles. We obtain the phase portrait  $L_{42}$  of Figure 2.3.1.
- (E.12) If  $c_0 \neq 0$ ,  $c_3^2 > 4c_0c_2$ ,  $c_2 < 0$ ,  $\mu < -1$ ,  $c_0(a_0 + c_0\mu)(2c_0c_2 - c_3^2 - c_3R_c) > 0$ ,  $c_0(R_c - c_3) > 0$  and  $(a_0 + c_0\mu)(2c_0c_2 - c_3^2 + c_3R_c) < 0$ , then  $S_0$  is an unstable node,  $S_1$  is a saddle and  $S_2$  is a stable node. We obtain the phase portrait  $L_{43}$  of Figure 2.3.1.
- (E.13) If  $c_0 \neq 0$ ,  $c_3^2 > 4c_0c_2$ ,  $c_2 < 0$ ,  $\mu < -1$ ,  $c_0 > 0$ ,  $(a_0 + c_0\mu)(2c_0c_2 - c_3^2 - c_3R_c) < 0$ ,  $R_c - c_3 > 0$ ,  $(a_0 + c_0\mu)(2c_0c_2 - c_3^2 + c_3R_c) < 0$ , then  $S_0$  is an unstable node and  $S_1$  and  $S_2$  are stable nodes. We obtain the phase portrait  $L_{44}$  of Figure 2.3.1.

Note that in phase portraits  $L_{22}$ ,  $L_{30}$ ,  $L_{33}$ ,  $L_{43}$ ,  $L_{46}$  and  $L_{47}$  of Figure 2.3.1 it is possible to consider hyperbolic sectors instead of the elliptic ones, but we have only represented the elliptic cases by the same reason given before for phase portraits  $L_8$ ,  $L_9$ ,  $L_{11}$  and  $L_{12}$ , i.e., because applying index theory to the phase portraits in the sphere  $\mathbb{S}^2$  described in Section 2.4, we prove that they are the only feasible.

Completed the study in the local chart  $U_1$ , we address the study of the origin of chart  $U_2$  which turned out to be much simpler. The systems in this chart have the expression

$$\begin{aligned} \dot{u} &= -c_1(\mu + 1)u^2v + (a_0 - c_0)uv^2 - c_3(\mu + 1)uv - c_2(\mu + 1)u, \\ \dot{v} &= -c_1uv^2 - c_0v^3 - c_3v^2 - c_2v. \end{aligned} \quad (2.3.15)$$

**Lemma 2.3.3.** *Assuming hypothesis  $H_2^1$ , the origin of chart  $U_2$  is an infinite singular point of systems (2.0.1). It is a saddle if  $\mu < -1$ , a stable node if  $c_2 > 0$  and  $\mu > -1$ , and an unstable node if  $c_2 < 0$  and  $\mu > -1$ .*

*Proof.* It is clear that the origin is a singular point of systems (2.3.15), and we denote it by  $O_2$ . The eigenvalues of the linear part at  $O_2$  are  $\lambda_1 = -c_2(\mu + 1)$  and  $\lambda_2 = -c_2$ , which are both non-zero, so the singular point is hyperbolic. By Theorem 1.2.1 we get the three possible phase portraits and the conditions defining them.  $\square$

## 2.4 Global phase portraits

Our aim in this section is to give the topological classification of all the global phase portraits of systems (2.0.1) by proving Theorem 2.0.1. To this end we bring together the local information obtained in the previous sections. We start our classification from cases in Tables 2.2.2 to 2.2.7. In some of them the conditions determine only one local phase portrait in each one of the infinite singular points but, in many others, we shall distinguish several possibilities. In some cases the local information gives rise to only one global phase portrait, this occurs when the separatrices can be connected in only one way, but in other cases several global possibilities appear, and we shall prove which of them are feasible.

In Table 2.4.1 we give, for each case of the Tables 2.2.2 to 2.2.7, the local phase portrait of the infinite singularities  $O_1$  and  $O_2$  (in most cases it depends on the parameters), and also the global phase portrait on the Poincaré disk obtained. Now we detail the reasonings in some cases, although they will not be showed in all cases to avoid repetitions.

We recall that we are denoting the origins of charts  $U_1$  and  $U_2$  as  $O_1$  and  $O_2$  respectively, and in this section, to simplify the explanations, we will denote by  $Q_1$  the origin of chart  $V_1$  and by  $Q_2$  the origin of  $V_2$ .

### 2.4.1 Cases with a totally-determined local phase portrait at infinity

First, we show an example of how to proceed in those cases where all local phase portraits of the singular points, both finite and infinite, are fully determined, and where, in addition, the separatrices can only be connected in one way.

**Case 1.2.** We must combine the local information to get the global phase portrait. The infinite singular point  $O_1$  has the local phase portrait  $L_3$  given in Figure 2.3.1, and  $O_2$  is a stable node. Regarding the finite singular points, in this case the systems have an unstable node  $P_2$  which is on the negative  $z$ -axis and a saddle  $P_4$  which is on the positive  $x$ -axis. The origin is a saddle-node and by the local configuration of the other singular points we can conclude that it has the three separatrices over the axes which connect with the singular points  $Q_1$ ,  $P_2$  and  $P_4$ . Also we know that the part of the  $x$ -axis which connects  $P_4$  with  $O_1$  is a separatrix. Apart from those, the systems have two separatrices which arrive at  $Q_1$  from the second and third quadrants, respectively, and two separatrices leaving the singular point  $P_4$  on the first and fourth quadrants, respectively, as can be seen in Figure 2.4.1.

There is only one possible connection for these separatrices: the ones that leave  $P_4$  go to  $O_2$  and  $Q_2$ , respectively; the separatrix that arrives to  $Q_1$  in the second quadrant comes from the origin and the one that arrives to  $Q_1$  from the third quadrant comes from the node  $P_2$ . Then we obtain phase portrait G2 in Figure 2.4.10, which has 19 separatrices and 6 canonical regions.

With the same reasonings we can obtain the global phases portraits in the following cases: 1.3 with  $\mu > -1$ ; 1.4; 1.7 with  $\mu > -1$  or  $\mu < -2$ ; 1.8; 1.12 with  $\mu > -1$ ; 1.13; 1.14; 1.16 with  $\mu > -1$ ; 1.18 with  $\mu < -2$ ; 1.20; 2.3 with  $\mu > -1$ ; 2.4; 2.5; 2.6 with  $c_1 = 0$  and  $\mu < -1$ ; 2.8; 2.9; 2.10; 3.2 with  $\mu \in (-1, 0)$ ; 3.4 with  $\mu < -2$ ; 3.5 with  $\mu \in (-1, 0)$ ; 3.7 with  $\mu > -1$ ; 3.8; 3.9; 4.1 with  $\mu = 0$  or with  $c_1 = 0$ ,  $\mu > -1$  and  $a_0 + c_0\mu > 0$ ; 4.2 with  $c_1 = 0$ ,  $\mu < -1$  and  $a_0 + c_0\mu > 0$ ; 4.3 with  $\mu > -1$ ; 4.4; 5.1 with  $\mu > -1$ ; 5.3 with  $\mu > -1$ ; 5.4 with  $\mu > -1$ ; 5.5; 6.1 with  $\mu > -1$ ; and 6.2.

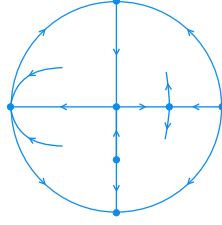


Figure 2.4.1: Separatrices provided by local information in case 1.2.

### 2.4.2 Cases with undetermined sectors at infinity

Here we give an example of how we deal with the cases in which there are infinite singular points whose local phase portrait is not totally determined in the results obtained by mean of the blow up technique. In these cases, the indeterminacy comes from the fact that some sectors could be either elliptic or hyperbolic. We apply the index theory introduced in Section 1.6 to show that only one of the options is possible.

**Case 1.1.** The infinite singular point  $O_1$  has the local phase portrait  $L_{12}$  given in Figure 2.3.1, and  $O_2$  is an unstable node. As we said in Section 2.3, the elliptic sectors appearing in phase portrait  $L_{12}$  could be hyperbolic sectors if we attend only to local results, but now having all the global information we can prove that they are elliptic by using index theory. By Theorem 1.6.1, the sum of the indices of all the singular points on the Poincaré sphere has to be 2. To compute this sum, we must consider that the finite singular points on the Poincaré disk appear twice on the sphere (on the northern hemisphere and on the southern hemisphere). Thus, if we denote  $ind_F$  the sum of the indices of finite singular points, and  $ind_I$  the sum of the indices of infinite singular points on the Poincaré disk, the equality  $2ind_F + ind_I = 2$  must be satisfied.

In this particular case, the finite singular points are a saddle-node, whose index is 0, and two saddles, whose index is -1, so  $ind_F = -2$ . We deduce that  $ind_I$  must be 6. The infinite singular points are  $O_1$  and  $O_2$ , the origins of the local charts  $U_1$  and  $U_2$ , and the origins of the symmetric local charts  $V_1$  and  $V_2$ , which have the same index. Since  $O_2$  is a node, and so it has index 1, we get that the sum of the indices of  $O_2$  and its symmetric must be 4, i.e., the index of  $O_2$  has to be 2. From the Poincaré formula for the index given in Section 1.6, we get

$$\frac{e-h}{2} + 1 = 2 \Rightarrow e-h = 2.$$

Hence only the case with the elliptic sectors on the local phase portrait  $L_{12}$  is possible, because if we had two hyperbolic sectors instead of the elliptic ones, the index of  $O_2$  would be zero.

Once determined the local phase portraits, by analyzing the possible connection of the separatrices we get that in this case 1.1 there is only one possible phase portrait on the Poincaré disk, which is G1 in Figure 2.4.10.

We recall that by an analogous application of index theory in the corresponding cases, it

can be concluded that elliptic sectors appearing on local phase portraits  $L_8, L_9, L_{11}, L_{22}, L_{30}, L_{33}, L_{43}, L_{46}$  and  $L_{47}$  of  $O_1$  are indeed elliptic rather than hyperbolic.

Then, this kind of arguments based on the index of the singular points allow us to complete the proof and determine the global phase portraits in the following cases: 1.1; 1.3 with  $\mu < -1$ ; 1.5; 1.7 with  $\mu < -1$ ; 1.9; 1.11; 1.12 with  $\mu < -1$ ; 1.15; 1.16 with  $\mu < -1$ ; 2.1; 2.3 with  $c_1 = 0$ , and  $\mu < -1$ ; 3.1; 3.2 with  $\mu < -1$ ; 3.5 with  $\mu < -1$ ; 3.6; 3.7 with  $\mu < -1$ ; 4.1 with  $c_1 = 0$  and  $\mu < -1$ ; 4.3 with  $c_1 = 0$  and  $\mu < -1$ ; 5.1 with  $\mu < -1$ ; 5.2; 5.3 with  $\mu < -1$ ; 5.4 with  $\mu < -1$ ; 6.1 with  $c_1 = 0$  and  $\mu < -1$ .

### 2.4.3 Cases with three possible global phase portraits

Here we focus on cases in which the separatrices can be connected in three different forms based on the local information obtained in the previous sections.

**Case 1.6.** In this case  $O_1$  has the local phase portrait  $L_3$  and  $O_2$  is a stable node. From the local results we can obtain three possible global phase portraits, given in Figure 2.4.2.

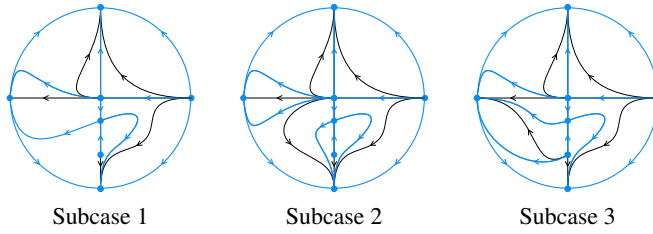


Figure 2.4.2: Possible global phase portraits in case 1.6.

By Theorem 2.1.10, on the straight lines  $z = z_0 \neq 0$  cannot be more than one contact point, but as it is shown in Figure 2.4.3, if subcases 1 and 2 are feasible, there exist straight lines  $z = z_0$  with  $-(R_c + c_3)/(2c_2) < z_0 < (R_c - c_3)/(2c_2)$  on which there exist two contact points, so we deduce that the only possible global phase portrait is the subcase 3, i.e., G10 of Figure 2.4.10.

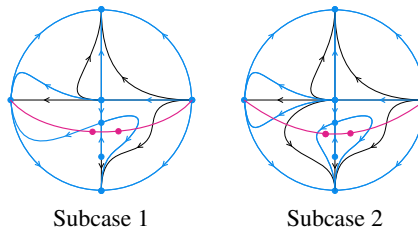


Figure 2.4.3: Straight lines with two contact points on the two first subcases of 1.6.

**Case 1.10.** In this case  $O_1$  has the local phase portrait  $L_6$  and  $O_2$  is an unstable node. From the local results we can obtain three possible global phase portraits, but in two of them shown



in Figure 2.4.4, we can find straight lines  $z = z_0 \neq 0$  with  $(R_c - c_3)/(2c_2) < z_0 < -(R_c + c_3)/(2c_2)$ , on which there are two contact points, so according to Theorem 2.1.10 they are not possible. Then, the only possibility is the phase portrait G20 of Figure 2.4.10.

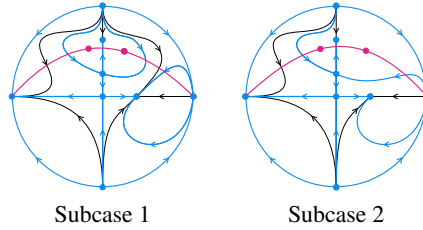


Figure 2.4.4: Lines with two contact points on two subcases of 1.10.

**Case 2.2.** In this case  $O_1$  has the local phase portrait  $L_{47}$  and  $O_2$  is an unstable node. We must use index theory, as in the previous section, to determine some sectors at infinity, obtaining that they are elliptic. Then, from the local results and applying Corollary 2.1.4 which states that the phase portrait is symmetric, we obtain three possible global phase portraits, the ones given in Figure 2.4.5. Note that if we were not guaranteed that the phase portraits are symmetric, there would be a total of nine possible connections for the separatrices.

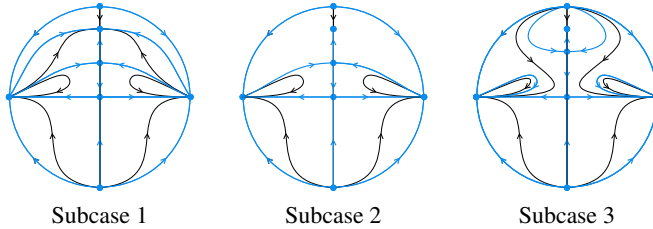


Figure 2.4.5: Possible global phase portraits in case 2.2.

By Theorem 2.1.10 we know that, under the conditions of this case, two invariant lines  $z = (R_c - c_3)/2c_2$  and  $z = -(R_c + c_3)/2c_2$  must exist, and it is only possible on subcase 1, which provides the phase portrait G42 of Figure 2.4.10.

**Case 2.6.** Here we distinguish three subcases and, in two of them, three global phase portraits appear, but in each case we use different arguments to prove which of the options is realizable.

If  $\mu = 0$ , then  $O_1$  has the local phase portrait  $L_5$  and  $O_2$  is a stable node. We obtain three phase portraits, but we conclude that two of them are not feasible because we can find straight lines  $z = z_0 \neq 0$  with two contact points, as it is shown in Figure 2.4.6. Therefore there is only one global phase portrait: G50 of Figure 2.4.10.

If  $c_1 = 0$  and  $\mu > -1$ , then  $O_1$  has the local phase portrait  $L_{38}$  and  $O_2$  is a stable node. We obtain three possible global phase portraits, the ones given in Figure 2.4.7. By Theorem 2.1.10 we know that, under the conditions of this case, two invariant lines  $z =$

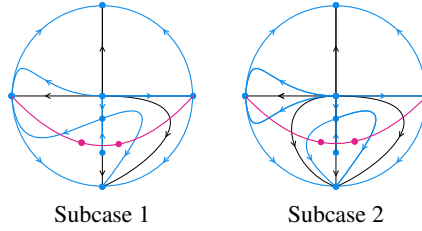


Figure 2.4.6: Straight lines with two contact points on two subcases of case 2.6 with  $\mu = 0$ .

$(R_c - c_3)/(2c_2)$  and  $z = -(R_c + c_3)/(2c_2)$  must exist, and it is only possible in the subcase 3, which provides the phase portrait G51 of Figure 2.4.10.

If  $c_1 = 0$  and  $\mu < -1$ , then  $O_1$  has the local phase portrait  $L_{41}$  and  $O_2$  is a saddle. In this case we obtain only one phase portrait which is G52 of Figure 2.4.10.

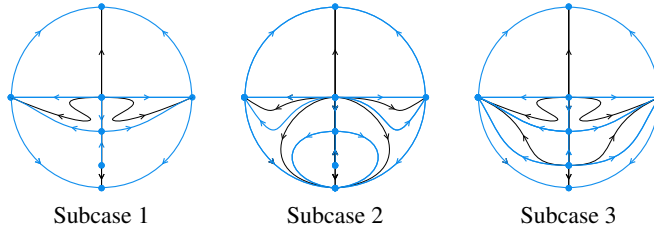


Figure 2.4.7: Possible global phase portraits in case 2.6 with  $c_1 = 0$  and  $\mu > -1$ .

**Case 3.2.** Here we distinguish three subcases and, in two of them, there is only one possible global phase portrait. More precisely, if  $\mu < -1$ , then  $O_1$  has the local phase portrait  $L_8$ ,  $O_2$  is a saddle and the global phase portrait is G64. If  $\mu \in (-1, 0)$ , then  $O_1$  has the local phase portrait  $L_{13}$ ,  $O_2$  is an unstable node and we obtain the phase portrait G65.

If  $\mu > 0$ , then  $O_1$  has the local phase portrait  $L_6$  and  $O_2$  is an unstable node, and we get three phase portraits, the ones given in Figure 2.4.8. By Theorem 2.1.10, there must exist a contact point on each straight line  $z = z_0$ , but if in subcases 1 and 2 if we take a straight line  $z = z_0$  with  $z_0 > -c_3/(2c_2)$ , there are not contact points on it, so those subcases are not feasible. The only possibility is the subcase 3, which provides the phase portrait G63 of Figure 2.4.10.

**Case 4.2.** Here we distinguish five different subcases. First if  $c_1 = 0$ ,  $\mu < -1$  and  $a_0 + c_0\mu > 0$ , then  $O_1$  has the local phase portrait  $L_{31}$  and  $O_2$  is a saddle. In this case we obtain the global phase portrait G90.

If  $c_1 = 0$ ,  $\mu < -1$  and  $a_0 + c_0\mu < 0$ , then  $O_1$  has the local phase portrait  $L_{32}$  and  $O_2$  is a saddle. By Corollary 2.1.5 the phase portrait must be symmetric so we obtain three possibilities, given in Figure 2.4.9. We further know that there must exist an invariant straight line  $z = -c_3/2c_2$ , so we can deduce that subcase 2 is not feasible because that invariant

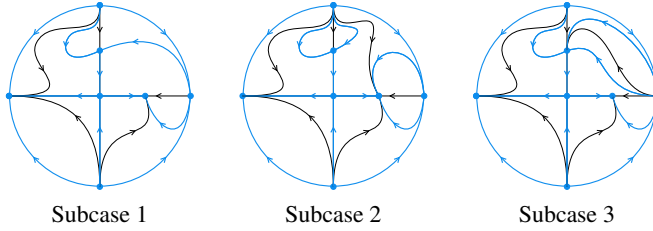


Figure 2.4.8: Possible global phase portraits in case 3.2 with  $\mu > 0$ .

straight line does not exist. As we also know that this invariant straight line is a separatrix in the local phase portrait of  $O_1$ , the one appearing in  $L_{32}$ , the subcase 3 is not feasible, because there would exist another separatrix over the invariant straight line that does not appear on  $L_{32}$ . So finally the only possible phase portrait is G91.

The same happens in the next cases in which we initially obtain three possibilities but we can discard two of them with the same arguments, so finally we get the next results. If  $\mu = 0$ , then  $O_1$  has the local phase portrait  $L_5$  and  $O_2$  is a stable node and we obtain the global phase portrait G87. If  $c_1 = 0$ ,  $\mu > -1$  and  $a_0 + c_0\mu > 0$ , then  $O_1$  has the local phase portrait  $L_{27}$ ,  $O_2$  is a stable node and we obtain the phase portrait G88. Finally, if  $c_1 = 0$ ,  $\mu > -1$  and  $a_0 + c_0\mu < 0$ , then  $O_1$  has the local phase portrait  $L_{28}$ ,  $O_2$  is a stable node, and the global phase portrait is G89.

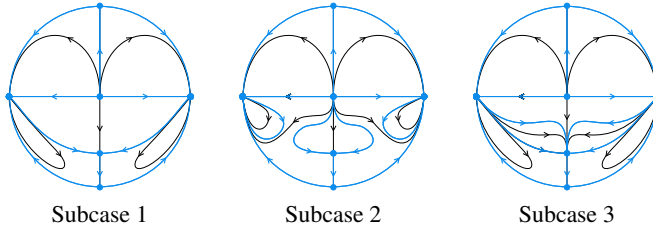


Figure 2.4.9: Possible global phase portraits in case 4.2 with  $c_1 = 0$ ,  $\mu < -1$  and  $a_0 + c_0\mu < 0$ .

The same methods that we have used in the previous cases for determine which of the global phase portraits are realizable, must be used in some other cases, namely: 1.17; 1.18 with  $\mu \geq -2$ ; 1.19; 2.7; 3.3; 3.4 with  $\mu \geq -2$ ; 3.5 with  $\mu > 0$ ; and finally, 4.1 with  $c_1 = 0$ ,  $\mu > -1$  and  $a_0 + c_0\mu < 0$ .

In subcases of 1.19 and 3.3 with  $\mu < -1$  it is also necessary to apply index theory to determine completely the local phase portraits at infinity, before obtaining the three possibilities for the global phase portraits.

## 2.4 Global phase portraits

Case	Conditions	$O_1$	$O_2$	Global
1.1		$L_{12}$	Unstable node	G1
1.2		$L_3$	Stable node	G2
1.3	$\mu < -1$	$L_8$	Saddle	G3
	$\mu \in (-1, 0)$	$L_{13}$	Unstable node	G4
1.4	$\mu < -2$	$L_1$	Saddle	G5
	$\mu \in (-1, 0)$	$L_4$	Saddle	G6
	$\mu \in (-2, -1)$	$L_{15}$	Saddle	G7
	$\mu = -2$	$L_{17}$	Saddle	G8
1.5		$L_{12}$	Unstable node	G9
1.6		$L_3$	Stable node	G10
1.7	$\mu \in (-1, 0)$	$L_{10}$	Stable node	G11
	$\mu < -1$	$L_{11}$	Saddle	G12
1.8	$\mu < -2$	$L_2$	Saddle	G13
	$\mu \in (-1, 0)$	$L_7$	Unstable node	G14
	$\mu \in (-2, -1)$	$L_{16}$	Saddle	G15
	$\mu = -2$	$L_{18}$	Saddle	G16
1.9		$L_9$	Stable node	G19
1.10		$L_6$	Unstable node	G20
1.11		$L_{12}$	Unstable node	G17
1.12	$\mu < -1$	$L_8$	Saddle	G21
	$\mu \in (-1, 0)$	$L_{13}$	Unstable node	G22
1.13		$L_3$	Stable node	G18
1.14	$\mu < -2$	$L_1$	Saddle	G23
	$\mu \in (-1, 0)$	$L_4$	Stable node	G24
	$\mu \in (-2, -1)$	$L_{15}$	Saddle	G25
	$\mu = -2$	$L_{17}$	Saddle	G26
1.15		$L_{12}$	Unstable node	G27
1.16	$\mu < -1$	$L_8$	Saddle	G35
	$\mu \in (-1, 0)$	$L_{13}$	Unstable node	G36
1.17		$L_3$	Stable node	G28
1.18	$\mu < -2$	$L_1$	Saddle	G37
	$\mu \in (-1, 0)$	$L_4$	Stable node	G38
	$\mu \in (-2, -1)$	$L_{15}$	Saddle	G39
	$\mu = -2$	$L_{17}$	Saddle	G40
1.19	$\mu \in (-1, 0)$	$L_{10}$	Saddle	G29
	$\mu < -1$	$L_{11}$	Saddle	G30
1.20	$\mu < -2$	$L_2$	Saddle	G31
	$\mu \in (-1, 0)$	$L_7$	Unstable node	G32
	$\mu \in (-2, -1)$	$L_{16}$	Saddle	G33
	$\mu = -2$	$L_{18}$	Saddle	G34

Table 2.4.1 (1 out of 3): Classification of global phase portraits of systems (2.0.1).

Case	Conditions	$O_1$	$O_2$	Global
2.1		$L_{46}$	Stable node	G41
2.2		$L_{47}$	Unstable node	G42
2.3	$\mu = 0$	$L_{14}$	Unstable node	G43
	$c_1 = 0, \mu > -1$	$L_{36}$		
	$c_1 = 0, \mu < -1$	$L_{43}$	Saddle	G44
2.4	$\mu = 0$	$L_5$	Stable node	G45
	$c_1 = 0, \mu > -1$	$L_{35}$	Stable node	G46
	$c_1 = 0, \mu < -1$	$L_{39}$	Saddle	G47
2.5	$\mu = 0$	$L_{14}$	Unstable node	G48
	$c_1 = 0, \mu > -1$	$L_{45}$		
	$c_1 = 0, \mu < -1$	$L_{44}$	Saddle	G49
2.6	$\mu = 0$	$L_5$	Stable node	G50
	$c_1 = 0, \mu > -1$	$L_{38}$	Stable node	G51
	$c_1 = 0, \mu < -1$	$L_{41}$	Saddle	G52
2.7	$\mu > -1$	$L_{37}$	Stable node	G53
	$\mu < -1$	$L_{40}$	Saddle	G54
2.8	$\mu > -1$	$L_{34}$	Unstable node	G55
	$\mu < -1$	$L_{42}$	Saddle	G56
2.9	$\mu = 0$	$L_{14}$	Unstable node	G57
	$c_1 = 0, \mu > -1$	$L_{24}$		
	$c_1 = 0, \mu < -1$	$L_{26}$	Saddle	G58
2.10	$\mu = 0$	$L_5$	Stable node	G59
	$c_1 = 0, \mu > -1$	$L_{23}$	Stable node	G60
	$c_1 = 0, \mu < -1$	$L_{25}$	Saddle	G61
3.1		$L_{12}$	Unstable node	G62
3.2	$\mu > 0$	$L_6$	Unstable node	G63
	$\mu < -1$	$L_8$	Stable node	G64
	$\mu \in (-1, 0)$	$L_{13}$	Unstable node	G65
3.3	$\mu > 0$	$L_3$	Stable node	G66
	$\mu < -1$	$L_{11}$	Stable node	G68
	$\mu \in (-1, 0)$	$L_{10}$	Stable node	G67
3.4	$\mu < -2$	$L_1$	Saddle	G69
	$\mu \in (-1, 0)$	$L_4$	Stable node	G70
	$\mu \in (-2, -1)$	$L_{15}$	Saddle	G71
	$\mu = -2$	$L_{17}$	Saddle	G72
3.5	$\mu > 0$	$L_3$	Stable node	G73
	$\mu \in (-1, 0)$	$L_{10}$	Stable node	G74
	$\mu < -1$	$L_{11}$	Saddle	G75
3.6		$L_{12}$	Unstable node	G76
3.7	$\mu < -1$	$L_8$	Saddle	G77
	$\mu \in (-1, 0)$	$L_{13}$	Unstable node	G78

Table 2.4.1 (2 out of 3): Classification of global phase portraits of systems (2.0.1).

## 2.4 Global phase portraits

Case	Conditions	$O_1$	$O_2$	Global
3.8		$L_3$	Stable node	G79
3.9	$\mu < -2$	$L_1$	Saddle	G80
	$\mu \in (-1, 0)$	$L_4$	Stable node	G81
	$\mu \in (-2, -1)$	$L_{15}$	Saddle	G82
	$\mu = -2$	$L_{17}$	Saddle	G83
4.1	$\mu = 0$	$L_{14}$	Unstable node	G84
	$c_1 = 0, \mu > -1, a_0 + c_0\mu > 0$	$L_{29}$		
	$c_1 = 0, \mu > -1, a_0 + c_0\mu < 0$	$L_{30}$	Unstable node	G85
	$c_1 = 0, \mu < -1$	$L_{33}$	Saddle	G86
4.2	$\mu = 0$	$L_5$	Stable node	G87
	$c_1 = 0, \mu > -1, a_0 + c_0\mu > 0$	$L_{27}$	Stable node	G88
	$c_1 = 0, \mu > -1, a_0 + c_0\mu < 0$	$L_{28}$	Stable node	G89
	$c_1 = 0, \mu < -1, a_0 + c_0\mu > 0$	$L_{31}$	Saddle	G90
	$c_1 = 0, \mu < -1, a_0 + c_0\mu < 0$	$L_{32}$	Saddle	G91
4.3	$\mu = 0$	$L_{14}$	Unstable node	G92
	$c_1 = 0, \mu > -1$	$L_{20}$		
	$c_1 = 0, \mu < -1$	$L_{22}$	Saddle	G93
4.4	$\mu = 0$	$L_5$	Stable node	G94
	$c_1 = 0, \mu > -1$	$L_{19}$	Stable node	G95
	$c_1 = 0, \mu < -1$	$L_{21}$	Saddle	G96
5.1	$\mu > 0$	$L_3$	Stable node	G97
	$\mu \in (-1, 0)$	$L_{10}$	Stable node	G98
	$\mu < -1$	$L_{11}$	Saddle	G99
5.2		$L_{12}$	Unstable node	G76
5.3	$\mu > 0$	$L_6$	Unstable node	G100
	$\mu < -1$	$L_8$	Saddle	G77
	$\mu \in (-1, 0)$	$L_{13}$	Unstable node	G78
5.4	$\mu > 0$	$L_3$	Stable node	G79
	$\mu \in (-1, 0)$	$L_{10}$	Stable node	G101
	$\mu < -1$	$L_{11}$	Saddle	G102
5.5	$\mu < -2$	$L_1$	Saddle	G80
	$\mu \in (-1, 0)$	$L_4$	Stable node	G81
	$\mu \in (-2, -1)$	$L_{15}$	Saddle	G82
	$\mu = -2$	$L_{17}$	Saddle	G83
6.1	$\mu = 0$	$L_{14}$	Unstable node	G92
	$c_1 = 0, \mu > -1$	$L_{20}$		
	$c_1 = 0, \mu < -1$	$L_{22}$	Saddle	G93
6.2	$\mu = 0$	$L_5$	Stable node	G94
	$c_1 = 0, \mu > -1$	$L_{19}$	Stable node	G95
	$c_1 = 0, \mu < -1$	$L_{21}$	Saddle	G96

Table 2.4.1 (3 out of 3): Classification of global phase portraits of systems (2.0.1).

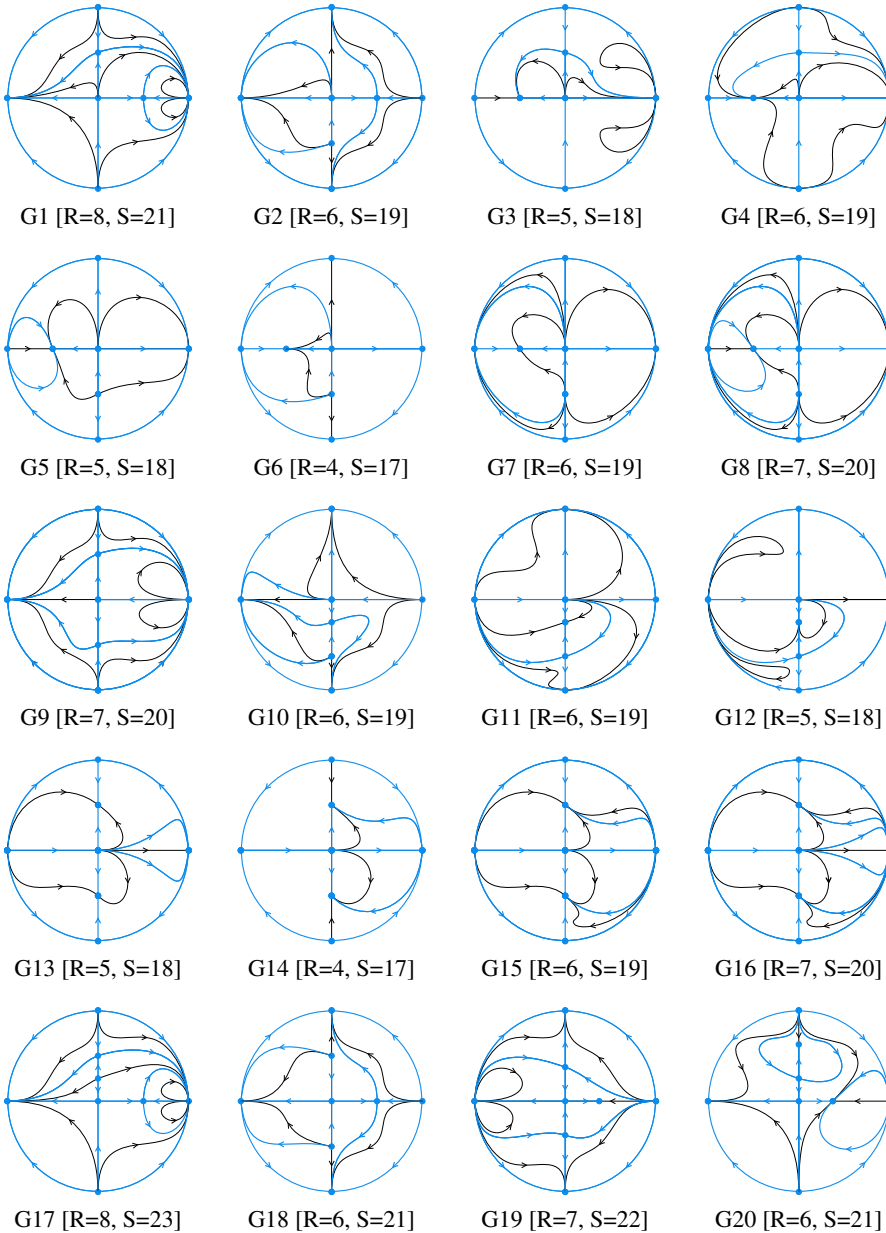


Figure 2.4.10 (1 out of 6): Global phase portraits of systems (2.0.1) on the Poincaré disk.

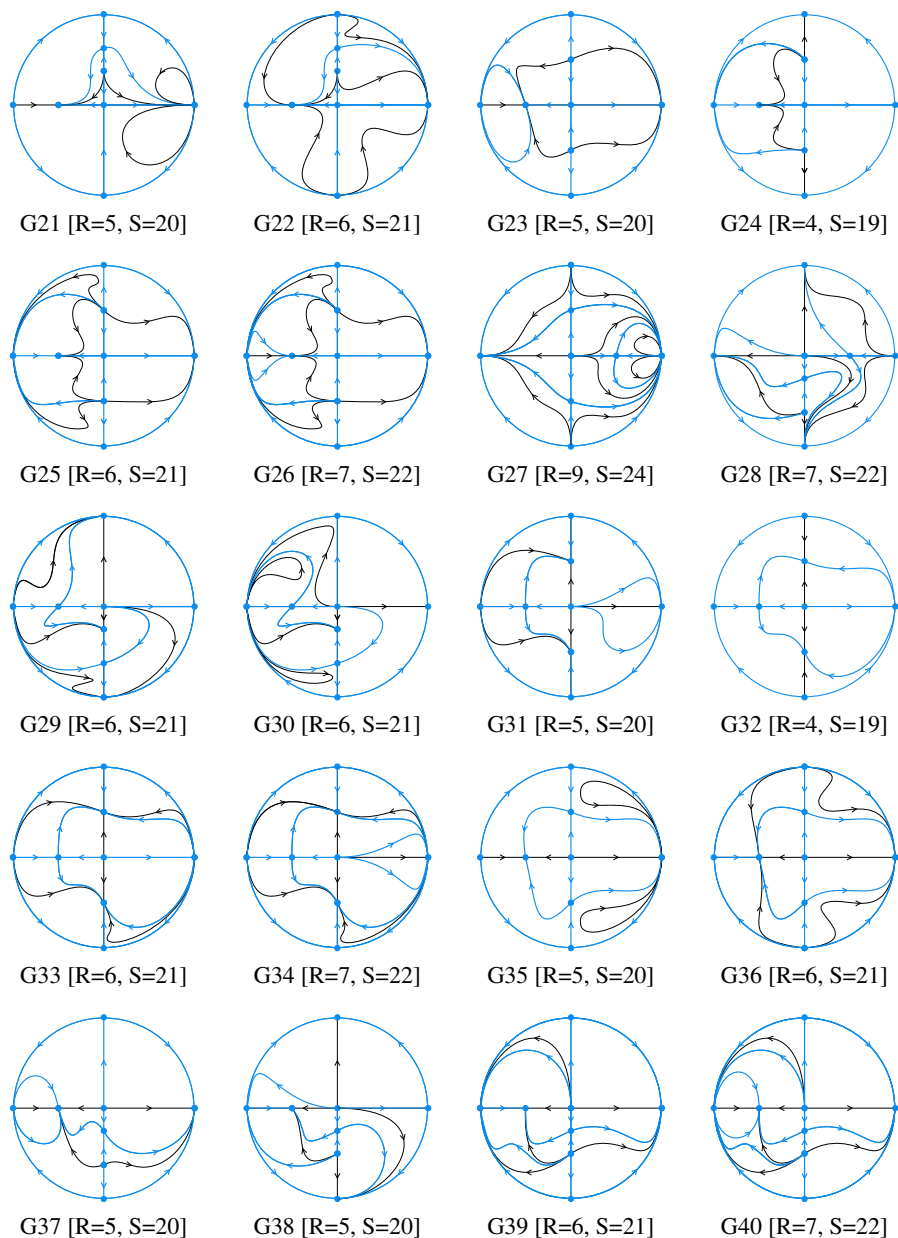


Figure 2.4.10 (2 out of 6): Global phase portraits of systems (2.0.1) on the Poincaré disk.



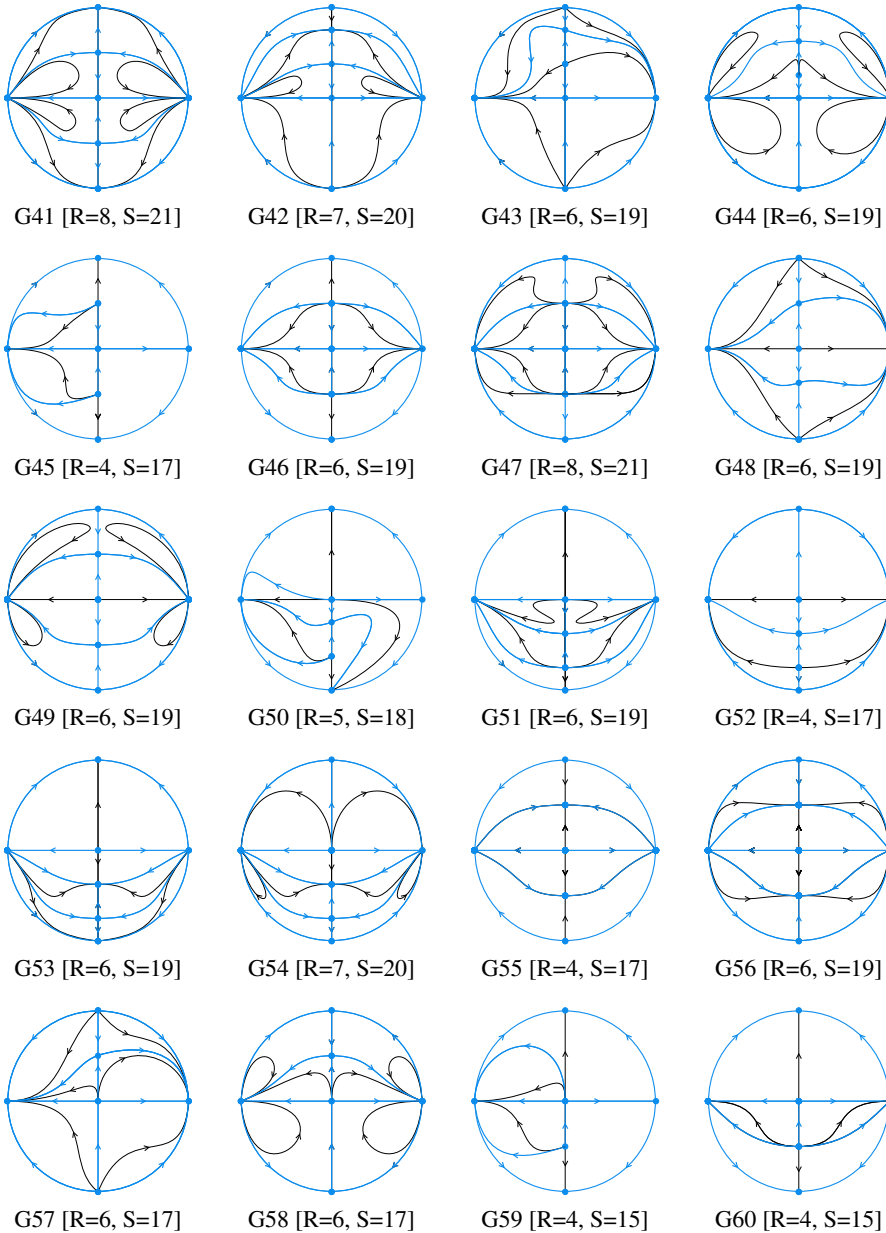


Figure 2.4.10 (3 out of 6): Global phase portraits of systems (2.0.1) on the Poincaré disk.

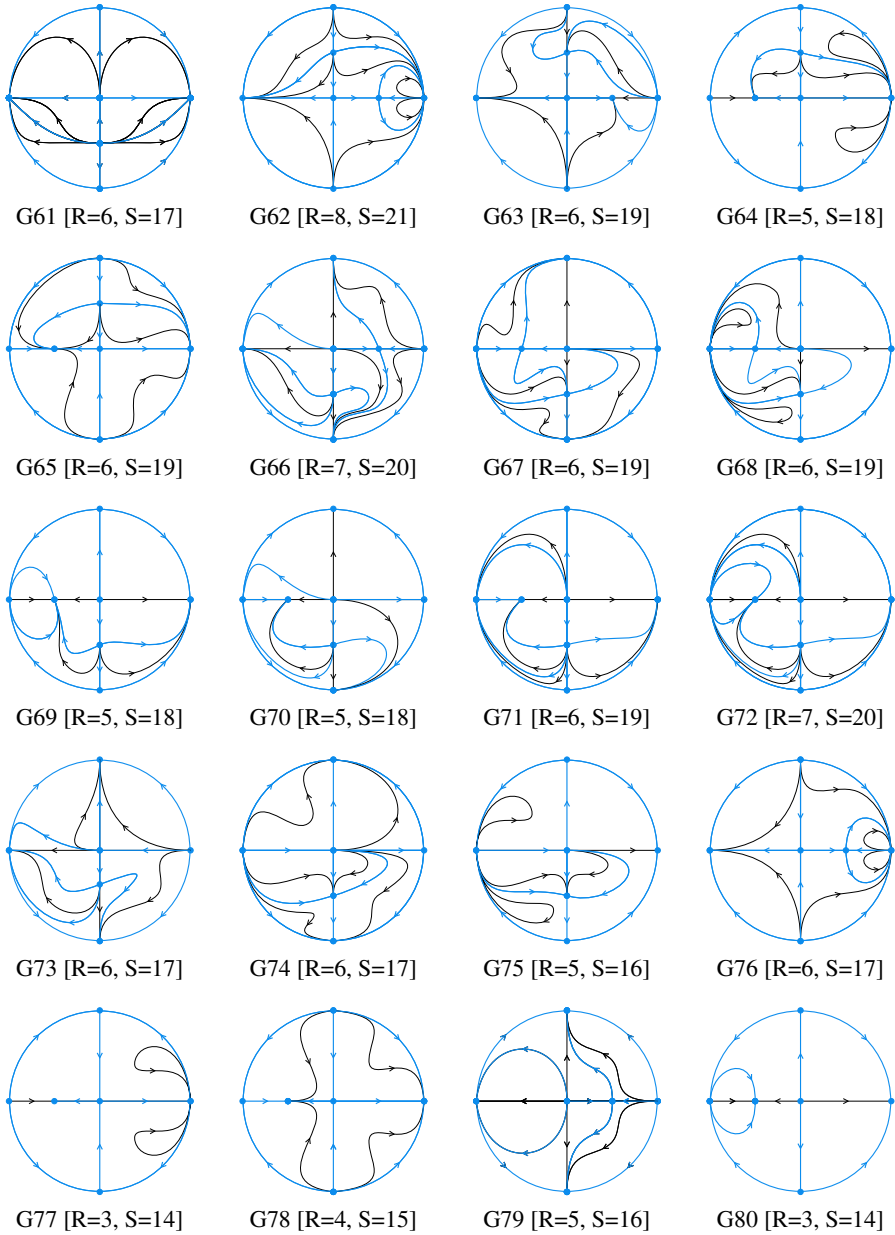


Figure 2.4.10 (4 out of 6): Global phase portraits of systems (2.0.1) on the Poincaré disk.

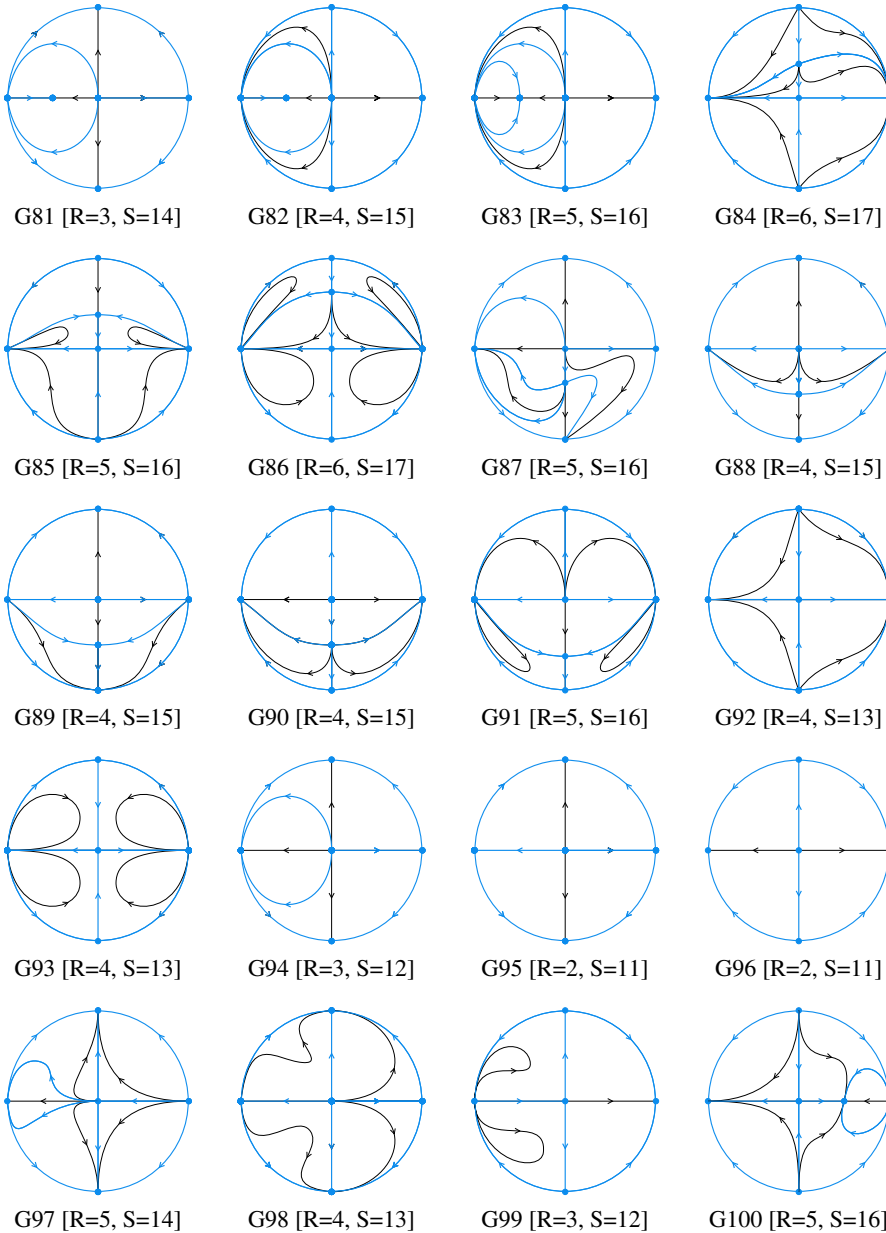


Figure 2.4.10 (5 out of 6): Global phase portraits of systems (2.0.1) on the Poincaré disk.

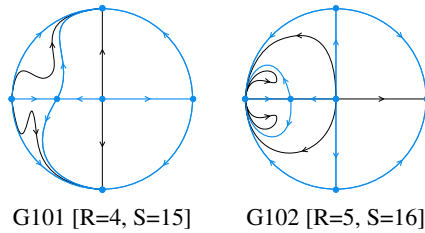


Figure 2.4.10 (6 out of 6): Global phase portraits of systems (2.0.1) on the Poincaré disk.

**Remark 2.4.1.** The global phase portraits  $G43$ ,  $G48$ ,  $G57$ ,  $G84$  and  $G92$  can appear both under condition  $c_1 = 0$  or  $c_1 \neq 0$ , so as we are interested in the topological classification we represent only the non-symmetric case respect to  $z$ -axis, but also the symmetric is possible.

The same situation occurs with global phase portraits  $G9$ ,  $G13$ – $G16$ ,  $G18$ ,  $G19$ ,  $G23$ – $G27$ ,  $G31$ – $G36$ ,  $G41$ ,  $G45$ – $G49$ ,  $G55$ ,  $G56$ ,  $G76$ – $G83$ ,  $G92$ – $G102$ , which can appear under condition  $c_3 = 0$  or  $c_3 \neq 0$ , so they can present the symmetric or the non-symmetric form respect to  $x$ -axis, although we only represent one of them because we are only interested on the topological classification.

## 2.5 Topological equivalences

In the previous sections we have obtained the 102 global phase portraits given in Figure 2.4.10. There are 19 different classes according to their number of canonical regions and separatrices, and within each class we distinguish which ones are topologically equivalent in the following result.

**Proposition 2.5.1.** For Kolmogorov systems (2.0.1) there are 19 classes according to the number of canonical regions and separatrices. Taking into account the topological equivalences, we get:

- (i) Four distinct phase portraits with 8 canonical regions and 21 separatrices.
- (ii) Thirteen distinct phase portraits with 6 canonical regions and 19 separatrices.
- (iii) Six distinct phase portraits with 5 canonical regions and 18 separatrices.
- (iv) Five distinct phase portraits with 4 canonical regions and 17 separatrices.
- (v) Seven distinct phase portraits with 7 canonical regions and 20 separatrices.
- (vi) One phase portrait with 8 canonical regions and 23 separatrices.
- (vii) Five distinct phase portraits with 6 canonical regions and 21 separatrices.
- (viii) Three distinct phase portraits with 7 canonical regions and 22 separatrices.
- (ix) Three distinct phase portraits with 5 canonical regions and 20 separatrices.

- (x) One phase portrait with 4 canonical regions and 19 separatrices.
- (xi) One phase portrait with 9 canonical regions and 24 separatrices.
- (xii) Six distinct phase portraits with 6 canonical regions and 17 separatrices.
- (xiii) Six distinct phase portraits with 4 canonical regions and 15 separatrices.
- (xiv) Seven distinct phase portraits with 5 canonical regions and 16 separatrices.
- (xv) Three distinct phase portraits with 3 canonical regions and 14 separatrices.
- (xvi) Three distinct phase portraits with 4 canonical regions and 13 separatrices.
- (xvii) Two distinct phase portraits with 3 canonical regions and 12 separatrices.
- (xviii) One phase portrait with 2 canonical regions and 11 separatrices.
- (xix) One phase portraits with 5 canonical regions and 14 separatrices.

*Proof.* We proof this proposition by studying the topological equivalences within each one of the 19 classes provided by the number of separatrices and canonical regions.

- (i) For systems (2.0.1) we have obtained four phase portraits with 8 canonical regions and 21 separatrices, namely, G1, G41, G47 and G62 of Figure 2.4.10. In the phase portraits G1 and G62 there are two elliptic sectors, in G41 there are four and in G47 there are no elliptic sectors. Furthermore in G1 there are two separatrices that connect the saddle-node with other finite singular points but in G62 there is only one. Then, all the phase portraits in this class are topologically distinct.
- (ii) For systems (2.0.1) we have obtained 19 phase portraits with 6 canonical regions and 19 separatrices, namely, G2, G4, G7, G10, G11, G15, G43, G44, G46, G48, G49, G51, G53, G56, G63, G65, G67, G68 and G71 of Figure 2.4.10. First we consider different subclasses attending to two invariants, the number of elliptic sectors and the sum of the indices at the finite singular points, denoted by  $ind_F$ .

The phase portraits G44 and G49 have 4 elliptic sectors and  $ind_F = -1$ . If we move the node to the origin in G44 we obtain G49, so they are topologically equivalent.

The only phase portrait with two elliptic sectors is the G68, so it is topologically distinct from all the others. The same occurs with phase portrait G56, which is the only with no elliptic sectors and  $ind_F = 3$ .

Phase portraits G43 and G48 have no elliptic sectors and  $ind_F = -1$ . They are topologically equivalent as we can obtain G48 by moving the node in G43 to the origin.

Phase portraits G7, G15 and G71 have no elliptic sectors and  $ind_F = 2$ . G7 is topologically equivalent to G71 after moving the node of G7 to the origin and doing a symmetry with respect to the  $x$ -axis. G7 is topologically distinct from G15 because in G7 there are five separatrices which arrive or leave the saddle-node and in G15 there are only four of those separatrices.

Phase portraits G46, G51 and G53 have no elliptic sectors and  $ind_F = 1$ . If we move the saddle in G51 to the origin we obtain G46, so they are topologically equivalent. G46 is distinct from G53 due to the relative position of the finite singular points, in both phase portraits the three finite singular points are on the  $z$ -axis, in G46 the saddle is between the nodes but in G53 it is not.

All the remaining phase portraits have no elliptic sectors and  $ind_F = 0$ .

G4 is topologically equivalent to G65 by moving the saddle in G4 to the origin and doing a symmetry with respect to the  $x$ -axis. G65 is equivalent to G67 by moving the saddle in G67 to the origin, doing a rotation of  $180^\circ$  and changing  $t$  by  $-t$ .

G4 is different from G2 and G63 because in G2 and G63 there are an infinite singular point which is connected with finite singularities by three separatrices and in G4 there is not such infinite singular point.

G2 is distinct from G10, G11 and G63 because in G2 the saddle has three separatrices that connect with infinite singular points but in G10, G11 and G63 only two separatrices of the saddle connect with the infinity.

In G4 there are two types of orbits in the parabolic sector at the saddle-node, the ones which go to a finite singular point and those who go to an infinite singular point. In G10 all the orbits on that sector go to the infinity and in G11 are three different types of orbit in that sector as they can go to two different infinite singular point or to a finite singular point. Then, G4, G10 and G11 are distinct.

Finally, G63 is distinct from G10 and G11. In G63 the two separatrices that separate the parabolic sector from the hyperbolic sectors in the saddle-node go to infinite singular points while in G10 and G11 one of them goes to a finite singular point.

Summarizing, we have thirteen distinct phase portraits which can be represented by G2, G4, G7, G10, G11, G15, G43, G44, G46, G53, G56, G63 and G68.

- (iii) For systems (2.0.1) we have obtained eight phase portraits with five canonical regions and 18 separatrices, namely, G3, G5, G12, G13, G50, G64, G69 and G70 of Figure 2.4.10. Attending to the number of elliptic sectors and the sum  $ind_F$  we have three subclasses.

First, G3, G12 and G64 have two elliptic sectors. G3 is topologically equivalent to G64 by moving the saddle in G3 to the origin and doing a symmetry with respect to the  $x$ -axis. G3 is distinct from G12 because in G3, to the infinite singular point at which arrive orbits from the parabolic sector of the saddle node, also arrive two separatrices from finite singular points but in G12 no separatrix arrives to that infinite singular point.

G50 is the only phase portrait with no elliptic sectors and  $ind_F = 1$ .

G5, G13, G69 and G70 have no elliptic sectors and  $ind_F = 2$ . G5 is topologically equivalent to G69 by moving the unstable node in G5 to the origin and doing a symmetry with respect to the  $x$ -axis. G5 is distinct from G13 because in G5 there are four separatrices that start or end in the saddle node, but in G13 there are five of those separatrices. Finally, G70 is distinct from G5 and G13 because in G70 there is an infinite

singular point connected with finite singularities by three separatrices and there is not such infinite singularity in G5 or G13.

Summarizing we have six different phase portraits in this class which can be represented by G3, G5, G12, G13, G50 and G70.

- (iv) For systems (2.0.1) we have obtained five phase portraits with 4 canonical regions and 17 separatrices, namely, G6, G14, G45, G52 and G55 of Figure 2.4.10. G45 and G52 have  $ind_F = 1$  and they are topologically distinct because in G45 there is an infinite singularity connected with finite singularities by three separatrices and in G52 there is not such infinite singular point. G6 and G14 have  $ind_F = 2$  and they are distinct because in G14 the two unstable separatrices which leave the saddle-node go to finite singular points, but in G6 one of them goes to a infinite singular point. Lastly, G55 is the only phase portrait with  $ind_F = 3$ .
- (v) For systems (2.0.1) we have obtained seven phase portraits with 7 canonical regions and 20 separatrices, namely, G8, G9, G16, G42, G54, G66 and G72 of Figure 2.4.10. In a first subclass, G9, G42 and G54 have two elliptic sectors and they are all topologically distinct as the sum  $ind_F$  in each of them is  $-2$ ,  $-1$  and  $1$  respectively. In a second subclass G8 and G66 have no elliptic sectors and  $ind_F = 0$ , and they are distinct because in G8 there is an infinite singular point which is connected by four separatrices with finite singular points and in G66 there is not such infinite singularity. Lastly, G16 and G72 have no elliptic sectors and they are distinct because in G6 the two unstable separatrices which leave the saddle-node go to finite singular points, but in G72 one of them goes to a infinite singularity. Then all the phase portraits in this class are topologically distinct.
- (vi) For systems (2.0.1) we have obtained only one phase portraits with 8 canonical regions and 23 separatrices, the G17 of Figure 2.4.10, so no proof is required.
- (vii) For systems (2.0.1) we have obtained nine phase portraits with 6 canonical regions and 21 separatrices, namely, G18, G20, G22, G25, G29, G30, G33, G36 and G39 of Figure 2.4.10. G30 is the only with two elliptic sectors so it is distinct from all the others. G25, G33 and G39 have no elliptic sectors and  $ind_F = 2$ , and they are all topologically equivalent. If we move the saddle in G33 to the origin, we do a symmetry with respect to the  $z$ -axis and we change  $t$  by  $-t$  we obtain G25. If we move the saddle to the origin in G39 we obtain G25.

In the last subclass, with no elliptic sectors and  $ind_F = 0$  we have the phase portraits G18, G20, G22, G29 and G36. If we move in G29 the saddle which is on the negative  $x$ -axis to the origin, we do a rotation of  $180^\circ$  and we change  $t$  by  $-t$  we obtain G22. If we move the unstable node in G22 to the origin we obtain G36, so these three phase portraits are topologically equivalent. G18 is distinct from G20 and G22 because in G18 there is an infinite singular point which is connected with finite singular points by three separatrices and there is not such infinite singular point in the other phase portraits. G20 is distinct from G22 because in G20 there are two infinite singular points which are connected with finite singular points by two separatrices, and in G22 there are not such infinite singularities.

- (viii) For systems (2.0.1) we have obtained five phase portraits with 7 canonical regions and 22 separatrices, namely, G19, G26, G28, G34 and G40 of Figure 2.4.10. G19 has two elliptic sectors and G28 has no elliptic sectors and  $ind_F = 0$  so they are different from all the other phase portraits which have no elliptic sectors and  $ind_F = 2$ . Those other phase portraits, G26, G34 and G40 are topologically equivalent. If we move the saddle in G26 to the origin we obtain G40. If we move the stable node in G26 to the origin, we do a symmetry with respect to the  $z$ -axis and we change  $t$  by  $-t$  we obtain G34.
- (ix) For systems (2.0.1) we have obtained six phase portraits with 5 canonical regions and 20 separatrices, namely, G21, G23, G31, G35, G37 and G38 of Figure 2.4.10. First, in G21 and G35 there are two elliptic sectors and these phase portraits are topologically equivalent by moving the node in G21 to the origin. The other phase portraits have no elliptic sectors. G23 is equivalent to G31 by moving the saddle in G31 to the origin, doing a symmetry with respect to the  $z$ -axis and changing  $t$  by  $-t$ . G23 is also equivalent to G37 by moving the saddle in G37 to the origin. Finally, G37 is distinct to G38 because in G38 there is an infinite singularity connected with finite singular points by three separatrices and in G37 there is not such infinite singularity. Thus we have three distinct phase portraits which can be represented by G23, G38 and G21.
- (x) For systems (2.0.1) we have obtained two phase portraits with 4 canonical regions and 19 separatrices, the G24 and the G32 of Figure 2.4.10. If we move the node in G24 to the origin, we do a symmetry with respect to the  $z$ -axis and we change  $t$  by  $-t$  we obtain G32, so both phase portraits are equivalent.
- (xi) For systems (2.0.1) we have obtained only one phase portrait with 9 canonical regions and 24 separatrices, the G27 of Figure 2.4.10, so no proof is required.
- (xii) For systems (2.0.1) we have obtained eight phase portraits with 6 canonical regions and 17 separatrices, namely, G57, G58, G61, G73, G74, G76, G84 and G86 of Figure 2.4.10. We consider subclasses depending on the number of elliptic sectors and the  $ind_F$ . First, G58 and G84 have four elliptic sectors, and they are topologically equivalent by moving the saddle in G58 to the origin and doing a symmetry with respect to the  $x$ -axis. G76 is the only phase portrait with two elliptic sectors and G61 is the only with no elliptic sectors and  $ind_F = 1$ , so they are not equivalent to any other. G57 and G84 have no elliptic sectors and  $ind_F = -1$  and they are topologically equivalent by moving the saddle in G57 to the origin and doing a symmetry with respect to the  $x$ -axis. Finally, G73 and G74 have no elliptic sectors and  $ind_F = 0$ , but their as distinct because in G73 there is an infinite singular point connected by three separatrices with finite singular points, and in G74 there is not such infinite singular point.
- (xiii) For systems (2.0.1) we have obtained eight phase portraits with 4 canonical regions and 15 separatrices, namely, G59, G60, G78, G82, G88, G89, G90 and G101 of Figure 2.4.10. First we divide the phase portrait attending to the  $ind_F$ . G82 is the only with  $ind_F = 2$ . G78 and G101 have  $ind_F = 0$ , and they are topologically equivalent as if we move in G78 the node to the origin, we do a symmetry with respect to the  $z$ -axis and we change  $t$  by  $-t$ , we obtain G101.



All the remaining phase portraits have  $\text{ind}_F = 1$ . G59 is different from G60, G89 and G90 as in G59 there is an infinite singular point which is the  $\omega$ -limit of three separatrices which start in finite singular points, and in G60, G89 and G90 there is not such infinite singular point. G60 is topologically equivalent to G88 by moving the node in G60 to the origin and doing a symmetry with respect to the  $x$ -axis. G89 is distinct from G88 and G90 because in G89 there are orbits which connect two infinite singular points and in G88 and G90 there are not such orbits. Lastly, G88 is distinct from G90 because in G88 there are two infinite singular points at which arrive two separatrices from finite singularities, and in G90 there are not such infinite singular points.

Summarizing we have six topologically different phase portraits which can be represented by G82, G78, G59, G60, G89 and G90.

- (xiv) For systems (2.0.1) we have obtained eight phase portraits with 5 canonical regions and 16 separatrices, namely, G75, G79, G83, G85, G87, G91, G100 and G102 of Figure 2.4.10. We focus on the number of elliptic sectors and the  $\text{ind}_F$  in each one of the phase portraits. G75, G85, G91 and G102 have two elliptic sectors, and the sum  $\text{ind}_F$  in each one of them is 0,  $-1$ , 1 and  $-2$  respectively, so they are all distinct. On the other hand G79, G83, G87 and G100 have no elliptic sectors. The sum  $\text{ind}_F$  is 2 in G83, 1 in G87 and 0 in G79 and G100, so we only have to prove if G79 and G100 are topologically equivalent, and indeed they are. If we move the node to the origin in G79, we do a symmetry with respect to the  $z$ -axis and we change the time variable  $t$  by  $-t$ , we get G100.
- (xv) For systems (2.0.1) we have obtained three phase portraits with 3 canonical regions and 14 separatrices, namely, G77, G80 and G81 of Figure 2.4.10. The phase portrait G77 has two elliptic sectors so it is topologically distinct from G80 and G81 which do not have elliptic sectors. In G80 and G81 there are two separatrices which connect a infinite singular point with a finite singular point, and in the region limited by those separatrices there is a finite singular point in G81 but none in G80.
- (xvi) For systems (2.0.1) we have obtained three phase portraits with 4 canonical regions and 13 separatrices, namely, G92, G93 and G98 of Figure 2.4.10. The phase portrait G93 which has four elliptic sectors is distinct from G92 and G98 which do not have any elliptic sector. G92 is also distinct from G98 as both have only one finite singular point which is a saddle in G92 and an unstable node in G98.
- (xvii) For systems (2.0.1) we have obtained two phase portraits with 3 canonical regions and 12 separatrices, the G94 and the G99 of Figure 2.4.10. These phase portraits are topologically distinct because G94 has two elliptic sectors and G99 has no elliptic sectors.
- (xviii) For systems (2.0.1) we have obtained two phase portraits with 2 canonical regions and 11 separatrices, the G95 and the G96 of Figure 2.4.10, and we can transform G96 into G95 with a rotation of  $90^\circ$ , so they are topologically equivalent.
- (xix) For systems (2.0.1) we have obtained only one phase portrait with 5 canonical regions and 14 separatrices, the G97 of Figure 2.4.10, so no proof is required. □

## 2.5 Topological equivalences

---

The classification given in Table 2.4.1 together with Proposition 2.5.1, prove our main result in this chapter, i.e., Theorem 2.0.1.

Figure 2.0.1 includes the representatives of each one of the topological equivalence classes, which correspond to the portraits in Figure 2.4.10 as indicated in Table 2.5.1

Representative	Phase portraits
R1	G1
R2	G2
R3	G3, G64
R4	G4, G65, G67
R5	G5, G69
R6	G6
R7	G7, G71
R8	G8
R9	G9
R10	G10
R11	G11
R12	G12
R13	G13
R14	G14
R15	G15
R16	G16
R17	G17
R18	G18
R19	G19
R20	G20
R21	G21, G35
R22	G22, G29, G36
R23	G23, G31, G37
R24	G24, G32
R25	G25, G33, G39
R26	G26, G34, G40
R27	G27
R28	G28
R29	G30
R30	G38
R31	G41
R32	G42
R33	G43, G48
R34	G44, G49
R35	G45
R36	G46, G51
R37	G47
R38	G50
R39	G52

Representative	Phase portraits
R40	G53
R41	G54
R42	G55
R43	G56
R44	G57, G84
R45	G58, G86
R46	G59
R47	G60, G88
R48	G61
R49	G62
R50	G63
R51	G66
R52	G68
R53	G70
R54	G72
R55	G73
R56	G74
R57	G75
R58	G76
R59	G77
R60	G78, G101
R61	G79, G100
R62	G80
R63	G81
R64	G82
R65	G83
R66	G85
R67	G87
R68	G89
R69	G90
R70	G91
R71	G92
R72	G93
R73	G94
R74	G95, G96
R75	G97
R76	G98
R77	G99
R78	G102

Table 2.5.1: Representatives of each equivalence class and their corresponding global phase portraits of systems (2.0.1).

# Classification of the first Kolmogorov family with non-isolated singularities

---

The current chapter includes the contents of the research article [45]<sup>1</sup>, in which we study systems (2.0.1) in the particular case with  $\mu = -1$ . In this case all the singular points at infinity are singular points. It was proved in Section 2.1 and Lemma 2.2.1 that systems (2.0.1) can be studied under conditions

$$H_1^1 = \{c_2 \neq 0, a_0 \geq 0, c_1 \geq 0, c_3 \geq 0, a_0 + c_0\mu \neq 0, a_0^2 + c_1^2\mu^2 \neq 0\},$$

as any other case can be reduced to satisfy such conditions either using symmetries, or eliminating known phase portraits as in the cases in which there exist infinitely many finite singular points. Then taking  $\mu = -1$  we will study the systems

$$\begin{aligned}\dot{x} &= x(a_0 + c_1x + c_2z^2 + c_3z), \\ \dot{z} &= z(c_0 + c_1x + c_2z^2 + c_3z),\end{aligned}\tag{3.0.1}$$

under conditions

$$\tilde{H}^1 = \{c_2 \neq 0, a_0 \geq 0, c_1 \geq 0, c_3 \geq 0, a_0 \neq c_0, a_0^2 + c_1^2 \neq 0\}.$$

Moreover, from Remark 2.1.8, when  $a_0$  is zero it is enough to study the case with  $c_0$  positive.

Our main objective in this chapter is to prove the following result, which provides the topological classification of all global phase portraits of systems (3.0.1) on the Poincaré disk.

**Theorem 3.0.1.** *Kolmogorov systems (3.0.1) under conditions  $\tilde{H}^1$  have 22 topologically distinct phase portraits in the Poincaré disk, given in Figure 3.0.1.*

---

<sup>1</sup>Érika Diz-Pita (Departamento de Estatística, Análise Matemática e Optimización, Universidade de Santiago de Compostela), Jaume Llibre (Departament de Matemàtiques, Universitat Autònoma de Barcelona) and María Victoria Otero-Espinar (Departamento de Estatística, Análise Matemática e Optimización, Universidade de Santiago de Compostela), *Phase portraits of a family of Kolmogorov systems with infinitely many singular points at infinity*, Communications in Nonlinear Science and Numerical Simulation, (ISSN:1007-5704, EISSN:1878-7274), **104** (2022), 106038. Published by Elsevier. The final authenticated version is available online at: <https://doi.org/10.1016/j.cnsns.2021.106038>

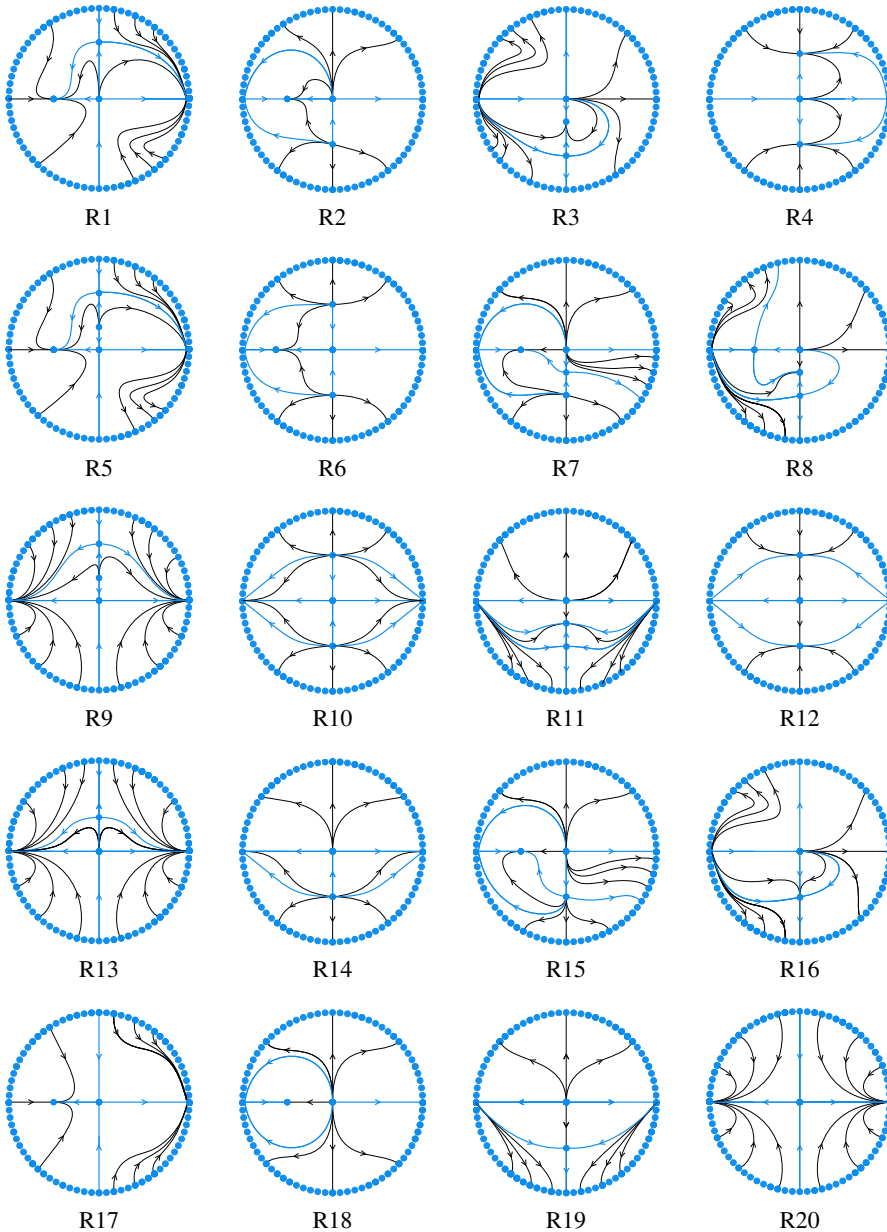


Figure 3.0.1 (1 out of 2): The topologically distinct phase portraits of systems (2.0.1) in the Poincaré disk.

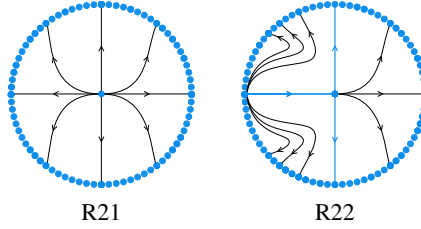


Figure 3.0.1 (2 out of 2): The topologically distinct phase portraits of systems (3.0.1) in the Poincaré disk.

This Chapter is organized as follows: In Section 3.1 we give the classification of the local phase portraits of the finite singular points, in Section 3.2 we study the local phase portraits at the infinite singular points, and finally in Section 3.3 we prove Theorem 3.0.1.

## 3.1 Local study of finite singular points

From Section 2.2, if we consider the condition  $\mu = -1$ , we get that the singular points of systems (3.0.1) are

$$P_0 = (0, 0), \quad P_1 = \left(0, \frac{R_c - c_3}{2c_2}\right) \quad \text{and} \quad P_2 = \left(0, -\frac{R_c + c_3}{2c_2}\right) \quad \text{if } c_3^2 > 4c_0c_2,$$

$$P_3 = \left(0, -\frac{c_3}{2c_2}\right) \quad \text{if } c_3^2 = 4c_0c_2 \quad \text{and} \quad P_4 = \left(-\frac{a_0}{c_1}, 0\right) \quad \text{if } c_1 \neq 0.$$

From Table 2.2.1 in Section 2.2, we get six cases depending on the coexistence of finite singular points, given in Table 3.1.1.

Case	Conditions	Finite singular points
1	$c_3^2 > 4c_0c_2, c_1 \neq 0$	$P_0, P_1, P_2, P_4$
2	$c_3^2 > 4c_0c_2, c_1 = 0, a_0 \neq 0$	$P_0, P_1, P_2$
3	$c_3^2 = 4c_0c_2, c_1 \neq 0$	$P_0, P_3, P_4$
4	$c_3^2 = 4c_0c_2, c_1 = 0, a_0 \neq 0$	$P_0, P_3$
5	$c_3^2 < 4c_0c_2, c_1 \neq 0$	$P_0, P_4$
6	$c_3^2 < 4c_0c_2, c_1 = 0, a_0 \neq 0$	$P_0$

Table 3.1.1: The different cases for the finite singular points.



From Lemma 2.2.9 and Tables 2.2.2 to 2.2.2 in Section 2.2, assuming the condition  $\mu = -1$ , we get the following classification for the local phase portraits of the finite singular points, with 34 subcases.

**Case 1:**  $c_3^2 > 4c_0c_2, c_1 \neq 0$

Sub.	Conditions	Classification
1.1	$a_0 > 0, c_0 = 0, c_2 < 0$	$P_0 \equiv P_1$ saddle-node, $P_2$ saddle, $P_4$ stable node
1.2	$a_0 > 0, c_0 = 0, c_2 > 0$	$P_0 \equiv P_1$ saddle-node, $P_2$ unstable node, $P_4$ stable node
1.3	$a_0 = 0, c_0 > 0, R_c - c_3 < 0, c_2 > 0$	$P_0 \equiv P_4$ saddle-node, $P_1$ stable node, $P_2$ saddle
1.4	$a_0 = 0, c_0 > 0, c_2 < 0, R_c - c_3 > 0$	$P_0 \equiv P_4$ saddle-node, $P_1$ stable node, $P_2$ stable node
1.5	$a_0 > 0, c_0 < 0, c_2 < 0, a_0 - c_0 > 0, (R_c - c_3) < 0$	$P_0$ saddle, $P_1$ unstable node, $P_2$ saddle, $P_4$ stable node
1.6	$a_0 > 0, c_0 < 0, a_0 - c_0 > 0, c_2 > 0, R_c - c_3 > 0$	$P_0$ saddle, $P_1$ unstable node, $P_2$ unstable node, $P_4$ stable node
1.7	$a_0 > 0, c_0 > 0, a_0 - c_0 > 0, c_2 < 0, R_c - c_3 > 0$	$P_0$ unstable node, $P_1$ saddle, $P_2$ saddle, $P_4$ stable node
1.8	$a_0 > 0, c_0 > 0, R_c - c_3 < 0, a_0 - c_0 > 0, c_2 > 0$	$P_0$ unstable node, $P_1$ saddle, $P_2$ unstable node, $P_4$ stable node
1.9	$a_0 > 0, c_0 > 0, a_0 - c_0 < 0, R_c - c_3 < 0, c_2 > 0$	$P_0$ unstable node, $P_1$ stable node, $P_2$ saddle, $P_4$ saddle
1.10	$a_0 > 0, c_0 > 0, a_0 - c_0 < 0, c_2 < 0, R_c - c_3 > 0$	$P_0$ unstable node, $P_1$ stable node, $P_2$ stable node, $P_4$ saddle

Table 3.1.2: Classification in case 1 of Table 3.1.1 according to the local phase portraits of finite singular points.

**Case 2:**  $c_3^2 > 4c_0c_2, c_1 = 0, a_0 > 0$

Sub.	Conditions	Classification
2.1	$c_0 < 0, a_0 - c_0 > 0, R_c - c_3 < 0, c_2 < 0$	$P_0$ saddle, $P_1$ unstable node, $P_2$ saddle
2.2	$c_0 < 0, a_0 - c_0 > 0, c_2 > 0, R_c - c_3 > 0$	$P_0$ saddle, $P_1$ unstable node, $P_2$ unstable node
2.3	$c_0 > 0, c_2(a_0 - c_0) < 0, R_c - c_3 > 0$	$P_0$ unstable node, $P_1$ saddle, $P_2$ saddle
2.4	$c_0 > 0, R_c - c_3 < 0, a_0 - c_0 > 0, c_2 > 0$	$P_0$ unstable node, $P_1$ saddle, $P_2$ unstable node
2.5	$c_0 > 0, a_0 - c_0 < 0, R_c - c_3 < 0, c_2 > 0$	$P_0$ unstable node, $P_1$ stable node, $P_2$ saddle
2.6	$c_0 > 0, a_0 - c_0 < 0, c_2 < 0, R_c - c_3 > 0$	$P_0$ unstable node, $P_1$ stable node, $P_2$ stable node
2.7	$c_0 = 0, a_0 > 0, c_2 < 0$	$P_0 \equiv P_1$ saddle-node, $P_2$ saddle
2.8	$c_0 = 0, a_0 > 0, c_2 > 0$	$P_0 \equiv P_1$ saddle-node, $P_2$ unstable node

Table 3.1.3: Classification in case 2 of Table 3.1.1 according to the local phase portraits of finite singular points.

### 3.1 Local study of finite singular points

**Case 3:**  $c_3^2 = 4c_0c_2, c_1 \neq 0$

Sub.	Conditions	Classification
3.1	$a_0 > 0, c_0 < 0, a_0 - c_0 > 0$	$P_0$ saddle, $P_3$ saddle-node, $P_4$ stable node
3.2	$a_0 > 0, c_0 > 0, a_0 - c_0 < 0$	$P_0$ unstable node, $P_3$ saddle-node, $P_4$ saddle
3.3	$a_0 > 0, c_0 > 0, a_0 - c_0 > 0$	$P_0$ unstable node, $P_3$ saddle-node, $P_4$ stable node
3.4	$a_0 = 0, c_0 > 0$	$P_0 \equiv P_4$ saddle-node, $P_3$ saddle-node
3.5	$c_0 = 0, a_0 > 0, c_2 < 0$	$P_0 \equiv P_3$ topological saddle, $P_4$ stable node
3.6	$c_0 = 0, a_0 > 0, c_2 > 0$	$P_0 \equiv P_3$ topological unstable node, $P_4$ stable node

Table 3.1.4: Classification in case 3 of Table 3.1.1 according to the local phase portraits of finite singular points.

**Case 4:**  $c_3^2 = 4c_0c_2, c_1 = 0, a_0 > 0$

Sub.	Conditions	Classification
4.1	$c_0 < 0$	$P_0$ saddle, $P_3$ saddle-node
4.2	$c_0 > 0$	$P_0$ unstable node, $P_3$ saddle-node
4.3	$c_0 = 0, c_2 < 0$	$P_0 \equiv P_3$ topological saddle
4.4	$c_0 = 0, c_2 > 0$	$P_0 \equiv P_3$ topological unstable node

Table 3.1.5: Classification in case 4 of Table 3.1.1 according to the local phase portraits of finite singular points.

**Case 5:**  $c_3^2 < 4c_0c_2, c_1 \neq 0$

Sub.	Conditions	Classification
5.1	$a_0 = 0$	$P_0 \equiv P_4$ saddle-node
5.2	$a_0 > 0, c_0 < 0, a_0 - c_0 > 0$	$P_0$ saddle, $P_4$ stable node
5.3	$a_0 > 0, c_0 > 0, a_0 - c_0 < 0$	$P_0$ unstable node, $P_4$ saddle
5.4	$a_0 > 0, c_0 > 0, a_0 - c_0 > 0$	$P_0$ unstable node, $P_4$ stable node

Table 3.1.6: Classification in case 5 of Table 3.1.1 according to the local phase portraits of finite singular points.

**Case 6:**  $c_3^2 < 4c_0c_2, c_1 = 0, a_0 > 0$

Sub.	Conditions	Classification
6.1	$c_0 < 0$	$P_0$ saddle
6.2	$c_0 > 0$	$P_0$ unstable node

Table 3.1.7: Classification in case 6 of Table 3.1.1 according to the local phase portraits of finite singular points.



### 3.2 Local study of infinite singular points

In order to study the behavior of the trajectories of systems (3.0.1) near infinity we consider the Poincaré compactification. We assume the hypothesis  $\tilde{H}^1$ . According to equations (1.3.9) and (1.3.10), we get the compactification in the local charts  $U_1$  and  $U_2$  respectively. To study all the infinite singular points, it is enough to study the singular points over  $v = 0$  in chart  $U_1$  and the origin of chart  $U_2$ .

We start with the study of the origin of chart  $U_2$ , which is simpler. The systems in this chart have the expression

$$\begin{aligned}\dot{u} &= (a_0 - c_0)uv^2, \\ \dot{v} &= -c_1uv^2 - c_0v^3 - c_3v^2 - c_2v.\end{aligned}$$

Over the line  $v = 0$  we get  $\dot{u}|_{v=0} = \dot{v}|_{v=0} = 0$ , then all points at infinity are singular points, including the origin which is the only one we must study in this chart. At the origin of this chart, one of the eigenvalues of the Jacobian matrix is zero and the other is  $-c_2$ . Applying Theorem 1.5.1 given in Section 1.5, we can conclude that if  $c_2 > 0$  there is exactly one orbit outside the infinity that goes to the origin of  $U_2$  and if  $c_2 < 0$  there is exactly one orbit from outside the infinity that leaves the origin of  $U_2$ .

Now we address the study of the infinite singular points in the local chart  $U_1$ , where the expression of the systems is

$$\begin{aligned}\dot{u} &= (c_0 - a_0)uv^2, \\ \dot{v} &= -c_2u^2v - c_3uv^2 - a_0v^3 - c_1v^2.\end{aligned}\tag{3.2.2}$$

Taking  $v = 0$  we get again that all points at infinity in this chart are singular points. At the origin, the eigenvalues of the Jacobian matrix are both zero. At a point  $(u_0, 0)$  with  $u_0 \neq 0$  the eigenvalues are one zero and the other  $-c_2u_0^2$  so, if  $c_2 > 0$ , then the nonzero eigenvalue is negative and exactly one orbit outside the infinity arrives at each infinite singular point on chart  $U_1$  distinct from the origin. If  $c_2 < 0$  the nonzero eigenvalue is positive so from each infinite singular point on chart  $U_1$  distinct from the origin leaves exactly one orbit from outside the infinity.

From the previous reasoning we can state the following result.

**Lemma 3.2.1.** *For any infinite singular point of systems (3.0.1) distinct from the origin of chart  $U_1$  the following statements hold:*

- If  $c_2 > 0$  exactly one orbit outside the infinity arrives to the singular point.
- If  $c_2 < 0$  exactly one orbit from outside the infinity leaves the singular point.

Now we must study in detail the origin of chart  $U_1$ , which we will name  $O_1$ . For this singular point we will prove the following result.

**Lemma 3.2.2.** *The origin of chart  $U_1$  is an infinite singular point of systems (3.0.1) and it has 12 distinct local phase portraits described in Figure 3.2.1.*

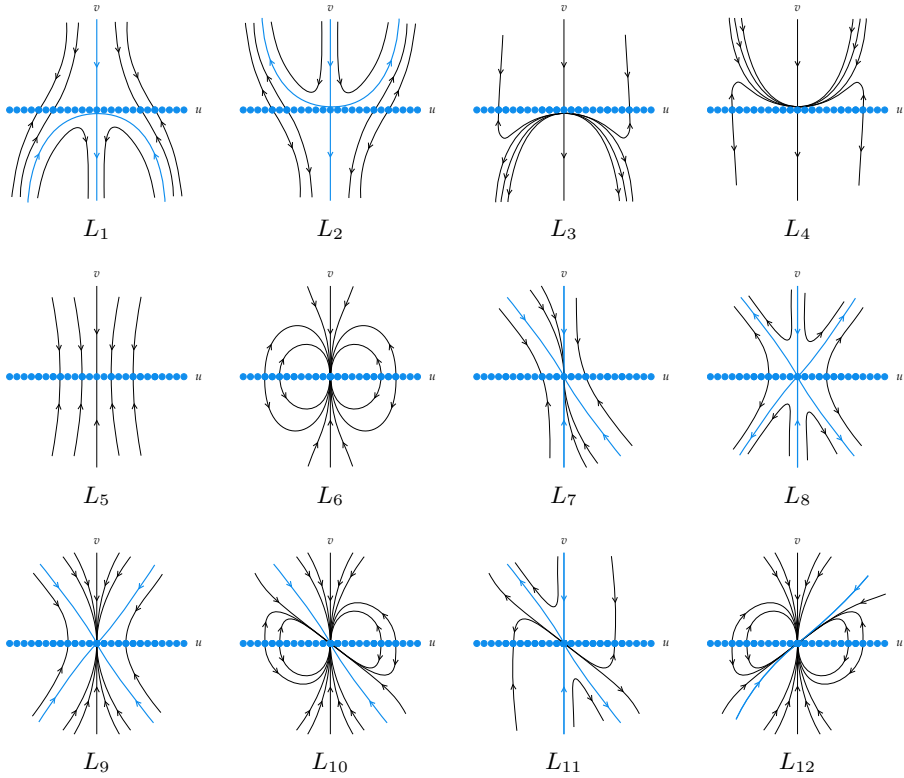


Figure 3.2.1: Local phase portraits at the infinite singular point  $O_1$ .

To prove Lemma 3.2.2, at first, we must eliminate a common factor  $v$  from systems (3.2.2) obtaining:

$$\begin{aligned}\dot{u} &= (c_0 - a_0)uv, \\ \dot{v} &= -c_2u^2 - c_3uv - a_0v^2 - c_1v.\end{aligned}\tag{3.2.3}$$

Now we must study the origin of these systems, which we name  $\tilde{O}_1$ , and which is now the only singular point over  $v = 0$ . The eigenvalues of the Jacobian matrix at  $\tilde{O}_1$  are zero and  $-c_1$ , so if  $c_1 \neq 0$  the singular point of systems (3.2.3) is semi-hyperbolic and we can study it applying Theorem 1.2.3. If  $c_1 = 0$  we must study this singular point with the blow up technique.

#### 3.2.1 Case with $\tilde{O}_1$ semi-hyperbolic

In order to apply the theorem for semi-hyperbolic singular points, we must change the sign of the flow, as the result requires the nonzero eigenvalue to be positive. We obtain systems

$$\begin{aligned}\dot{u} &= (a_0 - c_0)uv, \\ \dot{v} &= c_2u^2 + c_3uv + a_0v^2 + c_1v,\end{aligned}$$

and applying the mentioned result we get that the origin of these systems is a saddle point if  $c_2(a_0 - c_0) > 0$  and a topological unstable node if  $c_2(a_0 - c_0) < 0$ . Then, reversing the orientations, the singular point  $\tilde{O}_1$  is a saddle if  $c_2(a_0 - c_0) > 0$  and a topological stable node if  $c_2(a_0 - c_0) < 0$ . Before obtaining the corresponding phase portraits for  $O_1$ , we will distinguish four cases according to the sign of  $c_2$  and  $a_0 - c_0$ .

- (a) If  $c_2 > 0$  and  $a_0 - c_0 > 0$  then  $\tilde{O}_1$  is a saddle as in Figure 3.2.2(a). If we multiply by  $v$  to go back to systems (3.2.2), then all the points at the  $u$ -axis become singular points and the orientation of the orbits in the third and fourth quadrants is reversed. Thus, for  $O_1$  we obtain the local phase portrait in Figure 3.2.2(b), which is  $L_1$  of Figure 3.2.1.

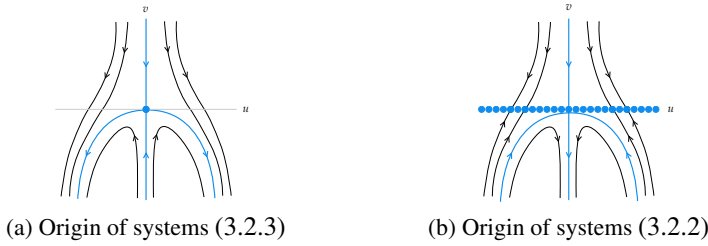


Figure 3.2.2: Local phase portraits of  $\tilde{O}_1$  and  $O_1$  with  $c_2 > 0$  and  $a_0 - c_0 > 0$ .

- (b) If  $c_2 < 0$  and  $a_0 - c_0 < 0$  then  $\tilde{O}_1$  is also a saddle, but with the sectors in a different position as in the previous case. Going back to systems (3.2.2) we obtain phase portrait  $L_2$  of Figure 3.2.1.
- (c) If  $c_2 > 0$  and  $a_0 - c_0 < 0$  then  $\tilde{O}_1$  is a stable topological node as represented in Figure 3.2.3(a). If we multiply by  $v$  to go back to systems (3.2.2), then all the points of the  $u$ -axis become singular points and the orientation of the orbits in the third and fourth quadrants is reversed. We obtain the local phase portrait in Figure 3.2.3(b), which is  $L_3$  of Figure 3.2.1.

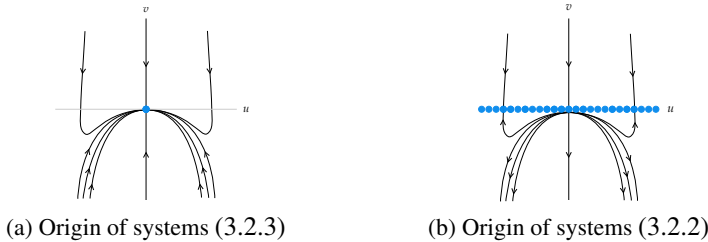


Figure 3.2.3: Local phase portraits of  $\tilde{O}_1$  and  $O_1$  with  $c_2 > 0$  and  $a_0 - c_0 < 0$ .

- (d) If  $c_2 < 0$  and  $a_0 - c_0 > 0$  then  $\tilde{O}_1$  is also a stable topological node, but with its orbits in a different position as in the previous case. Going back to systems (3.2.2) we obtain phase portrait  $L_4$  of Figure 3.2.1.

### 3.2.2 Case with $\tilde{O}_1$ linearly zero

In this subsection we study the local phase portrait of the origin of systems (3.2.3) assuming  $c_1 = 0$ . In order to do that we use the blow up technique. First we note that the characteristic polynomial is  $\mathcal{F} = -c_2u^3 - c_3u^2v - c_0uv^2$ , which cannot be identically zero because  $c_2 \neq 0$ , so the singular point  $\tilde{O}_1$  is nondicritical.

We introduce the variable  $w_1$  by means of the variable change  $uw_1 = v$ , and we obtain the systems:

$$\begin{aligned}\dot{u} &= (c_0 - a_0)u^2w_1, \\ \dot{w}_1 &= -c_0uw_1^2 - c_3uw_1 - c_2u.\end{aligned}$$

We eliminate a common factor  $u$  so we get

$$\begin{aligned}\dot{u} &= (c_0 - a_0)uw_1, \\ \dot{w}_1 &= -c_0w_1^2 - c_3w_1 - c_2.\end{aligned}\tag{3.2.4}$$

We must study the singular points of these systems over the line  $u = 0$ , which are the points with the first coordinate zero and the second one a solution of the equation  $-c_0w_1^2 - c_3w_1 - c_2 = 0$ . In the following we will distinguish several subcases.

- (A) If  $c_0 = 0$  and  $c_3 = 0$ , then there are no singular points over the line  $u = 0$ , as  $c_2 \neq 0$  by hypothesis.

**Subcase (A.1).** If  $c_2 > 0$ , we have for systems (3.2.4) the phase portrait given in Figure 3.2.4(a). If we multiply by  $u$ , then all the points over the  $w_1$ -axis become singular points, and the orbits on the second and third quadrants reverse their orientation, so we get the phase portrait in Figure 3.2.4(b). If we undo the blow up, contracting the exceptional divisor to the origin, and swapping the second and third quadrants, we obtain, for systems (3.2.3), the phase portrait in Figure 3.2.4(c). Lastly, if we multiply by  $v$  we get the local phase portrait for  $O_1$ , the origin of systems (3.2.2), which has a line consisting of singular points, the  $u$ -axis, and it is the phase portrait  $L_5$  given in Figure 3.2.1.

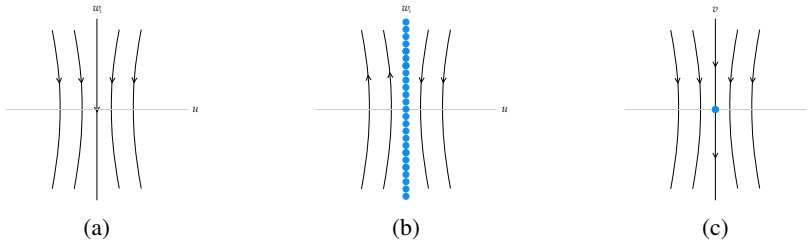


Figure 3.2.4: Desingularization of the origin of systems (3.2.2) with  $c_0 = c_1 = c_3 = 0$  and  $c_2 > 0$ .

**Subcase (A.2).** If  $c_2 < 0$  the vertical blow up does not determine the phase portrait, it only give us the information that over the  $u$ -axis the flow is vertical and it goes in the

positive sense. We must do a horizontal blow up to determine the phase portrait. In systems (3.2.3) we introduce the variable  $w_2$  by means of the change  $vw_2 = u$ , and with the hypothesis of this case we get the systems

$$\begin{aligned}\dot{w}_2 &= c_2 w_2^3 v, \\ \dot{v} &= -c_2 w_2^2 v - a_0 v^2.\end{aligned}\quad (3.2.5)$$

Eliminating a common factor  $v$  we obtain

$$\begin{aligned}\dot{w}_2 &= c_2 w_2^3, \\ \dot{v} &= -c_2 w_2^2 - a_0 v,\end{aligned}\quad (3.2.6)$$

and for these systems the only singular point over the line  $v = 0$  is the origin, which is semi-hyperbolic. Applying Theorem 1.2.3 we obtain that it is a stable topological node. The phase portrait around the origin for systems (3.2.6) is the one in Figure 3.2.5(a), and multiplying by  $v$ , the phase portrait for systems (3.2.5) is the one in Figure 3.2.5(b). Undoing the blow up, contracting the exceptional divisor into the origin and swapping the third and fourth quadrants, we get that in the first and second quadrants the orbits arrive to the origin tangent to the  $v$ -axis and in the third and fourth quadrants the orbits leave the origin tangent to the  $v$ -axis, this together with the information from the vertical blow up leads to the phase portrait in Figure 3.2.5(c). At last, if we multiply again by  $v$  we obtain the local phase portrait for  $O_1$  which is  $L_6$  of Figure 3.2.1.

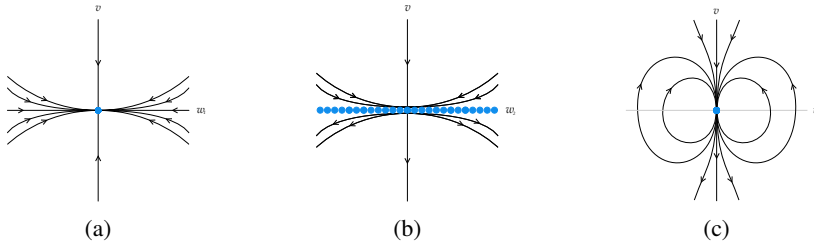


Figure 3.2.5: Desingularization of the origin of systems (3.2.2) with  $c_0 = c_1 = c_3 = 0$  and  $c_2 < 0$ .

- (B) If  $c_0 = 0$  and  $c_3 > 0$  then we have the hyperbolic singular point  $Q_1 = (0, -c_2/c_3)$ . At this point the eigenvalues of the Jacobian matrix are  $\lambda_1 = a_0 c_2/c_3$  and  $\lambda_2 = -c_3$  so we have two subcases.

**Subcase (B.1).** If  $c_2 > 0$  the vertical blow up does not determine the behavior of the orbits around the  $v$ -axis in the second and fourth quadrants. Then we do a horizontal blow up introducing the variable  $vw_2 = u$  in systems (3.2.3):

$$\begin{aligned}\dot{w}_2 &= c_2 w_2^3 v + c_3 w_2^2 v, \\ \dot{v} &= -c_2 w_2^2 v + c_3 w_2 v^2 - a_0 v^2,\end{aligned}\quad (3.2.7)$$

### 3.2 Local study of infinite singular points

and we eliminate a common factor  $v$ :

$$\begin{aligned}\dot{w}_2 &= c_2 w_2^3 - c_3 w_2^2, \\ \dot{v} &= -c_2 w_2^2 v - c_3 w_2 v - a_0 v.\end{aligned}\tag{3.2.8}$$

For systems (3.2.8) there are two singular points over the line  $v = 0$ , the origin which is a semi-hyperbolic saddle-node and the point  $(-c_3/c_2, 0)$  which is a saddle. The phase portrait around the  $w_2$ -axis for systems (3.2.8) is the one in Figure 3.2.6(a), and multiplying by  $v$ , the phase portrait for systems (3.2.7) is the one in Figure 3.2.6(b). Undoing the blow up we get the phase portrait in Figure 3.2.6(c). Finally, if we multiply again by  $v$ , we obtain the local phase portrait for  $O_1$  which is  $L_7$  of Figure 3.2.1.

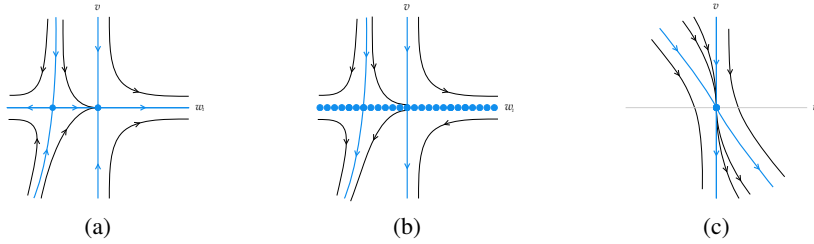


Figure 3.2.6: Desingularization of the origin of systems (3.2.2) with  $c_0 = c_1 = 0$ ,  $c_3 > 0$  and  $c_2 < 0$ .

**Subcase (B.2).** If  $c_2 < 0$  then  $Q_1$  is a stable node. We must do again a horizontal blow up to determine the local phase portrait, and thus we obtain again the phase portrait  $L_6$  of Figure 3.2.1.

(C) If  $c_0 \neq 0$ ,  $c_3 = 0$  and  $c_0 c_2 > 0$ , there are no singular points over  $u = 0$ .

**Subcase (C.1).** If  $c_0$  and  $c_2$  are positive, we obtain again the phase portrait  $L_5$  of Figure 3.2.1 by undoing the blow up.

**Subcase (C.2).** If  $c_0$  and  $c_2$  are negative, we obtain again the phase portrait  $L_6$  of Figure 3.2.1, but in this case it is necessary to do a horizontal blow up to conclude.

(D) If  $c_0 \neq 0$ ,  $c_3 = 0$  and  $c_0 c_2 < 0$ , there are two hyperbolic singular points over  $u = 0$ , namely,  $Q_2 = (0, \sqrt{-c_2/c_0})$  and  $Q_3 = (0, -\sqrt{-c_2/c_0})$ . By studying the eigenvalues of the Jacobian matrix at both points, we distinguish three subcases.

**Subcase (D.1).** If  $c_0 > 0$  and  $a_0 - c_0 > 0$  then  $Q_2$  is a stable node and  $Q_3$  is an unstable node. Undoing the blow up we obtain the phase portrait  $L_6$  of Figure 3.2.1.

**Subcase (D.2).** If  $c_0 > 0$  and  $a_0 - c_0 < 0$  then  $Q_2$  and  $Q_3$  are saddle points with the orientation of the hyperbolic orbits given in Figure 3.2.7(a). If we multiply by  $u$  and then we undo the blow up we obtain, respectively, the phase portraits in Figure 3.2.7(b) and

Figure 3.2.7(c). Multiplying by  $u$  again, we obtain that the local phase portrait for  $O_1$  is  $L_8$  of Figure 3.2.1.

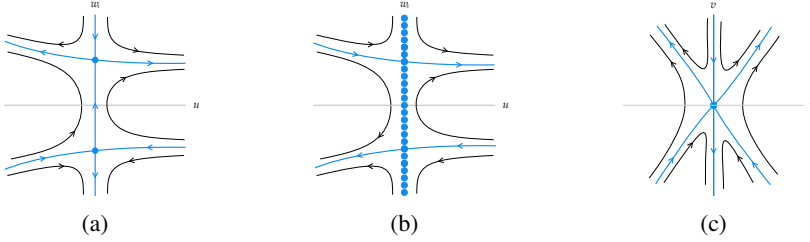


Figure 3.2.7: Desingularization of the origin of systems (3.2.2) with  $c_3 = 0$ ,  $c_0 > 0$ ,  $c_2 < 0$  and  $a_0 - c_0 < 0$ .

**Subcase (D.3).** If  $c_0 < 0$  and  $a_0 - c_0 > 0$  then  $Q_2$  and  $Q_3$  are saddle points with a different orientation than in the previous case. Now the vertical blow up does not determine the behavior of the orbits around the  $v$ -axis, so we must do a horizontal blow up introducing the variable  $w_2$  such that  $vw_2 = u$ . Then we obtain

$$\begin{aligned} \dot{w}_2 &= c_2 w_2^3 v + c_0 w_2 v, \\ \dot{v} &= -c_2 w_2^2 v - a_0 v^2, \end{aligned} \quad (3.2.9)$$

and if we eliminate a common factor  $v$ :

$$\begin{aligned} \dot{w}_2 &= c_2 w_2^3 + c_0 w_2, \\ \dot{v} &= -c_2 w_2^2 - a_0 v. \end{aligned} \quad (3.2.10)$$

For systems (3.2.10) there are three singular points over the line  $v = 0$ , the origin which is a stable node, and two saddle points  $(\pm\sqrt{-c_0/c_2}, 0)$ . The phase portrait around the  $w_2$ -axis for systems (3.2.10) is the one in Figure 3.2.8(a). If we multiply by  $v$  we get the phase portrait in Figure 3.2.8(b) for systems (3.2.9). Blowing down we obtain the phase portrait in Figure 3.2.8(c). If we multiply again by  $v$  we obtain the local phase portrait for  $O_1$  which is  $L_9$  of Figure 3.2.1.

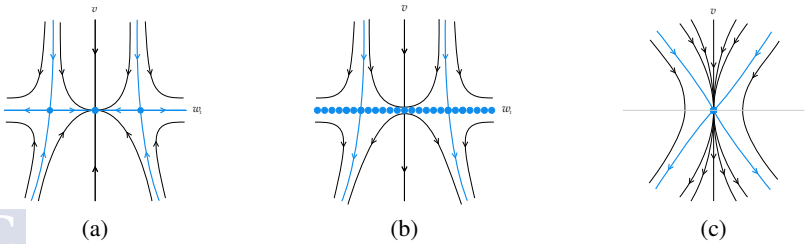


Figure 3.2.8: Desingularization of the origin of systems (3.2.2) with  $c_3 = 0$ ,  $c_0 < 0$ ,  $c_2 > 0$  and  $a_0 - c_0 > 0$ .

- (E) If  $c_0 \neq 0$ ,  $c_3 \neq 0$  and  $c_3^2 - 4c_0c_2 < 0$  then there are no singular points over the straight line  $u = 0$ .

**Subcase (E.1).** If  $c_2 > 0$  we obtain phase portrait  $L_5$  of Figure 3.2.1.

**Subcase (E.2).** If  $c_2 > 0$ , it is necessary to do a horizontal blow up, and thus we obtain the phase portrait  $L_6$  of Figure 3.2.1.

- (F) If  $c_0 \neq 0$ ,  $c_3 \neq 0$  and  $c_3^2 - 4c_0c_2 > 0$  then there are two hyperbolic singular points over  $u = 0$ , namely,

$$Q_4 = (0, -(c_3 + \sqrt{c_3^2 - 4c_0c_2})/(2c_0)) \text{ and } Q_5 = (0, -(c_3 - \sqrt{c_3^2 - 4c_0c_2})/(2c_0)).$$

We study these singular points and study separately the following six subcases.

**Subcase (F.1).** If  $a_0 - c_0 > 0$ ,  $c_0 > 0$  and  $R_c - c_3 > 0$  then  $Q_4$  is an unstable node and  $Q_5$  a stable node. Blowing down we obtain phase portrait  $L_6$  of Figure 3.2.1.

**Subcase (F.2).** If  $a_0 - c_0 > 0$ ,  $c_0 > 0$  and  $R_c - c_3 < 0$  then  $Q_4$  is an unstable node and  $Q_5$  a saddle. Blowing down we obtain phase portrait  $L_7$  of Figure 3.2.1.

**Subcase (F.3).** If  $a_0 - c_0 > 0$ ,  $c_0 < 0$  and  $R_c - c_3 > 0$  then  $Q_4$  and  $Q_5$  are saddle points, but the vertical blow up does not determine the behavior of the orbits around the  $v$ -axis. Doing a horizontal blow up we obtain phase portrait  $L_9$  of Figure 3.2.1.

**Subcase (F.4).** If  $a_0 - c_0 > 0$ ,  $c_0 < 0$  and  $R_c - c_3 < 0$  then  $Q_4$  is a saddle and  $Q_5$  is a stable node. Again the vertical blow up is not enough to determine the phase portrait. With a horizontal blow up we obtain phase portrait  $L_{10}$  of Figure 3.2.1.

**Subcase (F.5).** If  $a_0 - c_0 < 0$ ,  $c_0 > 0$  and  $R_c - c_3 > 0$  then  $Q_4$  and  $Q_5$  are saddle points. Blowing down we obtain phase portrait  $L_8$  of Figure 3.2.1.

**Subcase (F.6).** If  $a_0 - c_0 < 0$ ,  $c_0 > 0$  and  $R_c - c_3 < 0$  then  $Q_4$  is a saddle and  $Q_5$  is a stable node. Blowing down we obtain phase portrait  $L_{11}$  of Figure 3.2.1.

- (G) If  $c_0 \neq 0$ ,  $c_3 \neq 0$  and  $c_3^2 - 4c_0c_2 = 0$  then we have the singular point  $Q_6 = (0, -c_3/(2c_0))$ , which is a semi-hyperbolic saddle-node. Attending to the position of the different sectors we have the following cases.

**Subcase (G.1).** If  $c_0(a_0 - c_0) > 0$  and  $c_0 > 0$ , blowing down we obtain phase portrait  $L_7$  of Figure 3.2.1.

**Subcase (G.2).** If  $c_0(a_0 - c_0) < 0$  and  $c_0 > 0$ , blowing down we obtain phase portrait  $L_{11}$  of Figure 3.2.1.

**Subcase (G.3).** If  $c_0(a_0 - c_0) < 0$  and  $c_0 < 0$  the vertical blow up does not determine the phase portrait of  $O_1$ . Doing a horizontal blow up we get the phase portrait  $L_{12}$  of Figure 3.2.1.



### 3.3 Global phase portraits

In this section we bring together the local information obtained in Sections 3.1 and 3.2 to prove Theorem 3.0.1. In each case of Tables 3.1.2 to 3.1.7, the conditions determine the phase portrait of  $O_1$ , i.e., only one of the local phase portraits  $L_1$  to  $L_{12}$  in Figure 3.2.1 can appear in each case, except in case 4.2. In this case 4.2 we must distinguish two cases determined by the sign of  $a_0 - c_0$ .

Once determined the local phase portrait at the singular points, in most cases the place where born and die the separatrices is determined in a unique way. We draw these separatrices, one orbit in each canonical region which does not have an infinite number of singular points in the boundary, and three orbits (representing the infinite number of them existing) in each canonical region with an infinite number of singular points in the boundary. Thus we obtain the global phase portraits in Figure 3.3.6. In Table 3.3.1 we indicate which is the global phase portrait obtained in each case from the ones included in Figure 3.3.6.

Now we focus on the cases in which the separatrices can be connected in three different ways, namely 1.8, 1.9, 2.4, 2.5, 3.2 and 3.3. In the following we explain how it can be determined which of the three options is realizable.

**Case 1.8.** By Theorem 2.1.10(1) in Section 2.1 we know that on any straight line  $z = cte \neq 0$  there exists exactly one contact point. Two of the three global phase portraits obtained by connecting the separatrices contradict this result. In both cases, if we take the line  $z = (R_c - c_3)/2c_2$  we can find two contact points on it, one is the singular point  $P_1$  and the other is a point on the third quadrant, as shown in Figure 3.3.1. We can ensure the existence of this contact point as if we choose, for example, the point indicated with a square in Figure 3.3.1, the orbit passing through this point has as  $\alpha$ -limit the origin and as  $\omega$ -limit the singular point  $P_4$ , i.e., it is an orbit as the one drawn with dashed line, and that allows us to prove the existence of the contact point indicated with a cross. The same occurs in the two phase portraits included in Figure 3.3.1, then we can conclude that these two phase portraits are not realizable, and there is only one global phase portrait in case 1.8, and it is the G8 as it is indicated in Table 3.3.1.

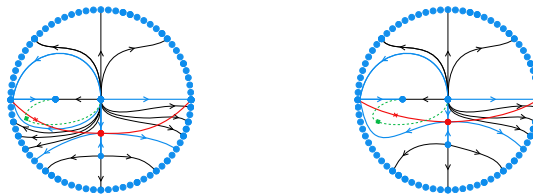


Figure 3.3.1: Global phase portraits appearing on case 1.8 that are not realizable.

**Case 1.9.** Here we can apply the same result than in the previous case to dismiss two global phase portraits. If we take a straight line  $z = z_0$  with  $-(R_c + c_3)/(2c_2) < z_0 < (R_c - c_3)/(2c_2)$ , then over this line there are two contact points, one in the third quadrant and other in the fourth quadrant, as shown in Figure 3.3.2. Thus the only global phase portrait in case 1.9 is the G9.

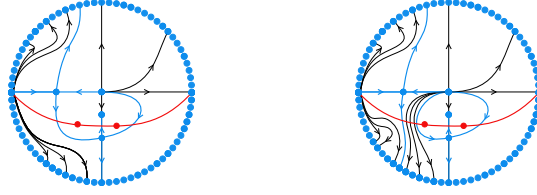


Figure 3.3.2: Global phase portraits appearing on case 1.9 that are not realizable.

**Case 2.4.** In this case we can connect the separatrices in three different ways by applying Corollary 2.1.4 in Section 2.1, because it ensures that the phase portraits must be symmetric with respect to the  $z$ -axis. Otherwise we would have more possible phase portraits. By Theorem 2.1.10(2) in Section 2.1, we know that there must exist two invariant straight lines  $z = (-c_3 \pm R_c)/(2c_2)$ , i.e., the lines  $z = cte$  passing through the singular points  $P_1$  and  $P_2$ . This is only possible in one of the three global phase portraits obtained by connecting the separatrices, namely in the G14 of Figure 3.3.6. In the other two global phase portraits these two invariant lines does not exist, as can be seen in Figure 3.3.3.

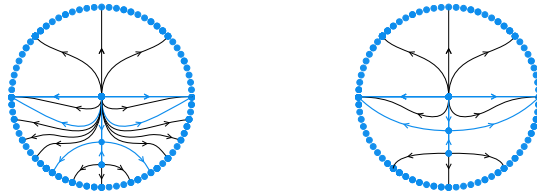


Figure 3.3.3: Global phase portraits appearing on case 2.4 that are not realizable.

**Case 2.5.** Here we can use the same arguments than in the previous case to prove that the only realizable phase portrait is the G15, so we do not give more details.

**Case 3.2.** We must apply again Theorem 2.1.10(1). In two of the three global phase portraits obtained by connecting the separatrices, if we take the line  $z = -c_3/(2c_2)$  we can find two contact points on it, one is the singular point  $P_3$  and the other is a point on the third quadrant, as shown in Figure 3.3.4. Thus, these two phase portraits are no realizable, and the only global phase portrait in case 3.2 is the G20, as indicated in Table 3.3.1.

**Case 3.3.** The same arguments that in the previous case are valid here. In Figure 3.3.5 the line with two contact points is represented in the two global phase portraits that are indeed not realizable. The only possible phase portrait in this case is the G21 of Figure 3.3.6.

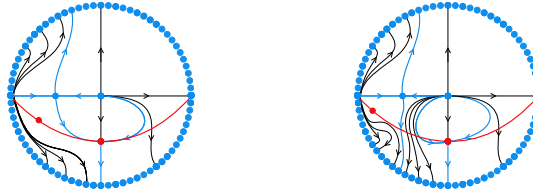


Figure 3.3.4: Global phase portraits appearing on case 3.2 that are not realizable.

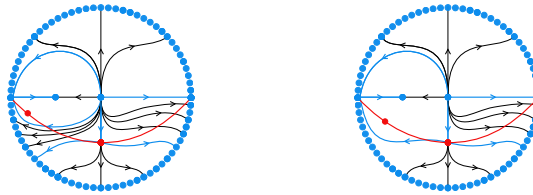


Figure 3.3.5: Global phase portraits appearing on case 3.3 that are not realizable.

Case	Subcase	$O_1$	Global
1.1		$L_4$	G1
1.2		$L_1$	G2
1.3		$L_3$	G3
1.4		$L_2$	G4
1.5		$L_4$	G5
1.6		$L_1$	G6
1.7		$L_4$	G7
1.8		$L_1$	G8
1.9		$L_3$	G9
1.10		$L_2$	G10
2.1		$L_{10}$	G11
2.2		$L_9$	G12
2.3		$L_6$	G13
2.4		$L_7$	G14
2.5		$L_{11}$	G15
2.6		$L_8$	G16
2.7		$L_6$	G17
2.8		$L_7$	G18

Case	Subcase	$O_1$	Global
3.1		$L_4$	G19
3.2		$L_3$	G20
3.3		$L_1$	G21
3.4		$L_3$	G22
3.5		$L_4$	G23
3.6		$L_1$	G24
4.1		$L_{12}$	G25
4.2	$a_0 - c_0 > 0$	$L_7$	G26
	$a_0 - c_0 < 0$	$L_{11}$	G27
4.3		$L_6$	G28
4.4		$L_5$	G29
5.1		$L_3$	G30
5.2		$L_4$	G23
5.3		$L_3$	G31
5.4		$L_1$	G24
6.1		$L_6$	G28
6.2		$L_5$	G29

Table 3.3.1: Classification of global phase portraits of systems (3.0.1).

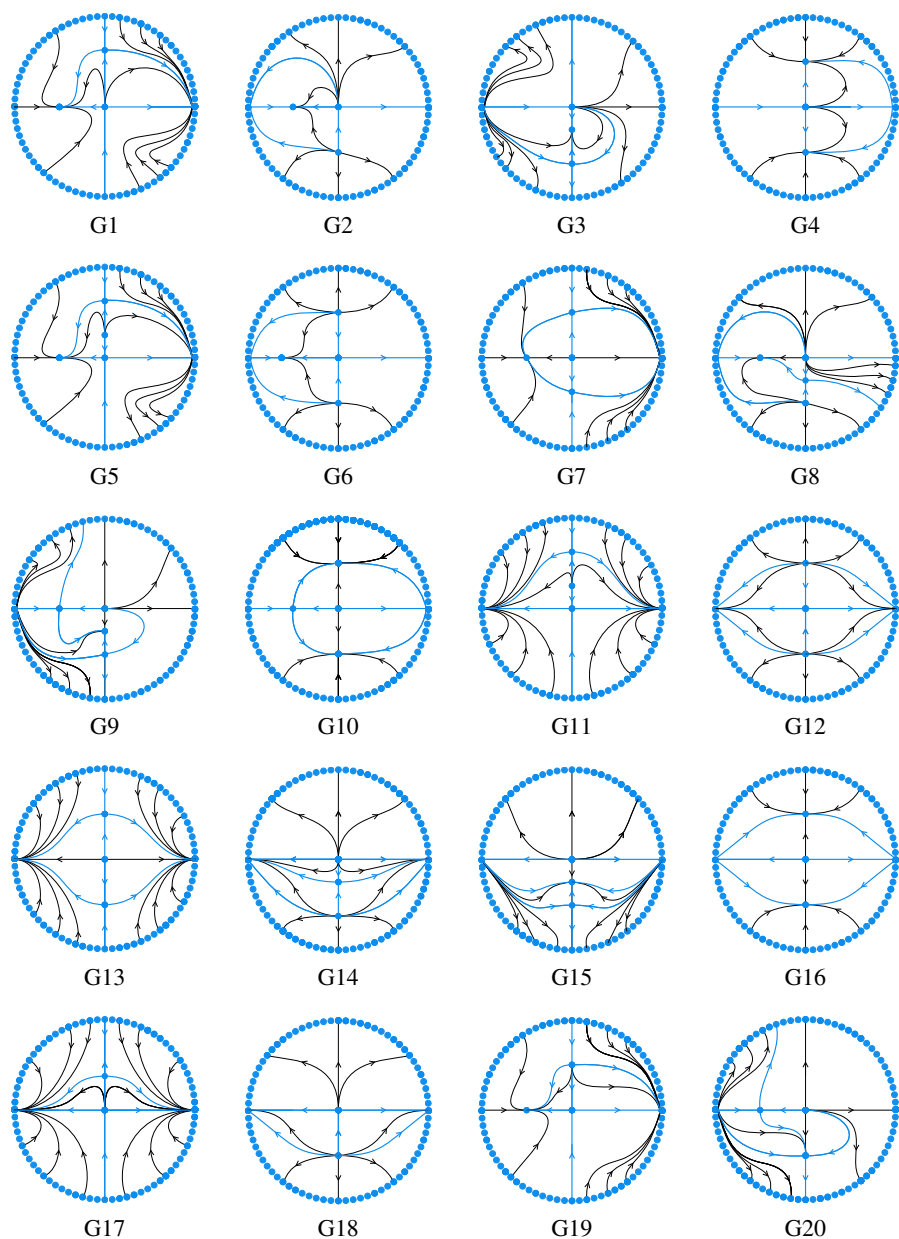


Figure 3.3.6 (1 out of 2): Global phase portraits of systems (3.0.1) in the Poincaré disk.

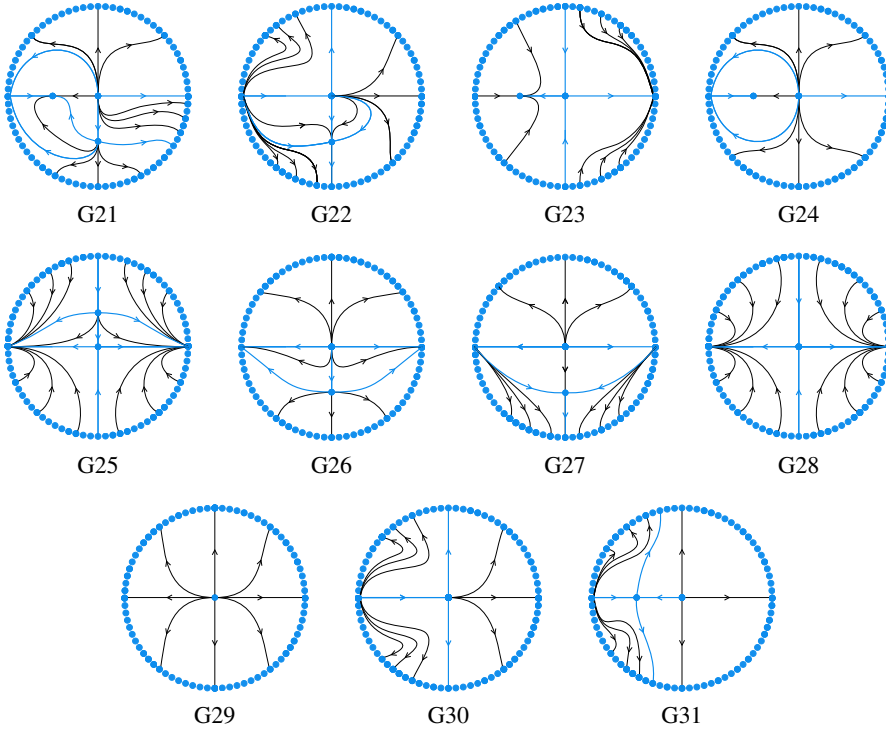


Figure 3.3.6 (2 out of 2): Global phase portraits of systems (3.0.1) in the Poincaré disk.

We have obtained 34 global phase portraits given in Figure 3.3.6, but some of them are topologically equivalent so we must study these equivalences. In order to apply Theorem 1.4.2 and determine which of them are topologically equivalent by studying the separatrix configurations, we consider only the open Poincaré disk. We will distinguish classes of equivalence according to the following invariants: the number of finite singular points and the sum of the indices at the finite singular points, denoted by  $ind_F$ . This classification is given in Table 3.3.2. Then within each class we prove which of the phase portraits are topologically equivalent and which are not.

**Class 1.** Global phase portrait G5 is topologically equivalent to G7 because if we move the unstable node in G5 to the origin we obtain G7. G5 is topologically distinct to G9 as in G9 all the orbits arriving to the stable node come from the unstable node or from a unique infinite singular point while in G5 there are orbits that arrive to the stable node from infinitely many infinite singular points. Then in this class there are two topologically different phase portraits represented by G5 and G9.

**Class 2.** G6 is topologically equivalent to G10 by moving the stable node in G6 to the origin, doing a symmetry with respect to the  $z$ -axis and doing a change of the time variable  $t$  by  $-t$ . G6 is different from G8 because in G6 there are four separatrices that connect infinite singular points with finite singular points and in G8 there are five separatrices of this kind. In this class there are two topologically different phase portraits represented by G6 and G8.

Class	N° finite singular points	$ind_F$	Global phase portraits
1	4	0	G5,G7,G9
2		2	G6,G8,G10
3	3	-1	G11,G13
4		0	G1, G3, G19, G20
5		1	G12,G14,G15
6		2	G2,G4,G21
7		3	G16
8	2	-1	G17, G25
9		0	G22, G23, G31
10		1	G18, G26, G27
11		2	G24
12	1	-1	G28
13		0	G30
14		1	G29

Table 3.3.2: Classes of equivalence according to the number of finite singular points and to the  $ind_F$ .

**Class 3.** G11 is topologically equivalent to G12 by moving the node in G11 to the origin. Then in this class there is only one topologically different phase portrait.

**Class 4.** G1 is different from G3 as to the node in G1 arrive orbits from infinitely many infinite singular points but in G3 only from one infinite singular point. G1 is topologically equivalent to G19 by moving the saddle in G1 to the origin and doing a symmetry with respect to the  $x$ -axis. G1 is topologically equivalent to G20: we must move the saddle in G20 to the origin and the unstable node to the positive  $x$ -axis, and then the saddle-node to the origin and the saddle to the positive  $z$ -axis. Then we must do a symmetry with respect to the  $z$ -axis and a change of the time variable  $t$  by  $-t$ . In this class there are two topologically different phase portraits represented by G1 and G3.

**Class 5.** G12 is topologically equivalent to G14 by moving the saddle in G14 to the origin. G14 is different from G15 because in both global phase portraits there are two nodes, but in G14 they have the same stability and in G15 one is stable and the other is unstable. In this class there are two topologically different phase portraits represented by G12 and G15.

**Class 6.** G2 is different from G4 because in both phase portraits there are two nodes, but in G2 they have different stability and in G4 the same. G21 is different from G2 and G4 because in G2 and G4 there are nine separatrices in the open Poincaré disk and in G21 there are 10 separatrices. Then in this class all the phase portraits are topologically different.

**Class 8.** G17 is topologically equivalent to G25 by moving the saddle-node in G17 to the origin and doing a symmetry with respect to the  $x$ -axis. Then in this class there is only one topologically different phase portrait.

**Class 9.** G22 is different from G23 because they have different kind of finite singular points. G23 is topologically equivalent to G31 by moving the node in G23 to the origin,

doing a symmetry with respect to the  $z$ -axis and a change of the time variable  $t$  by  $-t$ . In this class there are two topologically different phase portraits represented by G22 and G23.

**Class 10.** G18 is topologically equivalent to G26 by moving the node in G18 to the origin and doing a symmetry with respect to the  $x$ -axis. G26 is different from G27 because in G26 there are a separatrix that connects two finite singular points and in G27 there is not a such separatrix. In this class there are two topologically different phase portraits represented by G18 and G27.

Note that classes 7,11,12,13 and 14 have only one global phase portrait each of them. In summary, we have obtained 22 different phase portraits in the Poincaré disk for systems (3.0.1), so we have proved Theorem 3.0.1. This 22 phase portraits are described in Figure 3.0.1, where we include a representative of each one of the topological equivalence classes. These representatives correspond with the phase portraits in Figure 3.3.6 as indicated in Table 3.3.3.

Rep.	Phase portraits	Rep.	Phase portraits	Rep.	Phase portraits
R1	G1, G19, G20	R9	G11, G13	R17	G23, G31
R2	G2	R10	G12, G14	R18	G24
R3	G3	R11	G15	R19	G27
R4	G4	R12	G16	R20	G28
R5	G5, G7	R13	G17, G25	R21	G29
R6	G6, G10	R14	G18, G26	R22	G30
R7	G8	R15	G21		
R8	G9	R16	G22		

Table 3.3.3: Representatives of each equivalence class and their corresponding global phase portraits of systems (3.0.1).

# Classification of the second Kolmogorov family with isolated singularities

---

In this chapter we study the global dynamics of the second family of Kolmogorov systems obtained in Chapter 1, i.e., the systems

$$\begin{aligned}\dot{y} &= y(b_0 + b_1 yz + b_2 y + b_3 z), \\ \dot{z} &= z(c_0 - \mu(b_1 yz + b_2 y + b_3 z)),\end{aligned}\tag{4.0.1}$$

for which we give the topological classification of all the global phase portraits in the Poincaré disk. We prove that it is sufficient to study these systems under conditions

$$H_2^2 = \{b_1 \neq 0, b_0\mu + c_0 \neq 0, b_0 \geq 0, b_2 \geq 0, b_3 \geq 0, \mu^2 b_3^2 + c_0^2 \neq 0, b_2^2 + b_0^2 \neq 0, \mu \neq -1\},$$

since in any other case they can be reduced to simpler systems already studied, except the case with  $\mu = -1$ , in which there is a continuum of singular points at infinity, but we study that case in detail in Chapter 5. Our main result is the following.

**Theorem 4.0.1.** *Kolmogorov systems (4.0.1) under conditions  $H_2^2$  have 52 topologically distinct phase portraits in the Poincaré disk, given in Figure 4.0.1.*

Based on the contents of the research article [44]<sup>1</sup>, we give the complete proof of Theorem 4.0.1, organized as follows: In Section 4.1 we give some properties of the systems that are useful to simplify the task of determine all the topologically distinct phase portraits of the systems. In Section 4.2 we study the local phase portrait of the finite singular points, and in Sections 4.3 and 4.4 we do the same with the infinite singular points, applying the blow up technique. Finally, in Section 4.5 we prove Theorem 4.0.1.

---

<sup>1</sup>Erika Diz-Pita (Departamento de Estadística, Análise Matemática e Optimización, Universidade de Santiago de Compostela), Jaume Llibre (Departament de Matemàtiques, Universitat Autònoma de Barcelona) and María Victoria Otero-Espinar (Departamento de Estadística, Análise Matemática e Optimización, Universidade de Santiago de Compostela), *Planar Kolmogorov systems coming from spatial Lotka-Volterra systems*, International Journal of Bifurcation and Chaos, (ISSN:1007-5704, EISSN:1878-7274), **31**(3) (2021), 2150201. Published by World Scientific. The final authenticated version is available online at: <https://doi.org/10.1142/S0218127421502011>.



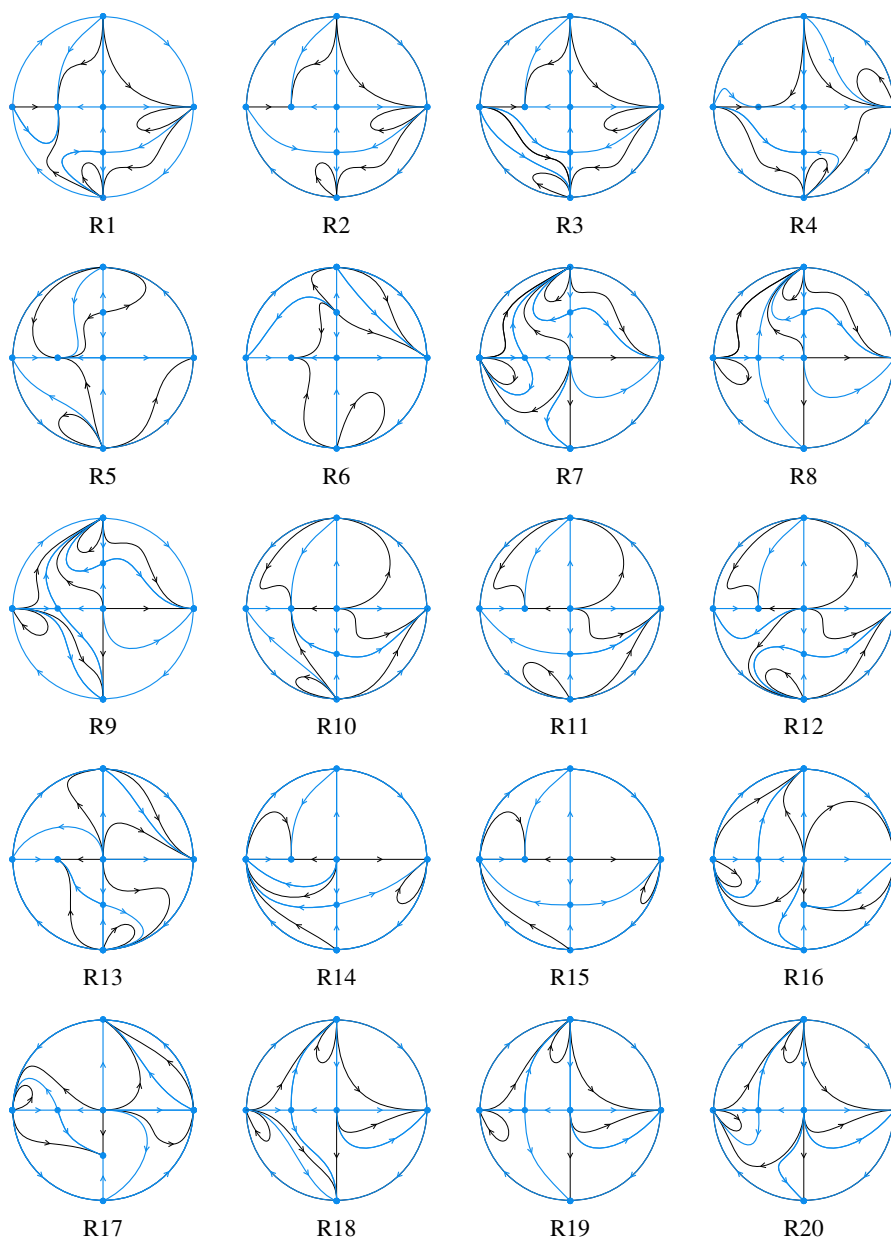


Figure 4.0.1 (1 out of 3): The topologically distinct phase portraits of systems (4.0.1) in the Poincaré disk.

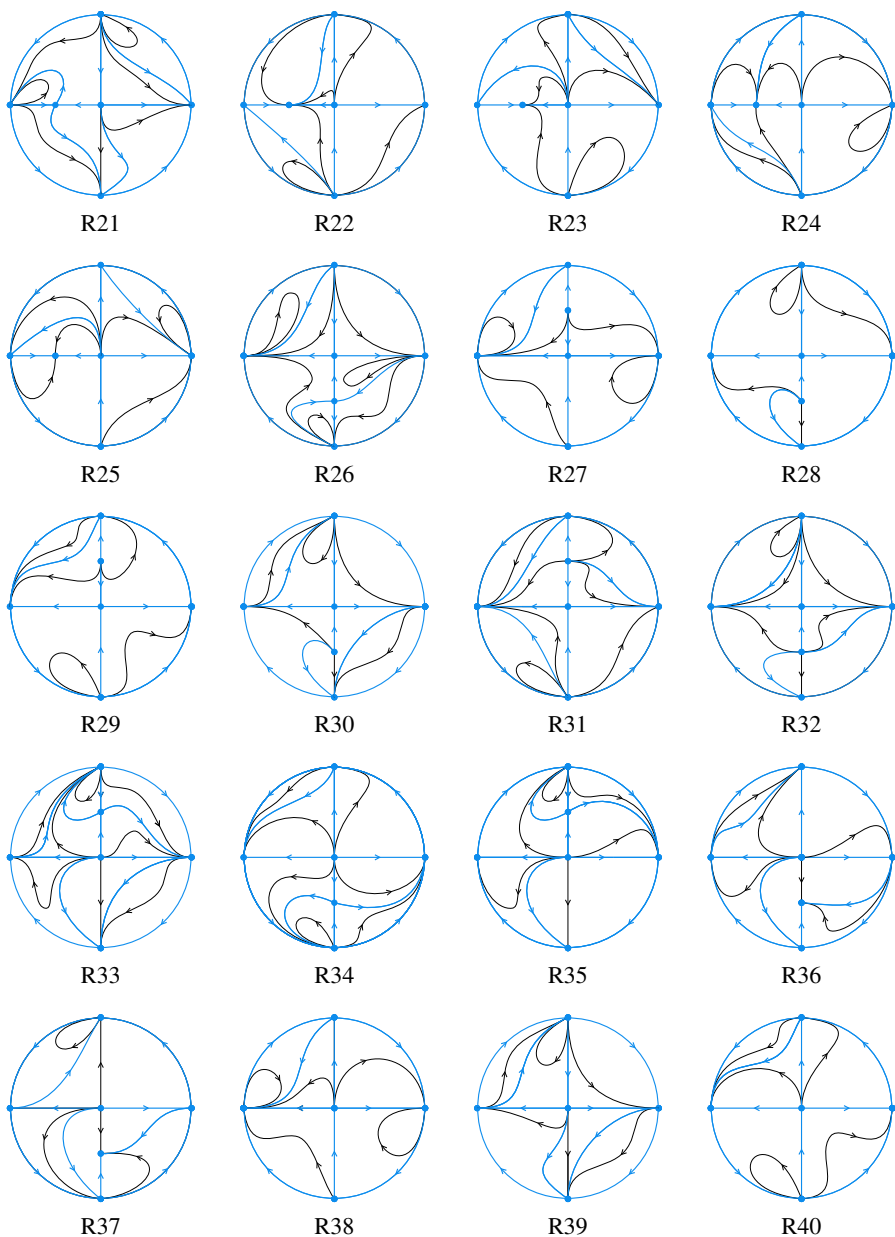


Figure 4.0.1 (2 out of 3): The topologically distinct phase portraits of systems (4.0.1) in the Poincaré disk.

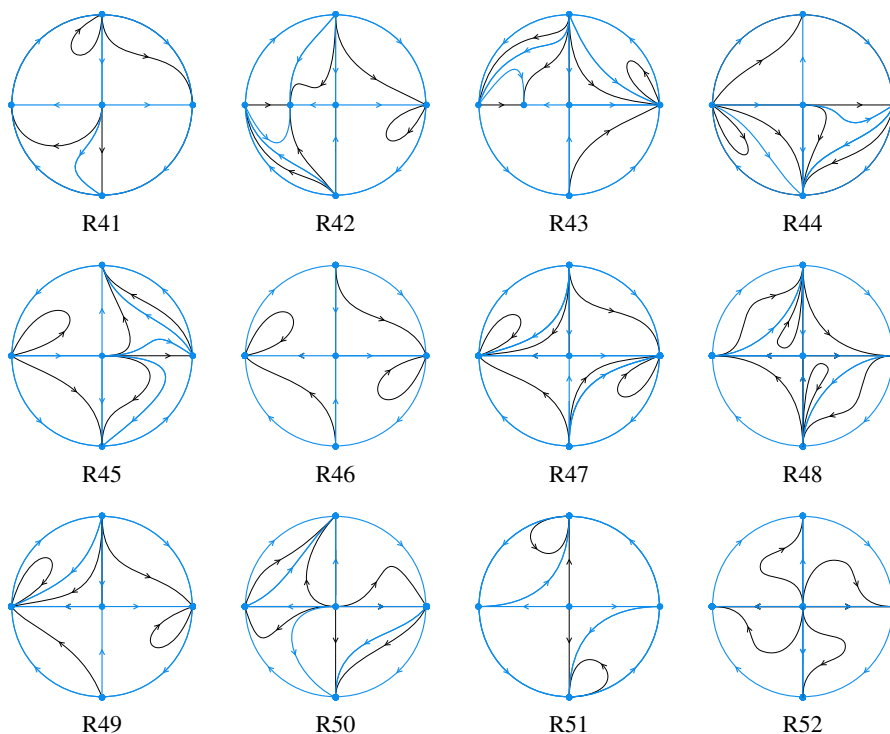


Figure 4.0.1 (3 out of 3): The topologically distinct phase portraits of systems (4.0.1) in the Poincaré disk.

## 4.1 Properties of the systems

In this section we state some results that will be useful to reduce the number of global phase portraits appearing. First, note that if  $b_1 = 0$ , then systems (4.0.1) are Lotka-Volterra systems in dimension two. A global topological classification of these systems has been completed in [117], so we limit our study to the case  $b_1 \neq 0$ .

We recall that for obtaining systems (4.0.1) we have supposed that systems (1.7.15) have the Darboux invariant  $y^\mu z e^{-t(c_0 + b_0 \mu)}$ , so it is required that  $c_0 + b_0 \mu \neq 0$ . The proofs of the next propositions are simple and analogous to those of the results in Section 2.1 so we omit them.

**Proposition 4.1.1.** *Let  $(\tilde{y}(t), \tilde{z}(t))$  be a solution of systems (4.0.1). In the next cases we obtain other systems with solution  $(-\tilde{y}(-t), -\tilde{z}(-t))$ .*

1. If  $c_0, b_0$  and  $b_1$  are not zero, and we change the sign of all of them.
2. If  $b_0 = 0$  and we change the sign of  $c_0$  and  $b_1$ , which are not zero.
3. If  $c_0 = 0$  and we change the sign of  $b_0$  and  $b_1$ , which are not zero.

**Remark 4.1.2.** By Proposition 4.1.1 we can limit our study to Kolmogorov systems (4.0.1) with  $b_0$  non-negative. In the cases with this parameter negative, we would obtain phase portraits symmetric to the ones obtained in the cases with the positive parameter. When  $b_0 = 0$  we will consider also  $c_0 > 0$ .

**Proposition 4.1.3.** Consider systems (4.0.1) and suppose that  $(\tilde{y}(t), \tilde{z}(t))$  is a solution of these systems. If we change  $b_1$  by  $-b_1$  and  $b_2$  by  $-b_2$  (respectively  $b_3$  by  $-b_3$ ), then  $(-\tilde{y}(t), \tilde{z}(t))$  (respectively  $(\tilde{y}(t), -\tilde{z}(t))$ ) is a solution of the obtained systems.

**Corollary 4.1.4.** Consider systems (4.0.1) and suppose  $(\tilde{y}(t), \tilde{z}(t))$  is a solution. If  $b_2 = 0$  (respectively  $b_3 = 0$ ) and we change  $b_1$  by  $-b_1$ , then  $(-\tilde{y}(t), \tilde{z}(t))$  (respectively  $(\tilde{y}(t), -\tilde{z}(t))$ ) is a solution.

**Remark 4.1.5.** In order to classify all the phase portraits of the Kolmogorov systems (4.0.1), according to the previous results, it is sufficient to consider  $b_2 \geq 0$  and  $b_3 \geq 0$ . When  $b_2 b_3 = 0$  we will consider also  $b_1 > 0$ .

**Remark 4.1.6.** In short, according to the previous results and considerations, from now on it will be sufficient to study the Kolmogorov systems (4.0.1) with their parameters satisfying

$$H^2 = \{b_1 \neq 0, c_0 + b_0\mu \neq 0, b_0 \geq 0, b_2 \geq 0, b_3 \geq 0\},$$

and with  $c_0 > 0$  if  $b_0 = 0$ , and  $b_1 > 0$  if  $b_2 b_3 = 0$ .

## 4.2 Finite singular points

Systems (4.0.1) have the following finite singularities:

$$P_0 = (0, 0), \quad P_1 = \left(0, \frac{c_0}{\mu b_3}\right) \text{ if } \mu b_3 \neq 0 \text{ and } P_2 = \left(-\frac{b_0}{b_2}, 0\right) \text{ if } b_2 \neq 0.$$

Moreover, if  $\mu b_3 = 0$  and  $c_0 = 0$ , all the points on the  $z$ -axis are singular points, and if  $b_2^2 + b_0^2 = 0$  all the points on the  $y$ -axis are singular points. In both cases the systems can be reduced to quadratic systems with an invariant straight line. More precisely, if  $\mu b_3 = 0$  and  $c_0 = 0$ , then by condition  $b_0\mu + c_0 \neq 0$  we must have  $b_3 = 0$ , and systems (2.0.1) are of the form

$$\begin{aligned} \dot{y} &= (b_0 + b_1 y z + b_2 y), \\ \dot{z} &= -\mu y z (b_1 z + b_2). \end{aligned}$$

If we introduce the time variable  $s$  such that  $ds = y dt$ , then we get the quadratic systems

$$\begin{aligned} \frac{dy}{ds} &= b_0 + b_1 y z + b_2 y, \\ \frac{dz}{ds} &= -\mu z (b_1 z + b_2). \end{aligned}$$

with the invariant line  $z = 0$ .

In the second case, if  $b_0^2 + b_2^2 = 0$  systems (2.0.1) write

$$\begin{aligned}\dot{y} &= y(b_1 y z + b_3 z), \\ \dot{z} &= z(c_0 - \mu b_1 y z - \mu b_3 z).\end{aligned}$$

If we introduce the time variable  $s$  such that  $ds = z dt$ , we obtain again quadratic systems:

$$\begin{aligned}\frac{dy}{ds} &= y(b_1 y + b_3), \\ \frac{dz}{ds} &= c_0 - \mu b_1 y z - \mu b_3 z.\end{aligned}$$

These systems also have an invariant line  $y = 0$ .

As this kind of systems have been already studied in [6], from now on we will consider the hypothesis

$$H_1^2 = \{b_1 \neq 0, b_0 \mu + c_0 \neq 0, b_0 \geq 0, b_2 \geq 0, b_3 \geq 0, (\mu b_3)^2 + c_0^2 \neq 0, b_2^2 + b_0^2 \neq 0\}.$$

**Theorem 4.2.1.** *Systems (4.0.1) have no limit cycles.*

*Proof.* The straight lines  $y = 0$  and  $z = 0$  are invariant sets and all the singular points of systems (4.0.1) are over these axes. If there were any periodic orbit in the plane, it would be surrounding one of the singular points, and therefore it would intersect an invariant set, which is not possible.  $\square$

Assuming  $H_1^2$  there are four different cases according to the finite singular points existing for systems (4.0.1), which are given in Table 4.2.1. Then we study the possible local phase portraits in each one of the finite singular points under the hypothesis  $H_1^2$ .

Case	Conditions	Finite singular points
1	$\mu b_3 \neq 0, b_2 \neq 0$	$P_0, P_1, P_2$
2	$\mu b_3 \neq 0, b_2 = 0, b_0 \neq 0$	$P_0, P_1$
3	$\mu b_3 = 0, c_0 \neq 0, b_2 \neq 0$	$P_0, P_2$
4	$\mu b_3 = 0, c_0 \neq 0, b_2 = 0, b_0 \neq 0$	$P_0$

Table 4.2.1: The different cases for the finite singular points.

The origin is always an isolated singular point for systems (4.0.1), and we have the next classification for its phase portraits: If  $b_0 c_0 \neq 0$  the origin is hyperbolic and two cases are possible, it is a saddle point if  $c_0 < 0$ , and it is an unstable node if  $c_0 > 0$ . If  $b_0 c_0 = 0$  the origin is a semi-hyperbolic saddle-node.

When  $P_1$  is a singular point of systems (4.0.1), it can present different phase portraits although it is always a hyperbolic singular point, except when it coincides with the origin. If

$c_0 \neq 0$ , then  $P_1$  is hyperbolic and it can present the following phase portraits: If  $c_0\mu(b_0\mu + c_0) > 0$ , then  $P_1$  is a saddle; if  $c_0 > 0$ ,  $\mu < 0$  and  $b_0\mu + c_0 > 0$ , it is a stable node; and finally, if  $c_0 < 0$  and  $\mu(b_0\mu + c_0) > 0$ , it is an unstable node. The singular point  $P_1$  collides with the origin if  $c_0 = 0$ .

When  $P_2$  is a singular point of systems (4.0.1), it is a saddle if  $b_0\mu + c_0 > 0$ , and it is a stable node if  $b_0\mu + c_0 < 0$ . If  $b_0 = 0$  then  $P_2$  collides with the origin.

Now, combining the classifications given above for the phase portraits of the singular points, we obtain the following result:

**Lemma 4.2.2.** *Assuming hypothesis  $H_1^2$  there are 22 different cases according to the local phase portrait of the finite singular points of systems (4.0.1), which are given in Tables 4.2.2 - 4.2.5.*

*Proof.* We have to analyze cases 1 to 4 in Table 4.2.1 and determine the local phase portraits of the singular points existing in each one of them, according to their individual classification.

We start with the first one, in which the conditions  $\mu b_3 \neq 0$  and  $b_2 \neq 0$  hold. The singular points are  $P_0$ ,  $P_1$  and  $P_2$ .

Consider the case with  $c_0 < 0$  and  $b_0 \neq 0$ , in which the origin is a saddle. Then  $P_1$  can be a saddle if  $\mu(b_0\mu + c_0) < 0$ , or an unstable node if  $\mu(b_0\mu + c_0) > 0$ . If  $P_1$  is a saddle, then  $P_2$  is a stable node, because if it was a saddle with  $b_0\mu + c_0 > 0$ , then  $\mu < 0$  and so  $b_0\mu < 0$  and  $b_0\mu + c_0 < 0$ , which is a contradiction. If  $P_1$  is an unstable node, then  $P_2$  can be either a saddle or a stable node. This leads to cases 1.1 to 1.3 in Table 4.2.2.

We continue with the case  $c_0 > 0$  and  $b_0 > 0$ , in which  $P_0$  is an unstable node. Now  $P_1$  can be a saddle or a stable node. If  $P_1$  is a saddle, then  $P_2$  can be a saddle or a stable node, but if  $P_1$  is a stable node, then  $b_0\mu + c_0 > 0$ , and so  $P_2$  is always a saddle. This leads to cases 1.4 to 1.6.

If  $P_0$  is a saddle-node with  $c_0 = 0$  and  $b_0 > 0$ , then  $P_1$  coincides with the origin and  $P_2$  can be a saddle or a stable node. If  $P_0$  is a saddle-node with  $b_0 = 0$  and  $c_0 > 0$ , then  $P_2$  coincides with the origin and  $P_1$  can be a saddle or a stable node. We recall that by the hypothesis it is not possible to have  $b_0$  and  $c_0$  simultaneously zero;  $b_0$  is non negative and if  $b_0 = 0$  then we consider  $c_0 > 0$  by Proposition 4.1.1, so this allows us to conclude the classification in case 1 of Table 4.2.1.

Now we study case 2 of Table 4.2.1, in which  $\mu b_3 \neq 0$ ,  $b_2 = 0$  and  $b_0 \neq 0$ . The singular points are  $P_0$  and  $P_1$ . If  $P_0$  is a saddle, then  $P_1$  can be only a saddle or an unstable node, by the sign of the parameter  $c_0$ . Likewise the sign of  $c_0$  determines that if  $P_0$  is an unstable node,  $P_1$  can be a saddle or a stable node. This leads to cases 2.1 to 2.4 of Table 4.2.3. At last, if  $c_0 = 0$  then  $P_1$  coincides with the origin and it is a saddle-node.

We address the case 3 of Table 4.2.1, in which  $\mu b_3 = 0$ ,  $c_0 \neq 0$  and  $b_2 \neq 0$ . The origin can be a saddle or an unstable node and in both cases  $P_2$  can be a saddle or a stable node, as  $b_0 \neq 0$ . If  $b_0 = 0$  then  $P_2$  coincides with the origin and it is a saddle-node.

Finally, in case 4 of Table 4.2.1, we have the conditions  $\mu b_3 = 0$ ,  $c_0 \neq 0$ ,  $b_2 = 0$  and  $b_0 \neq 0$ . The unique singular point is the origin and as  $c_0 b_0$  cannot be zero, it is either a saddle or an unstable node.

□

**Case 1:  $\mu b_3 \neq 0, b_2 \neq 0$** 

Sub.	Conditions	Classification
1.1	$b_0 > 0, c_0 < 0, \mu > 0, (b_0\mu + c_0) < 0$	$P_0$ saddle, $P_1$ saddle, $P_2$ stable node
1.2	$b_0 > 0, c_0 < 0, \mu > 0, b_0\mu + c_0 > 0$	$P_0$ saddle, $P_1$ unstable node, $P_2$ saddle
1.3	$b_0 > 0, c_0 < 0, \mu < 0, b_0\mu + c_0 < 0$	$P_0$ saddle, $P_1$ unstable node, $P_2$ stable node
1.4	$b_0 > 0, c_0 > 0, \mu > 0, b_0\mu + c_0 > 0$	$P_0$ unstable node, $P_1$ saddle, $P_2$ saddle
1.5	$b_0 > 0, c_0 > 0, \mu < 0, b_0\mu + c_0 < 0$	$P_0$ unstable node, $P_1$ saddle, $P_2$ stable node
1.6	$b_0 > 0, c_0 > 0, \mu < 0, b_0\mu + c_0 > 0$	$P_0$ unstable node, $P_1$ stable node, $P_2$ saddle
1.7	$c_0 = 0, \mu > 0$	$P_0 \equiv P_1$ saddle-node, $P_2$ saddle
1.8	$c_0 = 0, b_0 > 0, \mu < 0$	$P_0 \equiv P_1$ saddle-node, $P_2$ stable node
1.9	$b_0 = 0, \mu > 0$	$P_0 \equiv P_2$ saddle-node, $P_1$ saddle
1.10	$b_0 = 0, c_0 > 0, \mu < 0$	$P_0 \equiv P_2$ saddle-node, $P_1$ stable node

Table 4.2.2: Classification in case 1 of Table 4.2.1 according to the local phase portraits of finite singular points.

**Case 2:  $\mu b_3 \neq 0, b_2 = 0, b_0 \neq 0$** 

Sub.	Conditions	Classification
2.1	$b_0 > 0, c_0 < 0, \mu > 0, b_0\mu + c_0 < 0$	$P_0$ saddle, $P_1$ saddle
2.2	$b_0 > 0, c_0 < 0, \mu(b_0\mu + c_0) > 0$	$P_0$ saddle, $P_1$ unstable node
2.3	$b_0 > 0, c_0 > 0, \mu(b_0\mu + c_0) > 0$	$P_0$ unstable node, $P_1$ saddle
2.4	$b_0 > 0, c_0 > 0, \mu < 0, b_0\mu + c_0 > 0$	$P_0$ unstable node, $P_1$ stable node
2.5	$c_0 = 0, b_0 > 0$	$P_0 \equiv P_1$ saddle-node

Table 4.2.3: Classification in case 2 of Table 4.2.1 according to the local phase portraits of finite singular points.

**Case 3:  $\mu b_3 = 0, c_0 \neq 0, b_2 \neq 0$** 

Sub.	Conditions	Classification
3.1	$b_0 > 0, c_0 < 0, \mu > 0, b_0\mu + c_0 > 0$	$P_0$ saddle, $P_2$ saddle
3.2	$b_0 > 0, c_0 < 0, b_0\mu + c_0 < 0$	$P_0$ saddle, $P_3$ stable node
3.3	$b_0 > 0, c_0 > 0, b_0\mu + c_0 > 0$	$P_0$ unstable node, $P_2$ saddle
3.4	$b_0 > 0, c_0 > 0, \mu < 0, b_0\mu + c_0 < 0$	$P_0$ unstable node, $P_2$ stable node
3.5	$b_0 = 0, c_0 > 0$	$P_0 \equiv P_3$ saddle-node

Table 4.2.4: Classification in case 3 of Table 4.2.1 according to the local phase portraits of finite singular points.

### 4.3 Local study of infinite singular points in chart $U_1$

**Case 4:**  $\mu b_3 = 0, c_0 \neq 0, b_2 = 0, b_0 \neq 0$

Sub.	Conditions	Classification
4.1	$b_0 c_0 < 0$	$P_0$ saddle
4.2	$b_0 > 0, c_0 > 0$	$P_0$ unstable node

Table 4.2.5: Classification in case 4 of Table 4.2.1 according to the local phase portraits of finite singular points.

### 4.3 Local study of infinite singular points in chart $U_1$

In order to study the behavior of the trajectories of systems (4.0.1) near infinity, we consider its Poincaré compactification. For the moment we assume the same hypothesis  $H_1^2$  than in previous sections. From Section 1.3 it is enough to study the singular points over  $v = 0$  in chart  $U_1$  and the origin of chart  $U_2$ . We will deal with the study of the origin of chart  $U_2$  in Section 4.4, so now we focus on the chart  $U_1$ . According to equation (1.3.9) we get the compactification in the local chart  $U_1$ , where systems (4.0.1) write

$$\begin{aligned}\dot{u} &= -b_3(\mu + 1)u^2v + (c_0 - b_0)uv^2 - b_1(\mu + 1)u^2 - b_2(\mu + 1)uv, \\ \dot{v} &= -b_3uv^2 - b_0v^3 - b_1uv - b_2v^2.\end{aligned}\quad (4.3.2)$$

Taking  $v = 0$  we get  $\dot{u}|_{v=0} = -b_1(\mu + 1)u^2$  and  $\dot{v}|_{v=0} = 0$ . Therefore, if  $\mu = -1$ , all points at infinity are singular points, and we will not deal with this situation in this chapter. In other case, if  $\mu \neq -1$ , the only singular point is the origin of  $U_1$ , which we denote by  $O_1$ . As the linear part of systems (4.3.2) at the origin is identically zero, we use the blow up technique to study it, leading to the next result, which is proved in Subsections 4.3.1 and 4.3.2.

From now on we include the condition  $\mu \neq -1$  in our hypothesis, so we will work under conditions

$$H_2^2 = \{b_1 \neq 0, b_0\mu + c_0 \neq 0, b_0 \geq 0, b_2 \geq 0, b_3 \geq 0, \mu^2 b_3^2 + c_0^2 \neq 0, b_2^2 + b_0^2 \neq 0, \mu \neq -1\}.$$

**Lemma 4.3.1.** *Assuming hypothesis  $H_2^2$ , the origin of chart  $U_1$  is an infinite singular point of systems (4.0.1), and it has 27 distinct local phase portraits described in Figure 4.3.1.*

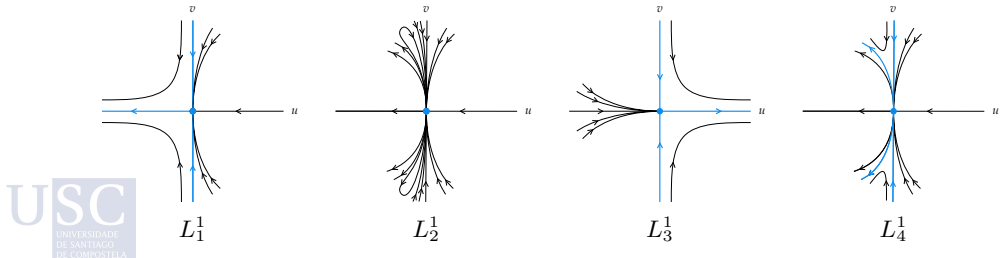
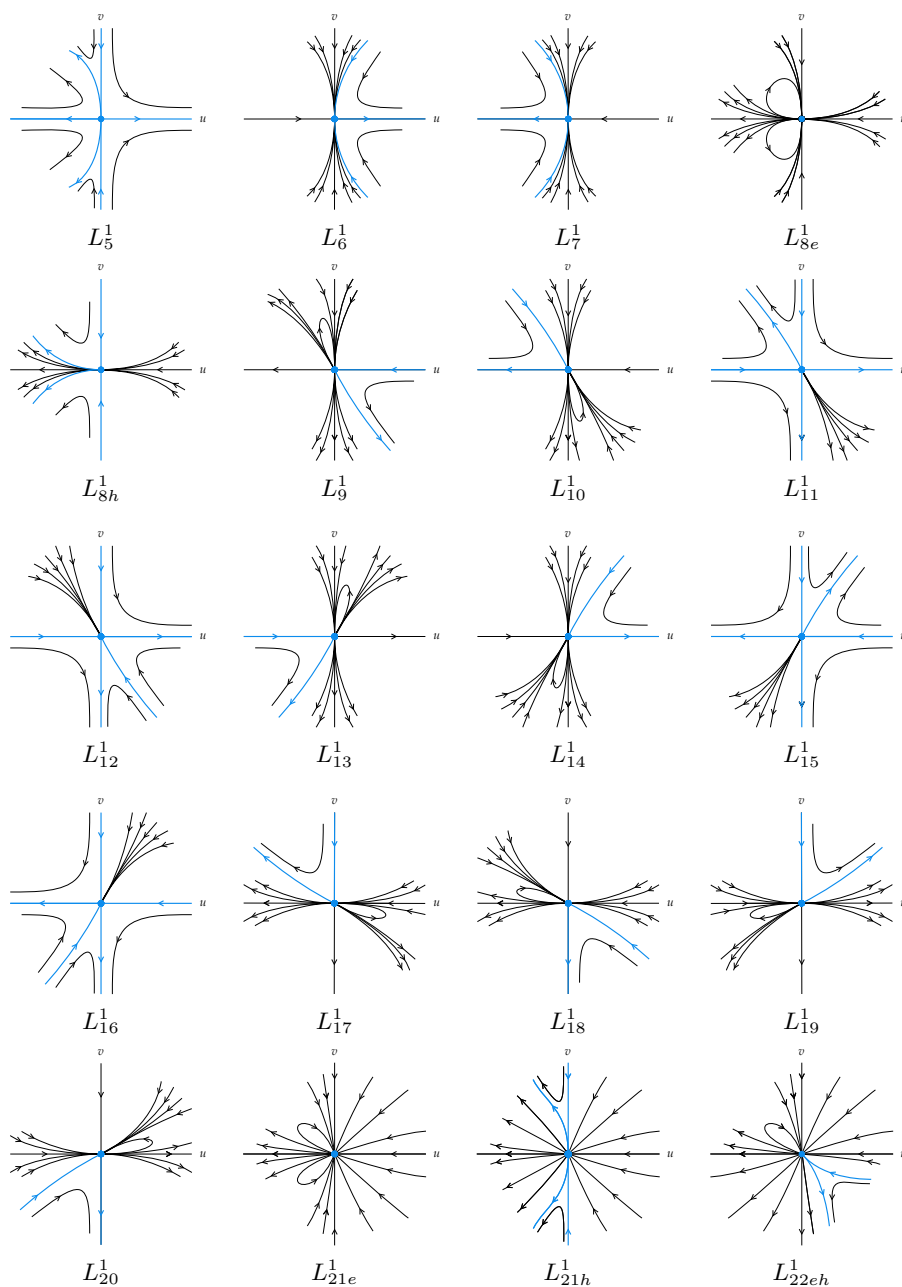
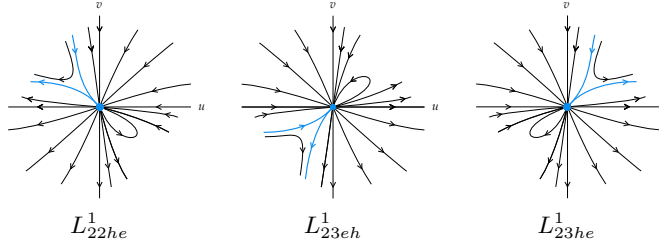


Figure 4.3.1 (1 out of 3): Local phase portraits of the infinite singular point  $O_1$ .




 Figure 4.3.1 (2 out of 3): Local phase portraits of the infinite singular point  $O_1$ .


 Figure 4.3.1 (3 out of 3): Local phase portraits of the infinite singular point  $O_1$ .

In the following subsections we prove Lemma 4.3.1. For systems (4.3.2) the characteristic polynomial is  $\mathcal{F} = b_2\mu uv^2 + b_1\mu u^2v$ , so the origin is a nondicritical singular point if  $\mu \neq 0$  and it is dicritical if  $\mu = 0$ . We will study these two cases separately.

We introduce the new variable  $w_1$  by means of the variable change  $uw_1 = v$ , and get the systems

$$\begin{aligned}\dot{u} &= (c_0 - b_0)u^3w_1^2 - b_3(\mu + 1)u^3w_1 - b_2(\mu + 1)u^2w_1 - b_1(\mu + 1)u^2, \\ \dot{w}_1 &= b_3\mu u^2w_1^2 - c_0u^2w_1^3 + b_2\mu uw_1^2 + b_1\mu ww_1.\end{aligned}$$

In the nondicritical case we have to cancel the common factor  $u$  obtaining

$$\begin{aligned}\dot{u} &= (c_0 - b_0)u^2w_1^2 - b_3(\mu + 1)u^2w_1 - b_2(\mu + 1)uw_1 - b_1(\mu + 1)u, \\ \dot{w}_1 &= b_3\mu uw_1^2 - c_0uw_1^3 + b_2\mu w_1^2 + b_1\mu w_1.\end{aligned}\tag{4.3.3}$$

In the dicritical case, when  $\mu = 0$ , we must cancel the common factor  $u^2$  and we obtain the systems

$$\begin{aligned}\dot{u} &= (c_0 - b_0)uw_1^2 - b_3uw_1 - b_2w_1 - b_1, \\ \dot{w}_1 &= -c_0w_1^3.\end{aligned}\tag{4.3.4}$$

### 4.3.1 Nondicritical case

At first, it is necessary to study the singular points of systems (4.3.3) on the exceptional divisor. The origin is always a singular point, and we denote it by  $Q_0$ . When  $b_2 \neq 0$  there is another singular point,  $Q_1 = (0, -b_1/b_2)$ .

The origin,  $Q_0$ , is always hyperbolic. It is a saddle if  $\mu \in (-\infty, -1) \cup (0, +\infty)$ , a stable node if  $\mu \in (-1, 0)$  and  $b_1 > 0$ , and an unstable node if  $\mu \in (-1, 0)$  and  $b_1 < 0$ . The singular point  $Q_1$  is always a semi-hyperbolic saddle-node. These conditions come together in the next five subcases.

- (A) If  $b_2 = 0$ ,  $b_0 \neq 0$  and  $\mu \in (-\infty, -1) \cup (0, +\infty)$ , then the only singular point on the exceptional divisor is  $Q_0$  which is a saddle. In this case the vertical blow up done does not provide a well determined phase portrait, so it is necessary to apply a horizontal

blow up. In order to do that, we introduce the variable  $w_1 = u/v$  on systems (4.3.2) obtaining:

$$\begin{aligned}\dot{w}_1 &= -\mu b_3 v^2 w_1^2 - \mu b_1 v w_1^2 + c_0 v^2 w_1, \\ \dot{v} &= -b_3 v^3 w_1 - b_1 v^2 w_1 - b_0 v^3,\end{aligned}\tag{4.3.5}$$

and eliminating a common factor  $v$  we get the systems

$$\begin{aligned}\dot{w}_1 &= -\mu b_3 v w_1^2 - \mu b_1 w_1^2 + c_0 v w_1, \\ \dot{v} &= -b_3 v^2 w_1 - b_1 v w_1 - b_0 v^2,\end{aligned}\tag{4.3.6}$$

for which the only singular point on the exceptional divisor is the origin, and it is linearly zero, so we have to repeat the process.

Now the characteristic polynomial is  $\mathcal{F} = b_1(\mu - 1)w_1^2 v - (b_0 + c_0)w_1 v^2$ , so the origin is always nondicritical. Note that, as  $b_1 \neq 0$ ,  $\mathcal{F} \equiv 0$  if and only if  $c_0 = -b_0$  and  $\mu = 1$ , but in that case  $b_0\mu + c_0 = 0$  which contradicts hypothesis  $H_2^2$ . Now we introduce the new variable  $w_2 = w_1/v$ , obtaining the systems

$$\begin{aligned}\dot{w}_2 &= -b_3(\mu - 1)w_2^2 v^2 - b_1(\mu - 1)w_2^2 v + (b_0 + c_0)w_2 v, \\ \dot{v} &= -b_3 w_2 v^3 - b_1 w_2 v^2 - b_0 v^2,\end{aligned}\tag{4.3.7}$$

and eliminating a common factor  $v$ , we get

$$\begin{aligned}\dot{w}_2 &= -b_3(\mu - 1)w_2^2 v - b_1(\mu - 1)w_2^2 + (b_0 + c_0)w_2, \\ \dot{v} &= -b_3 w_2 v^2 - b_1 w_2 v - b_0 v.\end{aligned}\tag{4.3.8}$$

The singular points of systems (4.3.8) on the exceptional divisor are the origin  $S_0$  and the singular point  $S_1 = ((b_0 + c_0)/(b_1(\mu - 1)), 0)$  if  $\mu \neq 1$  (note that it coincides with the origin if  $b_0 + c_0 = 0$ ). We determine their local phase portraits obtaining the classification given below. We start with the cases in which the only singular point on the exceptional divisor is the origin:

**Subcase (A.1).** If  $b_0 + c_0 = 0$  and  $\mu \neq 1$ , then the origin is a semi-hyperbolic saddle-node. The relative position and orientation of the hyperbolic and parabolic sectors depends on the sign of  $\mu$  and  $\mu - 1$ . Thus we deal with the following subcases.

**(A.1.1).** Let  $\mu > 1$ . This determines the sense of the flow on the  $w_2$ -axis, so the phase portrait around this axis for systems (4.3.8) is the one in Figure 4.3.2(a).

To return to systems (4.3.7) we multiply by  $v$ , thus the orbits in the third and fourth quadrants change their orientation. Moreover, all the points on the  $w_2$ -axis become singular points. The resultant phase portrait is given in Figure 4.3.2(b).

When going back to the  $(w_1, v)$ -plane, the third and fourth quadrants swap from the  $(w_2, v)$ -plane, and the exceptional divisor shrinks to a point, and hence the orbits are slightly modified. Attending to the expressions of  $\dot{w}_1|_{v=0} = -\mu b_1 w_1^2$  and  $\dot{v}|_{w_1=0} = -b_0 v^2$ , we know the sense of the flow along the axes. Following Proposition 1.2.6,

we get the phase portrait given in Figure 4.3.2(c), and multiplying again by  $v$ , the one given in Figure 4.3.2(d).

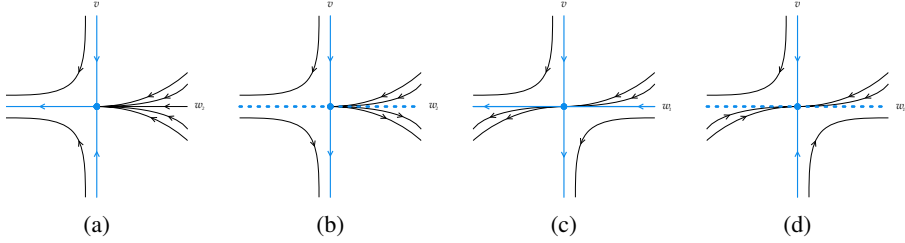


Figure 4.3.2: Desingularization of the origin of systems (4.3.2) in nondicritical case (A.1.1).

Finally, we must go back to the  $(u, v)$ -plane, swapping again the third and the fourth quadrants and contracting the exceptional divisor to the origin. The orbits tending to the origin in forward or backward time, became orbits tending to the origin in forward or backward time tangent to the  $v$ -axis. For the origin of systems (4.3.2) we get the local phase portrait  $L_1^1$  given in Figure 4.3.1.

**(A.1.2).** Let  $\mu \in (0, 1)$ . In this case the phase portrait around the  $w_2$ -axis for systems (4.3.8) is the one in Figure 4.3.3(a), and multiplying by  $v$ , the phase portrait for systems (4.3.7) is 4.3.3(b).

Here, if we try go back to the  $(w_1, v)$ -plane, swapping the third and fourth quadrants and shrinking the exceptional divisor, the phase portrait is not determined on the first and third quadrants and around the  $w_1$ -axis, and the only information we have is given in Figure 4.3.3(c). We must do a vertical blow up on systems (4.3.6). We introduce the new variable  $w_3 = v/w_1$  and get the systems

$$\begin{aligned}\dot{w}_1 &= -b_3\mu w_1^3 w_3 + c_0 w_1^2 w_3 - \mu b_1 w_1^2, \\ \dot{w}_3 &= b_3(\mu - 1)w_1^2 w_3^2 + b_1(\mu - 1)w_1 w_3.\end{aligned}\tag{4.3.9}$$

Now we eliminate a common factor  $w_1$ :

$$\begin{aligned}\dot{w}_1 &= -b_3\mu w_1^2 w_3 + c_0 w_1 w_3 - \mu b_1 w_1, \\ \dot{w}_3 &= b_3(\mu - 1)w_1 w_3^2 + b_1(\mu - 1)w_3.\end{aligned}\tag{4.3.10}$$

The only singular point on the exceptional divisor is the origin, which is a stable node. The phase portrait around the  $w_1$ -axis for systems (4.3.10) is the one in Figure 4.3.3(d), and multiplying by  $v$ , the phase portrait for systems (4.3.9) is the one in Figure 4.3.3(e). Undoing the vertical blow up we obtain Figure 4.3.3(f) where the behavior around the  $v$ -axis, in the colored regions, is not determined. Combining this phase portrait with the information in Figure 4.3.3(c), it is, that there are orbits which go to the origin tangent to the  $v$ -axis on the second quadrant, and there are orbits which leave the origin tangent to the  $v$ -axis on the fourth quadrant, we can conclude that for systems

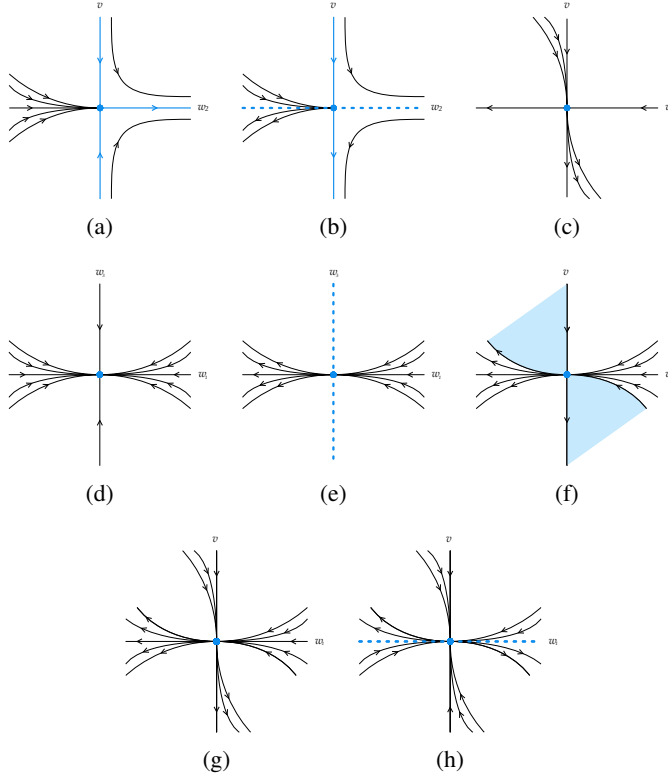


Figure 4.3.3: Desingularization of the origin of systems (4.3.2) in nondicritical case (A.1.2).

(4.3.6) we have phase portrait in Figure 4.3.3(g). In the second and fourth quadrants it would be possible to have a hyperbolic sector or an elliptic one, but we have proved in the global phase portraits, by applying index theory, that the only feasible option is the one with the elliptic sector.

We must multiply by  $v$  and we get the phase portrait given in Figure 4.3.2(h) for systems (4.3.5). Now we undo the first horizontal blow up done and hence we obtain for  $O_1$  the phase portrait  $L_2^1$  given in Figure 4.3.1, where the existence of the elliptic sector is proved in the global phase portraits, as we have just mentioned.

**(A.1.3).** Taking  $\mu < 0$  and similarly to the first subcase, we obtain for  $O_1$  the local phase portrait  $L_3^1$  given in Figure 4.3.1.

**Subcase (A.2).** If  $\mu = 1$  and  $b_0 + c_0 > 0$ , then the origin is a saddle. Here, when undoing the blow ups, it is necessary again to do a vertical blow up on systems (4.3.6), and after that we obtain the same phase portrait as in the first subcase, it is  $L_1^1$ .

**Subcase (A.3).** If  $\mu = 1$  and  $b_0 + c_0 < 0$ , then the origin is a stable node. Again, including a vertical blow up on systems (4.3.6), we obtain phase portrait  $L_2^1$ . As in

the first case in which we obtained this local phase portrait, the blow up does not determine if the elliptic sectors are indeed elliptic, but we prove it when analyzing the global phase portraits.

Now we consider the cases with two singular points on the exceptional divisor:

**Subcase (A.4).** If  $b_0 + c_0 > 0$  and  $(b_0\mu + c_0)(\mu - 1) < 0$ , then the origin and  $S_1$  are saddles. The phase portrait for systems (4.3.8) is in Figure 4.3.4(a) and multiplying by  $v$ , the phase portrait for systems (4.3.7) is in Figure 4.3.4(b).

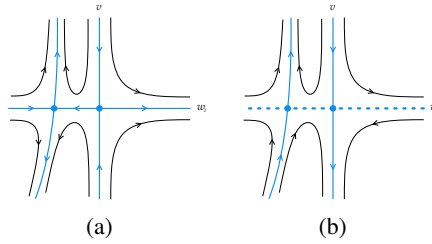


Figure 4.3.4: Desingularization of the origin of systems (4.3.2) in nondicritical case (A.4).

To go back to the  $(w_1, v)$ -plane we have to distinguish two cases, one with  $\mu < -1$  and other with  $\mu \in (0, 1)$ . In the first one, the subsequent phase portraits are well determined and we arrive easily to final phase portrait  $L_5^1$  in Figure 4.3.1. If  $\mu \in (0, 1)$ , the phase portrait for systems (4.3.6) is not determined. We must do a vertical blow up, introducing the variable  $w_3 = v/w_1$ . We get the systems

$$\begin{aligned}\dot{w}_1 &= -b_3\mu w_1^3 w_3 + c_0 w_1^2 w_3 - \mu b_1 w_1^2, \\ \dot{w}_3 &= b_3(\mu - 1)w_1^2 w_3^2 - (b_0 + c_0)w_1 w_3^2 + b_1(\mu - 1)w_1 w_3,\end{aligned}$$

and eliminating a common factor  $w_1$ :

$$\begin{aligned}\dot{w}_1 &= -b_3\mu w_1^2 w_3 + c_0 w_1 w_3 - \mu b_1 w_1, \\ \dot{w}_3 &= b_3(\mu - 1)w_1 w_3^2 - (b_0 + c_0)w_3^2 + b_1(\mu - 1)w_3.\end{aligned}\tag{4.3.11}$$

These systems have two singular points on the exceptional divisor: the origin, which is a stable node, and the point  $(0, b_1(\mu - 1)/(b_0 + c_0))$  which is a saddle. Studying the sense of the flow on the axes, we get that the phase portrait for systems (4.3.11) is the one in Figure 4.3.5(a). Multiplying by  $w_1$  and undoing the vertical blow up, we obtain, respectively, the phase portraits in Figure 4.3.5(b) and (c). Now the phase portrait for systems (4.3.6) is well determined, and we can go on undoing the first horizontal blow up, getting the final phase portrait  $L_4^1$ .

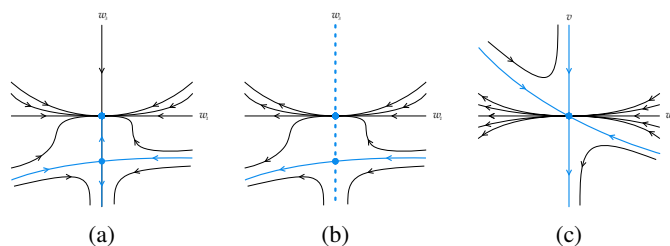


Figure 4.3.5: Vertical blow up on systems (4.3.6) in nondicritical case (A.4).

**Subcase (A.5).** If  $b_0 + c_0 > 0$  and  $(b_0\mu + c_0)(\mu - 1) > 0$ , then the origin is a saddle and  $S_1$  is a stable node. We must distinguish three cases in function of the sign of  $\mu - 1$ , which determines the position of the singular point  $Q_1$  on systems (4.3.8), and the sense of the flow on the axes on systems (4.3.6). We do not get any new phase portrait for  $O_1$  in this case. If we take  $\mu < 0$ , then we obtain the same phase portrait as in subcase A1.3, it is,  $L_3^1$ , and with  $\mu > 1$ , we obtain the phase portrait  $L_1^1$ . At last, with  $\mu \in (0, 1)$ , we obtain the phase portrait  $L_2^1$ , but in this case it is necessary to do a vertical blow up on systems (4.3.6) during the desingularization process.

**Subcase (A.6).** If  $b_0 + c_0 < 0$  and  $(b_0\mu + c_0)(\mu - 1) > 0$ , then the origin is a stable node and  $S_1$  is a saddle. This case is similar to the previous one and we should distinguish three cases: if  $\mu < 0$ , we obtain the phase portrait  $L_6^1$ ; if  $\mu > 1$ , we obtain phase portrait  $L_7^1$ ; and if  $\mu \in (0, 1)$ , we need to do a vertical blow up of systems (4.3.6) and we obtain phase portrait  $L_2^1$ . As we mentioned before, we have proved that the elliptic sectors are always elliptic in the global phase portraits, although it is not provided by the blow ups. Here, as in the first case in which we obtained this local phase portrait, the blow up does not determine that the elliptic sectors are indeed elliptic, but we prove it when analyzing the global phase portraits.

**Subcase (A.7).** If  $b_0 + c_0 < 0$  and  $(b_0\mu + c_0)(\mu - 1) < 0$ , then the origin is a stable node and  $S_1$  is an unstable node and we obtain again phase portrait  $L_2^1$ .

**(B)** If  $b_2 = 0$ ,  $b_0 \neq 0$  and  $\mu \in (-1, 0)$ , then  $Q_0$  is a stable node. We obtain phase portraits  $L_{8e}^1$  and  $L_{8h}^1$ . Note that the only difference is on the sectors that appear beside the  $v$ -axis on the second and third quadrants. On  $L_{8e}^1$  we have elliptic sectors and on  $L_{8h}^1$  we have hyperbolic sectors. It will be enough to apply index theory to know which of them appears in a global phase portrait, as we will detail on Section 4.5.

**(C)** If  $b_2 \neq 0$  and  $\mu \in (-\infty, -1) \cup (0, +\infty)$ , then  $Q_0$  is a saddle and  $Q_1$  a saddle-node. We must distinguish eight cases. At first, the sign of  $b_1$  determines if singular point  $Q_1$  is on the positive or the negative part of  $w_1$ -axis. Also we must fix the signs of  $\mu$  and  $b_0\mu + c_0$  as they determine the position and orientation of the sectors at the saddle-node. The different conditions to study and the corresponding results are given in Table 4.3.1

### 4.3 Local study of infinite singular points in chart $U_1$

Subcase	Conditions	Phase portrait of $O_1$
(C.1)	$b_1 > 0, \mu > 0, b_0\mu + c_0 < 0$	$L_9^1$
(C.2)	$b_1 > 0, \mu > 0, b_0\mu + c_0 > 0$	$L_{10}^1$
(C.3)	$b_1 > 0, \mu < -1, b_0\mu + c_0 > 0$	$L_{11}^1$
(C.4)	$b_1 > 0, \mu < -1, b_0\mu + c_0 < 0$	$L_{12}^1$
(C.5)	$b_1 < 0, \mu > 0, b_0\mu + c_0 < 0$	$L_{13}^1$
(C.6)	$b_1 < 0, \mu > 0, b_0\mu + c_0 > 0$	$L_{14}^1$
(C.7)	$b_1 < 0, \mu < -1, b_0\mu + c_0 > 0$	$L_{15}^1$
(C.8)	$b_1 < 0, \mu < -1, b_0\mu + c_0 < 0$	$L_{16}^1$

Table 4.3.1: Local phase portrait obtained for  $O_1$  in the subcases of case (C).

In subcases (C.1), (C.2), (C.5) and (C.6), it is necessary to do a horizontal blow up to completely determine the phase portrait of  $O_1$ . The process is the same in the four cases so we describe it only for the first one. If we introduce the variable  $w_1 = u/v$  in systems (4.3.2) and we eliminate a common factor  $v$  we get

$$\begin{aligned}\dot{w}_1 &= -\mu b_3 w_1^2 v - \mu b_1 w_1^2 - \mu b_2 w_1 + c_0 w_1 v, \\ \dot{v} &= -b_3 w_1 v^2 - b_1 w_1 v - b_0 v^2 - b_2 v.\end{aligned}\quad (4.3.12)$$

The singular points of systems (4.3.12) on the exceptional divisor are the origin, which in this case is a stable node, and the point  $(-b_2/b_1, 0)$  which is a saddle-node. Thus, attending to the sense of the flow on the axes, the phase portrait of these systems around the  $w_1$ -axis is the one in Figure 4.3.6(a). Multiplying by  $w_1$  we get the phase portrait in Figure 4.3.6(b). Then we undo the horizontal blow up: we swap the third and fourth quadrants, contract the exceptional divisor into the origin and modify the orbits according to Proposition 1.2.6. We recall that, for example, the separatrix of singular point  $(-b_2/b_1, 0)$  which is on the third quadrant, goes into a separatrix on the fourth quadrant that starts from the origin with slope  $-b_2/b_1$ . Now the phase portrait for systems (4.3.2) is well determined and, as we said, it is  $L_9^1$  in Figure 4.3.1.

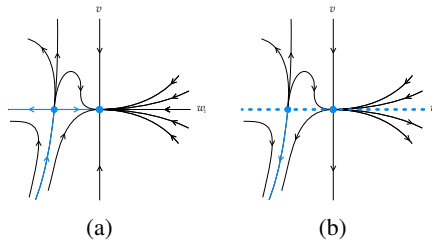


Figure 4.3.6: Horizontal blow up on systems (4.3.2) in nondicritical case (C.1).

- (D) If  $b_2 = 0, b_0 \neq 0$  and  $\mu \in (-\infty, -1) \cup (0, +\infty)$ , then  $Q_0$  is a stable node and  $Q_1$  a saddle-node. We separate two cases as the sign of  $b_0\mu + c_0$  determines the position



of the saddle-node sectors. If  $b_0\mu + c_0 > 0$ , we obtain phase portrait  $L_{17}^1$  and if  $b_0\mu + c_0 < 0$ , then we obtain phase portrait  $L_{18}^1$ .

- (E) If  $b_2 = 0$ ,  $b_0 \neq 0$  and  $\mu \in (-\infty, -1) \cup (0, +\infty)$ , then  $Q_0$  is an unstable node and  $Q_1$  a saddle-node. If  $b_0\mu > 0$ , we obtain phase portrait  $L_{19}^1$  and if  $b_0\mu < 0$ , then we obtain phase portrait  $L_{20}^1$ .

### 4.3.2 Dicritical case

Now we study the case with  $\mu = 0$ , i.e, the dicritical case. Systems (4.3.4) would have a singular point on the exceptional divisor if and only if  $c_0 = 0$  and  $b_2 \neq 0$ , but as we are considering  $\mu = 0$ , it is not possible because then we would have  $b_0\mu + c_0 = 0$ , which contradicts hypothesis  $H_2^2$ . Then there are no singular points on the exceptional divisor.

We must consider four cases depending on the sign of  $b_1$  and on whether  $b_2$  is zero or not. If  $b_2 = 0$  then the sign of  $\dot{u}$  does not change along the  $w_1$ -axis, but if  $b_2 \neq 0$ ,  $\dot{u}$  changes its sign at the point  $(0, -b_1/b_2)$ .

If  $b_2 = 0$ , (then we assume  $b_1 > 0$  by Remark 4.1.6), the flow around the  $w_1$  axis is as represented in Figure 4.3.7(a). Multiplying by  $u^2$  all the points on the  $w_1$ -axis become singular points, but the sense of the flow remains the same in all regions (see Figure 4.3.7(b)). At last, going back to the  $(u, v)$ -plane, we get that there are orbits which tend to the origin with any slope on quadrants first and fourth, and there are orbits leaving the origin with any slope on quadrant second and third, but also there are sectors which are not determined in these quadrants near the  $v$ -axis. These sectors, colored in Figure 4.3.7(c), can be elliptic or hyperbolic, and this can be determined on the global phase portraits by applying index theory, as we will explain on Section 4.5. As a result we can have phase portraits  $L_{21e}^1$  or  $L_{21h}^1$  in Figure 4.3.1.

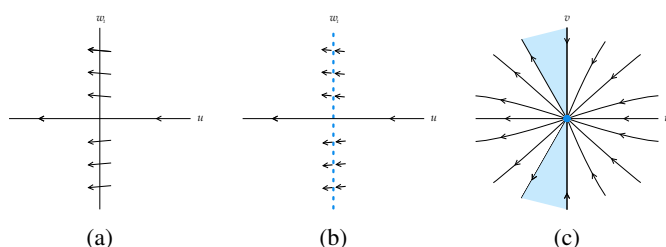


Figure 4.3.7: Desingularization of the origin of systems (4.3.2) in dicritical case with  $b_2 = 0$  and  $b_1 > 0$ .

If  $b_2 > 0$  and  $b_1 > 0$ , the flow on the  $w_1$  axis changes its direction at the point  $(0, -b_1/b_2)$ , as represented in Figure 4.3.8(a). Multiplying by  $u^2$  the sense of the flow does not change, but all the points on the  $w_1$ -axis become singular points (see Figure 4.3.8(b)). Going back to the  $(u, v)$ -plane, there are again two sectors that are not well determined, the ones colored in Figure 4.3.8(c) on quadrants second and fourth, and they can be either hyperbolic or elliptic. In this case, it can be proved by index theory that there are always a

#### 4.4 Local study of infinite singular points in chart $U_2$

hyperbolic sector and an elliptic sector, but their positions change depending on the global phase portrait we are studying. The two possibilities are  $L_{22eh}^1$  and  $L_{22he}^1$  in Figure 4.3.1.

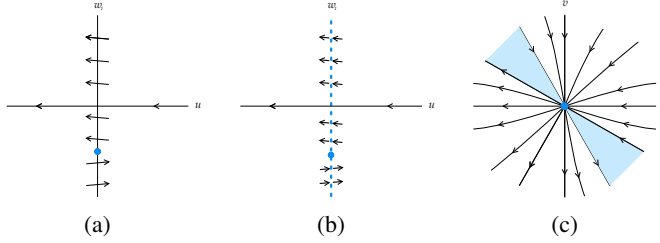


Figure 4.3.8: Desingularization of the origin of systems (4.3.2) in dicritical case with  $b_2 > 0$  and  $b_1 > 0$ .

If  $b_2 > 0$  and  $b_1 < 0$ , similarly to the previous case we obtain phase portraits  $L_{23eh}^1$  or  $L_{23he}^1$  in Figure 4.3.1.

We note that in this classification there are local phase portraits which are topologically equivalent, see for example in Figure 4.3.1 the phase portraits  $L_2^1$ ,  $L_{8e}^1$  and  $L_{22e}^1$ , but we maintain the distinction here as a result of the application of the blow up technique. In the final global classification the phase portraits which are topologically equivalent are unified.

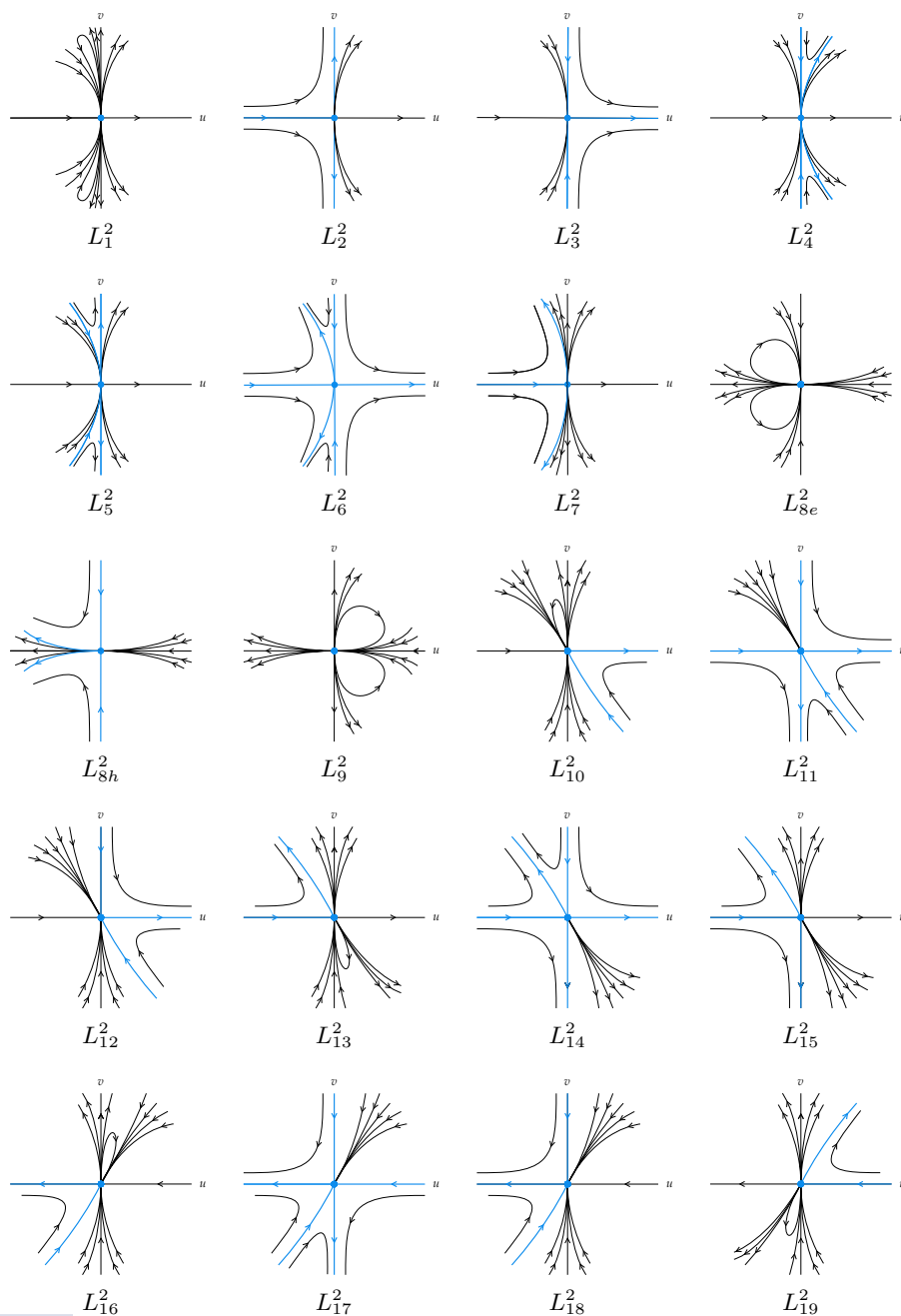
#### 4.4 Local study of infinite singular points in chart $U_2$

According to equation (1.3.10), we get the compactification in the local chart  $U_2$ , where systems (4.0.1) write

$$\begin{aligned} \dot{u} &= b_2(\mu + 1)u^2v + (b_0 - c_0)uv^2 + b_1(\mu + 1)u^2 + b_3(\mu + 1)uv, \\ \dot{v} &= b_2\mu uv^2 - c_0v^3 + b_1\mu uv + b_3v^2. \end{aligned} \quad (4.4.13)$$

In the local chart  $U_2$  we only need to study its singularity localized at the origin, denoted by  $O_2$ , because the other infinite singularities have already been studied in the local chart  $U_1$ . As the linear part of systems (4.4.13) at the origin is identically zero, we must use the blow up technique to study it. We obtain the next result, which is proved below.

**Lemma 4.4.1.** *Assuming hypothesis  $H_2^2$  the origin of the chart  $U_2$  is an infinite singular point of systems (4.0.1), and it has 26 distinct local phase portraits described in Figure 4.4.1.*


 Figure 4.4.1 (1 out of 2): Local phase portraits of the infinite singular point  $O_2$ .

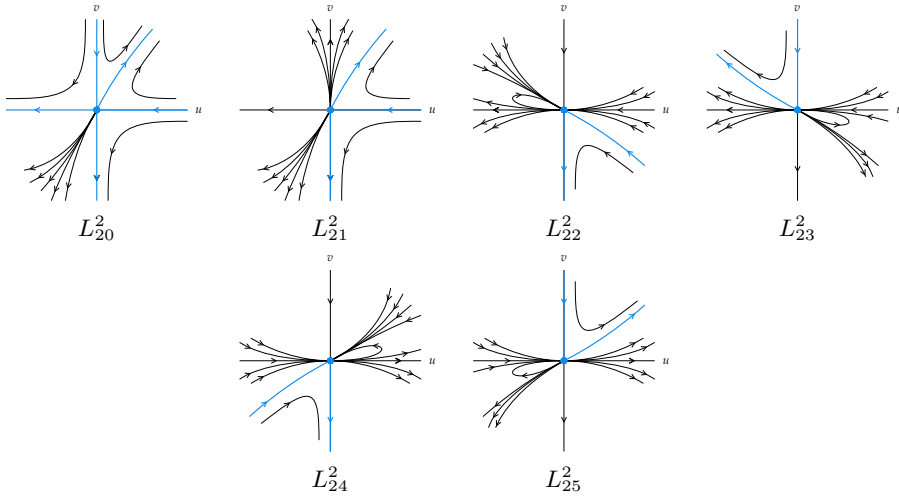


Figure 4.4.1 (2 out of 2): Local phase portraits of the infinite singular point  $O_2$ .

For systems (4.4.13), the characteristic polynomial is  $\mathcal{F} = -b_1 u^2 v - b_3 u v^2 \neq 0$ , so the origin is a nondicritical singular point. We introduce the variable  $w_1$  by means of the variable change  $uw_1 = v$  and we eliminate a common factor  $u$ , then we get the systems

$$\begin{aligned} \dot{u} &= (b_0 - c_0)u^2 w_1^2 + b_2(\mu + 1)u^2 w_1 + b_3(\mu + 1)u w_1 + b_1(\mu + 1)u \\ \dot{w}_1 &= -b_0 u w_1^3 - b_2 u w_1^2 - b_3 w_1^2 - b_1 w_1. \end{aligned} \quad (4.4.14)$$

The singular points on the exceptional divisor  $u = 0$  of systems (4.4.14) are the origin  $S_0$  and the singular point  $S_1 = (0, -b_1/b_3)$  if  $b_3 \neq 0$ . This point  $S_1$  is a semi-hyperbolic saddle-node whenever it exists, while the origin can be a saddle if  $\mu > -1$ , a stable node if  $\mu < -1$  and  $b_1 > 0$ , and an unstable node if  $\mu < -1$  and  $b_1 < 0$ . Then we must study five different subcases originated by these conditions.

- (a) If  $b_3 = 0$ ,  $c_0 \neq 0$  and  $\mu > -1$ , then  $S_0$  is a saddle. Note that once we fix  $b_3 = 0$  we can assume  $b_1 > 0$  by Remark 4.1.6. In this case the vertical blow up done does not provide a well determined phase portrait, so we must proceed similarly to the case (A) in Section 4.3, doing a horizontal blow up. In order to do that, we introduce the variable  $w_1 = u/v$  on systems (4.4.13) and eliminate a common factor  $v$  obtaining:

$$\begin{aligned} \dot{w}_1 &= b_2 w_1^2 v + b_1 w_1^2 + b_0 w_1 v, \\ \dot{v} &= b_2 \mu w_1 v^2 + b_1 \mu w_1 v - c_0 v^2, \end{aligned} \quad (4.4.15)$$

for which the only singular point on the exceptional divisor is the origin, and it is linearly zero, so we have to repeat the process. The characteristic polynomial is  $\mathcal{F} = b_1(\mu - 1)w_1^2 v - (b_0 + c_0)w_1 v^2$ , so the origin is always nondicritical by the same reasoning as in (A). Now we introduce the new variable  $w_2 = w_1/v$ , obtaining the

systems

$$\begin{aligned}\dot{w}_2 &= b_2(1 - \mu)w_2^2v^2 + b_1(1 - \mu)w_2^2v + (b_0 + c_0)w_2v, \\ \dot{v} &= b_2\mu w_2v^3 + b_1\mu w_2v^2 - c_0v^2,\end{aligned}\tag{4.4.16}$$

and eliminating a common factor  $v$ , we get

$$\begin{aligned}\dot{w}_2 &= b_2(1 - \mu)w_2^2v + b_1(1 - \mu)w_2^2 + (b_0 + c_0)w_2, \\ \dot{v} &= b_2\mu w_2v^2 + b_1\mu w_2v - c_0v.\end{aligned}\tag{4.4.17}$$

The singular points of systems (4.3.8) on the exceptional divisor are the origin  $Q_0$  and the singular point  $Q_1 = ((b_0 + c_0)/(b_1(\mu - 1)), 0)$  if  $\mu \neq 1$  (note that it coincides with the origin if  $b_0 + c_0 = 0$ ). We determine their local phase portraits obtaining the following classification. We start with the cases in which the only singular point on the exceptional divisor is the origin:

**Subcase (a.1).** If  $b_0 + c_0 = 0$  and  $\mu \neq 1$ , then the origin is a semi-hyperbolic saddle-node. If  $\mu > 1$ , it is necessary to do a vertical blow up of systems (4.4.15). We omit the details as the process is similar to the explained in case A.1.1 for the singular point  $O_1$ . The phase portrait obtained for  $O_2$  is  $L_1^2$  given in Figure 4.3.1. If  $\mu \in (-1, 1)$ , we obtain phase portrait  $L_2^2$ .

**Subcase (a.2).** If  $\mu = 1$  and  $c_0(b_0 + c_0) > 0$ , then the origin is a saddle. If  $b_0 + c_0 < 0$  and  $c_0 < 0$ , we obtain again phase portrait  $L_2^2$  and if  $b_0 + c_0 > 0$  and  $c_0 > 0$ , then we obtain phase portrait  $L_3^2$ . In both cases it is necessary to do a vertical blow up of systems (4.4.15).

**Subcase (a.3).** If  $\mu = 1$ ,  $c_0 < 0$ , and  $b_0 + c_0 > 0$ , then the origin is an unstable node. We obtain phase portrait  $L_1^2$ . Here the same consideration we made in case (a.1) about the elliptic sectors applies. The blow ups do not determine if the elliptic sectors appearing are indeed elliptic or hyperbolic, but this would be concluded analyzing the global phase portraits on Section 4.5. The same consideration applies also in (a.7) when  $\mu > 1$ .

Now we consider the cases with two singular points on the exceptional divisor:

**Subcase (a.4).** If  $c_0 > 0$ ,  $b_0 + c_0 > 0$  and  $(b_0\mu + c_0)(\mu - 1) < 0$ , then the origin is a saddle and  $Q_1$  a stable node. From these conditions we can deduce that  $\mu \in (-1, 1)$  and then we obtain only one phase portrait which is the same  $L_3^2$ .

**Subcase (a.5).** If  $c_0 < 0$ ,  $b_0 + c_0 < 0$  and  $(b_0\mu + c_0)(\mu - 1) > 0$ , then  $Q_0$  is a saddle and  $Q_1$  is an unstable node. If  $\mu > 1$ , it is necessary to do a vertical blow up of systems (4.4.15), and then we obtain phase portrait  $L_1^2$ . If  $\mu \in (-1, 1)$ , we obtain phase portrait  $L_2^2$ .

**Subcase (a.6).** If  $c_0(b_0 + c_0) > 0$  and  $(b_0 + c_0)(b_0\mu + c_0)(\mu - 1) > 0$ , then  $Q_0$  and  $Q_1$  are saddles. If  $\mu \in (-1, 1)$ ,  $b_0 + c_0 > 0$  and  $c_0 > 0$ , we easily obtain phase portrait  $L_6^2$ . If  $\mu > 1$ ,  $b_0 + c_0 > 0$  and  $c_0 > 0$ , we obtain phase portrait  $L_4^2$  and if  $\mu > 1$ ,

$b_0 + c_0 < 0$  and  $c_0 < 0$ , we obtain phase portrait  $L_5^2$ . In these two last cases it is necessary to do a vertical blow up of systems (4.4.15). We detail it for the first case, it is, with  $\mu > 1$ ,  $b_0 + c_0 > 0$  and  $c_0 > 0$ .

The phase portrait for (4.4.17) with the two saddles on the  $w_2$ -axis is given in Figure 4.4.2(a), and the corresponding for systems (4.4.16) is in Figure 4.4.2(b). If we undo the horizontal blow up, we must swap the third and fourth quadrants and shrink the  $w_2$ -axis into the origin. As a consequence, the separatrices of the saddle  $Q_1$  go into two separatrices with slope  $(b_0 + c_0)/(b_1(\mu - 1))$ , one of them goes to the origin in the third quadrant and the other leaves the origin in the first quadrant. There are four sectors, colored in Figure 4.4.2(c), in which the behavior is not determined, so we must do a vertical blow up.

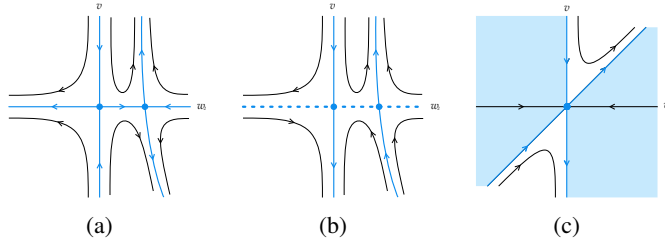


Figure 4.4.2: Desingularization of the origin of systems (4.4.13) case (a.6) with  $\mu > 1$ ,  $c_0 > 0$  and  $b_0 + c_0 > 0$ .

Let us introduce the variable  $w_3 = v/w_1$  and eliminate a common factor  $w_1$ . We get the systems

$$\begin{aligned}\dot{w}_1 &= b_2 w_1^2 w_3 + b_0 w_1 w_3 + b_1 w_1, \\ \dot{w}_3 &= b_2(\mu - 1) w_1 w_3^2 - (b_0 + c_0) w_3^2 + b_1(\mu - 1) w_3.\end{aligned}\tag{4.4.18}$$

These systems has two singular points on the exceptional divisor: the origin which is an unstable node, and the point  $(0, b_1(\mu - 1)/(b_0 + c_0))$  which is a saddle. Studying the sense of the flow on the axes, we get that the phase portrait for systems (4.4.18) is the one in Figure 4.4.3(a). Multiplying by  $w_1$  and undoing the vertical blow up, we obtain, respectively, the phase portraits in Figure 4.4.3(c) and (d). Now the phase portrait for systems (4.4.15) is well determined, and we just have to undo the first horizontal blow up, getting the final phase portrait  $L_4^2$ .

**Subcase (a.7).** If  $c_0 < 0$ ,  $b_0 + c_0 > 0$ , and  $(b_0\mu + c_0)(\mu - 1) > 0$ , then  $Q_0$  is an unstable node and  $Q_1$  is a saddle. If  $\mu > 1$ , we obtain phase portrait  $L_1^2$  and if  $\mu \in (-1, 1)$ , we obtain phase portrait  $L_7^2$ .

**Subcase (a.8).** If  $c_0 < 0$ ,  $b_0 + c_0 > 0$ , and  $(b_0\mu + c_0)(\mu - 1) < 0$ , then  $Q_0$  is an unstable node and  $Q_1$  is a stable node, and we obtain phase portrait  $L_1^2$ .

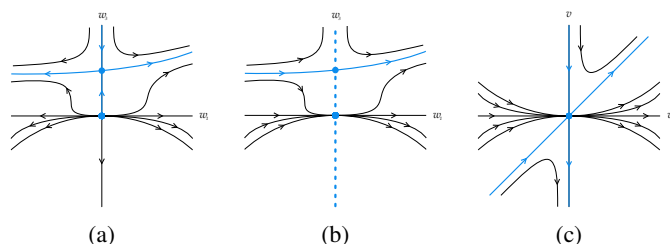


Figure 4.4.3: Desingularization of the origin of systems (4.4.13) case (a.6) with  $\mu > 1$ ,  $c_0 > 0$  and  $b_0 + c_0 > 0$ .

- (b) If  $b_3 = 0$ ,  $c_0 \neq 0$ ,  $\mu < -1$  and  $b_1 > 0$ , then the singular point  $S_0$  is a stable node. If  $c_0 > 0$ , we obtain phase portraits  $L_{8e}^2$  and  $L_{8h}^2$ , which differ on the sectors that appear beside the  $v$ -axis on the second and third quadrants. On  $L_{8e}^2$  we have elliptic sectors and on  $L_{8h}^2$  we have hyperbolic sectors. We apply index theory on the global phase portraits to know which of them appears (see Section 4.5). If  $c_0 < 0$ , the result is similar and an undetermined sector also appears when undoing the blow up. Nevertheless, in this case we have proved that in all the global phase portraits the undetermined sectors are elliptic, so we have always phase portrait  $L_9^2$ .
- (c) If  $b_3 > 0$  and  $\mu > -1$ , then the singular point  $S_0$  is a saddle and  $S_1$  is a saddle-node. We distinguish four cases in function of the sign of  $b_1$  which determines the position of  $S_1$ , and the sign of  $b_0\mu + c_0$  which determines the position of the sectors of that singular point. With these signs fixed, we can determine and represent the phase portrait of systems (4.4.17) and (4.4.16). Then, in each of the four cases, when going back to the  $(u, v)$ -plane we must distinguish three cases depending on whether  $\mu = 0$ ,  $\mu \in (-1, 0)$  or  $\mu > 0$ . In the cases with  $\mu > 0$  there appears an undefined sector which could be hyperbolic or elliptic. By doing a horizontal blow up in that cases, it can be determined that those sectors are always elliptic, but we omit the details as the process is the same that has been exposed in other cases. Another possibility is to prove directly on the global phase portrait, by applying index theory, that those sectors can only be elliptic. To avoid repetitions, we simply include the results obtained in each case in Table 4.4.1.
- (d) If  $b_3 > 0$ ,  $\mu < -1$  and  $b_1 > 0$ , then the singular point  $S_0$  is a stable node and  $S_1$  is a saddle-node. The sign of  $b_0\mu + c_0$  determines the position of the sectors of the saddle-node in systems (4.4.17), so we must distinguish two cases and undo the blow up in each of them. If  $b_0\mu + c_0 > 0$ , we obtain phase portrait  $L_{23}^2$  and if  $b_0\mu + c_0 < 0$ , we obtain  $L_{24}^2$ .
- (e) If  $b_3 > 0$ ,  $\mu < -1$  and  $b_1 < 0$ , then  $S_0$  is an unstable node and  $S_1$  is a saddle-node. As in the previous case we distinguish the case with  $b_0\mu + c_0 > 0$ , in which we obtain phase portrait  $L_{25}^2$ , and the case with  $b_0\mu + c_0 < 0$ , in which we obtain phase portrait  $L_{26}^2$ .

Subcase	Conditions		Phase portrait of $O_2$
(c.1)	$b_1 > 0, b_0\mu + c_1 > 0$	$\mu > 0$	$L_{10}^2$
		$\mu \in (-1, 0)$	$L_{11}^2$
		$\mu = 0$	$L_{12}^2$
(c.2)	$b_1 > 0, b_0\mu + c_1 < 0$	$\mu > 0$	$L_{13}^2$
		$\mu \in (-1, 0)$	$L_{14}^2$
		$\mu = 0$	$L_{15}^2$
(c.3)	$b_1 < 0, b_0\mu + c_1 > 0$	$\mu > 0$	$L_{16}^2$
		$\mu \in (-1, 0)$	$L_{17}^2$
		$\mu = 0$	$L_{18}^2$
(c.4)	$b_1 > 0, b_0\mu + c_1 < 0$	$\mu > 0$	$L_{19}^2$
		$\mu \in (-1, 0)$	$L_{20}^2$
		$\mu = 0$	$L_{21}^2$

Table 4.4.1: Local phase portraits for  $O_2$  obtained is the subcases of case (c).

## 4.5 Global phase portraits

In this section we give the topological classification of global phase portraits of systems (4.0.1) by proving Theorem 4.0.1.

We bring together the local information obtained in Sections 4.2, 4.3 and 4.4. We start our classification from the cases in Tables 4.2.2 to 4.2.5. In Table 4.5.1 we give, for each case of the Tables 4.2.2 to 4.2.5, the local phase portrait of the infinite singular points  $O_1$  and  $O_2$ . In some of them the conditions determine only one local phase portrait in each one of the infinite singular points, but in most cases, we shall distinguish several possibilities depending on the parameters. Also in Table 4.5.1 we give the global phase portrait on the Poincaré disk obtained. All these global phase portraits are given in Figure 4.5.5, where we also indicate the number of separatrices (S) and canonical regions (R) that each of them has. We detail the reasonings in some cases, although they will not be showed in all of them to avoid repetitions. We recall that we are denoting the origins of charts  $U_1$  and  $U_2$  as  $O_1$  and  $O_2$  respectively, and in this section, to simplify the explanations, we will denote by  $Q_1$  the origin of chart  $V_1$  and by  $Q_2$  the origin of  $V_2$ .

### 4.5.1 Cases with a totally-determined local phase portrait at infinity

First, we explain the process in a case where all local phase portraits are fully determined, and the separatrices can only be connected in one manner.

**Case 1.3.** Let us consider the conditions  $\mu < -1$  and  $b_1 > 0$ , so the infinite singular point  $O_1$  has the local phase portrait  $L_{12}^1$  given in Figure 4.3.1, and  $O_2$  has the phase portrait  $L_{23}^2$  given in 4.4.1. We must combine the local information to get the global phase portrait. The systems have an unstable node  $P_1$  which is on the positive  $z$ -axis and a stable node  $P_2$  which



is on the negative  $x$ -axis. The origin is a saddle and it has its four separatrices over the axes (as the axes are invariant). Also, by the local configurations of  $O_1$  and  $O_2$  we know that the part of the  $z$ -axis which connects  $P_1$  with  $O_1$  is a separatrix, and the part of the  $x$ -axis which connects  $P_2$  with  $Q_1$  is a separatrix. Apart from those, the systems have a separatrix leaving the singular point  $O_2$  in the second quadrant and a separatrix which arrives at  $Q_1$  on the third quadrant (see Figure 4.5.1). There is only one possible connection for these separatrices: the separatrix which leaves  $O_2$  goes to  $P_2$  and the separatrix which arrives at  $Q_1$  starts at  $Q_2$ . Then we obtain phase portrait G9 in Figure 4.5.5, which has 19 separatrices and 6 canonical regions.

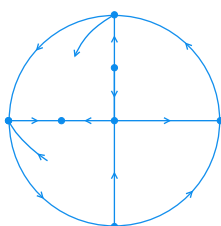


Figure 4.5.1: Separatrices provided by local information in case 1.3 with  $\mu < -1$  and  $b_1 > 0$ .

With the same reasonings we can obtain the global phase portraits in the other subcases of 1.3 and also in the following: the subcases in 1.5 and 1.6 with  $b_1 < 0$ ; all subcases in 1.8 and in 1.10; subcases in 2.2, 2.4 and 2.5 with  $\mu < -1$ ; subcases in 3.2 with  $\mu < -1$  or  $\mu \in (-1, 0)$ ; subcases in 3.3, 3.4 and 3.5 with  $\mu \in (-1, 0)$ ; subcases in 4.1 with  $\mu < -1$  and subcases in 4.2 with  $\mu \in (0, 1)$ ,  $\mu = 1$  or  $\mu > 1$ .

## 4.5.2 Cases with undetermined sectors at infinity

Now we will deal with some cases in which the local phase portrait of  $O_1$ ,  $O_2$  or both was not totally determined in Sections 4.3 and 4.4, in the sense that they present certain sectors which can be either hyperbolic or elliptic.

**Case 1.1.** We consider  $b_1 < 0$ . The infinite singular point  $O_1$  has the local phase portrait  $L_{13}^1$  given in Figure 4.3.1, and  $O_2$  the phase portrait  $L_{19}^2$  given in Figure 4.4.1. We must prove here that the elliptic sectors on both phase portraits are indeed elliptic.

The systems have a saddle  $P_1$  on the negative  $z$ -axis and a stable node  $P_2$  on the negative  $x$ -axis. The origin is a saddle and it has the four separatrices over the axes. The repelling separatrices of  $P_1$  are also over the  $z$ -axis, but the attracting ones should arrive to  $P_1$ , one in the third quadrant and other in the fourth quadrant. Also the systems have a separatrix leaving the singular point  $O_2$  in the first quadrant and a separatrix leaving  $Q_1$  on the second quadrant. Then, attending to the local phase portrait of each singular point, the only possible connection is the following: there is a separatrix which goes from  $Q_1$  to the point  $P_2$  and a separatrix from  $O_2$  to  $O_1$ , the attracting separatrix of  $P_1$  on the third quadrant starts in  $Q_1$  and the one in the fourth quadrant starts in  $Q_2$ . As a result, there is a canonical region delimited

by  $Q_2$ , the part of the  $z$ -axis which connects this point with  $P_1$ ,  $P_1$ , and its separatrix on the fourth quadrant (see Figure 4.5.2). If the sector on the local phase portrait of  $Q_2$  were hyperbolic, then there would not be any possible  $\alpha$  or  $\omega$ -limit on the boundary for the orbits in that region, but as it is not possible to have periodic orbits, this situation is not feasible, and this sector should be elliptic. The same happens with the elliptic sector at  $O_1$ . Anyway, this can be proved also analytically by applying index theory.

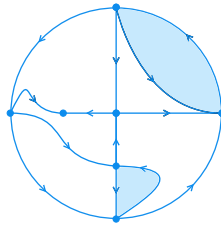


Figure 4.5.2: Separatrix configuration in case 1.1 with  $b_1 < 0$  and regions in which local phase portrait was not determined.

By Theorem 1.6.1 the sum of the indices of all the singular points on the Poincaré sphere has to be 2. To compute this sum we must consider that the finite singular points on the Poincaré disk appear twice on the sphere (on the northern hemisphere and on the southern hemisphere). Thus if we denote by  $ind_F$  the sum of the indices of the finite singular points, and by  $ind_I$  the sum of the indices of the infinite singular points, the equality  $2ind_F + ind_I = 2$  must be satisfied. In this particular case, the finite singular points are two saddles whose index is  $-1$ , and a stable node which index is  $1$ , so  $ind_F = -1$ . We deduce that  $ind_I$  must be  $4$ . The infinite singular points are  $O_1$  and  $Q_1$  which have the same index, and  $O_2$  and  $Q_2$  which have also the same index.

The singular point  $O_1$  has a hyperbolic sector so, if the non-determined sector is elliptic, from the Poincaré formula for the index given in Section 1.6,  $O_1$  has index  $1$ , and if the non-determined sector were hyperbolic,  $O_1$  would have index  $0$ . The same is valid for the singular point  $O_2$ . Then, if at any of these points  $O_1$  or  $O_2$  the sector were hyperbolic, the sum of the index of that point and its symmetric would be zero, and so the sum of the other point and its symmetric should be  $4$ , which is not possible.

In other words,

$$ind_I = 2 \left( \frac{e - h}{2} + 1 \right) + 2 \left( \frac{\tilde{e} - \tilde{h}}{2} - 1 \right),$$

where  $e$  and  $h$  are the number of elliptic and hyperbolic sectors of  $O_1$  and  $\tilde{e}$  and  $\tilde{h}$  are the number of elliptic and hyperbolic sectors of  $O_2$ . As we know that  $ind_I = 4$ , then we obtain

$$(e + \tilde{e}) - (h + \tilde{h}) = 0,$$

it is, considering both phase portraits of  $O_1$  and  $O_2$  together, there must be the same number of elliptic and hyperbolic sectors. As we have a hyperbolic sector in each of them, the two non-determined sectors must be elliptic.

**Case 3.3.** We consider  $\mu < -1$ . The infinite singular point  $O_1$  has the local phase portrait  $L_{11}^1$  given in Figure 4.3.1, and  $O_2$  has the phase portrait  $L_{8e}^2$ , but we must prove that we actually have  $L_{8e}^2$  instead of  $L_{8h}^2$ .

The origin is an unstable node and the systems have a saddle  $P_2$  on the negative  $x$ -axis. The attracting separatrices of  $P_2$  are over the  $x$ -axis, but the repelling separatrices should leave  $P_2$ , one in the second quadrant and other in the third quadrant. There is also a separatrix leaving the singular point  $O_1$  in the fourth quadrant. There is only one possible way to connect these separatrices: the systems have a separatrix which goes from  $P_2$  to  $O_2$ , another which goes from  $P_2$  to  $Q_2$  and the third one which goes from  $O_1$  to  $Q_2$ . Then we have two canonical regions, the ones colored in Figure 4.5.3, in which the only possibility is to have elliptic sectors whose orbits have as alpha and omega-limits the singular point  $O_2$  and  $Q_2$  respectively. We verify this with Theorem 1.6.1. As we have a finite saddle with index  $-1$  and a finite node with index 1, then  $ind_F = 0$ . From the equality  $2ind_F + ind_I = 2$  we know that  $ind_I$  must be 2.

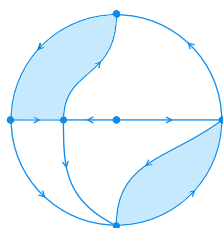


Figure 4.5.3: Separatrix configuration in case 3.3 with  $\mu < -1$  and regions in which local phase portrait was not determined.

The local phase portrait of  $O_1$  is well determined and it has four hyperbolic sectors and one parabolic sector, so

$$ind_{O_1} = \frac{e-h}{2} + 1 = \frac{0-4}{2} + 1 = -1,$$

and also we know that  $ind_{O_1} = ind_{Q_1}$  and  $ind_{O_2} = ind_{Q_2}$ . Then

$$ind_I = 2ind_{O_1} + 2ind_{O_2} \Rightarrow ind_{O_2} = 2,$$

and by the Poincaré formula, if  $e$  and  $h$  are the number of elliptic and hyperbolic sectors at  $O_2$ , then

$$\frac{e-h}{2} + 1 = 2 \Rightarrow e-h = 2,$$

and as we have only two sectors to determine whether they are elliptic or hyperbolic, the only possibility is that both are elliptic.

With similar reasonings we can conclude and prove the results in all the remaining subcases, except the ones included in the following subsection.

### 4.5.3 Cases with three possible global phase portraits

Here we focus on the cases in which the separatrices can be connected in three different manners. As can be seen in Table 4.5.1, this happens in the subcases of 1.1, 1.2, 1.5, 1.6 and 1.7 in which  $b_1 > 0$ , in both subcases of 1.4, in the subcase of 1.9 with  $b_1 < 0$ , and in the subcase of 3.3 with  $\mu = 0$ ,  $b_3 > 0$  and  $b_1 > 0$ . We give a detailed explanation in the following case:

**Case 1.5.** We consider the condition  $\mu < -1$  and  $b_1 > 0$ . The origin is an unstable node, there is a stable node  $P_2$  on the negative  $z$ -axis and saddle  $P_1$  on the negative  $x$ -axis. The two attracting separatrices of  $P_1$  are over the  $z$ -axis, and the repelling ones leave the origin in the third and fourth quadrants respectively. The infinite singular point  $O_1$  has the local phase portrait  $L_{12}^1$  of Figure 4.3.1, and  $O_2$  has the phase portrait  $L_{23}^2$  of Figure 4.4.1. According to these local phase portraits, the positive  $z$ -axis, the positive  $x$ -axis, and the part of the negative  $x$ -axis between  $Q_1$  and  $P_2$  are separatrices. Moreover, there is another separatrix which leaves  $O_2$  in the second quadrant and one that goes to  $Q_1$  in the third quadrant. There is only one possible connection for the separatrices on the second and fourth quadrant, as it is represented in Figure 4.5.4(a).

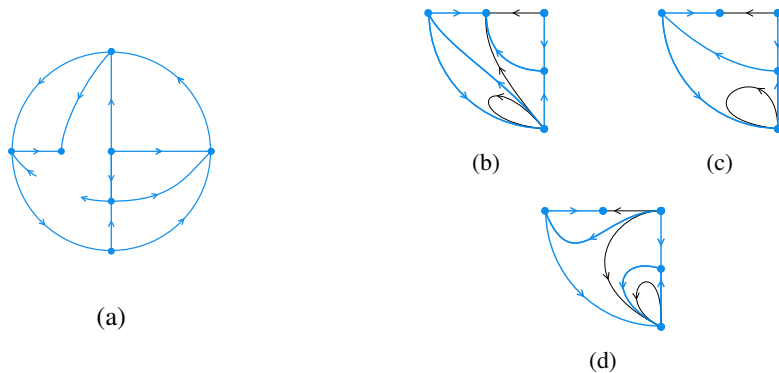


Figure 4.5.4: Separatrices and possible configurations on the third quadrant on case 1.5 with  $\mu < -1$  and  $b_1 > 0$ .

We focus now on the third quadrant. We know that there is a separatrix leaving the point  $P_1$  and another one going into  $Q_1$ . If we analyze the possible  $\omega$ -limits of the separatrix leaving  $P_1$  there are three options, the singular points  $Q_1$ ,  $Q_2$  and  $P_2$ . If the  $\omega$ -limit is  $Q_1$ , then both separatrices should be the same, as the point  $Q_1$  does not have parabolic sectors in the third quadrant. In that case, the configuration in the third quadrant is the one given in Figure 4.5.4 (c), and this leads to the global phase portrait G20.

If the  $\omega$ -limit is  $P_2$ , then only possibility for the other separatrix is that its  $\alpha$ -limit is  $Q_2$ . The configuration in the third quadrant is given in Figure 4.5.4(b), and this leads to the global phase portrait G19.

At last, if the  $\omega$ -limit is  $Q_2$ , then the  $\alpha$ -limit of the other separatrix is the origin. The configuration in the third quadrant is given in Figure 4.5.4(d), and this leads to the global phase portrait G21.

In phase portrait G20 we have proved that the connection of the separatrices takes place on the invariant straight line  $z = -1/2$  for the values of the parameters  $b_0 = b_2 = c_0 = 1$ ,  $b_1 = 2$  and  $\mu = -2$ . The two remaining phase portraits can be obtained by perturbing just one parameter.

We have also proved numerically, by using the program P4 (see [50, Chapter 9]), that the three global phase portraits are realizable.

In Table 4.5.2 we give the values of the parameters for which we have found each phase portrait, not only on this subcase but also in all the subcases in which three possibilities appear. In all of them we have checked that the three possibilities are realizable and in all the triplets we have proved that in the phase portraits in which two separatrices connect, this connection takes place on an invariant straight line. More precisely, in the phase portraits G2, G20, G24 and G45 the invariant line is  $z = c_0/\mu b_3$  and in the phase portraits G6, G14, G28, G32, G36 and G81 the invariant line is  $y = -b_0/b_2$ .

Case	Conditions	$O_1$	$O_2$	Global
1.1	$b_1 > 0$	$L_9^1$	$L_{13}^2$	G1, G2 or G3
	$b_1 < 0$	$L_{13}^1$	$L_{19}^2$	G4
1.2	$b_1 > 0$	$L_{10}^1$	$L_{10}^2$	G5, G6 or G7
	$b_1 < 0$	$L_{14}^1$	$L_{16}^2$	G8
1.3	$\mu < -1, b_1 > 0$	$L_{12}^1$	$L_{23}^2$	G9
	$\mu < -1, b_1 < 0$	$L_{16}^1$	$L_{25}^2$	G10
	$\mu \in (-1, 0), b_1 > 0$	$L_{18}^1$	$L_{14}^2$	G11
	$\mu \in (-1, 0), b_1 < 0$	$L_{20}^1$	$L_{20}^2$	G12
1.4	$b_1 > 0$	$L_{10}^1$	$L_{10}^2$	G13, G14 or G15
	$b_1 < 0$	$L_{14}^1$	$L_{16}^2$	G16, G17 or G18
1.5	$\mu < -1, b_1 > 0$	$L_{12}^1$	$L_{23}^2$	G19, G20 or G21
	$\mu < -1, b_1 < 0$	$L_{16}^1$	$L_{25}^2$	G22
	$\mu \in (-1, 0), b_1 > 0$	$L_{18}^1$	$L_{14}^2$	G23, G24 or G25
	$\mu \in (-1, 0), b_1 < 0$	$L_{20}^1$	$L_{20}^2$	G26
1.6	$\mu < -1, b_1 > 0$	$L_{11}^1$	$L_{22}^2$	G27, G28 or G29
	$\mu < -1, b_1 < 0$	$L_{15}^1$	$L_{24}^2$	G30
	$\mu \in (-1, 0), b_1 > 0$	$L_{17}^1$	$L_{11}^2$	G31, G32 or G33
	$\mu \in (-1, 0), b_1 < 0$	$L_{19}^1$	$L_{17}^2$	G34
1.7	$b_1 > 0$	$L_{10}^1$	$L_{10}^2$	G35, G36 or G37
	$b_1 < 0$	$L_{14}^1$	$L_{16}^2$	G38
1.8	$\mu < -1, b_1 > 0$	$L_{12}^1$	$L_{23}^2$	G39
	$\mu < -1, b_1 < 0$	$L_{16}^1$	$L_{25}^2$	G40
	$\mu \in (-1, 0), b_1 > 0$	$L_{18}^1$	$L_{14}^2$	G41
	$\mu \in (-1, 0), b_1 < 0$	$L_{20}^1$	$L_{20}^2$	G42

Table 4.5.1 (1 out of 3): Classification of global phase portraits of systems (4.0.1).

Case	Conditions	$O_1$	$O_2$	Global
1.9	$b_1 > 0$	$L_{10}^1$	$L_{10}^2$	G43
	$b_1 < 0$	$L_{14}^1$	$L_{16}^2$	G44, G45 or G46
1.10	$\mu < -1, b_1 > 0$	$L_{11}^1$	$L_{22}^2$	G47
	$\mu < -1, b_1 < 0$	$L_{15}^1$	$L_{24}^2$	G48
	$\mu \in (-1, 0), b_1 > 0$	$L_{17}^1$	$L_{11}^2$	G49
	$\mu \in (-1, 0), b_1 < 0$	$L_{19}^1$	$L_{17}^2$	G50
2.1		$L_2^1$	$L_{13}^2$	G51
2.2	$\mu \in (-1, 0)$	$L_{8e}^1$	$L_{14}^2$	G52
	$b_0 + c_0 = 0, \mu > 1$	$L_1^1$	$L_{10}^2$	G53
	$b_0 + c_0 > 0, \mu \geq 1$			
	$b_0 + c_0 \geq 0, \mu < -1$	$L_3^1$	$L_{23}^2$	G54
	$b_0 + c_0 > 0, \mu \in (0, 1)$	$L_4^1$	$L_{10}^2$	G55
	$b_0 + c_0 < 0, \mu < -1$	$L_6^1$	$L_{23}^2$	G56
	$b_0 + c_0 < 0, \mu > 1$	$L_7^1$	$L_{10}^2$	G57
2.3	$\mu \in (-1, 0)$	$L_{8e}^1$	$L_{14}^2$	G58
	$\mu \in (0, 1)$	$L_4^1$	$L_{10}^2$	G59
	$\mu < -1$	$L_3^1$	$L_{23}^2$	G60
	$\mu \geq 1$	$L_1^1$	$L_{10}^2$	G61
2.4	$\mu \in (-1, 0)$	$L_{8h}^1$	$L_{11}^2$	G62
	$\mu < -1$	$L_5^1$	$L_{22}^2$	G63
2.5	$\mu \in (-1, 0)$	$L_{8e}^1$	$L_{14}^2$	G64
	$\mu \in (0, 1)$	$L_4^1$	$L_{10}^2$	G65
	$\mu < -1$	$L_3^1$	$L_{23}^2$	G66
	$\mu \geq 1$	$L_1^1$	$L_{10}^2$	G67
3.1		$L_{10}^1$	$L_1^2$	G68
3.2	$b_0 + c_0 = 0, \mu > 0$	$L_9^1$	$L_2^2$	G69
	$b_0 + c_0 < 0, \mu \in (0, 1]$			
	$b_0 + c_0 < 0, \mu > 1$	$L_9^1$	$L_5^2$	G70
	$b_0 + c_0 < 0, \mu \in (0, 1)$	$L_9^1$	$L_7^2$	G71
	$\mu < -1$	$L_{12}^1$	$L_9^2$	G72
	$b_0 + c_0 \leq 0, \mu \in (-1, 0)$	$L_{18}^1$	$L_2^2$	G73
	$b_0 + c_0 \leq 0, \mu = 0, b_3 = 0$	$L_{22eh}^1$		
	$b_0 + c_0 > 0, \mu \in (-1, 0)$	$L_{18}^1$		
	$b_0 + c_0 > 0, \mu = 0, b_3 = 0$	$L_{22eh}^1$	$L_7^2$	G74
	$\mu = 0, b_3 > 0, b_1 > 0$	$L_{22eh}^1$		
	$\mu = 0, b_3 > 0, b_1 < 0$	$L_{23eh}^1$	$L_{15}^2$	G75
		$L_{23eh}^1$	$L_{21}^2$	G76

Table 4.5.1 (2 out of 3): Classification of global phase portraits of systems (4.0.1).

Case	Conditions	$O_1$	$O_2$	Global
3.3	$\mu \in (0, 1]$	$L_{10}^1$	$L_3^2$	G77
	$\mu > 1$	$L_{10}^1$	$L_4^2$	G78
	$\mu < -1$	$L_{11}^1$	$L_{8e}^2$	G79
	$\mu \in (-1, 0)$	$L_{17}^1$	$L^2 3$	G80
	$\mu = 0, b_3 = 0$	$L_{22he}^1$		
	$\mu = 0, b_3 > 0, b_1 > 0$	$L_{22he}^1$	$L_{12}^2$	G80, G81 or G82
	$\mu = 0, b_3 > 0, b_1 < 0$	$L_{23he}^1$	$L_{18}^2$	
3.4	$\mu < -1$	$L_{12}^1$	$L_{8h}^2$	G84
	$\mu \in (-1, 0)$	$L_{18}^1$	$L_6^2$	G85
3.5	$\mu \in (0, 1]$	$L_{10}^1$	$L_3^2$	G86
	$\mu > 1$	$L_{10}^1$	$L_4^2$	G87
	$\mu < -1$	$L_{11}^1$	$L_{8e}^2$	G88
	$\mu \in (-1, 0)$	$L_{17}^1$	$L_3^2$	G89
	$\mu = 0, b_3 = 0$	$L_{22he}^1$		
	$\mu = 0, b_3 > 0, b_1 > 0$	$L_{22he}^1$	$L_{12}^2$	G90
	$\mu = 0, b_3 > 0, b_1 < 0$	$L_{23he}^1$	$L_{18}^2$	G91
4.1	$b_0 + c_0 \leq 0, \mu = 0, b_3 = 0$	$L_{21e}^1$	$L_2^2$	G92
	$b_0 + c_0 \leq 0, \mu \in (-1, 0)$	$L_{8e}^1$		
	$b_0 + c_0 = 0, \mu \in (0, 1)$	$L_2^1$		
	$b_0 + c_0 < 0, \mu \in (0, 1]$	$L_2^1$		
	$b_0 + c_0 > 0, \mu = 0, b_3 = 0$	$L_{21e}^1$	$L_7^2$	G93
	$b_0 + c_0 > 0, \mu \in (-1, 0)$	$L_{8e}^1$		
	$b_0 + c_0 > 0, \mu \in (0, 1), b_0\mu + c_0 < 0$	$L_2^1$		
	$b_0 + c_0 = 0, \mu > 1$	$L_1^1$	$L_1^2$	G94
	$b_0 + c_0 > 0, \mu \geq 1$			
	$b_0 + c_0 \geq 0, \mu < -1$	$L_3^1$	$L_9^2$	G95
	$b_0 + c_0 > 0, \mu \in (0, 1), b_0\mu + c_0 > 0$	$L_4^1$	$L_1^2$	G96
	$b_0 + c_0 < 0, \mu < -1$	$L_6^1$	$L_9^2$	G97
	$b_0 + c_0 < 0, \mu > 1, b_0\mu + c_0 > 0$	$L_7^1$	$L_1^2$	G98
	$b_0 + c_0 < 0, \mu > 1, b_0\mu + c_0 < 0$	$L_2^1$	$L_5^2$	G99
	$\mu = 0, b_3 > 0$	$L_{21e}^1$	$L_{15}^2$	G100
4.2	$\mu = 0, b_3 > 0$	$L_{21h}^1$	$L_{12}^2$	G101
	$\mu = 0, b_3 = 0$	$L_{21h}^1$	$L_3^2$	G102
	$\mu \in (-1, 0)$	$L_{8h}^1$		
	$\mu \in (0, 1)$	$L_4^1$		
	$\mu < -1, b_0\mu + c_0 > 0$	$L_5^1$	$L_{8e}^2$	G103
	$\mu < -1, b_0\mu + c_0 < 0$	$L_3^1$	$L_{8h}^2$	G104
	$\mu = 1$	$L_1^1$	$L_3^2$	G105
	$\mu > 1$	$L_1^1$	$L_4^2$	G106

Table 4.5.1 (3 out of 3): Classification of global phase portraits of systems (4.0.1).

#### 4.5 Global phase portraits

Subcase	Phase portrait	Obtained for the values
<b>1.1</b> $b_1 > 0$	G1	$b_0 = 1/2, b_1 = b_2 = b_3 = 1, c_0 = -1, \mu = 1/2$
	G2	$b_0 = 1/2, b_1 = b_2 = b_3 = 1, c_0 = -1, \mu = 1$
	G3	$b_0 = 1/2, b_1 = b_2 = b_3 = 1, c_0 = -1, \mu = 5/4$
<b>1.2</b> $b_1 > 0$	G5	$b_0 = 2, b_1 = b_2 = b_3 = 1, c_0 = -1/2, \mu = 1$
	G6	$b_0 = b_1 = b_2 = b_3 = 1, c_0 = -1/2, \mu = 1$
	G7	$b_0 = 4/5, b_1 = b_2 = b_3 = 1, c_0 = -1/2, \mu = 1$
<b>1.4</b> $b_1 > 0$	G13	$b_0 = 2, b_1 = b_2 = b_3 = c_0 = \mu = 1$
	G14	$b_0 = b_1 = b_2 = b_3 = c_0 = \mu = 1$
	G15	$b_0 = 1/2, b_1 = b_2 = b_3 = c_0 = \mu = 1$
<b>1.4</b> $b_1 < 0$	G16	$b_0 = b_2 = b_3 = c_0 = \mu = 1, b_1 = -2$
	G17	$b_0 = 1, b_1 = -1, b_2 = b_3 = c_0 = \mu = 1$
	G18	$b_0 = b_2 = b_3 = c_0 = \mu = 1, b_1 = -1/2$
<b>1.5</b> $\mu < -1, b_1 > 0$	G19	$b_0 = b_2 = b_3 = c_0 = 1, b_1 = 1, \mu = -2$
	G20	$b_0 = b_2 = b_3 = c_0 = 1, b_1 = 2, \mu = -2$
	G21	$b_0 = b_2 = b_3 = c_0 = 1, b_1 = 4, \mu = -2$
<b>1.5</b> $\mu \in (-1, 0), b_1 > 0$	G23	$b_0 = 4, b_1 = 1, b_2 = b_3 = c_0 = 1, \mu = -1/2$
	G24	$b_0 = 4, b_1 = 1/2, b_2 = b_3 = c_0 = 1, \mu = -1/2$
	G25	$b_0 = 4, b_1 = 1/10, b_2 = b_3 = c_0 = 1, \mu = -1/2$
<b>1.6</b> $\mu < -1, b_1 > 0$	G27	$b_0 = 1/4, b_1 = b_2 = b_3 = 1, c_0 = 3, \mu = -2$
	G28	$b_0 = b_1 = b_2 = b_3 = 1, c_0 = 3, \mu = -2$
	G29	$b_0 = 5/4, b_1 = b_2 = b_3 = 1, c_0 = 3, \mu = -2$
<b>1.6</b> $\mu \in (-1, 0), b_1 > 0$	G31	$b_0 = b_1 = b_3 = 1, b_2 = 7/4, c_0 = 2, \mu = -1/2$
	G32	$b_0 = b_1 = b_2 = b_3 = 1, c_0 = 2, \mu = -1/2$
	G33	$b_0 = b_1 = b_3 = 1, b_2 = 1/4, c_0 = 2, \mu = -1/2$
<b>1.7</b> $b_1 > 0$	G35	$b_0 = b_2 = b_3 = \mu = 1, b_1 = 7/8, c_0 = 0$
	G36	$b_0 = b_1 = b_2 = b_3 = \mu = 1, c_0 = 0$
	G37	$b_0 = b_2 = b_3 = \mu = 1, b_1 = 9/8, c_0 = 0$
<b>1.9</b> $b_1 < 0$	G44	$b_0 = 0, b_1 = -1/2, b_2 = b_3 = c_0 = \mu = 1$
	G45	$b_0 = 0, b_1 = -1, b_2 = b_3 = c_0 = \mu = 1$
	G46	$b_0 = 0, b_1 = -2, b_2 = b_3 = c_0 = \mu = 1$
<b>3.3</b> $\mu = 0, b_3 > 0, b_1 > 0$	G80	$b_0 = 2, b_1 = b_2 = b_3 = c_0 = 1, \mu = 0$
	G81	$b_0 = b_1 = b_2 = b_3 = c_0 = 1, \mu = 0$
	G82	$b_0 = 1/2, b_1 = b_2 = b_3 = c_0 = 1, \mu = 0$

Table 4.5.2: Values of the parameters for which each global phase portrait is obtained in cases with three possible configurations.



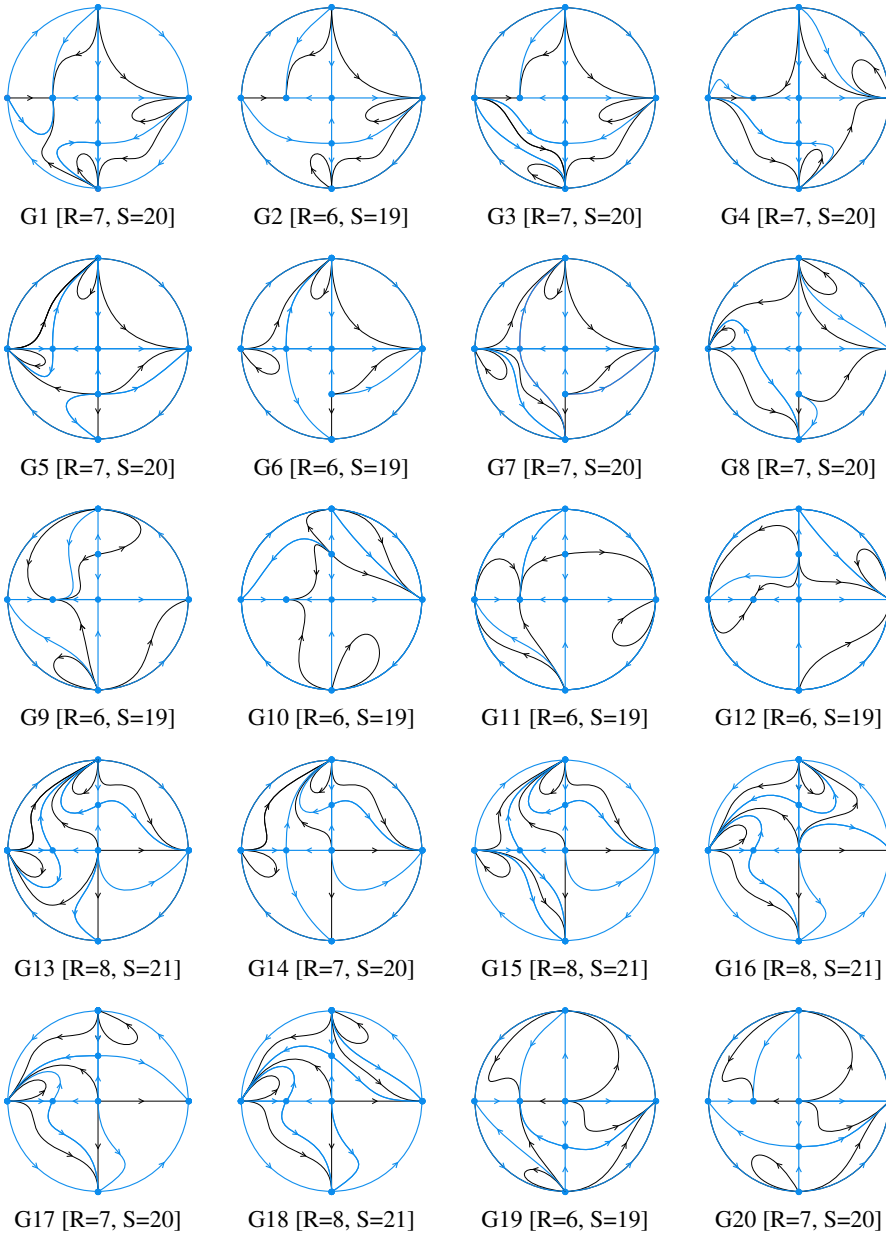


Figure 4.5.5 (1 out of 6): Global phase portraits of systems (4.0.1) in the Poincaré disk.

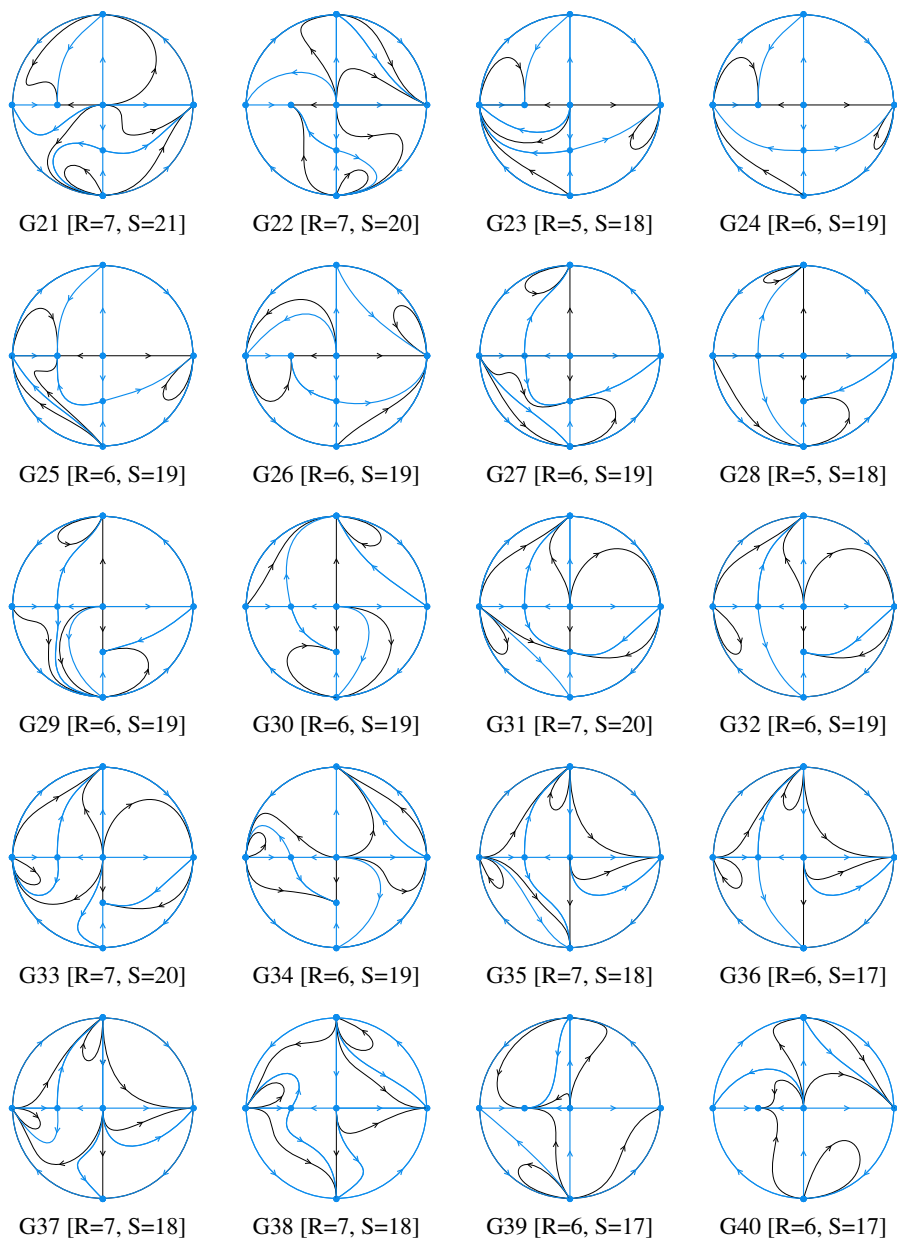


Figure 4.5.5 (2 out of 6): Global phase portraits of systems (4.0.1) in the Poincaré disk.

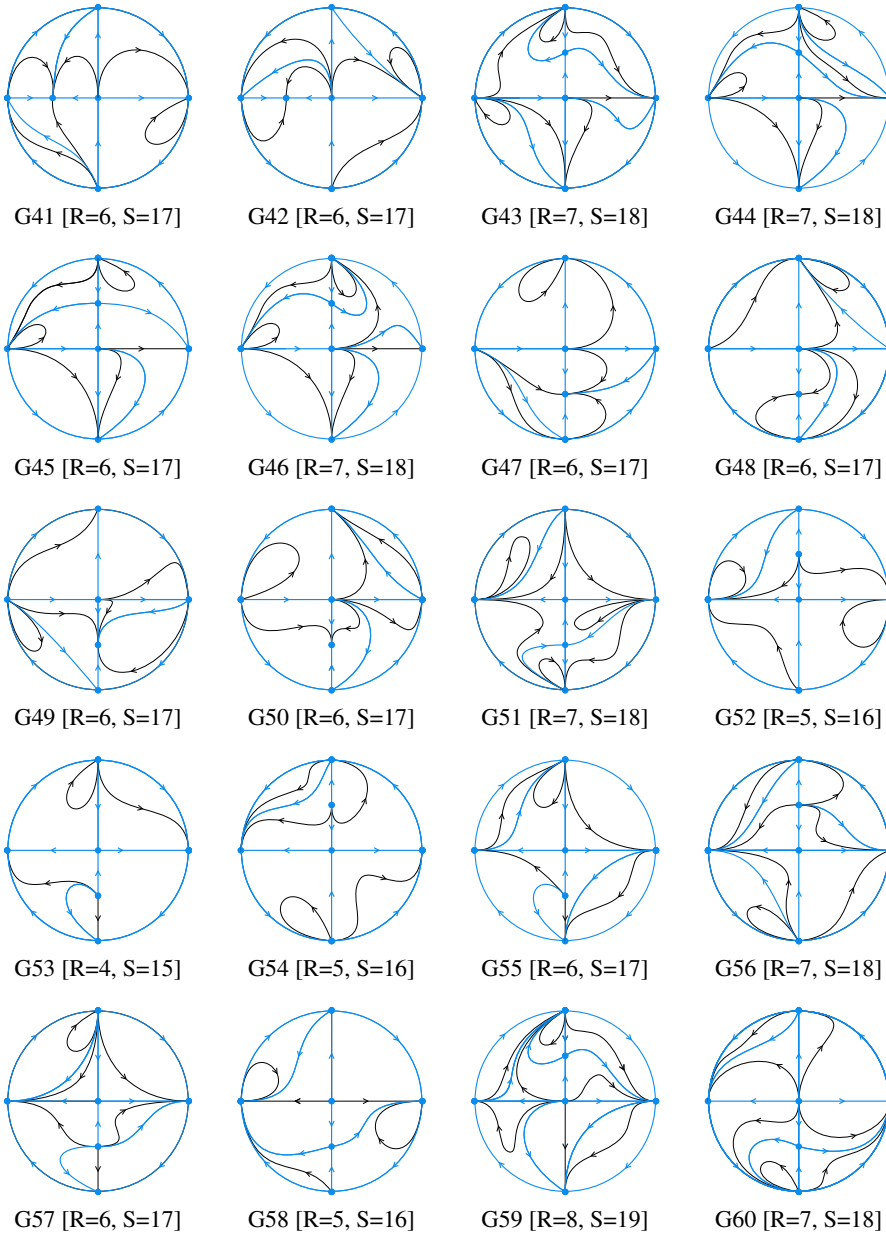


Figure 4.5.5 (3 out of 6): Global phase portraits of systems (4.0.1) in the Poincaré disk.

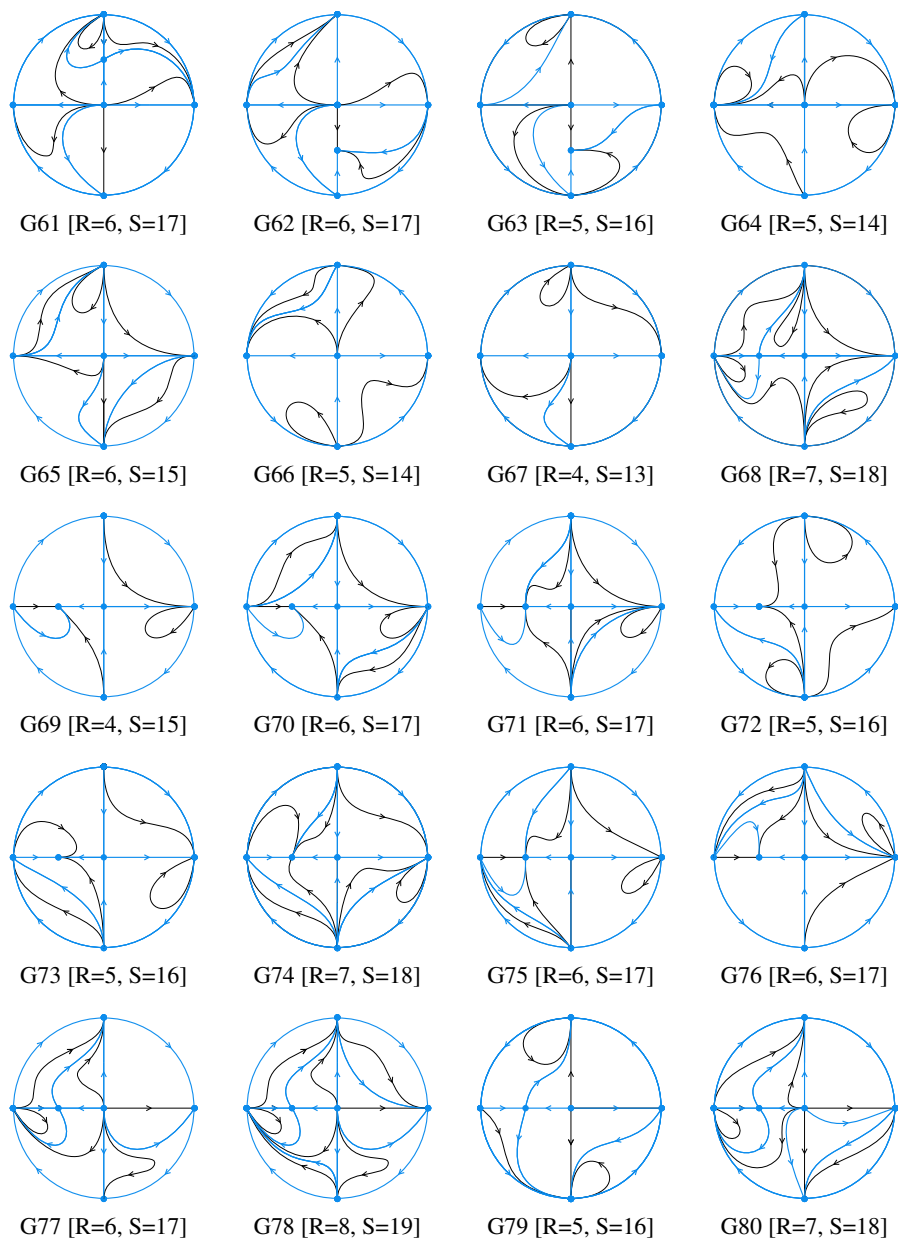


Figure 4.5.5 (4 out of 6): Global phase portraits of systems (4.0.1) in the Poincaré disk.

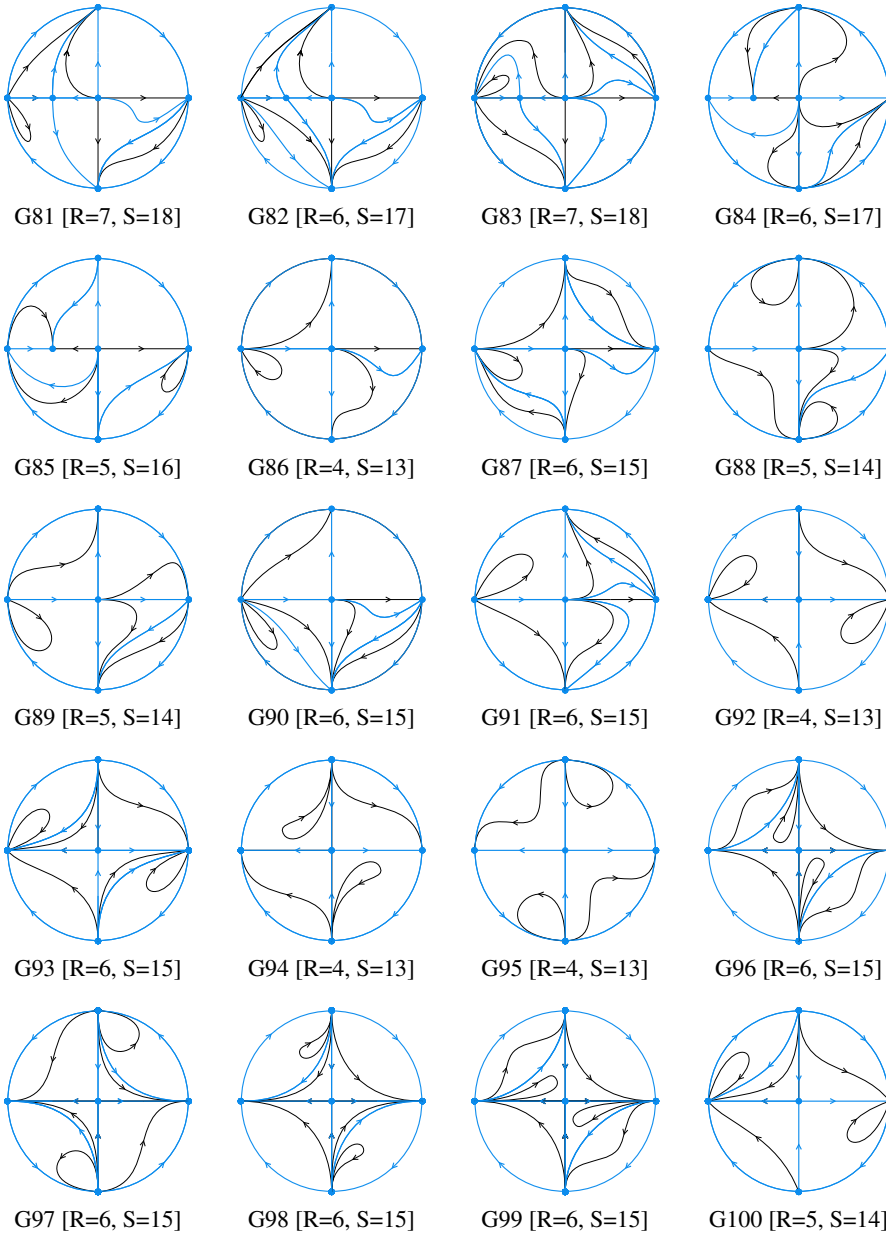


Figure 4.5.5 (5 out of 6): Global phase portraits of systems (4.0.1) in the Poincaré disk.

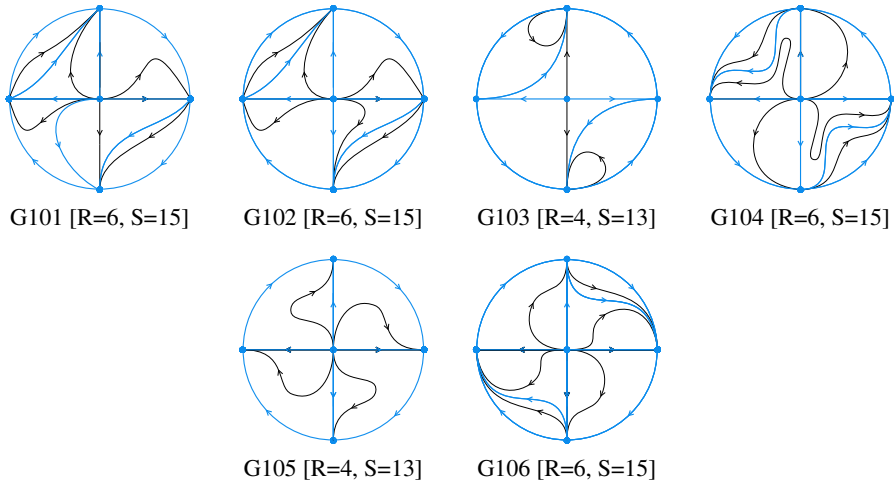


Figure 4.5.5 (6 out of 6): Global phase portraits of systems (4.0.1) in the Poincaré disk.

## 4.6 Topological equivalences

In the previous sections we have obtained the 106 global phase portraits given in Figure 4.5.5. There are 13 different classes according to the number of canonical regions and separatrices, and within each class we distinguish which ones are topologically equivalent in the following result.

**Proposition 4.6.1.** *For Kolmogorov systems (4.0.1) there are 13 classes according to the number of canonical regions and separatrices. Taking into account the topological equivalences, we get:*

- (i) Seven distinct phase portraits with 7 canonical regions and 20 separatrices.
- (ii) Six distinct phase portraits with 6 canonical regions and 19 separatrices.
- (iii) Two distinct phase portraits with 8 canonical regions and 21 separatrices.
- (iv) One phase portrait with 7 canonical regions and 21 separatrices.
- (v) One phase portrait with 5 canonical regions and 18 separatrices.
- (vi) Six distinct phase portraits with 7 canonical regions and 18 separatrices.
- (vii) Eleven distinct phase portraits with 6 canonical regions and 17 separatrices.
- (viii) Three distinct phase portraits with 5 canonical regions and 16 separatrices.
- (ix) One phase portrait with 4 canonical regions and 15 separatrices.
- (x) One phase portrait with 8 canonical regions and 19 separatrices.

- (xi) *Three distinct phase portraits with 5 canonical regions and 14 separatrices.*
- (xii) *Six distinct phase portraits with 6 canonical regions and 15 separatrices.*
- (xiii) *Four distinct phase portraits with 4 canonical regions and 13 separatrices.*

*Proof.* We do the proof for every one of the thirteen statements of the proposition.

- (i) For systems (4.0.1) we have obtained 12 phase portraits with 7 canonical regions and 20 separatrices, namely, G1, G3, G4, G5, G7, G8, G14, G17, G19, G22, G31 and G33 of Figure 4.5.5. At first we divide the phase portraits in two subclasses attending to the index of the finite singular points.

In G1, G3, G4, G5, G7, G8, G14 and G17 the sum of the indices of the finite singular points is -1, and in the other phase portraits it is 1. Now we analyze the first subclass. G1 and G3 are topologically different because the boundary of the elliptic sectors in each of them is topologically different, by the same reason G1 is topologically different from G4 and G3 topologically different from G4. G1 is topologically equivalent to G5 by doing a symmetry with respect to the line  $y - z = 0$  and a change of the time variable  $t$  by  $-t$ , and analogously G3 is topologically equivalent to G7 and G4 to G8. The phase portrait G14 is topologically different from G1 and G3 because in these two there are an elliptic sector with two finite singular points in the boundary which does not exist in G14. Also G14 is topologically different from G4 because the fourth quadrant of G14 is topologically different from all the quadrants of G4. This phase portrait G14 is topologically equivalent to G17 by a symmetry with respect to the line  $y + z = 0$ .

In the second subclass the phase portrait of G19 is topologically equivalent to G31 by a symmetry with respect to the line  $y - z = 0$ . The phase portrait of G19 is different from G22 and from G33, because the boundary of the elliptic sectors is different. G22 is topologically different from G33 because in the first one the saddle has two separatrices which connect to finite singular points and two separatrices which connect to infinite singular points, but in G33 there is only one separatrix which connects to a finite singular point.

Thus we have only seven topologically distinct phase portraits between the 12 phase portraits with 7 canonical regions and 20 separatrices, which can be represented by G1, G3, G4, G14, G19, G22 and G33.

- (ii) For systems (4.0.1) we have obtained 15 phase portraits with 6 canonical regions and 19 separatrices, namely, G2, G6, G9, G10, G11, G12, G20, G23, G25, G26, G27, G29, G30, G32 and G34 of Figure 4.5.5.

We can consider a first subclass with the phase portraits in which there are two elliptic sectors, i.e., G2 and G6, which are topologically equivalent by a symmetry with respect to the line  $y - z = 0$  and by changing the time variable  $t$  by  $-t$ .

Consider now a second subclass with the phase portraits with only one elliptic sector which has in the boundary two singular points; this occurs in G9, G12, G26, G30 and G34. Here G9 is topologically equivalent to G12 by a symmetry with respect to the line

$y - z = 0$  and a change of  $t$  by  $-t$ . G26 is the same as G12 if we move the saddle point to the origin, and G30 is the same as G26 with a symmetry along the line  $y - z = 0$ . At last, G30 and G34 are topologically different because the two singular points in the boundary of the elliptic sector in G30 are infinite and in G34 one is infinite and the other is finite.

In the remaining phase portraits there is only one elliptic sector and it has three singular points in the boundary. In the phase portraits G10, G11, G25 and G27 the saddle point has two separatrices which connect with infinite singular points. G10 is topologically equivalent to G11 by a symmetry along the line  $y + z = 0$  and a change of  $t$  by  $-t$ . G10 is also topologically equivalent to G25 after moving the saddle of G25 to the origin, doing a rotation of  $-90^\circ$ , a symmetry with respect to the  $z$ -axis and a change of  $t$  by  $-t$ . G25 is topologically equivalent to G27 with a symmetry along the line  $y - z = 0$ . In the phase portraits G20, G23, G29 and G32 the saddle point has three separatrices which connect with infinite singular points. Here G20 is topologically different from G23 because in both the position of the finite singular points is the same but the elliptic sector has a different position, so we can not get a transformation between them. By a symmetry with respect to the line  $y - z = 0$ . G23 is topologically equivalent to G29 and G20 topologically equivalent to G32.

Thus, we have six topologically different phase portraits between the 15 phase portraits with 6 canonical regions and 19 separatrices, which can be represented by G2, G9, G34, G10, G10 and G23.

- (iii) We have obtained for systems (4.0.1) four phase portraits with 8 canonical regions and 21 separatrices, namely, G13, G15, G16 and G18 of Figure 4.5.5. By a symmetry with respect to the line  $y + z = 0$ , G13 is topologically equivalent to G16, and G15 topologically equivalent to G18. G13 is topologically different from G15 because the boundary of the elliptic sectors is different.
- (iv) For systems (4.0.1) we have obtained only one phase portrait with 7 canonical regions and 21 separatrices, G21 of Figure 4.5.5.
- (v) We have obtained for systems (4.0.1) two phase portraits with 5 canonical regions and 18 separatrices, G24 and G28 of Figure 4.5.5. These phase portraits are topologically equivalent by doing a symmetry with respect to the line  $y - z = 0$ .
- (vi) We have obtained for systems (4.0.1) 14 phase portraits with 7 canonical regions and 18 separatrices, namely, G35, G37, G38, G43, G44, G46, G51, G56, G60, G68, G74, G80, G82 and G83 of Figure 4.5.5. We divide them into three subclasses attending to the number of elliptic sectors that they have.

First, in G56, G60, G74, G80, G82 and G83 there is only one elliptic sector. G56 is topologically different from G60 because in the second one there is a finite singular point in the boundary of the elliptic sector, but in the first one there is not. We can transform G56 into G74 with a rotation of  $-90^\circ$  and a change of  $t$  by  $-t$ ; G60 into G80 with a symmetry with respect to the line  $y - z = 0$ ; G80 into G83 with a symmetry with respect to the  $y$ -axis; and G82 into G56 by moving the saddle point to the origin and doing a symmetry with respect to the line  $y - z = 0$ .



We consider now the subclass with two elliptic sectors, in which we have G35, G37, G38, G43, G44 and G46. Here G35 is topologically different from G37 and G38 because the boundary of the elliptic sectors is different. Also G37 is topologically different from G38, as in the last one there is a separatrix which connects two infinite singular points, and it does not exist in G37. We have that G35 and G44, G37 and G46, G38 and G43 these are topologically equivalent with a symmetry with respect to the line  $y + z = 0$ .

Finally, in G51 and G68 there are three elliptic sectors, and both are topologically equivalent by a symmetry with respect to the line  $y - z = 0$  and changing  $t$  by  $-t$ .

Thus we have 6 topologically different phase portraits which can be represented by G56, G60, G35, G37, G38 and G51.

- (vii) For systems (4.0.1) we have obtained 21 phase portraits with 6 canonical regions and 17 separatrices, namely, G36, G39, G40, G41, G42, G45, G47, G48, G49, G50, G55, G57, G61, G62, G70, G71, G75, G76, G77, G81 and G84 of Figure 4.5.5. We divide them into four subclasses.

First, in G62 and G84 there are no elliptic sectors, and both phase portraits are symmetric with respect to the line  $y - z = 0$ .

Second, in G36 and G45 there are two elliptic sectors, and both are symmetric with respect to the line  $y + z = 0$ .

We consider now the phase portraits with one elliptic sector having the sum of the indices of the finite singular points equal to 1: G39, G40, G41, G42, G47, G48, G49 and G50. Due to the differences between the boundary of the elliptic sectors we get that G39 and G40, G39 and G41, G40 and G42, G41 and G42 are not topologically equivalent. Also G40 is not topologically equivalent to G41 because in G40 there are four separatrices which connect the origin with infinite singular points, but in G41 there are only three. Similarly, G39 is not topologically equivalent G42 because in G42 there are four separatrices which connect the finite saddle-node with infinite singular points, but in G39 there are only three. By doing a symmetry with respect to the line  $y - z = 0$  we get that G41 and G47, G42 and G48, G39 and G49, G40 and G50 are topologically equivalent.

Finally, we consider the phase portraits with one elliptic sector having the sum of the indices of the finite singular points equal to 0: G55, G57, G61, G70, G71, G75, G76, G77, G81. Again due to the differences between the boundary of the elliptic sectors we get that G55 and G57, G61 and G55, G61 and G57, G57 and G75, G61 and G75 are not topologically equivalent. G55 is topologically different from G75 because in G55 there are two separatrices which connect infinite points but in G75 there are only one. G76 is topologically different from G57 and from G61 because in G76 there are two separatrices which connect infinite points, in G57 one and in G61 none. We can transform G55 into G70 and G57 into G71 with a symmetry with respect to the line  $y - z = 0$  and a change of  $t$  for  $-t$ . If we rotate  $-90^\circ$  the phase portrait G77 we obtain G61, and at last if we move the stable node of G75 to the origin, we do a symmetry with respect to the  $z$ -axis and we change  $t$  by  $-t$  we obtain G81.

Thus we have 11 topologically different phase portraits between the 21 phase portraits with 6 canonical regions and 17 separatrices, that can be represented by G36, G39, G40, G41, G42, G55, G57, G61, G62, G75, G76.

- (viii) For systems (4.0.1) we have obtained eight phase portraits with 5 canonical regions and 16 separatrices.

In G52, G58, G72 and G79 there are two elliptic sectors, and these phase portraits are all topologically equivalent. If we move the node in G52 to the origin, we get G58; if we rotate  $90^\circ$  the phase portrait G52 we obtain G72, and with a symmetry with respect to the line  $y - z = 0$  we transform G58 into G79.

In G54, G63, G73 and G85 there are only one elliptic sector. G54 and G63 are topologically different because the boundary of the elliptic sector is different. G54 becomes G73 with a rotation of  $90^\circ$  and G63 becomes G85 with a symmetry with respect to the line  $y - z = 0$ .

Thus we have three distinct phase portraits which can be represented by G52, G54 and G63.

- (ix) For systems (4.0.1) we have obtained two phase portraits with 4 canonical regions and 15 separatrices, G53 and G69 of Figure 4.5.5. These phase portraits are topologically equivalent by doing a symmetry with respect to the line  $y - z = 0$  and changing the time variable  $t$  by  $-t$ .
- (x) For systems (4.0.1) we have obtained two phase portraits with 8 canonical regions and 19 separatrices, G59 and G78 of Figure 4.5.5. Both are topologically equivalent as we can obtain G78 if we do a rotation of  $90^\circ$  in G59.
- (xi) For systems (4.0.1) we have obtained five phase portraits with 5 canonical regions and 14 separatrices, namely, G64, G66, G88, G89 and G100 of Figure 4.5.5. G66 has two elliptic sectors so it is topologically different from G64 and G100 which have only one. G64 is topologically different from G100 because the only finite singular point is the origin, which is a saddle-node in the first one and a saddle in the second one. With a symmetry with respect to the line  $y - z = 0$ , we transform G64 into G88, and G66 into G89. Thus we have three distinct phase portraits represented by G64, G66 and G100.
- (xii) For systems (4.0.1) we have obtained 13 phase portraits with 6 canonical regions and 15 separatrices, namely, G65, G87, G90, G91, G93, G96, G97, G98, G99, G101, G102, G104 and G106 of Figure 4.5.5. We consider three subclasses depending on the number of the elliptic sectors.

In G65, G87, G90 and G91 there is only one elliptic sector. G65 is topologically equivalent to G87 with a rotation of  $90^\circ$ . G65 is topologically different from G90 because the boundary of the elliptic sectors is different, and by the same reason G95 is topologically different from G91, and G90 from G91.

In G93, G96, G97, G98 and G99 there are two elliptic sectors. G93 is topologically different from G96 because the boundary of the elliptic sectors is different. G93 is topologically equivalent to G98 with a symmetry with respect to the line  $y + z = 0$

and a change of  $t$  by  $-t$ ; the same occurs with G96 and G99. Also G97 and G98 are symmetric with respect to the  $z$ -axis.

In G101, G102, G104 and G106 there are no elliptic sectors, and all these phase portraits are topologically equivalent. G101 is topologically equivalent to G102 moving the separatrix in the third quadrant to the negative  $z$ -axis. G102 is symmetric to G104 with respect to the line  $y - z = 0$ , and G104 is symmetric to G106 with respect to the  $z$ -axis.

In summary we have six topologically different phase portraits represented by G65, G90, G91, G93, G96 and G101.

- (xiii) We have obtained for systems (4.0.1) seven phase portraits with 4 canonical regions and 13 separatrices, namely, G67, G86, G92, G94, G95, G103 and G105 of Figure 4.5.5. If we rotate  $90^\circ$  the phase portrait G67 we obtain G86. G67 is topologically different from G92 because they have a different number of elliptic sectors. G92 is topologically equivalent to G94 with a symmetry with respect to the line  $y + z = 0$  and a change of the time variable  $t$  by  $-t$ ; and G94 topologically equivalent to G95 with a symmetry with respect to the  $z$ -axis. In G92 the only finite singular point is the origin, which is a saddle, and it is a node in G103, so both phase portraits are distinct. With the same argument G67 is topologically different from G103, G92 from G105, and G67 from G103. Finally, G103 and G105 are topologically different because the first one has elliptic sectors but not the second one has none. Then we have four topologically different phase portraits represented by G67, G92, G103 and G105.

□

The classification given in Table 4.5.1, proved in Subsections 4.5.1, 4.5.2 and 4.5.3, together with Proposition 4.6.1, prove our main result, i. e., Theorem 4.0.1.

Figure 4.0.1 includes the representatives of each one of the topological equivalence classes, which correspond to the phase portraits in Figure 4.5.5 as indicated in Table 4.6.1

## 4.6 Topological equivalences

Representative	Phase portraits
R1	G1, G5
R2	G2, G6
R3	G3, G7
R4	G4, G8
R5	G9, G12, G26, G30
R6	G10, G11, G25, G27
R7	G13, G16
R8	G14, G17
R9	G15, G18
R10	G19, G31
R11	G20, G32
R12	G21
R13	G22
R14	G23, G29
R15	G24, G28
R16	G33
R17	G34
R18	G35, G44
R19	G36, G45
R20	G37, G46
R21	G38, G43
R22	G39, G49
R23	G40, G50
R24	G41, G47
R25	G42, G48
R26	G51, G68

Representative	Phase portraits
R27	G52, G58, G72, G79
R28	G53, G69
R29	G54, G73
R30	G55, G70
R31	G56, G74, G82
R32	G57, G71
R33	G59, G78
R34	G60, G80, G83
R35	G61, G77
R36	G62, G84
R37	G63, G85
R38	G64, G88
R39	G65, G87
R40	G66, G89
R41	G67, G86
R42	G75, G81
R43	G76
R44	G90
R45	G91
R46	G92, G94, G95
R47	G93, G97, G98
R48	G96, G99
R49	G100
R50	G101, G102, G104, G106
R51	G103
R52	G105

Table 4.6.1: Representatives of each equivalence class and their corresponding global phase portraits of systems (4.0.1).



---

## Chapter 5

# Classification of the second Kolmogorov family with non-isolated singularities

---

The current chapter includes the contents of the research article [46]<sup>1</sup>, in which we study systems (4.0.1) in the particular case with  $\mu = -1$ . In this case all the singular points at infinity are singular points. We recall that from Sections 4.1 and 4.2 we can study systems (4.0.1) under conditions

$$H_1^2 = \{b_1 \neq 0, b_0\mu + c_0 \neq 0, b_0 \geq 0, b_2 \geq 0, b_3 \geq 0, (\mu b_3)^2 + c_0^2 \neq 0, b_2^2 + b_0^2 \neq 0\},$$

as in any other case they can be reduced to satisfy such conditions either using symmetries, or eliminating known phase portraits, as in the cases in which there exist infinitely many finite singularities. Then taking  $\mu = -1$  on systems (4.0.1) we will study the systems

$$\begin{aligned}\dot{y} &= y(b_0 + b_1 yz + b_2 y + b_3 z), \\ \dot{z} &= z(c_0 + b_1 yz + b_2 y + b_3 z),\end{aligned}\tag{5.0.1}$$

under conditions

$$\tilde{H}^2 = \{b_1 \neq 0, c_0 - b_0 \neq 0, b_0 \geq 0, b_2 \geq 0, b_3 \geq 0, b_3^2 + c_0^2 \neq 0, b_2^2 + b_0^2 \neq 0\}.$$

Moreover if  $b_2 b_3 = 0$  then it is enough to study the case with  $b_1 > 0$ , and if  $b_0 = 0$  it is enough to consider  $c_0 > 0$ .

We give the topological classification of all global phase portraits of systems (5.0.1) on the Poincaré disk, and our main result is the following.

**Theorem 5.0.1.** *Kolmogorov systems (5.0.1) under conditions  $\tilde{H}^2$  have 13 topologically distinct phase portraits in the Poincaré disk, given in Figure 5.0.1.*

---

<sup>1</sup>Érika Diz-Pita (Departamento de Estatística, Análise Matemática e Optimización, Universidade de Santiago de Compostela), Jaume Llibre (Departament de Matemàtiques, Universitat Autònoma de Barcelona) and María Victoria Otero-Espinar (Departamento de Estatística, Análise Matemática e Optimización, Universidade de Santiago de Compostela), *Planar Kolmogorov systems with infinitely many singular points at infinity*, International Journal of Bifurcation and Chaos, (ISSN:0218-1274, EISSN:1793-6551), **32**(5) (2022), 106038. Published by World Scientific. The final authenticated version is available online at: <https://doi.org/10.1016/j.cnsns.2021.106038>

In this chapter we give the proof of Theorem 5.0.1 organized as follows: In Section 5.1 we give the classification of the local phase portraits of the finite singular points based on the results of Chapter 4, in Section 5.2 we study the local phase portraits at the infinite singular points, and finally in Section 5.3 we prove Theorem 5.0.1 by studying the global phase portraits in the Poincaré disk.

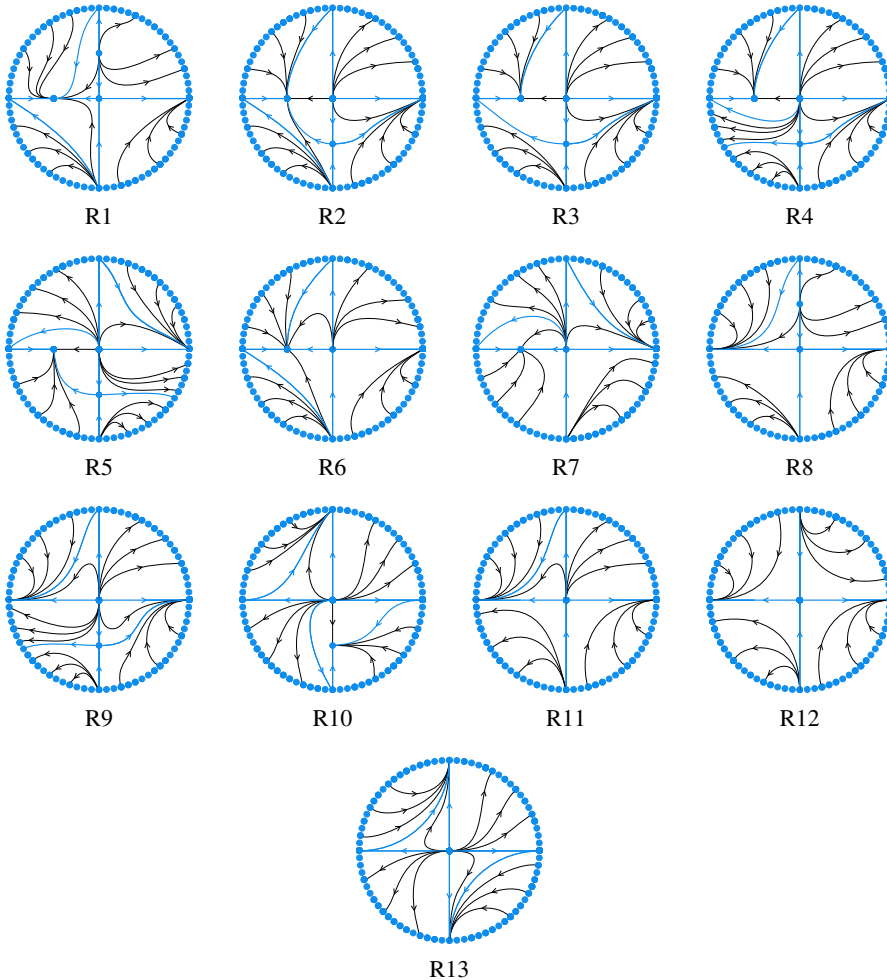


Figure 5.0.1: The topologically distinct phase portraits of systems (5.0.1) in the Poincaré disk.

## 5.1 Local study of finite singular points

Assuming the condition  $\mu = -1$ , from Section 4.2 in Chapter 4 we know that the singular points of systems (5.0.1) are

$$P_0 = (0, 0), \quad P_1 = \left(0, -\frac{c_0}{b_3}\right) \text{ if } b_3 \neq 0 \text{ and } P_2 = \left(-\frac{b_0}{b_2}, 0\right) \text{ if } b_2 \neq 0,$$

and from Table 4.2.1 we distinguish four cases depending on the existence of the singular points. These cases are given in Table 5.1.1.

Case	Conditions	Finite singular points
1	$b_3 \neq 0, b_2 \neq 0$	$P_0, P_1, P_2$
2	$b_3 \neq 0, b_2 = 0, b_0 \neq 0$	$P_0, P_1$
3	$b_3 = 0, c_0 \neq 0, b_2 \neq 0$	$P_0, P_2$
4	$b_3 = 0, c_0 \neq 0, b_2 = 0, b_0 \neq 0$	$P_0$

Table 5.1.1: The different cases for the finite singular points.

Also from the results in Chapter 4, taking  $\mu = -1$  in Lemma 4.2.2 and Tables 4.2.2 to 4.2.5, we get the following local classification in 15 subcases for the finite singular points.

**Case 1:**  $b_3 \neq 0, b_2 \neq 0$

Sub.	Conditions	Classification
1.1	$b_0 > 0, c_0 < 0$	$P_0$ saddle, $P_1$ unstable node, $P_2$ stable node
1.2	$b_0 > 0, c_0 > 0, c_0 - b_0 < 0$	$P_0$ unstable node, $P_1$ saddle, $P_2$ stable node
1.3	$b_0 > 0, c_0 > 0, c_0 - b_0 > 0$	$P_0$ unstable node, $P_1$ stable node, $P_2$ saddle
1.4	$c_0 = 0, b_0 > 0$	$P_0 \equiv P_1$ saddle-node, $P_2$ stable node
1.5	$b_0 = 0, c_0 > 0$	$P_0 \equiv P_2$ saddle-node, $P_1$ stable node

Table 5.1.2: Classification in case 1 of Table 5.1.1 according to the local phase portraits of finite singular points.

**Case 2:**  $b_3 \neq 0, b_2 = 0, b_0 \neq 0$

Sub.	Conditions	Classification
2.1	$b_0 > 0, c_0 < 0, c_0 - b_0 < 0$	$P_0$ saddle, $P_1$ unstable node
2.2	$b_0 > 0, c_0 > 0, c_0 - b_0 < 0$	$P_0$ unstable node, $P_1$ saddle
2.3	$b_0 > 0, c_0 > 0, c_0 - b_0 > 0$	$P_0$ unstable node, $P_1$ stable node
2.4	$c_0 = 0, b_0 > 0$	$P_0 \equiv P_1$ saddle-node

Table 5.1.3: Classification in case 2 of Table 5.1.1 according to the local phase portraits of finite singular points.



**Case 3:**  $b_3 = 0, c_0 \neq 0, b_2 \neq 0$

Sub.	Conditions	Classification
3.1	$b_0 > 0, c_0 < 0, c_0 - b_0 < 0$	$P_0$ saddle, $P_2$ stable node
3.2	$b_0 > 0, c_0 > 0, c_0 - b_0 > 0$	$P_0$ unstable node, $P_2$ saddle
3.3	$b_0 > 0, c_0 > 0, c_0 - b_0 < 0$	$P_0$ unstable node, $P_2$ stable node
3.4	$b_0 = 0, c_0 > 0$	$P_0 \equiv P_2$ saddle-node

Table 5.1.4: Classification in case 3 of Table 5.1.1 according to the local phase portraits of finite singular points.

**Case 4:**  $b_3 = 0, c_0 \neq 0, b_2 = 0, b_0 \neq 0$

Sub.	Conditions	Classification
4.1	$b_0 > 0, c_0 < 0$	$P_0$ saddle
4.2	$b_0 > 0, c_0 > 0$	$P_0$ unstable node

Table 5.1.5: Classification in case 4 of Table 5.1.1 according to the local phase portraits of finite singular points.

## 5.2 Local study of infinite singular points

Here we study the local phase portrait at the infinite singular points, and as it was said previously, we work under the hypothesis  $\tilde{H}^2$ . The expression of the Poincaré compactification of systems (5.0.1) in the local chart  $U_1$ , according to equations (1.3.9), is

$$\begin{aligned} \dot{u} &= (c_0 - b_0)uv^2, \\ \dot{v} &= -b_3uv^2 - b_0v^3 - b_1uv - b_2v^2. \end{aligned} \quad (5.2.2)$$

In chart  $U_2$ , according to equations (1.3.10), the expression is

$$\begin{aligned} \dot{u} &= (b_0 - c_0)uv^2, \\ \dot{v} &= -b_2uv^2 - c_0v^3 - b_1uv + b_3v^2. \end{aligned} \quad (5.2.3)$$

We want to study all the points at the infinity, which correspond with the line  $v = 0$  of these systems. To do that it is enough to study the singular points over  $v = 0$  in chart  $U_1$  and the origin of chart  $U_2$ .

We easily check in systems (5.2.2) that all points over the line  $v = 0$  are singular points. The eigenvalues of the Jacobian matrix at these singular points are both zero at the origin and at any other point  $(u_0, 0)$  the eigenvalues are zero and  $-b_1u_0$ . If  $b_1 > 0$  (respectively,  $b_1 < 0$ ), the nonzero eigenvalue is positive (respectively, negative) at the points on the negative  $u$ -axis, which correspond with the infinite singular points at the second and fourth quadrants of the Poincaré disk; the nonzero eigenvalue is negative for the infinite points at the first and third quadrants on the Poincaré disk (respectively, positive). Then, by Theorem 1.5.1, we get the following result:

**Lemma 5.2.1.** *For all the infinite singular point of systems (5.0.1) distinct from the origin of charts  $U_1$  and  $U_2$  the following statements hold.*

- *If  $b_1 > 0$ , to the points on the first and third quadrants arrives exactly one orbit from outside the infinity, and from the points on the second and fourth quadrants leaves exactly one orbit outside the infinity.*
- *If  $b_1 < 0$ , from the points on the first and third quadrants leaves exactly one orbit outside the infinity, and to the points on the second and fourth quadrants arrives exactly one orbit from outside the infinity.*

To study the origin of systems (5.2.2) we eliminate a common factor  $v$  from these systems and then study the singular points over the line  $v = 0$ . We do that on Subsection 5.2.1 and there we prove Theorem 5.2.2. The same occurs with the origin of chart  $U_2$ , as the origin of systems (5.2.3) is a singular point and the eigenvalues of the Jacobian matrix at that point are both zero. We study this point in Subsection 5.2.2 proving Theorem 5.2.4. Note that Theorem 5.2.2 and Theorem 5.2.4 determine the local phase portrait at the origin of charts  $U_1$  and  $U_2$  in the Poincaré disk, but also at the origins of charts  $V_1$  and  $V_2$ .

**Theorem 5.2.2.** *The origin of chart  $U_1$  is an infinite singular point of systems (5.0.1) and it has 3 topologically distinct local phase portraits, which taking into account the position of the sectors and orientation of the orbits, give raise to the 8 phase portraits described in Figure 5.2.1.*

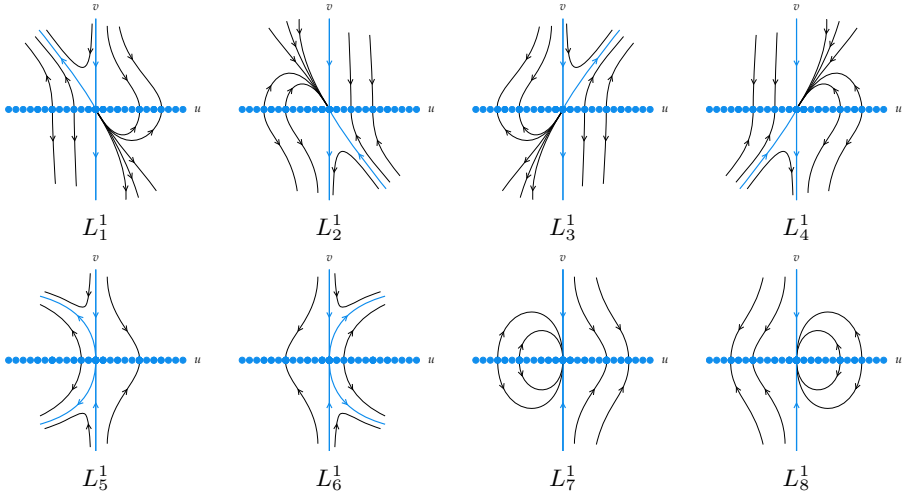


Figure 5.2.1: Local phase portraits at the infinite singular point  $O_1$ .

**Remark 5.2.3.** *Note that phase portraits  $L_1^1$  to  $L_4^1$  correspond to the first equivalence class,  $L_5^1$  and  $L_6^1$  to the second class, and  $L_7^1$  and  $L_8^1$  to the third class.*

**Theorem 5.2.4.** *The origin of chart  $U_2$  is an infinite singular point of systems (5.0.1) and it has 3 topologically distinct local phase portraits, which taking into account the position of the sectors and orientation of the orbits, give raise to the 10 phase portraits described in Figure 5.2.2.*

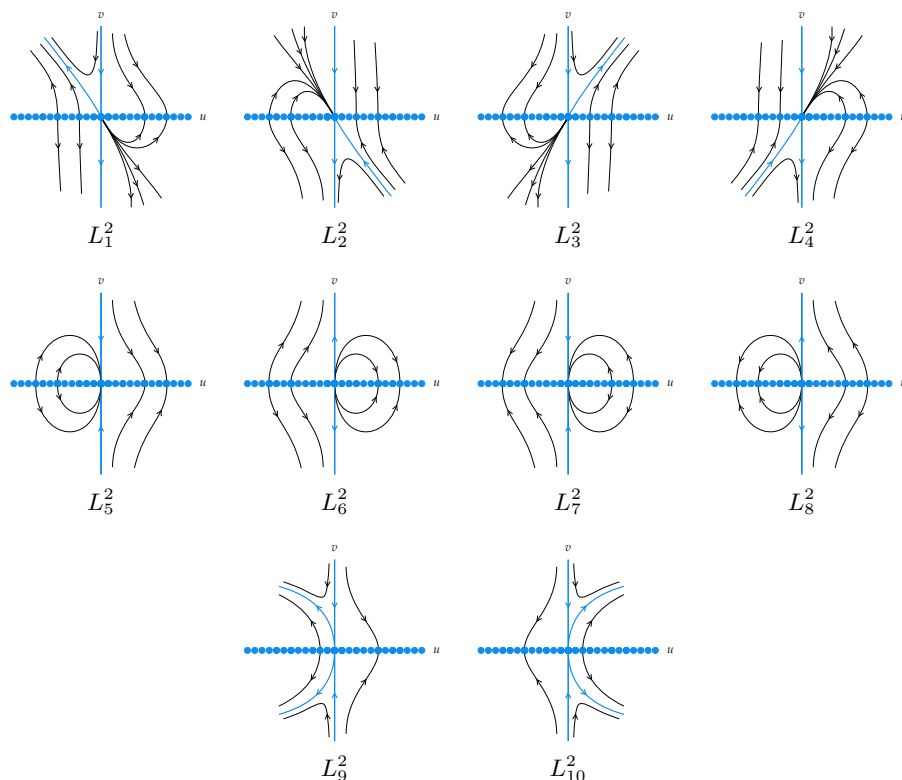


Figure 5.2.2: Local phase portraits at the infinite singular point  $O_2$ .

**Remark 5.2.5.** *Note that phase portraits  $L_1^1$  to  $L_4^1$  correspond to the first equivalence class,  $L_5^1$  to  $L_8^1$  to the second class, and  $L_9^1$  and  $L_{10}^1$  to the third class.*

### 5.2.1 Study of the origin of chart $U_1$

To study the origin of chart  $U_1$ , first we eliminate a common factor  $v$  from systems (5.2.2) obtaining:

$$\begin{aligned} \dot{u} &= (c_0 - b_0)uv, \\ \dot{v} &= -b_3uv - b_0v^2 - b_1u - b_2v. \end{aligned} \quad (5.2.4)$$

The only singular point of these systems over  $v = 0$  is the origin, and the eigenvalues of the Jacobian matrix at that point are zero and  $-b_2$ . Then, this singular point can be semi-

hyperbolic or nilpotent.

**Semi-hyperbolic case.** If  $b_2 \neq 0$ , then the origin of systems (5.2.4) is semi-hyperbolic, so its phase portrait can be determined by Theorem 1.2.3, concluding that it is always a saddle-node. In order to determine its local phase portrait it will be necessary to know the position of the different sectors and the orientation of the orbits in the saddle-node, so we must determine them depending on the parameters.

If  $b_1 > 0$ ,  $c_0 - b_0 > 0$  and  $b_0 = 0$ , then by the information given by the theorem and the sense of the flow in the different regions, the position of the sectors of the saddle-node and the orientation of the orbits for systems (5.2.4) is the one given in Figure 5.2.3(a). To obtain the local phase portrait at the origin of chart  $U_1$  we must multiply by  $v$ , so that all the points over the  $v$ -axis become singular points and the orbits on the third and fourth quadrants reverse their orientation. Thus we obtain the phase portrait of Figure 5.2.3(b), which is also  $L_1^1$  of Figure 5.2.1.

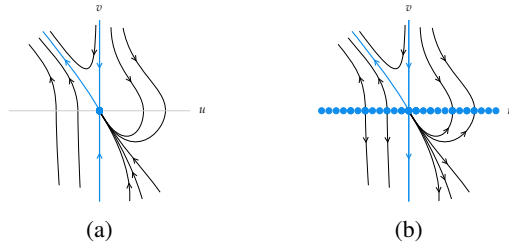


Figure 5.2.3: Local phase portraits of the origins of systems (5.2.4) and (5.2.2) with  $b_1 > 0$ ,  $c_0 - b_0 > 0$  and  $b_0 = 0$ .

If  $b_1 > 0$ ,  $c_0 - b_0 > 0$  and  $b_0 > 0$ , the fact that the parameter  $b_0$  is nonzero makes that systems (5.2.4) have a singular point on the negative  $v$ -axis, so that affects the phase portrait but not in a neighborhood of the origin. Then we obtain the same phase portrait for  $O_1$  as in the previous case,  $L_1^1$ .

Similarly we determine the position of the sectors and the orientation of the orbits in the remaining cases. If  $b_1 > 0$ ,  $c_0 - b_0 < 0$  and  $b_0 > 0$ , we obtain the phase portrait  $L_2^1$  of Figure 5.2.1. If  $b_1 < 0$ ,  $c_0 - b_0 > 0$  and  $b_0 \geq 0$ , we obtain the phase portrait  $L_3^1$ , and if  $b_1 < 0$ ,  $c_0 - b_0 < 0$  and  $b_0 > 0$ , the phase portrait is  $L_4^1$ .

**Nilpotent case.** If  $b_2 = 0$  then the origin of systems (5.2.4) is nilpotent so its phase portrait can be determined by Theorem 1.2.5, which concludes that in this case the singular point is either a saddle or it has a local phase portrait consisting of a hyperbolic sector and an elliptic sector, depending on the parameters. It is also necessary to determine the position of the sectors and the orientation of the orbits, and in order to do that we must take into account the information given by the theorem and also analyze the sense of the flow in the different regions depending on the parameters. Once we have determined the local phase portrait for systems (5.2.4), we must multiply by  $v$ , so all the points over the line  $v = 0$  become singular points, and the orientation of the orbits on the third and fourth quadrants is reversed. Thus we obtain for  $O_1$  the 8 phase portraits in Figure 5.2.2 under the following conditions:

If  $b_2 = 0$ ,  $b_0 > 0$ ,  $b_1 > 0$ ,  $c_0 - b_0 \neq 2b_0b_1$  and  $c_0 - b_0 > 0$ , the phase portrait at  $O_1$  is

$L_5^1$ . We obtain the same phase portrait if  $b_2 = 0$ ,  $b_0 > 0$ ,  $b_1 > 0$  and  $c_0 - b_0 = 2b_0b_1$ .

If  $b_2 = 0$ ,  $b_0 > 0$ ,  $b_1 > 0$ ,  $c_0 - b_0 \neq 2b_0b_1$  and  $c_0 - b_0 < 0$ , the phase portrait is  $L_7^1$ .

If  $b_2 = 0$ ,  $b_0 > 0$ ,  $b_1 < 0$ ,  $c_0 - b_0 \neq 2b_0b_1$  and  $c_0 - b_0 > 0$ , the phase portrait is  $L_6^1$ . The same result is obtained for  $b_2 = 0$ ,  $b_0 > 0$ ,  $b_1 < 0$  and  $b_0 - c_0 = 2b_0b_1$ .

If  $b_2 = 0$ ,  $b_0 > 0$ ,  $b_1 < 0$ ,  $c_0 - b_0 \neq 2b_0b_1$  and  $c_0 - b_0 < 0$ , the phase portrait is  $L_8^1$ .

## 5.2.2 Study of the origin of chart $U_2$

As in the previous section, to determine the phase portrait at the singular point  $O_2$ , we eliminate a common factor  $v$  from systems (5.2.3). Then we study the singular points over the line  $v = 0$  of systems

$$\begin{aligned}\dot{u} &= (b_0 - c_0)uv, \\ \dot{v} &= -b_2uv - c_0v^2 - b_1u + b_3v.\end{aligned}$$

The only singular point over that line is the origin, and it presents a similar behavior than in the previous case: it is semi-hyperbolic if  $b_3 \neq 0$  and it is nilpotent if  $b_3 = 0$ . In the semi-hyperbolic case the singular point is always a saddle-node, and attending to the information given by Theorem 1.2.3 and to the sense of the flow, we get four possibilities for the position and orientation of the sectors in the saddle-node, which are associated with their corresponding conditions in Table 5.2.1. In the nilpotent case the singular point can be a saddle or have a hyperbolic and an elliptic sector. In the first case we found two possibilities for the position of the saddle, and in the second case we found four different cases attending to the position and orientation of the two sectors. The results are given in Table 5.2.1.

Conditions	Phase portrait $O_2$
$b_3 \neq 0, b_1 > 0, b_0 - c_0 > 0$	$L_1^2$
$b_3 \neq 0, b_1 > 0, b_0 - c_0 < 0, c_0 > 0$	$L_2^2$
$b_3 \neq 0, b_1 < 0, b_0 - c_0 > 0$	$L_3^2$
$b_3 \neq 0, b_1 < 0, b_0 - c_0 < 0, c_0 > 0$	$L_4^2$
$b_3 \neq 0, c_0 \neq 0, b_1 > 0, b_0 - c_0 \neq 2b_1c_0, b_0 - c_0 < 0, c_0 > 0$	$L_5^2$
$b_3 \neq 0, c_0 \neq 0, b_1 > 0, b_0 - c_0 \neq 2b_1c_0, b_0 - c_0 > 0, c_0 < 0$	$L_6^2$
$b_3 \neq 0, c_0 \neq 0, b_1 > 0, b_0 - c_0 \neq 2b_1c_0, b_0 - c_0 > 0, c_0 > 0$	$L_9^2$
$b_3 \neq 0, c_0 \neq 0, b_1 > 0, b_0 - c_0 = 2b_1c_0, c_0 > 0$	
$b_3 \neq 0, c_0 \neq 0, b_1 < 0, b_0 - c_0 \neq 2b_1c_0, b_0 - c_0 < 0, c_0 > 0$	$L_{10}^2$
$b_3 \neq 0, c_0 \neq 0, b_1 < 0, b_0 - c_0 = 2b_1c_0, c_0 > 0$	
$b_3 \neq 0, c_0 \neq 0, b_1 < 0, b_0 - c_0 \neq 2b_1c_0, b_0 - c_0 > 0, c_0 > 0$	$L_7^2$
$b_3 \neq 0, c_0 \neq 0, b_1 < 0, b_0 - c_0 \neq 2b_1c_0, b_0 - c_0 < 0, c_0 < 0$	$L_8^2$

Table 5.2.1: Conditions for each local phase portrait of  $O_2$ .

## 5.3 Global phase portraits

In this section we prove Theorem 5.0.1 by obtaining all the possible global phase portraits from the local information analyzed in Sections 5.1 and 5.2. In each case of Tables 5.1.2 to

5.1.5 we must consider two subcases by setting the sign of  $b_1$ , and once this sign is fixed the local phase portrait at the infinite singular points is determined by Lemma 5.2.1 and Theorems 5.2.2 and 5.2.4. There is an exception to this, which is case 4.2 in Table 5.1.5, as in this case we must consider four subcases fixing also the sign of  $c_0 - b_0$ . Thus we have 32 cases.

According to Theorem 1.4.2, we have to draw the separatrix configuration in each case. We recall that the separatrices are the finite and infinite singular points, the limit cycles and the separatrices of the hyperbolic sectors. Systems (5.0.1) do not have any limit cycles as if they had a limit cycle, it must surround a finite singular point, but all the finite singular points are over invariant lines, particularly over the axes, so there are no limit cycles. Then we have to draw the local phase portraits of the singular points and the separatrices of the hyperbolic sectors for which we have to determine their  $\alpha$  and  $\omega$ -limits. In 30 of the 32 cases the place where the separatrices are born and die is determined in a unique way, so we obtain the corresponding global phase portrait by drawing them and one orbit in each canonical region which does not have an infinite number of singular points in the boundary, and three orbits (representing the infinite number of them existing) in each canonical region with an infinite number of singular points in the boundary.

The two remaining cases are 1.2 and 1.3 in Table 5.1.2, with  $b_1 > 0$ . In these cases the  $\alpha$  and  $\omega$ -limits are not determined in a unique way, and we can connect the separatrices in three different ways.

In case 1.2, if we fix  $b_1 > 0$ , we obtain the phase portraits G3, G4 and G5 of Figure 5.3.2, depending on how we connect the separatrices on the third quadrant. We know from the local information that there is a separatrix whose  $\omega$ -limit is the origin of chart  $V_1$  and a separatrix whose  $\alpha$ -limit the saddle  $P_1$  in the negative  $z$ -axis. Studying their possible  $\alpha$  and  $\omega$ -limits, respectively, we obtain the configurations given in Figure 5.3.1. Note that in the second case, the two separatrices are connected and so there is actually only one separatrix on the quadrant.

If  $b_2 = b_1 c_0 / b_3$ , then the connection of the separatrices takes place on the invariant straight line  $y = -c_0 / b_3$ , and we have the global phase portrait G4, as the configuration in the third quadrant is the one in Figure 5.3.1(b). The two remaining phase portraits can be obtained by perturbing just one parameter. For example, setting the values  $b_0 = 2$ ,  $b_1 = b_2 = b_3 = 1$ , we obtain the phase portrait G3 for  $c_0 = 1/2$ , G4 for  $c_0 = 1$  and G5 for  $c_0 = 3/2$ .

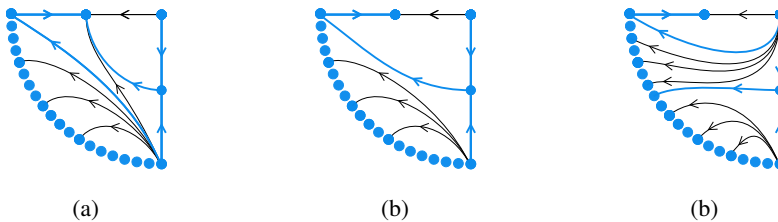


Figure 5.3.1: Possible configurations on the third quadrant on case 1.2 with  $b_1 > 0$ .

Similarly, if we fix  $b_1 > 0$  in case 1.3, we obtain three phase portraits, G7, G8 and G9 in Figure 5.3.2. The connection of the separatrices in G8 takes place on the invariant line

$y = -b_0/b_2$  when  $b_3 = b_1b_0/b_2$ . Fixed the values  $c_0 = 2$ ,  $b_1 = b_2 = b_3 = 1$ , we get the phase portrait G7 for  $b_0 = 1/2$ , G8 for  $b_0 = 1$  and G9 for  $b_0 = 3/2$ .

We include all the global phase portraits obtained in Figure 5.3.2 and in Table 5.3.1 we indicate which of them are obtained in each case.

Case	Subcase	$O_1$	$O_2$	Global
1.1	$b_1 > 0$	$L_2^1$	$L_1^2$	G1
	$b_1 < 0$	$L_4^1$	$L_3^2$	G2
1.2	$b_1 > 0$	$L_2^1$	$L_1^2$	G3, G4 or G5
	$b_1 < 0$	$L_4^1$	$L_3^2$	G6
1.3	$b_1 > 0$	$L_1^1$	$L_2^2$	G7, G8 or G9
	$b_1 < 0$	$L_3^1$	$L_4^2$	G10
1.4	$b_1 > 0$	$L_2^1$	$L_1^2$	G11
	$b_1 < 0$	$L_4^1$	$L_3^2$	G12
1.5	$b_1 > 0$	$L_1^1$	$L_2^2$	G13
	$b_1 < 0$	$L_3^1$	$L_4^2$	G14
2.1	$b_1 > 0$	$L_7^1$	$L_1^2$	G15
	$b_1 < 0$	$L_8^1$	$L_3^2$	G16
2.2	$b_1 > 0$	$L_7^1$	$L_1^2$	G17
	$b_1 < 0$	$L_8^1$	$L_3^2$	G18
2.3	$b_1 > 0$	$L_5^1$	$L_2^2$	G19
	$b_1 < 0$	$L_6^1$	$L_4^2$	G20
2.4	$b_1 > 0$	$L_7^1$	$L_1^2$	G21
	$b_1 < 0$	$L_8^1$	$L_3^2$	G22
3.1	$b_1 > 0$	$L_2^1$	$L_6^2$	G23
	$b_1 < 0$	$L_4^1$	$L_8^2$	G24
3.2	$b_1 > 0$	$L_1^1$	$L_5^2$	G25
	$b_1 < 0$	$L_3^1$	$L_7^2$	G26
3.3	$b_1 > 0$	$L_2^1$	$L_9^2$	G27
	$b_1 < 0$	$L_4^1$	$L_{10}^2$	G28
3.4	$b_1 > 0$	$L_1^1$	$L_5^2$	G29
	$b_1 < 0$	$L_3^1$	$L_7^2$	G30
4.1	$b_1 > 0$	$L_7^1$	$L_6^2$	G31
	$b_1 < 0$	$L_8^1$	$L_8^2$	G32
4.2	$b_1 > 0, c_0 - b_0 > 0$	$L_5^1$	$L_5^2$	G33
	$b_1 > 0, c_0 - b_0 < 0$	$L_7^1$	$L_9^2$	G34
	$b_1 < 0, c_0 - b_0 > 0$	$L_6^1$	$L_7^2$	G35
	$b_1 < 0, c_0 - b_0 < 0$	$L_8^1$	$L_{10}^2$	G36

Table 5.3.1: Classification of the global phase portraits of systems (5.0.1).

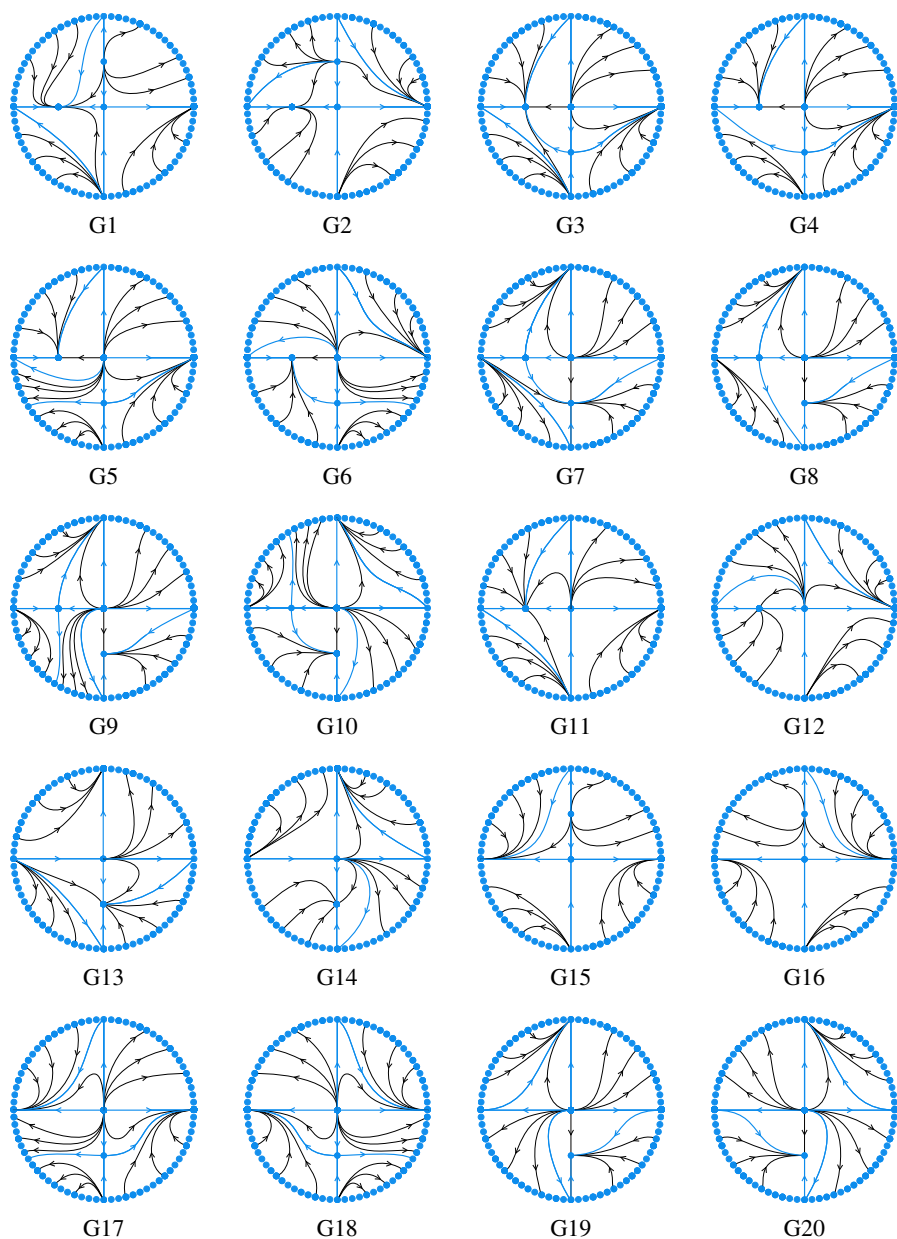


Figure 5.3.2 (1 out of 2): Global phase portraits of systems (5.0.1) in the Poincaré disk.



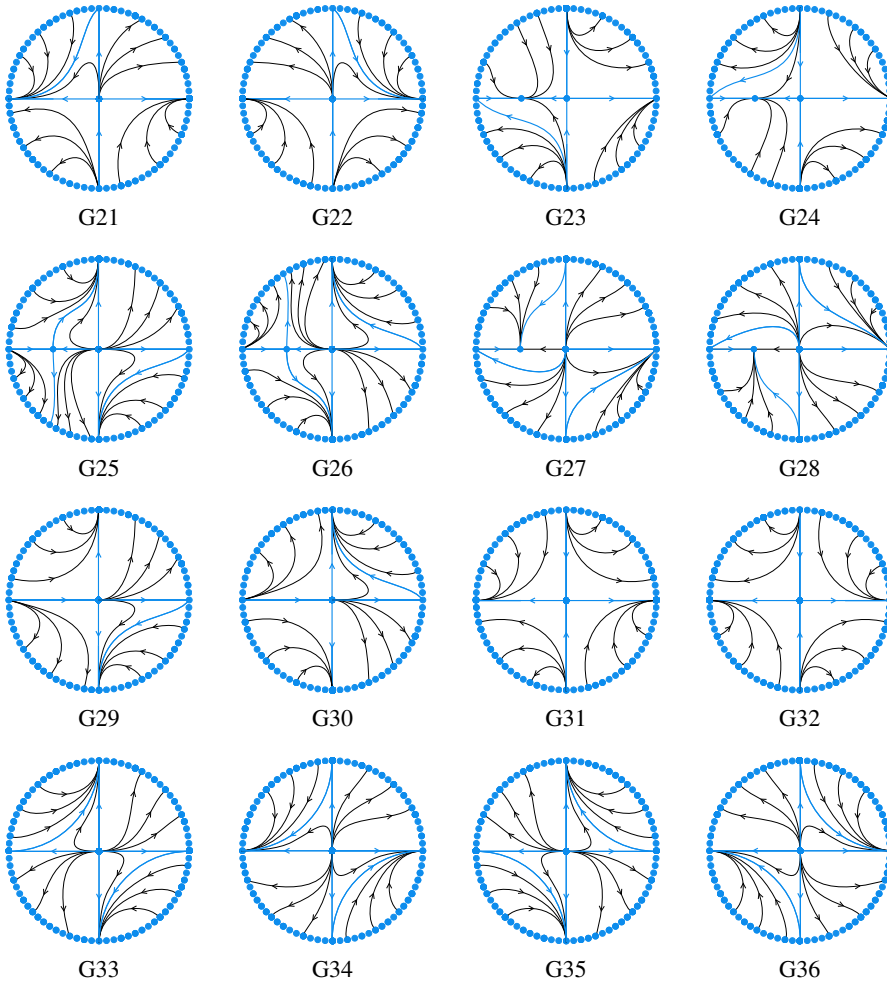


Figure 5.3.2 (2 out of 2): Global phase portraits of systems (5.0.1) in the Poincaré disk.

## 5.4 Topological equivalences

In the previous sections we have obtained the 36 global phase portraits given in Figure 5.3.2 and now we study which of them are topologically equivalent. As Theorem 1.4.2 only works in regions with a finite number of singular points, we will consider the equivalences on the open Poicaré disk, but this does not affect the result as if two separatrix configurations are topologically equivalent, they will be still equivalent if we add the boundary of the disk, because the boundary is filled of singular points. If they are not topologically equivalent they will not be equivalent by adding the boundary of the disk.

We will consider classes of equivalence according to the following invariants: the number

of finite singular points and the sum of the indices at the finite singular points, denoted by  $ind_F$ . We give this first classification in Table 5.4.1 and then, within each class, we prove which of the phase portraits are topologically equivalent.

Class	N° finite sing.	$ind_F$	Global phase portraits
1	3	1	G1, G2, G4, G4, G5, G6, G7, G8, G9, G10
2	2	1	G11, G12, G13, G14
3		0	G15, G16, G17, G18, G23, G24, G25, G26
4		2	G19, G20, G27, G28
5	1	0	G21, G22, G29, G30
6		-1	G31, G32
7		1	G33, G34, G35, G36

Table 5.4.1: Classes of equivalence according to the number of finite singular points and to the  $ind_F$ .

**Class 1.** First we can distinguish two subclasses depending on the number of separatrices in the open Poincaré disk. There are 11 separatrices in phase portraits G1, G2, G4 and G8, and 12 separatrices in phase portraits G3, G5, G6, G7, G9 and G10. In the first subclass, G1 is topologically equivalent to G2 by doing a symmetry with respect to the line  $z = -y$  and a change of the time variable  $t$  by  $-t$ . G1 is different from G4 as in G1 there are two separatrices that start in the unstable node and in G4 there are three. G1 is also different from G8 as in G1 there are two separatrices of the saddle that connect with the infinity and in G8 there are three. At last, G4 is topologically equivalent to G8 by doing a  $90^\circ$  rotation of G8 and then a symmetry with respect to the  $z$ -axis. In the second subclass, G3 is different from G5 as in G3 the saddle has two separatrices that connect with the infinity and in G5 it has three. By doing a symmetry with respect to the line  $y = z$  we transform G3 into G7, G5 into G9, and G6 into G10. G7 is different from G10 as in G7 there are three separatrices that start in the unstable node and in G10 there are four. G9 is different from G10 as in G10 there is a separatrix that connects two infinite singular points but in G9 there is not a such separatrix.

**Class 2.** G11 is different from G12 as in G11 the saddle-node has three separatrices that connect with infinite singular points and in G12 it has four. G11 is topologically equivalent to G13 and G12 to G14 by doing a symmetry with respect to the line  $y = z$ .

**Class 3.** G15 is topologically equivalent to G16 and G17 to G18 by doing a symmetry with respect to the  $z$ -axis. G15 is different from G17 as in G15 there are two separatrices that start at the node and in G17 there are four. G15 is topologically equivalent to G23 by doing a rotation of  $90^\circ$  in G15 and a change of the time variable  $t$  by  $-t$ . We can also transform G25 into G18 by a rotation of  $90^\circ$ . Lastly we can transform G23 into G24 and G25 into G26 with a symmetry with respect to the  $y$ -axis.

**Class 4.** G19 is topologically equivalent to G20 by a symmetry with respect to the  $z$ -axis, G19 to G27 by a symmetry with respect to the line  $z = y$ , and G27 to G28 by a symmetry with respect to  $y$ -axis.

**Class 5.** G21 is topologically equivalent to G22 by a symmetry with respect to the  $z$ -

axis, G21 to G29 by a symmetry with respect to the line  $z = y$ , and G29 to G30 by a symmetry with respect to  $y$ -axis.

**Class 6.** G31 is topologically equivalent to G32 by a symmetry with respect to the  $z$ -axis.

**Class 7.** G33 is topologically equivalent to G34 with a symmetry with respect to the line  $z = y$ , and by a symmetry with respect to the  $z$ -axis, G33 is topologically equivalent to G35 and G34 to G36.

In summary, among these seven classes, we have found 13 topologically different phase portraits in the Poincaré disk for systems (5.0.1), so we have proved Theorem 5.0.1. This 13 phase portraits are described in Figure 5.0.1, where we include a representative of each one of the topological equivalence classes. These representatives correspond with the phase portraits in Figure 5.3.2 as indicated in Table 5.4.2.

Rep.	Phase portraits	Rep.	Phase portraits	Rep.	Phase portraits
R1	G1, G2	R6	G11, G13	R10	G19, G20, G27, G28
R2	G3, G7	R7	G12, G14	R11	G21, G22, G29, G30
R3	G4, G8	R8	G15, G16, G23, G24	R12	G31, G32
R4	G5, G9	R9	G17, G18, G25, G26	R13	G33, G34, G35, G36
R5	G6, G10				

Table 5.4.2: Representatives of each equivalence class and their corresponding global phase portraits of systems (5.0.1).

Now we give a second proof that shows that these 13 phase portraits are indeed topologically distinct.

**Theorem 5.4.1.** *The 13 phase portraits of systems (5.0.1) included in Figure 5.0.1 are topologically distinct.*

*Proof.* We will consider six geometrical invariants in order to distinguish the phase portraits.

- ( $I_1$ ) Number of finite singularities. The values of this invariant for the phase portraits R1 to R13 are, respectively: 3, 3, 3, 3, 3, 2, 2, 2, 2, 2, 1, 1, 1.
- ( $I_2$ ) Sum of the index of the finite singularities. The values of this invariant for the phase portraits R1 to R13 are: 1, 1, 1, 1, 1, 1, 1, 0, 0, 2, 0, -1, 1.

With these two invariants we can already determine that the phase portraits R10, R11, R12 and R13 are topologically distinct between them and from all the others. We will not determine other invariants for them.

- ( $I_3$ ) Separatrices of the finite singularities connected with finite nodes. For the phase portraits R1 to R9 this invariant has the values: 2, 2, 1, 1, 2, 1, 1, 1, 1.
- ( $I_4$ ) Number of connections between separatrices of the finite singularities and separatrices of infinite singularities. The values of this invariant for the phase portraits R1 to R9 are: 2, 1, 2, 1, 1, 2, 2, 3, 1.

## 5.4 Topological equivalences

---

With the four previous invariants we can guarantee that the phase portraits R1, R3, R4, R8 and R9 are topologically distinct. Among the remaining phase portraits, R2 has the same invariants as R5 and R6 the same as R7, so we will distinguish between them with the two following invariants.

- ( $I_5$ ) Number of infinite singularities receiving an infinite number of orbits from a finite singularity. This invariant is 2 for R2 and 1 for R5.
- ( $I_6$ ) Number of separatrices that leave the finite saddle-node in its parabolic sector and go to an infinite singular point. This invariant is 1 for R6 and 2 for R7.

Then we have proved that all the 13 phase portraits are topologically distinct as they have different values for the mentioned invariants.

□



# Zero-Hopf bifurcation on Kolmogorov systems

In this chapter, although we continue with the study of the Kolmogorov systems, we do so from a different point of view, focusing our attention on the existence of limit cycles. More precisely, we study the limit cycles of the Kolmogorov systems of degree three in  $\mathbb{R}^3$  which appear by a zero-Hopf bifurcation of the singular points  $(a, b, c)$  which are not on the invariant planes  $x = 0$ ,  $y = 0$  and  $z = 0$ . The results of this chapter are included in the work published in [40]<sup>1</sup>. We consider the systems

$$\dot{x} = xP(x, y, z), \quad \dot{y} = yQ(x, y, z), \quad \dot{z} = zR(x, y, z),$$

with  $P$ ,  $Q$  and  $R$  polynomials of degree two. Doing the scaling  $(x, y, z) \rightarrow (x/a, y/b, z/c)$  we can assume without loss of generality that  $(a, b, c) = (1, 1, 1)$ . Therefore it is sufficient to study the limit cycles which can bifurcate from the singular point  $(1, 1, 1)$  of the systems

$$\begin{aligned} \dot{x} &= x \left( a_1(x-1) + a_2(y-1) + a_3(z-1) + a_4(x-1)^2 + a_5(x-1)(y-1) \right. \\ &\quad \left. + a_6(x-1)(z-1) + a_7(y-1)^2 + a_8(y-1)(z-1) + a_9(z-1)^2 \right), \\ \dot{y} &= y \left( b_1(x-1) + b_2(y-1) + b_3(z-1) + b_4(x-1)^2 + b_5(x-1)(y-1) \right. \\ &\quad \left. + b_6(x-1)(z-1) + b_7(y-1)^2 + b_8(y-1)(z-1) + b_9(z-1)^2 \right), \\ \dot{z} &= z \left( c_1(x-1) + c_2(y-1) + c_3(z-1) + c_4(x-1)^2 + c_5(x-1)(y-1) \right. \\ &\quad \left. + c_6(x-1)(z-1) + c_7(y-1)^2 + c_8(y-1)(z-1) + c_9(z-1)^2 \right), \end{aligned} \quad (6.0.1)$$

when this singular point is a *zero-Hopf equilibrium*, i.e., when the eigenvalues of the linear part of the systems at  $(1, 1, 1)$  are of the form  $0$  and  $\pm\beta i$  with  $\beta > 0$ . In the next result we characterize when the singular point  $(1, 1, 1)$  is zero-Hopf.

**Proposition 6.0.1.** *The singular point  $(1, 1, 1)$  of systems (6.0.1) is zero-Hopf if and only if one of the following sets of conditions hold, with  $\gamma = a_3b_3(b_2 - a_1) - a_2b_3^2 + a_3^2b_1$  and  $\beta > 0$ :*

<sup>1</sup>Erika Diz-Pita (Departamento de Estatística, Análise Matemática e Optimizaci3n, Universidade de Santiago de Compostela), Jaume Llibre (Departament de Matemàtiques, Universitat Aut3noma de Barcelona), Maria Victoria Otero-Espinar (Departamento de Estatística, Análise Matemática e Optimizaci3n, Universidade de Santiago de Compostela) and Claudia Valls (Departamento de Matemática, Instituto Superior T3cnico, Universidade de Lisboa), *The zero-Hopf bifurcations in the Kolmogorov systems of degree 3 in  $\mathbb{R}^3$* , Communications in Nonlinear Science and Numerical Simulation (ISSN: 1007-5704, EISSN: 1878-7274), **95** (2021), 105621, Published by Elsevier. The final authenticated version is available online at: <https://doi.org/10.1016/j.cnsns.2020.105621>.

- (i)  $\gamma \neq 0, c_3 = -a_1 - b_2, c_1 = \frac{1}{\gamma}(a_1^3 b_3 - a_1^2 a_3 b_1 - a_1(a_3 b_1 b_2 - b_3(2a_2 b_1 + \beta^2)) - b_1(a_2(a_3 b_1 - b_2 b_3) + a_3(\beta^2 + b_2^2)))$  and  $c_2 = \frac{1}{\gamma}(a_1^2 a_2 b_3 + a_1 a_2(b_2 b_3 - a_3 b_1) + a_2^2 b_1 b_3 - a_3 b_2(\beta^2 + b_2^2) + a_2(b_3(\beta^2 + b_2^2) - 2a_3 b_1 b_2))$ .
- (ii)  $\gamma \neq 0, a_3 b_3 \neq 0, a_2 = \frac{a_3 b_2}{b_3}, b_1 = \frac{a_1 b_3}{a_3}, c_2 = -\frac{(a_1 + b_2)^2 + a_3 c_1 + \beta^2}{b_3}$  and  $c_3 = -a_1 - b_2$ .
- (iii)  $\gamma \neq 0, b_3 \neq 0, a_1 = a_2 = a_3 = 0, c_2 = -\frac{b_2^2 + \beta^2}{b_3}$  and  $c_3 = -b_2$ .
- (iv)  $\gamma \neq 0, a_3 \neq 0, b_1 = b_2 = b_3 = 0, c_1 = -\frac{a_1^2 + \beta^2}{a_3}$  and  $c_3 = -a_1$ .
- (v)  $\gamma \neq 0, b_1 \neq 0, a_2 = -\frac{a_1^2 + \beta^2}{b_1}, a_3 = b_3 = c_3 = 0$  and  $b_2 = -a_1$ .

*Proof.* We want to characterize when the singular point  $(1, 1, 1)$  of systems (6.0.1) is a zero-Hopf equilibrium. At first, through the change of variables  $(x, y, z) \rightarrow (x+1, y+1, z+1)$ , we translate the point  $(1, 1, 1)$  to the origin of coordinates, obtaining the systems:

$$\begin{aligned} \dot{x} &= (1+x)(a_1 x + a_2 y + a_3 z + a_4 x^2 + a_5 xy + a_6 xz + a_7 y^2 + a_8 yz + a_9 z^2), \\ \dot{y} &= (1+y)(b_1 x + b_2 y + b_3 z + b_4 x^2 + b_5 xy + b_6 xz + b_7 y^2 + b_8 yz + b_9 z^2), \\ \dot{z} &= (1+z)(c_1 x + c_2 y + c_3 z + c_4 x^2 + c_5 xy + c_6 xz + c_7 y^2 + c_8 yz + c_9 z^2). \end{aligned} \quad (6.0.2)$$

In order that the origin of these systems (6.0.2) can exhibit a zero-Hopf bifurcation we must require that the eigenvalues of the linear part of the systems at the origin be of the form  $0$  and  $\pm\beta i$  with  $\beta > 0$ . We compute the characteristic polynomial and require that it has the form  $\lambda(\lambda^2 + \beta^2)$ . Solving the resultant equation we get the five solutions given in (i)–(v).  $\square$

The first of these five cases has been studied in [85]. More precisely, in Theorem 3 of [85] are provided sufficient conditions in order that the Kolmogorov systems (6.0.1) under conditions (i) exhibit a zero-Hopf bifurcation from which two limit cycles bifurcate. The kind of stability or instability of these limit cycles is also provided.

In the present chapter of this thesis we want to study the Kolmogorov systems (6.0.1) under conditions (ii)–(v). To this end we use the averaging theory of first order, introduced in Section 1.8, to study the limit cycles bifurcating from the zero-Hopf bifurcations of these systems. We consider conditions (ii) in Section 6.1, while conditions (iii) and (iv) are considered together in Section 6.2 as their study is analogous. Finally, in Section 6.3, we deal with conditions (v).

All the necessary computations for proving our results have been made with the algebraic manipulator Mathematica 12.0.0.0 (for Mac OS X x86) in a computer MacBook Air of 2019. The computations done with Mathematica were verified for family (ii) also with the software Maple. Some of the expressions obtained in these computations are particularly long, so

they are not included in the manuscript, but can be consulted in the downloadable documents at [41].

## 6.1 Kolmogorov systems under conditions (ii)

Our main result concerning the Kolmogorov systems (6.0.1) under conditions (ii) is the following. The expressions of  $A_i$ , with  $i = 0, \dots, 4$ ,  $K_1$  and  $N$  are defined in Section 6.4.

**Theorem 6.1.1.** *If  $a_3b_3 \neq 0$ ,  $N \neq 0$ ,  $a_2 = a_3b_2/b_3$ ,  $b_1 = a_1b_3/a_3$ ,  $c_3 = -a_1 - b_2$ ,  $c_2 = -((a_1+b_2)^2 + a_3c_1 + \beta^2)/b_3$ ,  $A_1 \neq 0$ ,  $A_2 \neq 0$ ,  $A_3 \neq 0$ , and  $A_0A_4(A_1A_2 - A_0A_3) > 0$ , then the Kolmogorov systems (6.0.1) have two limit cycles bifurcating from the zero-Hopf equilibrium point  $(1, 1, 1)$ . Moreover the following statements hold.*

(a) *If  $K_1 > 0$ ,  $A_2A_3(A_0A_3 - A_1A_2)N < 0$  and  $|2A_0A_3 - A_1A_2| < \sqrt{K_1}$ , then the two limit cycles have a stable manifold formed by two cylinders and an unstable manifold formed by two cylinders.*

(b) *If  $b_3A_2N > 0$ ,  $b_3A_3(A_0A_3 - A_1A_2) > 0$  and*

- *either  $K_1 > 0$ ,  $b_3A_1N(2A_0A_3 - A_1A_2 - \sqrt{K_1}) < 0$  and  $b_3A_1N(2A_0A_3 - A_1A_2 + \sqrt{K_1}) < 0$ ,*
- *or  $K_1 \leq 0$  and  $b_3A_1N(2A_0A_3 - A_1A_2) < 0$ ;*

*or if  $b_3A_2N < 0$ ,  $b_3A_3(A_0A_3 - A_1A_2) < 0$  and*

- *either  $K_1 > 0$ ,  $b_3A_1N(2A_0A_3 - A_1A_2 - \sqrt{K_1}) > 0$  and  $b_3A_1N(2A_0A_3 - A_1A_2 + \sqrt{K_1}) > 0$ ,*
- *or  $K_1 \leq 0$  and  $b_3A_1N(2A_0A_3 - A_1A_2) > 0$ ;*

*then one limit cycle is a local repeller, and the other is a local attractor.*

(c) *If  $b_3A_2N > 0$ ,  $b_3A_3(A_0A_3 - A_1A_2) > 0$ ,  $K_1 > 0$  and  $|2A_0A_3 - A_1A_2| < \sqrt{K_1}$ ; or if  $A_2A_3(A_0A_3 - A_1A_2)N < 0$  and*

- *either  $K_1 > 0$ ,  $b_3A_1N(2A_0A_3 - A_1A_2 - \sqrt{K_1}) > 0$  and  $b_3A_1N(2A_0A_3 - A_1A_2 + \sqrt{K_1}) > 0$ ,*
- *or  $K_1 \leq 0$  and  $b_3A_1(2A_0A_3 - A_1A_2)N > 0$ ;*

*then both limit cycles are unstable. One limit cycle is a local repeller, and the other has a stable manifold formed by two cylinders and an unstable manifold formed by two cylinders.*

(d) *If  $b_3A_2N < 0$ ,  $b_3A_3(A_0A_3 - A_1A_2) < 0$ ,  $K_1 > 0$  and  $|2A_0A_3 - A_1A_2| < \sqrt{K_1}$ ; or if  $A_2A_3(A_0A_3 - A_1A_2)N < 0$  and*

- *either  $K_1 > 0$ ,  $b_3A_1N(2A_0A_3 - A_1A_2 - \sqrt{K_1}) < 0$  and  $b_3A_1N(2A_0A_3 - A_1A_2 + \sqrt{K_1}) < 0$ ,*



- or  $K_1 \leq 0$  and  $b_3 A_1 (2A_0 A_3 - A_1 A_2) N < 0$ ;

then one limit cycle is a local attractor, and the other is unstable and has a stable manifold formed by two cylinders and an unstable manifold formed by two cylinders.

- (e) If  $K_1 < 0$ ,  $A_2 A_3 (A_0 A_3 - A_1 A_2) N < 0$  and  $2A_0 A_3 = A_1 A_2$ ; then one limit cycle is unstable and has a stable manifold formed by two cylinders and an unstable manifold formed by two cylinders and we cannot decide about the stability of the other.

*Proof of Theorem 6.1.1.* We consider systems (6.0.1) under conditions (ii) of Proposition 6.0.1, and we proceed to study the limit cycles bifurcating from the zero-Hopf equilibrium point, applying the averaging theory of first order, summarized in Theorem 1.8.3 of Section 1.8. To do so we perturb the parameters  $a_2$ ,  $b_1$ ,  $c_2$  and  $c_3$  which define the zero-Hopf equilibrium under the assumption (ii) as follows:

$$a_2 = \frac{a_3 b_2}{b_3} + \varepsilon a_{21}, \quad b_1 = \frac{a_1 b_3}{a_3} + \varepsilon b_{11},$$

$$c_2 = -\frac{(a_1 + b_2)^2 + a_3 c_1 + \beta^2}{b_3} + \varepsilon c_{21}, \quad c_3 = -a_1 - b_2 + \varepsilon c_{31},$$

where  $\varepsilon$  is a small parameter and  $\beta > 0$ .

We write the linear part of systems (6.0.2) at the origin in its real Jordan normal form

$$J = \begin{pmatrix} 0 & -\beta & 0 \\ \beta & 0 & 0 \\ 0 & 0 & 0 \end{pmatrix}. \quad (6.1.3)$$

The variables of the systems having its linear part in the real Jordan normal form are  $(X, Y, Z)$ . Then systems (6.0.1) under conditions (ii) of Proposition 6.0.1 become of the form

$$\begin{aligned} \dot{X} &= -\beta Y + O(\varepsilon), \\ \dot{Y} &= \beta X + O(\varepsilon), \\ \dot{Z} &= O(\varepsilon). \end{aligned}$$

The complete explicit expression of these systems is given in systems  $(\dot{X}, \dot{Y}, \dot{Z})$  in file ss[[2]], downloadable at [41].

We note that there are infinitely many linear changes of variables for writing the linear part of systems (6.0.2) at the origin in its real Jordan normal form. This forces to choose some of the entries (denoted by  $y_i$  for  $i = 1, \dots, 9$  in file ss[[2]]) of the changing matrix. Thus in the file ss[[2]] we choose  $y_1 = y_7 = 1$  and  $y_2 = 0$  in order to fix a unique changing matrix.

We note that the choice of the matrix  $J$  given in (6.1.3) instead of the matrix

$$J = \begin{pmatrix} 0 & 0 & 0 \\ 0 & -\beta & 0 \\ \beta & 0 & 0 \end{pmatrix}$$

is irrelevant. If we choose this last expression for the matrix in its real Jordan form, then instead of doing the change to cylindrical coordinates  $(X, Y, Z) \rightarrow (r \cos \theta, r \sin \theta, Z)$ , we must do the change  $(X, Y, Z) \rightarrow (X, r \cos \theta, r \sin \theta)$ . This change to cylindrical coordinates is necessary in order to arrive to write the differential systems in the normal form for applying the averaging theory described in Theorem 1.8.3

Now we want to write the systems in such a way that conditions of Theorem 1.8.3 are satisfied. For this we write the systems in cylindrical coordinates by means of the change of variables  $(X, Y, Z) \rightarrow (r \cos \theta, r \sin \theta, Z)$  obtaining systems  $(\dot{r}, \dot{\theta}, \dot{Z})$  of file ss[[2]].

In order to study the periodic solutions in a neighborhood of the origin, i.e., in a neighborhood of the zero-Hopf equilibrium, we do the scaling  $(r, Z) \rightarrow (\varepsilon R, \varepsilon Z)$ , where  $\varepsilon > 0$  is the same parameter used before. We obtain systems  $(\dot{R}, \dot{Z})$  of file ss[[2]].

We take the variable  $\theta$  as the new independent variable and so we obtain the system

$$R' = \varepsilon F_{11} + O(\varepsilon^2), \quad Z' = \varepsilon F_{12} + O(\varepsilon^2), \quad (6.1.4)$$

with coefficients  $F_{11}$  and  $F_{12}$  given in the file ss[[2]].

Note that systems (6.1.4) are in the normal form (1.8.17), so we can apply the averaging theory with  $T = 2\pi$ ,  $x = (R, Z)$ ,  $t = \theta$  and  $\varepsilon R(\theta, x, \varepsilon) = O(\varepsilon^2)$ . The functions  $F_{11}$ ,  $F_{12}$  and  $R$  are  $C^2$  in  $x$  and  $2\pi$ -periodic in  $\theta$ . Applying Theorem 1.8.3 we compute the averaging function of first order  $f_1 = (f_{11}(R, Z), f_{12}(R, Z))$ , and we obtain

$$f_{11} = \frac{\pi R(A_0 + A_1 Z)}{a_3^2 b_3 \beta^5}, \quad f_{12} = -\frac{\pi(A_2 Z + A_3 Z^2 + A_4 R^2)}{a_3^2 b_3 \beta^5 N}, \quad (6.1.5)$$

where  $A_i$ , for  $i = 0, \dots, 4$ ,  $K_1$  and  $N$  are given in Section 6.4.

We look for the isolated solutions of the equation  $(f_{11}(R, Z), f_{12}(R, Z)) = (0, 0)$ , and we obtain, apart from the origin, the solutions

$$(R_1, Z_1) = (0, -A_2/A_3) \text{ and } (R_2, Z_2) = \left( \pm \sqrt{A_0(A_1 A_2 - A_0 A_3)} / (A_1 \sqrt{A_4}), -A_0/A_1 \right).$$

We consider always the positive expression of  $R_2$ , i.e., we consider the positive sign if  $A_1 > 0$  and the negative sign if  $A_1 < 0$ .

We compute the Jacobian matrix of  $f_1$ , which is

$$\begin{pmatrix} \frac{\pi(A_0 + A_1 Z)}{a_3^2 b_3 \beta^5} & \frac{\pi R A_1}{a_3^2 b_3 \beta^5} \\ -\frac{2\pi R A_4}{a_3^2 b_3 \beta^5 N} & -\frac{\pi(A_2 + 2A_3 Z)}{a_3^2 b_3 \beta^5 N} \end{pmatrix},$$

and its determinant is  $\pi^2(-2A_1 A_4 R^2 + (A_0 + A_1 Z)(A_2 + 2A_3 Z)) / (a_3^4 b_3^2 \beta^{10} N)$ . Evaluating the determinant at the solution  $(R_1, Z_1)$  we get that it is equal to

$$\pi^2 A_2 (A_0 A_3 - A_1 A_2) / (a_3^4 b_3^2 A_3 \beta^{10} N),$$

and at the solutions  $(R_2, Z_2)$  we get that it is equal to

$$2\pi^2 A_0 (A_1 A_2 - A_0 A_3) / (a_3^4 b_3^2 A_1 \beta^{10} N).$$

From the hypothesis considered, these determinants are nonzero, therefore, it follows from Theorem 1.8.3 that for  $\varepsilon$  sufficiently small systems (6.1.4) have two  $2\pi$ -periodic solutions  $(R_1(\theta, \varepsilon), Z_1(\theta, \varepsilon))$  and  $(R_2(\theta, \varepsilon), Z_2(\theta, \varepsilon))$  such that  $(R_j(\theta, \varepsilon), Z_j(\theta, \varepsilon)) \rightarrow (R_j, Z_j)$  for  $j = 1, 2$  when  $\varepsilon \rightarrow 0$ .

Moreover the Jacobian matrix evaluated at the solution  $(R_1, Z_1)$  has eigenvalues equal to  $\pi A_2 / (a_3^2 b_3 \beta^5 N)$  and  $\pi(A_0 A_3 - A_1 A_2) / (a_3^2 b_3 A_3 \beta^5)$ . Since the eigenvalues of the Jacobian matrix evaluated at the solutions provide the stability of the fixed point corresponding to the Poincaré map defined in a neighborhood of the solution, we have that:

- If  $A_2 b_3 N > 0$  and  $A_3 b_3 (A_0 A_3 - A_1 A_2) > 0$ , then the fixed point of the Poincaré map has an unstable manifold of dimension two, and the corresponding periodic solution is unstable and has an unstable manifold of dimension three, which is equivalent to say that is a repelling periodic orbit.
- If  $A_2 b_3 N < 0$  and  $A_3 b_3 (A_0 A_3 - A_1 A_2) < 0$ , then the fixed point of the Poincaré map has a stable manifold of dimension two, and the associated periodic solution is stable and has a stable manifold of dimension three, which is equivalent to say that is a attracting periodic orbit.
- Finally, if  $A_2 A_3 N (A_0 A_3 - A_1 A_2) < 0$ , the fixed point of the Poincaré map is a saddle point with a stable manifold of degree one and an unstable manifold of degree one, and the corresponding periodic solution is unstable and has a stable manifold formed by two cylinders and an unstable manifold formed by two cylinders.

On the other hand, the Jacobian matrix evaluated at  $(R_2, Z_2)$  has eigenvalues equal to  $\pi(2A_0 A_3 - A_1 A_2 \pm \sqrt{K_1}) / (2a_3^2 b_3 A_1 \beta^5 N)$ , and so its stability is as follows:

- If  $K_1 > 0$ ,  $b_3 A_1 N(2A_0 A_3 - A_1 A_2 + \sqrt{K_1}) > 0$  and  $b_3 A_1 N(2A_0 A_3 - A_1 A_2 - \sqrt{K_1}) > 0$  or if  $K_1 < 0$  and  $b_3 A_1 N(2A_0 A_3 - A_1 A_2) > 0$ , then the fixed point of the Poincaré map has an unstable manifold of dimension two, and the periodic solution is unstable and has an unstable manifold of dimension three.
- If  $K_1 > 0$ ,  $b_3 A_1 N(2A_0 A_3 - A_1 A_2 + \sqrt{K_1}) < 0$  and  $b_3 A_1 N(2A_0 A_3 - A_1 A_2 - \sqrt{K_1}) < 0$  or if  $K_1 < 0$  and  $b_3 A_1 N(2A_0 A_3 - A_1 A_2) < 0$ , then the fixed point of the Poincaré map has an unstable manifold of dimension two, and the periodic solution is stable and has a stable manifold of dimension three.
- If  $K_1 > 0$  and  $-\sqrt{K_1} < 2A_0 A_3 - A_1 A_2 < \sqrt{K_1}$ , then the fixed point of the Poincaré map is a saddle point with a stable manifold of degree one and an unstable manifold of degree one, and the associated periodic solution is unstable and has a stable manifold formed by two cylinders and an unstable manifold formed by two cylinders.
- If  $K_1 < 0$  and  $A_1 A_2 = 2A_0 A_3$ , the fixed point of the Poincaré map associated with the periodic orbit is linearly stable, and we cannot decide about the stability of the periodic orbit.

Combining the above information of the eigenvalues of the Jacobian matrix for both  $(R_1, Z_1)$  and  $(R_2, Z_2)$  we get statements (a)–(e) in the theorem.

Now we shall go back through the changes of variables and we obtain two periodic solutions, for  $j = 1, 2$ ,  $(x_j(t, \varepsilon), y_j(t, \varepsilon), z_j(t, \varepsilon))$  bifurcating from  $(1, 1, 1)$  with a period tending to  $2\pi$  when  $\varepsilon \rightarrow 0$ . Moreover,  $(x_j(t, \varepsilon), y_j(t, \varepsilon), z_j(t, \varepsilon)) = (1, 1, 1) + O(\varepsilon)$  for  $j = 1, 2$ . This completes the proof of the theorem.  $\square$

### 6.1.1 Examples of Theorem 6.1.1

We provide examples showing that the conditions provided by Theorem 6.1.1 are non-empty. Only the values of the parameters which are nonzero are given. Systems (6.0.1) with the set of parameters

$$\left\{ \begin{array}{l} a_1 = a_3 = a_5 = b_1 = b_2 = b_3 = -1, \quad a_2 = -1 - \varepsilon, \quad a_4 = 1/2 \\ c_1 = 3/2, \quad c_2 = 7/2, \quad c_3 = 2, \quad c_6 = 4 \end{array} \right\}$$

have two limit cycles whose type of stability is given in statement (a) of Theorem 6.1.1. In this case, as an example, we illustrate the two limit cycles exhibited for systems (6.0.1) with this parameters, i.e.,

$$\begin{aligned} \dot{x} &= x \left( 2 + \frac{1}{2}(x-1)^2 - x - (x-1)(y-1) - z - (1+\varepsilon)(y-1) \right), \\ \dot{y} &= y(3 - x - y - z), \\ \dot{z} &= z \left( \frac{3}{2}(x-1) + \frac{7}{2}(y-1) + 2(z-1) + 4(x-1)(z-1) \right). \end{aligned} \tag{6.1.6}$$

For this differential system the two real zeros of the averaged functions (6.1.5) which provide the two limit cycles bifurcating from the equilibrium point  $(1, 1, 1)$  of system (6.1.6), when this point has been translated to the origin of coordinates, are

$$(R, Z) = (0, 4/3) \quad \text{and} \quad (R, Z) = (\sqrt{65/8}, -2).$$

Going back through the changes of variables of the proof of Theorem 6.1.1, we get that the initial conditions in the coordinates  $(x, y, z)$  at time  $t = 0$  for the two limit cycles are

$$(0, 4\varepsilon/3, -4\varepsilon/3) \quad \text{and} \quad ((-3 - 2\sqrt{10/13})\varepsilon, (-1 - 2\sqrt{10/13})\varepsilon, (4 + 7\sqrt{10/13})\varepsilon).$$

We compute numerically the two limit cycles starting at these initial conditions for the value  $\varepsilon = 5/1000$ , as can be seen in Figure 6.1.1.

The following sets of parameters satisfy, respectively, the four sets of conditions in statement (b) of Theorem 6.1.1, so for all of them systems (6.0.1) have two limit cycles whose type of stability is given in statement (b):

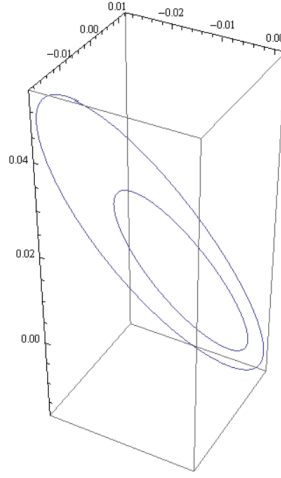


Figure 6.1.1: The two limit cycles which have bifurcated from the zero-Hopf equilibrium point  $(1, 1, 1)$  of system (6.1.6) with  $\varepsilon = 5/1000$ , when this point has been translated to the origin of coordinates.

$$\left\{ \begin{array}{l} a_1 = a_3 = -1, a_2 = -1 + \varepsilon, a_4 = -7/8, a_5 = 1, b_1 = b_2 = b_3 = -1, c_1 = 7/4, \\ c_2 = 37/16, c_3 = 2 + 5\varepsilon, c_6 = 6 \end{array} \right\},$$

$$\left\{ \begin{array}{l} a_1 = a_3 = b_1 = b_2 = b_3 = -1, a_2 = -1 + \varepsilon, a_4 = -1/2, a_5 = 1, c_1 = 3/2, \\ c_2 = 7/2, c_3 = 2 + \varepsilon, c_6 = 5 \end{array} \right\},$$

$$\left\{ \begin{array}{l} a_1 = a_3 = a_5 = b_2 = -1, a_2 = 1 + \varepsilon, a_4 = -7/8, b_1 = 1 + \varepsilon, b_3 = 1, \\ c_1 = 7/4, c_2 = -37/16, c_3 = 2 - 5\varepsilon, c_6 = 5 \end{array} \right\},$$

$$\left\{ \begin{array}{l} a_1 = a_3 = b_2 = -1, a_2 = 1 + \varepsilon, a_4 = 3/4, a_5 = b_1 = b_3 = 1, \\ c_2 = -5, c_3 = 2 - 3\varepsilon \end{array} \right\}.$$

The following sets of parameters satisfy, respectively, the three sets of conditions in statement (c) of Theorem 6.1.1, so for all of them, systems (6.0.1) have two limit cycles whose type of stability is given in statement (c):

$$\left\{ \begin{array}{l} a_1 = a_3 = a_5 = b_1 = b_2 = b_3 = -1, a_2 = -1 + \varepsilon, a_4 = 1/2, c_1 = 3/2, \\ c_2 = 7/2, c_3 = 2 + \varepsilon, c_6 = 4 \end{array} \right\},$$

$$\left\{ \begin{array}{l} a_1 = a_5 = b_3 = -1, a_2 = -3/4 - \varepsilon, a_3 = b_1 = 1, b_2 = 3/4, \\ c_2 = 17/16, c_3 = 1/4 + \varepsilon, c_6 = 2 \end{array} \right\},$$

$$\left\{ \begin{array}{l} a_1 = a_5 = b_2 = b_3 = c_2 = -1, a_2 = -3 - \varepsilon, a_4 = 1/2, \\ b_1 = -1/3, c_1 = c_6 = 2, c_3 = 2 + 2\varepsilon \end{array} \right\}.$$

The following sets of parameters satisfy, respectively, the three sets of conditions in statement (d) of Theorem 6.1.1, so for all of them, systems (6.0.1) have two limit cycles whose type of stability is given in statement (d):

$$\left\{ \begin{array}{l} a_1 = a_3 = a_5 = b_2 = -1, a_2 = 1 + \varepsilon, a_4 = -1/2, b_1 = b_3 = 1, c_1 = 3/2, \\ c_2 = -7/2, c_3 = 2 - \varepsilon, c_6 = 27/8 \end{array} \right\},$$

$$\left\{ \begin{array}{l} a_2 = -1/4 + \varepsilon, a_3 = b_2 = -1/2, a_4 = 3, a_5 = b_3 = -1, c_1 = -1/4, \\ c_2 = 393/1024, c_3 = 1/2 + 29\varepsilon, c_6 = 33 \end{array} \right\},$$

$$\left\{ \begin{array}{l} a_1 = a_3 = a_5 = b_2 = -1, a_2 = 1 + \varepsilon, a_4 = -2, b_1 = b_3 = 1, \\ c_1 = 3/2, c_2 = -7/2, c_3 = 2 - \varepsilon, c_6 = -1 \end{array} \right\}.$$

Finally, systems (6.0.1) with the set of parameters

$$\left\{ \begin{array}{l} a_1 = a_3 = b_1 = b_2 = b_3 = b_9 = -1, a_2 = -1 + \varepsilon, c_1 = 3/2, \\ c_2 = 7/2, c_3 = 2 + \varepsilon, c_6 = 44/3 \end{array} \right\}$$

have two limit cycles whose type of stability is given in statement (e) of Theorem 6.1.1.

## 6.2 Kolmogorov systems under conditions (iii) and (iv)

The main result concerning the Kolmogorov systems (6.0.1) under the conditions (iii) is the following. The expressions of  $B_i$  with  $i = 0, \dots, 4$ , and  $K_2$  are given in Section 6.4.

**Theorem 6.2.1.** *If  $b_3 \neq 0$ ,  $a_1 = a_2 = a_3 = 0$ ,  $c_2 = -(b_2^2 + \beta^2)/b_3$ ,  $c_3 = -b_2$ ,  $B_1 \neq 0$ ,  $B_2 \neq 0$ ,  $B_3 \neq 0$  and  $B_0B_4(B_1B_2 - B_0B_3) > 0$ , then the Kolmogorov systems (6.0.1) have two limit cycles bifurcating from the zero-Hopf equilibrium point  $(1, 1, 1)$ . Moreover the following statements hold.*

- (a) *If  $K_2 > 0$ ,  $B_2B_3(B_0B_3 - B_1B_2) > 0$  and  $|B_1B_2 - 2B_0B_3| < \sqrt{K_2}$ ; then the two limit cycles are unstable and have a stable manifold formed by two cylinders and an unstable manifold formed by two cylinders.*
- (b) *If  $B_2 < 0$ ,  $B_3(B_0B_3 - B_1B_2) > 0$ ,  $K_2 > 0$  and  $|B_1B_2 - 2B_0B_3| < \sqrt{K_2}$ ; or if  $B_2B_3(B_0B_3 - B_1B_2) > 0$ ,  $K_2 > 0$ ,  $B_1 < 0$  and  $B_1B_2 - 2B_0B_3 < -\sqrt{K_2}$ ; then both limit cycles are unstable. One limit cycle is a local repeller, and the other has a stable manifold formed by two cylinders and an unstable manifold formed by two cylinders.*
- (c) *If  $B_2 < 0$ ,  $B_3(B_0B_3 - B_1B_2) > 0$  and*
  - *either  $K_2 > 0$ ,  $B_1(B_1B_2 - 2B_0B_3 - \sqrt{K_2}) < 0$  and  $B_1(B_1B_2 - 2B_0B_3 + \sqrt{K_2}) < 0$ ,*
  - *or  $K_2 \leq 0$  and  $B_1(B_1B_2 - 2B_0B_3) < 0$ ;*

or if  $B_2 > 0$ ,  $B_3(B_0B_3 - B_1B_2) < 0$ ,  $K_2 > 0$ ,  $B_1 < 0$  and  $B_1B_2 - 2B_0B_3 < -\sqrt{K_2}$ ; then one limit cycle is a local attractor and the other limit cycle is a local repeller.

(d) If  $B_2 > 0$ ,  $B_3(B_0B_3 - B_1B_2) < 0$ ,  $K_2 > 0$  and  $|B_1B_2 - 2B_0B_3| < \sqrt{K_2}$ ; or if  $B_2B_3(B_0B_3 - B_1B_2) > 0$  and

- either  $K_2 > 0$ ,  $B_1(B_1B_2 - 2B_0B_3 - \sqrt{K_2}) < 0$  and  $B_1(B_1B_2 - 2B_0B_3 + \sqrt{K_2}) < 0$ ,
- or  $K_2 \leq 0$  and  $B_1(B_1B_2 - 2B_0B_3) < 0$ ,

then one limit cycle is a local attractor and the other limit cycle is unstable and has a stable manifold formed by two cylinders and an unstable manifold formed by two cylinders.

(e)  $B_2B_0 < 0$ ,  $K_2 < 0$  and  $B_1B_2 = 2B_0B_3$ ; then one limit cycle is unstable and has a stable manifold formed by two cylinders and an unstable manifold formed by two cylinders, and we cannot decide about the stability of the other limit cycle.

*Proof of Theorem 6.2.1.* We consider systems (6.0.1) under conditions (iii) of Proposition 6.0.1. In order to study the zero-Hopf bifurcation we perturb the parameters  $a_1$ ,  $a_2$ ,  $a_3$ ,  $c_2$  and  $c_3$  which define the zero-Hopf equilibrium under conditions (iii) as follows

$$a_1 = \varepsilon a_{11}, \quad a_2 = \varepsilon a_{21}, \quad a_3 = \varepsilon a_{31}, \quad c_2 = -\frac{b_2^2 + \beta^2}{b_3} + \varepsilon c_{21}, \quad c_3 = -b_2 + \varepsilon c_{31},$$

where  $\varepsilon$  is a parameter to be taken sufficiently small.

We write the lineal part of systems (6.0.2) at the origin in its real Jordan normal form, and the associated systems become systems  $(\dot{X}, \dot{Y}, \dot{Z})$  of file ss[[3]], downloadable at [41]. Then we write the systems in cylindrical coordinates obtaining systems  $(\dot{r}, \dot{\theta}, \dot{Z})$  in file ss[[3]], and we do the scaling  $(r, Z) \rightarrow (\varepsilon R, \varepsilon Z)$  obtaining systems  $(\dot{R}, \dot{Z})$  in file ss[[3]].

As in the proof of Theorem 6.1.1, in order to apply Theorem 1.8.3, we take the variable  $\theta$  as the new independent variable obtaining a system of the form

$$R' = \varepsilon F_{11} + O(\varepsilon^2), \quad Z' = \varepsilon F_{12} + O(\varepsilon^2),$$

whose coefficients  $F_{11}$  and  $F_{12}$  are given in the file ss[[3]]. The averaged function of first order  $f_1 = (f_{11}(R, Z), f_{12}(R, Z))$  is

$$f_{11} = \frac{\pi R(B_0 + B_1 Z)}{b_3^2 \beta^5}, \quad f_{12} = \frac{\pi(B_2 Z + B_3 Z^2 + B_4 R^2)}{b_3^2 \beta^5},$$

with  $B_i$ , for  $i = 0, \dots, 4$ , and  $K_2$  given in Section 6.4. Solving the equation

$$(f_{11}(R, Z), f_{12}(R, Z)) = (0, 0)$$

we obtain two solutions

$$(R_1, Z_1) = (0, -B_2/B_3) \text{ and } (R_2, Z_2) = \left( \pm \sqrt{B_0(B_1B_2 - B_0B_3)}/(B_1\sqrt{B_4}), -B_0/B_1 \right).$$

Again we consider always the positive expression of  $R_2$ . We compute the Jacobian matrix of  $f_1$  and we get

$$\begin{pmatrix} \frac{\pi(B_0 + B_1 Z)}{b_3^2 \beta^5} & \frac{\pi R B_1}{b_3^2 \beta^5} \\ \frac{2\pi R B_4}{b_3^2 \beta^5} & \frac{\pi(B_2 + 2B_3 Z)}{b_3^2 \beta^5} \end{pmatrix},$$

whose determinant is  $\pi^2(-2B_1 B_4 R^2 + (B_0 + B_1 Z)(B_2 + 2B_3 Z))/(b_3^4 \beta^{10})$ . The determinant at the solution  $(R_1, Z_1)$  is

$$\pi^2 B_2 (B_1 B_2 - B_0 B_3) / (b_3^4 B_3 \beta^{10}),$$

and at the solution  $(R_2, Z_2)$  is

$$2\pi^2 B_0 (B_0 B_3 - B_1 B_2) / (b_3^4 B_1 \beta^{10}).$$

From the hypothesis considered these determinants are nonzero, so it follows from Theorem 1.8.3 that for  $\varepsilon$  sufficiently small, systems (6.1.4) have two solutions  $(R_1(\theta, \varepsilon), Z_1(\theta, \varepsilon))$  and  $(R_2(\theta, \varepsilon), Z_2(\theta, \varepsilon))$  such that  $(R_j(\theta, \varepsilon), Z_j(\theta, \varepsilon)) \rightarrow (R_j, Z_j)$  for  $j = 1, 2$  when  $\varepsilon \rightarrow 0$ .

The Jacobian matrix evaluated at the solution  $(R_1, Z_1)$  has eigenvalues equal to

$$-\pi B_2 / (b_3^2 \beta^5) \quad \text{and} \quad \pi(B_0 B_3 - B_1 B_2) / (b_3^2 B_3 \beta^5).$$

We study the stability of the associated periodic orbit which is provided by these eigenvalues.

- If  $B_2 < 0$  and  $B_3(B_0 B_3 - B_1 B_2) > 0$ , the associated periodic solution is unstable and has an unstable manifold of dimension three.
- If  $B_2 > 0$  and  $B_3(B_0 B_3 - B_1 B_2) < 0$ , then the associated periodic solution is stable and has a stable manifold of dimension three.
- Finally, if  $B_2 B_3(B_0 B_3 - B_1 B_2) > 0$ , the periodic solution is unstable and has a stable manifold formed by two cylinders and an unstable manifold formed by two cylinders.

On the other hand, the Jacobian matrix evaluated at  $(R_2, Z_2)$  has eigenvalues equal to  $\pi(B_1 B_2 - 2B_0 B_3 \pm \sqrt{K_2}) / (2b_3^2 B_1 \beta^5)$ , and so

- If  $K_2 > 0$ ,  $B_1(B_1 B_2 - 2B_0 B_3 + \sqrt{K_2}) > 0$  and  $B_1(B_1 B_2 - 2B_0 B_3 - \sqrt{K_2}) > 0$ , or if  $K_2 < 0$  and  $B_1(B_1 B_2 - 2B_0 B_3) > 0$ , then the associated periodic solution is unstable and has an unstable manifold of dimension three.
- If  $K_2 > 0$ ,  $B_1(B_1 B_2 - 2B_0 B_3 + \sqrt{K_2}) < 0$  and  $B_1(B_1 B_2 - 2B_0 B_3 - \sqrt{K_2}) < 0$ , or if  $K_2 < 0$  and  $B_1(B_1 B_2 - 2B_0 B_3) < 0$ , then the associated periodic solution is stable and has a stable manifold of dimension three.
- If  $K_2 > 0$  and  $-\sqrt{K_2} < B_1 B_2 - 2B_0 B_3 < \sqrt{K_2}$ , then the associated periodic solution is unstable and has a stable manifold formed by two cylinders and an unstable manifold formed by two cylinders.



- If  $K_2 < 0$  and  $B_1B_2 - 2B_0B_3 = 0$ , the fixed point of the Poincaré map associated with the periodic orbit is linearly stable, and we cannot decide about the stability of the periodic orbit.

Combining the above information of the eigenvalues of the Jacobian matrix for both  $(R_1, Z_1)$  and  $(R_2, Z_2)$  we get statements (a)–(e) of the theorem.

Now we shall go back through the changes of variables and we obtain two periodic solutions, for  $j = 1, 2$ ,  $(x_j(t, \varepsilon), y_j(t, \varepsilon), z_j(t, \varepsilon))$  bifurcating from  $(1, 1, 1)$  with a period tending to  $2\pi$  when  $\varepsilon \rightarrow 0$ . Moreover,  $(x_j(t, \varepsilon), y_j(t, \varepsilon), z_j(t, \varepsilon)) = (1, 1, 1) + O(\varepsilon)$  for  $j = 1, 2$ . This completes the proof of the theorem.  $\square$

### 6.2.1 Examples of Theorem 6.2.1

We give examples showing that the conditions provided by Theorem 6.2.1 are non-empty. We give only the values of the parameters which are nonzero. Systems (6.0.1) with the set of parameters

$$\{a_1 = -2\varepsilon, a_2 = \varepsilon, a_4 = c_2 = 2, a_7 = b_1 = b_2 = b_3 = -1, c_3 = 1\}$$

have two limit cycles whose type of stability is given in statement (a) of Theorem 6.2.1.

The parameters

$$\{a_1 = -2\varepsilon, a_2 = \varepsilon, a_4 = -7/2, a_5 = 4, a_7 = b_1 = b_2 = -1, b_3 = c_3 = 1, c_2 = -2\}$$

satisfy the first set of conditions in statement (b) of Theorem 6.2.1, and the parameters

$$\{a_1 = -2\varepsilon, a_2 = \varepsilon, a_4 = -3, a_7 = b_3 = c_3 = 1, b_1 = b_2 = -1, c_2 = -2\}$$

satisfy the second set of conditions. For both of them there exist two limit cycles for systems (6.0.1) whose type of stability is given in statement (b).

The following sets of conditions satisfy, respectively, the three sets of conditions in statement (c) of Theorem 6.2.1, so for all of them, systems (6.0.1) have two limit cycles whose type of stability is given in statement (c):

$$\begin{aligned} &\{a_2 = -\varepsilon, a_4 = 4, a_5 = -2, a_7 = b_1 = b_2 = b_3 = -1, c_2 = 2, c_3 = 1\}, \\ &\{a_1 = 4\varepsilon, a_3 = -\varepsilon, a_4 = -2, a_6 = -1, a_7 = 1, b_1 = b_3 = -1, c_2 = 1\}, \\ &\{a_2 = -\varepsilon, a_4 = -2, a_7 = 1, b_1 = b_2 = b_3 = -1, c_2 = 2, c_3 = 1\}. \end{aligned}$$

The following sets of conditions satisfy, respectively, the three sets of conditions in statement (d) of Theorem 6.2.1, so for all of them, systems (6.0.1) have two limit cycles whose type of stability is given in statement (d):

$$\begin{aligned} &\{a_1 = 2\varepsilon, a_2 = -\varepsilon, a_4 = 1/2, a_7 = b_1 = b_2 = b_3 = -1, c_2 = 2, c_3 = 1\}, \\ &\{a_2 = \varepsilon, a_4 = -1/16, a_5 = -1/2, a_7 = b_3 = c_3 = 1, b_1 = b_2 = -1, c_2 = -2\}, \\ &\{a_1 = -2\varepsilon, a_3 = -\varepsilon, a_6 = a_7 = b_3 = 1, b_1 = c_2 = -1\}. \end{aligned}$$

Finally, systems (6.0.1) with parameters

$$\{a_3 = -\varepsilon, a_4 = a_7 = b_1 = b_3 = c_9 = -1, c_2 = 1\}$$

have two limit cycles whose type of stability is given in statement (e) of Theorem 6.2.1.

This section is entitled Kolmogorov systems under conditions (iii) and (iv), and for the moment we have only considered conditions (iii). This is enough as Kolmogorov systems (6.0.1) under conditions (iv) are the same as under conditions (iii) but interchanging the variables  $x$  and  $y$ , so if we change the conditions  $b_3 \neq 0, a_1 = a_2 = a_3 = 0, c_2 = -(b_2^2 + \beta^2)/b_3, c_3 = -b_2$  into  $a_3 \neq 0, b_1 = b_2 = b_3 = 0, c_1 = -(a_1^2 + \beta^2)/a_3, c_3 = -a_1$ , and redefine the constants  $B_i$  for  $i = 0, \dots, 4$  as it is indicated in Section 6.4, the same Theorem 6.2.1 holds.

### 6.3 Kolmogorov systems under conditions (v)

At last our main result concerning the Kolmogorov systems (6.0.1) under the conditions (v) is the following, with the expressions of  $D_i$ , for  $i = 0, \dots, 4$ , and  $K_4$  given in Section 6.4.

**Theorem 6.3.1.** *If  $b_1 \neq 0, a_3 = b_3 = c_3 = 0, a_2 = -(a_1^2 + \beta^2)/b_1, b_2 = -a_1, D_1 \neq 0, D_2 \neq 0, D_3 \neq 0$  and  $D_0 D_4 (D_1 D_2 - D_0 D B_3) > 0$ , then the Kolmogorov systems (6.0.1) have two limit cycles bifurcating from the zero-Hopf equilibrium point  $(1, 1, 1)$ . Moreover the following statements hold.*

- (a) *If  $K_4 > 0, D_2 D_3 (a_1 c_1 + b_1 c_2) (D_0 D_3 - D_1 D_2) > 0$  and  $|D_1 D_2 - 2D_0 D_3| < \sqrt{K_4}$ ; then the two limit cycles are unstable and have a stable manifold formed by two cylinders and an unstable manifold formed by two cylinders.*
- (b) *If  $b_1 D_2 (a_1 c_1 + b_1 c_2) < 0, b_1 D_3 (D_0 D_3 - D_1 D_2) > 0$  and*
  - *either  $K_4 > 0, b_1 D_1 (a_1 c_1 + b_1 c_2) (D_1 D_2 - 2D_0 D_2 - \sqrt{K_4}) < 0$  and  $b_1 D_1 (a_1 c_1 + b_1 c_2) (D_1 D_2 - 2D_0 D_2 + \sqrt{K_4}) < 0$ ,*
  - *or  $K_4 \leq 0$  and  $b_1 D_1 (a_1 c_1 + b_1 c_2) (D_1 D_2 - 2D_0 D_3) < 0$ ;*

*or if  $b_1 D_2 (a_1 c_1 + b_1 c_2) > 0, b_1 D_3 (D_0 D_3 - D_1 D_2) < 0$  and*

- *either  $K_4 > 0, b_1 D_1 (a_1 c_1 + b_1 c_2) (D_1 D_2 - 2D_0 D_2 - \sqrt{K_4}) > 0$  and  $b_1 D_1 (a_1 c_1 + b_1 c_2) (D_1 D_2 - 2D_0 D_2 + \sqrt{K_4}) > 0$ ,*
- *or  $K_4 \leq 0$  and  $b_1 D_1 (a_1 c_1 + b_1 c_2) (D_1 D_2 - 2D_0 D_3) > 0$ ;*

*then one limit cycle is a local repeller, and the other is a local attractor.*

- (c) *If  $b_1 D_2 (a_1 c_1 + b_1 c_2) < 0, b_1 D_3 (D_0 D_3 - D_1 D_2) > 0, K_4 > 0$  and  $|D_1 D_2 - 2D_0 D_3| < \sqrt{K_4}$ ; or if  $D_2 D_3 (a_1 c_1 + b_1 c_2) (D_0 D_3 - D_1 D_2) > 0$  and*

- *either  $K_4 > 0, b_1 D_1 (a_1 c_1 + b_1 c_2) (D_1 D_2 - 2D_0 D_2 - \sqrt{K_4}) > 0$  and  $b_1 D_1 (a_1 c_1 + b_1 c_2) (D_1 D_2 - 2D_0 D_2 + \sqrt{K_4}) > 0$ ,*

- or  $K_4 \leq 0$  and  $b_1 D_1(a_1 c_1 + b_1 c_2)(D_1 D_2 - 2D_0 D_3) > 0$ ;

then both limit cycles are unstable. One limit cycle is a local repeller, and the other has a stable manifold formed by two cylinders and an unstable manifold formed by two cylinders.

- (d) If  $b_1 D_2(a_1 c_1 + b_1 c_2) > 0$ ,  $b_1 D_3(D_0 D_3 - D_1 D_2) < 0$ ,  $K_4 > 0$  and  $|D_1 D_2 - 2D_0 D_3| < \sqrt{K_4}$ ; or if  $D_2 D_3(a_1 c_1 + b_1 c_2)(D_0 D_3 - D_1 D_2) > 0$  and

- either  $K_4 > 0$ ,  $b_1 D_1(a_1 c_1 + b_1 c_2)(D_1 D_2 - 2D_0 D_2 - \sqrt{K_4}) < 0$  and  $b_1 D_1(a_1 c_1 + b_1 c_2)(D_1 D_2 - 2D_0 D_2 + \sqrt{K_4}) < 0$ ,
- or  $K_4 \leq 0$  and  $b_1 D_1(a_1 c_1 + b_1 c_2)(D_1 D_2 - 2D_0 D_3) < 0$ ;

then one limit cycle is a local attractor, and the other is unstable and has a stable manifold formed by two cylinders and an unstable manifold formed by two cylinders.

- (e) If  $D_2 D_3(a_1 c_1 + b_1 c_2)(D_0 D_2 - D_1 D_2) > 0$ ,  $K_4 < 0$  and  $D_1 D_2 = 2D_0 D_3$ ; then one limit cycle is unstable and has a stable manifold formed by two cylinders and an unstable manifold formed by two cylinders and we cannot decide about the stability of the other.

*Proof of Theorem 6.3.1.* We consider systems (6.0.1) under conditions (v) of Proposition 6.0.1. In order to study the zero-Hopf bifurcation we perturb the parameters  $a_2$ ,  $a_3$ ,  $b_2$ ,  $b_3$  and  $c_3$  which define the zero-Hopf equilibrium point into the form

$$a_2 = -\frac{a_1^2 + \beta^2}{b_1} + \varepsilon a_{21}, \quad a_3 = \varepsilon a_{31}, \quad b_2 = -a_1 + \varepsilon b_{21}, \quad b_3 = \varepsilon b_{31}, \quad c_3 = \varepsilon c_{31},$$

where  $\varepsilon$  is a sufficiently small parameter.

We write the systems with the linear part at the origin in its real Jordan normal form, then we write it in cylindrical coordinates, and finally we do the scaling  $(r, Z) \rightarrow (\varepsilon R, \varepsilon Z)$ . Thus we obtain respectively systems  $(\dot{X}, \dot{Y}, \dot{Z})$ ,  $(\dot{r}, \dot{\theta}, \dot{Z})$  and  $(\dot{R}, \dot{Z})$  of file ss[[5]], downloadable at [41]. Taking  $\theta$  as the new independent variable we obtain systems in the form

$$R' = \varepsilon F_{11} + O(\varepsilon^2), \quad Z' = \varepsilon F_{12} + O(\varepsilon^2) \quad (6.3.7)$$

with coefficients  $F_{11}$  and  $F_{12}$  given in the file ss[[5]]. As in the previous proofs we are in conditions to apply Theorem 1.8.3. The averaged function of first order  $f_1 = (f_{11}(R, Z), f_{12}(R, Z))$  is

$$f_{11} = \frac{\pi R(D_0 + D_1 Z)}{b_1 \beta^5}, \quad f_{12} = \frac{\pi(D_2 Z + D_3 Z^2 + D_4 R^2)}{b_1(a_1 c_1 + b_1 c_2)\beta^5},$$

with  $D_i$ , for  $i = 0, \dots, 4$ , and  $K_4$  given in Section 6.4. We look for the solutions of

$$(f_{11}(R, Z), f_{12}(R, Z)) = (0, 0),$$

and we obtain

$$(R_1, Z_1) = (0, -D_2/D_3) \text{ and } (R_2, Z_2) = \left( \pm \sqrt{D_0(D_1 D_2 - D_0 D_3)} / (D_1 \sqrt{D_4}), -D_0/D_1 \right),$$

considering the positive expression of  $R_2$ .

We compute the Jacobian matrix of  $f_1$  and we get

$$\begin{pmatrix} \frac{\pi(D_0 + D_1 Z)}{b_1 \beta^5} & \frac{\pi R D_1}{b_1 \beta^5} \\ \frac{2\pi R D_4}{b_1 \beta^5 (a_1 c_1 + b_1 c_2)} & \frac{\pi(D_2 + 2D_3 Z)}{b_1 \beta^5 (a_1 c_1 + b_1 c_2)} \end{pmatrix},$$

whose determinant is  $\pi^2(-2D_1 D_4 R^2 + (D_0 + D_1 Z)(D_2 + 2D_3 Z))/(b_1^2 \beta^{10}(a_1 c_1 + b_1 c_2))$ . The determinant at the solution  $(R_1, Z_1)$  is

$$\pi^2 D_2 (D_1 D_2 - D_0 D_3) / (b_1^2 D_3 \beta^{10} (a_1 c_1 + b_1 c_2)),$$

and at the solution  $(R_2, Z_2)$  is

$$2\pi^2 D_0 (D_0 D_3 - D_1 D_2) / (b_1^2 D_1 \beta^{10} (a_1 c_1 + b_1 c_2)),$$

and both are nonzero by the hypotheses. By Theorem 1.8.3, for  $\varepsilon$  sufficiently small systems (6.3.7) have two solutions  $(R_1(\theta, \varepsilon), Z_1(\theta, \varepsilon))$  and  $(R_2(\theta, \varepsilon), Z_2(\theta, \varepsilon))$  such that, when  $\varepsilon \rightarrow 0$ ,  $(R_j(\theta, \varepsilon), Z_j(\theta, \varepsilon)) \rightarrow (R_j, Z_j)$  for  $j = 1, 2$ .

The Jacobian matrix evaluated at the solution  $(R_1, Z_1)$  has eigenvalues equal to

$$-\pi D_2 / (b_1 \beta^5 (a_1 c_1 + b_1 c_2)) \text{ and } \pi(D_0 D_3 - D_1 D_2) / (b_1 D_3 \beta^5).$$

We study the stability of the associated periodic orbit which is provided by these eigenvalues.

- If  $b_1 D_2 (a_1 c_1 + b_1 c_2) < 0$  and  $b_1 D_3 (D_0 D_3 - D_1 D_2) > 0$ , the associated periodic solution is unstable and has an unstable manifold of dimension three.
- If  $b_1 D_2 (a_1 c_1 + b_1 c_2) > 0$  and  $b_1 D_3 (D_0 D_3 - D_1 D_2) < 0$ , then the associated periodic solution is stable and has a stable manifold of dimension three.
- Finally, if  $D_2 D_3 (a_1 c_1 + b_1 c_2) (D_0 D_3 - D_1 D_2) > 0$ , the associated periodic solution is unstable and has a stable manifold formed by two cylinders and an unstable manifold formed by two cylinders.

On the other hand, the Jacobian matrix evaluated at  $(R_2, Z_2)$  has eigenvalues equal to

$$\pi(D_1 D_2 - 2D_0 D_3 \pm \sqrt{K_4}) / (2b_1 D_1 \beta^5 (a_1 c_1 + b_1 c_2)).$$

Then:

- If  $K_4 > 0$ ,  $b_1 D_1 (a_1 c_1 + b_1 c_2) (D_1 D_2 - 2D_0 D_3 + \sqrt{K_4}) > 0$  and  $b_1 D_1 (a_1 c_1 + b_1 c_2) (D_1 D_2 - 2D_0 D_3 - \sqrt{K_4}) > 0$ , or if  $K_4 < 0$  and  $b_1 D_1 (a_1 c_1 + b_1 c_2) (D_1 D_2 - 2D_0 D_3) > 0$ , then the associated periodic solution is unstable and has an unstable manifold of dimension three.
- If  $K_4 > 0$ ,  $b_1 D_1 (a_1 c_1 + b_1 c_2) (D_1 D_2 - 2D_0 D_3 + \sqrt{K_4}) < 0$  and  $b_1 D_1 (a_1 c_1 + b_1 c_2) (D_1 D_2 - 2D_0 D_3 - \sqrt{K_4}) < 0$ , or if  $K_4 < 0$  and  $b_1 D_1 (a_1 c_1 + b_1 c_2) (D_1 D_2 - 2D_0 D_3) < 0$ , then the associated periodic solution is stable and has a stable manifold of dimension three.

- If  $K_4 > 0$  and  $-\sqrt{K_4} < D_1 D_2 - 2D_0 D_3 < \sqrt{K_4}$ , then the associated periodic solution is unstable and has a stable manifold formed by two cylinders and an unstable manifold formed by two cylinders.
- If  $K_4 < 0$  and  $D_1 D_2 = 2D_0 D_3$ , the fixed point of the Poincaré map associated with the periodic orbit is linearly stable, and we cannot decide about the stability of the periodic orbit.

Combining the above information we get statements (a)–(e) in the theorem. Going back through the changes of variables we obtain two periodic solutions  $(x_j(t, \varepsilon), y_j(t, \varepsilon), z_j(t, \varepsilon))$  for  $j = 1, 2$  bifurcating from  $(1, 1, 1)$  with a period tending to  $2\pi$  when  $\varepsilon \rightarrow 0$ . Moreover,  $(x_j(t, \varepsilon), y_j(t, \varepsilon), z_j(t, \varepsilon)) = (1, 1, 1) + O(\varepsilon)$  for  $j = 1, 2$ . This completes the proof of the theorem.  $\square$

### 6.3.1 Examples of Theorem 6.3.1

We give examples showing that the conditions provided by Theorem 6.3.1 are non-empty. We give only the values of the parameters which are nonzero. Systems (6.0.1) with parameters

$$\{a_1 = a_9 = b_1 = c_1 = -1, a_2 = a_4 = 2, a_3 = \varepsilon, b_2 = 1 + 2\varepsilon\}$$

have two limit cycles whose type of stability is given in statement (a) of Theorem 6.3.1. The following sets of parameters satisfy, respectively, the four sets of conditions in statement (b) of Theorem 6.3.1, so for all of them systems (6.0.1) have two limit cycles whose type of stability is given in statement (b):

$$\begin{aligned} &\{a_1 = b_1 = c_1 = -1, a_2 = 2, a_3 = -\varepsilon, a_4 = -2, a_6 = 3, a_9 = 1, b_2 = 1 - (7/8)\varepsilon\}, \\ &\{a_1 = b_1 = -1, a_2 = 2, a_3 = \varepsilon, a_4 = -2, a_6 = -5, a_9 = 1, b_2 = c_1 = 1\}, \\ &\{a_1 = -1, a_2 = -2, a_3 = -\varepsilon, a_4 = 2, a_6 = 3, a_9 = -1, b_1 = b_2 = c_1 = 1\}, \\ &\{a_1 = a_9 = -1, a_2 = -2, a_3 = -\varepsilon, a_4 = 2, a_6 = 5, a_9 = -1, b_1 = b_2 = c_1 = 1\}. \end{aligned}$$

The following sets of parameters satisfy, respectively, the three sets of conditions in statement (c) of Theorem 6.3.1, so for all of them systems (6.0.1) have two limit cycles whose type of stability is given in statement (c):

$$\begin{aligned} &\{a_1 = a_9 = b_1 = -1, a_2 = 2, a_3 = \varepsilon, a_4 = 3, a_6 = -1, a_9 = -1, b_2 = c_1 = 1, c_9 = 2\}, \\ &\{a_1 = a_9 = -1, a_2 = -2, a_3 = -\varepsilon, a_6 = -1, a_9 = b_1 = c_1 = 1, b_2 = 1 + (7/8)\varepsilon\}, \\ &\left\{ \begin{aligned} &a_1 = a_9 = c_1 = -1, a_2 = -2, a_3 = -\varepsilon, a_4 = 1, a_6 = -1, a_9 = b_1 = 1, b_2 = 1 - 4\varepsilon, \\ &c_9 = -1/2 \end{aligned} \right\}. \end{aligned}$$

The following sets of parameters satisfy, respectively, the three sets of conditions in statement (d) of Theorem 6.3.1, so for all of them systems (6.0.1) have two limit cycles whose type of stability is given in statement (d):

$$\begin{aligned} &\{a_1 = -1, a_2 = -2, a_3 = -\varepsilon, a_4 = -3, a_6 = b_1 = b_2 = c_1 = 1, c_9 = -2\}, \\ &\{a_1 = b_1 = c_1 = -1, a_2 = 2, a_3 = \varepsilon, a_4 = -3, a_6 = b_1 = 1, b_2 = 1 + 2\varepsilon, c_9 = 2\}, \\ &\{a_1 = b_1 = c_1 = -1, a_2 = 2, a_3 = \varepsilon, a_4 = -1, a_6 = b_1 = 1, b_2 = 1 + 4\varepsilon, c_9 = 1/2\}. \end{aligned}$$

Finally, systems (6.0.1) with parameters

$$\{a_1 = a_6 = b_1 = -1, a_2 = 2, a_3 = (7/8)\varepsilon, b_1 = 1, b_2 = c_1 = 1, c_9 = 1/2\}$$

have two limit cycles whose type of stability is given in statement (e) of Theorem 6.3.1.

## 6.4 Notation

The expressions of  $A_i$  with  $i = 1, 2, 3, 4$ ,  $K_1$  and  $N$  used in Section 6.1 are the following.

$$A_0 = a_3\beta^2 \left( (a_3^2b_{11} - b_3^2a_{21})(a_1(a_1 + b_2) + a_3c_1) + a_3\beta^2(a_3b_{11} + b_3c_{31}) \right),$$

$$\begin{aligned} A_1 = & a_1^6(-2a_9b_3 + 2a_3b_9) + 2a_1^5(b_3(a_8b_3 - 4a_9b_2) - a_3^2b_6 + a_3(a_6b_3 - b_3b_8 + 4b_2b_9)) \\ & + a_3^2(2(-b_3(a_9b_2^2 + b_3(a_7b_3 - a_8b_2)) + a_3^3b_4 - a_3^2(a_4b_3 - b_3b_5 + b_2b_6) \\ & + a_3b_3(a_6b_2 - a_5b_3 + b_3b_7 - b_2b_8) + a_3b_2^2b_9)c_1^2 + c_1(4a_3^2b_4 - 2a_3b_2b_6 + a_3b_3 \\ & (3b_5 - 2a_4 + c_6) + b_3(a_6b_2 + b_2^2 + b_3(2b_7 - a_5 + c_8) + b_2(b_3 - b_8 - 2c_9)))\beta^2 \\ & + (2a_3b_4 + b_3(b_5 + c_6))\beta^4) + a_1a_3(-2a_3^3c_1(b_6c_1 - 2b_2b_4) + a_3^2(2c_1(-2b_2 \\ & (a_4b_3 - b_3b_5 + b_2b_6) + (a_6b_3 - b_3b_8 + 2b_2b_9)c_1) + (4b_2b_4 + (b_3 - 4b_6)c_1)\beta^2) \\ & + a_3(2c_1(2b_2b_3(a_6b_2 - a_5b_3 + b_3b_7 - b_2b_8) + 2b_2^3b_9 + b_3(a_8b_3 - 2a_9b_2)c_1) \\ & + (-2a_4b_2b_3 - 2b_2^2b_6 + 4b_2b_9c_1 + b_2b_3(3b_5 + 2c_1 + c_6) + b_3c_1(3a_6 - 3b_8 - 2c_9)) \\ & \beta^2 + (b_3 - 2b_6)\beta^4) + b_3(4b_2b_3(a_8b_2 - a_7b_3)c_1 + (a_6b_2^2 + b_2^3 + 2a_8b_3c_1 + b_2b_3 \\ & (2b_7 - a_5 + c_8) + b_2^2(b_3 - b_8 - 2c_9))\beta^2 + (a_6 + b_2 - b_8 - 2c_9)\beta^4 - 4a_9b_2c_1(b_2^2 \\ & + \beta^2))) + a_1^4(2a_3^3b_4 + 2a_3(3a_6b_2b_3 - a_5b_3^2 + b_3^2b_7 - 3b_2b_3b_8 + 6b_2^2b_9 - 2a_9b_3c_1) \\ & + a_3^2(2b_3b_5 - 2a_4b_3 - 6b_2b_6 + 4b_9c_1) + a_3(b_3 + 4b_9)\beta^2 - 2b_3(b_3(a_7b_3 - 3a_8b_2) \\ & + 2a_9(3b_2^2 + \beta^2))) + a_1^2(4a_3^4b_4c_1 + 2a_3^3(b_2^2b_4 - 4b_2b_6c_1 + c_1(2b_3b_5 - 2a_4b_3 + b_9c_1) \\ & + 2b_4\beta^2) + a_3(2b_2^2b_3(a_6b_2 - a_5b_3 + b_3b_7 - b_2b_8) + 2b_2^4b_9 - 4b_3(3a_9b_2^2 + b_3(a_7b_3 \\ & - 2a_8b_2))c_1 + (4a_6b_2b_3 + b_2^2(3b_3 + 4b_9) + b_3(-4a_9c_1 + b_3(2b_7 - a_5 + c_8)) \\ & + b_2b_3(b_3 - 4(b_8 + c_9)))\beta^2 + (b_3 + 2b_9)\beta^4) + a_3^2(-2b_2^3b_6 + 8b_2b_3(a_6 - b_8)c_1 \\ & - 2b_3c_1(2a_5b_3 - 2b_3b_7 + a_9c_1) + 2b_2^2(b_3b_5 + 6b_9c_1) + (b_2(b_3 - 6b_6) + 4b_9c_1 \\ & + b_3(3b_5 + c_1 + c_6))\beta^2 - 2a_4b_3(b_2^2 + \beta^2) - 2b_3(a_9(b_2^2 + \beta^2)^2 - b_2b_3(-a_7b_2b_3 \\ & + a_8(b_2^2 + \beta^2)))) + a_1^3(2a_3(b_2b_3(3a_6b_2 - 2a_5b_3 + 2b_3b_7 - 3b_2b_8) + 4b_2^3b_9 + 2b_3c_1 \\ & (a_8b_3 - 3a_9b_2)) + 4a_3^3(b_2b_4 - b_6c_1) + a_3(3a_6b_3 + 3b_2b_3 - 3b_3b_8 + 8b_2b_9 - 2b_3c_9) \\ & \beta^2 + a_3^2(-4a_4b_2b_3 - 6b_2^2b_6 + 4b_3(a_6 - b_8)c_1 + 4b_2(b_3b_5 + 3b_9c_1) + (b_3 - 4b_6)\beta^2) \\ & + 2b_3(-4a_9b_2(b_2^2 + \beta^2) + b_3(-2a_7b_2b_3 + a_8(3b_2^2 + \beta^2))))), \end{aligned}$$

$$\begin{aligned} A_2 = & -2a_3\beta^2 \left( (a_3^2b_{11} - b_3^2a_{21})(a_1(a_1 + b_2) + a_3c_1) + a_3^2b_{11}\beta^2 \right) \left( (a_1(a_1 + b_2) + a_3c_1)^2 \right. \\ & \left. + (2a_1^2 + 2a_1b_2 + b_2^2 + 2a_3c_1)\beta^2 + \beta^4 \right), \end{aligned}$$

$$\begin{aligned}
A_3 = & -2 \left( (a_1(a_1 + b_2) + a_3c_1)^2 + (2a_1^2 + 2a_1b_2 + b_2^2 + 2a_3c_1) \beta^2 + \beta^4 \right) (a_1^6 (a_3b_9 \\
& - a_9b_3) + a_1^5 (b_3 (a_8b_3 - 4a_9b_2) - a_3^2b_6 + a_3 (a_6b_3 - b_3b_8 + 4b_2b_9)) \\
& + a_3^2 ((-b_3 (a_9b_2^2 + b_3(a_7b_3 - a_8b_2)) + a_3^3b_4 - a_3^2 (a_4b_3 - b_3b_5 + b_2b_6) + a_3b_3 \\
& (a_6b_2 - a_5b_3 + b_3b_7 - b_2b_8) + a_3b_2^2b_9) c_1^2 + (b_3 (a_6b_2 - a_5b_3) + 2a_3^2b_4 \\
& + a_3 (b_3b_5 - 2a_4b_3 - b_2b_6)) c_1 \beta^2 + (a_3b_4 - a_4b_3) \beta^4) + a_1a_3 (a_3^3c_1 (2b_2b_4 - b_6c_1) \\
& + a_3^2 (c_1 (-2b_2 (a_4b_3 - b_3b_5 + b_2b_6) + (a_6b_3 - b_3b_8 + 2b_2b_9) c_1) + 2\beta^2 (b_2b_4 \\
& - b_6c_1)) + a_3 (c_1 (2b_2b_3 (a_6b_2 - a_5b_3 + b_3b_7 - b_2b_8) + 2b_2^2b_9 + b_3c_1 (a_8b_3 \\
& - 2a_9b_2)) + (b_2b_3b_5 - 2a_4b_2b_3 - b_2^2b_6 + 2a_6b_3c_1 - b_3b_8c_1 + 2b_2b_9c_1) \beta^2 - b_6\beta^4) \\
& + b_3 (2b_2b_3c_1 (a_8b_2 - a_7b_3) + (a_6b_2^2 - a_5b_2b_3 + a_8b_3c_1) \beta^2 + a_6\beta^4 - 2a_9b_2c_1 (b_2^2 \\
& + \beta^2))) + a_1^4 (a_3^3b_4 + a_3^2 (b_3b_5 - a_4b_3 - 3b_2b_6 + 2b_9c_1) + a_3 (3a_6b_2b_3 - a_5b_3^2 \\
& + b_3^2b_7 - 3b_2b_3b_8 + 6b_2^2b_9 - 2a_9b_3c_1 + 2b_9\beta^2) - b_3 (b_3 (a_7b_3 - 3a_8b_2) + 2a_9 (3b_2^2 \\
& + \beta^2))) + a_1^3 (2a_3^3 (b_2b_4 - b_6c_1) + a_3^2 (2b_2b_3(b_5 - a_4) - 3b_2^2b_6 + 2a_6b_3c_1 \\
& - 2b_3b_8c_1 + 6b_2b_9c_1 - 2b_6\beta^2) + a_3 (3b_2^2b_3(a_6 - b_8) - 2b_2b_3^2(b_7 - a_5) + 4b_2^3b_9 \\
& - 6a_9b_2b_3c_1 + 2a_8b_3^2c_1 + (2a_6b_3 - b_3b_8 + 4b_2b_9) \beta^2) + b_3 (-4a_9b_2 (b_2^2 + \beta^2) \\
& + b_3 (3a_8b_2^2 - 2a_7b_2b_3 + a_8\beta^2))) + a_1^2 (2a_3^4b_4c_1 + a_3^3 (b_2^2b_4 - 4b_2b_6c_1 + c_1 (2b_3b_5 \\
& - 2a_4b_3 + b_9c_1) + 2b_4\beta^2) - a_3^2 (b_2^2b_6 + 4b_2b_3c_1(b_8 - a_6) + b_3c_1 (2a_5b_3 - 2b_3b_7 \\
& + a_9c_1) - b_2^2(b_3b_5 + 6b_9c_1) + (3b_2b_6 - b_3b_5 - 2b_9c_1) \beta^2 + a_4b_3(b_2^2 + 2\beta^2)) \\
& + a_3 (b_2^2b_3^2b_7 - b_2^3b_3b_8 + b_2^2b_9 - 6a_9b_2^2b_3c_1 + 4a_8b_2b_3^2c_1 - 2a_7b_3^3c_1 + \beta^2 (-b_2b_3b_8 \\
& + 2b_2^2b_9 - 2a_9b_3c_1) + b_9\beta^4 - a_5b_3^2(b_2^2 + \beta^2) + a_6b_2b_3(b_2^2 + 3\beta^2)) + b_3 (-a_9 (b_2^2 \\
& + \beta^2)^2 + b_2b_3 (-a_7b_2b_3 + a_8(b_2^2 + \beta^2))))),
\end{aligned}$$

$$\begin{aligned}
A_4 = & -((a_1 + b_2) (a_1(a_1 + b_2) + a_3c_1) \beta + a_1\beta^2)^2 (a_3^3b_4 - a_3^2 (a_4b_3 - b_3b_5 + b_6(a_1 + b_2)) \\
& - b_3 (a_1^2a_9 + 2a_1a_9b_2 + a_9b_2^2 - a_1a_8b_3 - a_8b_2b_3 + a_7b_3^2 + a_9\beta^2) + a_3 (a_6b_2b_3 \\
& - a_5b_3^2 + b_3^2b_7 - b_2b_3b_8 + a_1^2b_9 + b_2^2b_9 + a_1 (a_6b_3 - b_3b_8 + 2b_2b_9) + b_9\beta^2)),
\end{aligned}$$

$$\begin{aligned}
K_1 = & A_1^2A_2^2 - 4A_0A_1A_2 (A_3 + 2A_1 ((a_1(a_1 + b_2) + a_3c_1)^2 + \beta^2 (2a_1^2 + 2a_1b_2 + b_2^2 + 2a_3c_1) \\
& + \beta^4)) + 4A_0^2A_3 (A_3 + 2A_1 (\beta^2 (2a_1^2 + 2a_1b_2 + 2a_3c_1 + b_2^2) + (a_1(a_1 + b_2) \\
& + a_3c_1)^2 + \beta^4))) ,
\end{aligned}$$

$$N = (a_1(a_1 + b_2) + a_3c_1)^2 + (2a_1^2 + 2a_1b_2 + b_2^2 + 2a_3c_1) \beta^2 + \beta^4.$$



Now we give the expressions of  $B_i$  with  $i = 1, 2, 3, 4$ , and  $K_2$  used in Section 6.2. Under conditions (iii) of Proposition 6.0.1, the expressions are the following.

$$\begin{aligned}
 B_0 &= \beta^2 b_3 ((b_1 b_2 + b_3 c_1)(a_{31} b_2 - a_{21} b_3) + \beta^2 (a_{31} b_1 + b_3 c_{31})), \\
 B_1 &= b_3 (b_1 b_2 + b_3 c_1) (2(a_8 b_2 - a_7 b_3)(b_1 b_2 + b_3 c_1) + \beta^2 (2a_8 b_1 + a_6 b_2 + b_2^2 + b_3(-a_5 \\
 &\quad + 2b_7 + c_8) + b_2(b_3 - b_8 - 2c_9))) + \beta^4 b_3 (b_3(b_5 + c_6) + b_1(a_6 + b_2 - b_8 - 2c_9)) \\
 &\quad - 2a_9(b_2 b_3 c_1 + b_1(b_2^2 + \beta^2))^2, \\
 B_2 &= 2b_3 \beta^2 ((b_1 b_2 + b_3 c_1)(a_{21} b_3 - a_{31} b_2) + \beta^2 (a_{11} b_3 - a_{31} b_1)), \\
 B_3 &= 2(b_3((a_7 b_3 - a_8 b_2)(b_1 b_2 + b_3 c_1)^2 - (a_8 b_1 + a_6 b_2 - a_5 b_3)(b_1 b_2 + b_3 c_1)\beta^2 \\
 &\quad + (a_4 b_3 - a_6 b_1)\beta^4) + a_9(b_2 b_3 c_1 + b_1(b_2^2 + \beta^2))^2), \\
 B_4 &= \beta^4 (b_3(a_7 b_3 - a_8 b_2) + a_9(b_2^2 + \beta^2)), \\
 K_2 &= B_1^2 B_2 (8B_0 + B_2) - 4B_0 B_1 (2B_0 + B_2) B_3 + 4B_0^2 B_3^2.
 \end{aligned}$$

On the other hand, under conditions (iv) of Proposition 6.0.1, the expression of  $K_2$  is the same as under conditions (iii) but we redefine the expressions of  $B_i$  with  $i = 0, \dots, 4$  as follows:

$$\begin{aligned}
 B_0 &= \beta^2 a_3 (a_1 a_2 + a_3 c_2) (b_{31} a_1 - b_{11} a_3) + \beta^4 a_3 (b_{31} a_2 + a_3 c_{31}), \\
 B_1 &= a_3 (a_1 a_2 + a_3 c_2) (2(b_6 a_1 - b_4 a_3)(a_1 a_2 + a_3 c_2) + \beta^2 (2a_2 b_6 + a_1 b_8 + a_1^2 + a_3(-b_5 \\
 &\quad + 2a_4 + c_6) + a_1(a_3 - a_6 - 2c_9))) + \beta^4 a_3 (a_3(a_5 + c_8) + a_2(b_8 + a_1 - a_6 \\
 &\quad - 2c_9)) - 2b_9(a_1 a_3 c_2 + a_2(a_1^2 + \beta^2))^2, \\
 B_2 &= 2a_3 \beta^2 ((a_1 a_2 + a_3 c_2)(b_{11} a_3 - b_{31} a_1) + \beta^2 (b_{21} a_3 - b_{31} a_2)), \\
 B_3 &= 2(a_3((a_3 b_4 - a_1 b_6)(a_1 a_2 + a_3 c_2)^2 - (b_6 a_2 + a_1 b_8 - a_3 b_5)(a_1 a_2 + a_3 c_2)\beta^2 \\
 &\quad + (a_3 b_7 - a_2 b_8)\beta^4) + b_9(a_1 a_3 c_2 + a_2(a_1^2 + \beta^2))^2), \\
 B_4 &= \beta^4 (a_3(a_3 b_4 - a_1 b_6) + b_9(a_1^2 + \beta^2)),
 \end{aligned}$$

Finally, the expressions of  $D_i$  with  $i = 1, 2, 3, 4$  and  $K_4$  used in Section 6.3 are the following.

$$\begin{aligned}
 D_0 &= (a_1 b_{31} - b_1 a_{31})(a_1 c_1 + b_1 c_2)\beta^2 + (b_1 b_{21} + c_1 b_{31})\beta^4, \\
 D_1 &= (a_1 c_1 + b_1 c_2)(2(a_1 b_9 - a_9 b_1)(a_1 c_1 + b_1 c_2) + (b_1(a_6 + b_8) + 2b_9 c_1)\beta^2), \\
 D_2 &= 2(a_1 c_1 + b_1 c_2)\beta^2 ((a_{31} b_1 - a_1 b_{31})(a_1 c_1 + b_1 c_2) + (b_1 c_{31} - b_{31} c_1)\beta^2) \\
 D_3 &= 2(a_1 c_1 + b_1 c_2)^2 ((a_9 b_1 - a_1 b_9)(a_1 c_1 + b_1 c_2) + (b_1 c_9 - b_9 c_1)\beta^2),
 \end{aligned}$$

$$\begin{aligned}
 D_4 = & (a_9b_1 - a_1b_9)(a_1c_1 + b_1c_2)^3 - (a_1c_1 + b_1c_2) (a_1^3b_4 + a_1^2b_1(b_5 - a_4) + a_1 (-a_5b_1^2 \\
 & + b_1^2b_7 + b_1b_8c_1 + 2b_9c_1^2 - b_1b_6c_2 - b_1c_1c_9) - b_1 (a_7b_1^2 + a_8b_1c_1 + a_9c_1^2 \\
 & - a_6b_1c_2 - b_9c_1c_2 + b_1c_2c_9)) \beta^2 + (-b_9c_1^3 + a_1^2(b_1c_4 - 2b_4c_1) + a_1b_1 (a_4c_1 \\
 & - b_5c_1 - b_4c_2 + b_1c_5) + b_1^3c_7 + b_1^2 (-c_1b_7 + a_4c_2 - c_2c_6 + c_1c_8) + b_1c_1 (-b_8c_1 \\
 & + b_6c_2 + c_1c_9)) \beta^4 + (b_1c_4 - b_4c_1)\beta^6, \\
 K_4 = & (D_1D_2 - 2D_0D_3)^2 + 8a_1c_1D_0D_1(D_1D_2 - D_0D_3) + 8b_1c_2D_0D_1(D_1D_2 - D_0D_3).
 \end{aligned}$$



# Applications: Differential systems modelizing population dynamics

---

In the previous chapters we dealt with the qualitative study of some general Lotka-Volterra and Kolmogorov systems. In the present chapter, by applying the techniques and results from the previous ones, we consider some more specific systems motivated by real problems. Since the Kolmogorov and Lotka-Volterra systems have their origin in the field of population dynamics, and their applications in this field have been growing and improving over time, we focus our attention on this branch.

First of all, in Section 7.1, we present the review work carried out in [43]<sup>1</sup>, which gives us a better understanding of how predator-prey models have advanced in recent years and which are the topics and characteristics that have particularly attracted the attention of researchers.

Next, in Section 7.2, we study a predator-prey system in the plane, for which we obtain its global phase portraits in the positive quadrant of the Poincaré disk. This work is based on the article [47]<sup>2</sup>.

Finally, Section 7.3 is based on the work published in [31]<sup>3</sup>. In that work we study a model in dimension three, with two prey and one predator, whose restriction to only two of the variables coincides with the previous model. For this three-dimensional model we study different aspects of its qualitative dynamics, including the existence of limit cycles.

---

<sup>1</sup>Érika Diz-Pita (Departamento de Estatística, Análise Matemática e Optimización, Universidade de Santiago de Compostela) and María Victoria Otero-Espinar (Departamento de Estatística, Análise Matemática e Optimización, Universidade de Santiago de Compostela), *Predator-prey models: a review on some recent advances*, Mathematics (EISSN: 2227-7390), **9** (2021), 1783. Published by MDPI. The final authenticated version is available online at: <https://doi.org/10.3390/math9151783>.

<sup>2</sup>Érika Diz-Pita (CITMaga; Departamento de Estatística, Análise Matemática e Optimización, Universidade de Santiago de Compostela), Jaume Llibre (Departament de Matemàtiques, Universitat Autònoma de Barcelona) and María Victoria Otero-Espinar (CITMaga; Departamento de Estatística, Análise Matemática e Optimización, Universidade de Santiago de Compostela), *Global phase portraits of a predator-prey system*, Electronic Journal of Qualitative Theory of Differential Equations, (ISSN: 1417-3875), **16** (2022), 1–13. Published by University of Szeged, Bolyai Institute. The final authenticated version is available online at: <https://doi.org/10.3390/math9151783>.

<sup>3</sup>Renato Colucci (Dipartimento di Ingegneria Industriale e Scienze Matematiche, Università Politecnica delle Marche), Érika Diz-Pita (Departamento de Estatística, Análise Matemática e Optimización, Universidade de Santiago de Compostela) and María Victoria Otero-Espinar (Departamento de Estatística, Análise Matemática e Optimización, Universidade de Santiago de Compostela), *Dynamics of a two prey and one predator system with indirect effect*, Mathematics (EISSN: 2227-7390), **9** (2021), 436. Published by MDPI. The final authenticated version is available online at: <https://doi.org/10.3390/math9040436>

## 7.1 Predator-prey systems: a review on some recent advances

Population dynamics is one of the most widely discussed topics within Biomathematics. The study of the evolution of different populations has always been of special interest, starting with populations of a single species, but evolving to more realistic models where different species live and interact in the same habitat. Among them we can find models that study competitive relationships, symbiosis, commensalism or predator-prey relationships.

In [43] we focus on predator-prey systems with the aim of give a state-of-art review of recent predator-prey models which include Allee effect, fear effect, cannibalism and immigration. We compare the qualitative results obtained for each of them, particularly regarding the singular points, local and global stability and the existence of limit cycles.

Probably the most famous predator-prey models are Lotka-Volterra systems, which on the other hand, have motivated the objectives of this thesis addressed in previous chapters

Actually, the study of predator-prey models has always been one of the hot spots in Biomathematics, so there is a very big number of works on this topic, especially in dimension two, it is, with one predator species and one prey species. For this reason we believe that the work done in [43] may be of particular interest to those researchers involved in modeling this kind of biological and ecological problems, allowing them to have an overview of the work who is currently being carried out.

Therefore, our objective is to analyze several adaptations of predator-prey models that have been done in the last years in order to model different real situations that appear in the field of population dynamics.

We have decided to focus on some special issues to which researchers have devoted special attention in recent years, particularly the study of the Allee effect, the influence of fear effect, cannibalism and immigration. We introduce some works with influences between them, which allow us to understand the importance of these biological aspects, through the study of several models that are completed and improved in successive works.

The Allee effect appears when a population of prey has a really small density, so it makes difficult for them to reproduce or survive. It was first introduced by Allee in [2]. There are several works in the literature that analyze this effect in different population models and conclude that it can have important effects on the system dynamics, including the stabilization or destabilization of a system. It also can cause that the solutions of a system take a much longer time to reach a stable equilibrium point.

Another issue to consider is that in certain ecosystems, prey may feel fear of predators and act accordingly, making hunting more difficult for the predators. The theoretical reasonings about the effect of fear behaviors are supported by real experiments. For example, Zanette, White, Allen and Clinchy [143] conducted an experiment on song sparrows during a whole breeding season by using electrical fence to eliminate direct predation of both juvenile and adult song sparrows. No direct killing can happen in the experiment; however, broadcast of vocal cues of known predators in the field was employed to mimic predation risk. Two groups of female song sparrows were tested, among which one group was exposed to predator sounds while the other group was not. The authors found that the group of song sparrows exposed to predator sounds produced 40% less offspring than the other group. They believe this is

because fewer eggs were laid, fewer eggs were successfully hatched, and fewer nestlings survived eventually. Also because there were behavioral changes including less time of adult song sparrows on brood and less feeding to nestlings during breeding period. Similar experiments on other birds and vertebrate species reported the same conclusions [34, 121, 139], it is, even though there is no direct killing between predators and prey, the presence of predators cause a reduction in prey population due to anti-predator behaviors.

We analyze different models with the presence of fear effect, combined with different functional responses, with both omnivorous and specialist predators, with hunting cooperation, with Allee effect and with prey refuge.

As we mentioned, we study ecosystems in which predators feed only on one prey species, which we will call specialists, and others in which predators are omnivorous, it is, they will be able to feed themselves from other resources. A special case of this is cannibalism, it is, the act of killing and at least partial consumption of conspecifics. Cannibalism actively occurs in more than 1300 species in the nature [111], and it has been mathematically modeled for some ecosystems, as for example the European regional seas ecosystem model (ERSEM) for the North Sea [9].

In the literature, one of the first contributions to the study of this topic was the work of Kohlmeir [75], who considered cannibalism in the predator in the classic Rosenzweig-McArthur model. In general, cannibalism has been considered primarily in predators, and the results agree that it has stabilizing effects, and can cause the survival of a species that would otherwise be driven to extinction. We have selected two works that illustrate well the different effects of cannibalism when we add it to already well-known models, as the Lotka-Volterra and the Holling-Tanner model. In addition, the inclusion of cannibalism is considered not only in the predator species as usual, but also in the prey species.

Just as cannibalism or omnivorism can be adaptation strategies to the lack or shortage of food, other types of strategies or behaviors can be induced by this lack of food or by the hostility of the habitat, such as migration. In fact, most predator-prey systems in the wild are not isolated, so it is important to consider the effects of the presence of some number of immigrants. In [43] we focus on the works that study how the inclusion of immigration changes the dynamics of the classic Rosenzweig-MacArthur and Lotka-Volterra models.

Although we have chosen the previous topics as the thread of our review, in many of the considered works these ones appear combined with other biological characteristics such as prey refugee, hunting cooperation or with different types of functional responses. Down below we make some considerations and give some references about these topics.

Firstly, we recall that in ecology, a functional response is the intake rate of a predator as a function of food density. The most usual classification of functional responses is the one given by C. S. Holling, in which three types of responses are considered. The type I functional response assumes that the consuming and hunting rates are linear up to a maximum where they become constant. This linear increase assumes that the time needed by the predator to process food is negligible and that consuming food does not interfere with searching food. This is the functional response used in the Lotka-Volterra model.

The type II functional response is given by  $f(x) = ax/(1 + ahx)$ , where  $x$  denotes the food or prey density,  $a$  is the rate at which the predator encounters food items per unit of food density, and  $h$  is the average time spent on processing a food item. This functional response assumes that the consumption rate is decelerated with increased population as a

consequence of a limited capacity in searching and processing food. This is the functional response considered in the Rosenzweig-MacArthur model [114], which is a classical model with logistic growth of the form:

$$\begin{aligned}\dot{x} &= rx \left(1 - \frac{x}{K}\right) - y \frac{mx}{b+x}, \\ \dot{y} &= y \left(-\delta + c \frac{mx}{b+x}\right).\end{aligned}$$

In type III functional response, the consumption rate is more than linear at low levels of resource. This is suitable for instance in a population of predators that has to learn how to hunt efficiently. This functional response is given by  $f(x) = nx^p/(a^p + x^p)$ , where  $a$  and  $n$  are positive and  $p$  is an integer with  $p > 1$ .

These three types of functional responses are widely used in population dynamics models and specially in predator-prey models, not only on ODE models but also on discrete models, diffusion models, stochastic or fractional order models. Some interesting recent works that study this kind of functional responses are [3, 25, 39, 102, 142, 146].

There are other types of functional responses, for example the one proposed by Taylor, also known sometimes as Holling type IV functional response, which is given by the function

$$h(x) = \frac{qx}{x^2 + bx + a},$$

where  $b \geq 0$ . Other models consider a functional response of ratio-dependent type, in which the consider function is  $h(x) = a/x$ , with  $a \in \mathbb{R}$ .

Regarding the existence of prey refuge, it has also special interest in the study of predator-prey populations, and many scholars have made great achievements in this aspect. There are interesting works on this subject apart from the ones that we include in [43], i.e., those related to the main topics of the work. Some interesting examples can be found in the following references [73, 74, 94, 101, 120].

Finally, we would like to note that the third characteristic that we have mentioned, hunting cooperation on predators, has been investigated by many authors in mathematical modeling, but most of the time independently of the effect of fear on prey [11, 48, 104, 112, 129]. In [43] we focus on the combination of both hunting cooperation and fear effect, which we believe is particularly important due to the ecological evidence. For example, wolves cooperate during hunting and when they are present, elks use anti-predator strategies and avoid areas frequented by the wolves [113]. Elks respond to the presence of wolves by altering foraging, vigilance, habitat selection, patterns of aggregation and sensitivity to environment [35, 36, 137, 138]. In the same way, while lionesses show cooperative hunting behaviors [126], zebras are affected by fear of predation risk, reaching areas where the encounter with lionesses is less frequent [33].

As we have said, in [43] we focus on models with Allee effect, with fear effect, with cannibalism and with immigration. We compare the proposed models whenever it is possible, and we analyze how the inclusion of different biological characteristics affects the dynamics.

Some of the stated models show a very rich dynamics which is much more realistic than the one of the first historical models. The following are some of the conclusions drawn from the review performed.

The inclusion of Allee effect in a predator-prey system can have important effects on the dynamics; it can stabilize or destabilize the system or cause that the solutions of the system take a much longer time to reach a stable equilibrium point as can be seen in [59, 100]. We note that the Allee effect can produce different consequences depending on whether it is considered in the prey species or in the predator species, see for example the works of Merdan [100] and Guan, Liu and Xie [61]. Also limit cycles can appear in systems with Allee effect, as analyzed in the work of Wang, Xi and Wei [134], and even two limit cycles can appear as proved in [58].

The conclusions about the influence of fear effect are not the same in all the studied models. Considering a system with linear functional response and specialist predators, in [135] the authors show that fear does not affect the dynamics, but considering omnivorous predators, in [145] it is shown that the increase of the fear constant decreases the population density of the species in the singular point and can even cause extinction. Also for the system considered in [135], it is proved that if we change the functional response from linear to Holling type II, then the fear affects the dynamics: a value large enough for the fear parameter can help to maintain the asymptotic stability of a singular point.

The stabilizing effect of fear is also showed when combined with other biological characteristics. In [105] the fear effect is combined with hunting cooperation and it is shown that when the system has oscillating behaviors, the increase of hunting cooperation or the increase of fear effect produces the stabilization. Also a stabilizing effect appears when combining the fear effect with prey refuge, as shown in [144].

In contrast, in [116] we see that the stabilizing effect does not appear when fear is combined with Allee effect. In this case the only consequence is a reduction of the population density in the positive singular point. Even replacing the usual Allee effect with a modified additive Allee effect, which in general gives rise to a more complex dynamics, similar conclusions are obtained. This is studied in [79].

Cannibalism had been principally considered in the predator species, and in that case the results agreed that cannibalism stabilizes the system and causes persistence in a population doomed to go extinct, but we have seen that considering cannibalism in prey species can produce the opposite result, as it can destabilize the system [10].

Regarding the presence of immigration we can observe that it has a stabilizing effect, reducing the amplitude of oscillations when they exist [127]. Even very small immigration can cause that cyclic populations be stabilized, as proved in [128]. Furthermore, this stabilization occurs whether immigration occurs on prey or predators.

We see, therefore, that population models have come a long way since the first Lotka-Volterra systems, and they are becoming more and more realistic. Even so, and after having analyzed the literature, there are still many open problems that are of interest to improve the existing models and that we plan to address in the future, as will be specified in the conclusions of the manuscript.

Finally, we would like to highlight that in most works studying populations dynamics, the authors start by doing variable changes to obtain equivalent systems, for example by writing them down in a dimensionless form, but, in many cases, those systems are transformed into Kolmogorov systems, which again reinforces the usefulness of these systems that we have been studying throughout the manuscript.



## 7.2 The Rosenzweig-MacArthur model as a Kolmogorov system

Rosenzweig and MacArthur introduced in [114] the following predator-prey model

$$\begin{aligned}\dot{x} &= rx \left(1 - \frac{x}{K}\right) - y \frac{mx}{b+x}, \\ \dot{y} &= y \left(-\delta + c \frac{mx}{b+x}\right),\end{aligned}$$

where the dot denotes the derivative with respect to the time  $t$ ,  $x \geq 0$  denotes the prey density and  $y \geq 0$  denotes the predator density. The parameter  $\delta > 0$  is the death rate of the predator, the function  $mx/(b+x)$  are the prey caught per predator per unit time, the function  $rx(1 - x/K)$  is the growth of the prey in the absence of predator, and  $c > 0$  is the rate of conversion of prey to predator. This Rosenzweig-MacArthur system is a particular system of the general predator-prey systems with a Holling type II functional response (see [69, 70]).

In [71] Huzak reduced the study of the Rosenzweig-MacArthur system to the study of a Kolmogorov polynomial differential system. In order to do that the first step is to do the rescaling  $(\bar{x}, \bar{y}, \bar{b}, \bar{c}, \bar{\delta}) = (x/K, (m/rK)y, b/K, cm/r, \delta/r)$ . After denoting again  $(\bar{x}, \bar{y}, \bar{b}, \bar{c}, \bar{\delta})$  by  $(x, y, b, c, \delta)$  and doing a time rescaling multiplying by  $b+x$ , the obtained Kolmogorov polynomial differential system of degree three is

$$\begin{aligned}\dot{x} &= x(-x^2 + (1-b)x - y + b), \\ \dot{y} &= y((c-\delta)x - \delta b),\end{aligned}\tag{7.2.1}$$

where  $b, c$  and  $\delta$  are positive parameters. It is interesting to study this system in the positive quadrant of the plane  $\mathbb{R}^2$ , where it has ecological meaning. The work of Huzak is focused in the study of the periodic sets that can produce the canard relaxation oscillations after perturbations. He finds three types of limit periodic sets and studies their cyclicity by using the geometric singular perturbation theory and the family blow up at  $(x, y, \delta) = (0, br/m, 0)$ . He proves that the upper bound on the number of limit cycles of the system is 1 or 2 depending on the parameters.

We want to complete the study of the dynamics of systems (7.2.1) by classifying all their phase portraits on the closed positive quadrant of the Poincaré disk, as in this way we also can control the dynamics of the system near the infinity. This classification is given in the following result, except for the case with the parameters satisfying  $0 < b\delta < c - \delta$ ,  $\delta(\delta(b+1) + c(b-1))^2 - 4c(c-\delta)^2(c-\delta(b-1)) < 0$  and  $1 + c - d - b - bd > 0$ , in which we make a conjecture about the expected global phase portrait.

**Theorem 7.2.1.** *The global phase portrait of system (7.2.1) in the closed positive quadrant of the Poincaré disk is topologically equivalent to one of the three phase portraits of Figure 7.2.1 in the following way:*

- If  $b\delta \geq c - \delta$ , the phase portrait is equivalent to phase portrait (A).
- If  $0 < b\delta < c - \delta$  and  $\delta(\delta(b+1) + c(b-1))^2 - 4c(c-\delta)^2(c-\delta(b-1)) \geq 0$ , the phase portrait is equivalent to phase portrait (B).

- If  $0 < b\delta < c - \delta$ ,  $\delta(\delta(b+1) + c(b-1))^2 - 4c(c-\delta)^2(c-\delta(b-1)) < 0$  and  $1 + c - d - b - bd < 0$ , the phase portrait is equivalent to phase portrait (C).

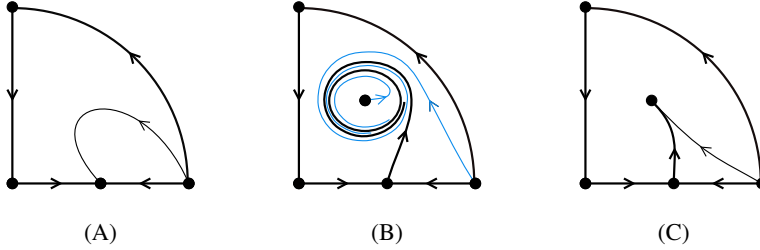


Figure 7.2.1: Phase portraits of system (7.2.1) in the positive quadrant of the Poincaré disk.

**Conjecture.** The global phase portrait of system (7.2.1) in the closed positive quadrant of the Poincaré disk if  $0 < b\delta < c - \delta$ ,  $\delta(\delta(b+1) + c(b-1))^2 - 4c(c-\delta)^2(c-\delta(b-1)) < 0$  and  $1 + c - d - b - bd > 0$ , is also topologically equivalent to the one in Figure 7.2.1(C).

In Figure 7.2.2 are represented the regions and surfaces in the parameters space in which each one of the phase portraits are realized. In the region I and over the surface  $S_1$  the phase portrait is the one in Figure 7.2.1(A), and in the region III the phase portrait is the one in Figure 7.2.1(B). In region II there are two subregions, II-a and II-b. It is proved that in the region II-a the phase portrait is the one in Figure 7.2.1(C) and we conjecture that the phase portrait is the same in the region II-b and over the surfaces  $S_2$  and  $S_3$ .

### 7.2.1 Finite singular points

First we study the finite singular points of system (7.2.1) in the closed positive quadrant. The origin  $P_0 = (0, 0)$  and the point  $P_1 = (1, 0)$  are singular points for any values of the parameters, and  $P_2 = (b\delta/(c-\delta), (-bc(\delta+b\delta-c))/(c-\delta)^2)$  is a positive singular point if  $c \neq \delta$  and  $0 < b\delta < c - \delta$ . Note that if  $b\delta = c - \delta$ , then  $P_1 = P_2$ .

Now we study the local phase portraits at these singular points. The origin is a saddle point, as the eigenvalues of the Jacobian matrix at this point are  $b$  and  $-\delta b$ . At the point  $P_1$  the eigenvalues are  $-b - 1$  and  $-\delta b + c - \delta$ . The first eigenvalue is always negative, but we distinguish three cases depending on the second one. If  $c - \delta < b\delta$ , then  $P_1$  is a stable node; if  $c - \delta > b\delta$ , then  $P_1$  is a saddle. If  $c - \delta = b\delta$ ,  $P_1$  is a semi-hyperbolic singular point, and from Theorem 1.2.3 we obtain that  $P_1 = P_2$  is a saddle-node.

At the singular point  $P_2$  the eigenvalues of the Jacobian matrix are

$$\lambda_{1,2} = \frac{2}{(c-\delta)^2} (A \pm \sqrt{\delta B}),$$

USC  
where

$$A = \delta(c-\delta) - b\delta(c+\delta) \quad \text{and} \quad B = \delta(\delta(b+1) + c(b-1))^2 - 4c(c-\delta)^2(c-\delta(b-1)).$$

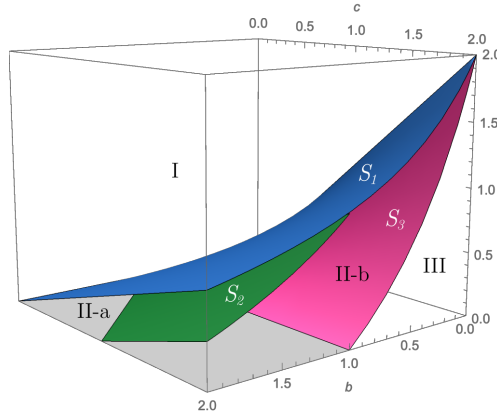


Figure 7.2.2: The regions I, II-a, II-b, III and the surfaces separating the different phase portraits:  $S_1 : \{d = c/(b+1) \mid b, c \geq 0\}$ ,  $S_2 : \{d = (1+c-b)/(b+1) \mid b, c \geq 0, (1+c-b)/(b+1) < c/(b+1)\}$  and  $S_3 : \{d = c(1-b)/(1+b) \mid b, c \geq 0\}$ .

If  $B < 0$ , then the eigenvalues are complex. In this case, for  $A > 0$ , the singular point  $P_2$  is an unstable focus, and for  $A < 0$  it is a stable focus. We deal with this case  $B < 0$  in Section 7.2.4, where we study the Hopf bifurcation which takes place at  $P_2$ .

If  $B = 0$ , we have  $\lambda_1 = \lambda_2 = A/(c-\delta)^2$  and in this case  $A$  cannot be zero, because if  $A = 0$ , then  $b = (c-\delta)/(c+\delta)$ , and replacing this expression,  $B = -4c^2(c-\delta)^3/(c+\delta)$ , so one of the conditions  $c = 0$  or  $c - \delta = 0$  must hold, but this is not possible as  $c > 0$  from the hypotheses, and if  $c = \delta$ , then  $b = 0$  and again this contradicts the hypotheses. Then  $A \neq 0$  and its sign determines if the singular point is either a stable or an unstable node.

If  $B > 0$  both eigenvalues are real. The determinant of the Jacobian matrix is

$$-\frac{b^2 c \delta}{(c-\delta)^2} (b\delta + \delta - c),$$

which is positive because the singular point  $P_2$  exists only if condition  $b\delta < c - \delta$  holds. Then both eigenvalues are nonzero and have the same sign, particularly, if  $A > 0$  both are positive and  $P_2$  is an unstable node, and if  $A < 0$  both are negative and  $P_2$  is a stable node.

The local phase portrait of the singular point  $P_2$  in the case with  $A = 0$  will be proved in Subsection 7.2.4.

In summary, we describe in Table 7.2.1 the finite singular points according to the values of the parameters  $b$ ,  $c$  and  $\delta$ .

Case	Conditions	Finite singular points
1	$b\delta > c - \delta$	$P_0$ saddle, $P_1$ stable node
2	$b\delta = c - \delta$	$P_0$ saddle, $P_1$ saddle-node
3	$0 < b\delta < c - \delta, B \geq 0, A > 0$	$P_0$ saddle, $P_1$ saddle, $P_2$ unstable node
4	$0 < b\delta < c - \delta, B \geq 0, A < 0$	$P_0$ saddle, $P_1$ saddle, $P_2$ stable node
5	$0 < b\delta < c - \delta, B < 0, A > 0$	$P_0$ saddle, $P_1$ saddle, $P_2$ unstable focus
6	$0 < b\delta < c - \delta, B < 0, A < 0$	$P_0$ saddle, $P_1$ saddle, $P_2$ stable focus
7	$0 < b\delta < c - \delta, B < 0, A = 0$	$P_0$ saddle, $P_1$ saddle, $P_2$ weak stable focus

Table 7.2.1: The finite singular points in the closed positive quadrant.

### 7.2.2 Infinite singular points

Now we consider the Poincaré compactification of system (7.2.1) as it allows us to study the behavior of the trajectories near infinity.

In chart  $U_1$  system (7.2.1) writes

$$\begin{aligned}\dot{u} &= uv^2 - b(\delta + 1)uv^2 + (b + c - \delta - 1)uv + u, \\ \dot{v} &= uv^2 - bv^3 + (b - 1)v^2 + v.\end{aligned}\tag{7.2.2}$$

The only singular point over  $v = 0$  is the origin of  $U_1$ , which we denote by  $O_1$ . The linear part of system (7.2.2) at the origin is the identity matrix, so  $O_1$  is an unstable node.

In chart  $U_2$  system (7.2.1) writes

$$\begin{aligned}\dot{u} &= -u^3 + (\delta + 1 - b - c)u^2v + b(\delta + 1)uv^2 - uv, \\ \dot{v} &= (\delta - c)uv^2 + b\delta v^3.\end{aligned}\tag{7.2.3}$$

The origin of  $U_2$  is a singular point,  $O_2$ , and the linear part of system (7.2.3) at  $O_2$  is identically zero, so we must use the blow up technique to study it. We do a horizontal blow up introducing the new variable  $w_1$  by means of the variable change  $vw_1 = u$ , and get the system

$$\begin{aligned}\dot{w}_1 &= v^2w_1^3 + (1 - b)v^2w_1^2 + bw_1v^2 - w_1v, \\ \dot{v} &= (\delta - c)w_1v^3 + b\delta v^3.\end{aligned}\tag{7.2.4}$$

Now rescaling the time variable we cancel the common factor  $v$ , getting the system

$$\begin{aligned}\dot{w}_1 &= vw_1^3 + (1 - b)vw_1^2 + bw_1v - w_1, \\ \dot{v} &= (\delta - c)w_1v^2 + b\delta v^2.\end{aligned}\tag{7.2.5}$$

The only singular point on  $v = 0$  is the origin, which is semi-hyperbolic. Applying Theorem 1.2.3 we conclude that it is a saddle-node. Studying the sense of the flow over the axis we determine that the phase portrait around the origin of system (7.2.5) is the one in Figure 7.2.3(a). If we multiply by  $v$  the sense of the orbits on the third and fourth quadrants changes

and all the points on the  $w_1$ -axis become singular points. With these modifications we obtain the phase portrait for system (7.2.4), given in Figure 7.2.3(b). Then we undo the blow up going back to the  $(u, v)$ -plane. We must swap the third and fourth quadrants and shrink the exceptional divisor to the origin. The phase portrait obtained for system (7.2.3) is not totally determined in the shaded regions of the third and fourth quadrants (see Figure 7.2.3(c)). This can be solved by doing a vertical blow up but, in our case, it is not necessary because we only need to know the phase portrait of  $O_2$  in the positive quadrant of the Poincaré disk, which corresponds with the positive quadrant in the plane  $(u, v)$ , in which the phase portrait is well determined.

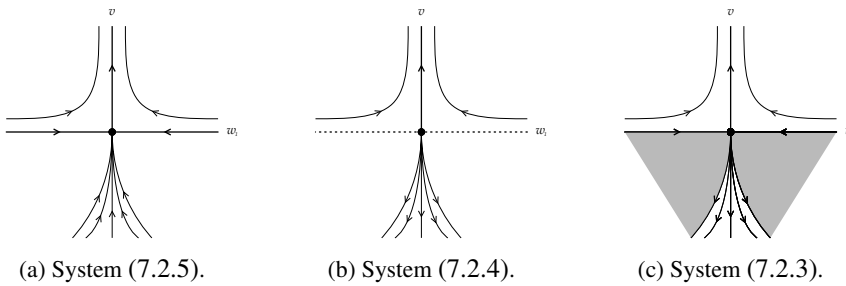


Figure 7.2.3: Desingularization of the origin of system (7.2.3).

As a conclusion the local phase portrait at the infinite singular points is the same independently of the values of the parameters, so in all cases of Table 7.2.1 the origin of chart  $U_1$ , i.e., the singular point  $O_1$ , is an unstable node and the origin of chart  $U_2$ , i.e., the singular point  $O_2$  has only one hyperbolic sector on the positive quadrant of the Poincaré disk being one separatrix at infinity and the other on  $x = 0$ .

### 7.2.3 Cases with no singular points in the positive quadrant

In the two first cases of Table 7.2.1 there are no singular points in the positive quadrant. The finite singular points are the origin, denoted by  $P_0$ , and  $P_1$ , which are both over the axes. The axes are invariant lines so there cannot exist a limit cycle surrounding these singular points. Therefore, as we have determined the local phase portrait at the finite and infinite singularities, and we know there are no limit cycles, we can study the global portrait in the first quadrant of the Poincaré disk.

In both cases we obtain the same result since in the case in which  $P_1$  is a saddle-node, studying the sense of the flow we determine that the parabolic sector of the saddle-node is always on the positive quadrant of the Poincaré disk. Analyzing all the possible  $\alpha$  and  $\omega$ -limits, the only possibility is that all the orbits leave the infinite singular point  $O_1$  and go to the finite singular point  $P_1$ . This phase portrait is given in Figure 7.2.1 (A).

## 7.2.4 Cases with singular points in the positive quadrant

### Existence of limit cycles

**Theorem 7.2.2.** *If  $0 < b\delta < c - \delta$  and  $A > 0$ , then there exists at least one limit cycle surrounding singular point  $P_2$ .*

*Proof.* If conditions  $0 < b\delta < c - \delta$  and  $A > 0$  hold, then we have case 3 or 5 of Table 7.2.1. In both cases singular point  $P_1$  is a saddle which has an unstable separatrix on the positive quadrant,  $P_2$  is either an unstable node or an unstable focus, and  $O_1$  is an unstable node. By Poincaré-Bendixon theorem, there must exist at least one limit cycle which is the  $\omega$ -limit of the orbits leaving  $O_1$ , the orbits leaving  $P_2$  and the separatrix of  $P_1$ , as there are no other singular points that can be the  $\omega$ -limit of all these orbits.  $\square$

In cases 5, 6 and 7 of Table 7.2.1, the Jacobian matrix at the point  $P_2$  has complex eigenvalues because  $B < 0$ . In these cases we study the existence of Hopf bifurcation, leading to the following result.

**Theorem 7.2.3.** *The equilibrium  $P_2$  of system (7.2.1) undergoes a supercritical Hopf bifurcation at  $b_0 = (c - \delta)/(c + \delta)$ . For  $b > b_0$  the system has a unique stable limit cycle bifurcating from the equilibrium point  $P_2$ .*

*Proof.* The Jacobian matrix at this equilibrium is

$$A(b) = \begin{pmatrix} -\frac{b\delta(c(b-1) + \delta(b+1))}{(c-\delta)^2} & -\frac{b\delta}{c-\delta} \\ -\frac{bc(b\delta + \delta - c)}{c-\delta} & 0 \end{pmatrix},$$

and it has eigenvalues  $\mu(b) \pm \omega(b)i$ , where

$$\mu(b) = \frac{b}{2(c-\delta)^2}A \quad \text{and} \quad \omega(b) = \frac{b}{2(c-\delta)^2}\sqrt{-\delta B}.$$

We get  $\mu(b_0) = 0$  for

$$b_0 = \frac{c-\delta}{c+\delta}.$$

We are working under condition  $B < 0$  and from this condition it can be deduced that  $c - \delta > 0$ , so the expression obtained for  $b_0$  is positive. Therefore, at  $b = b_0$ , the equilibrium point  $P_2$  has a pair of pure imaginary eigenvalues  $\pm i\omega(b)$  and the system will have a Hopf bifurcation if some Lyapunov constant is nonzero and  $(d\mu/db)(b_0) \neq 0$ .

The equilibrium is stable for  $b > b_0$  (i.e., for  $A < 0$ ) and unstable for  $b < b_0$  (i.e., for  $A > 0$ ). In order to analyze this Hopf bifurcation we will apply the results on Section 1.8, so we must prove if the genericity conditions are satisfied. We check that the transversality condition is satisfied as

$$\frac{d\mu}{db}(b_0) = -\frac{\delta}{2(c-\delta)} < 0,$$

and the sign is determined because  $c - \delta > 0$ .

To check the second condition we must compute the first Lyapunov constant. We fix the value  $b = b_0$  and then the equilibrium  $P_2$  has the expression

$$P_2 = \left( \frac{\delta}{c + \delta}, \frac{c^2}{(c + \delta)^2} \right).$$

We translate  $P_2$  to the origin of coordinates obtaining the system

$$\begin{aligned}\dot{\varepsilon}_1 &= -\varepsilon_1^3 - \frac{\delta}{c + \delta} \varepsilon_1^2 - \varepsilon_1 \varepsilon_2 - \frac{\delta}{c + \delta} \varepsilon_2, \\ \dot{\varepsilon}_2 &= (c - \delta) \varepsilon_1 \varepsilon_2 + \frac{c^2(c - \delta)}{(c + \delta)^2},\end{aligned}$$

which can be represented as

$$\dot{\varepsilon} = A\varepsilon + \frac{1}{2}B(\varepsilon, \varepsilon) + \frac{1}{6}C(\varepsilon, \varepsilon, \varepsilon),$$

where  $A = A(b_0)$  and the multilinear functions  $B$  and  $C$  are given by

$$\begin{aligned}B(\varepsilon, \eta) &= \begin{pmatrix} -\frac{2\delta}{c + \delta} \varepsilon_1 \eta_1 - \varepsilon_1 \eta_2 - \varepsilon_2 \eta_1 \\ (c - \delta) \varepsilon_1 \eta_2 + (c - \delta) \varepsilon_2 \eta_1 \end{pmatrix}, \\ C(\varepsilon, \eta, \zeta) &= \begin{pmatrix} 6\varepsilon_1 \eta_1 \zeta_1 \\ 0 \end{pmatrix}.\end{aligned}$$

We need to find two eigenvectors  $p, q$  of the matrix  $A$  satisfying

$$Aq = i\omega q, \quad A^T p = -i\omega p, \quad \text{and} \quad \langle p, q \rangle = 1,$$

as for example

$$q = \begin{pmatrix} -\frac{\delta}{c + \delta} \\ i\omega \end{pmatrix} \quad \text{and} \quad p = \begin{pmatrix} -\frac{c + \delta}{2\delta} \\ i\omega \frac{(c + \delta)^3}{2c^2\delta(c - \delta)} \end{pmatrix}.$$

Now we compute

$$\begin{aligned}g_{20} &= \langle p, B(q, q) \rangle = \frac{\omega^2(c + \delta)^5 - c^2\delta^2(c + \delta)}{2\delta c^4(c - \delta)} + \frac{\omega(c + \delta)^3}{2c^2\delta(c - \delta)} i, \\ g_{11} &= \langle p, B(q, \bar{q}) \rangle = -\frac{\delta(c + \delta)}{2c^2(c - \delta)}, \quad g_{21} = \langle p, C(q, q, \bar{q}) \rangle = -\frac{3(c + \delta)^4}{4c^4(c - \delta)^2},\end{aligned}$$

and the first Lyapunov coefficient

$$\ell_1 = \frac{1}{2\omega^2} \operatorname{Re}(ig_{20}g_{11} + \omega g_{21}) = -\frac{(c + \delta)^4}{4c^4\omega(c - \delta)^2},$$

which is negative for any values of the parameters, and so the second condition of theorem 1.8.4 is satisfied, and we can conclude that a unique stable limit cycle bifurcates from the equilibrium point  $P_2$  through a Hopf bifurcation for  $b < b_0$  with  $b_0 - b$  sufficiently small.  $\square$

**Proposition 7.2.4.** *If  $0 < b\delta < c - \delta$  and  $A > 0$ , the limit cycle surrounding singular point  $P_2$  is unique.*

*Proof.* This result follows from [83] by proving that system (7.2.1) with  $0 < b\delta < c - \delta$  and  $A > 0$  satisfies conditions (i)–(iv) in Section 2 of [83].

Condition (i) holds taking  $g(x) = (c - \delta)x$ , which satisfies  $g(0) = 0$  and  $g'(x) > 0$  for all  $x \geq 0$ , as we have assumed  $c - \delta > 0$ .

Condition (ii) holds for  $f(x) = -x^2 + (1 - b)x + b$ ,  $K = 1$  and  $a = (1 - b)/2$ . From condition  $A > 0$  we deduce that

$$\delta(c - \delta) - b\delta(c + \delta) > 0 \Rightarrow \frac{c - \delta}{c + \delta} > \frac{b\delta}{\delta} \Rightarrow 1 > \frac{c - \delta}{c + \delta} > b,$$

and condition  $b < 1$  guarantees that  $a > 0$ .

Condition (iii) holds for  $\lambda = b\delta$  and  $x^* = \delta b/(c - \delta)$ . It can be proved that with the expressions chosen for  $a$  and  $x^*$  the condition  $x^* < a$ , is equivalent to the condition  $A > 0$ :

$$x^* < a \Leftrightarrow \frac{\delta b}{c - \delta} < \frac{1 - b}{2} \Leftrightarrow 2\delta b < (1 - b)(c - \delta) \Leftrightarrow \delta b + bc < c - \delta \Leftrightarrow b < \frac{c - \delta}{c + \delta} \Leftrightarrow A > 0.$$

Condition (iv) is satisfied with

$$x^* = \frac{\delta b}{c - \delta} \quad \text{and} \quad \bar{x}^* = 1 - \frac{bc}{c - \delta}.$$

We have

$$\frac{d}{dx} \frac{xf'(x)}{g(x) - \lambda} = \frac{-2x^2(c - \delta) + 4x\delta b(b - 1)}{((c - \delta)x - \delta b)^2},$$

which is always negative as the polynomial in the numerator is negative in  $x = 0$  and has no real roots.

Then, as conditions (i)–(iv) hold for our systems, we can conclude that the limit cycle is unique.  $\square$

**Remark 7.2.5.** *Theorem 7.2.3 proves that the unique limit cycle of system (7.2.1) appears from the equilibrium point  $P_2$  in a Hopf bifurcation. From the proof of Theorem 7.2.3 the singular point  $P_2$  when  $B < 0$  and  $A = 0$  is a weak stable focus.*

So far we have not proved if in cases 4, 6, and 7 of Table 7.2.1 there are or not limit cycles. The following result proves that in some subcases there are not limit cycles.



**Theorem 7.2.6.** *If  $0 < b\delta < c - \delta$ ,  $A < 0$  and  $1 + c < d + b + bd$ , then system (7.2.1) does not have periodic orbits in the set  $\{(x, y) \in \mathbb{R}^2 : x, z \geq 0\}$ .*

*Proof.* Let

$$f(x, y) = x(-x^2 + (1 - b)x - y + b) \quad \text{and} \quad g(x, y) = y((c - \delta)x - \delta b).$$

In order to prove the non existence of periodic orbits we use Bendixson-Dulac Theorem that states that if there exists a function  $\varphi(x, y)$  such that the term

$$\Delta(x, y) = \frac{\partial(\varphi f)}{\partial x} + \frac{\partial(\varphi g)}{\partial y}$$

does not change sign in a simply connected set  $S$ , then there are no periodic orbits on  $S$ . We consider the function  $\varphi(x, y) = 1/x$ . Then:

$$\Delta(x, y) = 1 + c - d - 2x - \frac{b(d + x)}{x}.$$

We observe that there are no periodic orbits in the set

$$\{(x, y) \in \mathbb{R}_+^2 : x \geq 1\},$$

because  $\dot{x} < 0$  for all the points in this set, and for the same reason there are no periodic orbits crossing the line  $\{x = 1, y \geq 0\}$ . As a consequence we can restrict to the case  $x < 1$  for which we obtain

$$\Delta(x, y) < 1 + c - d - \frac{bd}{x} - b < 1 + c - d - bd - b.$$

Then  $\Delta(x, y) < 0$  in  $\{(x, y) \in \mathbb{R}^2 : 0 \leq x \leq 1, y \geq 0\}$  if  $1 + c - d - b - bd < 0$  and we conclude that there are no periodic orbits in the whole set  $\{(x, y) \in \mathbb{R}^2 : x \geq 0, y \geq 0\}$ .  $\square$

**Conjecture.** *If  $0 < b\delta < c - \delta$ ,  $A < 0$  (i. e, we are in cases 4, 6, or 7 of Table 7.2.1) and  $1 + c > d + b + bd$ , there are not limit cycles.*

We have numerical evidences that the conjecture holds.

### 7.2.5 Phase portraits on the positive quadrant of the Poincaré disk

Now we study the global phase portraits of system (7.2.1) on the positive quadrant of the Poincaré disk when there is a singular point in the positive quadrant, assuming the previous Conjecture.

In case 3 of Table 7.2.1, by Theorem 7.2.2 there exist a unique limit cycle which is the  $\omega$ -limit of all orbits leaving  $O_1$  and  $P_2$ , and also the  $\omega$ -limit of the unstable separatrix leaving  $P_1$  in the positive quadrant. Then the global phase portraits is the one in Figure 7.2.1(B).

In case 5 of Table 7.2.1 we have again that there exists a unique limit cycle attracting all orbits in the positive quadrant. The global phase portrait is the same as the one in case 3 but

here the singular point in the positive quadrant is an unstable focus instead of an unstable node. As the local phase portraits of these two singular points are topologically equivalent we have again phase portrait (B) of Figure 7.2.1.

In cases 4, 6 and 7 of Table 7.2.1, if  $1 + c < d + b + bd$ , we have proved that there are no limit cycles. In case 4 the only possibility is that the stable node  $P_2$  is a global attractor for all orbits in the positive quadrant, and we have the global phase portrait given in Figure 7.2.1(C). In cases 6 and 7 of Table 7.2.1,  $P_2$  is a stable focus and attracts all the orbits of the positive quadrant. As the local phase portrait of a stable focus is topologically equivalent to a stable node, we also have here the phase portrait of Figure 7.2.1(C).

In the cases 4, 6 and 7 of Table 7.2.1, if the conditions  $1 + c < d + b + bd$  does not hold, we have assumed that there are not limit cycles, so the conjectured phase portraits will be the same.

## 7.2.6 Conclusions

In this section we consider the Kolmogorov system (7.2.1), studied in [71] and obtained from the classical Rosenzweig-MacArthur model.

We study the global dynamics of system (7.3.11) and give their phase portraits in the closed positive quadrant of the Poincaré disk in Theorem 7.2.1.

If the parameters satisfy  $0 < b\delta < c - \delta$ ,  $\delta(\delta(b+1) + c(b-1))^2 - 4c(c-\delta)^2(c-\delta(b-1)) < 0$  and  $1 + c - d - b - bd > 0$ , we are not able to determine the global phase portrait but we make a conjecture which states that in that case the global phase portrait coincides with the one in Figure 7.2.1(C). This point remains as an open problem and it would be interesting to study it in the future.

Throughout this section we study the local phase portraits at the finite singular points, the dynamics at the points of the infinity by means of the Poincaré compactification, and we also analyze the existence of limit cycles.

We determine the conditions for which the system has at least one limit cycle in Theorem 7.2.2 and also more restrictive conditions for which the limit cycle is unique in Proposition 7.2.4 and for which it appears through a Hopf bifurcation in Theorem 7.2.3.

## 7.3 A two prey and one predator system

In ecosystems in which predators and prey coexist, predators can influence the evolution of their prey directly by eating them, but also indirectly. Theoretical biologists have pointed out that indirect effects can be comparable or even larger than the direct effects.

The role played by indirect effects in population dynamics has been investigated in the last decades, as can be seen for example in [13, 26, 57, 64, 93, 95, 99, 115, 123, 133, 140].

It has been pointed out that predator can alter the morphology or the behavior of the preys. In particular, the preys, in order to avoid contacts with predators, may reduce their normal activity or may stay hidden most of the time. An example (see [28]) is the case of indirect effects by the existence of prey refuges, a characteristic which has been previously mentioned in Section 7.1.

Many kinds of indirect effects have been described in the literature (see [99] for a detailed discussion), for example, indirect interactions in a plankton community were studied in [30]. The authors analyzed the effects of predator *Daphnia* over two groups of Phytoplankton of different morphology (see [95], [115]), having Phosphorous as resource (see [115] or [64]). In this case the predator prefers to predate the smaller size prey group and the other one take advantages of it. The model has been analytically studied in [30] by using persistence theory (see [122], [20]) and in [32] by bifurcation theory. Both studies suggest the importance of indirect effects of predation in order to describe cases of coexistence in real life. In [22] seasonal indirect effects have been considered showing the possibility of chaotic motion, while in [23, 24] the authors have considered also the stochastic version of the model.

In [119] the authors consider the following two-prey one-predator model:

$$\begin{aligned}\dot{x} &= rx \left(1 - \frac{x}{k}\right) - \frac{cxz}{a + \alpha\eta y + x}, \\ \dot{y} &= y(\beta - \delta z), \\ \dot{z} &= \frac{bxz}{a + \alpha\eta y + x} + \gamma yz - mz,\end{aligned}\tag{7.3.6}$$

where  $x, y, z$  represent the population densities of the two preys and of the predator respectively.

In this model, for the interaction between the first prey and the predator, they considered a Holling type II functional response, where the handling time of predator for the second prey is also involved, while for the interaction between the second prey and the predator they considered a Lotka-Volterra functional response. It is also assumed that there is no intraspecific interaction in the second prey population and its growth is exponential; as a consequence there is a huge availability of the second prey in the absence of predator and there is no searching time for the second prey population. They found necessary and sufficient conditions for existence and stability of a non trivial equilibrium (see [119]).

In order to recover a more complex and realistic behavior we consider a modification of the model which takes into account indirect effects of predation.

Regarding the model (7.3.6), since there is a higher availability of the second prey, it is natural to suppose that the predator prefers to predate the second prey and the first one take advantages of it. A simple way to model this situation consists in adding the indirect effect term  $-Lyz$  in the second equation and the term  $Lyz$  in the first one, with the parameter  $L > 0$  describing the intensity of indirect effects. The systems becomes

$$\begin{aligned}\dot{x} &= rx \left(1 - \frac{x}{k}\right) - \frac{cxz}{a + \alpha\eta y + x} + Lyz, \\ \dot{y} &= y(\beta - \delta z) - Lyz, \\ \dot{z} &= \frac{bxz}{a + \alpha\eta y + x} + \gamma yz - mz.\end{aligned}\tag{7.3.7}$$

We consider initial conditions  $x(0) \geq 0$ ,  $y(0) \geq 0$ ,  $z(0) \geq 0$  and we assume all the parameters are positive and with the following meaning:  $r$  and  $k$  are the intrinsic growth rate and carrying capacity of the first prey respectively;  $\beta$  and  $\delta$  are the intrinsic growth rate and predation rate of the second prey respectively;  $a$  is the half saturation value of the predator;

$b$  is the maximum growth rate of the predator;  $c$  is the maximum rate of predation for first prey item;  $m$  is the death rate of the predator in the absence of prey;  $\alpha$  is the quotient of the handling time of the predator per second prey item and the handling time of the predator per first prey item;  $\eta$  is the quotient of the capture rate of the second prey and the capture rate of the first prey; and finally,  $\gamma$  is the efficiency with which the second prey consumed by the predator gets converted into predator biomass (see [119] for more details).

We note that the system is not of Kolmogorov type, indeed the first equation cannot be written in the form

$$\dot{x} = x f(x, y, z).$$

Such systems can be regarded as semi-Kolmogorov systems using a terminology introduced in [22].

For system (7.3.7) we perform the stability analysis of singular points and we analyze the existence of limit cycles by Hopf bifurcation, as they play an important role in the qualitative theory of differential systems. The rest of the chapter is organized as follows: in Subsection 7.3.1 we present a preliminary analysis of the features of the model on the invariant planes, while in Subsection 7.3.2 we provide a study of the existence and stability of singular points. In Subsection 7.3.3 we discuss the problem of persistence of the three species while in Subsection 7.3.4 we present a case of Hopf bifurcation. Finally, Subsection 7.3.5 contains some conclusive remarks.

#### 7.3.1 Analysis of the system on the invariant planes

First, we show that the dynamics of the system, considering positive initial conditions, is contained in the first octant.

**Theorem 7.3.1.** *The set  $\{(x, y, z) \in \mathbb{R}^3 : x, y, z \geq 0\}$  is positively invariant for system (7.3.7).*

*Proof.* At first we must note that the planes  $z = 0$  and  $y = 0$  are invariant. On the plane  $x = 0$  we have  $\dot{x} = L y z > 0$ , then solutions do not leave the positive octant, that is, the set  $\{(x, y, z) \in \mathbb{R}^3 : x, y, z \geq 0\}$  is positively invariant.  $\square$

We analyze the dynamics on the boundary of  $\{(x, y, z) \in \mathbb{R}^3 : x, y, z \geq 0\}$ . In order to do that, we first study the dynamics on the coordinate axes and then on the planes  $y = 0$  and  $z = 0$ .

The three axes are invariant for the dynamics; in particular, any solution with initial conditions on the  $x$ -axis tends to the equilibrium  $(k, 0, 0)$ , any solution with initial conditions on the  $z$ -axis tends to the equilibrium  $(0, 0, 0)$ , and any solution with initial conditions on the  $y$ -axis satisfies that  $y(t)$  tends to infinity when  $t$  tends to infinity. See Figure 7.3.1.

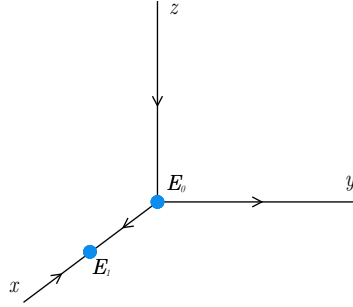


Figure 7.3.1: The dynamics on the axes.

Now we present some considerations about the dynamics on the invariant planes. On the invariant plane  $z = 0$  the system is

$$\begin{aligned}\dot{x} &= rx \left(1 - \frac{x}{k}\right), \\ \dot{y} &= \beta y,\end{aligned}$$

and for this system solutions are unbounded except that on the positive  $x$ -axis. The equilibrium points are  $(0, 0)$  and  $(k, 0)$ . The eigenvalues of  $DF(0, 0)$  are  $r$  and  $\beta$ , which are both positive, so this equilibrium is an unstable node. The eigenvalues of  $DF(k, 0)$  are  $-r$  and  $\beta$ , so the equilibrium point is a saddle.

On the plane  $y = 0$  the system is

$$\begin{aligned}\dot{x} &= rx \left(1 - \frac{x}{k}\right) - \frac{cxz}{a+x}, \\ \dot{z} &= \frac{bxz}{a+x} - mz,\end{aligned}\tag{7.3.8}$$

and the singular points are  $(0, 0)$ ,  $(k, 0)$ . If

$$kb > m(k + a),$$

there exists a further equilibrium point with coordinates  $(am/(b - m), \bar{z})$  where

$$\bar{z} = \frac{r}{c} \left( \frac{ba}{b - m} \right) \left( 1 - \frac{ma}{k(b - m)} \right).$$

The eigenvalues of  $DF(0, 0)$  are  $r$  and  $-m$ , so the origin is a saddle. The eigenvalues of  $DF(k, 0)$  are  $-r$  and  $bk/(a + k) - m$ . The first one is negative and the second changes its sign when  $bk = (a + k)m$ . When  $bk/(a + k) - m < 0$ , the singular point  $(k, 0)$  is a stable node, and when  $bk/(a + k) - m > 0$ , it loses its stability, it becomes a saddle and the third equilibrium appears.

The  $x$ -nullclines are  $x = 0$  and  $z = (r/(ck))(k - x)(a + x)$ . If  $bk/(a + k) = m$ , then  $\dot{z} = (ba(x - k))/((a + x)(a + k))z$  is positive if  $x > k$ , and negative if  $x < k$ . The local phase portrait in this case is given in Figure 7.3.2.

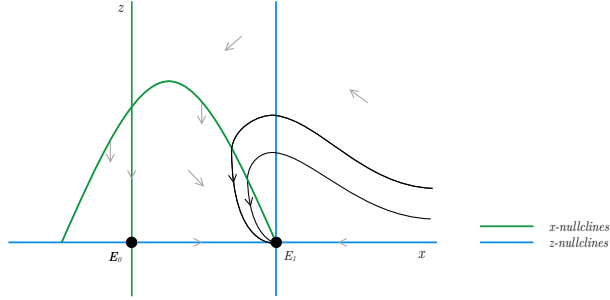


Figure 7.3.2: Phase portrait on the plane  $y = 0$  with  $bk/(a + k) = m$ .

When  $bk/(a + k) > m$ , the equilibrium  $(ma/(b - m), \bar{z})$  appears, as is it shown in Figure 7.3.3. The eigenvalues of the Jacobian matrix of system (7.3.8) at  $E_2$  are

$$\lambda_{1,2} = \frac{A_1 \pm \sqrt{A_2}}{A_3},$$

where

$$\begin{aligned} A_1 &= -cmr(k(m - b) + a(m + b)), \\ A_2 &= c^2mr \left( 4bk(b - m)^2(m(a + k) - bk) + mr(k(m - b) + a(m + b))^2 \right), \\ A_3 &= 2bck(b - m). \end{aligned} \quad (7.3.9)$$

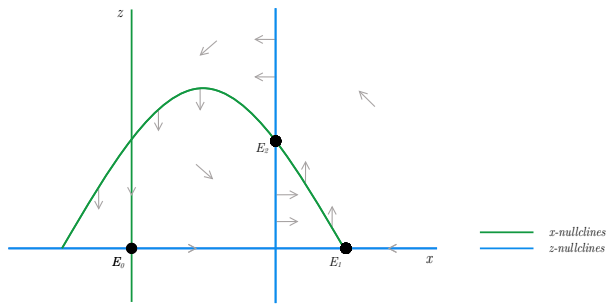


Figure 7.3.3: Phase portrait on the plane  $y = 0$  with  $bk/(a + k) > m$ .

Note that  $A_3 > 0$  by the existence conditions of the equilibrium point. These eigenvalues are complex if  $A_2 < 0$ , and in that case they have positive real part if

$$m < \frac{b(k - a)}{k + a}, \quad (7.3.10)$$

in which case  $E_2$  is unstable. If

$$m > \frac{b(k-a)}{k+a}, \quad (7.3.11)$$

the real part of the eigenvalues is negative, so  $E_2$  is asymptotically stable. In the case with  $A_2 > 0$ , as the determinant of the Jacobian matrix is positive, it is not possible that the eigenvalues have different sign. Then, if  $A_1$  is positive, both eigenvalues are positive and  $E_2$  is unstable. In other case, from the conditions  $A_1 + \sqrt{A_2} < 0$  and  $A_1 - \sqrt{A_2} < 0$ , we would get that  $A_1 < -\sqrt{A_2} < 0$ , which is a contradiction. In the same way we obtain that if  $A_1 < 0$ , then both eigenvalues are negative and  $E_2$  is asymptotically stable.

We give here some results about the possible existence of periodic orbits surrounding the equilibrium point  $E_2$  in the plane  $y = 0$ .

The equilibrium point  $E_2$  is a Hopf equilibrium if and only if  $A_1 = 0$  and  $A_2 < 0$ , it is, when  $m = b(k-a)/(k+a)$ . Note that this occurs only for  $a < k$ . We recall that, in general, when a differential system  $\dot{x} = F(x, \mu)$  in  $\mathbb{R}^n$  has an equilibrium  $x_0$  with eigenvalues  $\pm\omega i$ , it can exhibit a Hopf bifurcation, it is, a local bifurcation in which the equilibrium point loses stability as a pair of complex conjugate eigenvalues of the linearization around the equilibrium point cross the imaginary axis of the complex plane. To show that this bifurcation takes place, it is necessary to compute the first Lyapunov coefficient  $\ell_1(x_0)$  of the differential system at the equilibrium. When  $\ell_1(x_0) < 0$ , the equilibrium  $x_0$  is a weak focus of the differential system restricted to the central surface of  $x_0$ , associated to the pair of complex eigenvalues, which cross the imaginary axis, and the limit cycle that emerges from  $x_0$  is stable. In this case we say that the Hopf bifurcation is *supercritical*.

**Theorem 7.3.2.** *The equilibrium  $E_2$  of system (7.3.8) undergoes a supercritical Hopf bifurcation at  $m_0 = b(k-a)/(a+k) > 0$ . For  $m < m_0$  the system has a unique and stable limit cycle bifurcating from the equilibrium point  $E_2$ .*


*Proof.* We use the results presented on Section 1.8 for computing the first Lyapunov coefficient  $\ell_1$  at the equilibrium  $E_2$ . At first, to simplify calculations, we introduce in system (7.3.8) a new time variable  $\tau$  by  $dt = (a+x)d\tau$ , obtaining the polynomial system:

$$\begin{aligned} \dot{x} &= \frac{r}{k}x(k-x)(a+x) - cxz, \\ \dot{z} &= bxz - m(a+x)z. \end{aligned}$$

This system has the positive equilibrium

$$E_2 = \left( \frac{am}{b-m}, -\frac{abr(m(a+k)-bk)}{ck(b-m)^2} \right),$$

which is the same as  $(am/(b-m), \bar{z})$  with the notation previously introduced. The Jacobian matrix at this equilibrium is



$$A(m) = \begin{pmatrix} -\frac{amr(k(m-b)+a(b+m))}{k(b-m)^2} & -\frac{acm}{b-m} \\ -\frac{abr(m(a+k)-bk)}{ck(b-m)} & 0 \end{pmatrix},$$

and it has eigenvalues  $\mu(m) \pm \omega(m)i$ , where

$$\mu(m) = -\frac{amr(k(m-b) + a(b+m))}{2k(b-m)^2} \quad \text{and} \quad \omega(m) = \sqrt{-\frac{a^2bmr(m(a+k) - bk)}{k(b-m)^2}}.$$

We get  $\mu(m_0) = 0$  for

$$m_0 = \frac{b(k-a)}{a+k},$$

which is positive because as we have said before, a necessary condition for Hopf bifurcation is  $a < k$ . Moreover

$$\omega^2(m_0) = -\frac{abr(a-k)(a+k)}{4k} > 0.$$

Therefore, at  $m = m_0$ , the equilibrium point  $E_2$  has a pair of pure imaginary eigenvalues  $\pm i\omega(m)$  and the system has a Hopf bifurcation. The equilibrium is stable for  $m > m_0$  and unstable for  $m < m_0$ . In order to analyze this Hopf bifurcation we apply Theorem 1.8.4, so we must prove if the genericity conditions are satisfied. We check that the transversality condition is satisfied as

$$\mu'(m_0) = \frac{r(a-k)(a+k)^2}{8abk} < 0,$$

where ' represents the derivative with respect to  $m$ , and the sign is determined because  $a < k$ .

To check the second condition we must compute the first Lyapunov coefficient. We fix the value  $m = m_0$  and then the equilibrium  $E_2$  has the expression

$$E_2 = \left( \frac{k-a}{2}, \frac{r(a+k)^2}{4ck} \right).$$

We translate  $E_2$  to the origin of coordinates obtaining the system

$$\begin{aligned} \dot{\varepsilon}_1 &= -\frac{r}{k}\varepsilon_1^3 - \frac{r(k-a)}{2k}\varepsilon_1^2 - c\varepsilon_1\varepsilon_2 - \frac{ck(k-a)}{2k}\varepsilon_2, \\ \dot{\varepsilon}_2 &= \frac{2ab}{a+k}\varepsilon_1\varepsilon_2 + \frac{abr(a+k)^2}{2ck(a+k)}\varepsilon_1, \end{aligned}$$

which can be represented as

$$\dot{\varepsilon} = A\varepsilon + \frac{1}{2}B(\varepsilon, \varepsilon) + \frac{1}{6}C(\varepsilon, \varepsilon, \varepsilon),$$

where  $A = A(m_0)$  and the multilinear functions  $B$  and  $C$  are given by

$$B(\varepsilon, \eta) = \begin{pmatrix} -\frac{r(k-a)}{k}\varepsilon_1\eta_1 - c(\varepsilon_1\eta_2 + \varepsilon_2\eta_1) \\ \frac{2ab}{a+k}(\varepsilon_1\eta_2 + \varepsilon_2\eta_1) \end{pmatrix},$$



$$C(\varepsilon, \eta, \zeta) = \begin{pmatrix} \frac{-6r}{k} \varepsilon_1 \eta_1 \zeta_1 \\ 0 \end{pmatrix}.$$

We need to find two eigenvectors  $p, q$  of the matrix  $A$  satisfying

$$Aq = i\omega q, \quad A^T p = -i\omega p, \quad \text{and} \quad \langle p, q \rangle = 1,$$

as for example

$$q = \frac{1}{c(a-k)\omega} \begin{pmatrix} \frac{c(a-k)}{2} \\ \omega i \end{pmatrix} \quad \text{and} \quad p = \begin{pmatrix} \omega \\ \frac{c(a-k)}{2} i \end{pmatrix}.$$

Now we compute

$$g_{20} = \langle p, B(q, q) \rangle = \frac{4abk + r(a+k)(a-k)}{4k\omega(a+k)} + \frac{1}{k-a}i,$$

$$g_{11} = \langle p, B(q, \bar{q}) \rangle = \frac{r(a-k)}{4k\omega}, \quad g_{21} = \langle p, C(q, q, \bar{q}) \rangle = -\frac{3r}{4k\omega^2},$$

and the first Lyapunov coefficient

$$\ell_1 = \frac{1}{2\omega^2} \operatorname{Re}(ig_{20}g_{11} + \omega g_{21}) = -\frac{1}{4}r\omega k^3(a+k)^2.$$

This coefficient is negative for any values of the parameters, and so the second condition of Theorem 1.8.4 is satisfied and we can conclude that a unique and stable limit cycle bifurcates from the equilibrium point  $E_2$  through a Hopf bifurcation for  $m < m_0$ .  $\square$

Now we include some numerical experiments. We fix the parameters as follows:

$$r = k = 1, \quad a = 0.9, \quad b = 1.5, \quad c = 1.$$

In this case  $m_0 = 0.07894$  and the eigenvalues of  $J(E_2)$  are

$$\lambda_{1,2} = \pm 0.266557 i.$$

In Figure 7.3.4 we represent the case  $m = 0.18 > m_0$ , in which the equilibrium is locally asymptotically stable. In Figure 7.3.5 we represent the case  $m = 0.05 < m_0$ , in which the equilibrium loses stability and a limit cycle arises due to Hopf bifurcation.

### 7.3 A two prey and one predator system

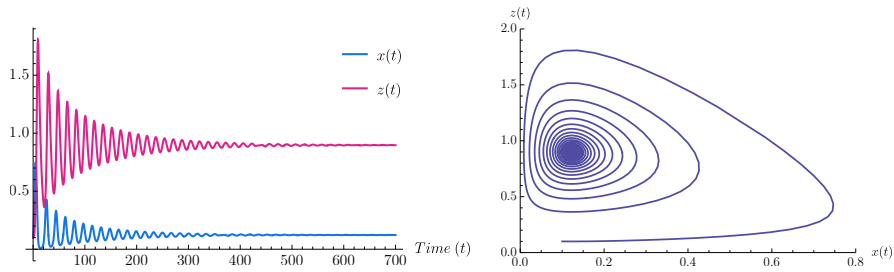


Figure 7.3.4: The time histories and the solution for  $m = 0.18 > m_0$ . In this case the equilibrium is locally asymptotically stable and nearby solutions converge to it.

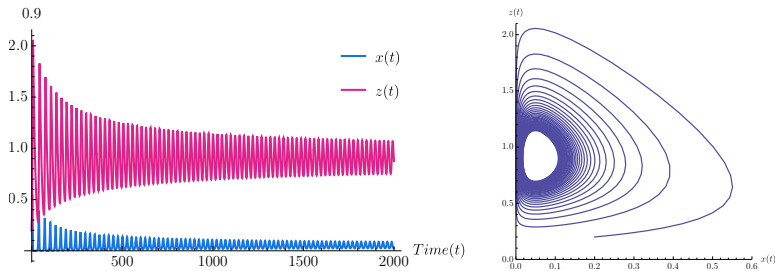


Figure 7.3.5: The time histories and the solution for  $m = 0.05 < m_0$ . In this case the equilibrium is no more locally asymptotically stable and a stable limit cycle attracts nearby solutions.

We conclude this section by determining a case in which there are no periodic orbits in  $\{y = 0\} \cap \mathbb{R}_+^3$ :

**Theorem 7.3.3.** *If*

$$r \left(1 - \frac{a}{k}\right) + \frac{bk - m(k + a)}{k} < 0,$$

*then system (7.3.8) does not admit periodic orbits in the set  $\{(x, z) \in \mathbb{R}^2 : x, z \geq 0\}$ .*

*Proof.* Let

$$f(x, z) = rx \left(1 - \frac{x}{k}\right) - \frac{cxz}{a + x} \quad \text{and} \quad g(x, z) = \frac{bxz}{a + x} - mz.$$

In order to prove the non existence of periodic orbits we use Bendixson-Dulac Theorem that states that if there exists a function  $\varphi(x, z)$  such that the term

$$\Delta(x, z) = \frac{\partial(\varphi f)}{\partial x} + \frac{\partial(\varphi g)}{\partial z}$$

does not change its sign in a simply connected set  $S$ , then there are no periodic orbits on  $S$ . We consider then function  $\varphi(y, z) = (a + x)/x$ , then:

$$\Delta(x, z) = r - \frac{a}{k}r + b - m - 2\frac{r}{k}x - \frac{am}{x}.$$

We observe that, since  $\dot{x} < 0$  for  $x \geq k$ , there are no periodic orbits in the set

$$\{(x, z) \in \mathbb{R}_+^2 : x \geq k\},$$

and for the same reason there are no periodic orbits crossing the half line  $\{x = k, z \geq 0\}$ . As a consequence we will restrict to the case  $x \leq k$  for which we obtain

$$\Delta(x, z) < r - \frac{a}{k}r + b - m - \frac{am}{k}.$$

Then  $\Delta(x, z) < 0$  in  $\{(x, z) \in \mathbb{R}_+^2 : x \leq k\}$  if  $r - \frac{a}{k}r + b - m - \frac{am}{k} < 0$  and we conclude that there are no periodic orbits in the whole set  $\{(x, z) \in \mathbb{R}_+^2\}$ .  $\square$

**Remark 7.3.4.** We observe that, for  $a < k$ , the condition of Theorem 7.3.3 on the non existence of periodic orbits

$$r \left(1 - \frac{a}{k}\right) + b < m \frac{a+k}{k},$$

that is

$$m > r \frac{k-a}{k+a} + \frac{bk}{k+a},$$

implies

$$m > b \frac{k-a}{k+a},$$

and then is compatible with the results of bifurcation analysis.

### 7.3.2 Existence and stability analysis of equilibria

The first step for studying the dynamics of the system (7.3.7) is to find all the equilibrium points and to analyze their stability.

**Theorem 7.3.5.** System (7.3.7) has the following boundary equilibria on  $\partial\mathbb{R}_+^3$ :

- $E_0 = (0, 0, 0)$  for any values of the parameters,
- $E_1 = (k, 0, 0)$  for any values of the parameters,
- If  $kb > m(a+k)$ , the equilibrium  $E_2 = (ma/(b-m), 0, \bar{z})$  with

$$\bar{z} = \frac{r}{c} \left( \frac{ba}{b-m} \right) \left( 1 - \frac{ma}{k(b-m)} \right).$$

*Proof.* This result is obtained from direct calculation.  $\square$

We also analyze the existence of non-trivial positive equilibria for system (7.3.7).

### 7.3 A two prey and one predator system

---

**Theorem 7.3.6.** *The system (7.3.7) has at least one positive equilibrium  $E^*(x^*, y^*, z^*)$  if and only if*

$$\beta cm - b(\delta + L)rx^* \left(1 - \frac{x^*}{k}\right) > 0, \quad (7.3.12)$$

where  $x^*$  is a solution of the equation

$$C_4x^4 + C_3x^3 + C_2x^2 + C_1x + C_0 = 0,$$

with the coefficients  $C_i$ ,  $i = 0, \dots, 4$  defined below.

*Proof.* By direct calculation we obtain the equilibrium  $E^* = (x^*, y^*, z^*)$ , where

$$z^* = \frac{\beta}{\delta + L},$$
$$y^* = \frac{mc}{\gamma c + bL} - \frac{(\delta + L)b}{\beta(\gamma c + bL)}rx^* \left(1 - \frac{x^*}{k}\right),$$

and  $x^*$  is the solution of the equation

$$C_4x^4 + C_3x^3 + C_2x^2 + C_1x + C_0 = 0. \quad (7.3.13)$$

We must require that  $x^*$  satisfies

$$\beta cm - b(\delta + L)rx^* \left(1 - \frac{x^*}{k}\right) > 0$$

so that  $y^*$  is positive. This is always satisfied if

$$kbr\frac{\delta + L}{\beta} < 4cm. \quad (7.3.14)$$

Otherwise this is satisfied when

$$x^* \in \left(0, \frac{k}{2} - \sqrt{\frac{k^2}{4} - \frac{k\beta cm}{br(\delta + L)}}\right) \cup \left(\frac{k}{2} + \sqrt{\frac{k^2}{4} - \frac{k\beta cm}{br(\delta + L)}}, \infty\right). \quad (7.3.15)$$

The expressions of the coefficients in equation (7.3.13) are given by

$$\begin{aligned}
 C_4 &= \frac{\gamma}{(\gamma c + bL)^2} \frac{(\delta + L)^2}{\beta^2} \frac{b^2 r^2}{k^2} \omega, \\
 C_3 &= \frac{\gamma}{(bL + c\gamma)^2} \frac{\delta + L}{\beta} \frac{br}{k} \left( -2 \frac{\delta + L}{\beta} \omega br + \gamma c + bL \right), \\
 C_2 &= \frac{\gamma}{(bL + c\gamma)^2} \frac{\delta + L}{\beta} \frac{br}{k} \left( m\omega \frac{c\gamma - bL}{\gamma} + (a - k)(\gamma c + bL) + \frac{\delta + L}{\beta} \omega br k \right), \\
 C_1 &= \frac{1}{(\gamma c + bL)^2} \left( br \frac{\delta + L}{\beta} ((m\omega - \gamma a)(\gamma c + bL) - 2m\omega \gamma c) + \gamma cm(\gamma c + bL) + \right. \\
 &\quad \left. (b - m)(\gamma c + bL)^2 \right), \\
 C_0 &= \left( ma + \frac{\omega m^2 c}{\gamma c + bL} \right) \left( \frac{\gamma c}{bL + c\gamma} - 1 \right).
 \end{aligned}$$

We apply Descartes rule of signs in equation (7.3.13) to study the existence of positive roots. The coefficient of degree zero,  $C_0$ , is always negative and the coefficient of degree four,  $C_4$ , is always positive. This means that there always exist a real positive and a real negative zero of the polynomial. The other two zeroes can be complex or real with the same sign.

The other coefficients of the polynomial can be positive, negative or zero and combining all the possible signs we obtain that:

- If one of the following conditions holds then there exists three or one positive roots of equation (7.3.13):
  - $C_1 > 0$  and  $C_3 < 0$ .
  - $C_1 > 0$ ,  $C_2 < 0$  and  $C_3 = 0$ .
  - $C_1 = 0$ ,  $C_2 > 0$  and  $C_3 < 0$ .
  - The signs of  $C_3$ ,  $C_1$  and  $-C_2$  are equal.
- In any other case, there exists one positive root of equation (7.3.13).

So that there exist at least one non-trivial interior equilibrium  $E^* = (x^*, y^*, z^*)$  of the system (7.3.7) if condition (7.3.12) is satisfied.  $\square$

**Corollary 7.3.7.** *A sufficient condition for system (7.3.7) has at least one positive equilibrium  $E^*(x^*, y^*, z^*)$  is*

$$kbr \frac{\delta + L}{\beta} < 4cm.$$

**Remark 7.3.8.** *The positive equilibria, if they exist, are all on the plane  $z = \beta/(\delta + L)$ .*

**Remark 7.3.9.** *Numerically, we have found different cases according to the existence of positive solutions for the equation (7.3.13) and the existence of positive equilibria  $E^*$ .*

### 7.3 A two prey and one predator system

---

- *There exist systems for which there is only one positive solution  $x^*$  of equation (7.3.13), and this solution is such that satisfies condition (7.3.12). As an example the system with parameters:*

$$a = 1/4, \quad b = m = 1/2, \quad c = \omega = r = \beta = \delta = L = k = \gamma = 1.$$

- *There are systems for which there is only one positive solution  $x^*$  of equation (7.3.13), and this solution does not satisfy condition (7.3.12), so there are no positive equilibria for system (7.3.7). As an example the system with parameters:*

$$a = b = c = r = \beta = \delta = k = \gamma = 1, \quad \omega = 4, \quad L = 1/4, \quad m = 0.2.$$

- *There are systems for which there are three positive solutions  $x^*$  of equation (7.3.13), and only for one of these solutions condition (7.3.12) holds, so there are one positive equilibrium for system (7.3.7). As an example the system with parameters:*

$$a = \beta = 1/10, \quad b = r = \delta = L = 1/2, \quad c = 1, \quad \omega = 2, \quad k = \gamma = 2, \quad m = 0.2.$$

- *Also there are systems for which there are three positive solutions  $x^*$  of equation (7.3.13), and none of them satisfies condition (7.3.12), so system (7.3.7) has none positive equilibria. As an example the system with parameters:*

$$a = \beta = 1/4, \quad b = \delta = L = 1/2, \quad c = 1, \quad \omega = k = \gamma = 2, \quad r = 1 \quad m = 0.2.$$

We have not found, numerically, any conditions for which equation (7.3.13) has three positive solutions  $x^*$  and the three of them satisfy condition (7.3.12), but we are not able to exclude this case analytically.

We analyze the local stability of the equilibria. To do this we consider the Jacobian matrix of the vector field

$$J(x, y, z) = \begin{pmatrix} f_{1x} & f_{1y} & f_{1z} \\ 0 & \beta - (\delta + L)z & -y(\delta + L) \\ f_{3x} & f_{3y} & f_{3z} \end{pmatrix}$$

where

$$\begin{aligned} f_{1x} &= r - \frac{2r}{k}x - \frac{(a + \omega y)cz}{(a + \omega y + x)^2} & f_{3x} &= \frac{(a + \omega y)bz}{(a + \omega y + x)^2}, \\ f_{1y} &= \frac{\omega cxz}{(a + \omega y + x)^2} + Lz, & f_{3y} &= -\frac{\omega bxz}{(a + \omega y + x)^2} + \gamma z, \\ f_{1z} &= -\frac{cx}{a + \omega y + x} + Ly, & f_{3z} &= \frac{bx}{a + \omega y + x} + \gamma y - m, \end{aligned}$$

and where we have set for simplicity  $\omega = \alpha\eta$ .

**Theorem 7.3.10.** *The stability of the boundary equilibria is the following:*

- The equilibrium point  $E_0$  is always a saddle, the  $z$ -axis is the stable manifold and it has an unstable manifold of dimension two.
- The equilibrium point  $E_1$  is a saddle with a stable manifold of dimension one if  $bk > m(a + k)$ , and with a stable manifold of dimension two if  $bk < m(a + k)$ .
- The equilibrium point  $E_2$  is unstable if  $\beta > \bar{z}(L + \delta)$  or if  $\beta < \bar{z}(L + \delta)$  and one of the following statements holds:
  - $A_2 < 0$  and condition (7.3.10) holds,
  - $A_2 > 0$  and  $A_1 > 0$ .

The equilibrium point  $E_2$  is asymptotically stable if  $\beta < \bar{z}(L + \delta)$  and one of the following statements holds:

- $A_2 < 0$  and condition (7.3.11) holds,
- $A_2 > 0$  and  $A_1 < 0$ ,

where the coefficients  $A_i$  are the ones given in (7.3.9).

*Proof.* The local stability analysis of the equilibria  $E_0$  and  $E_1$  is the same as in the case without indirect effects. For the equilibrium  $E_0 = (0, 0, 0)$  the Jacobian matrix is

$$J(E_0) = \begin{pmatrix} r & 0 & 0 \\ 0 & \beta & 0 \\ 0 & 0 & -m \end{pmatrix},$$

so there are two positive eigenvalues and one negative eigenvalue so that  $E_0$  is a saddle with a stable manifold of dimension one, which is the  $z$ -axis, and an unstable manifold of dimension two.

For the equilibrium  $E_1 = (k, 0, 0)$  we have

$$J(E_1) = \begin{pmatrix} -r & 0 & -\frac{ck}{a+k} \\ 0 & \beta & 0 \\ 0 & 0 & \frac{bk}{a+k} - m \end{pmatrix}.$$

Then, if

$$bk \neq m(a + k),$$

$E_1$  is a saddle, with two positive eigenvalues and one negative eigenvalue if

$$bk > m(a + k),$$

and with one positive eigenvalue and two negative eigenvalues if

$$bk < m(a + k).$$

### 7.3 A two prey and one predator system

When the value of  $bk$  surpasses the value of  $m(a+k)$ , a new equilibrium  $E_2 = (ma/(b-m), 0, \bar{z})$  appears, and the equilibrium  $E_1$  changes from having an unstable manifold of dimension two to an unstable manifold of dimension one. The Jacobian matrix of  $E_2$  is

$$J(E_2) = \begin{pmatrix} -\frac{mr(k(m-b) + a(m+b))}{bk(b-m)} & \frac{r(bk - m(a+k))(ab^2L + cm\omega(b-m))}{bck(b-m)^2} & -\frac{cm}{b} \\ 0 & \beta + \frac{abr(L+\delta)(m(a+k) - bk)}{ck(b-m)^2} & 0 \\ \frac{r(bk - m(a+k))}{ck} & \frac{r(bk - m(a+k))(ab\gamma + m\omega(m-b))}{ck(b-m)^2} & 0 \end{pmatrix}$$

with eigenvalues

$$\lambda_1 = \beta + \frac{ab(m(a+k) - bk)r(L+\delta)}{ck(b-m)^2}, \quad \lambda_{2,3} = \frac{A_1 \pm \sqrt{A_2}}{A_3},$$

and the coefficients  $A_i$  given in (7.3.9).

The sign of eigenvalues  $\lambda_{2,3}$  has been analyzed in Subsection 7.3.1. We note that the expression

$$\frac{-abr(L+\delta)(m(a+k) - bk)}{ck(b-m)^2}$$

can be written as  $\bar{z}(L+\delta)$ , so we conclude that the eigenvalue  $\lambda_1$  is positive if

$$\bar{z} < \frac{\beta}{L+\delta},$$

and it is negative in the other case. Combining the different possibilities for the three eigenvalues we obtain the conditions for the stability of  $E_2$ .  $\square$

**Remark 7.3.11.** We recall that in the case  $\beta = \bar{z}(L+\delta)$ , the equilibrium point  $E_2$  has two non-zero eigenvalues in the plane  $y = 0$ , as stated in Subsection 7.3.1, and the third eigenvalue is zero. The direction on the flow in the  $y$ -direction is determined by the  $z$  coordinate. Note that in this case  $\dot{y} = y(L+\delta)(\bar{z} - z)$ , so  $\dot{y}$  is positive if  $z < \bar{z}$  and  $\dot{y}$  is negative if  $z > \bar{z}$ .

**Remark 7.3.12.** We have seen that if (7.3.14) is satisfied, then there exists at least one positive equilibrium  $E^*$ . We can prove that, at least in this case, the first eigenvalue  $\lambda_1$  of  $J(E_2)$  is positive, that is  $E_2$  is unstable. We recall that  $\lambda_1$  is positive if

$$\bar{z} = \frac{r}{c} \left( \frac{ba}{b-m} \right) \left( 1 - \frac{ma}{k(b-m)} \right) \leq \frac{\beta}{L+\delta}.$$

In this case we observe that  $\bar{z} \leq \frac{kbr}{4cm}$ , in fact

$$\frac{r}{c} \left( \frac{ba}{b-m} \right) \left( 1 - \frac{ma}{k(b-m)} \right) \leq \frac{kbr}{4cm},$$

can be rewritten as

$$[k(b-m) - 2ma]^2 \geq 0,$$

which is always satisfied.



When all boundary equilibrium points are unstable we expect that there exist solutions that are attracted by an interior equilibrium or a limit cycle.

**Theorem 7.3.13.** *The positive equilibrium  $E^*$  is locally asymptotically stable if and only if  $s_1, s_2, s_3 > 0$  and  $s_1 s_2 - s_3 > 0$ , where the constants  $s_1, s_2, s_3$  are defined below.*

*Proof.* The characteristic polynomial of  $J(E^*)$  is given by the following expression:

$$\lambda^3 + s_1 \lambda^2 + s_2 \lambda + s_3 = 0,$$

where  $s_1 = -\text{Tr}(J(E^*))$ ,

$$s_2 = \begin{vmatrix} f_{1x} & f_{1y} \\ 0 & 0 \end{vmatrix} + \begin{vmatrix} f_{1x} & f_{1z} \\ f_{3x} & 0 \end{vmatrix} + \begin{vmatrix} 0 & -y^*(\delta + L) \\ f_{3y} & 0 \end{vmatrix},$$

and  $s_3 = -\det(J(E^*))$ , it is,

$$\begin{aligned} s_1 &= m + r \left( \frac{2x^*}{k} - 1 \right) - \gamma y^* + \frac{c\beta x^* - (c\beta + bx^*(L + \delta))(a + x^* + y^* \omega)}{(L + \delta)(a + x^* + \omega y^*)^2}, \\ s_2 &= m \left( r - \frac{2rx^*}{k} + \frac{c\beta(a + \omega y^*)}{(L + \delta)(a + x^* + \omega y^*)^2} \right) - \frac{1}{k(L + \delta)(a + x^* + \omega y^*)^3} \\ &\quad (\gamma y^*(L + \delta)(k(r + \beta) - 2rx^*)(a + x^* + \omega y^*)^3 + (bL(r(k - 2x^*)x^* - k\beta(x^* + y^*))) \\ &\quad + ck\beta\gamma y^* + b\delta x^*(kr - 2rx^* - k\beta))(a + x^* + \omega y^*)^2 + k\beta x^*(b(2c + L(a + x^* + y^*)) \\ &\quad + \delta(a + x^*) - c\gamma y^*))(a + x^* + \omega y^*) - 2bck\beta(x^*)^2), \\ s_3 &= \frac{\beta}{k(L + \delta)(a + x^* + \omega y^*)^4} (r\gamma y^*(k - 2x^*)(L + \delta)(a + x^* + \omega y^*)^4 + (bk(Lrx^* + L\beta y^* \\ &\quad + r\delta x^*) - ck\beta\gamma y^* - 2br(x^*)^2(L + \delta))(a + x^* + \omega y^*)^3 + x^*(abr(k - 2x^*)(L + \delta) \\ &\quad - ck\beta\gamma y^* - 2br(x^*)(L + \delta) + bk(Lrx^* - 2c\beta + L\beta y^* + r\delta x^*))(a + x^* + \omega y^*)^2 \\ &\quad + 2bck\beta x^*(a + 2x^*)(a + x^* + \omega y^*) - 2bck\beta(x^*)^2(a + x^*)). \end{aligned}$$

We use Hurwitz criterion to study the stability of the equilibrium point  $E^*$ , and we conclude that it is asymptotically stable if and only if  $s_1, s_2, s_3 > 0$  and also the expression  $s_1 s_2 - s_3$  is positive.  $\square$

**Remark 7.3.14.** *We observe that if*

$$x^* \in \left( \frac{k}{2} + \sqrt{\frac{k^2}{4} - \frac{k\beta cm}{br(\delta + L)}}, \infty \right),$$

*then  $f_{1x}$  is negative, that is  $\text{Trace}(J(E^*)) < 0$ . This means that at least one eigenvalue has negative real part.*

### 7.3.3 Some remarks about coexistence of the three species

The problem of the coexistence of the three species can be reformulated in mathematical terms by finding the conditions for which the positive solutions starting in the interior of  $\mathbb{R}_+^3$  do not approach the boundary of the set,  $\partial\mathbb{R}_+^3$  as  $t$  tends to infinity. These ideas can be made rigorous in the context of persistence theory (see [122]). There are several definitions that are used by mathematicians depending on the context. If we consider a nonlinear system of the form

$$\dot{x}(t) = f(x), \quad x \in \mathbb{R}_+^n \quad (7.3.16)$$

then we have *persistence* (see [52]) if

$$x_i(0) > 0, \quad i = 1, \dots, n \quad \Rightarrow \quad \limsup_{t \rightarrow +\infty} x_i(t) > 0, \quad i = 1, \dots, n,$$

while we have *permanence* (see [118]) if there exists  $m, M > 0$ , independent of  $x_i(0) > 0$ , such that

$$m \leq \liminf_{t \rightarrow +\infty} x(t) \leq \limsup_{t \rightarrow +\infty} x(t) \leq M.$$

Finally, we have *uniform persistence* (see [68]) if there exists  $\varepsilon > 0$ , independent of  $x_i(0) > 0$ , such that

$$\liminf_{t \rightarrow +\infty} x(t) \geq \varepsilon.$$

In many cases, the favorite choice for analysis is uniform persistence, since in real cases, requiring that  $\limsup_{t \rightarrow +\infty} x_i(t) > 0$  is not sufficient. In fact, a small stochastic or non-autonomous perturbations may lead solutions converge to the boundary. For this reason, in general, it is important to require that  $\limsup_{t \rightarrow +\infty} x_i(t) \geq \varepsilon > 0$ . We recall the definition introduced in [20]:

**Definition 7.3.15.** The system (7.3.16) is uniformly  $\rho$ -persistent if there exists  $\varepsilon > 0$  such that

$$\liminf_{t \rightarrow +\infty} \rho(x(t)) > \varepsilon,$$

for  $x(0)$  such that

$$\rho(x(0)) > 0, \quad x(0) \in \mathring{\mathbb{R}}_+^3,$$

and where

$$\rho(x) = \min\{x_1, x_2, \dots, x_n\}.$$

In order to prove uniform persistence (see Theorem 8.17 and Theorem 5.2 in [122]) we need to prove the following conditions:

(H1) There exists a compact attractor of bounded set.

(H2) The invariant sets of  $\partial\mathbb{R}_+^3$  are weakly  $\rho$ -repelling.

(H3) The invariant sets of  $\partial\mathbb{R}_+^3$  are acyclic.

Unfortunately, in the case of system (7.3.16), we cannot prove the existence of a compact attractor of bounded set of  $\mathbb{R}_+^3$  and as a consequence we are not able to obtain uniform persistence of the system. This lack of dissipativity can be guessed by considering the unbounded solutions on the invariant plane  $z = 0$ . Moreover, we recall that the divergence of the vector field  $F$  associated to the system,

$$\operatorname{div} F = f_{1x} + \beta - (\delta + L)z + f_{3z},$$

is related to the evolution of the three dimensional volumes elements under the flow of the system. We observe that it has a complex expression, in particular, there are no values of the parameters for which it has a negative sign (which means contraction), on a region of  $\partial\mathbb{R}_+^3$ . Moreover, while the first term and the second term are negative for high values of  $x$  and  $z$  respectively, the third term is positive for high value of  $y$ .

Then, we are able only to prove conditions (H2) – (H3) which only ensures that the invariant sets of  $\partial\mathbb{R}_+^3$  does not attracts positive solutions. For condition (H2) we first recall the definition:

**Definition 7.3.16.** A set  $M \subset \mathbb{R}_+^3$  is called is called weakly  $\rho$ -repelling if there is no solution  $x(t)$  of system (7.3.16) starting at  $x_0$ , with  $\rho(x_0) > 0$ , such that  $x(t) \rightarrow M$  as  $t \rightarrow +\infty$ .

**Theorem 7.3.17.** *We suppose that hypothesis of Theorem 7.3.3 is satisfied. Then the invariant set of  $\partial\mathbb{R}_+^3$  are weakly  $\rho$ -repelling in any of the following cases*

1.  $bk < k(a + m)$ ;
2.  $bk > k(a + m)$  and  $\beta > \frac{ab(bk - m(a + k))r(L + \delta)}{ck(b - m)^2}$ .

*Proof.* In order to prove the theorem it is sufficient to show that the stable manifolds of the invariant sets of  $\partial\mathbb{R}_+^3$  are all contained in  $\partial\mathbb{R}_+^3$ .

The equilibria  $E_0$  and  $E_1$  have their stable manifolds on  $\partial\mathbb{R}_+^3$  for any value of the parameters. Then if

$$b - k(m + a) < 0,$$

there are no further equilibria. Otherwise, if  $E_2$  exists, a sufficient condition that ensures that its stable manifold is in  $\partial\mathbb{R}_+^3$  consists in requiring that

$$\beta > \frac{ab(bk - m(a + k))r(L + \delta)}{ck(b - m)^2},$$

that is, its first eigenvalue is positive. To conclude the proof we have to exclude the existence of other invariant set contained in  $\partial\mathbb{R}_+^3$ . We use theorem 7.3.3 that guarantees the non existence of periodic orbits in the plane  $y = 0$ , that is, the only invariant sets of  $\partial\mathbb{R}_+^3$  are the equilibria.  $\square$

Now we pass to check condition (H3).

**Definition 7.3.18.** Let  $A, B \subset \partial\mathbb{R}_+^3$ . Then  $A$  is chained to  $B$  in  $\partial\mathbb{R}_+^3$ , and we write  $A \Rightarrow B$  if there exists a total trajectory  $x(t)$  with  $x(0) \notin A \cup B$  such that

$$x(-t) \rightarrow A, \quad x(t) \rightarrow B, \quad \text{for } t \rightarrow +\infty.$$

**Definition 7.3.19.** A finite collection  $\{M_1, \dots, M_k\}$  of subsets of  $\partial\mathbb{R}_+^3$  is called cyclic if after possibly renumbering

$$M_1 \Rightarrow M_1 \text{ or } M_1 \Rightarrow M_2 \Rightarrow \dots \Rightarrow M_j \Rightarrow M_1$$

in  $\partial\mathbb{R}_+^3$  for some  $j \in \{2, \dots, k\}$ . Otherwise it is called acyclic.

Thanks to this notion we are able to exclude the case in which orbits are attracted by an heteroclinic cycle that connects the equilibria such as in the well known case of [98].

**Theorem 7.3.20.** *If hypothesis of Theorem 7.3.3 is satisfied then the invariant sets  $\{E_0, E_1, E_2\}$  of  $\partial\mathbb{R}_+^3$  are acyclic.*

*Proof.* By hypothesis the only invariant sets of  $\partial\mathbb{R}_+^3$  are equilibria. The analysis of the previous sections is sufficient to exclude the existence of cycles between equilibria.

In Figure 7.3.6 below we represent the case in which there are only two boundary equilibria ( $E_0$  and  $E_1$ ) while in Figure 7.3.7 we represent the case in which we have also  $E_2$ . In the latter situation we distinguish two cases: both eigenvalues with positive and both with negative real part respectively.  $\square$

In conclusion, although we are not able to prove uniform persistence, the above results guarantee a sort of weak persistence of the three species.

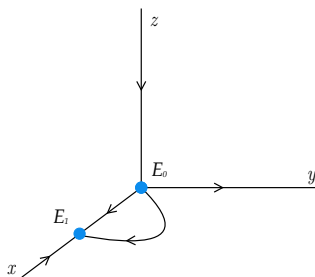


**Figure 7.3.6:** Possible connections in the cases in which there exist only two boundary equilibria.

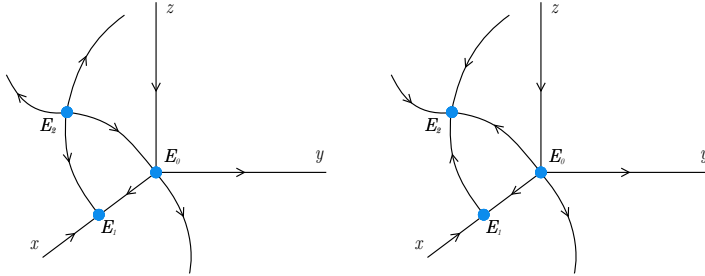


Figure 7.3.7: Possible connections in the cases in which there exists three boundary equilibria. In the first case the eigenvalues  $\lambda_{2,3}$  of  $J(E_2)$  both have positive real part while in the second they have negative real part.

### 7.3.4 Hopf bifurcation

In this section we analyze the possible existence of a limit cycle generated by Hopf bifurcation for the positive equilibrium  $E^*$ . We recall that Hopf bifurcation occurs when a pair of complex conjugate eigenvalues of the Jacobian matrix of an equilibrium crosses the imaginary axis. In this case a limit cycle arises and its stability character can be obtained by the analysis of the first Lyapunov coefficient. If it is negative, the limit cycle is stable and the bifurcation is called supercritical, otherwise it is unstable and the bifurcation is called subcritical.

Because of the complexity of the system and the high number of parameters, we are not able to perform a general bifurcation analysis. In this section we simplify this task by fixing the value of parameters and using  $m$  as bifurcation parameter.

In detail, we set:

$$a = b = c = \alpha = \eta = r = 1, \quad k = \beta = \frac{1}{2}, \quad \delta = \frac{4}{10}, \quad \gamma = L = \frac{1}{10}.$$

With the above choice of the parameters we have

$$\beta = \delta + L,$$

and as a consequence  $z^* = 1$ . In this case the equilibrium is:

$$E^* = (x^*, y^*, 1)$$

where

$$y^* = 5 [m - x^* + 2(x^*)^2]$$

and  $x^*$  is the solution of the equation

$$D_4 x^4 + D_3 x^3 + D_2 x^2 + D_1 x + D_0 = 0,$$

with

$$D_4 = 10 > 0, \quad D_3 = -9 < 0, \quad D_2 = 3 > 0, \quad D_1 = -\frac{1}{2}(m-1), \quad D_0 = -\frac{1}{2}m(1+5m).$$

Moreover the Jacobian matrix at  $E^*$  is

$$J(E^*) = \begin{pmatrix} f_{1x} & f_{1y} & f_{1z} \\ 0 & 0 & -\frac{1}{2}y^* \\ f_{3x} & f_{3y} & 0 \end{pmatrix}$$

where

$$\begin{aligned} f_{1x} &= 1 - 4x^* - \frac{(1+y^*)}{(1+x^*+y^*)^2}, & f_{3x} &= \frac{(1+y^*)}{(1+x^*+y^*)^2}, \\ f_{1y} &= \frac{x^*}{(1+x^*+y^*)^2} + \frac{1}{10}, & f_{3y} &= -\frac{x^*}{(1+x^*+y^*)^2} + \frac{1}{10}, \\ f_{1z} &= -\frac{x^*}{1+x^*+y^*} + \frac{1}{10}y^*. \end{aligned}$$

The characteristic polynomial is

$$p(\lambda) = \lambda^3 + s_1\lambda^2 + s_2\lambda + s_1$$

where

$$\begin{aligned} s_1 &= -f_{1x} = -\text{Tr}(J(E^*)), & s_2 &= -f_{1z}f_{3x} + y^*(\delta + L)f_{3y}, \\ s_3 &= -y^*(\delta + L) [f_{1x}f_{3y} - f_{1y}f_{3x}]. \end{aligned}$$

The Hurwitz matrix of the characteristic polynomial is given by

$$H(p) = \begin{pmatrix} 1 & s_2 & 0 \\ s_1 & s_3 & 0 \\ \frac{s_1s_2 - s_3}{s_1} & 0 & 0 \end{pmatrix}.$$

If  $s_1 > 0$ , we always have a negative real eigenvalue, while if  $p'(\lambda) > 0$ , that is  $s_1^2 - 3s_2 < 0$ , we ensure that the other two eigenvalues are complex conjugate. If  $s_1s_2 - s_3 > 0$  (respectively  $< 0$ ) then we have at least two eigenvalues with negative (respectively positive) real part. From Hurwitz-Routh criterion we obtain that a necessary condition for Hopf bifurcation in this case becomes

$$s_1s_2 - s_3 = f_{3x} \left[ f_{1x}f_{1z} - \frac{1}{2}y^*f_{1y} \right] = 0,$$

that is

$$f_{1x}f_{1z} - \frac{1}{2}y^*f_{1y} = 0.$$

We have numerically solved the previous equation by using the software Mathematica and we obtained the critical value

$$m_H = 0.2617.$$

For this value we obtain  $s_1 = 0.215694$ ,  $s_2 = -0.0410984$ ,  $s_3 = -0.0306826$  and  $s_1^2 - 3s_2 = 0.169819$ .

For  $m = m_H$  the eigenvalues of the Jacobian matrix  $J(E^*)$  are

$$\lambda_1 = -0.9395, \quad \lambda_{2,3} = \pm 0.2027i.$$

We will see below that as  $m$  passes through the value  $m = m_H$  the real part of the eigenvalues  $\lambda_{2,3}$  change sign from negative to positive. Then a limit cycle appears due to Hopf bifurcation of the equilibrium  $E^*$ . We are not able to exactly compute the first Lyapunov exponent of the system, however simulations and the sign of the term  $s_1 s_2 - s_3$  suggests that the cycle is stable and the equilibrium loses stability. In Figure 7.3.8 below we represent the solutions for  $m = m_H$ , as we expect, they converge to a periodic solution of period  $T = 2\pi/0.2027 = 30.9975$ .

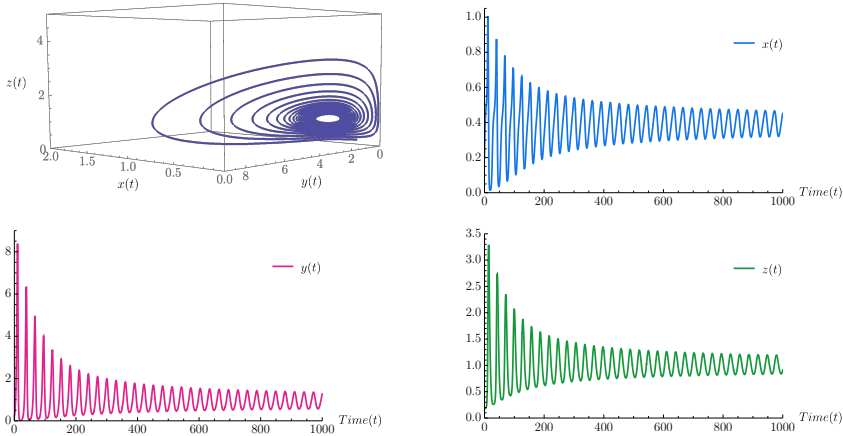


Figure 7.3.8: A limit cycle arises for  $m = m_H$ . We have represented the solution and its three components.

In order to illustrate the results of this section we present several numerical simulations. We fix the parameters as above and initial data as follows:

$$x(0) = y(0) = z(0) = \frac{1}{10}.$$

In a first numerical experiment we fix  $m = 2/10 < m_H$  and as we expect solutions converges to the equilibrium

$$E^* = (0.2668, 0.3778, 1)$$

as can be seen in Figure 7.3.9 below. In this case the eigenvalues of  $J(E^*)$  are

$$\lambda_1 = -0.5252, \quad \lambda_{2,3} = -0.0257 \pm 0.1898i,$$

and have negative real parts.

### 7.3 A two prey and one predator system

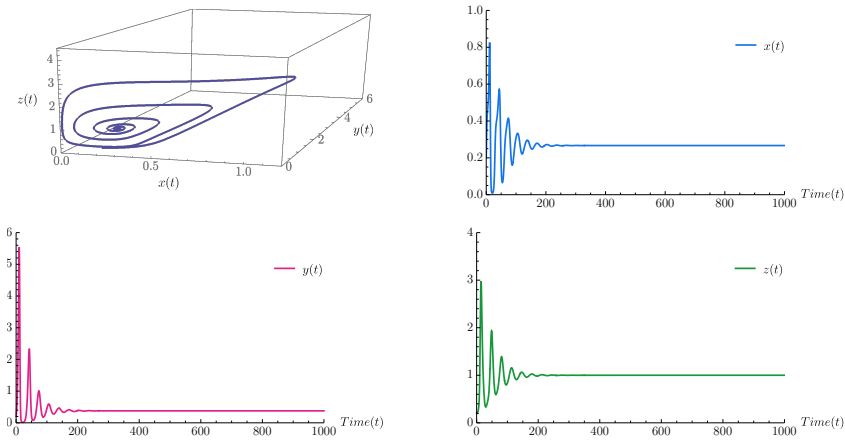


Figure 7.3.9: Graphic and time series of the solution for  $m = 2/10 < m_H$ . The positive equilibrium  $E^*$  is locally stable and nearby solutions converge to it.

In a second numerical experiment we set  $m = 4/10 > m_H$ . The positive equilibrium point

$$E^* = (0.595, 2.57, 1)$$

is unstable, the eigenvalues of  $J(E^*)$  are

$$\lambda_1 = -1.6157, \quad \lambda_{2,3} = 0.0136 \pm 0.3237i.$$

We observe that the eigenvalues  $\lambda_{2,3}$  now have positive real part and a Hopf bifurcation occurs at  $m_H = 0.2617$ . Solutions converge to a limit cycle as shown in Figure 7.3.10.

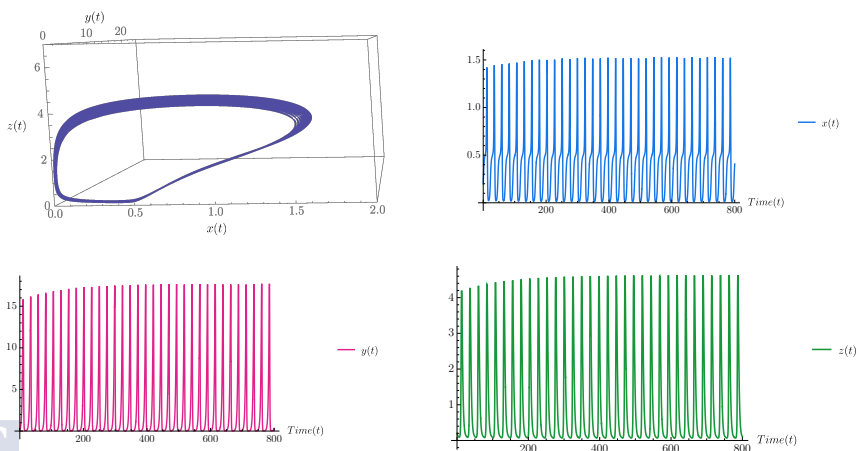


Figure 7.3.10: Graphic and time series of the solution for  $m = 4/10 > m_H$ . The positive equilibrium  $E^*$  is unstable and solutions converge to a stable limit cycle.



### 7.3.5 Conclusions

In this section we have considered a model describing the dynamics of an ecological system with two prey species and a predator species, which is a modification of the model proposed in [119]. In particular, due to the high availability of one of the two prey populations we supposed that the predator prefers to predate the more available prey population while the other one take advantages of it. Our main motivation for including this modification on the system proposed in [119] is the fact that in the literature, theoretical biologists have pointed out the importance of indirect effects in order to describe real cases of coexistence.

We have performed the stability analysis of equilibria and we have made a detailed analysis of the system on the invariant planes, including the study of the existence of Hopf bifurcation at the equilibrium point  $E_2$ . We have proved that through this bifurcation a stable limit cycle appears.

Regarding the existence of positive equilibria, the expression (7.3.13) and the verification of one of the conditions (7.3.14) or (7.3.15), give us all the positive equilibrium points. The expressions of the equilibria as a function of the parameters are too complicated and not easy to handle. Because of this, we have not been able to determine, in general, for which conditions appear none, one or three equilibria. We have obtained sufficient conditions for the existence of at least one positive equilibrium (see Corollary 7.3.7). Also, for fixed values of the parameters it is easy to compute the positive equilibria and maybe it would be possible for certain subfamilies on which less parameters are considered. We have found values of the parameters for which there exist one equilibrium point, and others for which there are not any positive equilibria, but numerically, we have not found values for which three positive equilibria exist, and therefore we think that probably this situation is not feasible, although we have not been able to prove it.

We have shown that Hopf bifurcation can occur also at the positive equilibrium  $E^*$  and as a consequence, coexistence of the three species via the existence of an attracting limit cycle is possible, by taking into account indirect effects of predation. It is worth mentioning that in [119] Hopf bifurcation is obtained only by considering a version of the model with time delay.

Furthermore, we have included a detailed discussion about the problem of persistence of the system. We have also included several numerical simulations in order to illustrate the theoretical results.

Due to the complexity of the model, we have not been able to perform a complete bifurcation analysis, then this point remains as an open problem and it would be interesting to study it in the future.

# General conclusions and future work

---

This work, which is developed in the field of qualitative dynamics of differential equations, includes some advances in the study of Lotka-Volterra and Kolmogorov systems.

First, we deal with the study of the dynamics of Lotka-Volterra systems in dimension three, for which there are, as far as we know, neither global results nor results concerning large subfamilies, but only works about very particular cases, with a reduced number of parameters, such as the May Leonard systems [12, 98].

In Chapters 2 to 5, which include the results from the articles [42, 44–46], we consider the Lotka-Volterra systems on dimension three, it is,

$$\begin{aligned}\dot{x} &= x(a_0 + a_1x + a_2y + a_3z), \\ \dot{y} &= y(b_0 + b_1x + b_2y + b_3z), \\ \dot{z} &= z(c_0 + c_1x + c_2y + c_3z),\end{aligned}$$

which have a rational first integral of degree two of the form  $x^{\lambda_1}y^{\lambda_2}z^{\lambda_3}$ . We characterize these systems by means of the Darboux theory of integrability, which allows us to reduce their study to the study of two families of planar Kolmogorov systems. As these two families turned out to be difficult to study in their totality, we have studied them with the restriction that they have a Darboux invariant of the form  $e^{st}x^{\lambda_1}z^{\lambda_2}$  for the first family, and a Darboux invariant of the form  $e^{st}y^{\lambda_1}z^{\lambda_2}$  for the second one.

While advancing in the study of Lotka-Volterra systems in dimension three, we have performed the topological classification of the global dynamics of the two families of Kolmogorov systems, each of them depending on six parameters. The results we obtain show a very rich dynamics, since for the first family we obtain a total of 100 topologically distinct global phase portraits and for the second one a total of 65.

Another field in which we have contributed has been the study of limit cycles. In particular, we have given sufficient conditions for Kolmogorov systems of degree three and dimension three to have two limit cycles appearing through a zero-Hopf bifurcation.

On the other hand, we made a review of works on population dynamics, and we have also studied two predator-prey models. First we studied a Rosenzweig-MacArthur predator-prey model, which we reduced to a Kolmogorov system in the plane. For this system we determined its possible phase portraits in the positive quadrant of the Poincaré disk, performing for this purpose a study of the dynamics at the finite and infinite singular points. We also studied the existence of limit cycles appearing by means of Hopf bifurcation. Then, we studied a system with one predator and two preys that takes into account indirect effects. For this model we studied the stability of its singular points and analyzed the existence of limit

cycles appearing through Hopf bifurcation. We also studied the restriction of this system to the invariant planes and discussed some results on persistence of the three species.

Therefore, there are different lines that have been started within this project, and we are willing to continue studying them. In particular, we plan to focus our future work on the topics that are commented below.

It is of special interest to continue the study of the global dynamics in the Poincare disk of other subfamilies of the Lotka-Volterra systems in dimension three. This can be addressed by setting other conditions directly on the Lotka-Volterra systems in dimension three (1.7.13), or by considering other conditions for the Kolmogorov systems (2.0.1) and (4.0.1).

The results about the existence of limit cycles for the Kolmogorov systems obtained in Chapter 6 can be extended to the Kolmogorov systems of higher dimension and higher degree.

Also for the Kolmogorov systems in dimension three and degree three that we have studied, we can apply the averaging theory of higher order, which may allow us to prove in some cases the existence of more than two limit cycles.

Another line of work shall be centered in the applications to real problems. From a theoretical point of view, the study of some existing population models can be improved. In the review work [43] we have detected, for example, that most of them do not address the study of the cases in which the singular points are not hyperbolic.

From our review we have found some characteristics that would be interesting to investigate more in detail. In the following we list some problems which we find interesting to address in the future.

- The functional response considered in the systems significantly affects their behavior. It seems possible that by changing the most classical functional responses and taking others as for example of Holling type III, the behavior becomes more realistic, so it would be interesting to study it.
- It would be interesting to consider models in which fear affects intraspecific competition, because as it is said in [135], there are arguments in support of this. It would be also important to get experimental evidence of this phenomenon to model it as realistic as possible.
- In some works, as [10], it is proved that cannibalism can lead to limit cycle dynamics, but it would be interesting to determine the uniqueness or non uniqueness of limit cycles for cannibalistic populations, and answer the question of how many limit cycles can appear.
- The effect of cannibalism on predator and prey simultaneously has not been studied as far as we know. But it is interesting to know what happens when both are considered and predator cannibalism has a stabilizing effect while prey cannibalism has a destabilizing effect.
- In some articles, as in [128], the authors consider small immigration in prey or in predator, but the case with immigration in both species is not studied. It would be interesting to study the effect of immigration in both species simultaneously.

Finally, we have started a work in which we are studying a problem of a different field: the study of the dynamics of the segmented disk dynamo. We are applying some of the techniques introduced in this thesis, as the Poincaré compactification or the blow up's, but also introducing some new and related results and tools, for example for dealing with the study of the existence of Darboux invariants.



# Bibliography

---

- [1] J. Alavez-Ramírez, G. Blé, V. Castellanos and J. Llibre, *On the global flow of a 3-dimensional Lotka-Volterra system*, Nonlinear Analysis, Theory, Methods and Applications, **75** (2012), 4114–4125.
- [2] W. C. Allee, *Animal aggregations: a study in general sociology*, University of Chicago Press, Chicago, 1931.
- [3] M. K. A. Al-Moqbali, N. S. Al-Salti, I. M. Elmojtaba, *Prey-Predator Models with Variable Carrying Capacity*, Mathematics, **6**(6) (2018), 102.
- [4] M. J. Álvarez, A. Ferragut and X. Jarque, *A survey on the blow up technique*, International Journal of Bifurcation and Chaos, **21**(11) (2011), 3103–3118.
- [5] A. A. Andronov, E. A. Leontovich, I. J. Gordon and A. G. Maier, *Qualitative Theory of 2nd Order Dynamic Systems*, J. Wiley & Sons, 1973.
- [6] J. C. Artés, *Sistemes diferencials quadràtics*, Universitat Autònoma de Barcelona, 1990.
- [7] J. C. Artés, F. Dumortier, C. Herssens, J. Llibre and P. De Maesschalck, *Computer program P4 to study Phase Portraits of Planar Polynomial differential equations*. <http://mat.uab.es/~artesp4/p4.htm>, 2005. [Online; accessed May 10, 2022]
- [8] J. C. Artés, J. Llibre D. Schlomiuk and N. Vulpe, *Geometric Configurations of Singularities of Planar Polynomial Differential Systems. A Global Classification in the Quadratic Case*, Birkhäuser, 2021.
- [9] J. W. Baretta, W. Ebenhöf and P. Ruudij, *The European regional seas ecosystem model, a complex marine ecosystem model*, Netherlands Journal of Sea Research, **33**(3,4) (1995), 233–246.
- [10] A. Basheer, E. Quansah, S. Bhowmick, R. D. Parshad, *Prey cannibalism alters the dynamics of Holling-Tanner-type predator-prey-models*, Nonlinear Dynamics, **85** (2016), 2549–2567.
- [11] L. Berec, *Impacts of foraging facilitation among predators on predator-prey dynamics*, Bulletin of Mathematical Biology, **72** (2010), 94–121.

- [12] G. Blé, V. Castellanos, J. Llibre and I. Quilantán, *Integrability and global dynamics of the May-Leonard model*, Nonlinear Analysis: Real World Applications, **14**(1) (2013), 280–293.
- [13] B. Bolker, M. Holyoak, V. Krivan, L. Rowe and O. Schmitz, *Connecting theoretical and empirical studies of trait-mediated interactions*, Ecology, **84**(5) (2003), 1101–1114.
- [14] P. Breitenlohner, G. Lavrelashvili and D. Maison, *Mass inflation and chaotic behaviour inside hairy black holes*, Nuclear Physics B, **524** (1998), 427–443.
- [15] L. Brenig, *Complete factorisation and analytic solutions of generalized Lotka-Volterra equations*, Physics Letters A, **133**(7) (1988), 378–382.
- [16] L. Brenig and A. Goriely, *Universal canonical forms for time-continuous dynamical systems*, Physical Review A, **40**(7) (1989), 4119–4122.
- [17] A. Buica and J. Llibre, *Averaging methods for finding periodic orbits via Brouwer degree*, Bulletin des Sciences Mathématiques, **28** (2004), 7–22.
- [18] A. Buica, J. Llibre and O. Y. Makarenkov, *On Yu. A. Mitropol'skii's Theorem on Periodic Solutions of System of Nonlinear Differential Equations with Nondifferentiable Right-Hand Sides*, Doklady Mathematics, **78** (2008), 525–527.
- [19] F. H. Busse, *Transition to turbulence via the statistical limit cycle route*, Synergetics, **39** (1978), Springer-Verlag, Berlin.
- [20] G. Butler, H. I. Freedman and P. Waltman, *Uniformly persistent systems*, Proceedings of the American Mathematical Society, **96** (3) (1968), 425–430.
- [21] L. Cairó and M. R. Feix, *Families of invariants of the motion for the Lotka-Volterra equations: the linear polynomials family*, Journal of Mathematical Physics, **33** (1992), 2440–2455.
- [22] T. Caraballo, R. Colucci and X. Han, *Non-autonomous dynamics of a semi-Kolmogorov population model with periodic forcing*, Nonlinear Analysis: Real World Applications, **31** (2016), 661–680.
- [23] T. Caraballo, R. Colucci and X. Han, *Semi-Kolmogorov models for predation with indirect effects in random environments*, Discrete and Continuous Dynamical Systems Journal, **21**(7) (2016), 2129–2143.
- [24] T. Caraballo, R. Colucci and X. Han, *Predation with indirect effects in fluctuating environments*, Nonlinear Dynamics, **84**(1) (2016), 115–126.
- [25] M. F. Carfora and I. Torricollo, *Cross-Diffusion-Driven Instability in a Predator-Prey System with Fear and Group Defense*, Mathematics, **8** (2020), 1244.
- [26] D. Cariveau, R. E. Irwin, A. K. Brody, L. S. Garcia-Mayeya and A. Von Der Ohe, *Direct and indirect effects of pollinators and seed predators to selection on plant and floral traits*, Oikos, **104**(1) (2004), 15–26.

- [27] T. Carleman, *Application de la théorie des équations intégrales linéaires aux systèmes d'équations différentielles non linéaires*, Acta Mathematica, **59** (1932), 63–87.
- [28] M. F. Carusela, F. R. Momo and L. Romanelli, *Competition, predation and coexistence in a three trophic system*, Ecological Modelling, **220**(19) (2009), 2349–2352.
- [29] C. J. Christopher, *Invariant algebraic curves and conditions for a center*, Proceedings of the Royal Society of Edinburgh, **124A** (1994), 1209–1229.
- [30] R. Colucci, *Coexistence in a one-predator, two-prey system with indirect effects*, Journal of Applied Mathematics, **2013** (2013), 625391.
- [31] R. Colucci, É. Diz-Pita and M. V. Otero-Espinar, *Dynamics of a two prey and one predator system with indirect effect*, Mathematics, **9** (2021), 436.
- [32] R. Colucci and D. Nuñez, *Periodic orbits for a three-dimensional biological differential systems*, Abstract and Applied Analysis, **2013** (2013), 465183.
- [33] N. Courbin, A. J. Loveridge, D. Macdonald, et al. *Reactive responses of zebras to lion encounters shape their predator-prey space game at large scale*, Oikos, **125** (2016), 829–838.
- [34] S. Creel, D. Christianson, S. Liley and J. A. Winnie, *Predation risk affects reproductive physiology and demography of elk*, Science, **315** (2007).
- [35] S. Creel and J. A. Winnie Jr., *Responses of elk herd size to fine-scale spatial and temporal variation in the risk of predation by wolves*, Animal Behaviour **69** (2005), 1181–1189.
- [36] S. Creel, J. A. Winnie Jr., B. Maxwell, et al., *Elk alter habitat selection as an anti-predator response to wolves*, Ecology, **86** (2005), 3387–3397.
- [37] M. Desai and P. Ormerod, *Richard Goodwin: A Short Appreciation*, The Economic Journal, **108**(450) (1998), 1431–1435.
- [38] R. L. Devaney, *Collision Orbits in the Anisotropic Kepler Problem*, Inventiones mathematicae, **45** (1978), 221–251.
- [39] W. Ding and W. Huang, *Global Dynamics of a Predator-Prey Model with General Holling Type Functional Responses*, Journal of Dynamics and Differential Equations **32** (2020), 965–978.
- [40] É. Diz-Pita, J. Llibre, M. V. Otero-Espinar and C. Valls, *The zero-Hopf bifurcations in the Kolmogorov systems of degree 3 in  $\mathbb{R}^3$* , Communications in Nonlinear Science and Numerical Simulation, **95** (2021), 105621.
- [41] É. Diz-Pita, J. Llibre, M. V. Otero-Espinar and C. Valls, *Supplementary Data to “The zero-Hopf bifurcations in the Kolmogorov systems of degree 3 in  $\mathbb{R}^3$ ”*,



- 
- [42] É. Diz-Pita, J. Llibre and M. V. Otero-Espinar, *Phase portraits of a family of Kolmogorov systems depending on six parameters*, Electronic Journal of Differential Equations, **35** (2021), 1–38.
  - [43] É. Diz-Pita and M. V. Otero-Espinar, *Predator-prey models: a review on some recent advances*, Mathematics, **9** (2021), 1783.
  - [44] É. Diz-Pita, J. Llibre and M. V. Otero-Espinar, *Planar Kolmogorov systems coming from spatial Lotka-Volterra systems*, International Journal of Bifurcation and Chaos, **31**(3) (2021), 2150201.
  - [45] É. Diz-Pita, J. Llibre and M. V. Otero-Espinar, *Phase portraits of a family of Kolmogorov systems with infinitely many singular points at infinity*, Communications in Nonlinear Science and Numerical Simulation, **104** (2022), 106038.
  - [46] É. Diz-Pita, J. Llibre and M. V. Otero-Espinar, *Planar Kolmogorov systems with infinitely many singular points at infinity*, International Journal of Bifurcation and Chaos, **32**(5) (2022).
  - [47] É. Diz-Pita, J. Llibre and M. V. Otero-Espinar, *Global phase portraits of a predator-prey system*, Electronic Journal of Qualitative Theory of Differential Equations, **16**, 1–13.
  - [48] J. Duarte, C. Januário, N Martins, et al., *Chaos and crises in a model for cooperative hunting: A symbolic dynamics approach*, Chaos, **19** (2009), 043102.
  - [49] F. Dumortier, *Singularities of vector fields on the plane*, Journal of Differential Equations, **23** (1977), 53–106.
  - [50] F. Dumortier, J. Llibre and J. C. Artés, *Qualitative Theory of Planar Differential Systems*, Universitext, Springer-Verlag, New York, 2006.
  - [51] J. Estes, K. Crooks and K., R. Holt, *Ecological Role of Predators*, Encyclopedia of Biodiversity, **4** (2001), 857–878.
  - [52] H. I. Freedman and P. Waltman, *Mathematical analysis of some three-species food chain models*, Mathematical Biosciences, **33** (1977), 257–276.
  - [53] B. R. de Freitas, J. Llibre and J. C. Medrado, *Limit cycles of continuous and discontinuous piecewise-linear differential systems in  $\mathbb{R}^3$* , Journal of Computational and Applied Mathematics, **338** (2018), 311–323.
  - [54] X. Fu, P. Zhang and J. Zhang, *Forecasting and analyzing internet user of China with Lotka-Volterra model*, Asia-Pacific Journal of Operational Research, **34**(1) (2017), 1740006.
  - [55] G. Gandolfo, *Economic dynamics*, Fourth edition. Springer, Heidelberg, 2009.
  - [56] G. Gandolfo, *Giuseppe Palomba and the Lotka-Volterra equations*, Rendiconti Lincei, **19**(4) (2008), 347–357.
-

- [57] J. Gomez and R. Zamora, *Top-down effects in a tritrophic system: parasitoids enhance plant fitness*, Ecology, **75** (1994), 1023–1030.
- [58] E. Gonzalez-Olivares, B. González-Yañez, J. Mena-Lorca, A. Rojas-Palma and J. D. Flores, *Consequences of double Allee effect on the number of limit cycles in a predator-prey model*, Computers & Mathematics with Applications, **62** (2011), 2449–3463.
- [59] E. Gonzalez-Olivares, J. Mena-Lorca, A. Rojas-Palma, et al., *Dynamical complexities in the Leslie-Gower predator-prey model as consequences of the Allee effect on prey*, Applied Mathematical Modelling, **35**(1) (2010), 366–381.
- [60] R. M. Goodwin, *A Growth Cycle*, C. H. Socialism, Capitalism and Economic Growth, Cambridge University Press, 1967.
- [61] X. Guan, Y. Liu and X. Xie, *Stability analysis of a Lotka-Volterra type predator-prey system with Allee effect on the predator species*, Communications in Mathematical Biology and Neuroscience, **9** (2018).
- [62] M. Han, J. Llibre and Y. Tian, *On the Zero-Hopf Bifurcation of the Lotka-Volterra Systems in  $\mathbb{R}^3$* , Mathematics, **8**(7) (2020), 1137.
- [63] R. H. Hering, *Oscillations in Lotka-Volterra systems of chemical reactions*, Journal of Mathematical Chemistry, **5** (1990), 197–202.
- [64] D. O. Hessen, T. Andersen, P. Brettum and B. A. Faafeng, *Phytoplankton contribution to sestonic mass and elemental ratios in lakes: implications for zooplankton nutrition*, Limnology and Oceanography: Methods, **48**(3) (2003).
- [65] D. Hilbert, *Mathematische Probleme*, Lecture, Second International Congress of Mathematicians (Paris, 1900), *Nachr. Ges. Wiss. Göttingen Math. Phys. Kl.* (1900), 253–297; English translation: Bulletin of the American Mathematical Society **8** (1902), 437–479; Bulletin (New Series) of the American Mathematical Society, **37** (2000), 407–436.
- [66] M. Hirsch, C. Pugh and M. Shub, *Invariant Manifolds*, Lecture Notes in Mathematics, Vol. 583. Springer-Verlag, 1977.
- [67] J. Hofbauer and K. Sigmund, *Evolutionary Games and Population Dynamics*, Cambridge University Press, Cambridge, 1988.
- [68] J. Hofbauer, *A general cooperation theorem for hypercycles*, Monatshefte für Mathematik, **91** (1981), 233–240.
- [69] C. S. Holling, *The components of predation as revealed by a study of small-mammal predation of the European pine sawfly*, The Canadian Entomologist, **91**(5) (1959), 293–320.
- [70] C. S. Holling, *Some characteristics of simple types of predation and parasitism*, The Canadian Entomologist, **91**(7) (1959), 385–398.

- [71] R. Huzak, *Predator-prey systems with small predator's death rate*, Electronic Journal of Qualitative Theory of Differential Equations, **86** (2018), 1–16.
- [72] Y. Ilyashenko, *Centennial history of Hilbert's 16th problem*, Bulletin (New Series) of the American Mathematical Society, **39** (2002), 301–354.
- [73] T. K. Kar, *Stability analysis of a prey-predator model incorporating a prey refuge*, Communications in Nonlinear Science and Numerical Simulation, **10** (2005), 681–691.
- [74] W. Ko and K. Ryu, *Qualitative analysis of a predator-prey model with holling type II functional response incorporating a prey refuge*, Journal of Differential Equations, **231**(2) (2006), 534–550.
- [75] C. Kohlmeier and W. Ebenhöh, *The stabilizing role of cannibalism in a predator-prey system*, Bulletin of Mathematical Biology, **57**(3) (1995), 401–411.
- [76] A. Kolmogorov, *Sulla teoria di Volterra della lotta per l'esistenza*, Giornale dell' Istituto Italiano degli Attuari, **7** (1936), 74–80.
- [77] R. Kon, *Stable Bifurcations in Multi-species Semelparous Population Models*, Advances in Difference Equations and Discrete Dynamical Systems, Springer Proceedings in Mathematics & Statistics, ICDEA, 2016, 3–25.
- [78] Y. Kuznetsov, *Elements of Applied Bifurcation Theory*, 2nd edition, Springer, 1998.
- [79] L. Lai, Z. Zhu and F. Chen, *Stability and Bifurcation in a Predator-Prey Model with the Additive Allee Effect and the Fear Effect*, Mathematics, **8** (2020), 1280.
- [80] W. E. Lamb, *Theory of an optical maser*, Physical Review Journals, **134** (1964), A1429–A1450.
- [81] G. Laval and R. Pellat, *Plasma Physics*, Proceedings of Summer School of Theoretical Physics, Gordon and Breach, NY, 1975.
- [82] J. Li, *Hilbert's 16th problem and bifurcations of planar polynomial vector fields*, International Journal of Bifurcation and Chaos, **13** (2003), 47–106.
- [83] L. P. Liou and K. S. Cheng, *On the uniqueness of a limit cycle for a predator-prey system*, SIAM Journal on Mathematical Analysis, **19**(4) (1988), 867–878.
- [84] J. Llibre and Y. P. Martínez, *Dynamics of a competitive Lotka-Volterra systems in  $\mathbb{R}^3$* , Acta Applicandae Mathematicae, **170** (2020), 569–577.
- [85] J. Llibre, Y. P. Martínez and C. Valls, *Limit cycles bifurcating of Kolmogorov systems in  $\mathbb{R}^2$  and in  $\mathbb{R}^3$* , Communications in Nonlinear Science and Numerical Simulation, **91** (2020), 105401.
- [86] J. Llibre, D. D. Novaes and M. A. Teixeira, *Higher order averaging theory for finding periodic solutions via Brouwer degree*, Nonlinearity, **27** (2014), 563–583.

- [87] J. Llibre and A. E. Teruel, *Introduction to the Qualitative Theory of Differential Equations*, Birkhäuser Advanced Texts, 2014.
- [88] J. Llibre and X. Zhang, *Darboux theory of integrability in  $\mathbb{C}^n$  taking into account the multiplicity*, Journal of Differential Equations, **246** (2009), 541–551.
- [89] J. Llibre and X. Zhang, *Darboux theory of integrability for polynomial vector fields in  $\mathbb{R}^n$  taking into account the multiplicity at infinity*, Bulletin des Sciences Mathématiques, **133** (2009), 765–778.
- [90] J. Llibre and X. Zhang, *Rational first integrals in the Darboux theory of integrability in  $\mathbb{C}^n$* , Bulletin des Sciences Mathématiques, **134** (2010), 189–195.
- [91] N. G. Lloyd, *Degree theory*, Cambridge Trends in Mathematics, 73, Cambridge University Press, 1978.
- [92] A. J. Lotka, *Elements of Physical Biology*, Waverly Press by the Williams and Wilkins Company, Baltimore, Md., U.S.A., 1925.
- [93] V. Lundgren and E. Granéli, *Grazer-induced defense in *Phaeocystis globosa* (Prymnesiophyceae): influence of different nutrient conditions*, Limnology and Oceanography: Methods, **55**(5) (2010).
- [94] Z. Ma, S. Wang, W. Li and Z. Li, *The effect of prey refuge in a patchy predator-prey system*, Mathematical Biosciences, **243**(1) (2013), 126–130.
- [95] R. Margalef, *Life forms of Phytoplanktos as survival alternative in an unstable environment*, Oceanologica Acta, **134** (1978).
- [96] L. Markus, *Global structure of ordinary differential equations in the plane*, Transactions of the American Mathematical Society, **76** (1954), 127–148.
- [97] R. M. May, *Stability and Complexity in Model Ecosystems*, Princeton NJ, 1974.
- [98] R. M. May and W. J. Leonard, *Nonlinear aspects of competition between three species*, SIAM Journal on Applied Mathematics, **29**(2) (1975), 243–253.
- [99] B. A. Menge, *Indirect effects in marine rocky intertidal interaction webs: patterns and importance*, Ecological Monographs, **65**(1) (1995), 21–74.
- [100] H. Merdan, *Stability analysis of a Lotka-Volterra type predator-prey system involving Allee effects*, The ANZIAM Journal, **52** (2010), 139–145.
- [101] D. Mukherjee, *The effect of prey refuges on a three species food chain model*, Differential Equations and Dynamical Systems, **22**(4) (2014), 413–426.
- [102] N. Neroual and T. A. Sari, *Predator-Prey System with Holling-Type Functional Response*, Proceedings of the American Mathematical Society, **148**(12) (2020), 5127–5140.

- 
- [103] D. A. Neumann, *Classification of continuous flows on 2-manifolds*, Proceedings of the American Mathematical Society, **48** (1975), 73–81.
  - [104] S. Pal, N. Pal and J. Chattopadhyay, *Hunting cooperation in a discrete-time predator-prey system*, International Journal of Bifurcation and Chaos, **28** (2018), 1850083.
  - [105] S. Pal, N. Pal, S. Samanta and J. Chattopadhyay, *Fear effect in prey and hunting co-operation among predators in a Leslie-Gower model*, Mathematical Biosciences and Engineering, **16**(5) (2019), 5146–5179.
  - [106] M. M. Peixoto, *Proceedings of a simposium held at the university of Bahia*, Academic Press, New York, 1973, 349–420.
  - [107] L. Perko, *Differential Equations and Dynamical Systems*, 3rd Edition, Texts in Applied Mathematics, Springer-Verlag, Berlin, 2001.
  - [108] H. Poincaré, *Sur les courbes définies par une équation différentielle*, Oeuvres complètes, Vol. 1, 1928.
  - [109] H. Poincaré, *Sur l'intégration des équations différentielles du premier ordre et du premier degré I*, Rendiconti del Circolo Matematico di Palermo, **5** (1891), 161–191.
  - [110] B. van der Pol, *On relaxation-oscillations*, The London, Edinburgh and Dublin Philosophical Magazine & Journal of Science, **2**(7) (1926), 978–992.
  - [111] G. A. Polis, *The evolution and dynamics of intraspecific predation*, Annual Review of Ecology and Systematics, **12** (1981), 225–251.
  - [112] L. Pribylová and A. Peniasková, *Foraging facilitation among predators and its impact on the stability of predator-prey dynamics*, Ecological Complexity, **29** (2017), 30–39.
  - [113] W. J. Ripple and E. J. Larsen, *Historic aspen recruitment, elk, and wolves in northern Yellowstone National Park*, Biological Conservation, **95** (2000), 361–370.
  - [114] M. Rosenzweig and R. MacArthur, *Graphical representation and stability conditions of predator-prey interaction*, The American Naturalist, **97** (1963), 209–223.
  - [115] O. Sarnelle, *Daphnia as keystone predators: effects on phytoplankton diversity and grazing resistance*, Journal of Plankton Research, **27**(12) (2005), 1229–1238.
  - [116] S. K. Sasmal, *Population dynamics with multiple Allee effect induced by fear factors - A mathematical study on prey-predator interactions*, Applied Mathematical Modelling, **64** (2018).
  - [117] D. Schlomiuk and N. Vulpe, *Global topological classification of Lotka-Volterra quadratic differential systems*, Electronic Journal of Differential Equations, **64** (2012), 1–69.
  - [118] P. Schuster, K. Sigmund and R. Wolff, *Dynamical systems under constant organization III. Cooperative and competitive behaviour in hypercycles*, Journal of Differential Equations, **32** (1979), 357–368.
-

## BIBLIOGRAPHY

---

- [119] S. Sharma and G. P. Samanta, *Dynamical behaviour of a two prey and one predator system*, Differential Equations and Dynamical Systems, **22** (2014), 125–145.
- [120] S. Sarwardi, P. K. Mandal and S. Ray, *Analysis of a competitive prey-predator system with a prey refuge*, Biosystems, **110**(3) (2012), 133–148.
- [121] M. J. Sheriff, C. J. Krebs and R. Boonstra, *The sensitive hare: sublethal effects of predator stress on reproduction in snowshoe hares*, Journal of Animal Ecology, **78** (2009), 1249–1258.
- [122] H. L. Smith and H. R. Thieme, *Dynamical Systems and Population Persistence*, American Mathematical Society, Providence, 2011.
- [123] W. E. Snyder and A. R. Ives, *Generalist predators disrupt biological control by a specialist parasitoid*, Ecology, **82**(3) (2001), 705–716.
- [124] S. Solomon and P. Richmond, *Stable power laws in variable economies; Lotka-Volterra implies Pareto-Zipf*, The European Physical Journal B, **27** (2002), 257–261.
- [125] A. Seidenberg, *Reduction of singularities of the differential equation  $Ady = Bdx$* , American Journal of Mathematics, **90** (1968), 248–269.
- [126] P. E. Stander, *Cooperative hunting in lions: the role of the individual*, Behavioral Ecology and Sociobiology, **29** (1992), 445–454.
- [127] J. Sugie and Y. Saito, *Uniqueness of limit cycles in a Rosenzweig-MacArthur model with prey immigration*, SIAM Journal on Applied Mathematics, **72**(1) (2012), 299–316.
- [128] T. Tahara, M. K. Areja, T. Kawano, et al., *Asymptotic stability of a modified Lotka-Volterra model with small immigrations*, Nature Scientific Reports, **8** (2018), 7029.
- [129] M. Teixeira-Alves and F. M. Hilker, *Hunting cooperation and Allee effects in predators*, Journal of Theoretical Biology, **419** (2017), 13–22.
- [130] A. Van den Essen, *Reduction of Singularities of the Differential Equation  $Ady = Bdx$* , Lecture Notes in Mathematics, **712** (1979), 248–269.
- [131] F. Vehrulst, *Nonlinear differential equations and dynamical systems*, Universitext, Springer, 1996.
- [132] V. Volterra, *Variazione fluttuazioni del numero d'individui in specie animali conienti*, Atti della Accademia nazionale dei Lincei, **2** (1926), 31–113.
- [133] M. R. Walsh and D. N. Reznick, *Interactions between the direct and indirect effects of predators determine life history evolution in a killifish*, Proceedings of the National Academy of Sciences of the United States of America, **105**(2) (2008), 594–599.
- [134] J. Wang, J. Shi and J. Wei, *Predator-prey system with strong Allee effect in prey*, Journal of Mathematical Biology, **62**(3) (2011), 291–331.

- [135] X. Wang, L. Zanette and X. Zou, *Modelling the fear effect in predator-prey interactions*, Journal of Mathematical Biology, **73**(5) (2016) 1179–1204.
- [136] A. W. Wijeratne, F. Yi and J. Wei, *Bifurcation analysis in the diffusive Lotka-Volterra system: an application to market economy*, Chaos Solitons Fractals, **40**(2) (2009), 902–911.
- [137] J. A. Winnie Jr., D. Christianson, S. Creel et al. *Elk decision-making rules are simplified in the presence of wolves*, Behavioral Ecology and Sociobiology, **61** (2006), 277.
- [138] J. A. Winnie Jr. and S. Creel, *Sex-specific behavioural responses of elk to spatial and temporal variation in the threat of wolf predation*, Animal Behaviour, **73** (2007), 215–225.
- [139] A. J. Wirsing and W. J. Ripple, *A comparison of shark and wolf research reveals similar behavioural responses by prey*, Frontiers in Ecology and the Environment, **9** (2011), 335–341.
- [140] J. T. Wootton, *Indirect effects, prey susceptibility, and habitat selection: impacts of birds on limpets and algae*, Ecology, **73**(3) (1992), 981–991.
- [141] X. Xie and L. Niu, *Global stability in a three-species Lotka-Volterra cooperation model with seasonal succession*, Mathematical Methods in the Applied Sciences, **44**(18) (2021), 14807–14822.
- [142] Y. Xie, Z. Wang, B. Meng and Z. Huang, *Dynamical analysis for a fractional-order prey-predator model with Holling III type functional response and discontinuous harvest*, Applied Mathematics Letters, **106** (2020), 106342.
- [143] L. Y. Zanette, A. F. White, M. C. Allen and M. Clinchy, *Perceived predation risk reduces the number of offspring songbirds produce per year*, Science, **334** (2011), 1398–1401.
- [144] H. Zhang, Y. Cai, S. Fu and W. Wang, *Impact of the fear effect in a prey-predator model incorporating a prey refuge*, Applied Mathematics and Computation, **356** (2019), 328–337.
- [145] Z. Zhu, R. Wu, L. Lai and X. Yu, *The influence of fear effect to the Lotka-Volterra predator-prey system with predator has other food resource*, Advances in Difference Equations, **237** (2020).
- [146] X. Zou, Y. Zheng, L. Zhang and J. Lv, *Survivability and stochastic bifurcations for a stochastic Holling type II predator-prey model*, Communications in Nonlinear Science and Numerical Simulation, **83** (2020), 105136.



# Further information

---

## Articles and journals

In compliance with the rules of doctoral studies at Universidade de Santiago de Compostela in *Regulamento dos estudos de doutoramento na USC, DOG de 16 de setembro de 2020*, we provide some information regarding the articles on which this work is based and the journals that published those articles. In particular we give the names of the authors, the title of the journals, the year each article was published, the ISSN (or EISSN), the publisher, the DOI-type link, the Journal Impact Factor and the quartile from the Journal Citation Reports, the CiteScore rating and the quartile from Scopus, and some relevant information regarding copyright and use of the articles. The links have been checked on May 10, 2022.

### Chapter 2. Article [42].

TITLE: Phase portraits of a family of Kolmogorov systems depending on six parameters.

AUTHORS: É. Diz-Pita, J. Llibre and M. V. Otero-Espinar.

JOURNAL: Electronic Journal of Differential Equations.

YEAR: 2021.

ISSN: 1072-6691.

PUBLISHER: Texas State University.

LINK: <https://ejde.math.txstate.edu/Volumes/2021/35/diz.pdf>

JOURNAL IMPACT FACTOR: The data from 2021 is still not available. The data from 2020: 1.282 [Q2 in Mathematics (106/330)].

CITESCORE: The data from 2021 is still not available. The data from 2020: 1.7 [Q2 in Mathematics - Analysis (72/164)].

INFORMATION REGARDING COPYRIGHT AND USE. The Electronic Journal of Differential Equations is an open access journal. See the website <https://ejde.math.txstate.edu>, in which the following statement can be found:

*This work is licensed under a Creative Commons Attribution 4.0 International License. This is an open access journal which means that all content is freely available without charges. Users are allowed to read, download, copy, distribute, print, search, or link to the full texts of the articles in this journal without asking prior permission from the publisher. This is in accordance with the BOAI definition of open access. Authors hold their copyrights. (Also we do not have page charges or access fees).*



**Chapter 3. Article [45].**

TITLE: Phase portraits of a family of Kolmogorov systems with infinitely many singular points at infinity.

AUTHORS: É. Diz-Pita, J. Llibre and M. V. Otero-Espinar.

JOURNAL: Communications in Nonlinear Science and Numerical Simulation.

YEAR: 2022.

ISSN: 1007-5704.

PUBLISHER: Elsevier.

LINK: <https://doi.org/10.1016/j.cnsns.2021.106038>.

JOURNAL IMPACT FACTOR: The data from 2022 is still not available. The data from 2020: 4.260 [Q1 in Applied Mathematics (5/265), in Mathematics, Interdisciplinary Applications (11/108) and in Mathematical Physics (3/55)].

CITESCORE: The data from 2022 is still not available. The data from 2020: 7.9 [Q1 in Mathematics-Applied Mathematics (15/548), in Mathematics-Numerical Analysis (3/66) and in Mathematics-Modeling and Simulation (16/290)].

INFORMATION REGARDING COPYRIGHT AND USE: Information about permissions can be found in the website: <https://www.elsevier.com/about/policies/copyright/permissions>. Furthermore, permission was directly requested from the publisher for the inclusion of the article in this thesis, and the following information was received:

*As a journal author, you retain rights for large number of author uses, including use by your employing institute or company. These rights are retained and permitted without the need to obtain specific permission from Elsevier. These include the right to include the article in full or in part in a thesis or dissertation (provided that this is not to be published commercially).*

**Chapter 4. Article [44].**

TITLE: Planar Kolmogorov systems coming from spatial Lotka-Volterra systems.

AUTHORS: É. Diz-Pita, J. Llibre and M. V. Otero-Espinar.

JOURNAL: International Journal of Bifurcation and Chaos.

YEAR: 2021.

ISSN: 0218-1274.

PUBLISHER: World Scientific Publishing.

LINK: <https://doi.org/10.1142/S0218127421502011>.

JOURNAL IMPACT FACTOR: The data from 2021 is still not available. The data from 2020: 2.836 [Q2 in Mathematics, Interdisciplinary Applications (30/108) and in Multidisciplinary Sciences (29/72)].

CITESCORE: The data from 2021 is still not available. The data from 2020: 4.2 [Q1 in Mathematics-Applied Mathematics (81/548), in Mathematics-Modeling and Simulation (64/290), in Multidisciplinary (13/110) and in Engineering-Miscellaneous (15/77)]

INFORMATION REGARDING COPYRIGHT AND USE: As indicated by the journal, a license has been requested and accepted through Copyright Clearance Center (see Permissions).

**Chapter 5. Article [46].**

TITLE: Planar Kolmogorov systems with infinitely many singular points at infinity.

AUTHORS: É. Diz-Pita, J. Llibre and M. V. Otero-Espinar.

JOURNAL: International Journal of Bifurcation and Chaos.

YEAR: 2022.

ISSN: 0218-1274.

EISSN: 1793-6551.

PUBLISHER: World Scientific Publishing.

LINK: <https://doi.org/10.1142/S0218127422500651>.

JOURNAL IMPACT FACTOR: The data from 2022 is still not available. The data from 2020: 2.836 [Q2 in Mathematics, Interdisciplinary Applications (30/108) and in Multidisciplinary Sciences (29/72)].

CITESCORE: The data from 2021 is still not available. The data from 2020: 4.2 [Q1 in Mathematics-Applied Mathematics (81/548), in Mathematics-Modeling and Simulation (64/290), in Multidisciplinary (13/110) and in Engineering-Miscellaneous (15/77)]

INFORMATION REGARDING COPYRIGHT AND USE: As indicated by the journal, a license has been requested and accepted through Copyright Clearance Center (see Permissions).

**Chapter 6. Article [40].**

TITLE: The zero-Hopf bifurcations in the Kolmogorov systems of degree 3 in  $\mathbb{R}^3$ .

AUTHORS: É. Diz-Pita, J. Llibre, M. V. Otero-Espinar and C. Valls.

JOURNAL: Communications in Nonlinear Science and Numerical Simulation.

YEAR: 2021.

ISSN: 1007-5704.

PUBLISHER: Elsevier

LINK: <https://doi.org/10.1016/j.cnsns.2020.105621>.

JOURNAL IMPACT FACTOR: The data from 2021 is still not available. The data from 2020: 4.260 [Q1 in Applied Mathematics (5/265), in Mathematics, Interdisciplinary Applications (11/108) and in Mathematical Physics (3/55)].

CITESCORE: The data from 2022 is still not available. The data from 2020: 7.9 [Q1 in Mathematics-Applied Mathematics (15/548), in Mathematics-Numerical Analysis (3/66) and in Mathematics-Modeling and Simulation (16/290)].

INFORMATION REGARDING COPYRIGHT AND USE: Information about permissions can be found in the website: <https://www.elsevier.com/about/policies/copyright/permissions>. Furthermore, permission was directly requested from the publisher for the inclusion of the article in this thesis, and the following information was received:

*As a journal author, you retain rights for large number of author uses, including use by your employing institute or company. These rights are retained and permitted without the need to obtain specific permission from Elsevier. These include the right to include the article in full or in part in a thesis or dissertation (provided that this is not to be published commercially).*

**Chapter 7. Article [43].**

TITLE: Predator-prey models: a review on some recent advances.

AUTHORS: É. Diz-Pita and M. V. Otero-Espinar.

JOURNAL: Mathematics.

YEAR: 2021.

EISSN: 2227-7390.

PUBLISHER: MDPI.

LINK: <https://doi.org/10.3390/math9151783>.

JOURNAL IMPACT FACTOR: The data from 2021 is still not available. The data from 2020: 2.258 [Q1 in Mathematics (24/330)].

CITESCORE: The data from 2021 is still not available. The data from 2020: 2.2 [Q1 in Mathematics-General Mathematics (75/378)].

INFORMATION REGARDING COPYRIGHT AND USE: Information about permissions can be found in the website: <https://www.mdpi.com/authors/rights> where the following statement is placed:

*For all articles published in MDPI journals, copyright is retained by the authors. Articles are licensed under an open access Creative Commons CC BY 4.0 license, meaning that anyone may download and read the paper for free. In addition, the article may be reused and quoted provided that the original published version is cited. These conditions allow for maximum use and exposure of the work, while ensuring that the authors receive proper credit.*

**Chapter 7. Article [47].**

TITLE: Global phase portraits of a predator-prey system.

AUTHORS: É. Diz-Pita, J. Llibre and M. V. Otero-Espinar.

JOURNAL: Electronic Journal of Qualitative Theory of Differential Equations.

YEAR: 2022.

ISSN: 1417-3875.

PUBLISHER: University of Szeged, Bolyai Institute.

LINK: <https://doi.org/10.14232/ejqtde.2022.1.16>.

JOURNAL IMPACT FACTOR: The data from 2022 is still not available. The data from 2020: 1.874 [Q1 in Mathematics (44/330), Q2 in Applied Mathematics (85/265)].

CITESCORE: The data from 2022 is still not available. The data from 2020: 1.7 [Q3 in Mathematics-Applied Mathematics (303/548)].

INFORMATION REGARDING COPYRIGHT AND USE: The Electronic Journal of Qualitative Theory of Differential Equations is a completely open access journal available online, as can be seen in the website <https://www.math.u-szeged.hu/ejqtde/subscrib.html>, where the following statement can be found:

*The Electronic Journal of Qualitative Theory of Differential Equations is an open access journal which means that all content is freely available without charge to the user or his/her institution. Users are allowed to read, download, copy, distribute, print, search, or link to*

*the full texts of the articles, or use them for any other lawful purpose, without asking prior permission from the publisher or the author. This is in accordance with the BOAI definition of open access. There are no charges and fees for publication, either.*

### **Chapter 7. Article [31].**

TITLE: Dynamics of a two prey and one predator system with indirect effect.

AUTHORS: R. Colucci, É. Diz-Pita and M. V. Otero-Espinar.

JOURNAL: Mathematics.

YEAR: 2021.

EISSN: 2227-7390.

PUBLISHER: MDPI.

LINK: <https://doi.org/10.3390/math9040436>.

JOURNAL IMPACT FACTOR: The data from 2021 is still not available. The data from 2020: 2.258 [Q1 in Mathematics (24/330)].

CITESCORE: The data from 2021 is still not available. The data from 2020: 2.2 [Q1 in Mathematics-General Mathematics (75/378)].

INFORMATION REGARDING COPYRIGHT AND USE: Information about permissions can be found in the website: <https://www.mdpi.com/authors/rights> where the following statement is placed:

*For all articles published in MDPI journals, copyright is retained by the authors. Articles are licensed under an open access Creative Commons CC BY 4.0 license, meaning that anyone may download and read the paper for free. In addition, the article may be reused and quoted provided that the original published version is cited. These conditions allow for maximum use and exposure of the work, while ensuring that the authors receive proper credit.*

## **Author contributions**

The contributions of the Ph.D. candidate were essential in all the included articles. The candidate contributed to the design of the research and proofs, to the analysis of the results and to the writing of the manuscripts.

## **Funding Information**

- Former Ministerio de Educación, Cultura y Deporte, Government of Spain. Contract FPU17/02125.
- As part of the Research Group GI-2136, Grupo de Investigación en Matemáticas (Universidade de Santiago de Compostela) both Xunta de Galicia (fund number ED431C 2019/10 with FEDER funds) and Agencia Estatal de Investigación of Spain (fund numbers MTM2016-79661-P with FEDER funds and PID2020-115155GB-I00).
- As part of the Grup de sistemes dinàmics (Universitat Autònoma de Barcelona), the Agencia Estatal de Investigación of Spain (fund number MTM2016-7727-P and number PID2019-104658GB-I00 with FEDER funds).

# Permissions

16/5/22, 11:07

<https://marketplace.copyright.com/rs-ui-web/mp/license/2e7da54e-acdf-4a12-b30a-183b242a92f9/0f8dc4f9-efd8-4adf-9e28-5fb7ce614f2a>

This is a License Agreement between Érika Diz Pita, Universidade de Santiago de Compostela ("User") and Copyright Clearance Center, Inc. ("CCC") on behalf of the Rightsholder identified in the order details below. The license consists of the order details, the CCC Terms and Conditions below, and any Rightsholder Terms and Conditions which are included below.

All payments must be made in full to CCC in accordance with the CCC Terms and Conditions below.

Order Date	16-May-2022	Type of Use	Republish in a thesis/dissertation
Order License ID	1221674-1	Publisher Portion	WSPC Chapter/article
ISSN	1793-6551		

## LICENSED CONTENT

Publication Title	International Journal of Bifurcation and Chaos	Country	Singapore
Date	01/01/1991	Rightsholder	World Scientific Publishing Co., Inc.
Language	English	Publication Type	e-Journal

## REQUEST DETAILS

Portion Type	Chapter/article	Distribution	Other territories and/or countries
Page range(s)	1-36	Enter territories/countries	Spain
Total number of pages	36	Translation	Original language of publication
Format (select all that apply)	Print, Electronic	Copies for the disabled?	No
Who will republish the content?	Academic institution	Minor editing privileges?	Yes
Duration of Use	Life of current edition	Incidental promotional use?	No
Lifetime Unit Quantity	Up to 499	Currency	EUR
Rights Requested	Main product		

## NEW WORK DETAILS

Title	Qualitative dynamics of planar and spatial Lotka-Volterra and Kolmogorov systems	Institution name	Universidade de Santiago de Compostela
Instructor name	Jaume Llibre and M. Victoria Otero Espinar	Expected presentation date	2022-07-08

## ADDITIONAL DETAILS

Order reference number	N/A	The requesting person / organization to appear on the license	Érika Diz Pita, Universidade de Santiago de Compostela
------------------------	-----	---	--

## REUSE CONTENT DETAILS

Title, description or numeric reference of the portion(s)	Planar Kolmogorov systems coming from spatial Lotka-Volterra systems	Title of the article/chapter the portion is from	Kolmogorov systems coming from spatial Lotka-Volterra systems
---	--	--	---


<https://marketplace.copyright.com/rs-ui-web/mp/license/2e7da54e-acdf-4a12-b30a-183b242a92f9/0f8dc4f9-efd8-4adf-9e28-5fb7ce614f2a>

1/4

## Further information

---

16/5/22, 11:07	<a href="https://marketplace.copyright.com/rs-ui-web/mp/license/2c7da54e-acdf-4a12-b30a-183b242a92f9/0f8dc4f9-efd8-4adf-9c28-5fb7ce614f2a">https://marketplace.copyright.com/rs-ui-web/mp/license/2c7da54e-acdf-4a12-b30a-183b242a92f9/0f8dc4f9-efd8-4adf-9c28-5fb7ce614f2a</a>		
Editor of portion(s)	N/A	Author of portion(s)	Érika Diz-Pita, Jaume Llibre, M. Victoria Otero-Espinar
Volume of serial or monograph	31		
Page or page range of portion	1-36	Issue, if republishing an article from a serial	N/A
		Publication date of portion	2021-06-12

## RIGHTSHOLDER TERMS AND CONDITIONS

1. This journal may publish some Open Access articles. Permission for reuse of all or part of these articles is granted subject to the terms of the License under which the work was published.
2. Please refer to the article's abstract page for any Open Access indication for the work that you wish to reuse. Where permission is not required for your specific reuse, please note that full and appropriate attribution must be given. This permission expressly excludes any third party copyright material which may appear in the requested work.
3. For queries, please email [openaccess@wspc.com](mailto:openaccess@wspc.com).

## CCC Terms and Conditions

1. Description of Service; Defined Terms. This Republication License enables the User to obtain licenses for republication of one or more copyrighted works as described in detail on the relevant Order Confirmation (the "Work(s)"). Copyright Clearance Center, Inc. ("CCC") grants licenses through the Service on behalf of the rightsholder identified on the Order Confirmation (the "Rightsholder"). "Republication", as used herein, generally means the inclusion of a Work, in whole or in part, in a new work or works, also as described on the Order Confirmation. "User", as used herein, means the person or entity making such republication.
2. The terms set forth in the relevant Order Confirmation, and any terms set by the Rightsholder with respect to a particular Work, govern the terms of use of Works in connection with the Service. By using the Service, the person transacting for a republication license on behalf of the User represents and warrants that he/she/it (a) has been duly authorized by the User to accept, and hereby does accept, all such terms and conditions on behalf of User, and (b) shall inform User of all such terms and conditions. In the event such person is a "freelancer" or other third party independent of User and CCC, such party shall be deemed jointly a "User" for purposes of these terms and conditions. In any event, User shall be deemed to have accepted and agreed to all such terms and conditions if User republishes the Work in any fashion.
3. Scope of License; Limitations and Obligations.
  - 3.1. All Works and all rights therein, including copyright rights, remain the sole and exclusive property of the Rightsholder. The license created by the exchange of an Order Confirmation (and/or any invoice) and payment by User of the full amount set forth on that document includes only those rights expressly set forth in the Order Confirmation and in these terms and conditions, and conveys no other rights in the Work(s) to User. All rights not expressly granted are hereby reserved.
  - 3.2. General Payment Terms: You may pay by credit card or through an account with us payable at the end of the month. If you and we agree that you may establish a standing account with CCC, then the following terms apply: Remit Payment to: Copyright Clearance Center, 29118 Network Place, Chicago, IL 60673-1291. Payments Due: Invoices are payable upon their delivery to you (or upon our notice to you that they are available to you for downloading). After 30 days, outstanding amounts will be subject to a service charge of 1-1/2% per month or, if less, the maximum rate allowed by applicable law. Unless otherwise specifically set forth in the Order Confirmation or in a separate written agreement signed by CCC, invoices are due and payable on "net 30" terms. While User may exercise the rights licensed immediately upon issuance of the Order Confirmation, the license is automatically revoked and is null and void, as if it had never been issued, if complete payment for the license is not received on a timely basis either from User directly or through a payment agent, such as a credit card company.
  - 3.3. Unless otherwise provided in the Order Confirmation, any grant of rights to User (i) is "one-time" (including the editions and product family specified in the license), (ii) is non-exclusive and non-transferable and (iii) is subject to any and all limitations and restrictions (such as, but not limited to, limitations on duration of use or circulation) included in the Order Confirmation or invoice and/or in these terms and conditions. Upon completion of the licensed use, User shall either secure a new permission for further use of the Work(s) or immediately cease any new use of the Work(s) and shall render inaccessible (such as by

<https://marketplace.copyright.com/rs-ui-web/mp/license/2c7da54e-acdf-4a12-b30a-183b242a92f9/0f8dc4f9-efd8-4adf-9c28-5fb7ce614f2a>

2/4

16/5/22, 11:07

<https://marketplace.copyright.com/rs-ui-web/mp/license/2e7da54e-acdf-4a12-b30a-183b242a92f9/0f8dc4f9-efd8-4adf-9e28-5fb7ce614f2a>

deleting or by removing or severing links or other locators) any further copies of the Work (except for copies printed on paper in accordance with this license and still in User's stock at the end of such period).

- 3.4. In the event that the material for which a republication license is sought includes third party materials (such as photographs, illustrations, graphs, inserts and similar materials) which are identified in such material as having been used by permission, User is responsible for identifying, and seeking separate licenses (under this Service or otherwise) for, any of such third party materials; without a separate license, such third party materials may not be used.
- 3.5. Use of proper copyright notice for a Work is required as a condition of any license granted under the Service. Unless otherwise provided in the Order Confirmation, a proper copyright notice will read substantially as follows: "Republished with permission of [Rightsholder's name], from [Work's title, author, volume, edition number and year of copyright]; permission conveyed through Copyright Clearance Center, Inc. " Such notice must be provided in a reasonably legible font size and must be placed either immediately adjacent to the Work as used (for example, as part of a by-line or footnote but not as a separate electronic link) or in the place where substantially all other credits or notices for the new work containing the republished Work are located. Failure to include the required notice results in loss to the Rightsholder and CCC, and the User shall be liable to pay liquidated damages for each such failure equal to twice the use fee specified in the Order Confirmation, in addition to the use fee itself and any other fees and charges specified.
- 3.6. User may only make alterations to the Work if and as expressly set forth in the Order Confirmation. No Work may be used in any way that is defamatory, violates the rights of third parties (including such third parties' rights of copyright, privacy, publicity, or other tangible or intangible property), or is otherwise illegal, sexually explicit or obscene. In addition, User may not conjoin a Work with any other material that may result in damage to the reputation of the Rightsholder. User agrees to inform CCC if it becomes aware of any infringement of any rights in a Work and to cooperate with any reasonable request of CCC or the Rightsholder in connection therewith.
4. Indemnity. User hereby indemnifies and agrees to defend the Rightsholder and CCC, and their respective employees and directors, against all claims, liability, damages, costs and expenses, including legal fees and expenses, arising out of any use of a Work beyond the scope of the rights granted herein, or any use of a Work which has been altered in any unauthorized way by User, including claims of defamation or infringement of rights of copyright, publicity, privacy or other tangible or intangible property.
5. Limitation of Liability. UNDER NO CIRCUMSTANCES WILL CCC OR THE RIGHTSHOLDER BE LIABLE FOR ANY DIRECT, INDIRECT, CONSEQUENTIAL OR INCIDENTAL DAMAGES (INCLUDING WITHOUT LIMITATION DAMAGES FOR LOSS OF BUSINESS PROFITS OR INFORMATION, OR FOR BUSINESS INTERRUPTION) ARISING OUT OF THE USE OR INABILITY TO USE A WORK, EVEN IF ONE OF THEM HAS BEEN ADVISED OF THE POSSIBILITY OF SUCH DAMAGES. In any event, the total liability of the Rightsholder and CCC (including their respective employees and directors) shall not exceed the total amount actually paid by User for this license. User assumes full liability for the actions and omissions of its principals, employees, agents, affiliates, successors and assigns.
6. Limited Warranties. THE WORK(S) AND RIGHT(S) ARE PROVIDED "AS IS". CCC HAS THE RIGHT TO GRANT TO USER THE RIGHTS GRANTED IN THE ORDER CONFIRMATION DOCUMENT. CCC AND THE RIGHTSHOLDER DISCLAIM ALL OTHER WARRANTIES RELATING TO THE WORK(S) AND RIGHT(S), EITHER EXPRESS OR IMPLIED, INCLUDING WITHOUT LIMITATION IMPLIED WARRANTIES OF MERCHANTABILITY OR FITNESS FOR A PARTICULAR PURPOSE. ADDITIONAL RIGHTS MAY BE REQUIRED TO USE ILLUSTRATIONS, GRAPHS, PHOTOGRAPHS, ABSTRACTS, INSERTS OR OTHER PORTIONS OF THE WORK (AS OPPOSED TO THE ENTIRE WORK) IN A MANNER CONTEMPLATED BY USER; USER UNDERSTANDS AND AGREES THAT NEITHER CCC NOR THE RIGHTSHOLDER MAY HAVE SUCH ADDITIONAL RIGHTS TO GRANT.
7. Effect of Breach. Any failure by User to pay any amount when due, or any use by User of a Work beyond the scope of the license set forth in the Order Confirmation and/or these terms and conditions, shall be a material breach of the license created by the Order Confirmation and these terms and conditions. Any breach not cured within 30 days of written notice thereof shall result in immediate termination of such license without further notice. Any unauthorized (but licensable) use of a Work that is terminated immediately upon notice thereof may be liquidated by payment of the Rightsholder's ordinary license price therefor; any unauthorized (and unlicensable) use that is not terminated immediately for any reason (including, for example, because materials containing the Work cannot reasonably be recalled) will be subject to all remedies available at law or in equity, but in no event to a payment of

<https://marketplace.copyright.com/rs-ui-web/mp/license/2e7da54e-acdf-4a12-b30a-183b242a92f9/0f8dc4f9-efd8-4adf-9e28-5fb7ce614f2a>

3/4

## Further information

---

16/5/22, 11:07 <https://marketplace.copyright.com/rs-ui-web/mp/license/2e7da54e-acdf-4a12-b30a-183b242a92f9/0f8dc4f9-efd8-4adf-9e28-5fb7ce614f2a>

less than three times the Rightsholder's ordinary license price for the most closely analogous licensable use plus Rightsholder's and/or CCC's costs and expenses incurred in collecting such payment.

### 8. Miscellaneous.

- 8.1. User acknowledges that CCC may, from time to time, make changes or additions to the Service or to these terms and conditions, and CCC reserves the right to send notice to the User by electronic mail or otherwise for the purposes of notifying User of such changes or additions; provided that any such changes or additions shall not apply to permissions already secured and paid for.
- 8.2. Use of User-related information collected through the Service is governed by CCC's privacy policy, available online here: <https://marketplace.copyright.com/rs-ui-web/mp/privacy-policy>
- 8.3. The licensing transaction described in the Order Confirmation is personal to User. Therefore, User may not assign or transfer to any other person (whether a natural person or an organization of any kind) the license created by the Order Confirmation and these terms and conditions or any rights granted hereunder; provided, however, that User may assign such license in its entirety on written notice to CCC in the event of a transfer of all or substantially all of User's rights in the new material which includes the Work(s) licensed under this Service.
- 8.4. No amendment or waiver of any terms is binding unless set forth in writing and signed by the parties. The Rightsholder and CCC hereby object to any terms contained in any writing prepared by the User or its principals, employees, agents or affiliates and purporting to govern or otherwise relate to the licensing transaction described in the Order Confirmation, which terms are in any way inconsistent with any terms set forth in the Order Confirmation and/or in these terms and conditions or CCC's standard operating procedures, whether such writing is prepared prior to, simultaneously with or subsequent to the Order Confirmation, and whether such writing appears on a copy of the Order Confirmation or in a separate instrument.
- 8.5. The licensing transaction described in the Order Confirmation document shall be governed by and construed under the law of the State of New York, USA, without regard to the principles thereof of conflicts of law. Any case, controversy, suit, action, or proceeding arising out of, in connection with, or related to such licensing transaction shall be brought, at CCC's sole discretion, in any federal or state court located in the County of New York, State of New York, USA, or in any federal or state court whose geographical jurisdiction covers the location of the Rightsholder set forth in the Order Confirmation. The parties expressly submit to the personal jurisdiction and venue of each such federal or state court. If you have any comments or questions about the Service or Copyright Clearance Center, please contact us at 978-750-8400 or send an e-mail to [support@copyright.com](mailto:support@copyright.com).

v 1.1

<https://marketplace.copyright.com/rs-ui-web/mp/license/2e7da54e-acdf-4a12-b30a-183b242a92f9/0f8dc4f9-efd8-4adf-9e28-5fb7ce614f2a>

4/4



13/5/22, 12:45

<https://marketplace.copyright.com/rs-ui-web/mp/license/865109af-c72f-448e-9e2e-543f7846d9b3/93fb4bb9-c5a8-49be-9aad-bb613ff4fe9a>

This is a License Agreement between Érika Diz Pita, Universidade de Santiago de Compostela ("User") and Copyright Clearance Center, Inc. ("CCC") on behalf of the Rightsholder identified in the order details below. The license consists of the order details, the CCC Terms and Conditions below, and any Rightsholder Terms and Conditions which are included below.

All payments must be made in full to CCC in accordance with the CCC Terms and Conditions below.

Order Date	13-May-2022	Type of Use	Republish in a thesis/dissertation
Order License ID	1220969-1	Publisher	WSPC
ISSN	1793-6551	Portion	Chapter/article

## LICENSED CONTENT

Publication Title	International Journal of Bifurcation and Chaos	Country	Singapore
Date	01/01/1991	Rightsholder	World Scientific Publishing Co., Inc.
Language	English	Publication Type	e-Journal

## REQUEST DETAILS

Portion Type	Chapter/article	Distribution	Other territories and/or countries
Page range(s)	1-16	Enter territories/countries	Spain
Total number of pages	16	Translation	Original language of publication
Format (select all that apply)	Print, Electronic	Copies for the disabled?	No
Who will republish the content?	Academic institution	Minor editing privileges?	Yes
Duration of Use	Life of current edition	Incidental promotional use?	No
Lifetime Unit Quantity	Up to 499	Currency	EUR
Rights Requested	Main product		

## NEW WORK DETAILS

Title	Qualitative dynamics of planar and spatial Lotka-Volterra and Kolmogorov systems	Institution name	Universidade de Santiago de Compostela
Instructor name	Jaume Llibre and M. Victoria Otero-Espinar	Expected presentation date	2022-07-15

## ADDITIONAL DETAILS

Order reference number	N/A	The requesting person / organization to appear on the license	Érika Diz Pita, Universidade de Santiago de Compostela
------------------------	-----	---	--

## REUSE CONTENT DETAILS

Title, description or numeric reference of the portion(s)	Planar Kolmogorov systems with infinitely many singular points at infinity	Title of the article/chapter the portion is from	Planar Kolmogorov systems with infinitely many singular points at infinity
---	--	--	--

<https://marketplace.copyright.com/rs-ui-web/mp/license/865109af-c72f-448e-9e2e-543f7846d9b3/93fb4bb9-c5a8-49be-9aad-bb613ff4fe9a>

1/4

## Further information

---

13/5/22, 12:45	<a href="https://marketplace.copyright.com/rs-ui-web/mp/license/865109af-c72f-448e-9e2e-543f7846d9b3/93fb4bb9-c5a8-49be-9aad-bb613ff4fe9a">https://marketplace.copyright.com/rs-ui-web/mp/license/865109af-c72f-448e-9e2e-543f7846d9b3/93fb4bb9-c5a8-49be-9aad-bb613ff4fe9a</a>			
Editor of portion(s)	N/A	Author of portion(s)	N/A	
Volume of serial or monograph	32	Issue, if republishing an article from a serial	N/A	
Page or page range of portion	1-16	Publication date of portion	2022-04-22	

## RIGHTSHOLDER TERMS AND CONDITIONS

1. This journal may publish some Open Access articles. Permission for reuse of all or part of these articles is granted subject to the terms of the License under which the work was published.
2. Please refer to the article's abstract page for any Open Access indication for the work that you wish to reuse. Where permission is not required for your specific reuse, please note that full and appropriate attribution must be given. This permission expressly excludes any third party copyright material which may appear in the requested work.
3. For queries, please email [openaccess@wspc.com](mailto:openaccess@wspc.com).

## CCC Terms and Conditions

1. Description of Service; Defined Terms. This Republication License enables the User to obtain licenses for republication of one or more copyrighted works as described in detail on the relevant Order Confirmation (the "Work(s)"). Copyright Clearance Center, Inc. ("CCC") grants licenses through the Service on behalf of the rightsholder identified on the Order Confirmation (the "Rightsholder"). "Republication", as used herein, generally means the inclusion of a Work, in whole or in part, in a new work or works, also as described on the Order Confirmation. "User", as used herein, means the person or entity making such republication.
2. The terms set forth in the relevant Order Confirmation, and any terms set by the Rightsholder with respect to a particular Work, govern the terms of use of Works in connection with the Service. By using the Service, the person transacting for a republication license on behalf of the User represents and warrants that he/she/it (a) has been duly authorized by the User to accept, and hereby does accept, all such terms and conditions on behalf of User, and (b) shall inform User of all such terms and conditions. In the event such person is a "freelancer" or other third party independent of User and CCC, such party shall be deemed jointly a "User" for purposes of these terms and conditions. In any event, User shall be deemed to have accepted and agreed to all such terms and conditions if User republishes the Work in any fashion.
3. Scope of License; Limitations and Obligations.
  - 3.1. All Works and all rights therein, including copyright rights, remain the sole and exclusive property of the Rightsholder. The license created by the exchange of an Order Confirmation (and/or any invoice) and payment by User of the full amount set forth on that document includes only those rights expressly set forth in the Order Confirmation and in these terms and conditions, and conveys no other rights in the Work(s) to User. All rights not expressly granted are hereby reserved.
  - 3.2. General Payment Terms: You may pay by credit card or through an account with us payable at the end of the month. If you and we agree that you may establish a standing account with CCC, then the following terms apply: Remit Payment to: Copyright Clearance Center, 29118 Network Place, Chicago, IL 60673-1291. Payments Due: Invoices are payable upon their delivery to you (or upon our notice to you that they are available to you for downloading). After 30 days, outstanding amounts will be subject to a service charge of 1-1/2% per month or, if less, the maximum rate allowed by applicable law. Unless otherwise specifically set forth in the Order Confirmation or in a separate written agreement signed by CCC, invoices are due and payable on "net 30" terms. While User may exercise the rights licensed immediately upon issuance of the Order Confirmation, the license is automatically revoked and is null and void, as if it had never been issued, if complete payment for the license is not received on a timely basis either from User directly or through a payment agent, such as a credit card company.
  - 3.3. Unless otherwise provided in the Order Confirmation, any grant of rights to User (i) is "one-time" (including the editions and product family specified in the license), (ii) is non-exclusive and non-transferable and (iii) is subject to any and all limitations and restrictions (such as, but not limited to, limitations on duration of use or circulation) included in the Order Confirmation or invoice and/or in these terms and conditions. Upon completion of the licensed use, User shall either secure a new permission for further use of the Work(s) or immediately cease any new use of the Work(s) and shall render inaccessible (such as by deleting or by removing or severing links or other locators) any further copies of the Work (except for copies printed on paper in accordance with this license and still in User's stock at the end of such period).

<https://marketplace.copyright.com/rs-ui-web/mp/license/865109af-c72f-448e-9e2e-543f7846d9b3/93fb4bb9-c5a8-49be-9aad-bb613ff4fe9a>

2/4

13/5/22, 12:45

<https://marketplace.copyright.com/rs-ui-web/mp/license/865109af-c72f-448e-9e2e-543f7846d9b3/93fb4bb9-e5a8-49be-9aad-bb613ff4fe9a>

- 3.4. In the event that the material for which a republication license is sought includes third party materials (such as photographs, illustrations, graphs, inserts and similar materials) which are identified in such material as having been used by permission, User is responsible for identifying, and seeking separate licenses (under this Service or otherwise) for, any of such third party materials; without a separate license, such third party materials may not be used.
- 3.5. Use of proper copyright notice for a Work is required as a condition of any license granted under the Service. Unless otherwise provided in the Order Confirmation, a proper copyright notice will read substantially as follows: "Republished with permission of [Rightsholder's name], from [Work's title, author, volume, edition number and year of copyright]; permission conveyed through Copyright Clearance Center, Inc. " Such notice must be provided in a reasonably legible font size and must be placed either immediately adjacent to the Work as used (for example, as part of a by-line or footnote but not as a separate electronic link) or in the place where substantially all other credits or notices for the new work containing the republished Work are located. Failure to include the required notice results in loss to the Rightsholder and CCC, and the User shall be liable to pay liquidated damages for each such failure equal to twice the use fee specified in the Order Confirmation, in addition to the use fee itself and any other fees and charges specified.
- 3.6. User may only make alterations to the Work if and as expressly set forth in the Order Confirmation. No Work may be used in any way that is defamatory, violates the rights of third parties (including such third parties' rights of copyright, privacy, publicity, or other tangible or intangible property), or is otherwise illegal, sexually explicit or obscene. In addition, User may not conjoin a Work with any other material that may result in damage to the reputation of the Rightsholder. User agrees to inform CCC if it becomes aware of any infringement of any rights in a Work and to cooperate with any reasonable request of CCC or the Rightsholder in connection therewith.
4. Indemnity. User hereby indemnifies and agrees to defend the Rightsholder and CCC, and their respective employees and directors, against all claims, liability, damages, costs and expenses, including legal fees and expenses, arising out of any use of a Work beyond the scope of the rights granted herein, or any use of a Work which has been altered in any unauthorized way by User, including claims of defamation or infringement of rights of copyright, publicity, privacy or other tangible or intangible property.
5. Limitation of Liability. UNDER NO CIRCUMSTANCES WILL CCC OR THE RIGHTSHOLDER BE LIABLE FOR ANY DIRECT, INDIRECT, CONSEQUENTIAL OR INCIDENTAL DAMAGES (INCLUDING WITHOUT LIMITATION DAMAGES FOR LOSS OF BUSINESS PROFITS OR INFORMATION, OR FOR BUSINESS INTERRUPTION) ARISING OUT OF THE USE OR INABILITY TO USE A WORK, EVEN IF ONE OF THEM HAS BEEN ADVISED OF THE POSSIBILITY OF SUCH DAMAGES. In any event, the total liability of the Rightsholder and CCC (including their respective employees and directors) shall not exceed the total amount actually paid by User for this license. User assumes full liability for the actions and omissions of its principals, employees, agents, affiliates, successors and assigns.
6. Limited Warranties. THE WORK(S) AND RIGHT(S) ARE PROVIDED "AS IS". CCC HAS THE RIGHT TO GRANT TO USER THE RIGHTS GRANTED IN THE ORDER CONFIRMATION DOCUMENT. CCC AND THE RIGHTSHOLDER DISCLAIM ALL OTHER WARRANTIES RELATING TO THE WORK(S) AND RIGHT(S), EITHER EXPRESS OR IMPLIED, INCLUDING WITHOUT LIMITATION IMPLIED WARRANTIES OF MERCHANTABILITY OR FITNESS FOR A PARTICULAR PURPOSE. ADDITIONAL RIGHTS MAY BE REQUIRED TO USE ILLUSTRATIONS, GRAPHS, PHOTOGRAPHS, ABSTRACTS, INSERTS OR OTHER PORTIONS OF THE WORK (AS OPPOSED TO THE ENTIRE WORK) IN A MANNER CONTEMPLATED BY USER; USER UNDERSTANDS AND AGREES THAT NEITHER CCC NOR THE RIGHTSHOLDER MAY HAVE SUCH ADDITIONAL RIGHTS TO GRANT.
7. Effect of Breach. Any failure by User to pay any amount when due, or any use by User of a Work beyond the scope of the license set forth in the Order Confirmation and/or these terms and conditions, shall be a material breach of the license created by the Order Confirmation and these terms and conditions. Any breach not cured within 30 days of written notice thereof shall result in immediate termination of such license without further notice. Any unauthorized (but licensable) use of a Work that is terminated immediately upon notice thereof may be liquidated by payment of the Rightsholder's ordinary license price therefor; any unauthorized (and unlicensable) use that is not terminated immediately for any reason (including, for example, because materials containing the Work cannot reasonably be recalled) will be subject to all remedies available at law or in equity, but in no event to a payment of less than three times the Rightsholder's ordinary license price for the most closely analogous licensable use plus Rightsholder's and/or CCC's costs and expenses incurred in collecting such payment.
8. Miscellaneous.

<https://marketplace.copyright.com/rs-ui-web/mp/license/865109af-c72f-448e-9e2e-543f7846d9b3/93fb4bb9-e5a8-49be-9aad-bb613ff4fe9a>

3/4

## Further information

---

13/5/22, 12:45

<https://marketplace.copyright.com/rs-ui-web/mp/license/865109af-c72f-448e-9e2e-543f7846d9b3/93fb4bb9-e5a8-49be-9aad-bb613ff4fe9a>

- 8.1. User acknowledges that CCC may, from time to time, make changes or additions to the Service or to these terms and conditions, and CCC reserves the right to send notice to the User by electronic mail or otherwise for the purposes of notifying User of such changes or additions; provided that any such changes or additions shall not apply to permissions already secured and paid for.
- 8.2. Use of User-related information collected through the Service is governed by CCC's privacy policy, available online here: <https://marketplace.copyright.com/rs-ui-web/mp/privacy-policy>
- 8.3. The licensing transaction described in the Order Confirmation is personal to User. Therefore, User may not assign or transfer to any other person (whether a natural person or an organization of any kind) the license created by the Order Confirmation and these terms and conditions or any rights granted hereunder; provided, however, that User may assign such license in its entirety on written notice to CCC in the event of a transfer of all or substantially all of User's rights in the new material which includes the Work(s) licensed under this Service.
- 8.4. No amendment or waiver of any terms is binding unless set forth in writing and signed by the parties. The Rightsholder and CCC hereby object to any terms contained in any writing prepared by the User or its principals, employees, agents or affiliates and purporting to govern or otherwise relate to the licensing transaction described in the Order Confirmation, which terms are in any way inconsistent with any terms set forth in the Order Confirmation and/or in these terms and conditions or CCC's standard operating procedures, whether such writing is prepared prior to, simultaneously with or subsequent to the Order Confirmation, and whether such writing appears on a copy of the Order Confirmation or in a separate instrument.
- 8.5. The licensing transaction described in the Order Confirmation document shall be governed by and construed under the law of the State of New York, USA, without regard to the principles thereof of conflicts of law. Any case, controversy, suit, action, or proceeding arising out of, in connection with, or related to such licensing transaction shall be brought, at CCC's sole discretion, in any federal or state court located in the County of New York, State of New York, USA, or in any federal or state court whose geographical jurisdiction covers the location of the Rightsholder set forth in the Order Confirmation. The parties expressly submit to the personal jurisdiction and venue of each such federal or state court. If you have any comments or questions about the Service or Copyright Clearance Center, please contact us at 978-750-8400 or send an e-mail to [support@copyright.com](mailto:support@copyright.com).

v 1.1

<https://marketplace.copyright.com/rs-ui-web/mp/license/865109af-c72f-448e-9e2e-543f7846d9b3/93fb4bb9-e5a8-49be-9aad-bb613ff4fe9a>

4/4



Ordinary differential equations are an important tool for the study of many real problems. In this thesis we focus on the qualitative dynamics of some ordinary differential systems, particularly, the Lotka-Volterra and Kolmogorov systems. We accomplish the study of some Lotka-Volterra systems on dimension three, which we characterize in two families of planar Kolmogorov systems. We give the complete classification of the global phase portraits in the Poincaré disk for those families. We also analyze the limit cycles of the three-dimensional Kolmogorov systems of degree three which appear through a zero-Hopf bifurcation. Some particular systems that model real problems in the field of population dynamics are also studied.